Wayne State University Dissertations

1-1-2016

# Development Of Gamma-Modified Atp Analogs To Study Kinase-Catalyzed Phosphorylations

Ahmed Eid Fouda
*Wayne State University,*

Follow this and additional works at: https://digitalcommons.wayne.edu/oa_dissertations

Part of the Biochemistry Commons, and the Organic Chemistry Commons

# DEVELOPMENT OF γ-MODIFIED ATP ANALOGS TO STUDY KINASE-CATALYZED PHOSPHORYLATIONS

by

**AHMED EID FOUDA**

**DISSERTATION**

Submitted to the Graduate School of

Wayne State University,

Detroit, Michigan

in partial fulfillment of the requirements

for the degree of

**DOCTOR OF PHILOSOPHY**

2016

MAJOR: CHEMISTRY (Organic)


Approved By:

_____

Advisor                                    Date


_____


_____


_____

# DEDICATION

**To my mother, my father, my wife and my children**
**The most important people in my life**

**To my grandmother who died of terminal kidney failure in October 2015**

**To all Fouda family**

# ACKNOWLEDGEMENTS

provided valuable suggestions during my projects. Also, I would like to thank Dr Mohamed Ammesou from pathology department for his great effort with me during performing the microscopy experiments. I would like to thank the members of the M. Greenberg laboratory, and Dr. X.-D. Zhang for technical support and usage of the fluorescence microscope

Lastly, I would like to thank my wife for her great support. I will not be able to achieve and reach this moment without her tremendous effort. She was taking care of everything during this long journey.

# TABLE OF CONTENTS

## CHAPTER 3 CHITOSAN-ASSISTED CELL PERMEABILIZATION OF ATP-BIOTIN FOR LIVE CELL KINASE-CATALYZED BIOTINYLATION

# LIST OF TABLES

# LIST OF FIGURES

# LIST OF SCHEMES

# LIST OF ABBREVIATIONS

## Amino Acids

A or Ala – alanine

P or Pro - proline

W or Trp - tryptophan

N or Asn - asparagine

I or Ile – isoleucine

R or Arg - arganine

V or Val - valine

H or His – histidine

Q or Gin - glutamine

G or Gly – glycine

D or Asp – aspatate

S or Ser - serine

C or Cys – cysteine

T or Thr - threonine

F or Phe – phenylalanine

E or Glu – glutamate

Y or Try - thyrosine

K or Lys – lysine

L or Leu – leucine

M or Met – Methionin

X- any amino acid

Z – hydrophobic residue

## Nucleic Acids

AMP – adenosine 5'-monophosphate

ADP - adenosine 5'-diphosphate

ATP - adenosine 5'-trihosphate

ATP-$\gamma$S– adenosine 5'-($\gamma$-thio)triphosphate

cAMP – cyclic 3',5'-monophosphate

RNA – ribonucleic acid

NADH – nicotinamide adenine dinucleotide

## Proteins

Abl – Abelson kinase

Akt1- v-akt murine thymoma viral oncogene homolog 1

CAMK4- calcium/calmodulin-dependent protein kinase IV

CBP – CREB binding protein

CDK1- cyclin-dependent kinase 1

CHK1- checkpoint kinase 1

CK1 – casein kinase

CK2 – casein kinase 2

CREB – cAMP responsive element binding protein

DFG – Aspartate Phenyl alanine Glycine

EGFR – endothelial growth factor receptor

ERK1 – extracellular signal-regulated kinase 1

GRK5- G - protein-coupled receptor kinase 5

GSK3β- glycogen synthase kinase 3 beta

HIPK1- homeodomain interacting protein kinase 1

JAK – janus kinase

MAPK – mitogen activated protein kinase

MBP– myelin basic protein

MEKK– MAPK/Erk kinase kinase

mTOR – mammalian target of rapamycin

PDK– 3- phosphoinositide -dependent protein kinase

PI3K – phosphoionositide 3 kinase

PKA – protein kinase A or cAMP regulated protein kinase

PP1 – protein phosphatase 1

Raf – protein kinase produced by the raf gene

Ras – protein kinase produced by the ras gene

RHEB – Ras homolog enriched in brain

SA-Cy5 – streptavidin –Cy5

SRC- v-src sarcoma (Schmidt-Ruppin A-2) viral oncogene homolog (avian)

STAT– signal transducer and activator of transcription

TPK – tyrosine protein kinase

TSC – Tuberous sclerosis complex

**Reagents**

APB – ATP-polyamine-biotin

BME – β-mercaptoethanol

BOC-ON – 2-(tert-butoxycarbonyloxyimino)-2-phenylacetonitrile

CDI – carbonyldiimidazole

DC – deacetylated chitosan

DMAC dimethylacetamide

DMF – dimethylformamide

DTT – dithiothreitol

EDC hydrochloride – 1-ethyl-3-(3-dimethyl aminopropyl) carbodiimide hydrochloride

FBS – fetal bovine serum

HCL – HeLa cell lysates

HDL – heat denatured HeLa cell lysates

NHS – N-hydroxy succinimide

PNBM – *p*-nitrobenzylmethylate

PVDF – polyvinylidene difluoride

SA-HRP – streptavidine- horseradish peroxidase

SA-Cy5- streptavidine-indodicarbocyanine

STSP – staurosporine

TBTU – [benzotriazol-1-yloxy(dimethylamino)methylidene]-dimethylazanium

tetrafluoroborate

TEA – triethylamine

TEAB – triethylammonium bicarbonate

TFA – trifluoroacetic acid

Tris– 2-amino-2-hydroxymethyl-propane-1,3-diol

**Techniques**

HCD – high energy collision dissociation


HPLC – high pressure liquid chromatography

MALDI-TOF – matrix assisted laser desorption/ionization time-of-flight

MS – mass spectrometry

MS/MS – tandem mass spectrometry

SDS-PAGE – sodium dodecyl sulfate polyacrylamide gel electrophores

IP – immune precipitation

K-CLIP – Kinase-CrossLinking and ImmunoPrecipitation

**Miscellaneous**

PTMs – Posttranslational modifications

# CHAPTER 1 INTRODUCTION: EXPANDING THE ENCODING GENOMES AND POST-TRANSLATIONAL MODIFICATION

(Some of the text in this chapter were reprinted or modified from: "A cell permeable ATP analog for kinase-catalyzed biotinylation". *Angew Chem Int. Ed.*, 2015, 54, 9618)[1]

The coding genome (coding DNA) is smaller by two to three fold compared to proteomes magnitude (types and numbers of proteins). The reason of the high proteome magnitude is the derivatization of proteins by two mechanisms.[2] The first is pretranslational modification and the second is posttranslational modification. In the pretranslational modification, alternative RNA splicing results in protein diversification by selective joining of the 5' and 3' splicing sites.[3] In posttranslational modifications (PTMs), proteins are derivatized after translation of RNA. PTMs diversification occur either by cleavage of a part of the protein through proteases or by covalent addition of certain groups. Examples of covalent PTMs are acetylation, acylation, adenylation, glycosylation, methylation, phosphorylation, etc.[2] PTMs allow the acquisition of new properties of proteins, such as change in protein function or access of modified proteins by proteolytic enzymes.[2] PTMs can be dynamically installed and removed as a part of controlling living cells by regulating a variety of cell signaling pathways in both normal and diseased cells.[2] Therefore, studying PTMs is important for understanding cell signaling and cell biology.

## 1.1.  Protein phosphorylation

Protein phosphorylation is a ubiquitous PTM that is catalyzed by protein kinases. Protein kinases catalyze phosphorylation of hydroxyl containing amino acids serine, threonine and tyrosine,[4-7] while dephosphorylation of phosphoproteins is catalyzed by a group of proteins called phosphatases (Figure 1).[4,5] Kinases utilize Adenosine 5'-triphosphate (ATP) as a phosphate donor, where the hydroxyl group of serine, threonine

or tyrosine on protein substrates attacks the γ-phosphate of ATP resulting in the formation of negatively charged phosphoproteins.[8] Phosphorylation and dephosphorylation dynamically regulate many cell functions by installing or removing a negatively charged phosphate group on proteins instead of neutral hydroxyl group.[9-11] For example, protein kinases regulate metabolism, transcription, cell cycle progression, cytoskeletal rearrangement, apoptosis, intracellular communications and differentiation.[12] Mutations and irregularities of protein kinases play a major role in several diseases, such as cancer, Alzheimers, Parkinsons and many others.[10,13-16] Studying kinases and their substrates is essential for drug discovery and understanding of pathogenesis of many diseases.
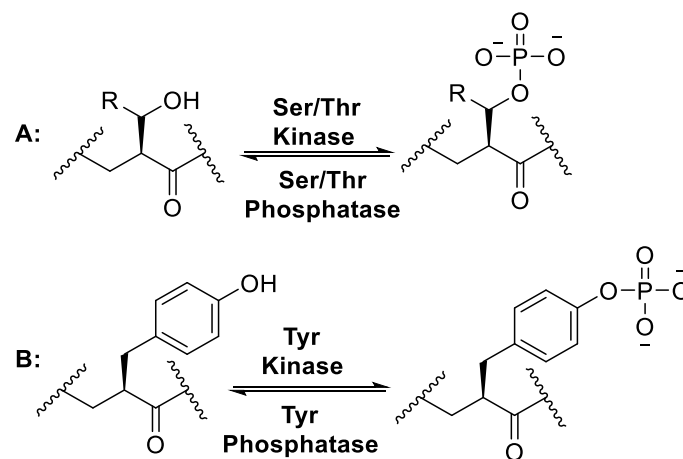


**Figure 1. 1:** Protein phosphorylation of A) Serine (R=H) and threonine (R=Me), or B) tyrosine

## 1.2.    The role of protein phosphorylation in cell biology

Protein phosphorylation regulates many cell signaling pathways that control many cell functions through protein kinases. Cell functions regulated by kinase-catalyzed phosphorylation are broad and diverse, including immunity, signal transduction in nervous system, morphogenesis, cell cycle progression, and etc. Studying kinase-catalyzed phosphorylation will provide a comprehensive understanding of cell biology, which will positively impact drug discovery.

### 1.2.1. Kinases and immunity

Many kinases control defense mechanisms through regulating the innate immunity and inflammatory responses.[11] For example, Janus (JAK) tyrosine kinases are associated with the cytoplasmic domain of cytokine receptor.[17] During inflammation, cytokines bind to cytokine receptors on cells leading to dimerization of JAKs and their activation. Upon activation of JAKs, JAKs phosphorylate several protein substrates, such as signal transducers and activators of transcription (STAT) transcription factors. STATs phosphorylation lead to their dimerization and migration to nucleus to initiate cytokines mediated responses (Figure 1.2).[11,18]
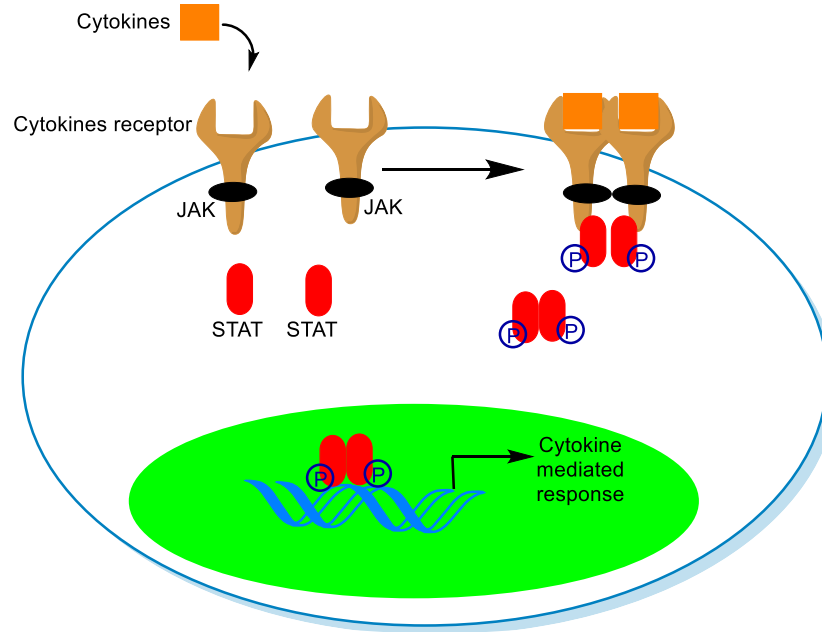
**Figure 1.2: Schematic diagram of the effect of cytokines on JAK/STAT pathway**. Upon cytokine binding to their receptor, receptor dimerization lead to JAK dimerization and activation. JAK activation leads to STAT phosphorylation, which translocate to nucleus to start an immune response.[18]

## 1.2.2. Kinases and nervous system

Transportation of proteins, lipids, and RNA along the axon of neuronal cells is called axonal transport. Axonal transport is regulated by various kinases through phosphorylation of motor and adapter proteins or through modification of microtubules. For instance, axonal transport from the cell body towards axial tips is mediated by kinesin protein and is called anterograde axonal transport. However, axonal transport in the opposite direction is called retrograde axonal transport and is mediated by cytoplasmic dynein (Figure 3). Protein kinases regulate axonal transport by phosphorylation of kinesin and dynein proteins. For example, extracellular signal-regulated kinase 1 and 2 (ERK1/2) directly phosphorylates kinesin and dynein to regulate their association with cargoes. ERK1/2 phosphorylates dynein intermediate chain 1 B (DIC1B) and 2C (DIC2C), which results in increasing dynein association with

TrkB/Rab7-positive signaling endosomes. The association leads to elevation in signaling endosomes quantities moving in the retrograde direction. On the other hand, ERK 1/2 phosphorylates the light chain of kinesin (KLC1) at Ser460 resulting in unbinding of the motor to amyloid precursor proteins (APP)-labeled vesicles, leading to slowdown in the anterograde transport. Other kinases involved in axonal transports are GSK3B, JNK, p38 MAPK, AKT, PKA, Cdk5, PKC, and PINK1.[19]
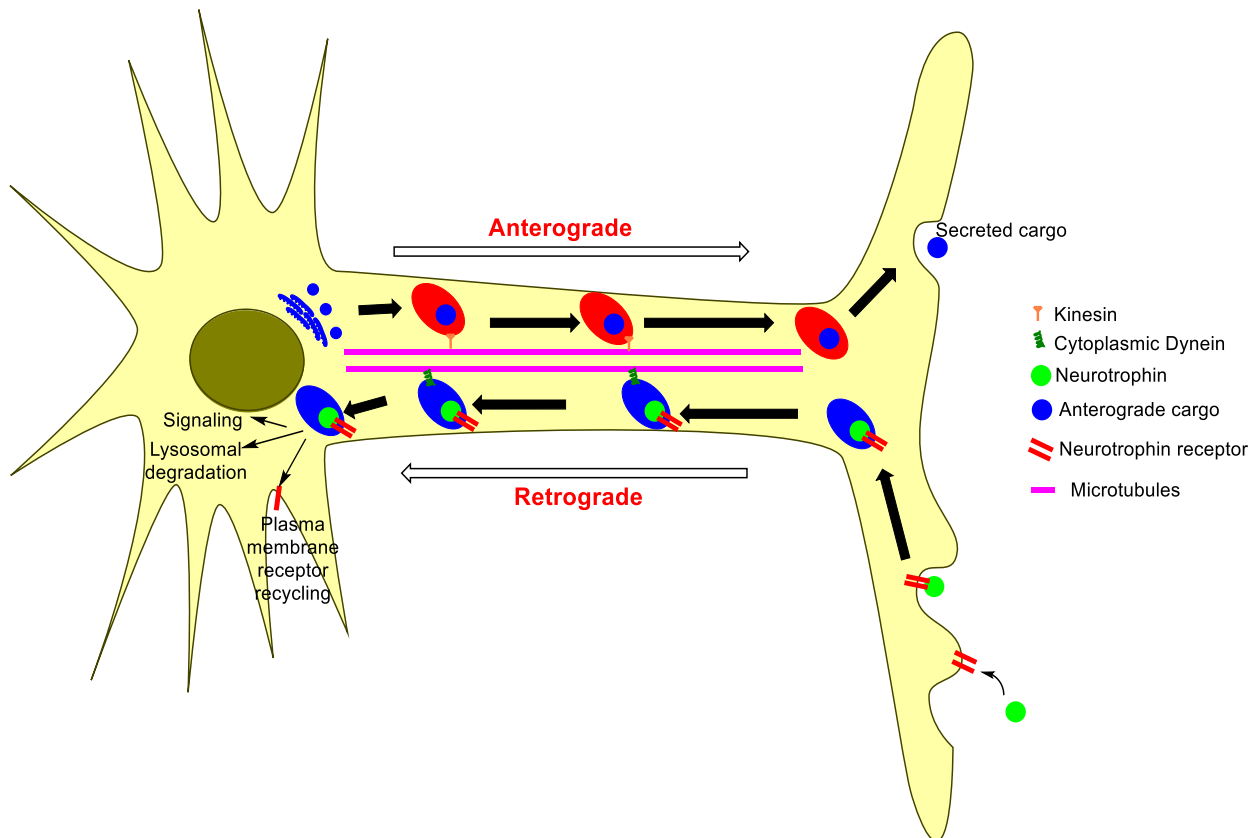


**Figure 1.3: Schematic diagram representing anterograde and retrograde axonal transport.** Anterograde transport occurs via kinesin, while retrograde transport undergo through cytoplasmic dynein.[19]

### 1.2.3. Kinases and cell signaling pathways

Cell growth, arrest and apoptosis are regulated by kinase protein. For example, cell growth is mediated through PI3K/Akt signaling pathway (Figure 4). Upon activation of receptor tyrosine kinase, autoinhibition of PI3K is removed and the enzyme becomes

catalytically active. Activated PI3K will catalyze the phosphorylation of phosphatidylinisitol diphosphate (PIP2) into phosphatidylinisitol triphosphate (PIP3). [20]PIP3 activates PDK1 by binding to its pleckstrin homology domain. Afterwards, activated phosphoinositide-dependent kinase 1 (PDK1) phosphorylates Akt1 at Thr308.[21] Akt1 is then activated by phosphorylation at Ser473 by mTORC2 resulting in signaling events.[21] Activated Akt1 phosphorylates its substrates, which prime cell cycle progression, survival, migration, and metabolism (Figure 1.4).[21] Several reports revealed numerous non redundant Akt1 substrates, which are involved in different aspects of cell function.[22-24]
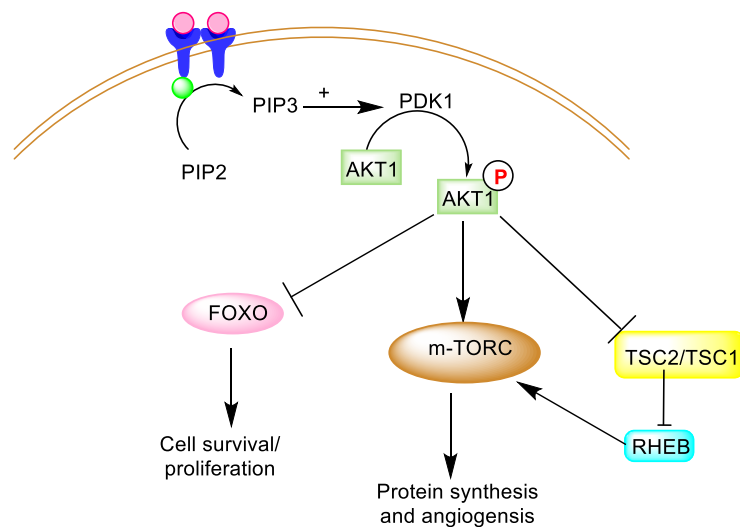


**Figure 1.4: Schematic diagram representing PI3K/Akt pathway[21]**

### 1.2.4. Phosphorylation and protein-protein interactions

Phosphorylation plays a crucial role in protein-protein interactions, which regulate trafficking in cells. For example, CREB (cyclic adenosine 3', 5'-monophosphate responsive element binding) -CBP (CREB binding protein) interaction is dependent on phosphorylation of CREB.[25,26] CREB is phosphorylated at serine-133 to yield a negatively charged phosphoserine residue. The phosphorylation of CREB induces a

hydrogen bond between CREB S-133 and Y-658 on CBP, which induces their interactions.[25] The CREB-CBP interaction positively induces the transcriptional activity of CREB.

## 1.3.    The role of kinases in formation of diseases

Kinase enzymes are involved in many diseases such as rheumatoid arthritis,[27] diabetes,[28] Parkinsons,[29,30] cardiovascular diseases,[31,32] and cancer.[33] For instance, MAPK pathway is hyperactivated by cytokines, such as TNF-α, in rheumatoid arthritis patient. Upon activation of the pathway, MAPK kinase kinase phosphorylates MAPK kinases (MKK) that consequently phosphorylates MAPK. MAPK includes extracellular signal-regulated kinases (ERK) and the p38 kinase (p38) that activate several transcriptional factors upon MAPK phosphorylation (Figure 1.5).[27]
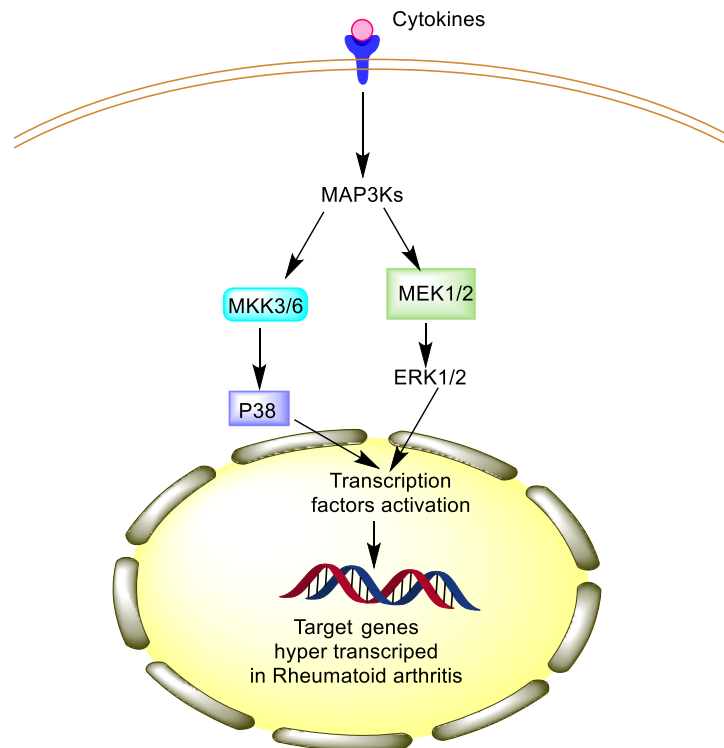


**Figure 1.5: Schematic diagram representing the role of several kinases in Rhematoid arthritis.[27]**

Another example, epidermal growth factor receptor tyrosine kinases (EGFR-TKs) is associated with cancer. In normal cells, epidermal growth factor (EGF) binds to cell surface receptor of EGFR-TK, which leads to dimerization of the cell surface receptor of EGFR-TK (Figure 1.6).[33,34] Dimerization of the EGFR-TK receptor triggers the activation of signal transduction pathway. In tumor cells, EGFR-TK receptors are elevated or hyperactivated due to excess ligand, which leads to higher expression of cell surface receptor or mutations and aberrant cell growth and malignancy.[33,34] As a third example example, BRAF kinase is mutated in 66% of melanomas.[35] Mutation of BRAF kinase lead to increase of its activity, which increases cancer proliferation.[35] Lastly in Parkinsons disease, a mutation in leucine rich repeat kinase 2 (LRRK2) increases its activity, which elevates phosphorylation of its substrates. [30,36] Therefore, further studies are needed to explore the function of LRRK2 and the relation between LRRK2 and Parkinsons. In the last few decades, scientists in drug discovery have targeted many protein kinases with small molecules or antibodies to treat many diseases.[33]
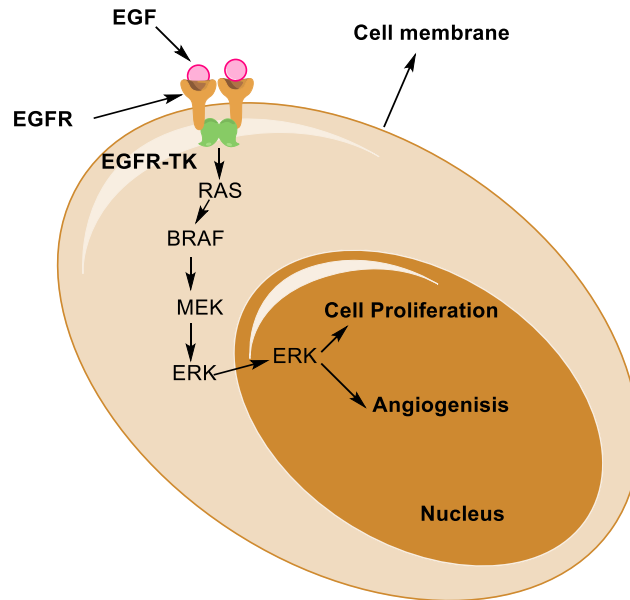
**Figure 1.6: Cell signal pathway for epidermal growth factor tyrosine kinase.**[34] Epidermal growth factor (EGF) binds to cell surface receptor of EGFR-TK, which leads to dimerization of the cell surface receptor of EGFR-TK. Dimerization of the EGFR-TK triggers the activation of RAS protein, which activates downstream signal until it reaches the nucleus.

## 1.4. Kinase inhibitors

Phosphorylation/dephosphorylation constitutes the key player in several diseases, such as rheumatoid arthritis,[27] diabetes,[28] Parkinsons,[29,30] cardiovascular diseases,[31,32] and cancer[33]. Dysregulation of phosphorylation/dephosphorylation balance results in the emergence of a disease. Many of these diseases are due to hyperactivation or overexpression of kinases that infers an over phosphorylation events. The hyperactivated or overexpressed kinase is a candidate target to treat the resulted disease. Pharmaceutical companies have developed many drugs targeting kinases; some are FDA approved and some still in clinical trials. A list of some FDA approved drugs is shown in table 1.1.[10,37-39]

**Table 1. 1: List of some of FDA approved drugs and their targeted kinase[9,36-38]
Structure of the compounds are shown in figure 1.8**

| Inhibitor/ Drug | Disease | Targeted kinase | Company | Year approved by FDA |
|---|---|---|---|---|
| Lenvatinib | Thyroid cancer | VEGFR | Eisai Co | 2015 |
| Palbocicnib | ER-positive and HER2-negative breast cancer | CDK4/CDK6 | Pfizer | 2015 |
| Afatinib | Non-small cell lung cancer | EGFR/ErbB2 | Boehringer Ingelheim | 2013 |
| Crizotinib | NSCLC with Alk mutation | ALK/ROS1 | Pfizer | 2011 |
| Dasatinib | Chronic myelogenous leukemia | multiple targets | BMS | 2006 |
| Ibrutinib | Mantle cell lymphoma | BTK | Pharmacyclics | 2013 |
| Pazopanib | (RCC) | VEGFR2/PDGFR/c-kit | GlaxoSmithKline | 2009 |
| Ruxolitinib | (Myelofibrosis) | JAK | Incyte | 2011 |
| Sunitinib | RCC & GIST | multiple targets | SUGEN/ Pfizer | 2006 |
| Vemurafenib | Aug Melanoma | BRAF | Roche | 2011 |
| Axitinib | Renal cell carcinoma | VEGFR1/VEGFR2/VEGFR3/PDGFRB/c-KIT | Pfizer | 2012 |
| Bosutinib | Chronic myelogenous leukemia | Bcr-Abl /SRC | Pfizer | 2012 |

Kinase inhibitors are classified into 2 major groups: reversible or irreversible inhibitors. The irreversible inhibitors react with a cysteine residue proximal to the ATP binding site, leading to blockage of active site. The reversible inhibitors can be further classified into four groups, according to the conformation of the binding pocket and the

DFG motif. Type 1 inhibitors are ATP-competitive inhibitors, in which the aspartate residue of the DFG motif is pointing into the active site (Figure 1.7). Type 2 inhibitors bind to the inactive form of kinases and the aspartate residue of DFG motif is pointing out of the ATP binding pocket, which provides accessibility of type 2 inhibitors to additional pocket adjacent to the ATP-binding site (Figure 1.7). The third type of inhibitors bind non-competitively to an allosteric site adjacent to ATP-binding pocket (Figure 1.7). On the other hand, type 4 inhibitors bind to allosteric site non-adjacent to ATP-binding pocket (Figure 1.7).[37]
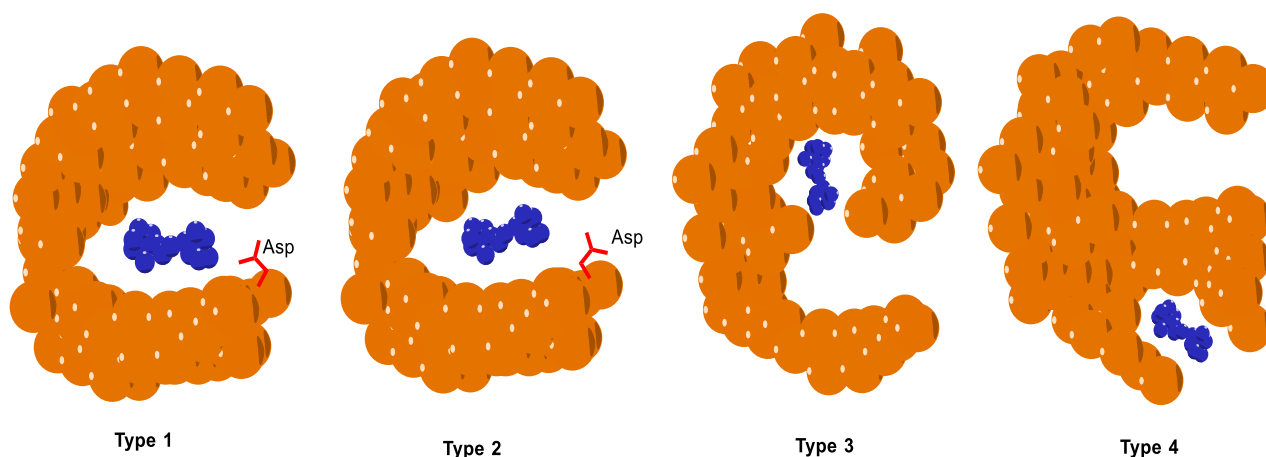


**Figure 1.7: The four types of reversible kinase inhibitors.**[37]
The kinase active site is represented in orange and the kinase inhibitor is represented in blue. Type 1 inhibitors are ATP-competitive inhibitors in which the aspartate residue (red) of the DFG motif is pointing into the active site. Type 2 inhibitors bind to the inactive form of kinase and the aspartate residue (red) of DFG motif is pointing out of the ATP binding pocket. The third type of inhibitors bind non-competitively to an allosteric site adjacent to ATP-binding pocket, while type 4 inhibitors bind to allosteric site non-adjacent to ATP-binding pocket

Although there are over 500 kinases, they share a highly conserved active site. This similarity results in a challenge in designing kinase inhibitors due to nonspecific binding of kinase inhibitors to several kinases.[10] The first rationally designed selective kinase inhibitor is Gleevec® (Imatinib) (Figure 1.8), which selectively inhibits tyrosine

kinase Bcr-Abl, an oncogene for chronic myeloid leukemia. [33,37]   Other examples of selective kinase inhibitors are Sprycelare[®33] (Bcr-Abl kinase inhibitor) and Tykerb[®] (EGFR family members, which blocks the tumorigenic effects of these RTKs).[33] In addition, there are other FDA non-organic compounds, such as monoclonal antibody Herceptin[®], which is used against receptor tyrosine kinases (RTKs) to treat breast cancer.[33] In addition, many natural products, such as staurosporine, are potent inhibitor against kinases, which are used in biological assays.[33]
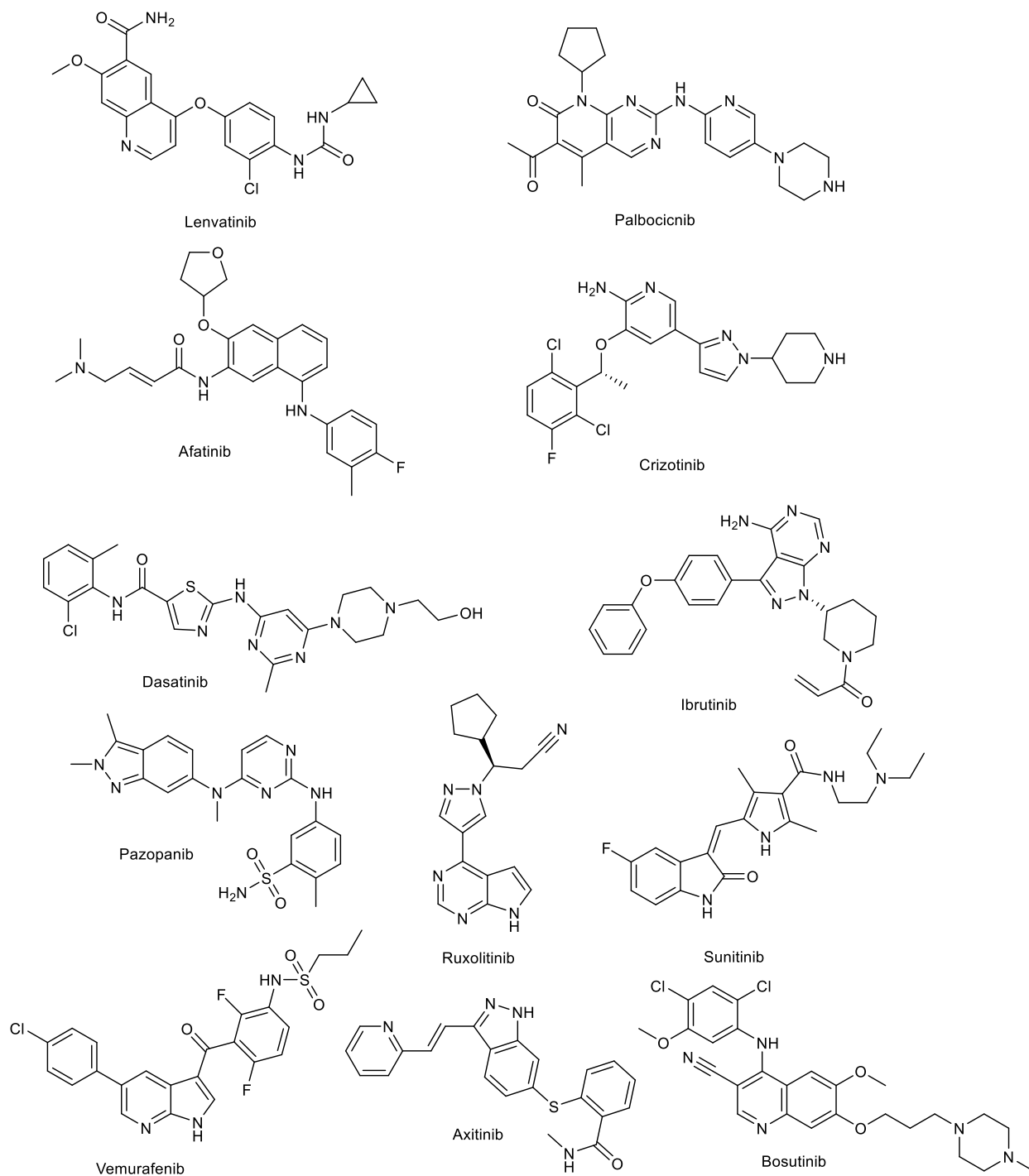
**Figure 1.8: Structure of kinase inhibitors in Table 1.1 and discussed in text.**

## 1.5.    Protein Kinases, mechanism of phosphorylation, and substrate specificity

There are over 500 protein kinases, which belong to two major classes. The first class is tyrosine kinases that catalyze the phosphorylation of tyrosine residues. The second class is serine/threonine kinases, which catalyze the phosphorylation of serine and threonine residues. Another classification divides human kinases into eight subgroups according to sequence similarities in their catalytic sites (Figure 1.9).[12]
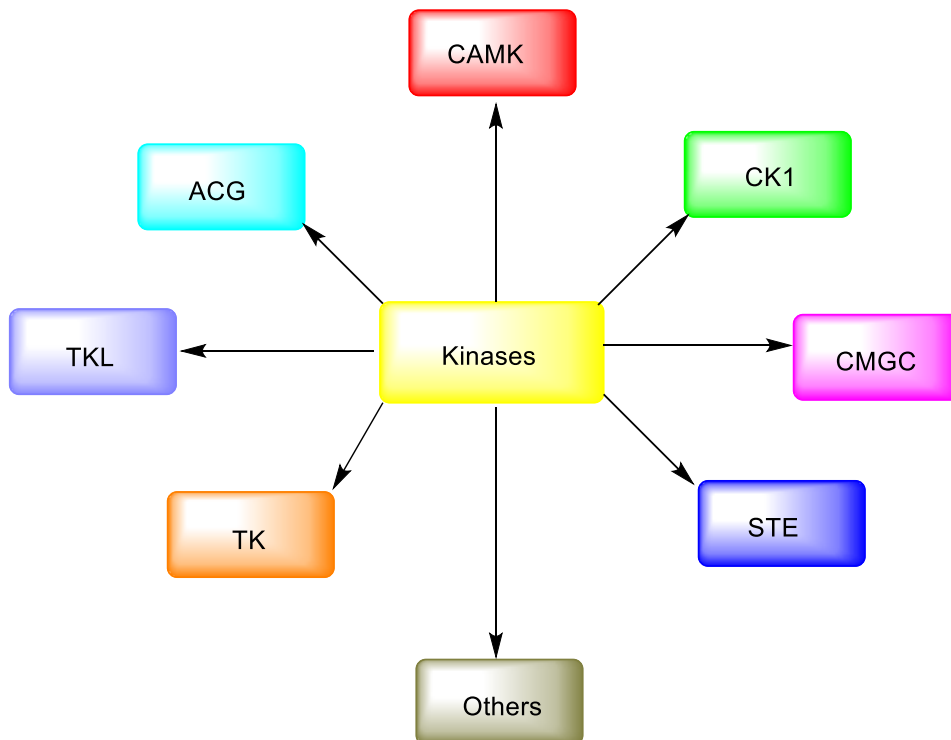


**Figure 1.9: Classifcation of Human Kinases.[12]**
Human kinases are classified into 7 groups: 1) **ACG:** Containing PKA, PKG, PKC families; 2) **CAMK:** Calcium/calmodulin-dependent protein kinase; 3) **CK1:** Casein kinase 1 family; 4) **CMGC:** Containing CDK, MAPK, GSK3, CLK families; 5) **STE:** Homologs of yeast Sterile 7, Sterile 11, Sterile 20 kinases; 6) **TK:** Tyrosine kinase family; 7) **TKL:** Tyrosine kinase-like family. **Other:** other kinases that do not belong to specific group.

Kinase enzymes catalyze the phosphorylation of protein substrates using ATP as a phosphate donor.[8] Kinases possess two binding sites: one to bind ATP and the other to bind protein substrate.[6] The ATP-binding pocket is formed between β-sheets (N-

terminal loop) connected through hinge region to α-helices (C-terminal loop).[37,40] The α-helices contains the substrate binding site, which has specific amino acids that binds the substrate (Figure 1.10).[6]
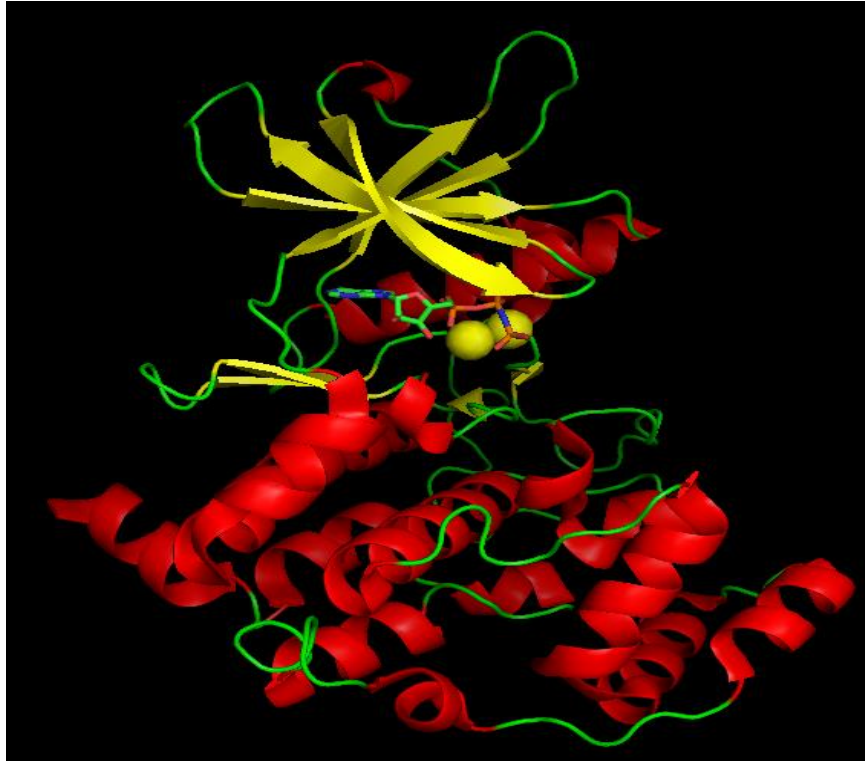


**Figure 1.10:** Crystal structure of CK2 downloaded from protein data bank (Pdb ID: 1DAW). Kinase crystal structure consists of β-sheet (N-loop, yellow) and α-helices (C-loop, red) connected with hinge region (green). The image shows binding of ANP (phosphoaminophosphonic acid-adenylate ester), which is analogous to ATP. ANP binds between N- and C-loop. ANP is color-coded (C = green; H = grey; N = blue; O = red; P = orange). For clarity, the atomic radius of $Mg^{2+}$ was reduced to 0.5 Å.

The active site is conserved among all protein kinases and contains nine highly conserved amino acids in the catalytic site (G52, K72, Q91, D166, N171, D184, G186, Q208, and R280, Figure 1.11).[41] Therefore, the general mechanism for protein phosphorylation is almost the same among the kinase family. The binding site for the ATP cosubstrate contains two divalent metal ion, $Mg^{2+}$ or $Mn^{2+}$, which stabilize the binding of ATP to the enzyme (Figure 1.11).[6] The divalent metal acts a bridge between

amino acids in the ATP binding site and the ATP cosubstrate. During phosphorylation, the hydroxyl group in the protein substrate is deprotonated by an aspartate residue (D166, Figure 1.11). Deprotonation of the hydroxyl group will increase its nucleophilicity and facilitate the attack on the $\gamma$-phosphate of ATP (Figure 1.11).[6]
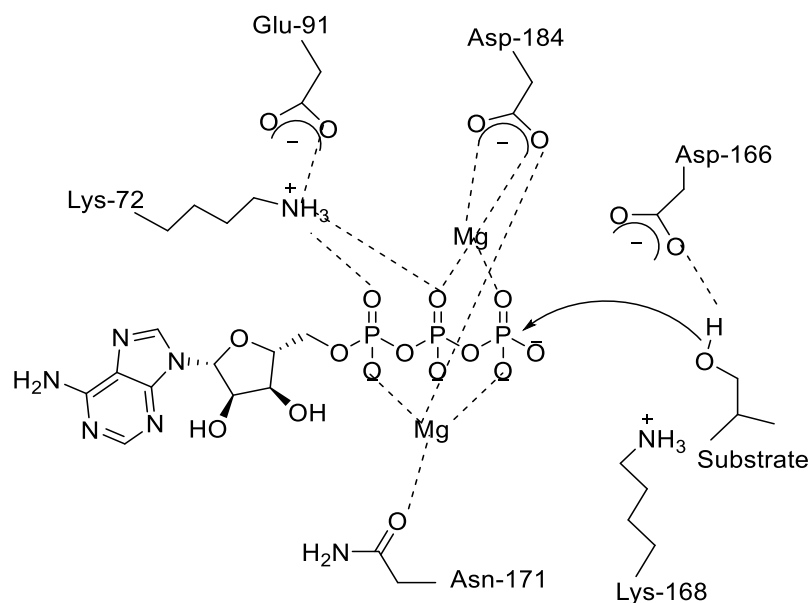


**Figure 1.11: Catalytically relevant residues in the active site of PKA kinase and their interaction with ATP cosubstrate and protein substrate[6,41]**

There are two theories regarding the mechanism of kinase-catalyzed phosphorylation.[42,43] The first mechanism is an associative mechanism, in which the hydroxyl group of substrate attacks the $\gamma$-phosphate of ATP at the same time the bond between the $\gamma$-phosphate and ADP molecule is breaking (Figure 1.12).[44] The second type is dissociative mechanism. In the dissociative mechanism, the bond between ADP and $\gamma$-phosphate breaks, followed by the attack of hydroxyl group of substrate. Recent studies suggests that the dissociative mechanism is more accurate.[42,43,45]
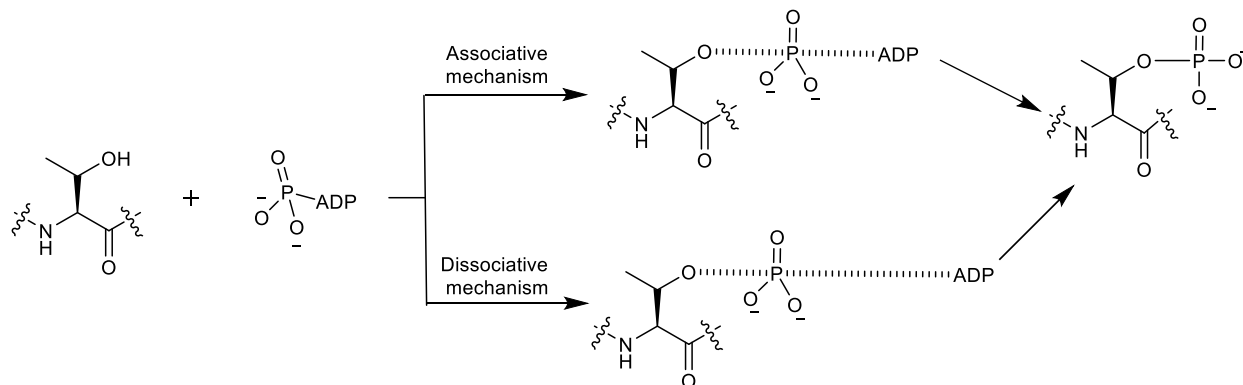
**Figure 1.12: Associative mechanism versus dissociative mechanism of kinase-catalyzed phosphorylation.** In the associative mechanism, nucleophilic oxygen of substrate attacks ATP at the same time as ADP leaves. In the dissociative mechanism, ADP leaves before the attack of nucleophilic oxygen of substrate onto ATP.

Kinase substrate phosphorylation is contingent upon recognition of protein or peptide substrate by its corresponding kinase. The recognition depends on a certain sequence on the substrate called consensus sequence.[6] The consensus sequence is a sequence of amino acid present in the protein or peptide substrate, including the hydroxyl containing amino acid target. Specifically, the amino acids surrounding the hydroxyl containing amino acid plays a crucial role in kinase recognition. Consensus sequence may contain acidic, basic, hydrophobic, or proline residues. For instance, PKA and Akt1 are serine/threonine kinases and recognize basic consensus sequences.[46] Representative examples of consensus sequence of selected kinases are presented in table 1.2.[46-49]

**Table 1. 2: Consensus sequences of selected kinases.**[49] X – any residue, Z-hydrophobic residue, pS is phosphorylated serine, Green/Bold is the site of phosphorylation

| Kinase | Consensus sequence | Nature of amino acids |
|--------|--------------------|-----------------------|
| Abl | I/V/L-**Y**-X-X-P/F | Hydrophobic |
| Akt1 | R-X-R-X-X-**S/T** | Basic |
| PKA | R-R-X-**S/T**-Z | Basic |
| CK1 | pS-X-X-**S/T** | Phosphoserine |
| CK2 | **S/T**-D/E-X-D/E | Acidic |
| CHK 1 | R-X-X-**S/T** | Basic |
| Aurora | A R/K/N-R-X-**S/T**-B | Acidic |
| SRC | E-E-I-**Y**-E/G-X-F | Acidic |
| ERK 2 | P-X-**S/T**-P | Proline |
| EGFR | E-E-E-**Y**-F | Acidic |

## 1.6. Kinase substrate identification

With over 500 kinases and thousands of substrates, kinase-substrate identification is a complex process. Kinase-substrate identification is used to reveal the molecular details of cell signaling pathway and understanding many diseases. Many tools were developed to identify kinase-substrate pairs, including *in vitro*

phosphorylation, pull down assays, yeast two-hybrid systems, and chemical approaches, such as ATP analogs. ATP analogs have been used extensively to study kinases and their substrates. They were used to identify kinase-substrate pairs and kinome profile. However, it is still challenging to determine kinase activities and its effectors in cell signaling pathways. Therefore, development of novel methods to identify kinase-substrate pairs in a kinase-catalyzed phosphorylation manner will allow a better deciphering of cell signaling events. Detailed discussion of current tools to identify kinase-substrate pairs is presented in chapter 4 (Section 4.1.3). In addition, we will present our latest contribution to develop new tool to identify kinase-substrate pairs using novel ATP analogs.

## 1.7.    Kinase cosubstrate promiscuity

Enzyme cosubstrate promiscuity were reported for several PTMs.[50-59] Cosubstrate promiscuity occurs when an enzyme utilize a modified cosubstrate similar to the natural one. Examples of enzymes that exhibit cosubstrate promiscuity are acetyltransferase, transglutaminase, galactosyltransferase, etc. In particularly, kinase enzymes also showed cosubstrate promiscuity. ATP is a kinase cosubstrate and it is the phosphoryl donor to phosphorylate proteins (Figure 1.13). ATP binds into ATP binding pocket of kinases, where adenine moiety binds deep into the active site with the triphosphate protruding into the solvent exposed area of the pocket (Figure 1.13). Modifications on $\gamma$-phosphate were accepted promiscuously by kinases.

### 1.7.1. ATP-$\gamma$S

The earliest reported $\gamma$-modified ATP analog was ATP $\gamma$-S.[60]  Protein kinases were reported to show promiscuity using ATP $\gamma$-S, producing thiophorylated products

(Figure 1.13).[60-63] ATP γ-S was first reported in the context of glycerokinase, hexokinase, and pyruvate kinase.[64] Indeed, ATP γ-S was also used with protein kinases to produce thiophosphorylated products (Figure 1.13).[63] Thiophosphorylation with ATP γ-S was used as a tool to purify and identify kinase substrates (Figure 1.13). The purification can be done by several methods. The first example used iodoacetyl-linked biotin affinity tags that promote subsequent avidin enrichment (Figure 1.13).[65,66] By maintaining low pH, thiophosphorylated products are more nucleophilic than other amino acid residues, which allows selective purification of thiophosphorylated products. In a second method, thiophosphorylated products were reacted iodoacetyl-linked resins that capture both thiophosphorylated and cysteine containing products.[67-69] However, selective elution of thiophosphorylated captured products was done by peroxides. The third method includes pretreatment of samples containing thiophosphorylated products with a capping reagent.[70,71] The capping reagent reacts with cysteines through thiol-ene reaction, leaving thiophosphorylated products. The thiophosphorylated products were then labeled with iodoacetly BODIPY fluorophore. The fourth method depends on capture of thiophosphorylated products via disulfide linkage.[72,73] This method captures both thiophosphorylated products and cysteine residues. However, thiophosphorylated products were selectively eluted via sodium hydroxide. The last method includes immunoaffinity purification of thiophosphorylated products.[74-76] The sample was first treated with *p*-nitrobenzylmethylate (PNBM) to alkylate all nucleophilic groups, including cysteines and thiophosphorylated proucts. Afterwards, alkylated thiophosphorylated products were purified by paranitrobenzylthiophosphoryl polyclonal antibodies (IgY and

IgG). Interestingly, ATP-γS was coupled with the as-kinase strategy to identify specific substrate kinase relationship, as discussed in chapter 4 (Section 4.3.1.2).[74]
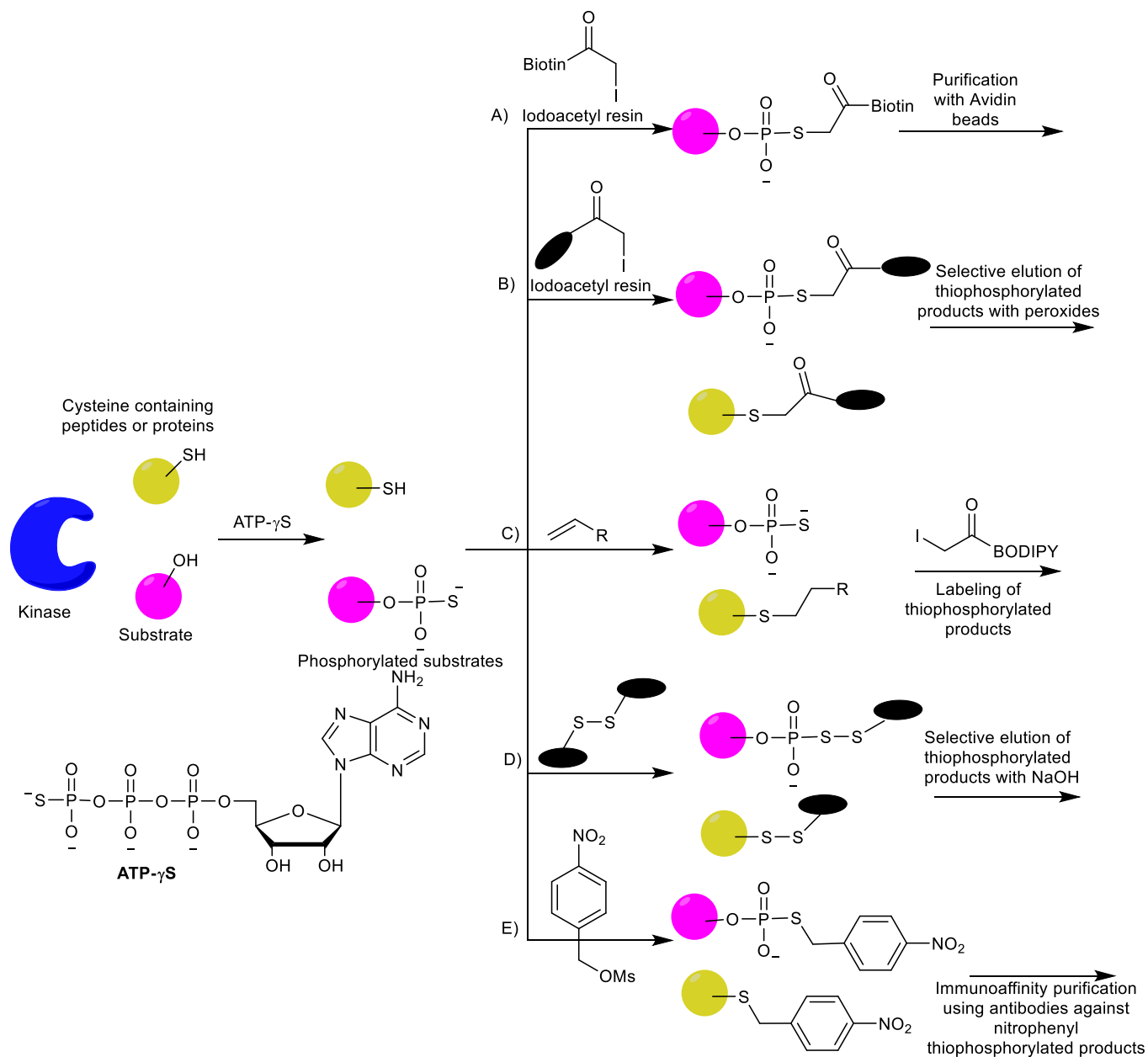


**Figure 1.13: Methods of purification of thiophosphorylated products.** ATP-γS was incubated with a sample containing kinases and protein substrates to produce thiophosphorylated products. The reaction mixture was purified by A) iodoacetyl biotin, B) iodoacetyl resin, C) thiol-ene reaction followed by iodoacetyl-BODIPY, D) disulfide resin followed by treatment with NaOH, and E) *p*-nitrobenzylmesylate followed by immunoaffinity prurification.

### 1.7.2. ATP-biotin

Kinase cosubstrate promiscuity was extended by attaching several groups to γ-phosphate beyond ATP-γS. Attaching a probe or a large group to the γ-phosphate results in the transfer of the γ-phosphate together with the probe onto protein substrate in a kinase-catalyzed reaction (Figure 1.14).[77] The group should be attached to the γ-phosphate via a linker. The structure activity relationship of the nature and size of both the linker and the attached group will be discussed later in chapter 5 (Section 5.1.1). Several groups were attached to the γ-phosphate of ATP. The first example is biotin (Figure 1.14, ATP-biotin **1a)**.[77] ATP-biotin was initially tested by Pflum lab for kinase promiscuity by incubating with recombinant kinases and peptide substrates. (Figure 1.14). Three kinases with their corresponding peptide substrates were used: PKA, CK2, and Abl. The first two are serine/threonine kinases and the last is tyrosine kinase. The biochemical reaction results were assessed by a quantitative mass spectrometric (MS) analysis, assuming that the reaction with ATP is providing 100% conversion. ATP-biotin was accepted by all three kinases and the percentage conversion is shown in Table 1.3.[77] Afterwards, ATP-biotin was used with full length proteins and recombinant kinases. For example, ATP-biotin was incubated with CK2 kinase and β-casein protein substrate. The reaction mixture were analyzed by SDS-PAGE gel electrophoresis, followed by transferring onto PVDF (polyvinylidene difluoride) membrane. Biotinylation was detected on the membrane using SA-HRP (Streptavidin-horseradish peroxidase) conjugate.[77] In addition, incubation of ATP-biotin with cell lysates resulted in biotinylation of protein substrates, which is consistent with that biotinylation as a generally kinase-catalyzed phenomenon.[77,78]
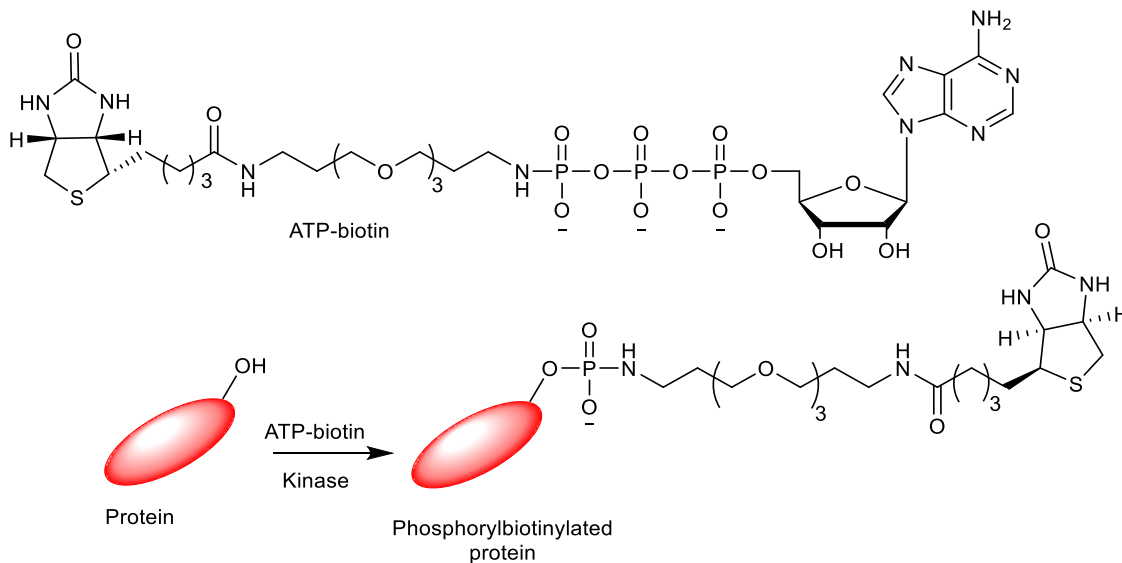
**Figure 1.14: Kinase-Catalyzed Biotinylation.**
Kinase enzyme catalyzes the phosphoryl biotinylation of protein substrate with ATP-biotin

To test the generality of biotinylation, the Pflum lab selected 25 kinases throughout the kinome tree to test if ATP-biotin is generally accepted by kinases.[79] Both kinetic analysis and percentage phosphorylation using each kinase with ATP-biotin were performed. The efficiency of biotinylation was determined by comparing percentage phoshphorylation and $K_m/K_{cat}$ using ATP-biotin to ATP, taking in consideration that ATP gives 100% phosphorylation. All 25 kinases accepted ATP-biotin with different kinetic efficiencies. The most efficient kinase with highest percentage conversion was SCR (96%±7). Also, SCR showed the highest catalytic efficiency, which is the most similar to ATP. By analyzing the results using docking studies for selective kinases, we found that the most efficient kinases positioned the $\gamma$-phosphate of ATP-biotin proximal to catalytic lysine as ATP.[79] With generality of biotinylation with protein kinases, ATP-biotin can be used with cell lysates to study dynamic phosphoproteomics.[80,81]

**Table 1.3: Quantitative mass spectrometry of the kinase-catalyzed phosphorylation using previously reported ATP analogs[77,82,83]**

|  | PKA | CK2 | Abl |
|---|---|---|---|
| **ATP-biotin** | 79% | 56% | 80% |
| **ATP-dansyl** | 91% | 81% | 87% |
| **ATP-Ar-N$_3$** | 86% | 51% | 78% |

### 1.7.3. ATP-dansyl

After establishing kinase-catalyzed biotinylation, kinase cosubstrate promiscuity was shown by other commercially available ATP analogs. Specifically, commercially available ATP-dansyl (Figure 1.15) was incubated with selected kinases (Abl, PKA, and CK2) with their corresponding peptides. The reaction mixtures were analyzed by quantitative mass spectrometry (MS) (Table 1.3). The results showed that ATP-dansyl was also accepted with diverse kinases. Subsequently, kinetic analysis was performed using an absorbance assay in presence of PKA and either ATP-dansyl or ATP. ATP-dansyl and ATP exhibits similar $K_m$ (23 µM and 24 µM respectively). However, ATP-dansyl had 9 fold reduced $K_{cat}$ than ATP. Reduced $K_{cat}$ indicates that kinase-catalyzed dansylation is slower than phosphorylation reaction using ATP.[82]
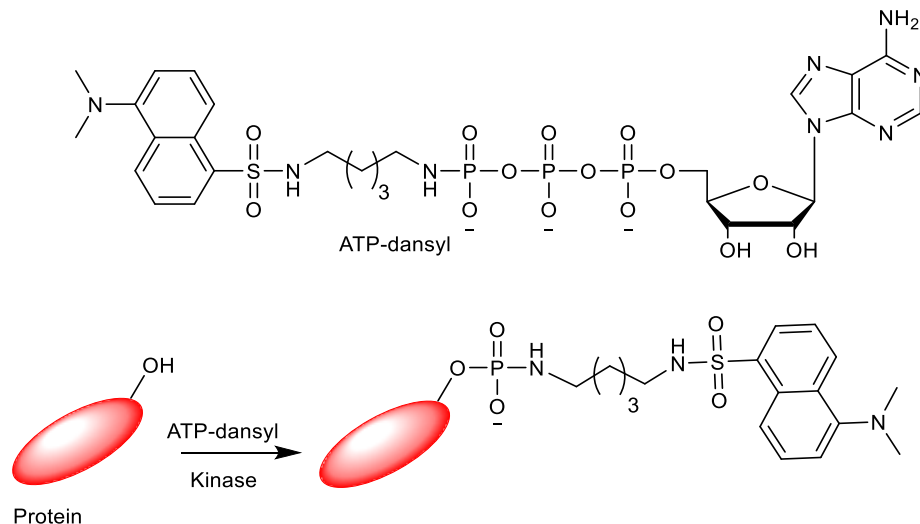
**Figure 1.15: Kinase-Catalyzed dansylation using ATP-dansyl.**

### 1.7.4. ATP-Aryl-Azide (ATP-ArN$_3$)

To expand the applications of ATP analogs, other ATP analogs were developed. Interestingly, an ATP analog with a photocrosslinker (ATP-ArN$_3$) was developed by Pflum lab to crosslink protein kinase to its substrate in a phosphorylation dependent reaction (Figure 1.16). First, ATP-ArN$_3$ was tested for its efficiency as a kinase cosubstrate using three kinases (PKA, CK2, and Abl) with their corresponding peptides using quantitative MS/MS assay (Table 1.3). MS/MS analysis revealed that ATP-ArN$_3$ can act as a kinase cosubstrate with different efficiency from one enzyme to another (Table 1.3). After confirming the ability of ATP-ArN$_3$ to work as a kinase cosubstrate, Pflum lab tested the validity of the analog as a kinase-substrate crosslinker. ATP-ArN$_3$ was incubated with CK2 and its substrate casein in the presence of UV light. The reaction mixture was separated by SDS-PAGE analysis, followed by transferring onto PVDF membrane to analyze crosslinked complex via western blotting. Western blotting analysis showed a higher molecular weight complex equal to the sum of the molecular weight of CK2 and casein (Figure 1.16). The higher molecular weight complex was

visualized in gel via protein stain and western blot using CK2 antibody. In contrast, no crosslinked complex was observed in absence of ATP-ArN$_3$ or UV. All these observations suggested that ATP-ArN$_3$ can result into a kinase-dependent photocrosslinking of kinases to their substrates. Other ATP-photocrosslinkers are being developed and are discussed in chapter 4.[83]
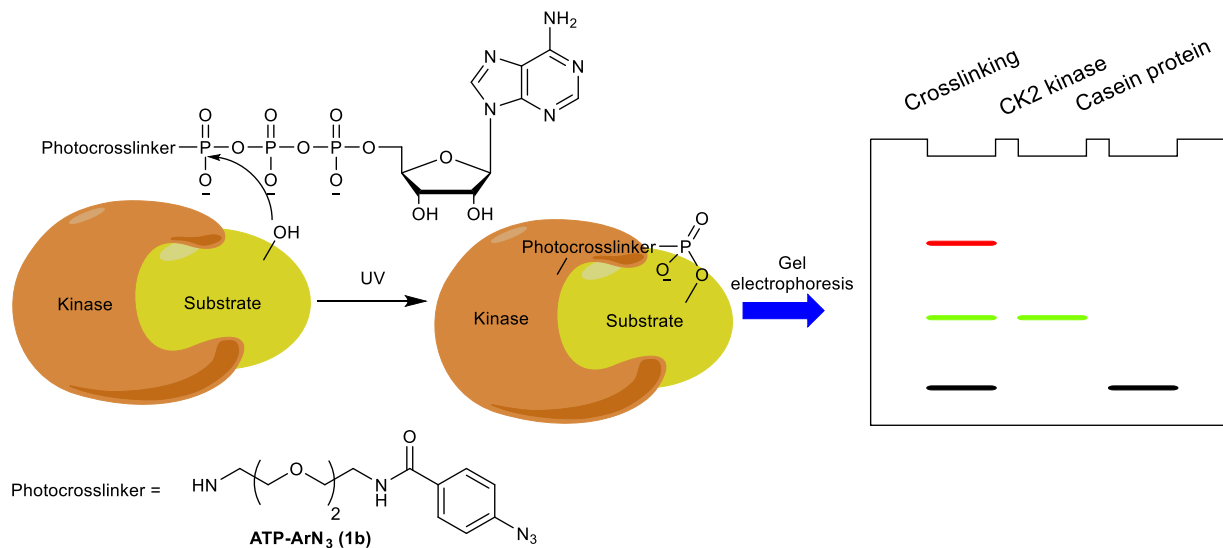


**Figure 1.16: Kinase-catalyzed photocrosslinking of CK2 kinase enzyme to casein protein substrate using ATP-ArN3.**
The gel electrophoresis showed the presence of higher molecular weight complex or bands equal to the sum of molecular weight of CK2 and casein protein, which indicates their crosslinking

## 1.7.5. ATP-Ferrocene

ATP-Ferrocene was developed by the Kraatz lab to transfer a ferrocene-phosphate group onto peptide or protein through a kinase-catalyzed reaction (Figure 1.17). Ferrocene-phosphate transfer was confirmed by antiferrocene antibodies. Interestingly, ATP-ferrocene was used to detect kinase activity by electrochemical

monitoring of ferrocene transfer onto protein or peptide substrate. Also, this assay was used to identify kinase inhibitors.[84,85]
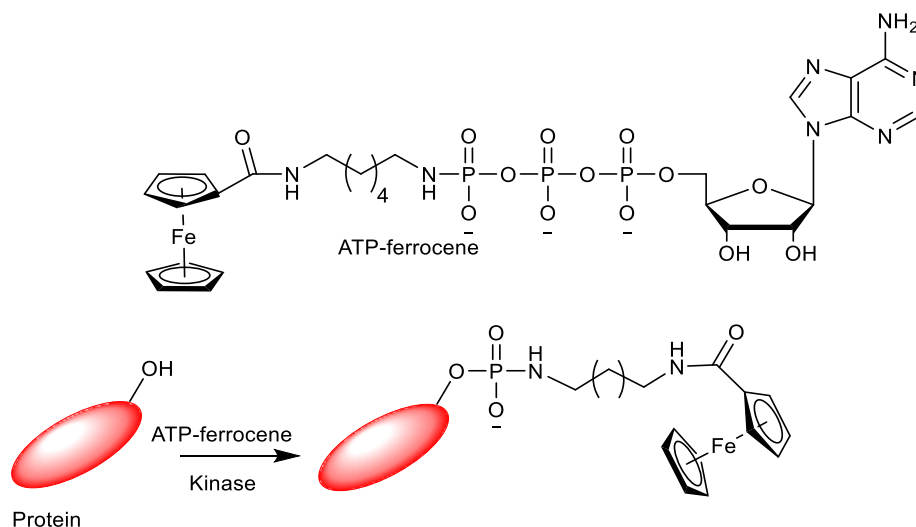


**Figure 1.17: Kinase-Catalyzed phosphate ferrocene transfer using ATP-ferrocene.**

## 1.7.6. Manns/Governeau's ATP analogs

The Mann and Governeau Labs developed a new generation of $\gamma$ -modified ATP analogs with alkynes, azides, and alkenes on the $\gamma$-phosphate (Figure 1.18). These analogs are useful for subsequent click chemistry or Staudinger ligation. Mann lab utilized cyclin E1/cdk2 kinase to test the cosubstrate promiscuity related to their analogs. They incubated their analogs with cyclin E1/cdk2 kinase and protein substrate, followed by SDS-PAGE gel analysis and western blotting. Their ATP analogs demonstrated successful phosphorylation using western blotting and phosphor antibodies. However, the studies of these analogs were limited and Mann lab did not use their analogs with click chemistry or Staudinger ligation.[86]

**Figure 1.18: Structures of Mann and Governeau's ATP analogs**[86]

### 1.7.7. Clickable ATP-Ferrocene (Fc-CO-Lys-ATP)

Recently, the Kraatz and Mann labs developed a clickable ATP-Ferrocene analog, Fc-CO-Lys-ATP for measuring kinases activity (Figure 1.19). Three kinases were used in this study: Sarcoma-related kinase (Src), cyclin-dependent kinase (CDK2), or casein kinase II (CK2a). Fc-CO-Lys-ATP was incubated together with the selected kinases and its corresponding peptide substrate fixed to gold particles. The kinase-catalyzed Ferrocen-phosphorylation of peptide gold particle was detected electrochemically or with antiferrocene antibodies as in section 1.6.5. Importantly, probing the Ferrocene-phosphorylated of peptide gold particle using click chemistry allowed visualization of ferrocene-phosphorylation by microscopy (Figure 1.19). The latter assay can be used to replace the well-established immunoassay. In conclusion, Fc-CO-Lys-ATP can be further applied to multiplex assays.[87]

**Figure 1.19: Kinase-catalyzed ferrocyl-phosphorylation using clickable ATP-Ferrocene (Fc-CO-Lys-ATP)**

## 1.7.8. ATP-acyl-biotin (X-probe)

$\gamma$-Modified ATP analogs were not only used to label kinase substrates but also used to identify and label kinases themselves. For example, ATP-acyl-biotin was utilized to identify many kinases.[88,89] Generally, kinases have two conserved lysine residues in the active site, which are positioned proximal to β- and γ-phosphate.[12,90,91] Interestingly, ATP-acyl-biotin binds to the active site of kinase and then the amine group of the lysine residue attacks the acyl-phosphate group and releases ATP. This reaction forms a covalent bond between the kinase and the acyl-biotin. The biotin tag allows purification

of the kinase by streptavidin beads and the kinase can be identified by MS/MS analysis.[88,89]
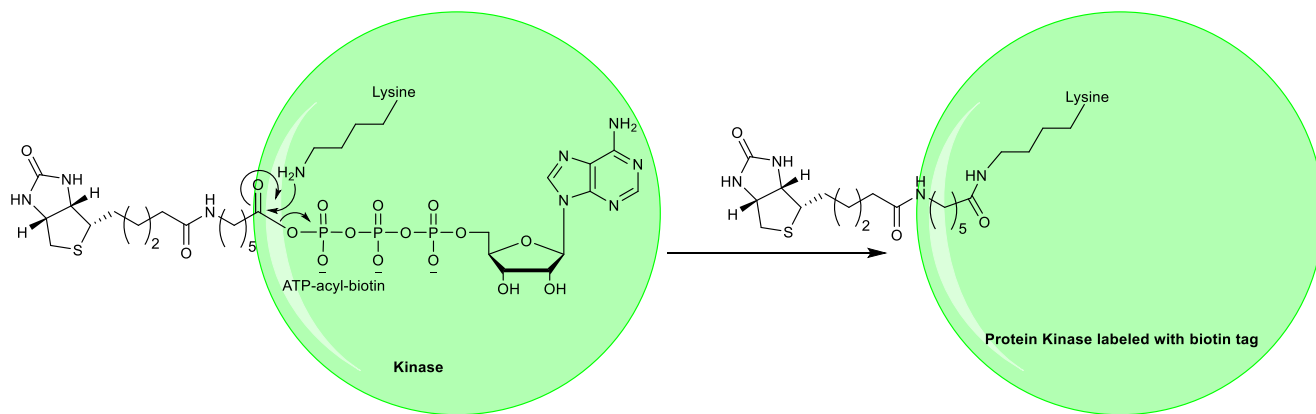


**Figure 1.20: Kinase labeling with ATP-acyl-biotin.**

## 1.8. Thesis projects

Kinase-catalyzed phosphorylation is critical in regulating cell signaling. With a large number of kinases and protein substrates, continuous development of tools to study kinase-catalyzed phosphorylation events is needed to decipher the molecular details of cell signaling cascades. The Pflum lab and others developed several ATP analogs to study kinase-catalyzed phosphorylation. However, ATP analogs applications were limited to *in vitro* usage due to cell impermeability of ATP analogs. In vitro studies may be less relevant than in cellulo experiments due to absence of compartments in lysates. To utilize our γ-modified ATP analogs in vitro, we developed two strategies to permeablize cells toward ATP analogs. The first one is synthesizing and developing a cell permeable ATP analog by attaching a polyamine to ATP analog (Chapter 2). The second strategy is the usage of an external polyamino-carbohydrate additive to

permeabilize ATP analogs (Chapter 3). Both strategies were successfully applied and showed that ATP analogs can pass cell mebrane using polymamines.

Previously, we developed a kinase cosubstrate photocosslinker, ATP-ArN$_3$ (Chapter 1. Section 1.7.4). ATP-ArN$_3$ can crosslink kinase enzymes to their protein substrates. However, the azide group of ATP-ArN$_3$ is converted to a very reactive species that can crosslink with proximal many proteins, which leads to non-specificity. Therefore, we developed an affinity-based ATP crosslinking analogs, ATP-acrylamides (Chapter 4). ATP-acrylamides have an acrylamide group instead of azide group, which crosslink only cysteine containing kinases.

My last project is a comparative study of the effect of different atoms attached to $\gamma$-phosphate on the ability of analog to act as kinase cosubstrate (chapter 5). Specifically, we synthesized three $\gamma$-modified ATP analogs with different atom attached to $\gamma$-phosphate. We studied the effect of different atoms on both the kinase cosubstrate ability and efficiency. Detailed kinetic studies were performed for all analogs.

## CHAPTER 2 DEVELOPMENT OF A CELL PERMEABLE ATP ANALOG FOR KINASE CATALYZED-BIOTINYLATION

(Some of the text in this chapter were reprinted or modified from: "A cell permeable ATP analog for kinase-catalyzed biotinylation". *Angew. Chem. Int. Ed.*, **2015**, 54, 9618)[1]

### 2.1    Introduction

In this chapter, we discuss the development of the first cell permeable ATP analog for kinase-catalysed labelling. The Pflum lab and others have utilized $\gamma$-phosphate modified ATP analogs as tools to study kinase-catalysed phosphorylation.[74,75,78,84-86,92-97]    As discussed in chapter 1, ATP-biotin (**1**) is promiscuously accepted as a cosubstrate by protein kinases to phosphorylbiotinylate substrates.[79,92,95,98]   After kinase-catalyzed biotinylation with ATP-biotin, the biotin group facilitates analysis of phosphoproteins using various commercial streptavidin-conjugated reagents.[92,99] Unfortunately, due to the impermeability of ATP analogs, ATP-biotin has been used *in vitro* only.[95] The ability to utilize ATP-biotin in living cells would promote the study of protein kinases in more physiologically relevant conditions. Here, we describe the first cell permeable ATP-biotin analog for live cell kinase-catalysed biotinylation. A summary of methods used to permeabilize phosphate containing compounds is also discussed in this chapter

### 2.1.1  Cell delivery of ATP analogs

ATP analogs have been extensively used in studying kinase-catalyzed phosphorylation. ATP analogs in kinase-catalyzed phosphorylation studies were extensively applied *in vitro,* with less applications *in cellulo* due to cell impermeability of ATP analogs. The cell impermeability of ATP analogs is a result of the negatively charged triphosphates. Several reports documented the usage of permeabilizing agents, such as digitonin, to deliver ATP analogs.[100] These methods suffer from several

drawbacks that limited their applications, which will be discussed extensively in chapter 3. In this chapter, we are discussing the development of the first intrinsically cell permeable ATP analog for kinase-catalyzed labeling studies. The cell permeable ATP analog does not require externally added additives, which suffers from several drawbacks such as incompatability with growing cell media or the usage of less physiologically relevant conditions.

### 2.1.2 Methods used to intrinsically permeabilize phosphate-containing compounds

Phosphate-containing compounds, such as ATP and phosphatidylinositol triphosphates, are cell impermeable due to the presence of highly polar negative charge on phosphates. Several approaches were used to permeabilize phosphate containing compounds to be used for different applications. Cell permeabilzation of phosphate-containing compounds depends on neutralizing the negative charge of phosphate groups to promote the cell permeability of compounds.[101-103] For example, phosphatidylinositol triphosphate (PIP3) (Figure 2.1.A) is a key factor in the EGF/PIP3K signaling pathway.[101] Studying the effect of PIP3 alteration within a cell is ubiquitous to understand its subsequent cell signaling events. Due to cell impermeability of PIP3, utilization of PIP3 to alter cellular levels is challenging. One reported approach to enhance cell permeability of PIP3 was to develop a membrane permeant derivative (PIP3/Ac) by masking the charges of the phosphate groups with acetoxymethyl ester (Figure 2.1.A). Acetoxymethyl esters are bioactive and will be hydrolyzed by cellular carboxyhydrolases, liberating free PIP3 (Figure 2.1.A). Also, an additional butyrate group was installed on free hydroxyl groups of PIP3 to assist cell permeability, which were and then removed by carboxyhydrolases after passing cell membrane.

Furthermore, installing an additional phosphate on the protected PIP3 resulted in a more potent cell permeable PIP3 alternative (PIP4/Ac) (Figure 2.1.A), which is more synthetically feasible.[101] This protection/enzyme deprotection strategy was also used to enhance the cell permeability of bisphosphonate anticancer drugs and increase their potency (Figure 2.1.B).[102]
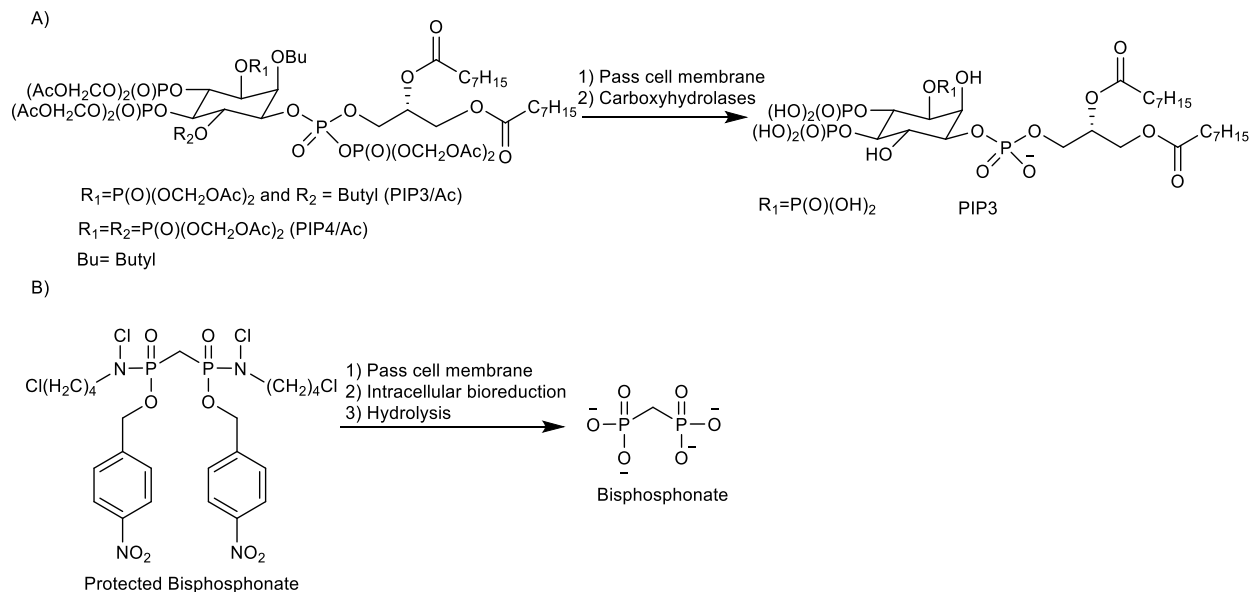


**Figure 2.1:** A) Schematic diagram of conversion of protected phosphatidylinositol triphosphates derivatives (PIP3/Ac and PIP4/Ac) to free phosphatidylinositol triphosphates (PIP3). B) Schematic diagram of conversion of protected bisphosphonate to free bisphosphonate after passing the cell membranes.

Another alternative to enhance the permeability of phosphate containing compounds is the usage of photoactivatable protecting group (Figure 2.2).[103] For instance, photoactivatable protected PIP3 (PA PIP3) was used to deliver PIP3 into cells. After cell delivery of PA PIP3, the photoactivable group was removed to liberate free PIP3 (Figure 2.2). PA PIP3 has the advantage of providing a fast release of PIP3 in more physiologically relevant quantities that acetoxymethyl esters.[103]
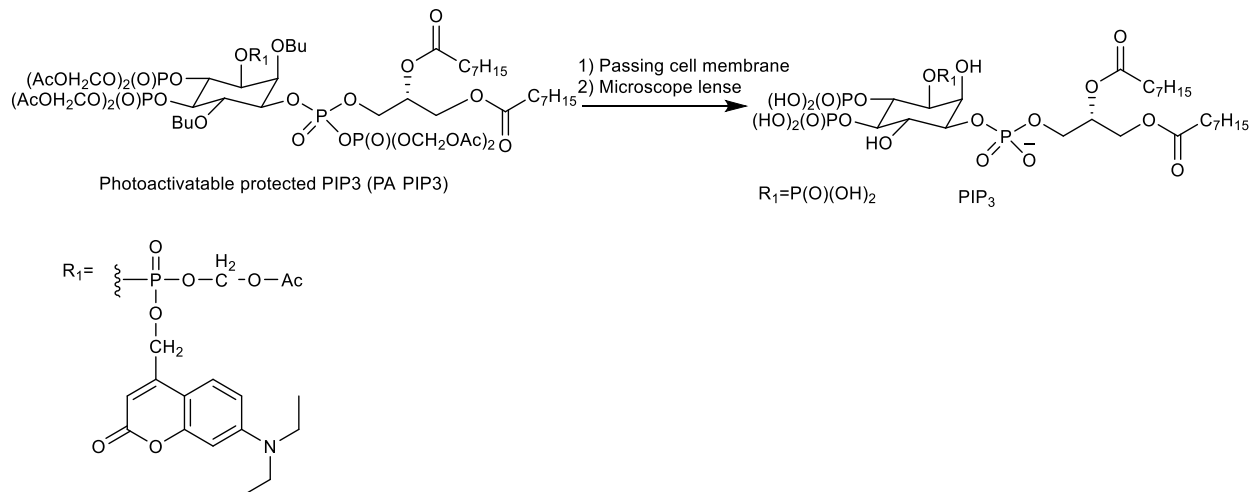
**Figure 2.2:** Schematic diagram of conversion of photoactivatable protected PIP3 (PA PIP3) to free PIP3

A third example of enhancing the cell permeability of phosphate-containing compounds is the usage of polyamines.[104] Polyamines are positively charged under physiological conditions and can chelate negatively charged phosphates to form cell permeable complexes. Aminoglycoside derivatives such as neomycin were incubated with PIP3 to form a cell permeable complex (Figure 2.3). In addition, polybasic proteins, such as histones, were also used to deliver PIP3.[104]
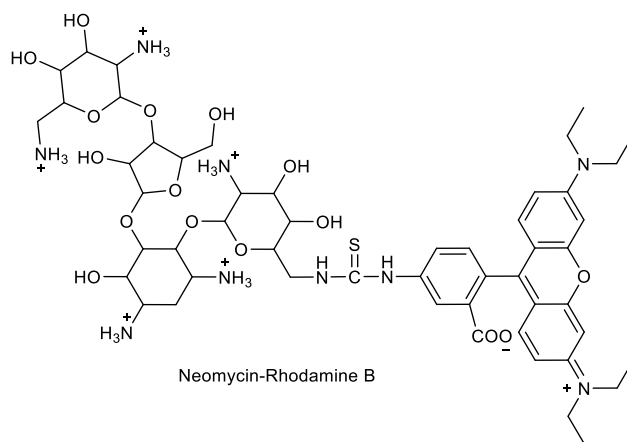


**Figure 2. 3:** Structure of Neomycin-Rhodamine B

In summary, phosphate-containing compounds are cell impermeable. To develop cell permeable phosphate-containing compounds, the negative charges of phosphates

should be masked by either protection with bioactive or photoactivatable protecting group or by using polyamine deliver agent. These findings guided us through our project to develop the first cell permeable ATP analog.

## 2.2 Development of cell permeable ATP analog for kinase-catalyzed biotinylation

In our lab and several other groups, $\gamma$-phosphate modified ATP analogs were utilized to study kinase-catalysed phosphorylation.[74,75,78,84-86,92-97] An important example developed by our lab is ATP-biotin (**1**, Figure 2.4 B). ATP-biotin phosphorylbiotinylates protein substrates and peptides through a kinase-catalyzed reaction (Figure 2.4 A).[79,92,95,98] Following kinase-catalyzed biotinylation with ATP-biotin, the biotin group can facilitate analysis of phosphoproteins using various commercial streptavidin-conjugated reagents.[92,99] Unfortunately, ATP-biotin has been used *in vitro* only due to the cell impermeability of ATP analogs as a result of the presence of highly polar negative charged phosphates.[95] Permeabilizing cells towards ATP-biotin would promote the study of protein kinases in more physiologically relevant conditions. In this chapter, we focus on systemic development of the first intrinsic cell permeable ATP-biotin analog for live cell kinase-catalyzed biotinylation (**2**, Figure 2.4).[1] Our developing strategy depended on previous finding of permeabilizing phosphate containing compounds.
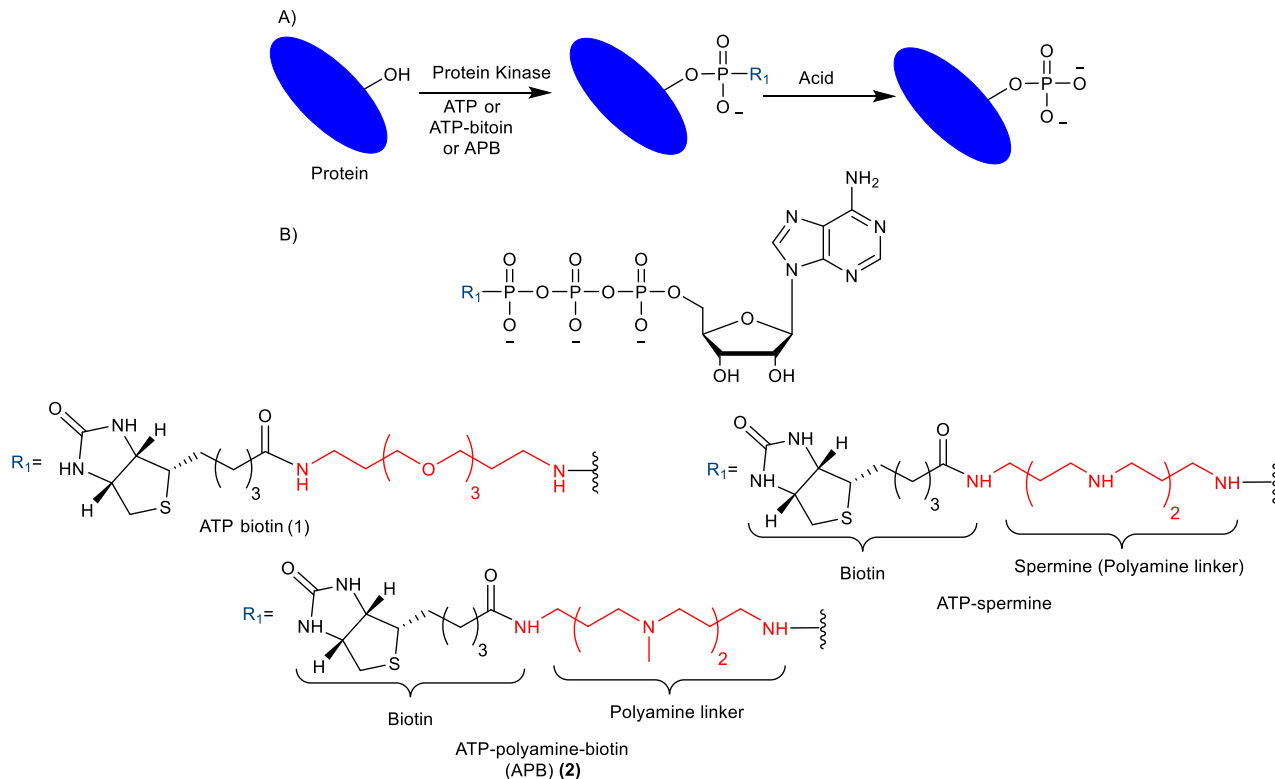
**Figure 2.4:** (A) Kinase-catalyzed phosphorylation of a protein substrate (green) with (B) ATP (R = O⁻) or ATP analogs ATP-biotin (1), or APB (2).

## 2.2.1 Results and discussion

Building on previous precedents of cell delivering phosphate containing compounds, we replaced the PEG linker of ATP-biotin with a polyamine linker to create ATP-spermine (Figure 2.4). Polyamines are known cell delivery vehicles for phosphate containing compounds.[105,106] In the case of ATP-spermine, the polyamine linker will be positively charged under physiological conditions to partially neutralize the triphosphate charge and promote cell permeability. We chose spermine as the linker because its size mimics the original poly ethylene glycol (PEG) linker in ATP-biotin (Figure 2.4).

To test our hypothesis, ATP-spermine was synthesized according to scheme 2.1. Biotin was selectively coupled to one primary amine of commercially available spermine

to give Biotin-spermine in 67% yield. Biotin-spermine was then coupled to ATP in a pH dependent reaction to afford ATP-spermine in 35% yield (Scheme 2.1).

**Scheme 2. 1:** Synthesis of ATP-spermine.
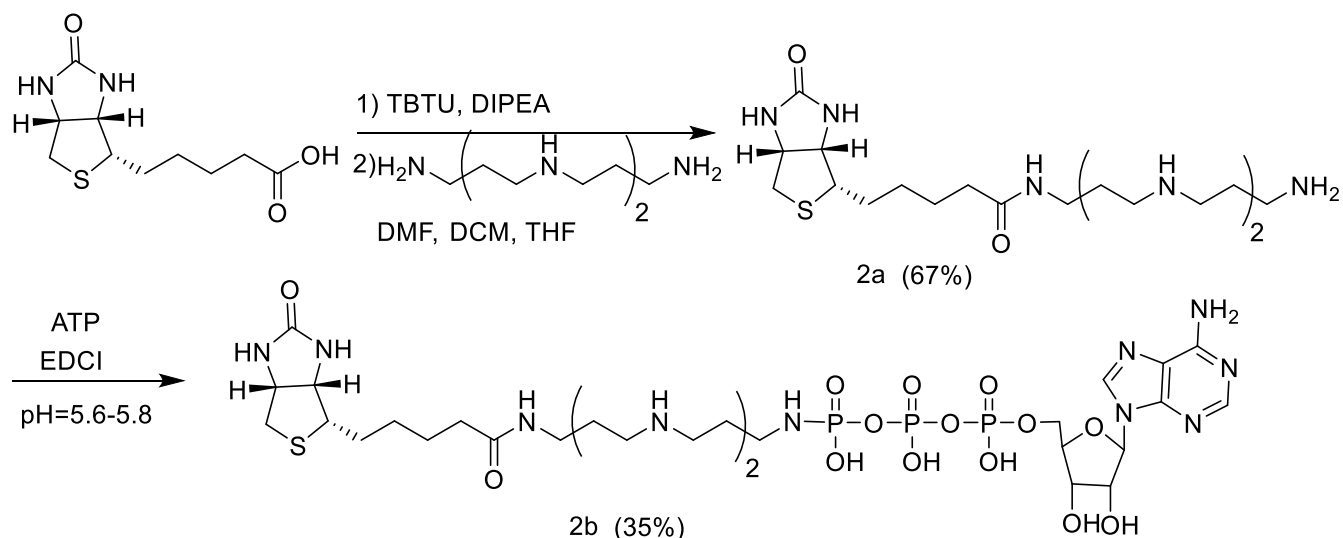


Before testing the cell permeability of ATP-spermine, We tested its ability to work *in vitro* as a kinase-cosubstrate. We chosed a well stablished system in our lab, where the kinase is PKA and the protein substrate is mylein basic protein (MBP). ATP-spermine was incubated with PKA and MBP, followed by SDS-PAGE analysis and protein transfer on PVDF membrane. Kinase-catalyzed biotinylation was then detected by streptavdinCy5. Unfortunately, ATP-spermine showed biotinylation in presence and abscence of PKA (lane 2 and 4, Figure 2.5), The biotinylation in presence and abscence of kniase may be due side reactions of the nucleophilic secondary amines.[1]
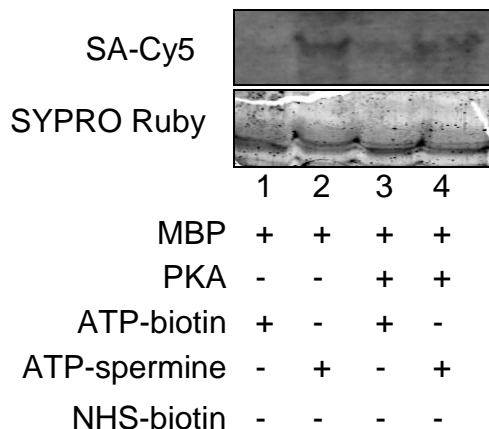
**Figure 2.5:** Kinase-catalyzed biotinylation of MBP with ATP-spermine. MBP was incubated with ATP-spermine and PKA in the manufacture provided buffer. The labeled mixtures were separated by SDS-PAGE and visualized by SYPRO® Ruby to see total proteins (bottom gel) or streptavdin Cy-5 (SA-Cy5, Life Technologies) to detect biotinylation (Top gel).

To solve the problem of non-specficity of ATP-spermine, we redesigned our ATP analog. We hyptheized that methylating the secondary nitrogen of spemine linker will decrease the reactivity of such nitrogen. To test the validity of the approach, we designed a new ATP-biotin with a polyamine linker, ATP-polyamine-biotin (APB). APB has a methylated nitrogen on the linker in cotrast to ATP-spermine, which may eliminate the non-specfic biotinylation.

### 2.2.1.1 Docking Studies of APB with PKA crystal structure.

Since APB has a methylated linker, which may affect the kinase-cosubstrate properties of ATP analogs, we computationally analyzed the kinase compatibility of APB. Docking studies with the PKA kinase crystal structure[107] were performed using the Autodock program.[108] Nearly identical PKA binding was observed with of APB (Figure 2.6 A), ATP-biotin (Figure 2.6 C), and ATP (Figure 2.6 E). The biotin group protrudes from the active site, while the triphosphate is positioned in a close proximity to the co-crystallized peptide. The $\alpha$-phosphate of APB is 3.8 Å from the catalytic amino acid

K72, as compared to 3.7 and 3.2 Å with ATP or ATP-biotin, respectively (Figure 2.6), suggesting that the three ATP molecules bind similarly in the active site. In contrast, the γ-phosphate of APB is 3.9 Å from K168 (Figure 2.6 B), as compared to 2.4 Å with both ATP-biotin and ATP (Figure 2.6 D and F). The docking studies suggest that APB is a potential kinase cosubstrate due to the similar active site binding. However, the long distance between the γ-phosphate of APB and K168 suggests that APB may be a less efficient cosubstrate compared to ATP or ATP-biotin.[1]

A)

B)

C)

D)

E)

F)
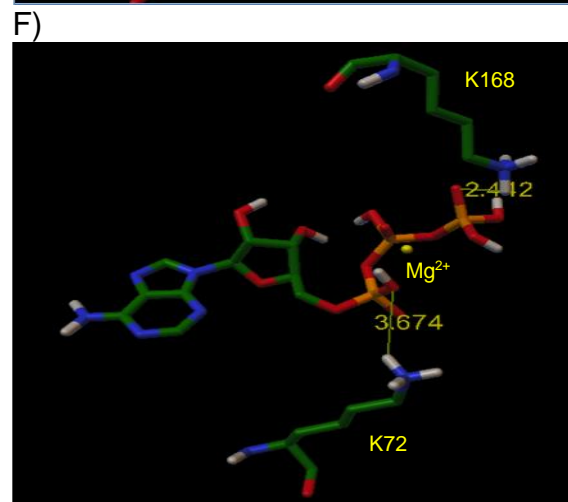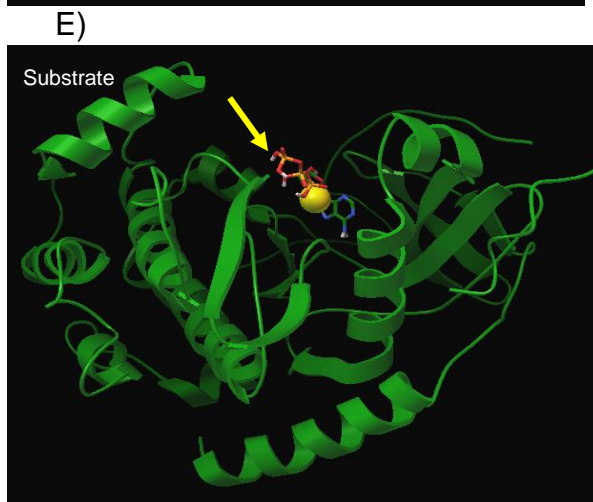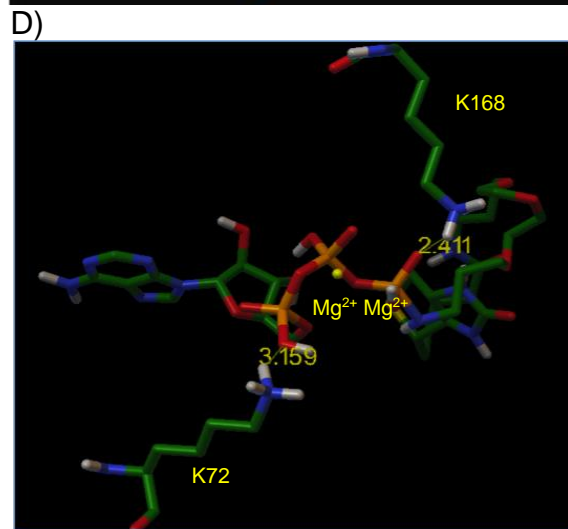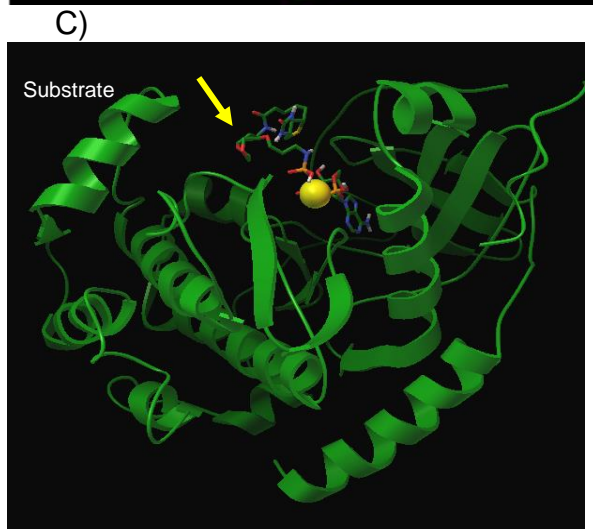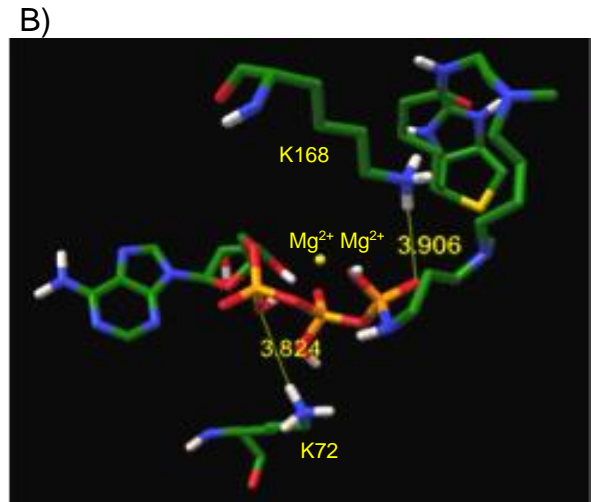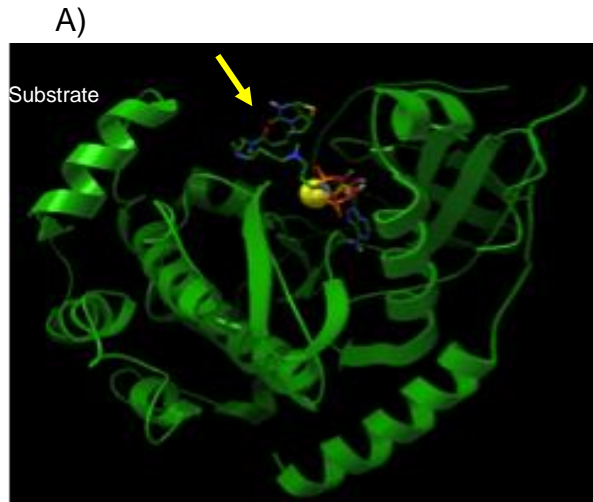
**Figure 2.6**: Docking of APB (A), ATP (C), and ATP-biotin (E) into the crystal structure of the catalytic active site of PKA kinase co-crystallized with peptide substrate (pdb: 4DH1)[107] using Autodock 4.2.[108] The arrow points to the solvent exposed biotin group in case of APB and ATP-biotin. Enlarged view of the interaction of APB (B), ATP (D), and ATP-biotin (F) with the catalytic $Mg^{2+}$ metal (yellow orb) and amino acids K72 and K168. The $\gamma$-phosphate of APB, ATP, and ATP-biotin is positioned in a close proximity to K168 while the $\alpha$-phosphate lies near K72. The APB, ATP, and ATP-biotin atoms are color-coded (C = green; H = grey; N = blue; O = red; P = orange). For clarity, the atomic radius of $Mg^{2+}$ was reduced to 0.5 Å.

## 2.2.1.2 Synthesis of APB with PKA crystal structure.

To experimentally test APB as a kinase cosubstrate, it was first synthesized from commercially available spermine (Scheme 2.2).[1] Spermine (**3**) was protected at the primary amines using 2-(t-Butoxycarbonyloxyimino)-2-phenylacetonitrile (BOC-ON) to yield protected spermine (**4**) in 80% yield. Compound **4** was methylated by reductive amination at secondary nitrogen using formaldehyde and sodium cyanoborohydride to give Boc-protected methylated spermine (**5**) in 98% yield.[109] Compound **5** was deprotected by 4M HCl in dioxane to give methylated spermine (**6**) in 90% yield. After deprotection,[109] the NHS-ester of biotin was synthesized as reported[110] and coupled to give polyamine biotin (**7**) in 40% yield.[111] Finally, polyamine-biotin (**7**) was coupled with ATP to obtain APB (**2**).[112]

**Scheme 2. 2:** Synthesis of ATP-polyamine-biotin **2** (APB)
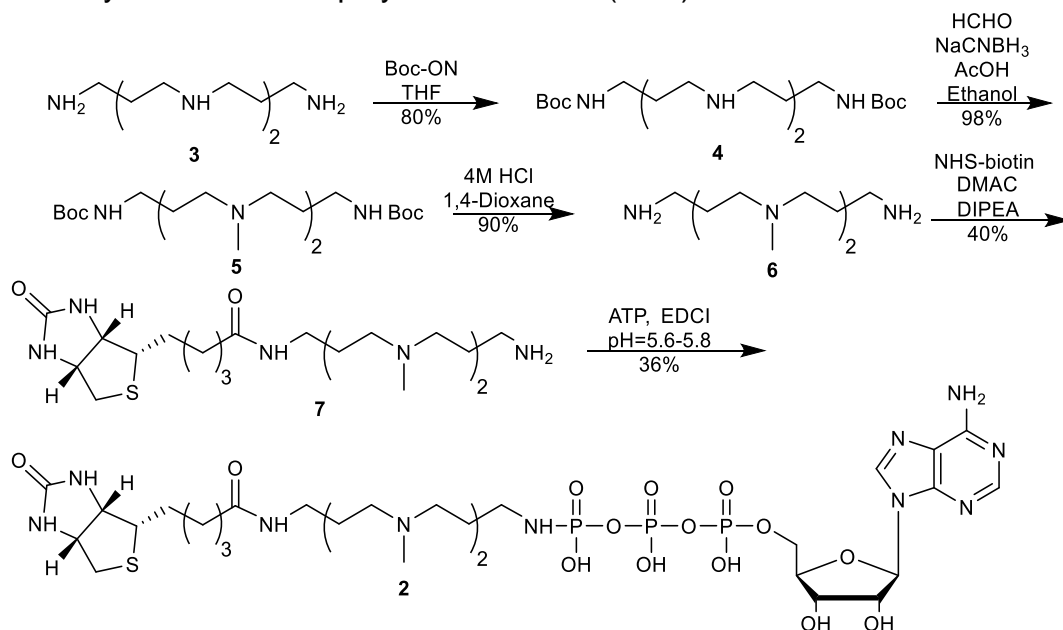


### 2.2.1.3 *In vitro* testing of APB.

To test compatibility with kinase-catalyzed biotinylation, APB was incubated with PKA kinase and full-length protein substrate, myelin basic protein (MBP). As a control, we performed the experiment in abscence of PKA or in presence of a panel kinase inhibitor, staurosporine. In addition, we treated the reaction mixture with acid after the incubation time as another control reaction. The acid should break the phosphoramidate bond and remove biotinylation. Biotinylation was visualized after SDS-PAGE gel separation, transfer to PVDF membrane, and staining with a streptavidin-Cy5 conjugate (Figure 2.7). Biotinylation was observed only in presence of kinase (Figure 2.7, compare lanes 3 and 4). In addition, MBP biotinylation was lost in the absence of APB (Figure 2.7, lane 2), in presence of the kinase inhibitor staursporine (Figure 2.7, compare lanes 7 and 8) or upon incubation with acid (Figure 2.7, lane 5) due to cleavage of phosphoramidate bond (Figure 2.4A). This experiment suggests that APB is a kinase-cosubstrate and it can be used for a kinase-catalyzed biotinylation reactions.

|  | 1 | 2 | 3 | 4 | 5 | 6 | 7 | 8 |
|---|---|---|---|---|---|---|---|---|
| MBP | + | + | + | + | + | + | + | + |
| PKA | - | + | - | + | + | - | + | + |
| ATP | - | + | - | - | - | - | - | - |
| APB | - | - | + | + | + | - | + | + |
| 50% TFA | - | - | - | - | + | - | - | - |
| STSP | - | - | - | - | - | - | - | + |
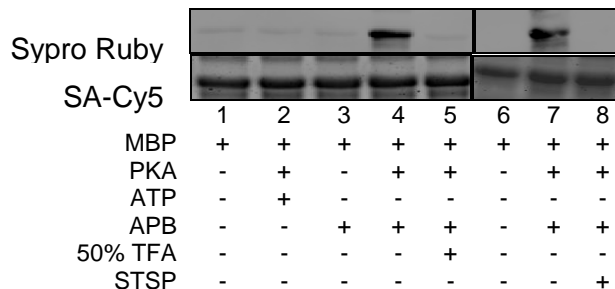
**Figure 2.7:** Kinase-catalyzed biotinylation of MBP with APB. MBP was incubated with APB and PKA in the manufacture provided buffer. As a control, TFA (50%) was added after biotinylation labeling to assure biotinylation via an acid-labile phosphoramidate bond (lane 5). A kinase inhibitor, Staursporine (STSP) was preincubated with PKA to confirm biotinylation via a kinase-catalyzed reaction (lane 8). The labeled mixtures were separated by SDS-PAGE and visualized by SYPRO® Ruby to see total proteins (A) or streptavdin Cy-5 (SA-Cy5, Life Technologies) to detect biotinylation (B). The images are representative of at least three independent trials (Figure A 2.17).

To further confirm kinase-catalyzed biotinylation by APB, a mass spectrometric (MS) study was performed. In this case, the PKA peptide substrate kemptide was incubated with APB and PKA before MALDI-TOF MS analysis. Biotinylated kemptide product was observed only in the presence of APB cosubstrate (Figure 2.8, m/z 1332.490 (M+H)[+]). The combined gel and MS analyses confirm that APB is a kinase cosubstrate.[1]
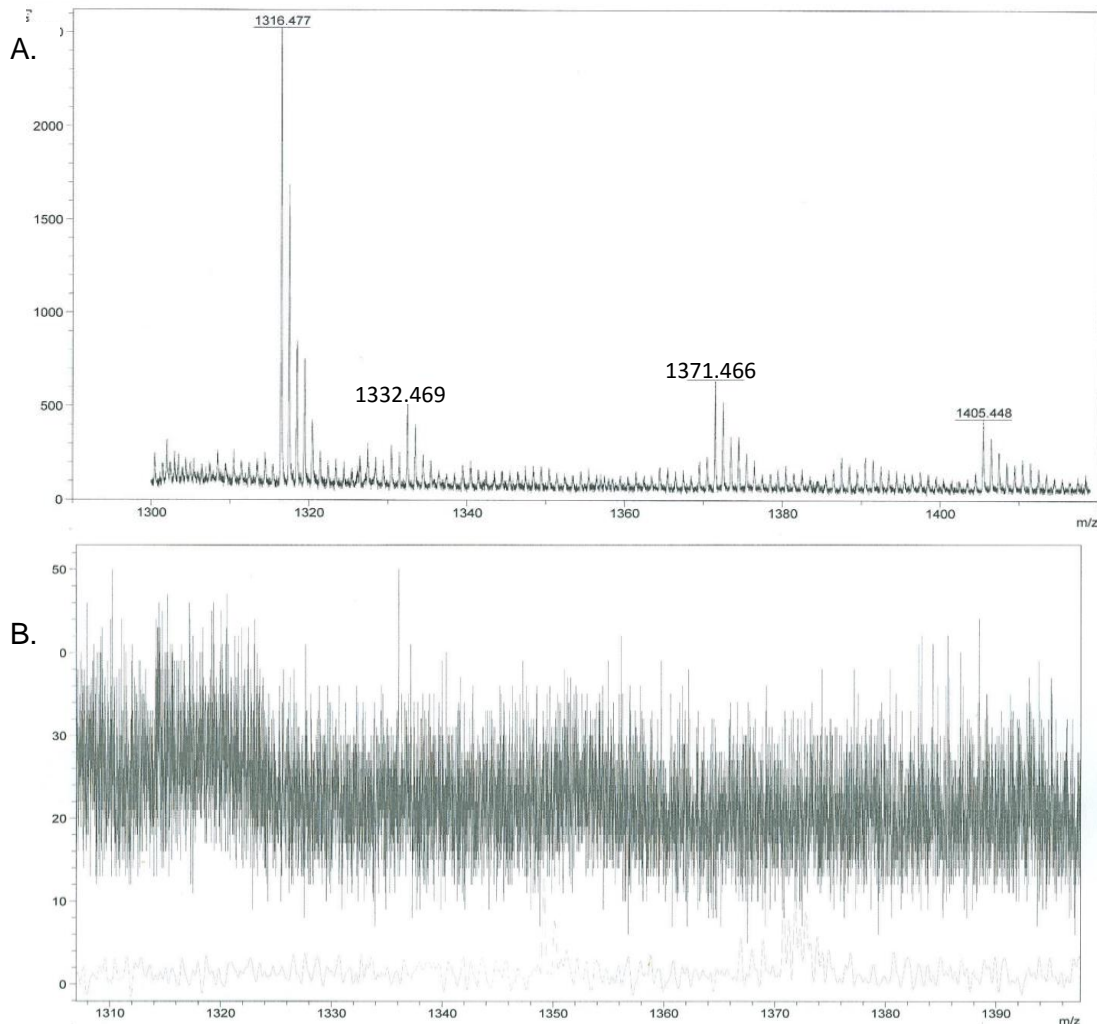
**Figure 2.8:** MALDI-TOF spectra of a kinase-catalyzed phosphobiotinylation reaction of N-acetylated kemptide with PKA in positive ion mode. A) Reaction in the presence of APB: ((M+H)$^+$ for $C_{56}H_{107}N_{19}O_{14}PS$, Calculated: 1332.7698; Observed: 1332.469,; (M+K)$^+$ for $C_{56}H_{106}KN_{19}O_{14}PS$, Calculated: 1371.7151; Observed: 1371.466 B) Reaction in the absence of APB showing no product peaks in the same m/z range. The data represent at least three repetitive trials (Figure A 2.18).

## 2.2.1.4 Determination of APB efficiency as a kinase-cosubstrate.

To investigate the efficiency of biotinylation using APB, both quantitative percentage conversion and kinetic studies were performed. For quantitative conversion studies, APB, ATP-biotin, and ATP were separately incubated with MBP and PKA, followed by cleavage of the phosphoramidate bond with acid to produce phosphoprotein

products with all ATP analogs (Figure 2.4), which allowed quantitative comparison. The

reaction mixtures were then separated by SDS-PAGE with phosphoproteins visualized

by ProQ diamond stain (Figure 2.9), as previously reported.[95] Quantification showed 55

± 6 % conversion with APB compared to ATP (Figure 2.9, lane 4), while ATP-biotin

showed 72 ± 7 % conversion compared to ATP (Figure 2.9, lane 3).[1]  Biotinylation was

less efficient with APB compared to ATP-biotin, as predicted by the docking studies.

However, the observed quantitative analysis confirmed that APB is a kinase

cosubstrate.
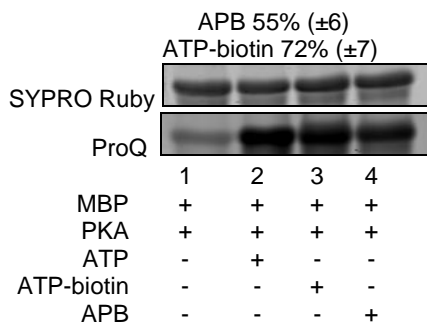


**Figure 2.9:** Quantitative analysis of MBP phosphorylation in presence of PKA with either ATP (lane 2), ATP-biotin **1** (lane 3), or APB **2** (lane 4). The reaction mixtures were separated by SDS-PAGE and visualized by SYPRO® Ruby stain (top gel) to ensure homogeneity of protein loading in all lanes or ProQ diamond stain (bottom gel) to detect phosphorylation of MBP. MBP degree of phosphorylation was quantified from the ProQ diamond stained gel (bottom gel) and the percentage of phosphorylation was calculated by comparison with phosphorylation with ATP (100%). The quantitative analysis is a representation of at least three independent trials (Figure A 2.19)

Next, kinetic studies were performed by incubating APB or ATP (0.5-100 µM)

with PKA and kemptide peptide substrate. APB revealed a reduced $K_M$ (0.87±0.21 µM)

compared to ATP (2.3±0.6 µM), but ATP showed better $k_{cat}$ (1.2±0.1 s$^{-1}$) compared to

APB (0.22±0.01 s$^{-1}$) (Figure 2.10). In sum, APB exhibited a reduced $k_{cat}$/$K_M$ (0.25 s$^{-1}$µM$^{-1}$) compared to ATP (0.52 s$^{-1}$µM$^{-1}$) (Figure 2.10). However, The reduced $k_{cat}$/$K_M$ is

similar to those observed with other ATP analogs used for kinase studies, including the

γ-phosphate modified ATP analog ATP-dansyl,[82] or the base-modified analogs N[6]-benzyl ATP or N[6]-(2-phenethyl) ATP.[113,114]   In total, both quantitative conversion and kinetics studies confirm that APB is an efficient kinase cosubstrate with conversions and kinetics similar to other known ATP analogs.[1]

A

**ATP and PKA**



| y = Vmax*x/(KM+x) | | |
|---|---|---|
| ATP | Value | Error |
| Vmax | 3.5 | 0.2 |
| KM | 2.3 | 0.64 |
| Chisq | 0.47 | NA |
| R | 0.97 | NA |

B

**APB and PKA**



| y = Vmax*x/(KM+x) | | |
|---|---|---|
| APB | Value | Error |
| Vmax | 0.64 | 0.028 |
| KM | 0.87 | 0.22 |
| Chisq | 0.013 | NA |
| R | 0.95 | NA |

C    934.272

| | ATP | APB |
|---|---|---|
| $K_M$ (µM) | 2.3 ± 0.6 | 0.87 ± 0.21 |
| $V_{max}$ (µM/min) | 3.5 ± 0.2 | 0.64 ± 0.02 |
| $k_{cat}$ (s$^{-1}$) | 1.2± 0.1 | 0.22± 0.01 |
| $k_{cat}/K_M$ (µM s)$^{-1}$ | 0.52 | 0.25 |
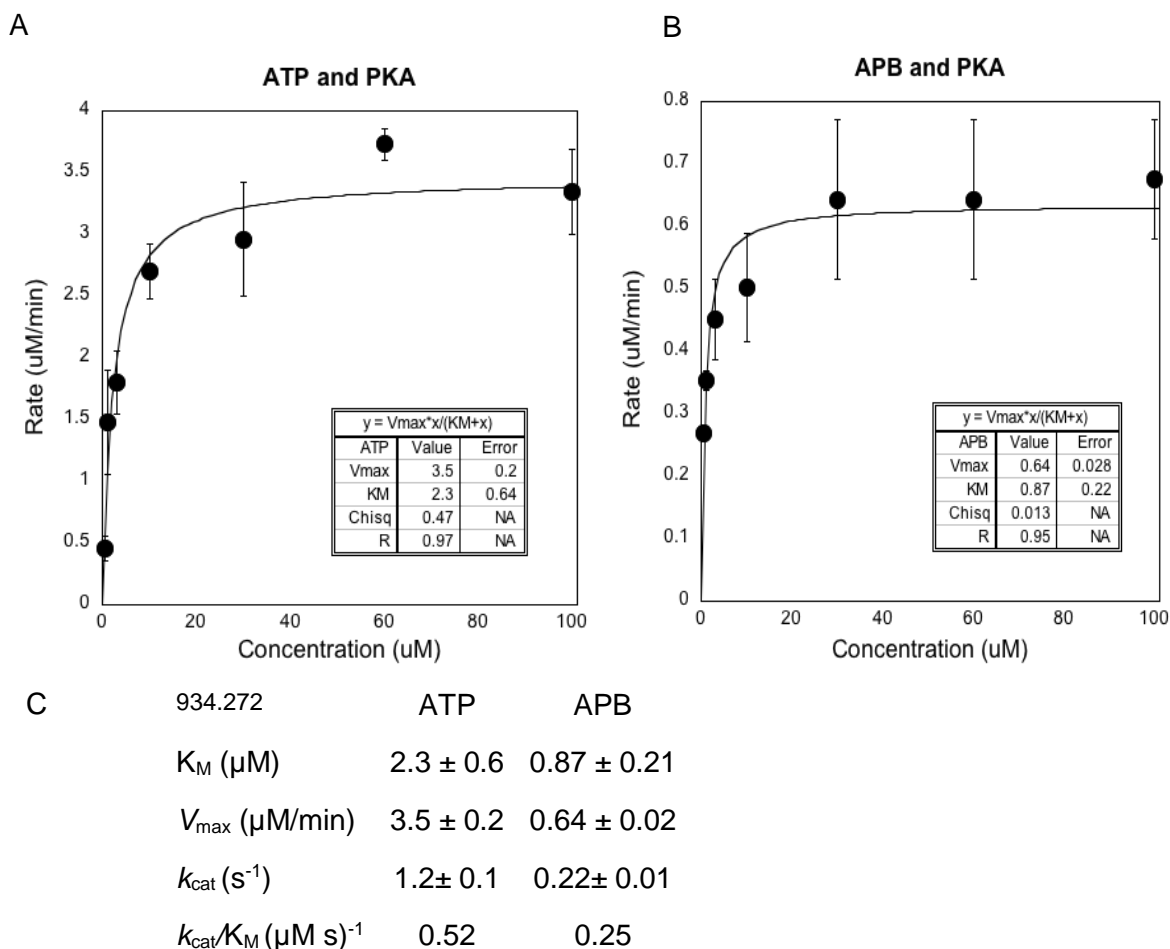
**Figure 2.10:** Michaelis-Menton curve fits for reaction containing ATP (A) or APB (B) as the cosubstrate, with kinetic analysis comparison between ATP and APB in the table (C).

To analyze the compatibility of APB with cellular kinases, HeLa cell lysates were incubated with APB, followed by SDS-PAGE analysis.[1] Biotinylation of proteins was detected in the APB reaction (Figure 2.11 , lane 4), showing the promiscuity of cellular kinases for APB.   Similar levels of labeling were observed comparing APB and ATP-

biotin (Figure 2.11, lane 4 versus 7). As a control, heat denatured lysates generated low levels of biotinylation with both APB and ATP-biotin (Figure 2.11, lanes 3 and 6), which confirmed the kinase-dependence of biotinylation. Acid treatment also reduced biotinylation (Figure 2.11, lane 5), which indicated labeling via the phosphoramidate bond in APB (Figure 2.4). To assess the quality of biotinylation in the various labeling reactions, another control reaction was performed by incubating cell lysates with the non-specific biotinylation reagent, NHS-biotin. Different biotinylated protein bands were observed with NHS-biotin treatment compared to kinase-catalyzed reactions with APB or ATP-biotin (Figure 2.11, compare lane 2 to lanes 4 and 7), suggesting kinase-selective biotinylation of lysates. These studies in lysates further establish the compatibility of APB with a range of cellular kinases and substrates, similar to ATP-biotin.[92,95]
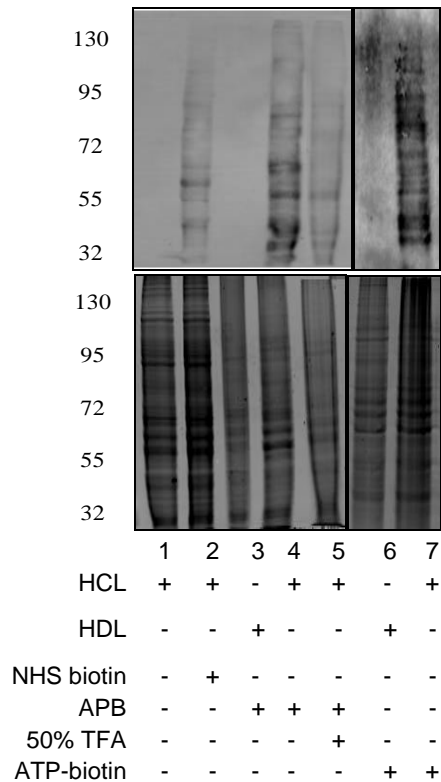
**Figure 2.11:** Kinase-catalyzed biotinylation of HeLa cell lysates (HCL) or heat-inactivated HeLa cell lysates (HDL) with APB and ATP-biotin. Acid (50% trifluoroacetic acid final concentration) was added after biotin labeling to cleave the biotin tag (lane 5). NHS-biotin was used to assess nonspecific biotinylation. Reaction mixture were separated by SDS-PAGE and visualized with streptavidin-Cy5 (SA-Cy5, top gel) or SYPRO® Ruby total protein stain (bottom gels). The gels are representative of at least three independent trials (Figre A 2.20).

## 2.2.1.5 Evaluation of APB cytotoxicity.

To assess if APB is cytotoxic to cells or not, a dose-dependent cell viability assay was performed.  The cytotoxicity studies will rule out the activation of alternative cell signaling pathways due to cell death, which may affect the results gahtered from APB biotinylation assays. An increasing concentrations of APB were incubated with HeLa cells, followed by washing and staining with trypan blue. Viable cells were counted and compared with untreated control cells. APB showed a cytotoxicity $EC_{50}$ value of 19 ± 1 mM (Figure 2.12A).  Importantly, 96 ± 1 % cell viability was observed with the 5 mM

concentration of APB that we planned to use in the cell labeling assay (Figure 2.12B). The cell-based studies show that APB is cell permeable and nontoxic at low mM concentrations, with cell penetration and labeling dependent on the polyamine linker.[1]

A)



| $y = 100/(1+(x/EC50)^n)$ | | |
|---|---|---|
| | Value | Error |
| EC50 | 0.019 | 0.00087 |
| n | 2 | 0.22 |
| Chisq | 60 | NA |
| R | 0.99 | NA |

B)

| Concentration (mM) | % cell viability |
|---|---|
| 0.0 | 100% |
| 1.0 | 99 ± 3 % |
| 5.0 | 96 ± 1 % |
| 10 | 80 ± 4 % |
| 15 | 60 ± 6 % |
| 20 | 43 ± 3 % |
| 30 | 34 ± 2 % |
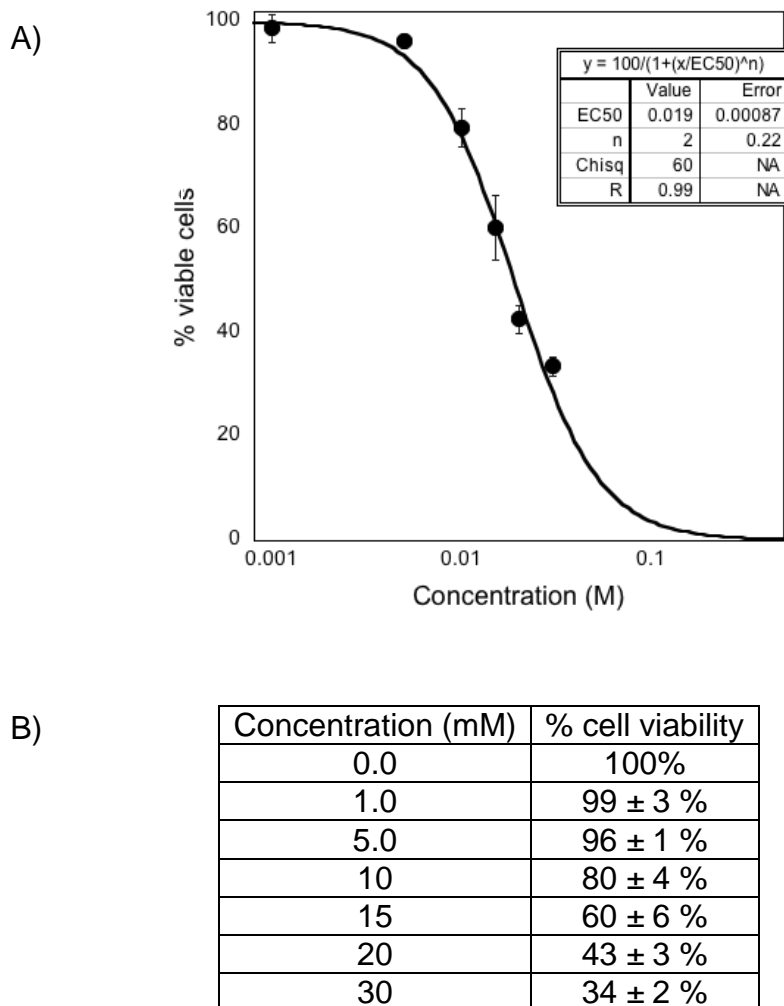
**Figure 2.12:** Cell viability assays with varying concentrations of APB. A) Dose response curve of APB with 1, 5, 10, 15, 20, 30 mM final concentrations. The $EC_{50}$ of APB is 19 ± 1. B) Table with the percentage viability data plotted in part A.  The concentration of APB used in kinase-catalyzed labeling of cells was 5 mM.

**2.2.1.6 Evaluation of APB cell permeability and live cell biotinylation**

Having confirmed the kinase compatibility of APB *in vitro* and low cytotxicity, we next sought to test kinase-catalyzed biotinylation of live cells. As a first step, fluorescence microscopy was used to confirm the cell permeability of APB. Hela cells were incubated with APB, followed by washing, fixation, and visualization with streptavidin-Cy5 to observe biotin. Cells treated with APB showed fluorescence corresponding to the presence of biotin (Figure 2.13). As controls, untreated cells (Figure 2.13) or cells incubated with ATP or ATP-biotin showed no biotin signal (Figure 2.13), which indicated that the polyamine linker in APB was required to promote cell permeability. These microscopy studies confirm that APB is cell permeable and validate the use of a polycationic groups to enhance the permeability of ATP analogs.[1]
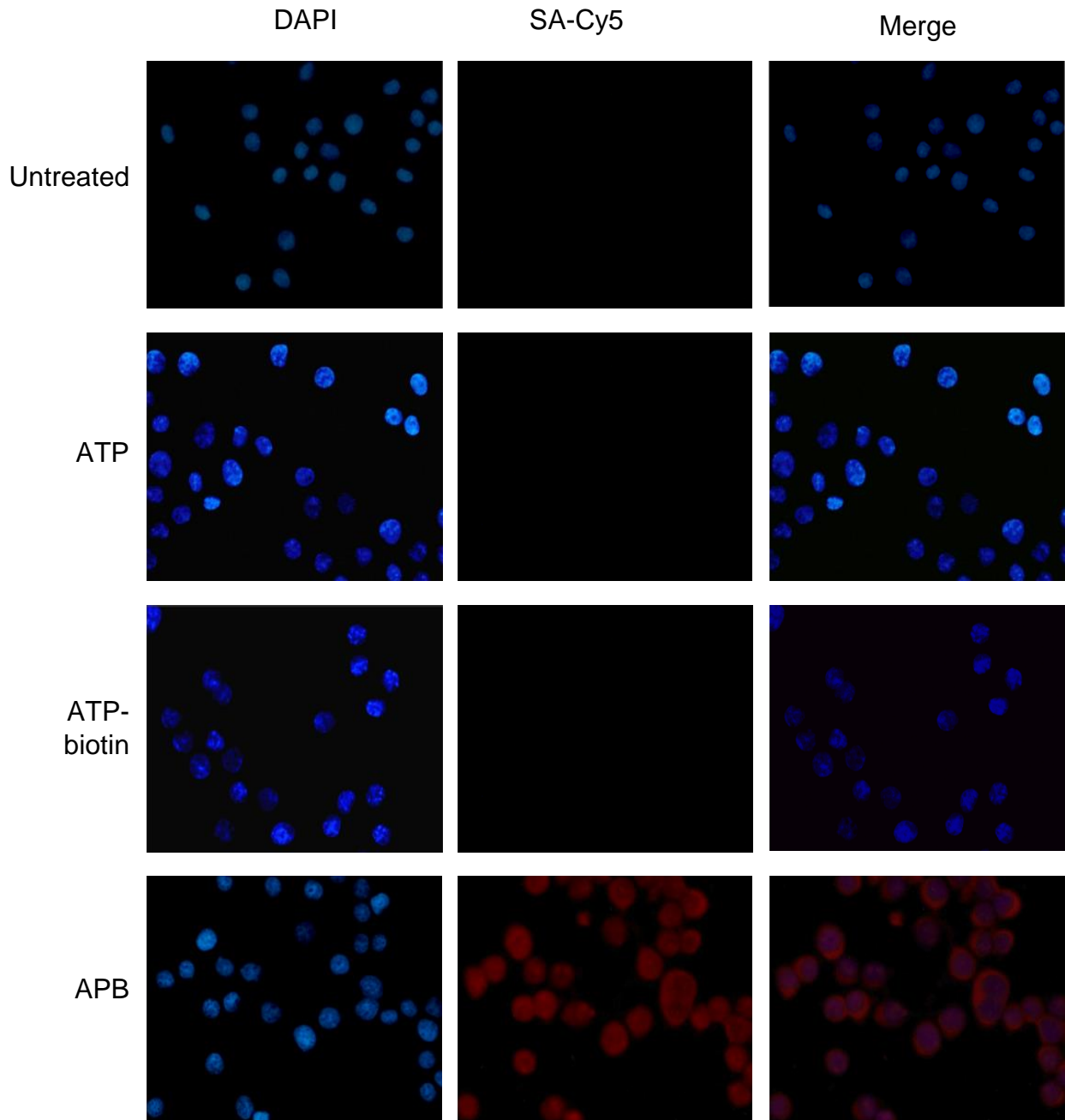
**Figure 2.13:** Microscopy studies of ATP-biotin or APB cell permeability. HeLa cells were untreated or treated with ATP, ATP-biotin or APB before visualization with the nuclear stain DAPI or biotin stain streptavidin-Cy5 (SA-Cy5).  These images are representative of three independent trials. One trial is shown here and the rest of trials are shown in figure A 2.21.

With the cell permeability of APB confirmed, live cell biotinylation with ABP was performed. HeLa cells were incubated with APB, washed to remove excess analog, lysed, and then analyzed by SDS-PAGE. Cells incubated with APB showed protein biotinylation (Figure 2.14, lane 4), which is consistent with cell permeability. Biotinylation was absent with ATP-biotin under the same conditions (Figure 2.14, lane 2), further confirming that the polyamine linker is necessary to enhance cell permeability. Also, pre-treating cells with the kinase inhibitor staursporine reduced biotinylation (Figure 2.14, lane 3), indicating that the labeling is kinase-dependent. Treatment with APB was accompanied by a modest loss of total protein (Figure 2.14, lane 3 and 4, bottom gel) compared with controls (Figure 2.14, lane 3 and 4, bottom gel), which is similar to the levels of protein loss observed in previous cell permeability studies,[115,116] including experiments with the widely used cationic-based permeabilization reagents.[117] This experiment confirms that APB is cell permeable and can *in cellulo* biotinylate protein substrates through a kinase-catalyzed reaction.
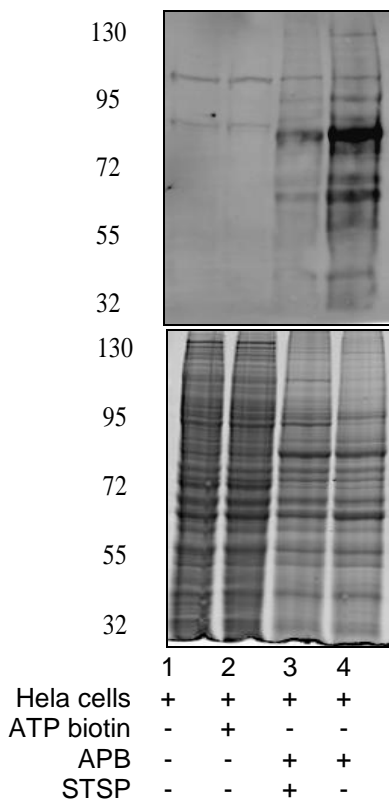
**Figure 2.14:** *In cellulo* kinase-catalyzed biotinylation with ATP-biotin or APB in HeLa cells. As a control, kinase inhibitor staurosporine (STSP) was pre-incubated with cells to prevent kinase catalysis (lane 3). Reaction mixtures (A and C) were separated by SDS-PAGE and visualized with streptavidin-Cy5 (SA-Cy5, top gel) or SYPRO® Ruby total protein stain (bottom gels). The gels are representative of at least three independent trials. One trial is shown here and the rest of trials are shown in figure A 2.22.

## 2.3 Conclusion and future directions

In conclusion, we report the first cell permeable ATP analog compatible with kinase-catalyzed biotinylation. APB acted as a cosubstrate with protein kinases *in vitro* and *in cellulo*. While the percentage conversion and kinetic efficiency was reduced compared to ATP or ATP-biotin in vitro, APB was able to label phosphoproteins in live cells. Importantly, a comparison of APB labeling reactions in lysates (Figure 2.11, lane 4) and cells (Figure 2.14, lane 4) revealed different biotinylated protein products, which indicated that *in cellulo* labeling is distinct from labeling in lysates. We speculate that the

difference in live cell versus lysates labeling may be due to compartmentalization inside the cell, which suggests that *in cellulo* labeling studies will better interrogate the phosphoproteome for cell signaling studies.[1] This difference in biotinylated proteins argue that labeling *in cellulo* will better reflect the cellular phosphoproteome. These results lay the foundation for future work using APB and kinase-catalyzed biotinylation as tools to identify and isolate phosphoproteins from cells, which will enhance cell signaling research. More generally, these studies establish that cationic groups attached to ATP analogs promote cell permeability, which provides a general strategy for creation of other ATP analogs for live cell labeling studies.

## 2.4 Experimental

### 2.4.1 Materials

Spermine, pyruvate kinase/lactate dehydrogenase, NADH, phosphoenol pyruvic acid and alpha-cyano-4-hydroxycinnamic acid were purchased from Sigma Aldrich. ATP was purchased from MP Biomedicals. Dimethyl acetamide (DMAC), 2-(tert-butoxycarbonyloxyimino)-2-phenylacetonitrile (Boc-ON), 1-(3-Dimethylaminopropyl)-3-ethylcarbodiimide hydrochloride (EDCI), diisopropyl ethyl amine (DIPEA), N-hydroxy succinimide (NHS), and N,N,N',N'-Tetramethylethylenediamine for electrophoresis were purchased from Acros. The NHS-biotin ester was synthesized according to prior literature.[110] Sodium cyanoborohydride, formaldehyde, silica, DEAE sephadex A-25, and ammonium persulfate (APS) for electrophoresis were bought from Fisher Scientific. Dichloromethane (DCM), acetic acid, hydrochloric acid, ammonium hydroxide, and HPLC grade acetonitrile were purchased from EMD. Ethanol was obtained from Decon lab. 40% Bis-acrylamide (37.5:1) for gel electrophoresis and Bradford reagent were purchases from Biorad. Myelin basic protein (MBP), F-12 media and trypan blue were bought from Invitrogen. PKA kinase was purchased from New England Biolabs. Antibiotic and Dulbecco's Phosphate Buffered Saline (DPBS) for cell culture were purchased from HyClone. 3-Hydroxypicolinic acid was bought from Fluka.

### 2.4.2 Instruments

$^1$H NMR, $^{13}$C NMR, $^{31}$P NMR (Varian Mercury-400), and high resolution mass spectra (HRMS) (LCT Premier XT (Waters)) were used to characterize the final APB analog. $D_2O$ was observed at $\delta$ 4.63 in $^1$H NMR. The peaks at $\delta$ 1.08 (t) and 3.01 in $^1$H NMR, and $\delta$ 8.29 and 46.59 in $^{13}$C NMR of ABP corresponded to the triethylamine

counter ion. Absorbance of APB was measure by UV-Vis spectrophotometer (Shimadzu 2101 PC). A Lyophilizer (VirTis BT 3.3 EL Benchtop) and Speed-vac (ThermoSAVANT, SPD131 DDA) were used during synthesis of APB. RP-HPLC was performed with Waters 1525 binary HPLC pump, Waters 2998 photodiode array detector, and Reverse phase C-18 column (YMC America, INC 250×4.6 mm, 4µm, 8 nm). Bradford assay was done using a fluorimeter (GENios Plus Tecan). SDS-PAGE apparatus were bought from BioRad (Protean III). Protein transfer was performed using the Mini-Transblot Electrophoretic Transfer Cell apparatus from BioRad. SDS gels and PVDF membranes were visualized by a Typhoon 9210 scanner (Amersham Biosciences). Immunofluorescence images were visualized by Olympus fluorescence microscope (BX 41). Peptide masses was detected using MTP Plate (Bruker) and MALDI-TOF (Bruker Ultraflex).

### 2.4.3  Docking Studies

The crystal structure of PKA was downloaded from RCSB Protein Data Bank (pdb ID: 4DH1). The co-crystallized peptide, ATP, and water were deleted using Pymol 1.5.0.5 (Schrodinger, LLC). All hydrogen atoms, Gasteiger charges and merging non polar hydrogen were added by AutoDock Tools 1.5.6, followed by generation of pdbqt output file. The charge of Mg was changed from zero to +2 manually. A grid box with a spacing of 0.375 Å, size of 74 X 70 X 70, and coordinates for the center of the grid box (-9.145, 13.434, -21.018) were used. The grid map files required for docking calculations were generated by AutoGrid 4.2. APB was drawn in ChemBioDraw Ultra and MM2 energy minimization was done by Chem 3D Pro. AutoDock Tools 1.5.6 was used again to add hydrogens, compute Gasteiger charges, merge nonpolar hydrogens,

choose torsions, and generate a pdbqt file. All acyclic bonds were rotatable except amide bonds. We then used AutoDock 4.2 to run docking calculations using the genetic algorithm, and a pdbqt file was generated. The pdbqt file for PKA was set as a rigid macromolecule and the genetic algorithm search parameters were set to 100 GA runs with a population size of 150, a maximum number of $2.5 \times 10^5$ energy evaluations, a maximum number of $2.7 \times 10^4$ generations, a mutation rate of 0.2, and a crossover rate of 0.8. Default docking parameters were used and the output DLG file was converted to pdbqt extension. Image was created using Autodock Tools 1.5.6.

### 2.4.4 Synthesis of ATP-polyamine-biotin (ABP)
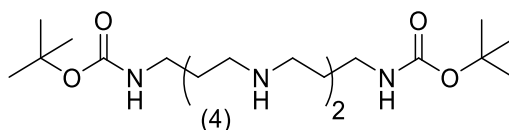


#### 2.4.4.1 Amine-protection of spermine: Synthesis of di-tert-butyl ((butane-1,4-diylbis(azanediyl))bis(propane-3,1-diyl))dicarbamate (4)

Compound **4** was synthesized according to literature, as follows.[118] Spermine (**3**, 1g, 4.9 mmol) was dissolved in THF (15 mL) at 0 °C. A solution of BOC-ON (2.42 g, 9.8 mmol) in THF (30 mL) was added drop wise under argon at 0 °C. After stirring at 0 °C for 2 minutes, the solution was stirred at room temperature for 1 hour. The reaction was quenched with saturated sodium carbonate (45 mL) and extracted with dichloromethane (135 mL). The organic layer was evaporated *in vacuo* and then the residue was purified by chromatography using silica and 5% ammonia in ethanol as eluting solvent to obtain **4** as a white solid (1.7 g, 80% yield). Spectral characterization was consistent with prior literature.[118] $H^1$NMR (400 MHz, CDCl$_3$): 1.2 (m, 2H), 1.4 (s, 18H), 1.55 (s, 4H), 1.65 (t,

4H), 2.6 (m, 8H), 3.1 (m, 4H), 5.3 (s, 2H). $C^{13}$NMR (100 MHz, CDCl$_3$): 27, 28, 30, 39, 47, 49, 79, 156.



(5)
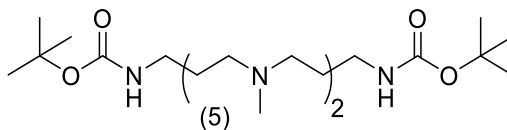
### 2.4.4.2 Synthesis of di-tert-butyl ((butane-1,4-diylbis(methylazanediyl)) bis(propane-3,1-diyl))dicarbamate (5)

Compound **5** was synthesized according to literature[118]. Compound **4** (1.7 g, 3.9 mmol) was dissolved in ethanol (45 mL) together with a 37% formaldehyde solution (17.3 mL, 213.1 mmol). Acetic acid (11.5 mL) was added, followed by sodium cyanoborohydride (4.3 g, 68.4 mmol). The reaction was stirred overnight and then quenched with saturated sodium carbonate solution until effervescence ceased, followed by extraction with dichlormethane (3 times). The organic layer was evaporated *in vacuo*. The residue was purified by chromatography using silica and 5% ammonia in ethanol as eluting solvent to obtain **5** as yellowish oil (1.8 mL, 98% yield). The spectral characterization was consistent with prior literature.[118] ESI (M+H)$^+$ for $C_{22}H_{47}N_4O_4$: calc. 431.6, found 431.6



(6)
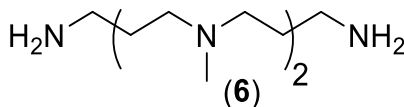
### 2.4.4.3 Synthesis N1,N1'-(butane-1,4-diyl)bis(N1-methylpropane-1,3-diamine) (6)

Compound **6** was synthesized according to literature.[118] Compound **5** (1.83 g, 4.2 mmol) was dissolved in 1,4-dioxane (40 mL) at 0 °C, followed by addition of 4N HCl (40 mL). The reaction was stirred at room temperature for 4 hours and then the solvent was evaporated *in vacuo*. The residue was crystallized with methanol/ethylacetate to give white crystals of compound **6** as a chloride salt (1.3 g, 90% yield). The spectral

characterization was consistent with prior literature.[118] ESI (M+1)$^+$ for $C_{12}H_{31}N_4$: calc. 231.4, found 231.5



(**7**)
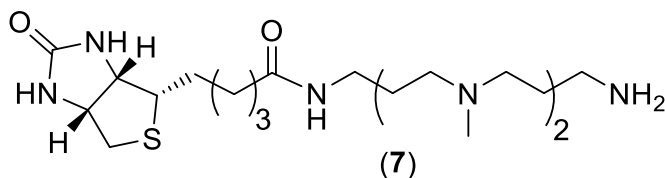
### 2.4.4.4 Synthesis of polyamine-biotin (using methylated spermine) (7)

Polyamine-biotin (**7**) was synthesized according to literature[119] with some modifications to the procedure. Methylated spermine (**6**) (0.78 g, 2.5 mmol) was dissolved in a mixture of DMAC (25 mL) and DIPEA (3.3 mL) at 0 °C. A solution of NHS biotin ester[110] (350 mg, 1 mmol) in DMAC (30 mL) was added dropwise over an hour under argon and the reaction mixture was stirred overnight at room temperature, followed by addition of diethyl ether (30 mL) to precipitate the product. The precipitate was filtered and then purified by chromatography using silica and ethanol:THF:DCM: ammonia (4:4:2:1) as an eluting solvent. Polyamine-biotin (**7**) was obtained as oil (0.5 g, 44%). The spectral data was consistent with literature.[119] $^1$H NMR (400 MHz, CD$_3$OD):δ 1.15-1.19 (m, 6H), 1.39-1.47 (m, 3H), 1.52-1.63 (m, 4H),1.64-1.82 (m, 6H), 2.19-2.34 (m, 7H), 2.45-2.61 (m,7H), 2.90-2.98 (m, 2H), 3.18-3.30(m, 2H), 4.30-4.48 (t, 1H), 4.49-4.91 (d, 1H).$^{13}$C NMR (100 MHz, CD$_3$OD): 23.40, 25.77, 28.47, 28.64, 29.52, 32.66, 35.66, 38.86, 39.33, 55.87, 59.63, 61.18, 61.48 163.15, 172.22.
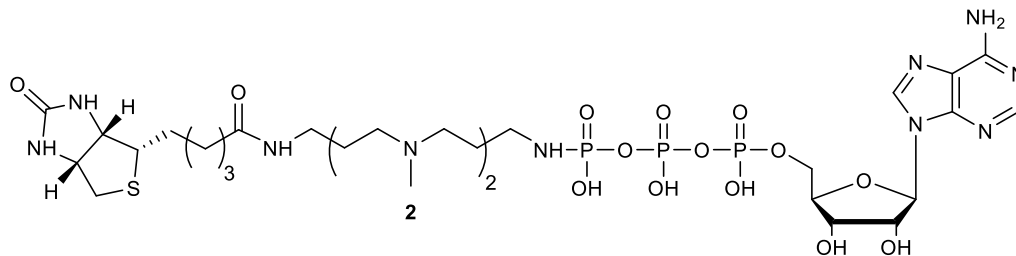
### 2.4.4.5 Synthesis of ATP-polyamine-biotin (ABP, 2)

The disodium salt of ATP (32 mg, 0.059 mmol) was dissolved in water (5 mL) and then the pH was adjusted to 7.0 with NaOH (0.5 M). EDCI (452.5 mg, 2.36 mmol) was added and the pH was readjusted to 5.6-5.8 with HCl (0.5 M). Polyamine-biotin (**7**) (114 mg, 0.25 mmol) in water (2 mL) was added and the pH was readjusted to 5.6-5.8 with HCl (0.5 M). The solution was stirred for 3 hours with control of pH at 5.6-5.8. The solution was brought to a pH of 8.5 uisng triethylamine and the product was separated by anion exchange column (A-25 sephadex, 5 gm) with 0.1-1 M triethyl ammonium carbonate buffer (pH 8.5) as eluent. Fractions containing APB were combined, lyophilized to dryness, and stored at -80 °C as a white solid (18.9 mg, 36%). Purity (95%) was assessed by RP-HPLC with triethyl ammonium acetate buffer (TEAAB, buffer A: 100 mM TEAAB in HPLC water) and acetonitrile (buffer B: 100% acetonitrile) using constant 5% buffer B for 10 minutes and then a gradient of 5% to 40% buffer B over 40 minutes. $^1$H NMR (400 MHz, D$_2$O): δ 0.92 (4H, t), 1.24 (6H, t), 1.50-1.53 (3H, m), 1.66 (3H, m), 2.05 (1H, t), 2.45 (2H, t), 2.58 (3H, s), 2.71-2.90 (m, 9H), 3.15-3.21 (6H, q), 4.00 (2H, d), 4.18-4.21 (2H, m), 4.35-4.39 (2H, m), 5.91 (2H, d), 8.07 (1H, s), 8.37 (1H, s). $^{13}$C NMR (100 MHz, D$_2$O): δ 25.1 (2), 25.9, 27.6, 27.9, 35.4 (2), 42.2, 44.7, 45.3, 45.4, 47.2 (2), 47.9 (2), 48.6 (2), 53.7 (2), 55.3, 60.1 (2), 61.9, 67.4, 86.5, 118.3, 123.7, 127.7, 139.9, 152.9, 167.6 (2C). $^{31}$P NMR (162 MHz, D$_2$O): -1.8 (d), -11.8 (d), -

23.1 (t). UV/Vis spectroscopy (H$_2$O): λ 260 nm (ε=154000). HRMS: (M-1)$^-$ for C$_{32}$H$_{57}$N$_{11}$O$_{14}$P$_3$S: calc. 944.3020, found 944.3046.

## 2.4.5 Synthesis of ATP-biotin (1)

### 2.4.5.1 Synthesis of biotin amine (1a):



**1a**
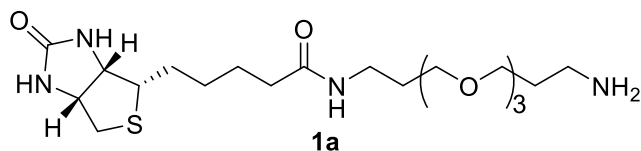
In 250 mL flask, TBTU (828 mg, 2.5 mmol) and biotin (509 mg, 2.08 mmol) were added into a mixture of DMF (5 mL) and DCM (15 mL). DIPEA (413 ul, 2.5 mmol) was added and the mixture was stirred until a heavy precipitate is formed. The precipitate was filtered, suspended in DCM (50 mL) and then added into a solution of PEG amine **1b** (1.14 ml, 5.2 mmol) in DCM (300 mL) portion wise. After stirring overnight, the solution was concentrated by evaporation under reduced pressure and purified using silica with solvent system of ethanol: DCM: ammonia in ratio 3:1:0.01 to give **1a** as white solid (600 mg, 80%).

### 2.4.5.2 Synthesis of ATP-biotin (1):



**1**
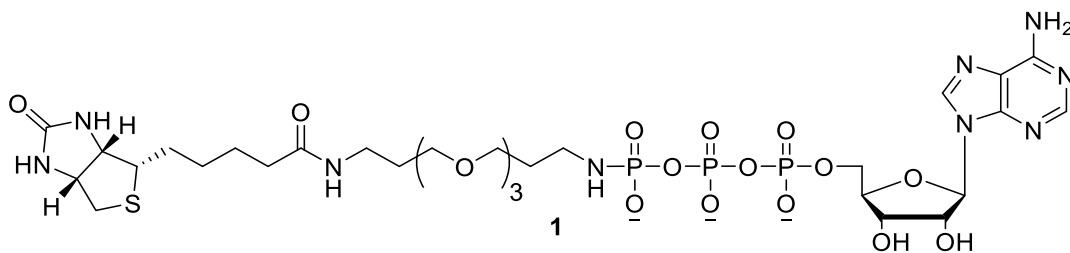
ATP (32 mg, 0.059 mmol) was dissolved in 5mL water and then pH was adjusted to 7. EDCI (452.5 mg, 2.36 mmol) was added and the pH was readjusted to 5.6-5.8 with HCl (0.5 M). Biotin amine (**1a**) (423 mg, 0.1.18 mmol) in water (2 mL) was added and the pH was readjusted to 5.6-5.8 with HCl (0.5 M). The solution was stirred for 3 hours

with control of pH at 5.6-5.8. The solution was brought to a pH of 8.5 using one drop triethylamine and the product was separated by anion exchange column (A-25 sephadex, 5 gm) with 0.1-1 M triethyl ammonium carbonate buffer (pH 8.5) as eluent. Fractions containing ATP-biotin were combined, lyophilized to dryness, and stored at -80 °C as a white solid (25 mg, 45%). $H^1$NMR ($D_2O$): 1.2 (s 2H), 1.6(m, 8H), 2.1 (s, 2H), 2.6 (d, 2H), 2.8 (m, 5H), 3.1 (s,2H), 3.4 (m, 11H), 4.1 (d, 2H), 4.21(s, 2H), 4.4(s, 2H), 6.00 (s, 1H), 8.1(s,1H), 8.4 (s, 1H). $P^{31}$NMr: -1.3(d), -11.6(d), -23.069 (t). MALDI-TOF: (M-1)$^-$ for $C_{32}H_{58}N_{11}O_{14}P_3S$: calc. 935.2415, found 934.523.

### 2.4.6  Preparation of triethyl ammonium carbonate buffer (TEAB)

To generate TEAB (1M), triethyl amine (139 mL) was mixed with water (861 mL). Dry ice was added to the mixture untill pH equaled 8.5 and the buffer was stored at 4 °C.

### 2.4.7  Synthesis of N-acetylated kemptide (AcLRRASLG)

Acetyl kemptide was synthesized by Fmoc based solid phase peptide solid according to literature.[82,120] The peptide was purified by RP-HPLC and characterized by MALDI-TOF, (M+1)$^+$ for $C_{34}H_{63}N_{13}O_{10}{}^+$: Calc. 814.4894, found 814.372.

### 2.4.8  *In vitro* kinase-catalyzed biotinylation of MBP with PKA

Kinase-catalyzed biotinylation was performed by incubating ATP or APB analog (5 mM), PKA enzyme (5µg/mL, 500U), and myelin basic protein (MBP) (1 µg/µL) in the PKA kinase buffer provided by the manufacturer (1X) (50 mM Tris-HCl, 10 mM $MgCl_2$, 0.1 mM EDTA, 2 mM DTT, 0.01% Brij 35, pH 7.5 at 25°C). The final volume for the reaction was 20 µL. The reaction mixture was incubated at 31 °C for 2 hours. Reactions without PKA and/or APB were conducted as control experiments. Reactions in the

presence of the kinase inhibitor staursporine (1 µM final concentration) were also performed where inhibitor and PKA were preincubated for 30 minutes before addition of APB. Another control experiment was performed by adding TFA (50% final conc.) and incubating at 45 °C for 1 hr with shaking at 700 rpm to cleave the phosphoramidate bond. TFA was evaporated using speed vac, followed by neutralization of the remaining TFA with 1.5 M Tris base (pH=8.8, 10 µL). All reaction mixtures were separated by 16% SDS-PAGE and visualized with SYPRO® Ruby or transferred onto a polyvinylidene difluoride membrane (Immobilon-P, Milipore) and visualized with streptavidin-Cy5 (Life Technologies).  Repetitive trials are shown in Figure 2.7 and A 2.17.

### 2.4.9  Sodium Dodecyl Sulfate-Polyacrylamide Gel Electrophoresis (SDS-PAGE)

The SDS-PAGE gels were prepared as described in Molecular Cloning, (Appendix 8.40-8.45) and Chamara Senevirathne's thesis.[121,122] Gels were prepared in 10% or 16% SDS-PAGE according to the needs of the experiments.

### 2.4.10 Visualization of biotinylation

To transfer proteins separated by SDS-PAGE, we used a polyvinylidene difluoride (PVDF) membrane (Immobilon P, Millipore). After wetting the PVDF membrane with methanol, a Mini-Transblot Electrophoretic Transfer Cell apparatus from BioRad was used to transfer the proteins in CAPS buffer (0.01 M CAPS (N-cyclohexyl-3-aminopropanesulfonic acid) at pH 10.5, containing 10% methanol). The apparatus was set at constant voltage (90 V) for 120 minutes. The membrane was air dried after protein transfer and then re-wetted with methanol. The membrane was incubated overnight in a blocking buffer (5% (w/v) non-fat milk in PBST (137 mM NaCl, 2.7mM KCl, 10 mM $Na_2HPO_4$, 2 mM $KH_2PO_4$, pH 7.4 and 0.1% Tween-20) at 4ºC. The

membrane was rinsed with PBST twice (10 mL each) and then incubated for 1 hour with streptavidinCy5 in blocking buffer (1:2000). Membrane was washed with PBST for 5 minutes twice (10 mL each) and visualized using the Typhoon 9400 scanner at 650/670 nm excitation and emission, respectively.

### 2.4.11 Sypro Ruby staining protocol

The SDS-polyacrylamide gel was incubated with fixing solution (100 mL, 50% methanol and 7% acetic acid in water) with gentle rocking at room temperature for one hour. The fixed solution was discarded and Sypro Ruby gel stain (100 mL, Invitrogen) was added in dark. The gel was incubated with Sypro Ruby stain at room temperature overnight, with gentle rocking and covered from light. The gel stain was removed and then destaining solution (10% methanol and 7% acetic acid in water) was added. The gel was incubated at room temperature for 30 minutes, followed by washing with distilled $H_2O$ for 5 minutes to remove excess acid. The stained gel was visualized using the Typhoon scanner at an excitation/emission wavelengths of 450 nm and 610 nm respectively.

### 2.4.12 *In vitro* MS analysis of kinase-catalyzed biotinylation

APB analog (5 mM) was incubated with PKA enzyme (20µg/mL, 2000U) and N-acetylated kemptide (1 mM) in the PKA kinase buffer provided by the manufacturer (1X). The final volume for the reaction was 10 µL. The reaction mixture was incubated at 31 °C for 2 hours. A reaction without PKA was conducted as a control experiment. The reactions were subsequently mixed with an equal volume (10 µL) of a saturated solution of a 1:1 mixture of 3-hydroxyalpha picolinic acid and alpha-cyano-4-hydroxycinnamic acid in 50% acetonitrile, then spotted on a MALDI plate. The spot was

left to dry and analyzed by MALDI-TOF (Bruker). Phosphorylbiotinylated peptide masses were detected at high laser power. Repetitive trials are shown in Figure 2.8 and A 2.18.

### 2.4.13 ProQ diamond gold staining protocol

The SDS-polyacrylamide gel was incubated with fixing solution (100 mL, 50% methanol and 10% acetic acid in water) overnight. The solution was discarded, followed by rinising the gel with distilled water for 30 minutes, three times. Pro-Q Diamond gel stain (100 mL, Invitrogen) was added and incubated with the gel at room temperature for 60-90 minutes, with gentle rocking and covered from light. The stain was removed and the gel was washed by destaining solution (100 mL, 20% acetonitrile, 50 mM sodium acetate pH 4) was added and incubated with the gel at room temperature for 30 minutes, three times. After removing the destaining solution, the gel was washed with distilled water for 5 minutes. The Pro-Q stained gel was visualized using the Typhoon scanner at an excitation/emission wavelengths of 532 nm and 555 nm, respectively.

### 2.4.14 *In vitro* quantification of kinase-catalyzed biotinylation of MBP with PKA

Kinase-catalyzed phosphorylation and biotinylation reactions were performed as in section 2.4.8, followed by incubation with TFA (50% final conc.) for 1 hour at 45 $^{\circ}$C with shaking at 700 rpm. The TFA incubation was necessary to cleave the phosphoramidate bond in the ATP-biotin products to create a phosphoprotein for quantitative analysis. TFA was evaporated using speed vac, followed by neutralization of the remaining TFA, as described in section 2.4.8. The reaction mixtures were separated by SDS-PAGE (16%) gel electrophoresis and visualized by SYPRO® Ruby or Pro-Q diamond stain according to the manufacturer's instructions. Quantification of

MBP phosphorylation on the Pro-Q diamond stained gel image was performed with ImageQuant 5.2 by drawing the same-sized rectangle on each MBP protein band. The MBP phosphorylation signal was background corrected by subtracting the signal after kinase reaction by the signal of untreated MBP.  Percentage phosphorylation was calculated by dividing the background-corrected MBP phosphorylation signal in ATP-biotin or APB reactions by the signal in ATP reactions (set as 100% phosphorylation) and multiplying by 100. Repetitive trials are shown in Figure 2.9 and A 2.19.

### 2.4.15 Kinetic analysis of APB with PKA

An NADH-dependent coupled assay was used to perform kinetic analysis, as previously described[7] with some exceptions. The assay was performed using NADH (0.5 mM), pyruvate kinase (24 units/mL), lactic acid dehydrogenase (36 units/mL), PKA (2.5 µg/mL, 61 nM), ATP or ATP-biotin (final concentrations of 0.5, 1, 3, 10, 30, and 100 µM), and absorbance at 360 nm taken every 30 second for 60 min. Kaleidagraph software (Synergy Software) and non-linear regression analysis was used to obtain $K_M$ and $V_{max}$ values from the Michaelis-Mentor equation ($v = V_{max}*(S)/(K_M + (S))$, where $v =$ initial rate of the reaction and (S)= substrate concentration). $k_{cat}$ was calculated by dividing $V_{max}$ by the concentration of PKA enzyme.

### 2.4.16 Starting a New Cell Culture

HeLa cells (HeLa S3 obtained from ATCC (American Type Culture Collection) was used. Cell aliquots (1.0 mL, $10 \times 10^6$ cells) were stored in cryogenic vials in a liquid nitrogen storage tank upon receipt. To start a new cell culture, an aliquot was thawed quickly in a 37 °C water bath. The solution of cells was mixed with Ham's F-12 media containing 10% v/v fetal bovine serum (FBS, Invitrogen) (10 mL) and centrifuged at

1000 rpm for approximately 5 minutes. The supernatant was removed and cells were resuspended into Ham's F-12 media (10 mL). The cells suspension were added to cell culture flask (75 mL, Corning) and grown at 37°C under a 5% $CO_2$ environment with 95% relative humidity in Hams F12 media containing 10% FSB, penicillin (9 units), and streptomycin (9 units).

## 2.4.17 Long Term Cell Storage

After growing cells to 90% confluency, cells ($1 \times 10^6$ cells per mL) were collected by centrifugation at 1000 rpm for 5 minutes. Ham's F-12 media (1 mL) with 10% v/v FBS, containing 10% v/v DMSO was used to suspended cell pellet. The cells were slowly cooled in a cryogenic vial (Corning) till the temperature reach -80 °C, followed by storing in a liquid nitrogen storage tank (Thermolyne).

## 2.4.18 Collection of Cells for Experiment

Trypsin triple express (5mL) was added to a flask containing HeLa cells at 90% confluency to cover the surface and was incubated at 37 °C for 5 minutes. Cells were removed and transferred to a centrifuge tube. After centrifugation at 1000 rpm for 5 minutes, the supernatant was removed and cells were washed with phosphate buffered saline (PBS, 137 mM NaCl, 2.7 mM KCl, 10 mM $Na_2HPO_4$, 2 mM $KH_2PO_4$, pH 7.4) and centrifuged between washings at 1000 rpm for 5 minutes. The pellets was used or stored as needed.

## 2.4.19 Bradford Assay

Bradford assay was used to measure the total protein concentration in cell lysates. The procedure was followed according to Chamara Senevirathne's thesis.[122]

**2.4.20 HeLa cells lysis procedure**

HeLa cells (National Cell Culture Center, Biovest) ($20 \times 10^6$) were lysed in lysis buffer (50 mM Tris, pH 8.0, 150 mM NaCl, 0.5% Triton X-100, 10% glycerol, and 1X protease inhibitor cocktail (GenDepot); 1 mL) with rotation for an hour at 4°C. Cell debris was removed by centrifugation at 13,200 rpm for 10 minutes at 4 °C. The supernatant was collected and protein concentration was determined by Bradford assay. Protein content was brought to a working concentration (10 mg/mL) using lysis buffer before storage at -80 °C.

**2.4.21 Kinase-catalyzed biotinylation of Hela cell lysates**

APB (5 mM) or ATP-biotin (5 mM) was incubated with HeLa cell lysates (4 µg/µL) at 30°C for 2 hours. The final volume of the reaction was 20 µL. Heat-inactivated HeLa cell lysates were produced by heating at 95°C for 5 min before adding APB. NHS-biotin (0.5 mM) was incubated with cell lysates (4 µg/µL) as a positive biotinylation control reaction. As a control to cleave the phosphoramidate bond, TFA (50% final conc.) was added after reaction and incubated for 1 hour at 31°C with shaking at 800 rpm, followed by evaporation using speed vac, and neutralization by adding 1.5 M Tris base (pH=8.8, 10 µL). The reaction mixtures were separated by SDS-PAGE (10%) and visualized by SYPRO® Ruby or transferred onto a polyvinylidene difluoride membrane (Immobilon-P, Milipore) and visualized with streptavidin-Cy5 (Life Technologies). Repetitive trials are shown in Figure 2.11 and A 2.20.

**2.4.22 Cell viability assay[123]**

Hela cells (100,000) were incubated in a 24 well plate and allowed to grow for 48 h in F-12 growth media at 37°C in a 5% $CO_2$ environment. APB (1, 5, 10, 15, 20, 30

mM) in growth media (200 uL) was added to cells and cells were incubated for an hour. The media was removed and cells were washed twice with DPBS (400uL), followed by trypsinization (section 2.4.18). Cells were collected by centrifugation at 4 $^{\circ}$C at 1000 rpm for 5 minutes, followed by washing twice with DPBS (100 uL). Cells were resuspended in an equal volume of cell suspension was mixed with trypan blue (0.4%) and counted using a hemocytometer. As a control, untreated cells were counted after subjecting them to the same washing conditions. Percentage viability was calculated by dividing the number of treated live cells by untreated ones. Kaleidagraph software (Synergy Software) was used to calculate EC$_{50}$ of APB. The results are from three independent trials (Figure 2.12).

## 2.4.23 Fluorescence microscopy assay.

Hela cells (80,000) were grown on a cover slip in a 24 well plate overnight in F-12 growth media (500 $\mu$L) at 37°C in a 5% CO$_2$ environment until 80% confluency. The cells were then incubated in serum free media for 2 hours, followed by incubation with APB (5 mM) in serum free media (500 $\mu$L) for 1 hour. Cells were washed with DPBS (500$\mu$L) 3 times, followed by PBS (500 $\mu$L, 137mM NaCl, 27 KCl, 10 mM Na$_2$HPO$_4$, 2 mM KH$_2$PO$_4$) three times. Cells were incubated with paraformaldehyde in water (4%, 500 $\mu$L) for 20 minutes at room temperature, then washed with PBS (500 $\mu$L) three times. Triton-X100 (0.2 % in PBS) was added and incubated with cells for 5 minutes at room temperature, followed by washing with PBS (500 $\mu$L) 3 times each for 5 min. Blocking buffer (2% BSA, 2% normal goat serum, and 0.2 % gelatin in 1X PBS) was incubated with cells for 1 hour at room temperature. Streptavidin-Cy5 (10 ug/mL) in blocking buffer (50 $\mu$L) was added and incubated with cells for 30 minutes. Cells were

washed with 0.1% BSA in PBS (500µL) 3 times each for 5 minutes. Cells were incubated with DAPI (100 µg/mL) for 5 minutes, followed by washing with 1X PBS (500 µL) 3 times each for 5 min. The cover slips were washed in water then installed on a glass slide containing Mowiol mounting solution (50 µL, Sigma Aldrich) saturated with DABCO (Sigma Aldrich). The slide was incubate at 31 $^o$C for 30 minutes, and then kept at 4 $^o$C until microscopy. Fluorescence photos were generated on an Olympus fluorescence microscope (BX 41) using laser wavelengths corresponding to DAPI (350 nm) and Cy5 (650nm). DAPI photos were generated at 10 ms and Cy5 at 200 ms. Merged images were created using Adobe Photoshop.  Repetitive trials are shown in Figure 2.13 and A 2.21.

## 2.4.24 Kinase-catalyzed biotinylation of live HeLa cells

Hela cells (200,000 cells) were added to 12-well plates and allowed to grow for 48 h in Ham's F-12 growth media (F-12 media contains 10% FBS, penicillin (9 units), and streptomycin (9 units)) at 37°C in a 5% $CO_2$ environment. The cells were then incubated with ATP-biotin (5 mM) or APB (5 mM) dissolved in F-12 growth media (400mL) for 1 hr under the same growth conditions as above. As a control, one well was preincubated with staurosporine (1 µM final concentration) in F-12 growth media for 1 hour before adding media containing APB. The media was removed and cells were washed with DPBS (400 µL) two times, scraped, and collected by centrifugation at 1000 rpm for 5 min at 0°C. Cell pellets were lysed in lysis buffer (31 µL) on ice for 30 minutes and then lysates were collected as in section VII. The lysate mixtures were separated by 10 % SDS-PAGE and visualized by SYPRO® Ruby or transferred onto a polyvinylidene

difluoride membrane (Immobilon-P, Milipore) and visualized with streptavidin-Cy5 (Life

Technologies). Repetitive trials are shown in Figure 2.14 and A 2.22.

**CHAPTER 3 CHITOSAN-ASSISTED CELL PERMEABILIZATION OF ATP-BIOTIN FOR LIVE CELL KINASE-CATALYZED BIOTINYLATION**

## 3.1  Introduction

In this chapter, a general method to permeabilize ATP analogs for kinase-catalyzed labelling is discussed using an additive, which is an easier alternative method to the synthesis of a cell permeable ATP analog discussed in chapter 2. We chose ATP-biotin as our model analog as ATP-biotin results in biotinylation of proteins, which can be easily analysed using various commercial streptavidin-conjugated reagents.[92,99] We used deacetylated chitosan as an additive to permeabilize cells towards ATP-biotin. Deacetylated chitosan has an advantage of biocompatibility with cell media, which overcomes draw backs for previously reported ATP analogs permeabilizing additives. A summary of methods used to permeabilize cells towards ATP analogs using an external additives with comparison to our newly reported method, is also discussed in this chapter.

### 3.1.1  Using additives to permeabilize cells toward ATP analogs

ATP analogs have been used to study kinase-catalyzed phosphorylation. Due to the cell impermeability of ATP analogs, *in cellulo* application of ATP analogs must be coupled with the usage of cell permeabilizing agent. Several methods were used to permeabilize cells to access protein phosphorylation systems.[100,124] Each method has its own advantages and limitations. In this chapter, we discuss these methods and compare it with our newly introduced procedure.

One of the most frequently used permeabilizing agents is digitonin Figure 3.1). Digitonin has been used to permeabilize cells towards ATP analogs to identify kinase substrates *in cellulo.* Digitonin permeabilize cells by binding to cholesterol in cell

membrane forming tubular structure.[100] Pores introduced by digitonin are big enough to allow large molecules such as polypeptides and ATP analogs to pass the cell membrane. The extent of permeabilization depends on the amount of cholesterol in the membrane. Digitonin permeabilization can lead to damage of intracellular membranes, but this effect can attenuated by proper control of digitonin concentration and exposure time.[100] Ionic strength and nature of growth should be considered with the application of digitonin in cell permeabilization. Many ions such as calcium can decrease the extent of cell permeabilization by resealing cell membrane. Also, glutamate in cell media increases phosphorylation rates when used with digitonin, affecting the physiological relevance of the experiment.[100] Therefore, most experiments reported the usage of digitonin in phosphorylation buffer rather than in cell media,[75,125] resulting in less physiologically relevant cell based experiment.
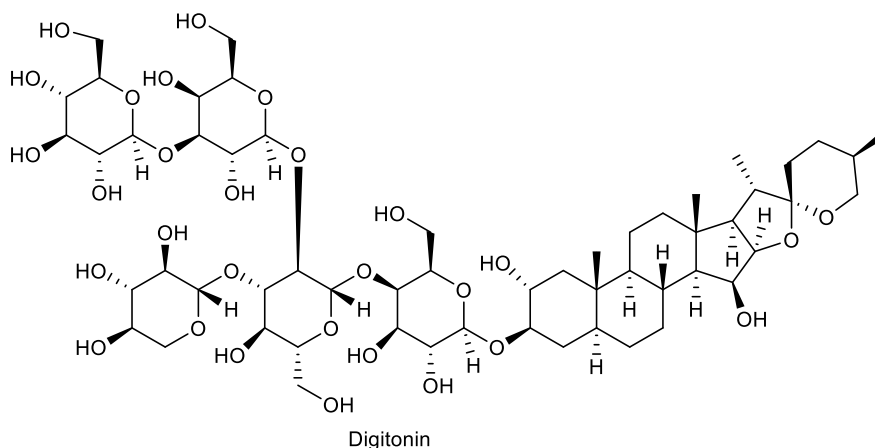


Digitonin

**Figure 3. 1: Structue of digitonin**

Another cell permeabilizing additive used with ATP analogs is streptolysin-O protein.[126] Streptolysin-O is a streptococcal hemolytic exotoxin that permeabilize cells by binding to cholesterol, similar to digitonin.[100] Like digitonin, streptolysin-O can permeabilize cells to allow entry of large molecules, but the toxicity of the reagent

should be monitored. Cell permeabilization with streptolysin-O should be controlled as it can cause damaged to intracellular membranes.[100] Unlike digitonin, streptolysin-O is unstable, which make it less favorable than digitonin. On the other hand, streptolysin-O can be used with cell growing media, without interference from media components.[100,126] In addition to digitonin and streptolysin-O, more examples of cell permeabilizing agents are present, but less frequently applied to phosphorylation studies with ATP analogs such as alpha toxin and electroporation.[100]

### 3.1.2  Deacetylated chitosan (DA)

Recently, we reported the first cell permeable ATP analog, APB (Figure 2.4, 2), compatible with kinase-cosubstrate promiscuity (Chapter 1). APB can help in studying cellular phosphorylation. The cell permeability of APB is due to the replacement of PEG by a polyamine linker, which is positively charged under physiological conditions and neutralizes the negative charge of the triphosphates. This approach can be used in general to promote the cell permeability of $\gamma$-modified ATP analogs. Attaching a polyamine to ATP analogs requires synthesis of the analog, which may have its own synthetic challenge and may affect the activity of the ATP analog. In this chapter, we report the first usage of deacetylated chitosan (DC) (Figure 3.1) as a vehicle to deliver an ATP analog into cells for kinase-catalyzed biotinylation. DC allows us to perform all permeabilizing experiments in cell media, in contrast to other previously reported cell delivery methods.[100]

Deacetylated chitosan (DC) is a polymer of deacetylated N-acetylglucosamine with a varying degree of deacetylation (Figure 3.1A). Due to the high proportion of free amines, DC was used recently in cell delivery of ATP and nucleotide drugs. DC deliver

ATP to cells through forming nanoparticles with the negatively charged nucleotides (Figure 3.1B).[127] DC cell permeability depended on the ratio of positively charged nitrogens in DC to the negatively charged phosphates in ATP (N/P ratio). In addition, DC was used under normal cell growth conditions with media, reflecting more physiologically relevant experimental conditions. In this chapter, we introduce coupling DC cell permeabilization with *in cellulo* kinase-catalyzed labelling and phosphorylation studies. DC permeabilization offers a powerful alternative to synthesis of intrinsically permeable ATP analog or use of physiologically-compromised digitonin permeabilization.
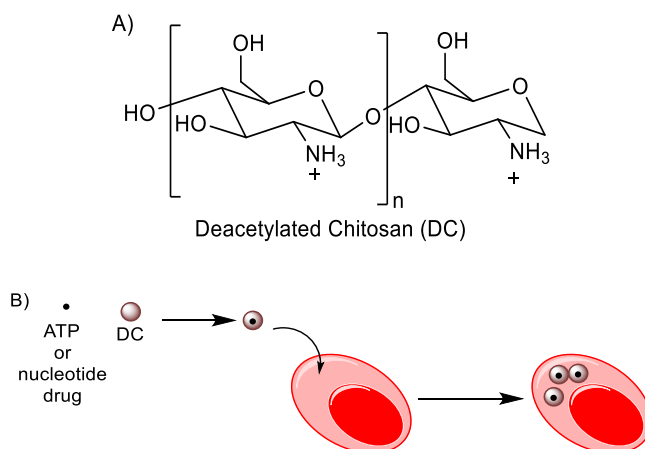


**Figure 3. 2:** A) Structure of deacetylated chitosan. B) Cell delivery of ATP or nucleotide drugs via deacetylated chitosan (DC)

## 3.2    Results

### 3.2.1  Cell permeability studies

To test if DC can enhance the cell permeabilization of ATP-biotin, fluorescence microscopy was performed. ATP-biotin and DC were first preincubated to form the ATP-biotin/DC complex. ATP-biotin/DC complex was incubated with HeLa cells in growth media under normal cell growth conditions (37 °C, 5% $CO_2$, and humidity), followed by washing, fixing, permeabilizing, staining with streptavdin-Cy5 to detect biotin, and

followed by DAPI to detect nucleus. As controls, untreated cells or cells treated with ATP-biotin only or DC only were also considered. Indeed, only cells treated with ATP-biotin/DC complex showed fluorescence signal (Figure 3.3 and A3.1). However, cells treated with ATP-biotin did not show fluorescence corresponding to biotin, which indicates the necessity of DC for cell permeabilization. Also, cells treated with DC only did not show any fluorescence, which rule out the possibility of auto-fluorescence from DC (Figure 3.3 and A3.1). These experiments indicated that DC promotes the cell permeability of ATP analogs.
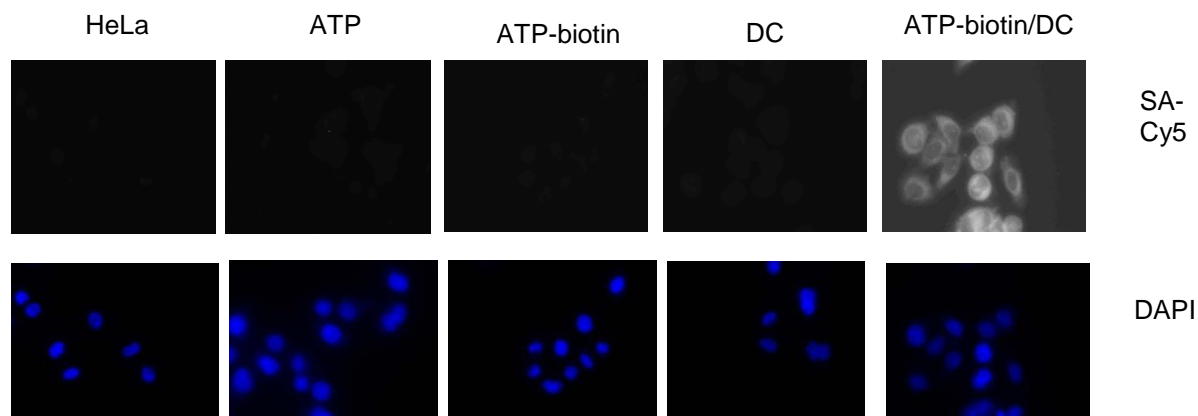


**Figure 3.3:** Fluorescence microscopy with DC. HeLa cells were incubated with ATP, ATP-biotin, DC, or the ATP-biotin/DC complex, followed by washing, fixing, and visualizing with Streptavidin Cy5 (Top) and DAPI (bottom). The images are representative of three independent trials. One trial is shown here and the rest of trials are in figure A3.1

As a secondary method to confirm ATP-biotin cell delivery by DC, mass spectrometry analysis was used. HeLa cells were incubated with the ATP-biotin/DC complex, washed, and analyzed by MALDI-TOF (Mass assisted laser ionization-time of flight) MS. Only cells treated with ATP-biotin/DC complex showed a peak at m/z 934 corresponding to ATP-biotin (Figure 3.4 and A3.2). Cells treated with ATP-biotin alone

did not show the presence of m/z 934 peak (Figure 3.4 and A3.2). The results confirm

that DC promotes the cell permeability of ATP-biotin.
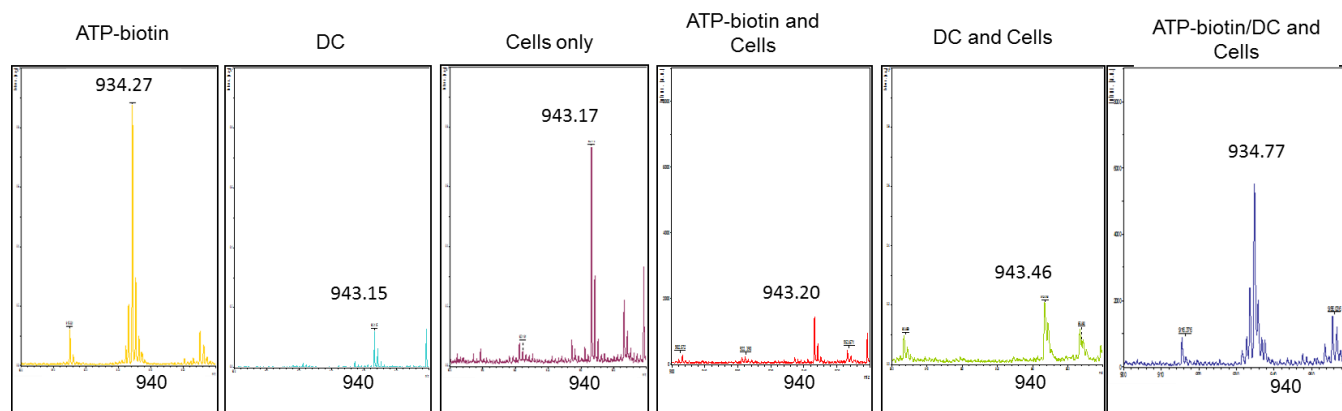


**Figure 3.4**: MALDI *in cellulo* imaging of ATP-biotin. HeLa cells were incubated with ATP-biotin, DC, or the ATP-biotin/DC complex followed by washing and mixing with alpha picolinic acid in 50% acetonitrile. The mixture was spotted on Bruker MALDI plate for analysis. The data represents at least three independent trials. One trial is shown here and the rest of trials are in figure A3.2

### 3.2.2  DC and cytotoxicity studies

In preparation for cell labeling, we assessed the dose dependent cytotoxicity of

increasing concentrations of ATP-biotin/DC in HeLa cells. Increasing concentrations of

ATP-biotin/DC (while maintaining N/P ratio at 1:1) are incubated with HeLa cells. HeLa

cells were washed, followed by resuspension in PBS buffer, and mixing with equal

amount of trypan blue. Viable cells were counted and compared with the numbers

obtained from untreated cells. The ATP-biotin/DC complex showed an $EC_{50}$ of 7.38±0.5

mg of DC (Figure 3.5). Importantly, HeLa cells exhibited cell viability of more than 80%

for ATP-biotin/DC complex concentration (2mM/1.88 mg/mL) used in the cell imaging

fluorescence assay. Cytotoxicity studies indicated that DC is not cytotoxic at cell

permeability condition experiments.

A)



| ATP-biotin (mM) | DC concentration (mg/mL) | % viable cells |
|---|---|---|
| 1 | 0.9 | 95 ± 7.2 |
| 2 | 1.88 | 85 ± 8.2 |
| 4 | 3.75 | 79 ± 4.7 |
| 8 | 7.5 | 52 ± 3.7 |
| 10 | 9.4 | 37 ± 0.8 |

B)
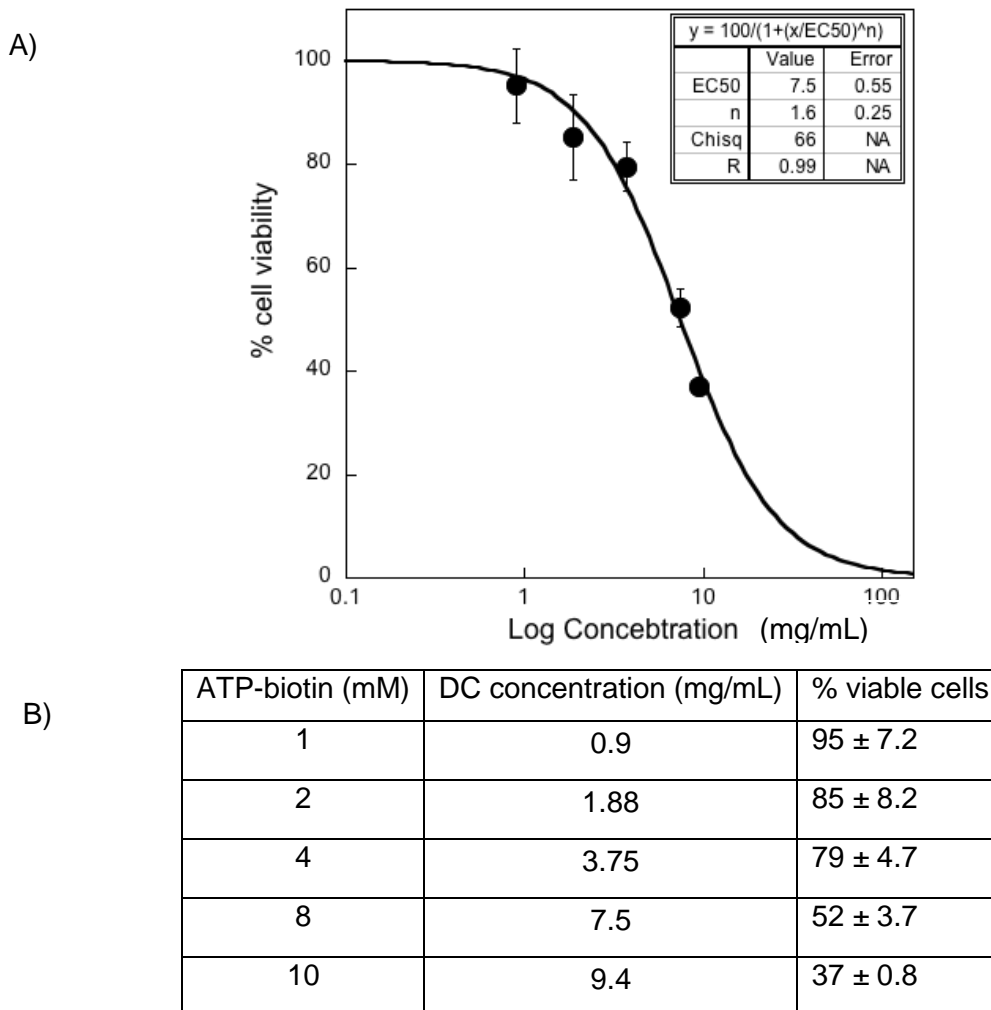
**Figure 3.5:** A) Dose dependent cell viability of ATP-biotin/DC complex. B) DC concentrations used to draw the curve.

### 3.2.3  Live cells kinase-catalyzed biotinylation

Having confirmed the cell permeability and low toxicity of DC, kinase-catalyzed biotinylation in live cells was tested. HeLa cells in growth media under normal growth conditions were incubated with ATP-biotin/DC complex (4mM/3.75 mg/mL), followed by washing, harvesting, lysis, and separation of proteins by SDS-PAGE. Biotinylation was observed in cells treated with the ATP-biotin/DC complex, which is consistent with cell permeability (Figure 3.6A and A3.3A, lane 6). As a control, HeLa cells pretreated with the kinase inhibitor, staurosporine, showed reduced biotinylation (Figure 3.6A and

A3.3A, lane 5), which confirms that biotinylation is kinase dependent. ATP-biotin alone did not show labeling (Figure 3.6A and A3.3A, lane 3), which indicates that DC is required for cell permeability. These live-cell labeling experiments show that DC-permeabilization is compatible with live cells labeling at high efficiency.



|  | 1 | 2 | 3 | 4 | 5 | 6 | 7 | 8 | 9 | 10 |
|---|---|---|---|---|---|---|---|---|---|---|
| Protein Ladder | + |  |  |  |  |  | + |  |  |  |
| Hela cells |  | + | + | + | + | + |  |  |  |  |
| Lysates |  |  |  |  |  |  |  | + |  | + |
| HD Lysates |  |  |  |  |  |  |  |  | + |  |
| ATP-biotin |  |  | + |  | + | + |  |  | + | + |
| DC |  |  |  | + | + | + |  |  |  |  |
| STSP |  |  |  |  | + |  |  |  |  |  |
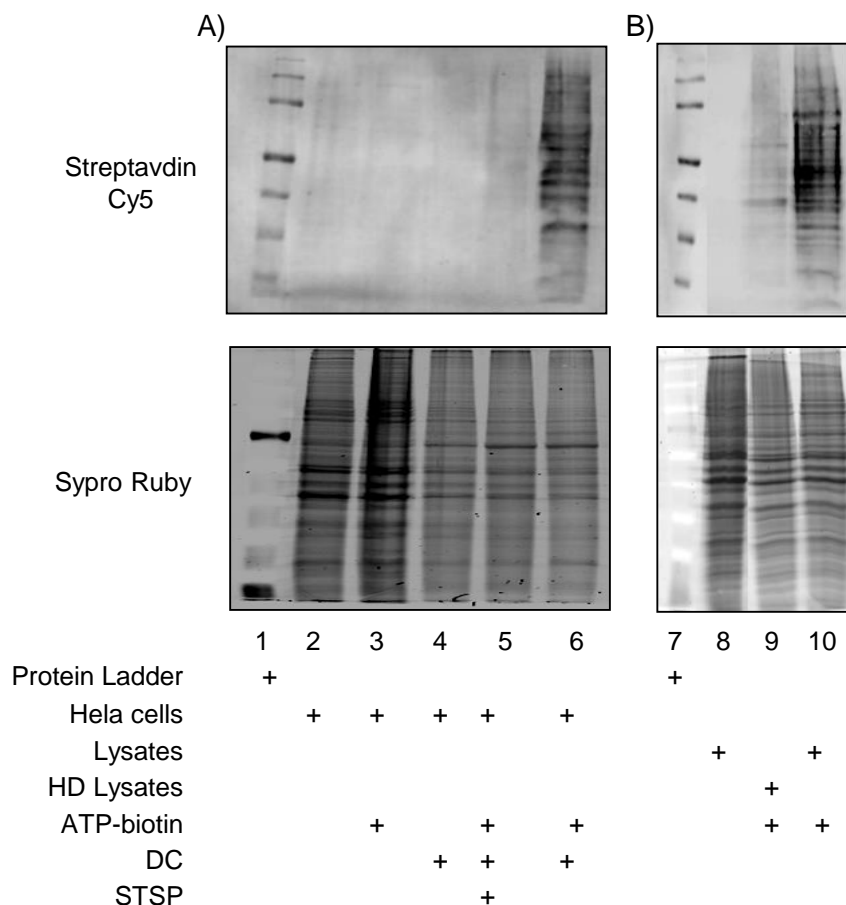
**Figure 3.6:** A) In cellulo kinase-catalyzed biotinylation of HeLa cells with ATP-biotin or ATP-biotin/DC complex. As a control, HeLa cells were preincubated with kinase inhibitor staurosporine (STSP) to prevent kinase catalysis (lane 5). B) In vitro kinase-catalyzed biotinylation of HeLa cell lysates with ATP-biotin. As a negative control, ATP-biotin was incubated with heat-denatured HeLa cell lysates (HDL). SDS-PAGE gel analysis was used to separate reaction mixtures and gels were visualized with streptavidin-Cy5 (SA-Cy5, top gel) or SYPRO® Ruby total protein stain (bottom gels). The protein ladder contains proteins of the following sizes: 170, 130, 100, 72, 55, 43, 34, and 26 kDa. All images are representative of at least three independent trials. One trial is shown here and the two trials are shown in figure A3.3.

We analyzed the quality of biotinylation of the *in cellulo* DC-assisted kinase-catalyzed biotinylation (Figure 3.4A and A3.3A) to *in vitro* labeling (Figure 3.4B and A3.3B). The extent of biotinylation was different in lysates as comparative to live cells (Figure 3.4A and A3.3A, lane 6 versus Figure 3.4B and A3.3B, lane 10). The reactions with lysates showed different bands of protein biotinylation than *in cellulo* labeling (Figure 3.4B and A3.3B, lane 10). This difference may be due to compartmentalization in cells. Therefore, this difference suggests that *in cellulo* ATP-biotin labeling is a better reflection of phosphoproteomes than lysates.

### 3.3 Conclusion and future directions

In conclusion, DC can permeabilize ATP analog through neutralizing of negative charges on the triphosphates. DC was compatible with cell growth conditions and maintained low cytotoxicity. ATP-biotin/DC showed fluorescence in cells corresponding to biotin when used with live cells. The florescence indicates that DC permeablized cells towards ATP-biotin. Our results were confirmed by MALDI mass that detected ATP-biotin in cells in presence of DC only. Importantly, using ATP-biotin/DC complex revealed biotinylation of protein substrates, which was detected by SDS-PAGE analysis. Unlike digitonin, DC can be used with cell growth media. Moreover, digitonin suffers from resealing of permeabilized cells when used with ATP analogs, in contrast to DC. Also, we compared between digitonin and DC permeabilization. Digitonin permeabilization was performed by my colleague Maheeka Embogama. The comparison experiments revealed that DC is a more efficient permeabilizing agent, which gave a better quality gels and fluorescence microscopy images. Therefore, we recommend to use DC in future with ATP analogs to study kinases.

In addition to previously discussed advantages of DC, *In cellulo* kinase-catalyzed biotinylation using ATP-biotin/DC showed different biotinylated proteins than *in vitro* biotinylation, which may reflect compartmentalization inside cells. DC cell permeabilzation of ATP-biotin can be used to reveal a more physiologically relevant kinase enzyme signaling pathways. A paper describing this work is in final stage of writing. Indeed, ATP-biotin/DC provides an alternative method to the cell permeable ATP analogs (APB) discussed in chapter 1. DC provides an easier and cheaper method for in cellulo kinase-catalyzed studies using ATP analogs because there is no need to synthesize a new analog with DC. Also, DC is more feasible when synthesis of cell permeable ATP analog is not accessible. However, cell permeable ATP analog (APB) discussed in chapter 1 is less cytotoxic than DC. Therefore, the usage of either APB or ATP-biotin/DC should be selected depending on pros and cons of each method.

In future, we are going to couple in cellulo kinase-catalyzed biotinylation with streptavidin columns to purify dynamically phosphorylated proteins. After purification, we will use Ms/Ms proteomic analysis to identify the purified proteins. Interestingly, DC can be used with other ATP analogs, such as ATP crosslinking analogs (discussed in chapter 4), to identify kinase-substrate pairs. The later method will provide a more physiologically data because kinase-substrate pairs identified from this method will reflect the compartmentalization inside the cells.

## 3.4 Experimental

### 3.4.1 Materials

ATP-biotin was synthesized as previously reported.[80,128] Low molecular weight deacetylated chitosan (75-85% deacetylation), digitonin, 1,4-Diazabicyclo(2.2.2)octane (DABCO), and Mowiol® 4-88 were purchased from Sigma Aldrich. ATP was bought from MP Biomedicals. 1-(3-Dimethylaminopropyl)-3-ethylcarbodiimide hydrochloride (EDCI) and N,N,N',N'-Tetramethylethylenediamine for electrophoresis were purchased from Acros. Silica, DEAE sephadex A-25, and ammonium persulfate (APS) for electrophoresis were bought from Fisher Scientific. Dichloromethane (DCM), acetic acid, and hydrochloric acid were bought from EMD. 40% Bis-acrylamide (37.5:1) for gel electrophoresis was purchases from Biorad. F-12 media were bought from Invitrogen. Antibiotic and Dulbecco's Phosphate Buffered Saline (DPBS) for cell culture were purchased from HyClone. DAPI was purchased from Life-Technology.

### 3.4.2 Instruments

A Lyophilizer (VirTis BT 3.3 EL Benchtop) and Speed-vac (ThermoSAVANT, SPD131 DDA) were used during synthesis of ATP-biotin. The SDS-PAGE instrument were purchased from BioRad (Protean III). Mini-Transblot Electrophoretic Transfer Cell apparatus from BioRad was used in Protein transfer. Typhoon 9210 scanner (Amersham Biosciences) was used to visualize SDS gels and PVDF membranes. Olympus immunofluorescence microscope (Model BX 41) was used to visualize fluorescence images. ATP-biotin mass was detected using MTP Plate (Bruker) and MALDI-TOF (Bruker ultraflex).

### 3.4.3  Synthesis of ATP-biotin

ATP-biotin was synthesized as previously reported, as discussed in chapter 2 (Section 2.11.5).[80]

### 3.4.4  Preparation of 10 mg/mL deacetylated chitosan

Deacetylated chitosan (75%, 500 mg) was triturated with 1.75% acetic acid in water (50 mL) till a homogenous. The mixture was stirred overnight at room temperature to produce homogenous solution.

### 3.4.5  Preparation of ATP-biotin/chitosan mixture

ATP-biotin (32 mM in water, 50 µL) was added portion wise to the deacetylated chitosan solution (10 mg/mL, 150 µL) with vortexing. The mixture was diluted with either water (4 µL) or staurosporine in water (4µL, 1 uM final) and volume was adjusted to 400 µL using media containing 10% FBS, penicillin (9 units), and streptomycin (9 units) to yield ATP-biotin at a final concentration of 4mM and DC at a final concentration of 3.75 mg/mL. The concentrations was adjusted when using higher or lower concentrations of ATP-biotin.

### 3.4.6  Fluorescence microscopy assay.[1]

HeLa cells (160,000 cells) were grown on a cover slip in a 12 well plate overnight in F-12 media (500 µL) containing 10% FBS, penicillin (9 units), and streptomycin (9 units) at 37°C in a 5% $CO_2$ environment. Cells were incubated in serum free media for 1 hour at 37°C in a 5% $CO_2$ environment. Media was removed and cells were incubated with a mixture of ATP-biotin (2 mM)/ DC (1.9 mg/mL) complex (section 3.4.5) in media at 37C in a 5% $CO_2$ environment for 2 hour. Cells were washed with DPBS (500µL) 3 times, followed by washing with PBS (500 µL) 3 times.

Paraformaldehyde (4% in water, 500 μL) was added and incubated for 20 minutes at room temperature to fix cells, followed by washing with PBS (500 μL) three times. Cells were incubated with TritonX 100 (0.2 % in PBS, 500 μL) for 5 minutes at room temperature, followed by washing with PBS (500 μL) 3 times each for 5 min. Cells were incubated with blocking buffer (2% BSA, 2% normal goat serum, and 0.2 % gelatin in PBS) for 1 hour at room temperature, followed by incubation of cells with streptavidin-Cy5 (10 μg/mL) in blocking buffer (50 μL) for 30 minutes. Cells were washed with BSA (0.1% in 1X PBS, 500μL) 3 times, each for 5 minutes. DAPI (100 μg/mL in blocking buffer, 50 μL) was added to cells for 5 minutes, followed by washing with PBS (500 μL) 3 times each for 5 min. Cover slips were immersed in water then fixed on a glass slide containing a Mowiol solution (6 μL) saturated with DABCO. The slide was incubate at 31°C for 30 minutes, then kept at 4 °C. An Olympus fluorescence microscope was used to generate fluorescence photos using laser wavelengths corresponding to DAPI (Excitation/emission maximum 358/461 nm) and Cy5 (Excitation/emission maximum 678/694 nm). DAPI photos were generated at 10 ms and Cy5 at 500 ms. Repeatitive trials are shown in Figure 3.3 and A3.1

### 3.4.7 MALDI in cellulo imaging of ATP-biotin

HeLa cells (20,000 cells) were suspended in F-12 growth media (50 μL), then added to a 96 well plate. An equal volume (50 μL) of ATP-biotin (4 mM), DC (3.75 mg/mL) or ATP-biotin (4 mM)/DC (3.75 mg/mL) mixture was added to give a final concentration of 4 mM of ATP-biotin and 3.75 mg/mL of DC. Cells were incubated for 2 hours at 37°C in a 5% $CO_2$ environment. As a control, one well without ATP analog or DC was used as a reference. All reaction volumes were 100 μL. Cells were collected

by centrifugation at 1000 rpm for 5 min at 4 °C, then washed twice with DPBS (100 μL).

Cell pellets were resuspended in water (20 μL). The cell suspension (1μL) was mixed

with saturated solution of α-picolinic acid in 50% acetonitrile (1 μL), and then applied to

a MALDI plate (Bruker) for MS analysis using MALDI-TOF spectrometer (Bruker). MS

spectrum was analyzed for the presence of ATP-biotin at m/z 934. Repetitive trials are

shown in Figure 3.4 and A3.2.

### 3.4.8  Cell viability assay for DC

HeLa cells (100,000 cells) were grown in a 12 well plate for 48 h in F-12 media

containing 10% FBS, penicillin (9 units), and streptomycin (9 units) at 37°C in a 5%

$CO_2$ environment. Increasing concentrations of ATP-biotin (1, 2, 4, 8, 10 mM)/DC (0.9.

1.88, 3.75, 7.5, and 9.4 mg/mL) complex respectively, were mixed as in section III-3

and the mixture was added to cells. Cells were incubated for 2 hours and then the

media were removed. Cells were washed twice with DPBS (400 μL), followed by gentle

scraping. Cells were collected by centrifugation at 4 °C, 1000 rpm for 5 minutes,

followed by resuspension in DPBS (100 μL). Equal volume of cell suspension was

mixed with trypan blue (0.4%) and cells were counted using Hemocytometer. As a

control, untreated cells were grown and counted as described. Percentage cell viability

was calculated by dividing the number of treated live cells by untreated ones and

multiplying by 100. Kaleidagraph software (Synergy Software) was used to calculate

$EC_{50}$ of ATP-biotin/DC.  The results are from three independent trials (Figure A 3.1).

### 3.4.9  Visualization of biotinylation

Refer to Chapter 2 (section 2.4.10)

### 3.4.10 Sypro Ruby gel staining

Refer to Chapter 2 (section 2.4.11)

### 3.4.11 Starting a new cell culture

Refer to Chapter 2 (section 2.4.16)

### 3.4.12 DC-assisted kinase-catalyzed biotinylation of HeLa cells

HeLa cells (200,000 cells) were grown in 12-well plates for 48 h in F-12 growth media at 37°C in a 5% $CO_2$ environment. The cells were then incubated with ATP-biotin (4 mM) alone or ATP-biotin (4 mM)/DC (3.75 mg/mL) complex in F-12 growth media for 2 hours under the same cell growing conditions. As a control, cells were preincubated with staurosporine (1 µM) in F-12 growth media at 37°C in a 5% $CO_2$ environment for 1 hour before adding the ATP-biotin/DC mixture in media containing staurosporine (1 µM). The media was removed and cells were washed with DPBS (400 µL) two times, harvested by scraping, and collected by centrifugation at 1000 rpm for 5 min at 0°C. Lysis buffer (21 µL, 50 mM Tris, pH 8.0, 150 mM NaCl, 0.5% Triton X-100, 10% glycerol, and 1X protease inhibitor cocktail (GenDepot)) was added to cell pellets on ice for 30 minutes with rocking and then lysates were collected by removing cell debris through centrifugation at 13,200 rpm for 10 minutes at 4 °C. SDS-PAGE gel analysis (10%) was used to separate cell lysates and total proteins were visualized by SYPRO® Ruby. Biotinylation was detected with streptavidin-Cy5 (Life Technologies) (dilution 1:2000), after transferring the lysate mixture onto a polyvinylidene difluoride membrane (Immobilon-P, Milipore). Repetitive trials are shown in Figure 3.5A and A3.3A.

### 3.4.13 Kinase-catalyzed biotinylation of HeLa cell lysates.[1]

HeLa cells (200,000 cells) were grown in 12-well plates for 48 h in F-12 media containing 10% FBS, penicillin (9 units), and streptomycin (9 units) at 37°C in a 5% $CO_2$ environment. Cell were collected and lysates were prepared as in section 3.4.12 and section 2.4.20. Lysates were incubated with ATP-biotin (4 mM) for 2 hours at 37°C. As a control, ATP-biotin (4mM) was incubated with heat denatured cell lysates (heated at 95 °C for 1 min). SDS-PAGE (10%) analysis was used to separate reaction mixtures and total proteins were visualized by SYPRO® Ruby. Biotinylation was detected with streptavidin-Cy5 (Life Technologies), after transferring lysate mixture onto a polyvinylidene difluoride membrane (Immobilon-P, Milipore). Repetitive trials are shown in Figure 3.5A and A3.3A.

# CHAPTER 4 DEVELOPMENT OF AN AFFINITY BASED ATP ANALOG FOR KINASE-CATALYZED CROSSLINKING

## 4.1 Introduction

Many cell signaling pathways are regulated through kinase-catalyzed phosphorylation biochemical reactions. Through phosphorylation, transcription of specific genes can be turned on followed by a specific response. Identifying kinase-substrate pairs can reveal the details of signaling pathways that control cell function. In this chapter, different methods of kinase substrate identification are discussed. Also, we introduce the first affinity-based crosslinking ATP cosubstrates to identify substrates for cysteine-containing kinases. Akt1 was used as an example for those cysteine-containing kinases. In addition, a brief discussion of various types of affinity-based crosslinking groups are discussed.

### 4.1.1 Introduction to affinity based crosslinkers

Cell signaling events are regulated through many biochemical reaction, such as phosphorylation, acetylation, methylation, etc.[2] The biochemical reactions can govern protein-protein interactions, conformational changes, enzymatic function, etc. Many methods have been used to purify protein bound to enzymes to identify the substrates of the biochemical reactions, such as co-immunoprecipitation, bimolecular fluorescence complementation (BiFC), mass spectrometry, and tandem affinity purification.[129] An alternative method to identify protein-protein interactions is the use of affinity-based crosslinkers (ABCL).[129] In ABCL, a bifunctional cosubstrate or reagent bearing two reactive chemical group is introduced to cells or lysates. Physically interacting proteins react with the bifunctional reagent resulting in crosslinking of the interacting protein (Figure 4.1). The crosslinked protein complexes have a higher

molecular weight equal to the sum of the molecular weight of individual proteins. The crosslinked complex can be detected by SDS-PAGE gel analysis and western blotting with a corresponding antibody.[130]
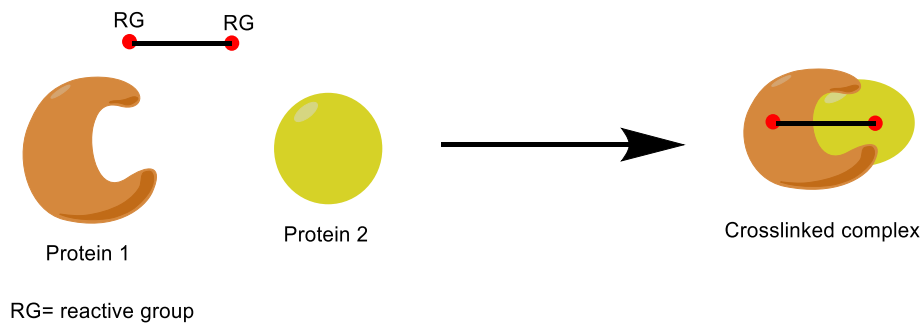


**Figure 4. 1:** Diagram deciphering affinity based crosslinking of two interacting proteins. RG is a reactive group.

Many reactive chemical groups have been used to crosslink enzymes to their interacting substrates via a covalent bond (Table 4.1). The reactive groups can crosslink with specific amino acids in close proximity on the interacting proteins. An ideal crosslinker should be water soluble and should form stable covalent bond. A summary of the most important affinity based crosslinkers with their possible reacting amino acids is shown in table 4.1.

**Table 4.1:** Types of affinity based crosslinkers[130]

| Crosslinker reactive group | Structure of crosslinker | Functional group target on amino acid | Reference |
|---|---|---|---|
| NHS ester |  | Amine (Primary or secondary) | 130 |
| Imidoester |  | | 130 |
| Pentafluorophenyl esters (PFP) |  | | 131 |
| Dichlorotriazine |  | | 132 |
| Maleimide |  | Sulfhydryl (Cysteine) | 130 |
| Acrylamides |  R= H or methyl | | 133 |
| Haloacetyl (e.g. bromo and iodo) |  X= Bromo or Iodo | | 134 |
| Pyridyldisulfide |  | | 131 |
| Vinyl sulfone |  | | 131,135 |
| p-chloronitrobenzene |  | | 132 |
| Hydrazide |  | Aldehyde (in oxidized carbohydrates) | 124 |
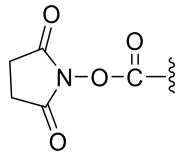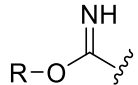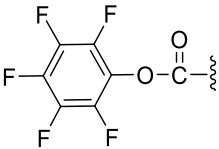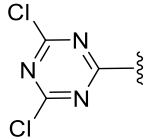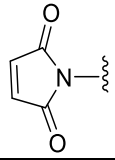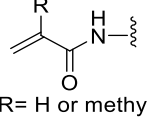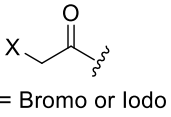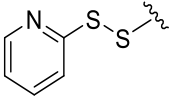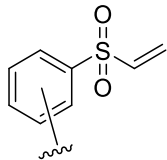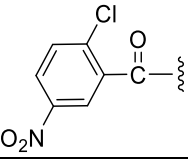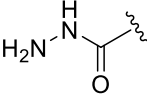
## 4.1.2 Photo affinity crosslinkers

Another type of crosslinking reaction to identify interacting proteins is photo affinity labeling (PAL).[130,136] In PAL, a photo-crosslinker, such as phenyl azide, benzophenone, or diazirine[137-147] is installed on one protein. The modified protein can be used with lysates to crosslink with interacting proteins in presence of light (Figure 4.2). A photo-crosslinker should possess four main criteria for successful PAL.[147] First, it should be inert to absence of light. Second, the photo-crosslinker should be mildly activated without destructing the targeted biological system. Third, the life time of interacting proteins should be longer than the life time of activated photo-crosslinker. Lastly, the activated photo-crosslinker should be able to form stable covalent bond with proximal interacting proteins. A brief review of selected photo-crosslinkers is presented in next sections.



PAC= Photo Affinity Crosslinker
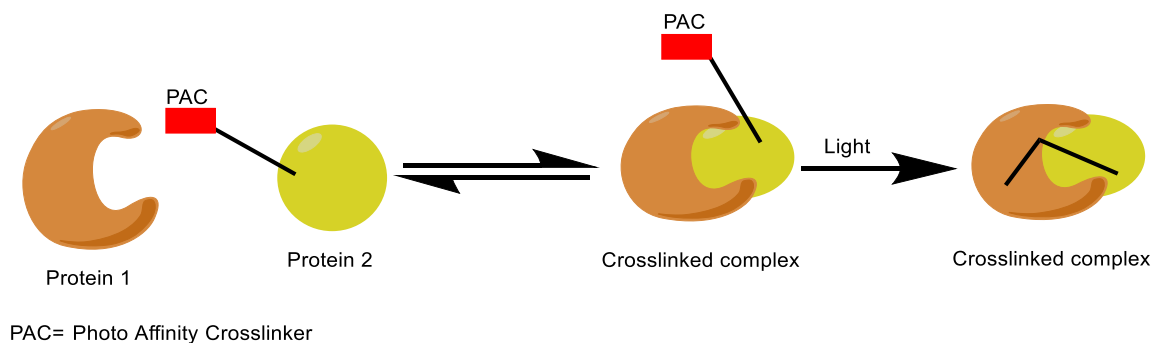
**Figure 4.2:** Diagram deciphering protein-protein photo affinity crosslinking

## 4.1.2.1 Aryl Azide

Phenyl azides are well known photo-crosslinkers and are more stable than alkyl azides. Phenyl (aryl) azides can be excited using UV light to form a reactive nitrene (Figure 4.3).[148,149] The nitrene intermediate inserts into different bonds, such as C-H, O-H, N-H, and S-H bonds of adjacent protein. Also, the nitrene can insert into the

phenyl ring to govern a ring expansion to form ketenimine. Ketemine can react with nearby nucleophiles on protein (Figure 4.3).[150] The phenyl azide has an advantage of its broad reactivity with many functional groups. However, the high reactivity can lead to nonspecificity.
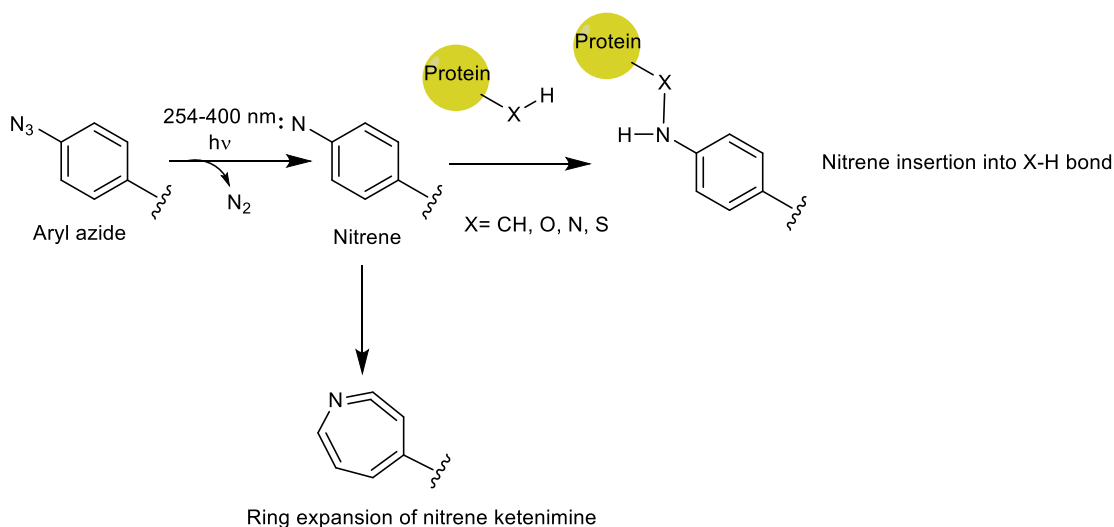


Figure 4. 3: Reactivity of phenyl azides upon photolysis

### 4.1.2.2 Diazirines

Similar to aryl azides, diazirines form highly reactive carbene intermediates upon photolysis at λ 350 nm (Figure 4.4). The carbene can insert into different bonds, such as C-H, O-H, N-H, and S-H bonds of adjacent proteins.[151,152] The formed carbene has the advantage of smaller size compared with the nitrene formed from aryl azides. The smaller size of carbene is more compatible with biomolecules. Unfortunately, carbenes suffer from the same nonspecific crosslinking as nitrenes.
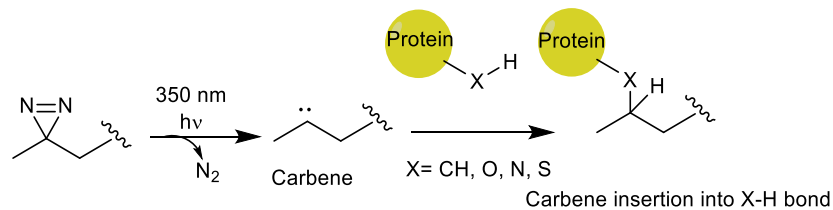


Figure 4. 4: Reactivity of diazirene upon photolysis

### 4.1.2.3  Benzophenones

Benzophenones differ from azides and diazirenes by forming a diradical species upon photolysis at λ 350-360 nm (Figure 4.5). The diradical species can insert into different functional groups, as in case of azides or diazirenes. Unlike azides and diazirenes, benzophenones can relax to its original state if not inserted into another functional group (Figure 4.5).[153] Benzophenones have many disadvantages, such as its bulky size, its preference to methionine,[154] and requirement of long irradiation time [155] when compared to azides and diazirenes.
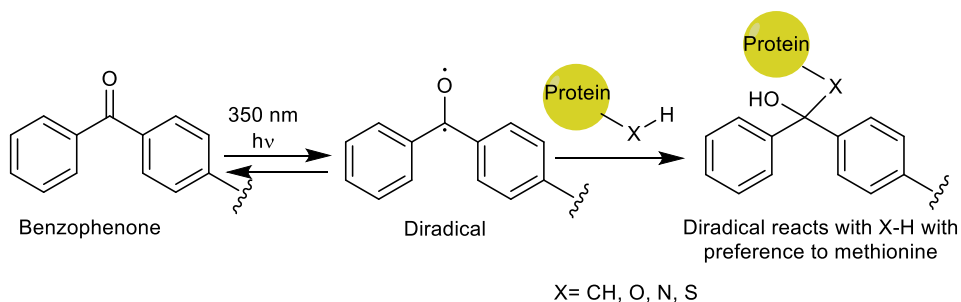


**Figure 4. 5:** Reactivity of benzophenone upon photolysis

The Pflum lab has used modified ATP analogs with photo-crosslinkers on the γ-phosphate for kinase-catalyzed substrate identification. A summary of kinase-substrate pairs identification methods are discussed later together with Pflum lab method. Also, the synthesis and applications of novel affinity based ATP analog crosslinkers are introduced later in this chapter.

### 4.1.3  Current methods for identification of kinase-substrate pairs

With increasing research reporting the involvement of kinases in several diseases, development of novel methods to identify kinase-substrate pairs is important to decipher molecular details of cell signaling. Depending on the crystal structures and the mechanisms of many kinases, many research groups have introduced various

techniques to identify kinase-substrate pairs. The techniques include *in vitro* phosphorylation, pull down assays, yeast two-hybrid systems, and chemical approaches, such as mechanism based crosslinkers and bifunctional photocrosslinkers. However, it is still challenging to determine kinase activities and its effectors in cell signaling pathways. Therefore, development of novel methods to identify kinase-substrate pairs in a kinase-catalyzed phosphorylation manner will allow a better deciphering of cell signaling events. In the next section, several existing kinase-substrate identification methods are discussed. Kinase-substrate identification methods fall in four main categories: *in vitro* phosphorylation, physical association, genetic approach, and chemical approach.

### 4.1.3.1  In vitro phosphorylation

### 4.1.3.1.1  ($\gamma$-$^{32}$P) ATP

In vitro phosphorylation is the most commonly used method to confirm kinase-substrates. In early studies, radiolabeled ($\gamma$-$^{32}$P) ATP was incubated with a particular kinase and substrate or cell lysates. The reaction mixture was then analyzed by SDS-PAGE gel analysis.[156] Later on, this technique was coupled to mass spectrometry to detect both kinase-substrates and phosphosites by quantifying the difference between ($\gamma$-$^{32}$P) ATP treated and untreated lysates.

### 4.1.3.1.2  As-kinase and kinase-substrate identification

Shokat and his coworkers introduced the analog sensitive kinase (as-kinase) technique in late nineties to discover novel kinase substrates.[60] In the as-kinase technique, a particular kinase was mutated in the ATP binding pocket at an certain amino acid called gate keeper to accommodate a bulkier N6-modified ATP to

phosphorylate protein substrates (Figure 4.6).[157] The gate keeper mutation should follow certain criteria. First, the mutation at the ATP binding pocket should allow the kinase to accept the bulky ATP analog. Second, the mutation should not affect the activity of kinases. Lastly, it should preserve protein substrate specificity for the mutated kinase. Also, the bulky ATP analog should act as a cosubstrate to mutated kinase only, not the wild type.[157]



R= -OCH$_3$, -OCH$_2$CH$_3$, -COCH$_3$,- OCH ((CH$_3$)$_2$), -CH$_2$Ph, -OCH$_2$Ph
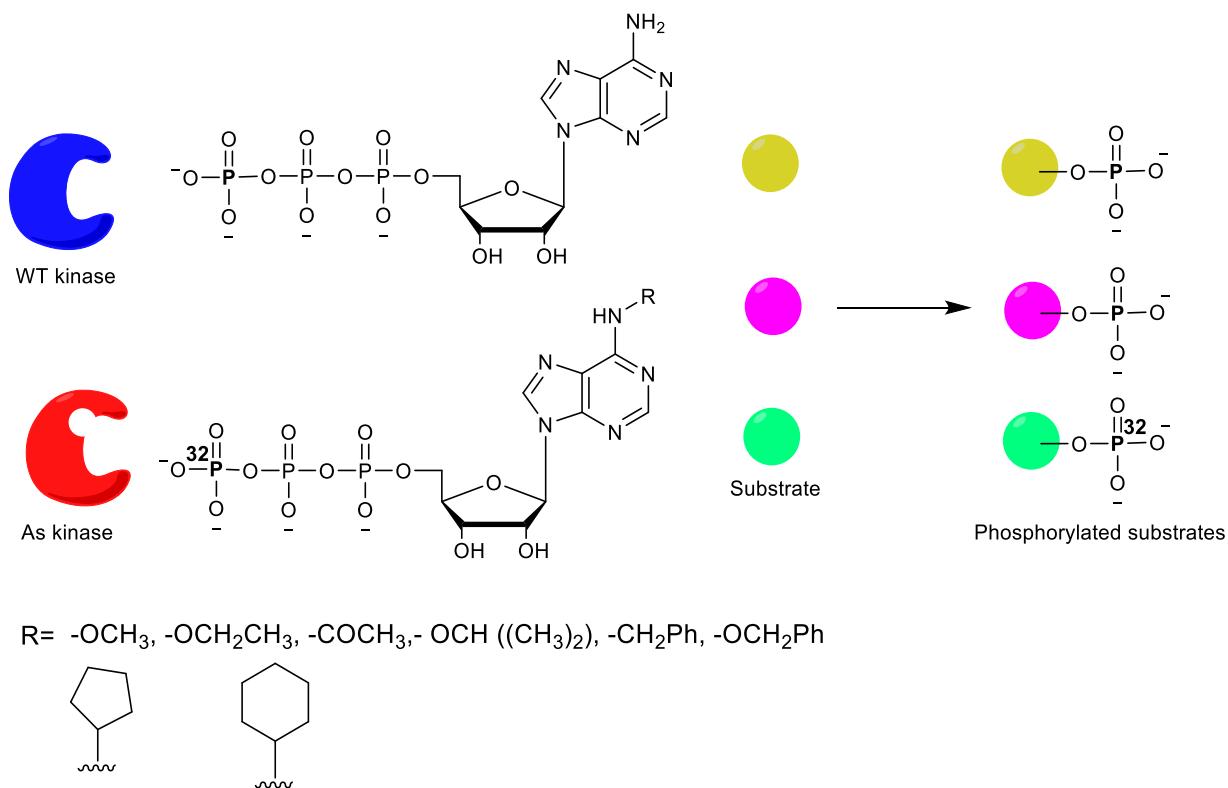
**Figure 4. 6: Schematic diagram of phosphorylation using as-kinases.** N6-modified ($\gamma-^{32}$P) ATP analog was incubated with as-kinase and cell lysates. The as-kinase accepts the N6-modified ($\gamma-^{32}$P) ATP analog and phosphorylate its substrates, while wild (WT) kinases will not accept the N6-($\gamma-^{32}$P) ATP analog and only accept normal ATP. Radiolabeled proteins can be separated by SDS-PAGE analysis and they constitutes the substrates for the as-kinase only.[60]

In the as-kinase technique, the mutated kinase was incubated with cell lystates and ($\gamma-^{32}$P) N-6-modified-ATP. The modified ATP was accepted by the as-kinase and phosphorylation of its substrates was detected by autoradiography (Figure 4.6). In case

of tyrosine kinases, non-radioactive N-6-modified-ATP were used and the phosphorylation was detected by phosphotyrosine antibody.[158] Also, N-6-modified-ATP $\gamma$-S was used to identify kinase-substrates. The $\gamma$-S group can facilitate purification of phosphorylated substrates using iodoacetyl resin resulting in easier less tedious method (Figure 4.7).[67,68] The as-kinase technique was used to identify substrates for several kinases such as v-Src, cSrc, ERK2, Cdk1-cyclinB, Cdk7, etc.[159-164]
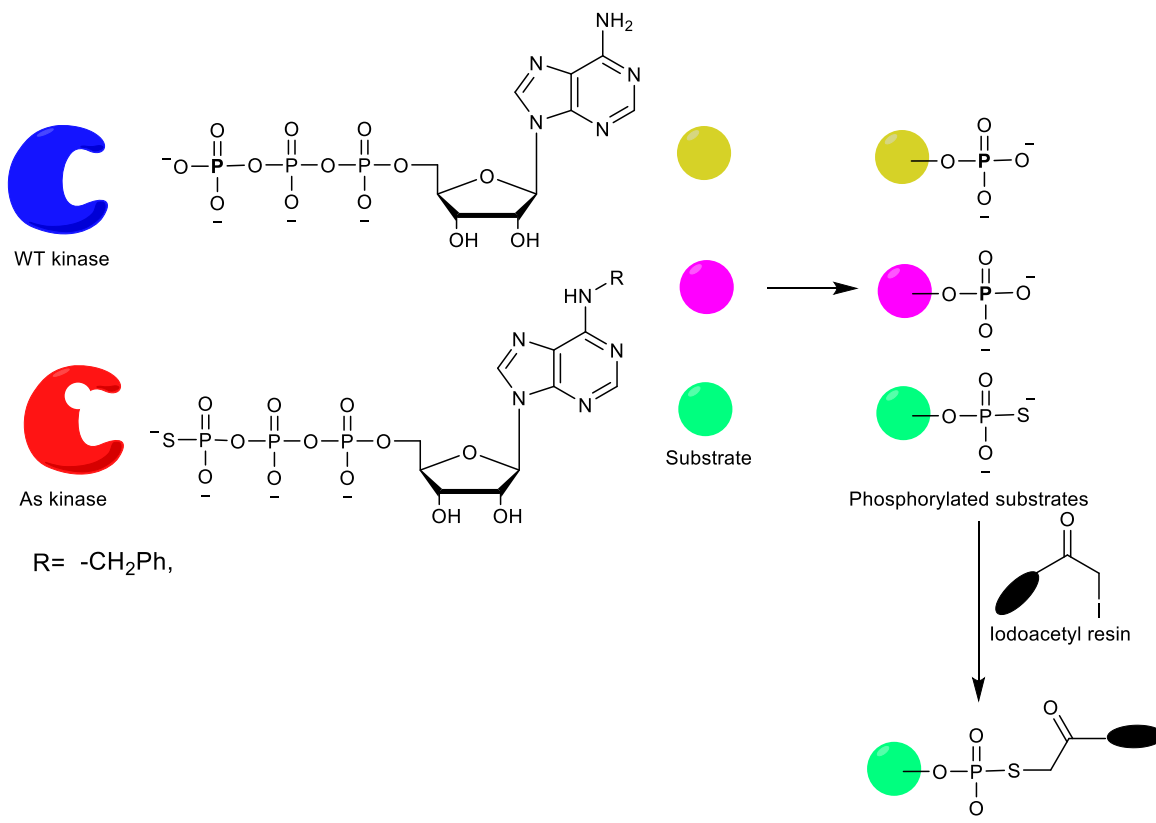


**Figure 4.7: Schematic diagram of phosphorylation using as-kinases and** N6-modified ATP $\gamma$-S**.** N6-modified ATP $\gamma$-S was incubated with the as-kinase and cell lysate. The as-kinase accepts the ATP analog and thiophosphorylates its substrates, while wild (WT) kinases will accept only normal ATP. Thiophosphorylated substrates can be purified by thio-capture reagent such as iodoacetyl resins and they represent as-kinase substrates only without interference from other kinases.

### 4.1.3.1.3  Yeast two hydrid (Y2H)

Y2H is a technique used mainly to detect protein-protein interaction.[165] A protein containing the active site of a kinase is fused to the DNA-binding domain of a

transcription factor, such as bacteria LexA is constructed. On the other hand, a group of substrates to an activation domain are assembled. Upon co-expression of the two fusion proteins, the binding of the kinase to its substrate activates the DNA-binding domain, which lead to formation of a signal, such as production of galactosidase or change in color (Figure 4.8). Y2H technique can be used with cells in the native conformation of kinase-substrate interaction. Many substrates were identified for several proteins using Y2H such as PKC.[166-168] Y2H suffers from few disadvantages such as over expression of proteins and abnormal protein activities, which limits its usage in kinase substrate pair identification.
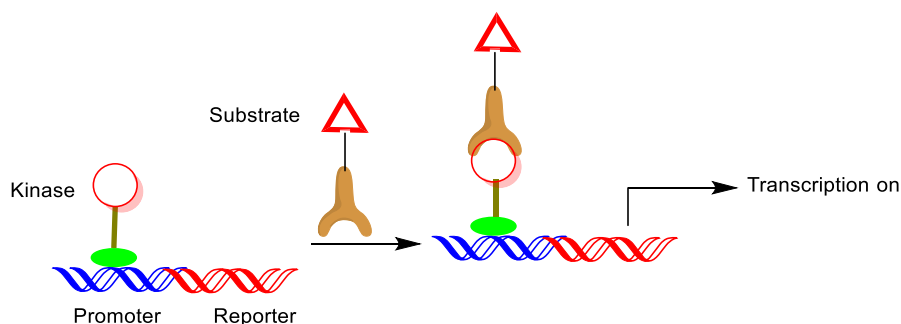


**Figure 4.8: Schematic diagram of yeast two hybrid assay.** DNA binding domain of a transcription factor is fused to the catalytic subunit of certain kinase. On the other hand, an engineered activation domain is fused to kinase-substrate. Upon binding of the kinase to its substrate, the two domains interacts with each other and expression is turned on resulting in a signal, which can be change in color or production of galactosidase, etc.[165]

### 4.1.3.1.4 Chemical genetic crosslinking of kinase-substrate pairs.

Since kinase-substrate interaction is transient, a chemical method involved a kinase-substrate crosslinking via a covalent bond have been used. The crosslinking of kinase to its substrate lead to higher molecular weight complex that can be detected by SDS-PAGE, western blotting, or mass spectrometry (Section 4.1.1). A summary of

several chemical genetic kinase-substrate crosslinking approaches is discussed in the following section.

## 4.1.3.1.4.1   Mechanism based crosslinking approach

Shokat and his coworkers have reported a mechanism based approach to crosslink of kinases to their substrates.[169] They used adenosine attached to o-phthaldialdehyde through 5'-hydroxyl group (Figure 4.9A). Upon binding of the adenosine moiety to the ATP binding site of kinase, the nearby lysine residue in the active site reacts with the aldehyde group of o-phthaldialdehyde resuling into imine group (Figure 4.9A). Cysteine containing kinase-substrates reacts with the imine group via free sulfhydryl group (Figure 4.9B).[169] Many biotinylated peptide substrates and their kinases were used to demonstrate this approach. Due to high reactivity of aldehyde groups, this approach suffers from non-specificity when used with lysates.
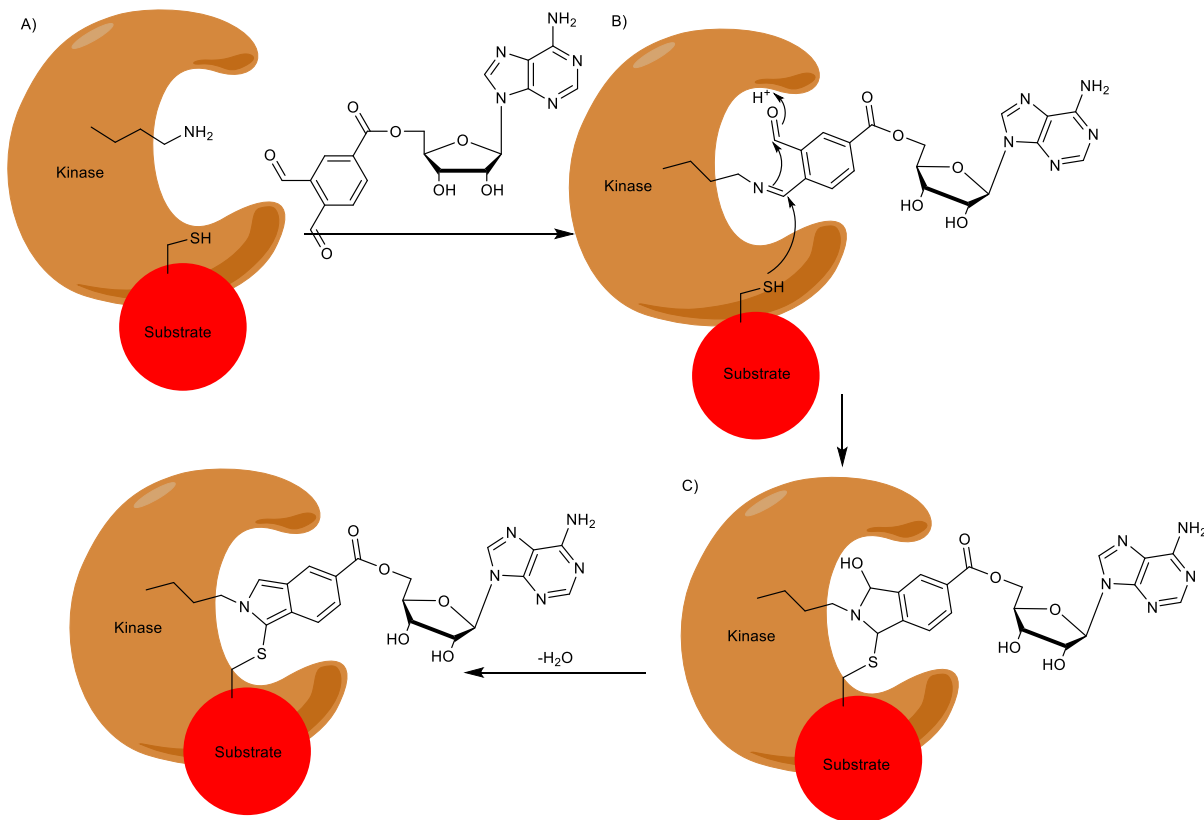
**Figure 4.9: Schematic diagram of mechanism based crosslinking.** Reaction of lysine side chain of kinase with o-phthaldialdehyde and sulfhydryl group on substrate results in crosslinking of the kinase to its substrate.[169]

Second and third generation mechanism-based crosslinkers were developed to reduce the non-specificity associated with the approach (Figure 4.10). In the second generation, the o-phthaldialdehyde group was replaced with a naphthalene-2,3-dialdehyde (NAD) (Figure 4.10A). The second generation of mechanism based crosslinkers were used in presence and absence of lysates with many kinases and fluorophore labeled peptide.[170] In third generation of mechanism based crosslinkers, 3-aminopyrazole, potent kinase inhibitor moiety, replaced the adenosine moiety (Figure 4.10B). Also, the o-phthaldialdehyde was replace by thiophene-2,3-dialdehyde (Figure 4.10C). The third generation crosslinker was able to crosslink Akt1 to fluorophore labeled peptide in lystates with lower non-specificity.[171]
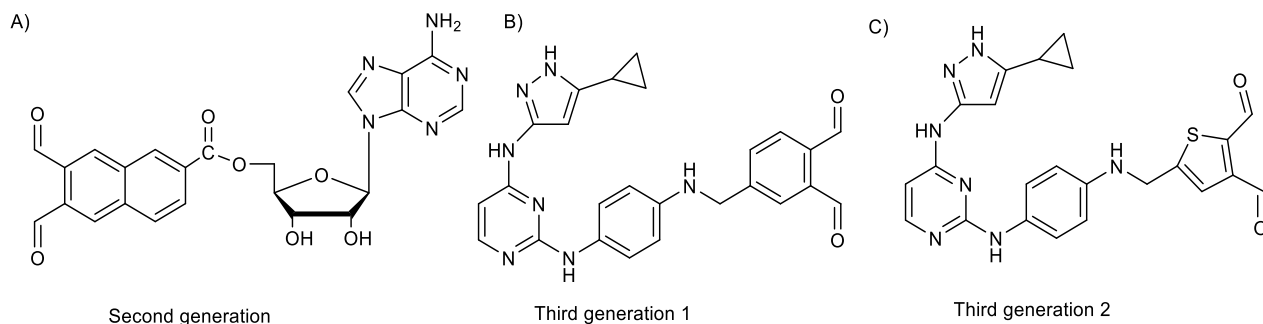


**Figure 4.10:** Structure of the A) second and B) and C) third generation of mechanism-based crosslinkers

A fourth generation of mechanism based crosslinkers were introduced by Shokat and his coworker.[133] An ATP analog with acrylic group attached directly to γ-phosphate was created (Figure 4.11A). This compound binds to kinase through adenosine moiety, followed by the attack of lysine residue of the kinase onto acyl group on γ-phosphate of ATP (Figure 4.11A). The cysteine containing substrate reacts with

the β-carbon of the acrylic group via Michael reaction, resulting in crosslinking of kinase to substrate (Figure 4.11B).[133] The fourth generation of crosslinkers are more specific than former generations when used with lysates. The mechanism-based crosslinking requires a substrate with amino acid mutated to cysteine.[133] However, the fourth generation has not yet further adopted for kinase-substrate pair identification.
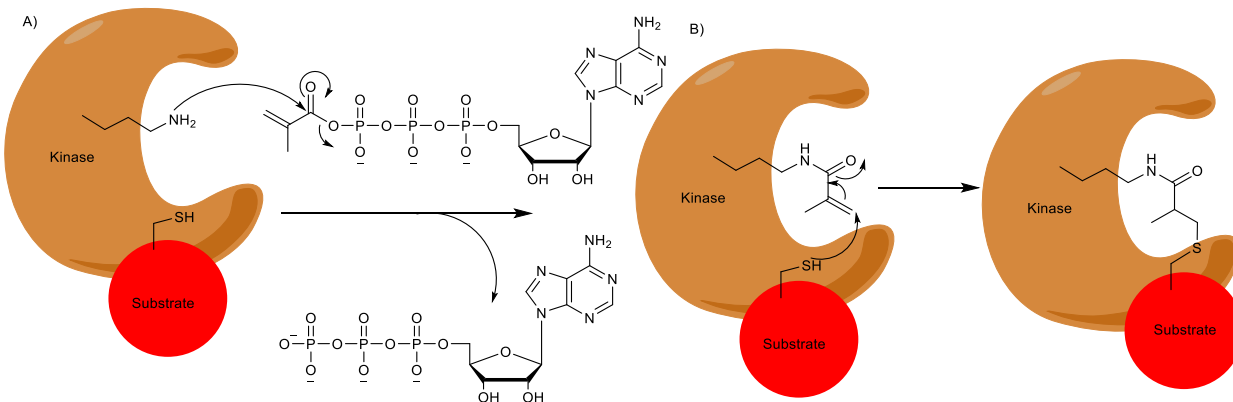


**Figure 4.11: Schematic diagram of the mechanism based crosslinking with fourth generation crosslinkers.** Reaction of lysine side chain of kinase with acyl group, followed by Michael reaction of sulfhydryl group on substrate resulting in crosslinking of the kinase to its substrate.[133]

### 4.1.3.1.4.2  Bifunctional crosslinker ATP analog

An ATP analog with azide photocrosslinkers on both the adenine moiety and gamma phosphate was introduced (Figure 4.12).[112] Upon photoactivation, the azide on the adenine ring can crosslink with the kinase, while the azide on the gamma phosphate can crosslink with substrate (Figure 4.12).[112] This bifunctional crosslinker was used to crosslink Src kinase to Csk substrate. However, no further application has been reported beyond Src and Csk examples.
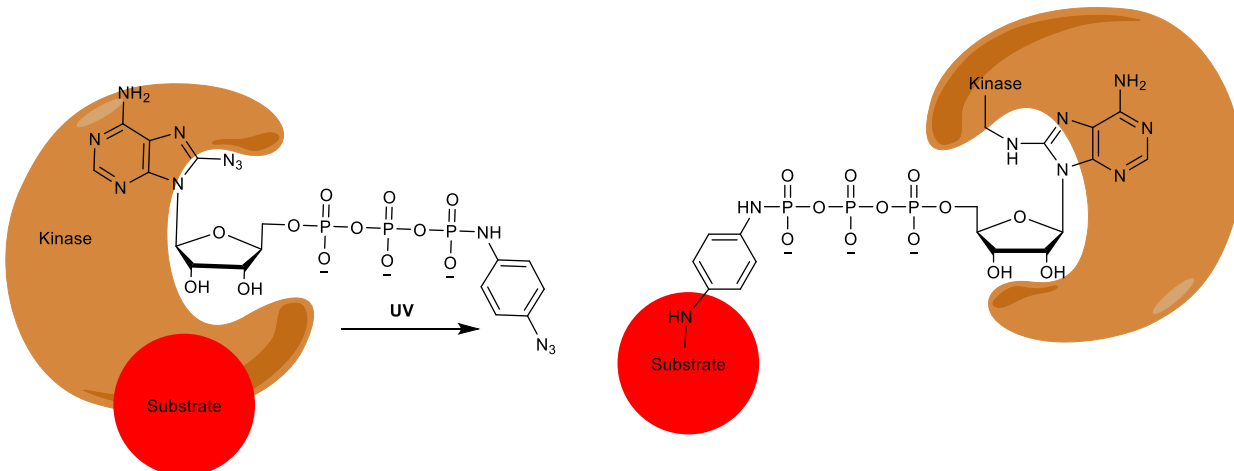
**Figure 4.12:** Schematic diagram of kinase-substrate crosslinking using bifunctional photo-crosslinking ATP analog[112]

### 4.1.3.1.4.3   Phosphorylation dependent kinase-catalyzed crosslinking

The kinase cosubstrate promiscuity introduced by Pflum lab (chapter 1) was developed into a kinase-substrate crosslinking tool. ATP analogs with $\gamma$-photocrosslinkers were utilized as a phosphorylation-dependent crosslinkers of protein kinases with their substrates in presence of UV light.[83,97] Examples of the photocrosslinking ATP analogs are ATP-ArN$_3$ and ATP-BP (Figure 4.13).[83,97] Incubation of the photocrosslinking ATP analog with protein substrate and kinase leads to phosphorylation of their substrates. Simultaneously, UV radiation activates the photocrosslinking group to crosslink with the kinase (Figure 4.13). SDS-PAGE or western-blotting analysis of the reaction mixture shows the presence of a higher molecular weight band corresponding to the kinase-substrate crosslinked complex. Photocrosslinking of kinases to their substrates can provide a tool to discover either new kinases or kinase-substrate pairs in their native environment without any modification.
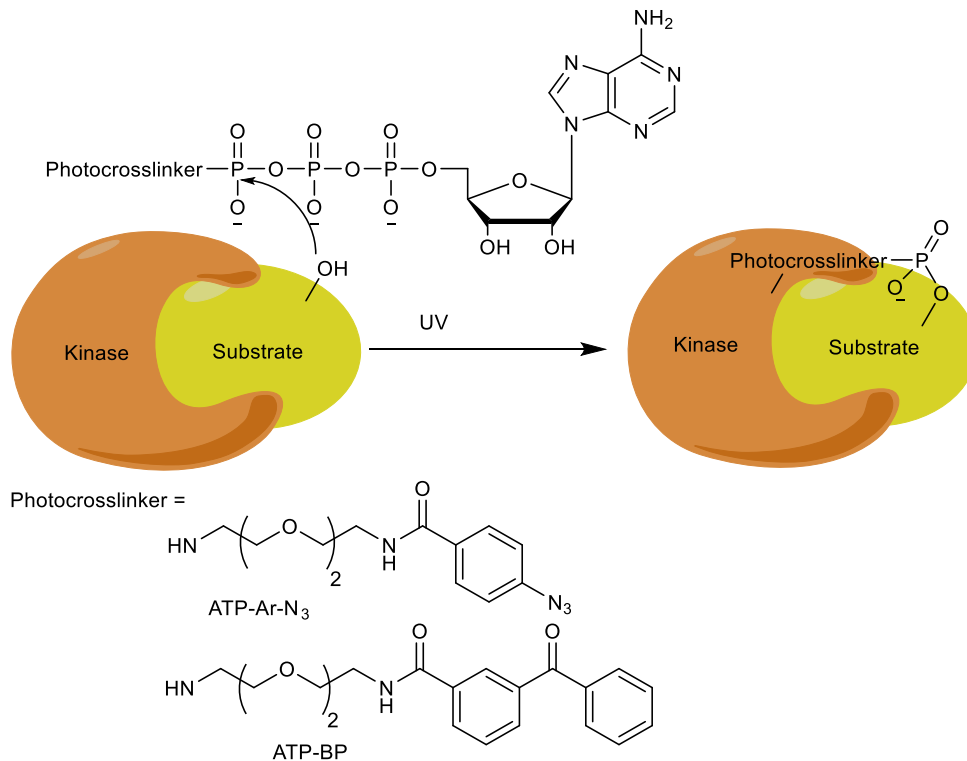
**Figure 4.13:** A) Schematic diagram of phosphorylation-dependent kinase-substrate crosslinking. B) Structure of the photocrosslinking ATP analogs developed by the Pflum lab. ATP-Ar-N3 (ATP-aryl-azide) and ATP-BP (ATP-benzophenone).[83,97]

One limitation for phosphorylation-dependent photo-crosslinking method is that the photo-crosslinking exhibits non-specificity due to the conversion of the photo-crosslinker to very reactive species (as discussed in section 4.2), which can crosslink with many proteins in the reaction medium. Therefore, developing phosphorylation-dependent affinity based crosslinking ATP analog that can crosslink specifically to only amino acids in close proximity will be a valuable addition.

## 4.2 Development of phosphorylation-dependent affinity based crosslinking ATP analog

With over 500 protein kinases, developing a more specific tool to study certain kinases would provide a valuable contribution to study cell signaling. Genome sequencing reveled that about 200 kinases have cysteine residues within or near the

ATP binding pocket, which can be classified into 5 groups (Figure 4.14).[172] Group one involves kinases with cysteines in the glycine rich loop or P-loop, such as Src. Group two contain kinases with cysteines located on the roof of the ATP-binding pocket, such as PLK1. Group 3 includes kinases with cysteines located in the hinge region and front pocket such as EGFR. Group 4 comprises kinases with cysteines adjacent to DFG-motif, such as ERK1. Lastly, group 5 contains kinases with cysteine residues positioned in the activation loop, such as AKT1.[172]

Considering that some kinases contain cysteines, we developed ATP-analogs that can specifically crosslink cysteine-containing kinases to their substrates to identify kinase-substrate pairs. Here, we created an ATP analogs with an acrylamide crosslinking group (ATP-acrylamides) (Figure 4.15) that can act as kinase cosubstrate. ATP-acrylamides can phosphorylate kinase substrates and react simultaneously with the cysteine residues in close proximity, resulting in crosslinking of kinase enzyme to its substrate (Figure 4.15). ATP-acrylamides were then used to crosslink Akt1 kinase to its substrates in HEK293 lysates. Crosslinked complexes were analyzed by SDS-PAGE and western blotting, followed by tandem MS/MS proteomic analysis. Several known Akt1 substrates and physical interactors are identified. Interestingly, other proteins may comprise candidate Akt1 substrates.
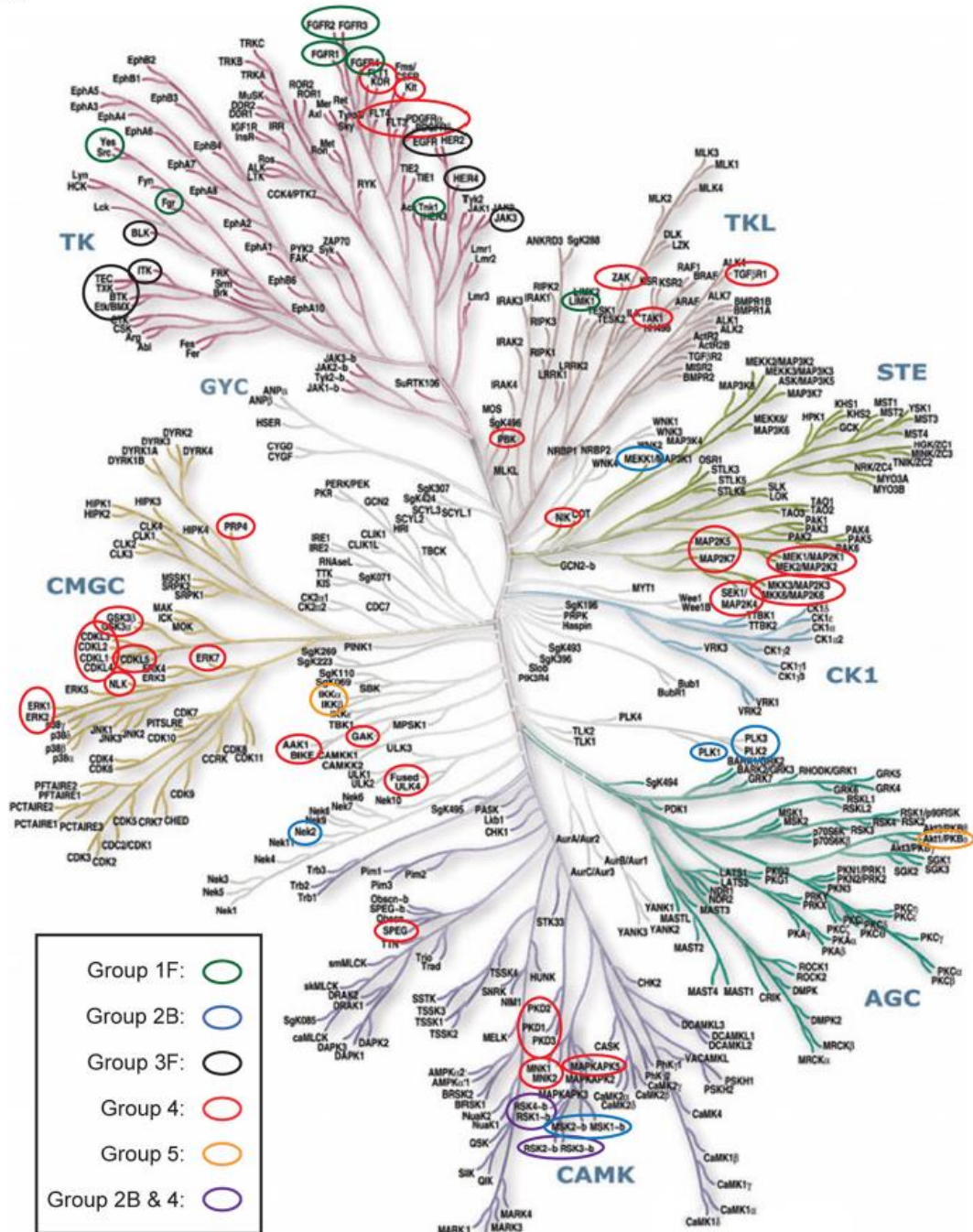
**Figure 4.14:** Classification of human protein kinases family.[12]  Protein kinases fall into 8 classes (CMGC, GYC, TK, TKL, STE, CL1, AGC, CAMK). Each class contains kinases with cysteine residues within or near kinase active site. Kinase containing cysteines fall into five classes and each class is assigned with different colour. Group 1B (green), Group 2B (blue), Group 3F (black), Group 4 (red), and Group 5 (orange). Some kinases have cysteines from both group 2B and 4, which are assigned in purple.[172]

### 4.2.1 Results

Here, we synthesized two analogs with different linkers between ATP and the acrylamide group; ATP-HEX-Acr **11** and ATP-PEG-Acr **12**. These two compounds have an acrylamide, which can react with cysteine-containing kinases (Figure 4.15). The two linkers were chosen to examine the adequate length needed to position the acrylamide group near the cysteine residues of the kinase. ATP-HEX-Acr **11** has 8 atoms linker to crosslink nearby cysteines, while ATP-PEG-Acr **12** has 15 atoms linker to crosslink far cysteines and provides flexibility for the molecule to bind to ATP binding site and simultaneously crosslink to cysteines.
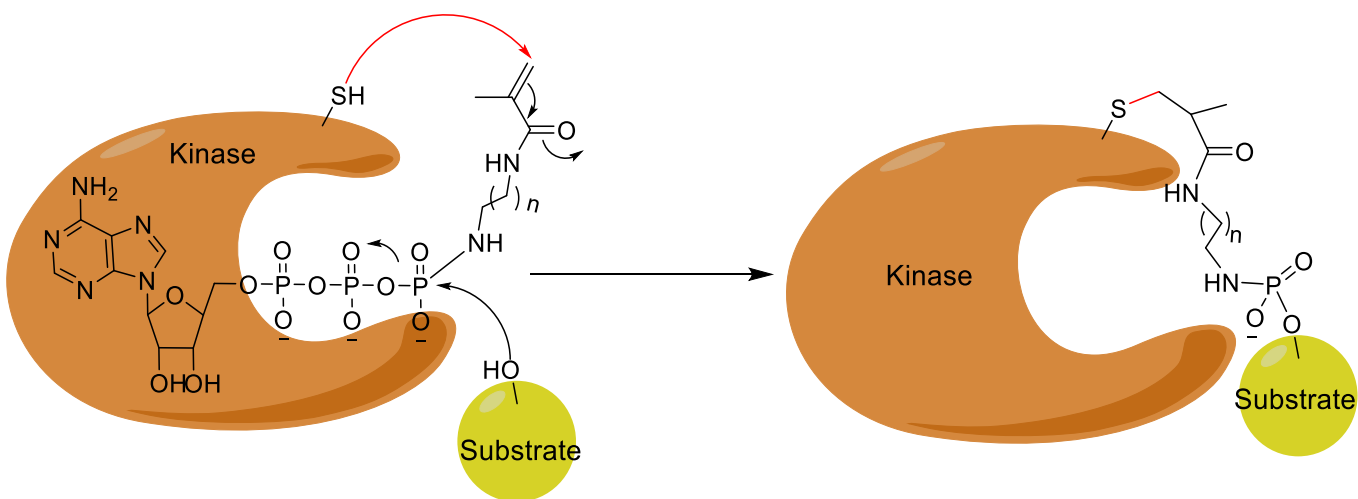


**Figure 4.15:** Schematic diagram of cross linking of kinase with protein substrate using ATP-acrylamide based crosslinker.

### 4.2.2 Synthesis of ATP-acrylamides (11 and 12)

Compound **11** and **12** were synthesized by reacting their corresponding amine (**14** and **16** respectively) with methacrylic anhydride (**13**) (Scheme 4.1 A and B) to yield **15** and **17** in 96 and 90% yield, respectively. Compound **15** and **17** were coupled with

ATP under pH controlled condition to yield compound **11** and **12** in 41 and 34%,

respectively (Scheme 4.1 A and B).

**Scheme 4. 1:** A) Synthesis of ATP-Hex-Acry (**11**). B) Synthesis of ATP-PEG-Acry (**12**). C) Synthesis of thiol containing fluorophore (**17**).
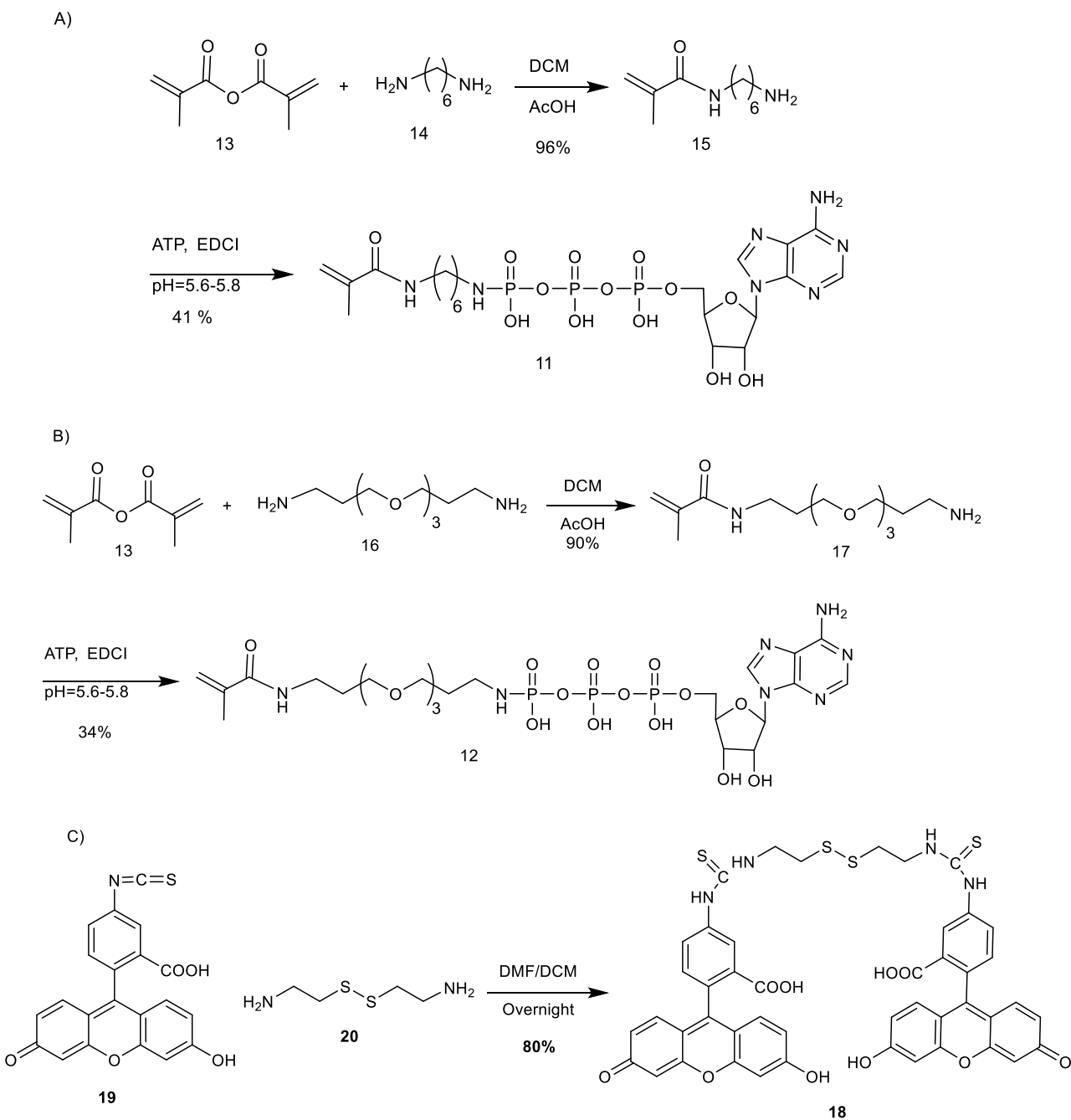
### 4.2.3 Detection of phosphorylation of mylein basic protein (MPB) with PKA and ATP-acrylamides using mercapto containing fluorophore (18)

In order to test the reactivity of the ATP-acrylamides (**11** and **12**) as crosslinkers of cysteines through Michael reaction, we designed a model assay to simulate the crosslinking conditions. First, we synthesized a disulfide containing fluorophore (**18**) to act as a Michael donor fluorescein isothiocyanate (FITC) (**19**) and cystamine (**20**) (Scheme 4.1C). Second, we incubated **18** with ATP-acrylamides (**11** and **12**), PKA kinase, and MBP protein substrate under reducing conditions (Figure 4.16A and B). The expectation was that PKA would catalyze the phosphoacrylamide transfer from ATP-acrylamides (**11** and **12**) to MBP. Simultaneously, the fluorophore (**18**) would be reduced to a free thiol (**21**) (Figure 4.16 B) that would label the acrylamide group through a Michael reaction, resulting in fluorescence of MBP. As expected, MBP was fluorophore labeled in the presence of PKA and ATP-acrylamides (Figure 4.16 C, lane 4 and 6). Reactions without PKA or in presence of staursporine, a kinase inhibitor, did not show labeling (Figure 4.16 C, lane 3, 5, 7, and 8), which indicates kinase dependency. Also, reactions without ATP-acrylamides (**11** and **12**) did not show any labeling (Figure 4.16 C, lane 2), which suggests that ATP-acrylamides are kinase cosubstrates. In summary, this experiment confirmed that ATP-acrylamides (**11** and **12**) are kinase cosubstrates and can act as a Michael acceptor to cysteine containing proteins.

A)



B)



C)



| | 1 | 2 | 3 | 4 | 5 | 6 | 7 | 8 |
|---|---|---|---|---|---|---|---|---|
| MBP | + | + | + | + | + | + | + | + |
| PKA | + | + | | + | | + | + | + |
| 11 | | | + | + | | | + | |
| 12 | | | | | + | + | | + |
| STSP | | | | | | | + | + |
| 18 | | + | + | + | + | + | + | + |
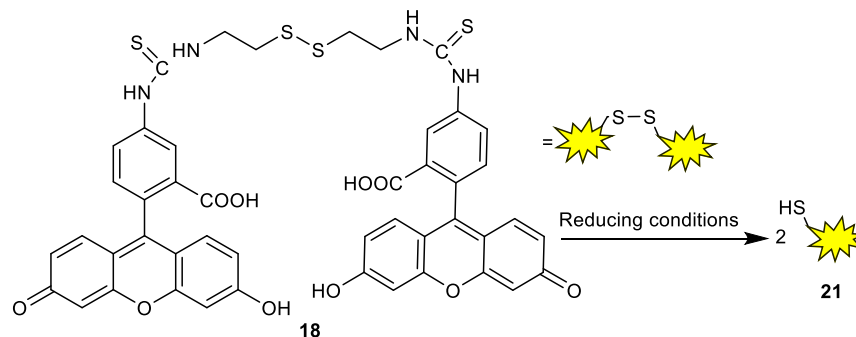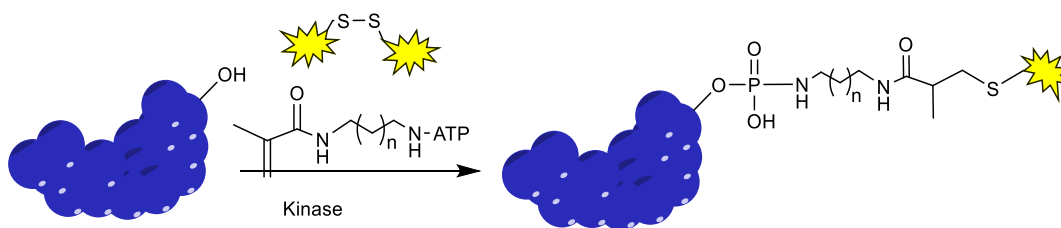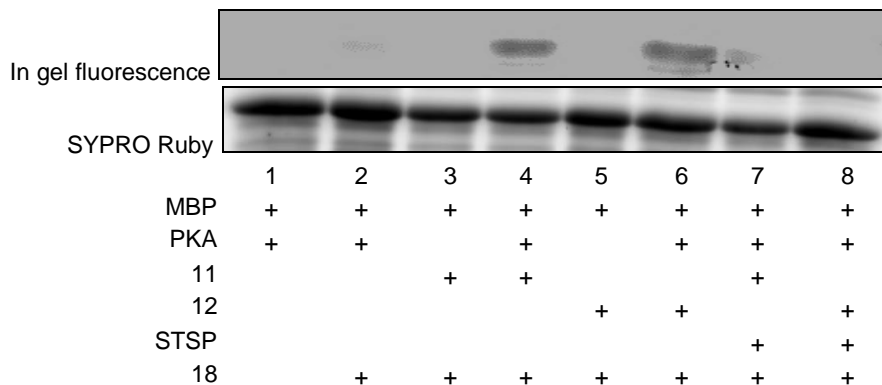
**Figure 4.16:** A) structure of DiFITCI-cystamine (20). B) Kinase-catalyzed labeling of MBP in presence of DIFITC-cystamine **18** and ATP-acrylamides (**11** and **12**). C) Detection of kinase-catalyzed phosphorylation of MPB with PKA and ATP-acrylamides in presence of DiFTC-cystamine (**18**). ATP-Hex-Acr **11** or ATP-PEG-Acr **12** were incubated with MBP, PKA, and DIFITC-cystamine (**18**). The reaction mixtures were separated by SDS-PAGE gel analysis. As a control, the reaction was performed in presence of staurosporine (STSP), kinase inhibitor. Top gel is visualized by typhoon scanning for in gel fluorescence (excitation/emission=495/519 nm) and bottom gel was visualized by SYPRO® Ruby total protein stain. These gel images is representative of at least three independent trials (Figure A4.18)

### 4.2.4 Exploring the efficiency of ATP-acrylamides (11 and 12)

Having confirmed the cosubstrate properties of ATP-acrylamides, we studied the efficiency of such analogs as kinase-cosubstrates by quantifying the extent of phosphorylation. ATP, ATP-Hex-Acr **11**, and ATP-PEG-Acr **12** were incubated with MPB and PKA, followed by cleavage of the acrylamide group with TFA. The reaction mixtures were analyzed by SDS-PAGE separation and staining with phosphoprotein stain ProQ diamond. Phosphorylation was quantified by ImageQuant 5.2 of the ProQ diamond stained gel. Compound **11** showed 60±9% conversion while ATP-PEG-Acr **12** showed 68±9% compared to ATP (100%, Figure 4.17). This data suggests that both analogs have an acceptable similar efficiency but less than ATP.
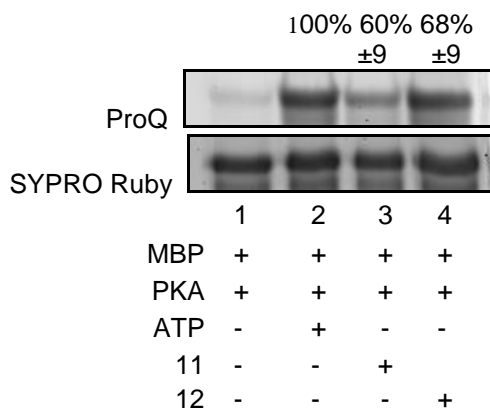


**Figure 4.17:** Quantitative analysis of MPB phosphorylation in the presence of PKA and incubated with either ATP (lane 2), ATP-Hex-Acr (lane 3), or ATP-PEG-Acr (lane 4), then treated with TFA. The reaction mixtures were analyzed by SDS-PAGE analysis, followed by staining with ProQ diamond phosphoprotein stain (top) or SYPRO® Ruby total protein stain (bottom). The mean percentage of phosphorylation of MBP from four trials is shown on the top of the ProQ diamond gel. Full gel images and repetitive trials are shown in figure A4.19

### 4.2.5 Kinase-catalyzed crosslinking of cysteine containing kinases to its substrates using affinity based crosslinking ATP-acrylamides (11 and 12)

Having confirmed the ability of ATP-acrylamides (**11** and **12**) to act as both kinase cosubstrate and Michael acceptor, we moved to the next step by using these

analogs to crosslink cysteine-containing kinases to their substrates. We chose Akt1 as our model kinase. Akt1 has 7 cysteine residues.[172] Of these residues Cys 296 and 310 are within close proximity to ATP-binding pocket (Figure 4.18). Using our ATP-acrylamide analogs **11** and **12** with Akt1 can provide a tool to identify Akt1 substrates by crosslinking the Akt1 through Cys 296 and Cys 310 to their corresponding substrates.

Akt1 has a key role in PI3K/Akt1 pathway, which controls many cell functions, such as cell growth, apoptosis, etc (Chapter 1, section 1.2.3). Also, Akt1 is an interesting target because it is hyperactivated in many types of cancers, such as lung, colon, prostate, skin cancer, etc.[24] For instance, in melanoma formation, Akt1 is overexpressed. Interstingly, 49% of melanomas contain pAkt1 that activates mTORC, which enhances tumor angiogenesis (Chapter 1, section 1.2.3).[24] Therefore, Akt1 is an ideal kinase for this study.

### 4.2.5.1 Docking of ATP-acrylamides into Akt1 kinase crystal structure

To test the compatibility of ATP-acrylamides with Akt1, we docked ATP-acrylamides into the crystal structure of Akt1 using Autodock. Both ATP-acrylamides showed binding to Akt1 similar to ATP with the adenine moiety binding into active site and the $\gamma$-phosphate protruding from the binding pocket (Figure 4.18). ATP-Hex-Acr (**11**) showed a distance of 18.6 and 14.8 Å from Cys 296 and 310, respectively (Figure 4.18), while ATP-PEG-Acr (**12**) showed a distance of 18 and 19 Å from Cys 296 and 310 (Figure 4.18), respectively. ATP-Hex-Acr has a short linker so the acrylamide group may not reach the cysteine residues, while ATP-PEG-Acr has a flexible long linker that may reach the cysteine residues and at same time phosphorylate Akt1

substrates. The docking studies suggests that ATP-acrylamides are kinase-cosubstrates but ATP-PEG-Acr may be a better crosslinker due to its long linker.
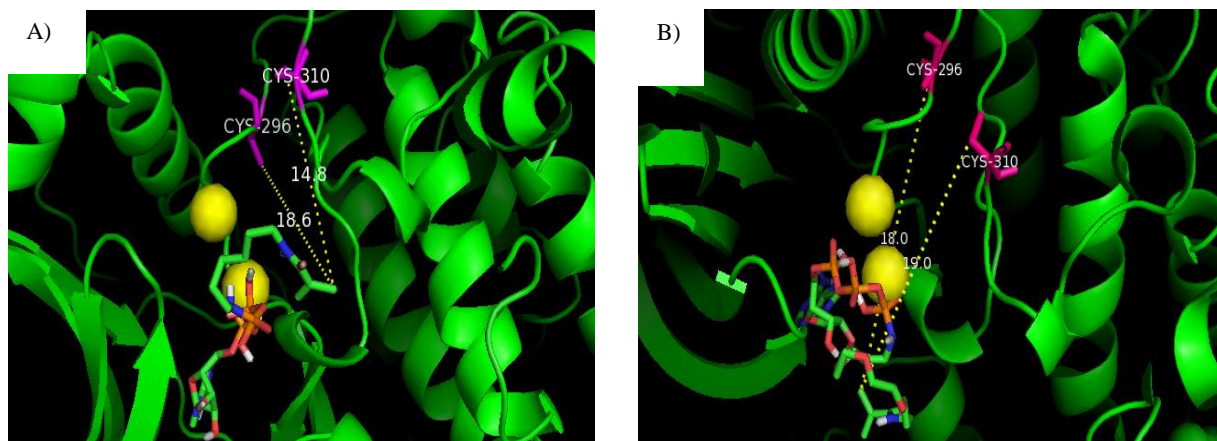


**Figure 4.18:** Crystal structure image of the catalytic active site of AKT1 kinase (pdb: 4EKK) docked with compound **11**(A) and **12** (B). Each atom of the ATP analogs is color-coded (C = green; H grey; N = blue; O = red; p = orange). ATP analogs were docked into the active site of Akt1 using AutoDock 4.2. Cysteine residues (C296 and C310) were shown in magenta red. The generated data was analyzed by both Auto dock tools 1.5.6 and PyMOL 1.5.0.5 (Schrodinger, LLC).

### 4.2.5.2 *In vitro* Akt1 crosslinking to its substrates using ATP-acrylamides

Since docking suggested that ATP-acrylamides can act as cosubstrates to Akt1, we tested the ability of ATP-acrylamides to crosslink Akt1 to its substrate in cell lysates. ATP-acrylamides were incubated with HEK293 cell lysates, followed by SDS-PAGE gel separation, and analysis by Sypro Ruby total protein stain or an Akt1 antibody after transferred to a PVDF membrane. As a control, the experiment was performed either without the ATP-acrylamides or with HEK293 lysates preincubated with staurosporine, a pan kinase inhibitor. Lysates treated with ATP-acrylamides showed high molecular weight complexes (Figure 4.19, lane 4 and 6), which may be due to crosslinking of Akt1 to its substrates. Staurosporine preincubated lysates showed reduced amount of the higher molecular weight complexes (Figure 4.19, lane 3

and 6), which confirm kinase dependence. Interestingly, ATP-PEG-Acr **12** showed a larger amount of higher molecular weight complexes (Figure 4.19, lane 6) when compared to ATP-Hex-Acr **11** (Figure 4.19, lane 4). The difference suggests that ATP-acrylamide **12** may be a more efficient crosslinker due to its longer linker that can reach cysteine residues of AKT1.
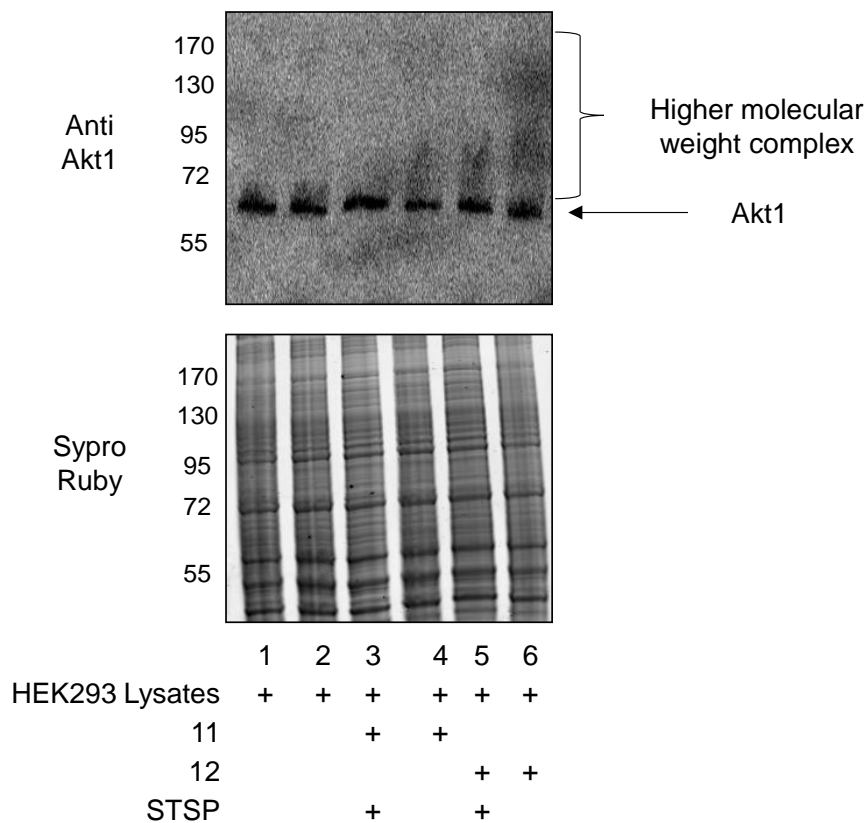


**Figure 4.19:** Kinase-catalyzed crosslinking of AKT with its substrates in HEK293 lysates using ATP-acrylamides (**11 and 12**). HEK293 lysates were incubated with ATP-acrylamides in presence of TCEP (tris(2-carboxyethyl)phosphine). TCEP was used to form necessary reducing conditions for cysteine reaction. As a control, the reaction was performed in presence of staurosporine (STSP), a kinase inhibitor. The reaction mixtures were separated by SDS-PAGE and transfered onto PVDF membrane as a western blotting. Top gel is visualized by treating with anti-AKT1 antibody followed by secondary HRP, while the bottom gel was visualized by SYPRO Ruby. These gel images is representative of at least three independent trials (Figure A4.20).

### 4.2.5.3 Akt1 substrate identification with ATP-acrylamides using K-CLIP (Kinase-CrossLinking and ImmunoPrecipitation)

With evidence that ATP-acrylamides can crosslink Akt1 to its substrates, we moved forward by evaluating and identifying the Akt1 crosslinked complexes. We developed an assay called Kinase-CrossLinking and ImmunoPrecipitation or K-CLIP, where crosslinking is coupled to immunoprecipitation (Figure 4.20 A). ATP-acrylamides (**11** and **12**) were incubated with HEK293 lysates, followed by immunoprecipitation of Akt1, SDS-PAGE gel analysis, and western blotting (Figure 4.20 A). The resulting higher molecular weight bands with **11** and **12** (Figure 4.20 B, lane 3 and 5) were excised from gel, trypsinized, and analyzed by MS/MS proteomics analysis. As a control, lanes from staursporine, a kinase inhibitor, treated lysates (Figure 4.20 B, lane 2 and 4) and untreated lysates (Figure 4.20 B, lane 1) were also analyzed.

A)



B)
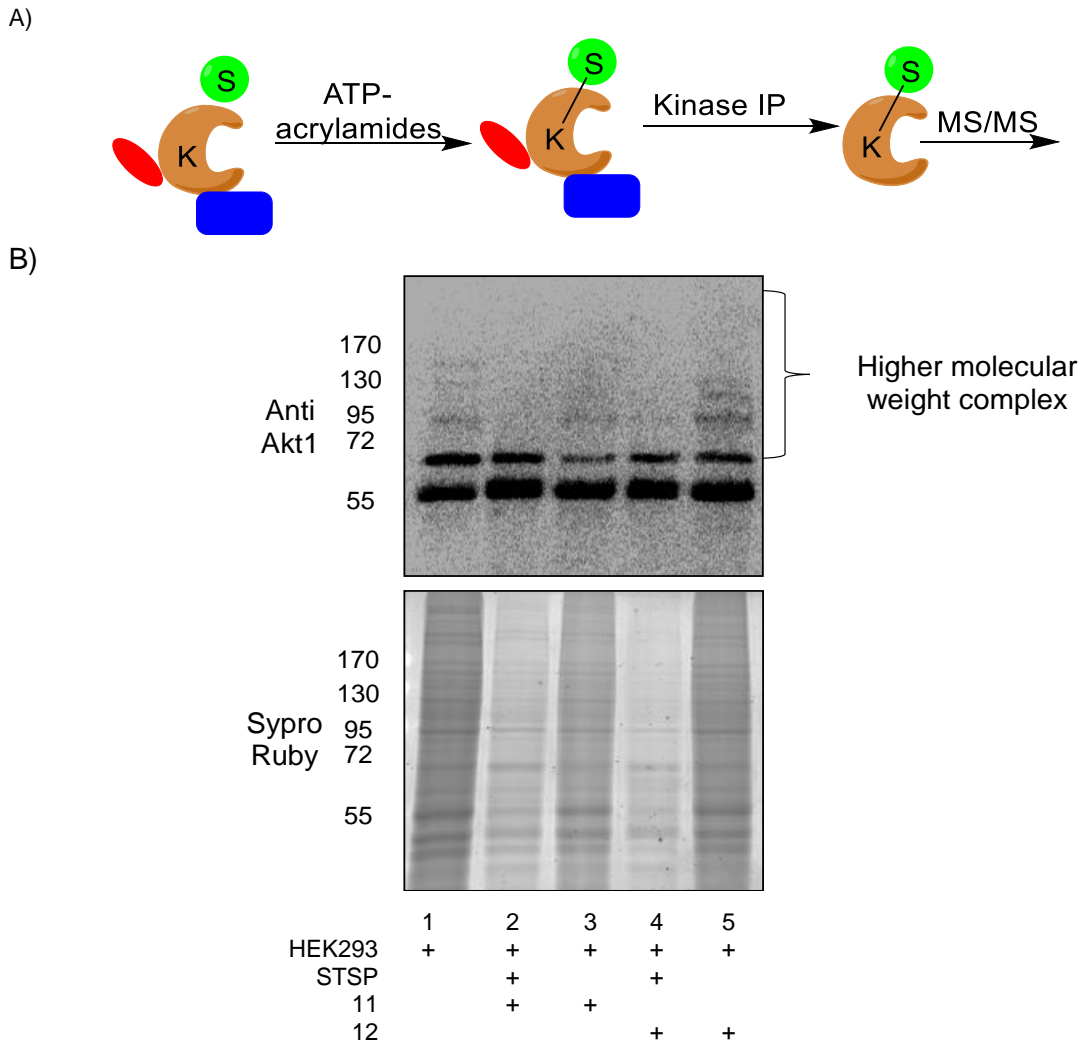


**Figure 4.20:** A) AKT1 substrate identification with ATP-acrylamides using K-CLIP (Kinase-CrossLinking and ImmunoPrecipitation. K=kinase or AKT1 and S=substrates. B) Kinase-catalyzed crosslinking of AKT with its substrates in HEK293 lysates using ATP-acrylamides (**11 and 12**). HEK293 lysates were incubated with ATP-acrylamides followed by immunoprecipitation with anti Akt1 antibody and agarose beads. As a control, the reaction was performed in presence of staurosporine (STSP), kinase inhibitor. The reaction mixtures were separated by SDS-PAGE electrophoresis and transferring onto PVDF membrane as a western blotting. Top gel is visualized by treating with anti-AKT1 antibody followed by secondary HRP, while the bottom gel was visualized by SYPRO Ruby. At least three independent trials were performed (Figure A4.21) but only two trials were used for in gel digestion and further Ms/Ms analysis.

After analyzing the data, the number of unique peptides identified for each

protein in the crosslinked Akt1 with ATP-Hex-Acr **11** (lane 3, Figure 4.20) or ATP-PEG-

Acr **12** (lane 5, Figure 4.20) were divided by number of unique peptides identified from

corresponding staursporine treated HEK293 (lane 3 and 4 respectively, Figure 4.20) or non-crosslinked Akt1 (lane 1, Figure 4.20) to obtain peptide ratio of crosslinking reaction for both analogs. Only proteins with peptide ratio >1 for both untreated and staursporine experiments from two independent trials were considered for further analysis. The peptide ratio analysis revealed 116 proteins enriched from lysates treated with ATP-acrylamide **12** with peptide ratio >1 (Table A4.1), while only 17 proteins were enriched in samples treated with ATP-acrylamide **11** with peptide ratio >1 (Table A4.2). The difference in detected proteins between the 2 samples may be due to the longer linker of ATP-acrylamide **12**, which can led to access of cysteine residue of AKT1. The observed results from proteomic analysis is consistent with both the computational (Figure 4.18) and the gel analysis experiments (Figure 4.19, lane 6 and lane 4).

Since ATP-acrylamide **12** showing more effective crosslinking of Akt1 substrates, we decided to continue our analysis only from compound **12** samples. A deeper analysis of ATP-acrylamide **12** proteomic data reveals that 11 out of the 116 proteins are known interactors or substrates (Table 4.2 and Figure 4.21, inner circle blue color), which confirm the validity of the experiment. Interestingly, we found that many of the detected proteins are physical interactors to the 11 know interactors/substrates (indirect interactors) (Figure 4.21, Outer circles red, green, orange and yellow). The presence of AKT1 indirect interacting protein may be due to their interaction with AKT1 or its substrates when AKT1 signaling is active. In addition, sixty proteins are not known interacting/substrates with AKT1 or its known interactors. The detected proteins that are not AKT1 substrates represents prospective AKT1

substrate candidates or phosphorylation-dependent AKT1 interactors. As a future direction, several proteins will be selected for validation as AKT1 substrates.

**Table 4.2: Proteins identified from crosslinking of Akt1 with ATP-PEG-Acr in HEK293.**

| No | Protein identified | Gene | Accession number | Mol. Wt (kDa) |
|---|---|---|---|---|
| 1. | Stress-70 protein, mitochondrial | HSPA9 | GRP75 | 74 |
| 2. | Vesicle-fusing ATPase | NSF | NSF | 83 |
| 3. | Heat shock protein HSP 90-alpha | HSP90AA1 | HS90A | 85 |
| 4. | Heat shock protein HSP 90-beta | HSP90AB1 | HS90B | 83 |
| 5. | Heat shock cognate 71 kDa protein | HSPA8 | HSP7C | 71 |
| 6. | Creatine kinase B-type | CKB | KCRB | 43 |
| 7. | L-lactate dehydrogenase A chain | LDHA | LDHA | 37 |
| 8. | Transitional endoplasmic reticulum ATPase | VCP | TERA | 89 |
| 9. | Pre-mRNA-processing factor 19 | PRPF19 | PRP19 | 55 |
| 10. | T-complex protein 1 subunit beta | CCT2 | TCPB | 57 |
| 11. | Zyxin | ZYX | ZYX | 61 |

After IP of Akt1 as in figure 4.20, Protein lists obtained from Ms/Ms analysis. Number of unique peptides identified for each protein in the crosslinked Akt1 with ATP-PEG-Acr lane (lane 5, Figure 4.20) were divided by number of unique peptides identified from staursporine treated HEK293 (lane 4, Figure 4.20) or non-crosslinked Akt1 (lane 1, Figure 4.20) to obtain peptide ratio of ATP-PEG-Acr. Only peptide ratio that is more than one and present in two independednt trials is considered to be solely phosphorylation dependent crosslinking and shown in the following table. Proteins from 1-7 are known Akt1 physical interactor (as reported in Biogrid database) and proteins from 8-11 are known Akt1 substrates (as reported in phosphosite database). The rest of proteins can be substrate candidates for Akt1

**Figure 4.21:** Proteomic analysis diagram showing the relation of 50% of AKT1-crosslinked proteins to AKT1. AKT1 is represented in black and direct interacting/substrate proteins are represented in blue (inner circle). Lines represent the presence of interactions between proteins. The analysis were performed by Genemania application in Cytoscape 3.3.0 program. AKT1 substrates and direct interacting proteins were determined by Phosphosite Plus and Biogrid respectively. The diagram was generated by Cytoscape 3.3.0.

## 4.3 Conclusions and future directions

In summary, we developed ATP-acrylamides that act as both kinase cosubstrates and affinity crosslinking ATP-analogs. We used a fluorescence gel analysis assay to show that ATP-acrylamides can act as kinase-cosubstrates and Michael acceptors. Importantly, ATP-acrylamides crosslink selectively cysteine containing kinases and their substrates that was demonstrated via Akt1 kinase. Coupling phosphorylation-dependent crosslinking using ATP-acylamides to immunoprecipitation followed by MS/MS analysis was able to separate and identify Akt1 substrates. ATP-PEG-Acr **12** with a long linker more efficiently crosslinked Akt1 to its substrates compared to ATP-Hex-Acr **11** with short linker. ATP-PEG-Acr **12** crosslinked 116 proteins to Akt1 kinase, while ATP-Hex-Acrylamide **11** crosslinked 17 proteins only. Out of the 116 crosslinked proteins via ATP-PEG-Acr **12**, 11 proteins are known Akt1 interacting proteins or substrates. Interestingly, 44 proteins are indirectly interacting proteins to Akt1. The rest of the proteins can be either Akt1 substrates or interacting proteins. Lastly, coupling ATP-acrylamide crosslinking with immunoprecipitation created a new tool to discover new kinase substrates. In future, several of the crosslinked proteins will be chosen for validation as Akt1 substrates. *In vitro* phosphorylation experiments will represent the key studies to show Akt1 kinase relation to the selected proteins.

Establishing affinity based crosslinking ATP analogs as a phosphorylation-dependent kinase-substrate crosslinking tool will promote cell signaling studies. Also, having a cysteine specific crosslinker as ATP-acrylamides decrease the non-specificity and increase the confidence in the data obtained in the crosslinking. Furthermore,

developing other affinity based crosslinking ATP analogs with different crosslinker will be helpful and may reduce non-specificity with such experiments. In contrast to other kinase-substrate crosslinking approaches, phosphorylation dependent kinase-substrate crosslinking requires the ATP analog to participate in phosphorylation as well as crosslinking. This methodology provides a powerful tool to identify kinases, their substrates, and phosphorylation-dependent interactions in cell signaling pathways when coupled to mass spectrometry.

## 4.4 Experimental

### 4.4.1 Materials

TCEP (tris(2-carboxyethyl)phosphine hydrochloride), iodoacetamide, proteomics grade trypsin, and ammonium bicarbonate were purchased from Sigma Aldrich. ATP was purchased from MP Biomedicals. 1-(3-Dimethylaminopropyl)-3-ethylcarbodiimide hydrochloride (EDCI), and N,N,N',N'-Tetramethylethylenediamine (TEMED) for electrophoresis were purchased from Acros. Methacrylic anhydride, hexane diamine, silica gel, DEAE sephadex A-25, and Ammonium persulfate (APS) for electrophoresis were bought from Fisher Scientific. Dichloromethane (DCM), acetic acid, hydrochloric acid, ammonium hydroxide, and HPLC grade acetonitrile were purchased from EMD. Ethanol was obtained from Decon lab. 40% Bis-acrylamide (37.5:1) for gel electrophoresis and Bradford reagent were purchases from Biorad. Myelin basic protein (MBP) and trypan blue were bought from Invitrogen. DMEM high glucose media was purchased from Gibco. PKA kinase was purchased from New England Biolabs. Antibiotic and Dulbecco's Phosphate Buffered Saline (DPBS) for cell culture were purchased from HyClone. AntiAkt1 and Goat Anti-Rabbit HRP Secondary antibodies were bought from cell signaling. HRP developer was purchased from Enzo life.

### 4.4.2 Instruments

$^1$H NMR, $^{13}$C NMR, $^{31}$P NMR (Varian Mercury-400), and High resolution mass spectra (HRMS) (LCT Premier XT (Waters)) were used to characterize the final ATP analogs. $CD_3OD$, $D_2O$, and trimethylamine chemical shifts are shown in charts in Appendix 4. Absorbance of ATP analogs was measure by UV-Vis spectrophotometer (Shimadzu 2101 PC). A Lyophilizer (VirTis BT 3.3 EL Benchtop) and Speed-vac

(ThermoSAVANT, SPD131 DDA) were used during synthesis of ATP analogs. Bradford assay was done using a fluorimeter (GENios Plus Tecan). SDS-PAGE apparatus were bought from BioRad (Protean III). Protein transfer was performed using the Mini-Transblot Electrophoretic Transfer Cell apparatus from BioRad. SDS gels and PVDF membranes were visualized by a Typhoon 9210 scanner (Amersham Biosciences).

### 4.4.3  Synthesis of ATP-Hex-Acrylamide

### 4.4.3.1 Synthesis of N-(aminohexyl)methacrylamide (15)
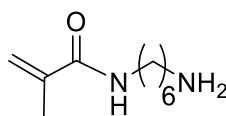


**15**

Hexane diamine **14** (1.25 g, 10.75 mmol) was dissolved in DCM (300 mL) then glacial acetic acid (183 uL) was added. A solution of methacrylic anhydride **13** (0.48 mL, 3.2 mmol) in DCM (50 mL) was added drop wise and stirred at room temperature for 3 hours. The solvent was removed *in vacuo* and the residue was dissolved in saturated solution of sodium carbonate (100 mL) until slightly basic. The aqueous solution was extracted with DCM (100 mL, three times) and the combined organic layer was dried over anhydrous sodium sulfate. The organic solvent was removed *in vacuo* and the residue was purified using silica column with a solvent mixture of *ethanol*: DCM in a 3:1 ratio containing ammonia (1%). Compound **15** was obtained as a white solid (0.56 g, 96%). $^1$HNMR (CD$_3$OD, 400 Hz): δ 1.88-1.92 (4H, m), 2.05-2.11 (4H, m), 2.46 (3H, s), 3.31 (2H, t), 3.76 (2H, t), 5.88 (1H, s), 6.19 (1H, s). $^{13}$CNMR (CD$_3$OD, 100 Hz): 17.39, 25.88, 26.15, 28.86, 29.34, 38.98, 39.96, 118.727, 140.06, 169.83.   ESI MS Calculated $(M+H)^{+1}$ for C$_{10}$H$_{21}$N$_2$O: 185.17; Observed 185.17. Data shown in figure A4.1-A4.3)

**4.4.3.2 Synthesis of ATP-Hex-Acr (11)**



**11**
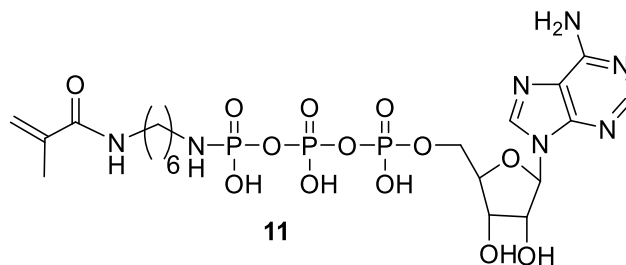
ATP disodium salt (32 mg, 0.059 mmol) was dissolved in water (5 mL) and the pH was adjusted to 7 using NaOH (0.5 M) and a pH meter. EDCI (452.5 mg, 2.36 mmol) was added and the pH was adjusted to 5.6-5.8 using HCl (0.5 M). A solution of N-(aminohexyl)methacrylamide (**15**) (206 mg, 1.12 mmol) in water (2 mL) was added and the pH was readjusted to 5.6-5.8. The solution was stirred for 3 hours with control of pH and monitoring the progress of reaction by TLC (isopropanol:water:ammonia in 3:1.5:0.5 ratio). The solution was brought to pH 8.5 using triethyl amine and the product was separated by anion exchange column (A-25 sephadex) with 0.1-1 M triethyl ammonium carbonate buffer (pH 8.5, section 2.4.6) as eluent. All liquids were lyophilized to dryness and solid compound was stored at -20 $^{\circ}$C. ATP-Hex-Acr **11** was obtained as a white solid (14 mg, 41%). UV/Vis spectroscopy ($H_2O$): $\lambda$ 260 cm$^{-1}$. $^{1}$HNMR (CD$_3$OD, 400 Hz): δ 1.02 (2H, m), 1.14 (6H, m), 1.74 (3H, m), 2.80 (2H, m), 3.38 (2H, q), 4.09 (3H, d), 4.23 (1H,s), 4.59 (1H, s), 5.23 (1H, d), 5.45 (1H, d), 5.987 (1H, d), 8.14 (1H, s), 8.43 (1H, s). $^{13}$CNMR (CD$_3$OD, 100 Hz): 7.11, 17.62, 25.11-25.65 (1C), 26.50, 27.99-28.087 (1C), 39.21-39.46 (1C), 58.56, 65.11, 70.34, 74.28, 84.11, 86.89, 97.22, 120.52, 139.22, 140.36, 148.98, 151.52, 169.58, 198.80. $^{31}$PNMR (D2O): -3.41 (d), -11.32- -11.46 (d), -23.1**3** (t). ESI HRMs, (M-H)$^{-}$ for C$_{20}$H$_{33}$N$_7$O$_{13}$P$_3$: calc. 672.1349, found 672.1316.

### 4.4.4 Synthesis of ATP-PEG-Acrylamide (12)

### 4.4.4.1 N-(3-(2-(2-(3-aminopropoxy)ethoxy)ethoxy)propyl)methacrylamide (17)



**17**
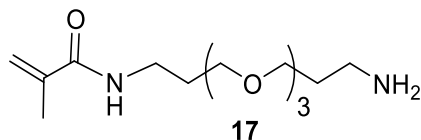
PEG diamine **16** (2.35 mL, 10.75 mmol) was dissolved in DCM (300 mL), followed by addition of acetic acid (183 uL). A solution of methacrylic anhydride **13** (0.48 mL, 3.2 mmol) in DCM (50 mL) was added drop wise and stirred at room temperature for 3 hours. The solvent was removed *in* vacuo and the residue was dissolved in a saturated solution of sodium carbonate (100 mL) until slightly basic. The aqueous solution was extracted by DCM (100mL, three times) and the organic layer was dried over anhydrous sodium sulfate. The organic solvent was removed *in vacuo* and the residue was purified using silica column chromatography with a solvent mixture of ethanol: DCM (3:1) containing ammonia (1%). Compound **17** was obtained as yellow oil (0.83 g, 90%). $^1$HNMR (CD$_3$OD, 400 Hz): δ 1.74-1.81 (4H, m), 1.93 (3H, s), 2.77-2.81 (2H, m), 3.51-3.63 (14H, m), 5.35 (1H, s), 5.69 (1H, s). $^{13}$CNMR (CD$_3$OD, 100 Hz): 17.46, 29.00, 31.04, 36.93, 38.68, 68.80, 68.99, 69.77, 69.86, 70.07, 70.11, 118.95, 139.96, 169.57. ESI pos. mass for $C_{14}H_{29}N_2O_4$ (M+H)$^+$, calc. 289.21, found 289.21.

### 4.4.4.2 Synthesis of ATP-PEG-Acr (12)
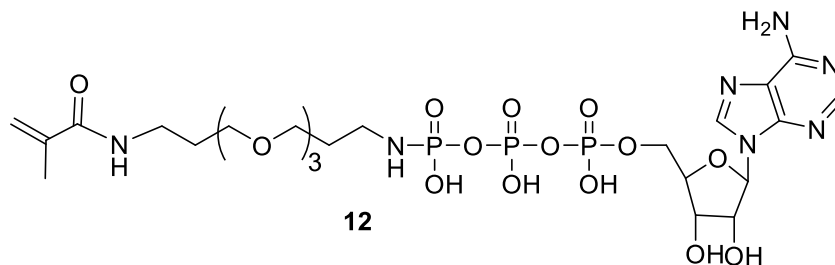


ATP (32 mg, 0.059 mmol) was dissolved in water (5 mL) and then the pH was adjusted to 7 using NaOH (0.5 M) and pH meter. EDCI (453 mg, 2.36 mmol) was added and the pH was adjusted to 5.6-5.8 using aqueous HCl (0.5 M). Compound (**17**) (288 mg, 1mmol) in water (2 mL) was added and the pH was readjusted to 5.6-5.8. The solution was stirred for 3 hours with control of pH and monitoring the progress of reaction by TLC (isopropanol:water:ammonia in 3:1.5:0.5 ratio). The solution was brought to a pH 8.5 using triethyl amine and the product was separated by anion exchange column (A-25 sephadex) with 0.1-1 M triethyl ammonium carbonate buffer (pH 8.5, section 2.4.6) as eluent. All fractions containing product were lyophilized to dryness and solid compound was stored at -80 °C. ATP-PEG-Acr **12** was obtained as a white solid (13.2 mg, 34%). UV/Vis spectroscopy ($H_2O$): $\lambda$ 260 cm$^{-1}$. $^1$HNMR ($D_2O$, 400 Hz): $\delta$ 1.60 (4H, t), 2.08 (2H, m), 2.17 (3H, s), 3.57 (2H, t), 3.87 (13H, m), 4.52 (2H,s), 4.67 (1H, s), 4.87 (1H, s), 5.69 (1H, s), 5.92 (1H, s), 6.41 (1H, d), 8.62 (1H, s), 8.87 (1H, s). $^{13}$CNMR ($D_2O$, 100 Hz): 7.05, 17.57, 26.41, 28.14, 36.63, 37.56, 58.46, 65.07, 68.19, 68.51, 69.23-69.50 (2C), 70.27, 74.39, 84.08, 87.13, 120.72, 139.10 (2C), 140.999 (2C), 148.69 (2C), 171.78. $^{31}$PNMR (D2O): -11.31- -10.91(d), -11.62- -11.49 (d), -23.14 (t). ESI HRMs, (M-H)$^-$ for $C_{24}H_{41}N_7O_{16}P_3$: calc. 776.1823, found 776.1822.

### 4.4.5 Scheme 4: Synthesis of 5,5'-(((((disulfanediylbis(ethane-2,1-diyl))bis(azanediyl))bis(carbonothioyl))bis(azanediyl))bis(2-(6-hydroxy-3-oxo-3H-xanthen-9-yl)benzoic acid)= DiFITC-cystamine (18)



**18**
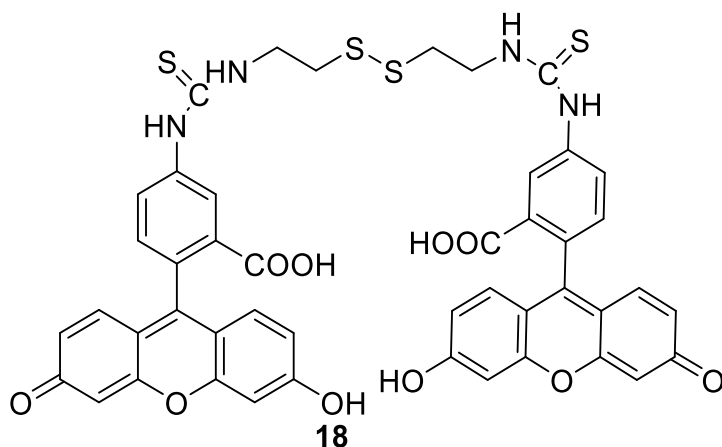
FITC **19** (216.9 mg, 0.56 mmol) and cystamine **20** (54 mg, 0.24 mmol) were dissolved in DMF (15 mL). DIPEA (1.225 mL, 2.04 mM) was added and the solution was stirred overnight at room temperature. DMF was removed *in vacuo* and the residue was purified by silica column chromatography using DCM : Ethanol (1:3) to get compound **18** as red solid (178 mg, 80%). $^1$HNMR (CD$_3$OD, 400 Hz): $\delta$ 3.06 (4H, t), 3.96 (4H, t), 6.49-6.52 (4H, m), 6.64-6.65 (8H, m), 7.12-7.14 (2H, d), 7.72-7.75 (2H, dd), 8.15 (2H, d). $^{13}$CNMR (CD$_3$OD, 100 Hz) $\delta$ 43.11, 62.99, 102.10, 110.08, 112.31, 118.81, 124.45, 127.79, 128.96, 130.58, 140.74, 152.81, 160.16, 169.74, 181.48. ESI HRMs, (M+1)$^+$ for C$_{46}$H$_{35}$N$_4$O$_{10}$S$_4$, calc. 931.1236, found 931.1240.[188]

### 4.4.6 Kinase-catalyzed in gel fluorescence of MBP using ATP-acrylamides and DIFITCI-cystamine

Kinase-catalyzed labeling was performed by incubation of ATP-Hex-Acr or ATP-PEG-Acr analogs (5 mM), PKA enzyme (5µg/mL, 500U), DIFITCI-cystamine (0.1 mM), TCEP (5.5 mg/mL, 22 mM) and myelin basic protein (MBP) (4 µg/ul) in the kinase reaction buffer (10 mM Tris, 1 mM MgCl$_2$, pH 7.5). The final volume for the reaction

was 20 µL. The reaction mixture was incubated at 31°C for 3 hours at 31 °C with shaking (300 rpm), followed by incubation with iodoacetamide (15 mM, 2.8 mg/mL in 0.13 M Tris buffer, pH=6.8) for 30 min at room temperature in dark to alkylate unreacted FITCI-cystamine. Acetone (80 µL) was added to reaction mixtures and incubated at -20 °C for 1 hour, followed by centrifugation at 13000 rpm for 10 min. The supernatant was removed and the residue was dissolved in Tris buffer (20 µL, 1M, pH=6.8), followed by precipitation by acetone (80 µL) and reincubation at -20°C for 1 hour. The mixture were centrifuged at 13000 rpm for 10 minutes and the residue were dissolved in Tris buffer (10 µL, 1.5 M, pH=8.8). Reactions without MBP, PKA and/or ATP-Hex-acrylamide or ATP-PEG-acrylamide analogs were conducted as control experiments. Also, as a control, the reaction was run with PKA preincubated for 30 min with staursporine (1µM). The precipitated products were separated by SDS-PAGE (16% of acrylamide:Bis-acrylamide solution (37.5:1)) and gel image was produced by scanning the gel with Typhoon at $\lambda$ 624, nm then visualized by SYPRO®Ruby (Figure 4.16 and A4.18).

### 4.4.7  *In vitro* quantification of ATP-acrylamides with PKA

ATP, ATP-Hex-Acr or ATP-PEG-Acr (5 mM) were incubated with PKA enzyme (500U) and myelin basic protein (MBP) (1 µg/ml) in the buffer provided by the company (1X). The final volume of the reaction was 20 µl. The reaction mixtures were incubated at 31°C for 2 hours. TFA (50% final conc.) was added and incubated for 1 hour at 45 °C with shaking at 700 rpm. TFA was evaporated using speed vac, followed by neutralization of the remaining TFA. The reaction mixtures were separated by SDS-PAGE (16%) gel electrophoresis and visualized by SYPRO Ruby or Pro-Q diamond

stain. Quantification of phosphorylation of MBP was done by ImageQuant 5.2 on the gel stained by Pro-Q diamond stain by drawing a same-sized rectangle on MBP. MBP phosphorylation by ATP, ATP-Hex-Acr, and ATP-PEG-Acr was background corrected by subtracting the signal after kinase reaction to the signal of untreated MBP. The percentage of phosphorylation by ATP-Hex-Acr and ATP-PEG-Acr was calculated by dividing the signal for ATP-Hex-Acr and ATP-PEG-Acr reactions to the signal with ATP (100% phosphorylation) and multiplying by 100 (Figure 4.17 and A4.19).

### 4.4.8  Docking of ATP-HEX-Acrylamide and ATP-PEG-Acrylamide

The crystal structure of Akt1 was downloaded from RCSB Protein Data Bank (pdb ID: 4EKK). Pymol 1.5.0.5 (Schrodinger, LLC) was used to delete the co-crystalized ligand and water. AutoDock Tools 1.5.6 was used to add all hydrogen atoms, Gasteiger charges and merging non polar hydrogen, followed by generation of pdbqt output file. The charge of Mn was changed from zero to +2 manually. A grid box with a spacing of 0.375 Å, size (90, 90, 60), and coordinates for the center of the grid box (63.202, 2.170, 24.916) were used. AutoGrid 4.2 was used to generate the grid maps file required for docking calculation. ATP, ATP-Hex-Acrylamide, and ATP-PEG-Acrylamide were drawn in ChemBioDraw Ultra and MM2 energy minimization was done by Chem 3D Pro. AutoDock Tools 1.5.6 was used again to add hydrogens compute Gasteiger charges, merge nonpolar hydrogens, choose torsions, and generate a pdbqt file and all acyclic bonds were set rotatable except amide bonds. Docking calculations were generated by AutoDock 4.2 using genetic algorithm and a pdbqt file was generated. The pdbqt file for Akt1 was set as a rigid macromolecule, and the genetic algorithm search parameters were set to 100 GA runs with a population

size of 150, a maximum number of $2.5 \times 105$ energy evaluations, a maximum number of $2.7 \times 104$ generations, a mutation rate of 0.2, and a crossover rate of 0.8. Default docking parameters were used and the output DLG file was converted to pdbqt extension. PyMOL 1.5.0.5 (Schrodinger, LLC) was used to create images (Figure 4.18).

### 4.4.9 Kinase-catalyzed crosslinking of Akt1 to its substrates using affinity based crosslinking ATP-acrylamides

Kinase-catalyzed crosslinking was performed by incubation of ATP-Hex-acrylamide or ATP-PEG-acrylamide (5 mM), HEK293 lysates (150 ug) in kinase buffer (5 mM MOPS, 5 mM $MgCl_2$, 1mM EGTA, 0.4 mM EDTA, pH 7.2) and TCEP (1.25 mM). The final volume for the reaction was 20 µL. The reaction mixture was incubated at 31°C for 3 hours with shaking at 300 rpm. Reactions without ATP analogs or in presence of lysates preincubated with staursporine (1uM), a pan kinase inhibitor, for 30 minutes were conducted as control experiments. The reaction mixtures were separated by SDS-PAGE (10% of acrylamide:Bis-acrylamide solution (37.5:1)) and visualized by SYPRO®Ruby total protein stain. Also, protein were transferred onto a polyvinylidene difluoride membrane (Immobilon-P, Milipore) and visualized with primary rabbit antiAKT followed by secondary antirabbit HRP (Figure 4.19 and A4.20).

### 4.4.10 AKT1 substrate identification with ATP-acrylamides using K-CLIP (Kinase-CrossLinking and ImmunoPrecipitation)

Kinase-catalyzed crosslinking was performed by incubation of ATP-Hex-acrylamide or ATP-PEG-acrylamide (5 mM), HEK293 lysates (500 µg) in the kinase buffer (5 mM MOPS, 5 mM $MgCl_2$, 1mM EGTA, 0.4 mM EDTA, pH 7.2) and TCEP (1.25 mM). The final volume for the reaction was 30 µL. The reaction mixture was incubated at 31°C for 3 hours with shaking at 300 rpm. Reactions without ATP analogs

or in presence of lysates preincubated for 30 min with staursporine (1µM), kinase inhibitor, were conducted as control experiments. The reaction mixture was immunoprecipitated (IP) by incubation with Anti AKT (6 µL, 1:50 dilution, cell signaling) in Lysis buffer (50 mM Tris, pH 7.4, 150 mM NaCl, 0.5% Triton X-100, 10% glycerol, and 1X protease inhibitor cocktail (GenDepot); 1 µL) up to final volume 300 uL, at 4 °C with rotation overnight. A/G PLUS-Agarose beads (20 µL slurry, Santa Cruz) were washed 3 times with lysis buffer (200 µL) and the lysates mixtures containing the antibody were incubated with the beads (20 µL slurry) with rotation for 4 hours at 4 °C. The reaction mixtures were centrifuged at 1 rcf/1min, washed 3 times with lysis buffer (200 µL), centrifuged to collect the beads (1 rcf for 1 min). The supernatant was removed, SDS loading dye (2x, 40 µL) was added, and the mixture was heated at 100 °C for 5 min, followed by addition of β-mercaptoehtanol (BME, 4 µL), and heating for another 1 min. The reaction mixture was separated by SDS-PAGE (10% acrylamide:Bis-acrylamide solution (37.5:1)) and visualized by SYPRO®Ruby or transferred onto a polyvinylidene difluoride membrane (Immobilon-P, Milipore) and visualized with primary rabbit antiAKT followed by secondary antirabbit HRP (Figure 4.20 and A4.21).

**4.4.11 Starting a new HEK293 cell culture and growing HEK293 cells**

Refer to chapter 2 (Section 2.4.16) but we used DMEM media for HEK293 cells (not F-12).

**4.4.12 Lysis procedure of HEK293 cells**

Same as HeLa cells lysis procedure in chapter 2 (Section 2.11.12).

**4.4.13 Sodium Dodecyl Sulfate-Polyacrylamide Gel Electrophoresis (SDS-PAGE)**

Refer to chapter 2 (Section 2.4.9).

### 4.4.14 SyproRuby Staining

Refer to chapter 2 (Section 2.4.11).

### 4.4.15 Pro-Q diamond phosphoprotein staning

Refer to chapter 2 (Section 2.4.13).

### 4.4.16 Western Blotting

To transfer proteins separated by SDS-PAGE, we used a polyvinylidene difluoride (PVDF) membrane (Immobilon P, Millipore). After wetting the PVDF membrane with methanol, a Mini-Transblot Electrophoretic Transfer Cell apparatus from BioRad was used to transfer the proteins in CAPS buffer (0.01 M CAPS (N-cyclohexyl-3-aminopropanesulfonic acid) at pH 10.5, containing 10% methanol). The apparatus was set at constant voltage (90 V) for 120 minutes. The membrane was air dried after protein transfer and then re-wetted with methanol. The membrane was incubated for an hour in a blocking buffer (5% (w/v) BSA in TBST (150 mM NaCl, 50 mM Tris chloride, pH 7.6 and 0.1% Tween-20). The membrane was rinsed with TBST twice (10 mL each) and then incubated overnight at $4^{\circ}C$ in the recommended dilution of Anti Akt1 primary antibody (1: 1000, cell signaling) in blocking buffer. The membrane was washed with TBST twice (10 mL each) for 5 minutes to remove excess antibody. Rabbit HRP secondary antibody (Cell signaling) diluted in PBST (137 mM NaCl, 2.7mM KCl, 10 mM $Na_2HPO_4$, 2 mM KH2PO4, pH 7.4 and 0.1% Tween-20) (1: 2000) was added and incubated for 1 hour, and then washed with TBST for 5 minutes twice (10 mL each). HRP substrate (1 mL, ThermoFischer) was used to develop the PVDF

membrane and proteins were visualized using the Typhoon 9400 scanner in chemiluminescence mode at 600 PTM.

## 4.4.17 In gel tryptic digestion of Akt1 crosslinked substrates

In gel tryptic digestion and sample preparation for proteomics was performed according to a protocol adapted from Bruker Daltonic and previously published reports.[173] SYPRO®Ruby stained gel was kept overnight in destaining buffer (100 mL, 10% methanol and 7% acetic acid in distilled water). Gel was washed twice with water (100 mL) for 10 minutes, followed by cutting of protein lanes above 55 KD into 1mm-cubes. Gel pieces were transferred into 2 mL low binding protein tubes and then washed with a 1:1 mixture of $NH_4HCO_3$ (50 mM):acetonitrile (500 μL) for 15 minutes. The supernatant was removed and acetonitrile (500 μL) was added and left until gel pieces shrank. Acetonitrile was removed and gel pieces were rehydrated with $NH_4HCO_3$ (50 mM, 500 μL). After 5 minutes, an equal volume of acetonitrile (500 μL) was added to the gel pieces and incubated for 15 minutes, followed by removing of supernatant and incubation with acetonitrile (500 μL) till gel pieces dried. Acetonitrile were then removed and gel pieces were dried under vacuum. A solution of TCEP (tris(2-carboxyethyl)phosphine, 25 mM) in $NH_4HCO_3$ (50 mM, 500 μL) was added to gel pieces and incubated at room temperature for 15 minutes. The liquid was removed, replaced by a solution of iodoacetamide (55 mM) in $NH_4HCO_3$ (50 mM, 500 μL), and incubated 30 minutes in dark at room temperature. The iodoacetamide solution was removed and gel pieces were washed with 1:1 mixture of $NH_4HCO_3$ (50 mM) and acetonitrile (500 μL) for 15 minutes, followed by removal of liquid mixture and incubation with acetonitrile (500 μL) till gel pieces shrank. The acetonitrile was

removed and gel pieces were dried under vacuum. A solution of trypsin was freshly prepared by constituting one vial trypsin (Sigma Aldrich, 20 µg) in aqueous HCl (100 µL, 1mM), followed by addition of a solution of $NH_4HCO_3$ (40 mM) in acetonitrile (9%) in water (900 µL). The final concentration of trypsin was 20 µg/mL. The trypsin solution (100µL) was added to gel pieces at 37 °C for 30 minutes.  A solution of $NH_4HCO_3$ (40 mM) in acetonitrile (9%) in water was added to keep gel pieces wet if needed and then left overnight at 37 °C. The trypsinized peptide solution was transferred into low protein binding tubes and a solution of 0.1 % formic acid in 50% acetonitrile solution in water was added to gel pieces to extract any remaining peptides, followed by sonication for 30 minutes. The extracting solution was removed and added to the tryptic-digestion solution, followed by addition of acetonitrile (500 µL) till gel pieces shrank. Acetonitrile was transferred to the tryptic-digestion solution and the mixture was dried under vacuum. The residue was analyzed by MS/MS tandem mass spectrometry to identify separated proteins.

**4.4.18 MS/MS tandem mass spectrometry**

MS/MS tandem mass spectrometry of trypsinized peptides was performed by Dr Joseph Caruso at Proteomics facility, Wayne State University, according to the following protocol.

Trypsinized peptides were desalted with C18 tips (Pierce ThermoFischer), followed by separation on a nanoflow HPLC instrument (Easy-nLC 1000, Thermo Scientific) using reverse phase chromatography (Acclaim PepMap100 C18 pre-column, Acclaim PepMapRSLC C18 analytical column, Thermo Scientific). A linear gradient was used in HPLC. The gradient started with 95% buffer A (0.1% formic acid in water)

with 5% buffer B (acetonitrile) and continued for 2 minutes until it reached 90% buffer A. Then, the gradient changed to 68% buffer A over 30 minutes at a flow rate of 300 nL/min for separation. Thermo Xcalibur 2.2 SP1.48 software (Thermo) was used to control pumps and instrument methods. After separation, peptides were ionized with a Nanospray Flex Ion Source (Proxeon Biosystems A/S), followed by spray into a Q Exactive mass spectrometer (Thermo Scientific) operated in positive mode and data was acquired using a data-dependent top 12 method. High energy collisional dissocation (HCD) was used to fragment the 12 most abundant ions from the full MS scan (375-1600 m/z). Dynamic exclusion was applied with the following parameters: 12.0 s duration and precursor isolation width set to 3.0 m/z. Resolution of full MS and HCD scans were as follow: 70,000 at 375 m/z and 17,500 at 200 m/z, respectively. Normalized collision energy for HCD spectra was set at 30 eV with aquiring data in profile mode. Lastly, we enabled isotope exclusion, singly charged and unrecognized charged ion exclusion.

### 4.4.19 Peptide Spectrum Matching and Data Analysis

Analysis of raw data was performed with Proteome Discoverer 1.4.0.288 (Thermo) using the Mascot search algorithm (Matrix Science, London, UK; version 1.4.1.14) and Sequest (Thermo Fisher Scientific, San Jose, CA, USA; version 1.4.1.14). Mascot was set up to search Uniprot human database assuming the digestion enzyme trypsin. Sequest was set up to search uniprot human also assuming trypsin. Mascot and Sequest were searched with a fragment ion mass tolerance of 0.020 Da and a parent ion tolerance of 10.0 PPM. To calculate false discovery rates (FDR), the SwissProt database was utilized against human protein sequences and the

reverse decoy protein database. Carbamidomethyl of cysteine (+57) was specified in Mascot and Sequest as a fixed modification. Deamidated of asparagine and glutamine, oxidation of methionine (+16), acetyl of the n-terminus (+42), alkylation of cysteine with acrylamides (184 for ATP-Hex-Acr experiments and 288 for ATP-PEG-Acr), were specified in Mascot as variable modifications. Enzyme specificity was assigned for trypsin as c-terminal to lysine and arginine with 1 missed cleavage site allowed.

Scaffold (version Scaffold_4.4.8, Proteome Software Inc., Portland, OR) was used to validate MS/MS based peptide and protein identifications. Peptide identifications were accepted if they could be established at greater than 100.0% probability to achieve an FDR less than 1.0% by the Scaffold Local FDR algorithm. Protein identifications were accepted if they could be established at greater than 99.0% probability and contained at least 1 identified peptide. Protein probabilities were assigned by the Protein Prophet algorithm.[174] Proteins that contained similar peptides and could not be differentiated based on MS/MS analysis alone were grouped to satisfy the principles of parsimony.

## 4.4.20 Proteomics MS/MS analysis procedure

Protein lists were obtain for untreated lysates or lysates treated with ATP-acrylamides in presence and absence of staursporine (kinase inhibitors). Peptide ratios for ATP-acrylamides were calculated by dividing peptide count obtained from lysates treated with ATP-acrylamides by either untreated lysates or lysates treated with both acrylamides and staursporine. Only proteins with peptides ratios greater than 1 were taken for further analysis in case of both untreated or staursporine treated lystaes. The interactome analysis was performed using the Genemania application in Cytoscape

3.3.0 program. AKT1 substrates and direct interacting proteins were determined by Phosphosite Plus and Biogrid, respectively. A diagram was generated by Cytoscape 3.3.0 to show the relation of all isolated proteins to Akt1.

# CHAPTER 5 SYNTHESIS AND STRUCTURAL ANALYSIS OF THE EFFECT OF DIFFERENT BOND LINKAGE ON THE γ-PHOSPHATE OF γ-MODIFIED ATP ANALOGS ON KINASE-COSUBSTRATE PROMISCUITY

## 5.1 Introduction

Several techniques have been developed to study kinase-catalyzed phosphorylation, such as $^{32}$P radio-labeling, covalent modification of phosphate, and gel based visualization of phosphoproteins.[175-180] Most recently, the Pflum lab reported that γ-modified ATP analogs were promiscuously accepted by protein kinases. Several γ-modified ATP analogs were developed to study enzymatic phosphorylation of proteins and peptides (Section 1.6, Chapter 1).[79,85,86,92,128,181-184] Importantly, the modifications reported to date were installed on the γ-phosphate through a phosphoramidate bond. In this chapter, we replace the nitrogen of the phosphoramidate bond with other atoms to study the ability of ATP analogs to act as kinase cosubstrates (Figure 5.1). Also, we discusse the structure activity relationship of γ-modified ATP analogs as kinase cosubstrates.

### 5.1.1 Kinase-cosubstrate promiscuity

Many γ-modified ATP analogs, such as ATP-γ-S and ($\gamma^{32}$P)-ATP (Chapters 1 and 4), are accepted promiscuously by protein kinases and participate in kinase-catalyzed phosphorylation reactions to furnish a modified phosphoproteins. Most recently, γ-modified ATP analogs with a tag such as biotin,[79,92,128,181,182] aryl-azide[185] or ferrocene[85] were developed, and the modification has attached to the γ-phosphate via a phosphoramidate bond (Figure 1.6). The tag can allow visualization of protein substrates, purification of phosphorylated proteins (as in ATP-biotin, Section 1.6.2, Chapter 1), or crosslinking of protein substrates to their corresponding kinases (as in

ATP-Ar-azide, Section 1.6.4, Chapter 1).[181,185] In this chapter, the structural analysis and requirements of the γ-modification to allow the promiscuity of kinase is explored.[94] Also, replacement of the phosphoramidate bond with other bonds, such as phosphodiester, is discussed. This work was performed in collaboration with my colleague Thilani Anthony.

## 5.1.2  Structure analysis of γ-modified ATP analogs

Many γ-modified ATP analogs are accepted by protein kinases depending on certain structure requirements. The functional group on the ATP molecule should be attached to γ-phosphate by a linker. The Pflum lab explored the structure requirements for the linker, as well as the function group.[94] First, the nature and size of the functional group on γ-phosphate affect the efficiency of the ATP analog as a kinase cosubstrate. Small groups such as acetyl group (Entry a-c, Figure 5.1) furnished better activity than large groups such as aryl group (Entry d-k, Figure 5.1). Also the type of functional group affects the efficiency. For instance, higher conversion was detected when the terminal group had a sulfonamide functional group (Entry k versus Entry h, Figure 5.1), which indicates that a more polar functional group on ATP-γ-modification is better for kinase activity. In addition, the length and nature of the linker affect the kinase activity. ATP analog with a longer linker (Entry i, Figure 5.1) were more efficient than an ATP analog with a shorter linker (Entry g, Figure 5.1), especially when the size of the functional group was big. Also, an ATP analog with a more hydrophilic linker such as 2,2'-ethylenedioxybis-(ethylamine) (Entry j, Figure 5.1) has more efficiency as a kinase cosubstrate than those analogs with a more hydrophobic linker (Entry i, Figure 5.1).
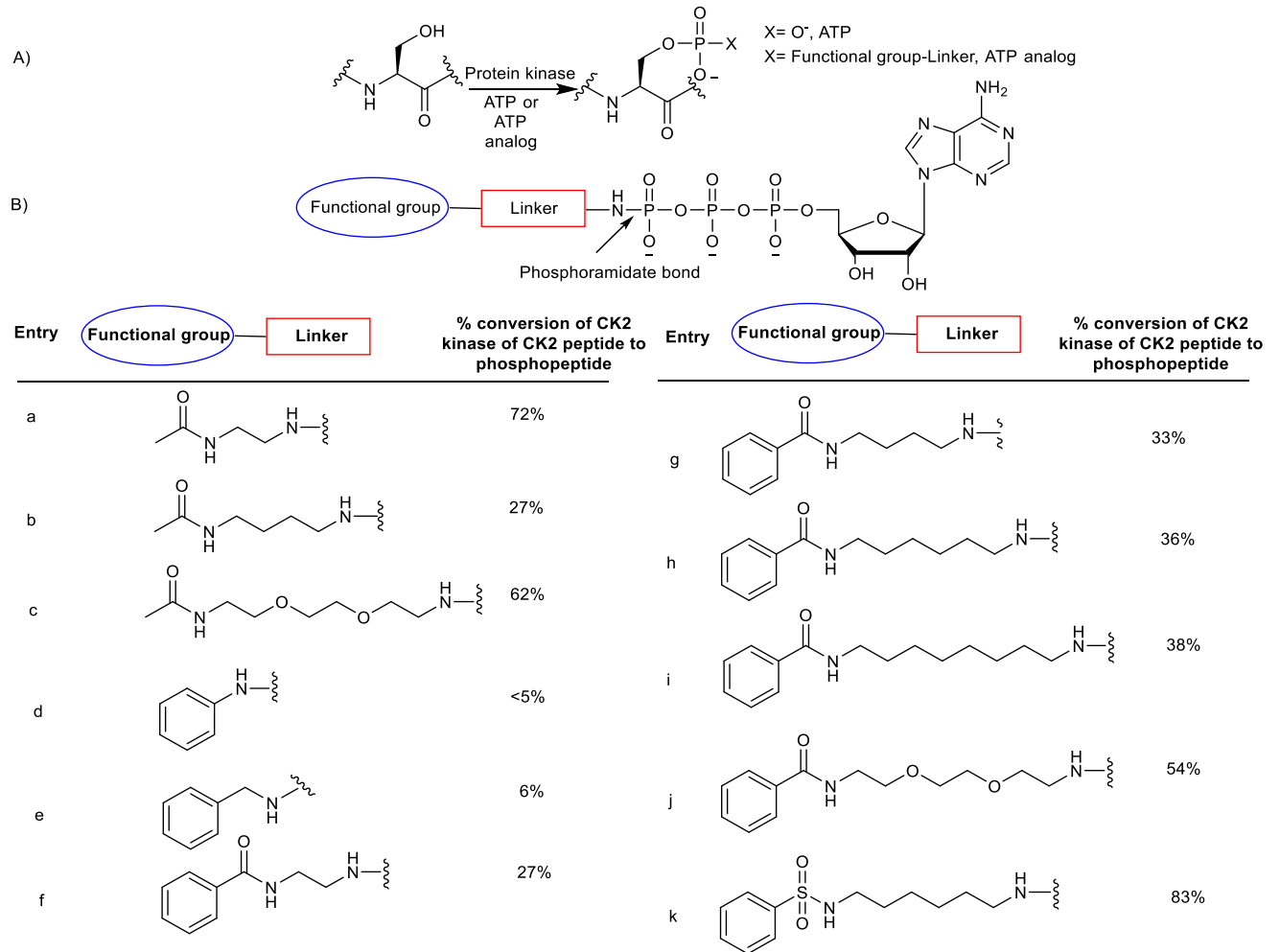
**Figure 5. 1:** A) Kinase-catalyzed phosphorylation of proteins or peptides using ATP or ATP analogs B) Percentage phosphorylation of CK2 peptide using CK2 and different ATP analogs with different linker sizes and functional groups.[94]

### 5.1.3  Development of γ-modified ATP analogs with phosphodiester bond

Mann and coworkers developed a new generation of γ -modified ATP analogs containing a phosphodiester bond at the γ-phosphate. The developed ATP analogs had alkynes, azides, and alkenes as γ-modification (Figure 1.18), which are useful for subsequent click chemistry or Staudinger ligation (Chapter 1, Section1.66). Their analogs were accepted by cyclin E1/cdk2 kinase, as demonstrated using western blotting and phosphor specific antibodies. Unfortunately, the phosphodiester analogs were not well studied. They did not show the kinetics for their analogs or confirmed the phosphorylation of kinase substrate using mass spectrometry. A more detailed discussion of Mann work and the structure of their ATP analogs were discussed in chapter 1 (Section 1.66).[86]

As a continuation of our previous studies, we studied the effect of directly attaching different atoms to the γ-phosphate on the ability of ATP analog to act as a kinase cosubstrate. We synthesized γ-modified ATP analogs with phosphoramidate, phosphodiester, and phosphonate bonds on the γ-phosphate (Figure 5.2 and Scheme 5.1). We studied their kinase cosubstrate ability, including detailed kinetics and mass identification of phosphorylated products.
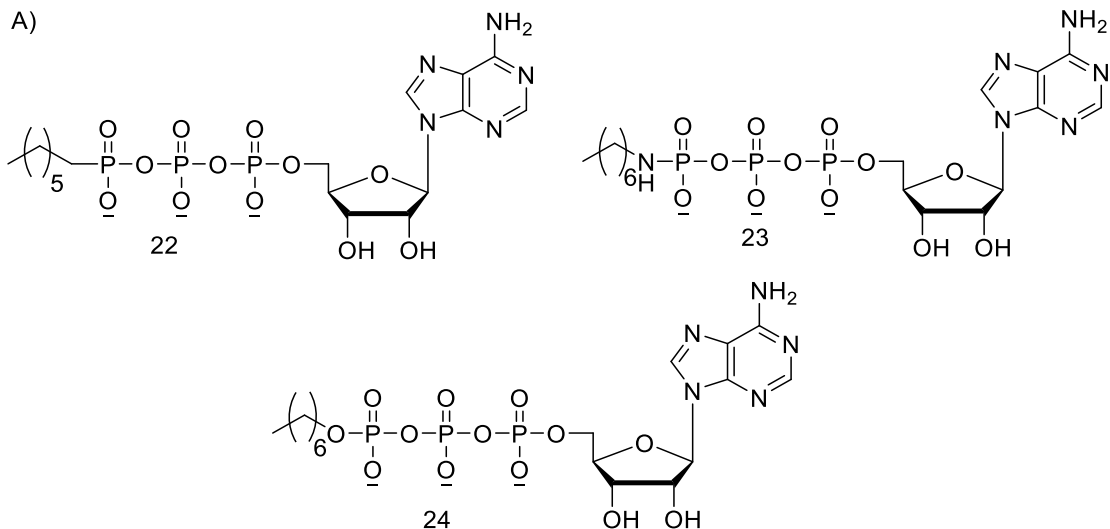
**Figure 5. 2:** ATP analogs (**22-24**) with different first atom linked to γ-phosphate. The figure shows ATP-C-heptyl with phosphonate bond, ATP-N-heptyl with phosphoramidate bond, and ATP-O-heptyl phosphodiesterbond

## 5.2 Results

### 5.2.1 Synthesis of ATP analogs

ATP analogs with heptyl groups attached to the γ-phosphate through different atom linkage (C, N, O) were synthesized (compounds **22-24**, Scheme 5.1). We selected heptyl group on γ-phosphate as it is a long and not bulky, which simulate our previously synthesized analogs and rules out any steric factors. The ATP-phosphonate (ATP-C-heptyl, **22**) was synthesized by my colleague, Thilani Anthony, (Scheme 5.1 A). The ATP-phosphoramidate analog (ATP-N-heptyl, **23**) was synthesized by coupling ATP with heptyl amine (Scheme 5.1B). ATP-phosphodiester (ATP-O-heptyl, **24**) was synthesized from ADP according to previously reported procedure.[86] Heptyl alcohol **29** was reacted with phosphorus oxychloride, followed by addition of triethylamine carbonate buffer (pH=7) (Scheme 5.1C). The resulting mixture was coupled without

purification with ADP tributyl ammonium salt **28** to give ATP-phosphodiester analog (**24**)

(Scheme 5.1C).

**Scheme 5. 1:** Synthesis of ATP analogs ATP-C-heptyl (22), ATP-N-heptyl (23), and ATP-O-heptyl (24).

A)
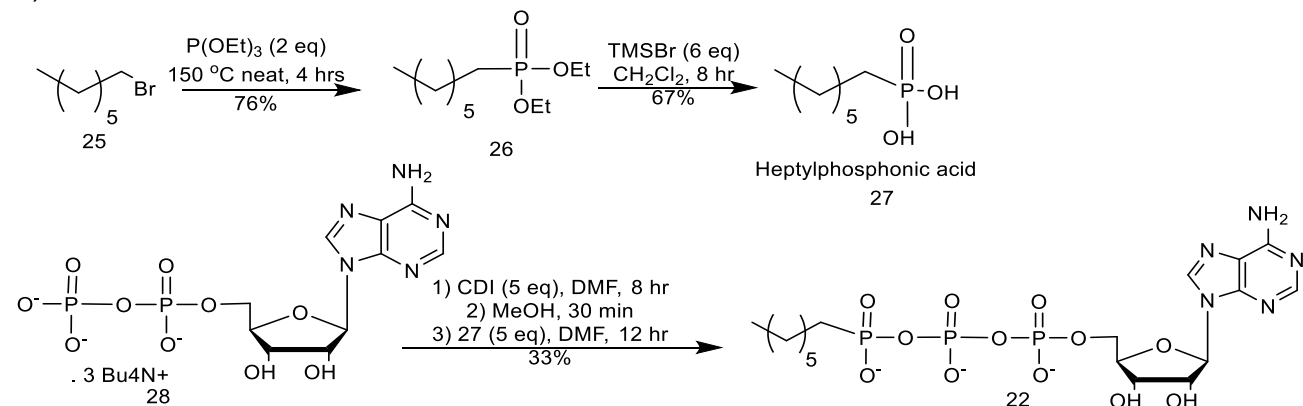


B)
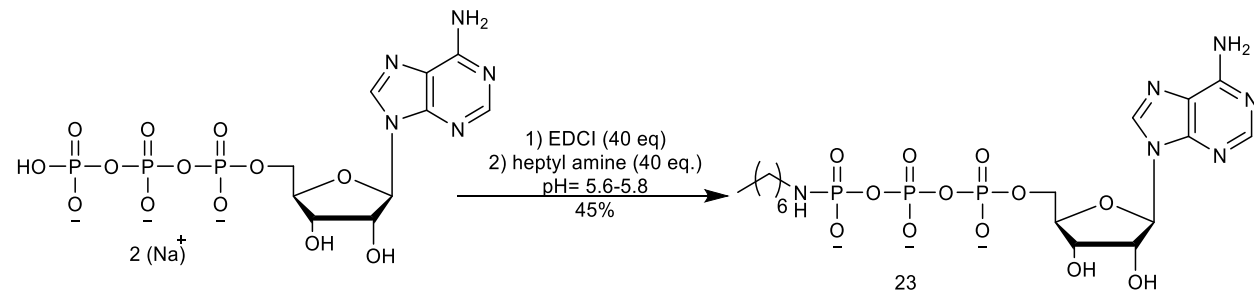


C)
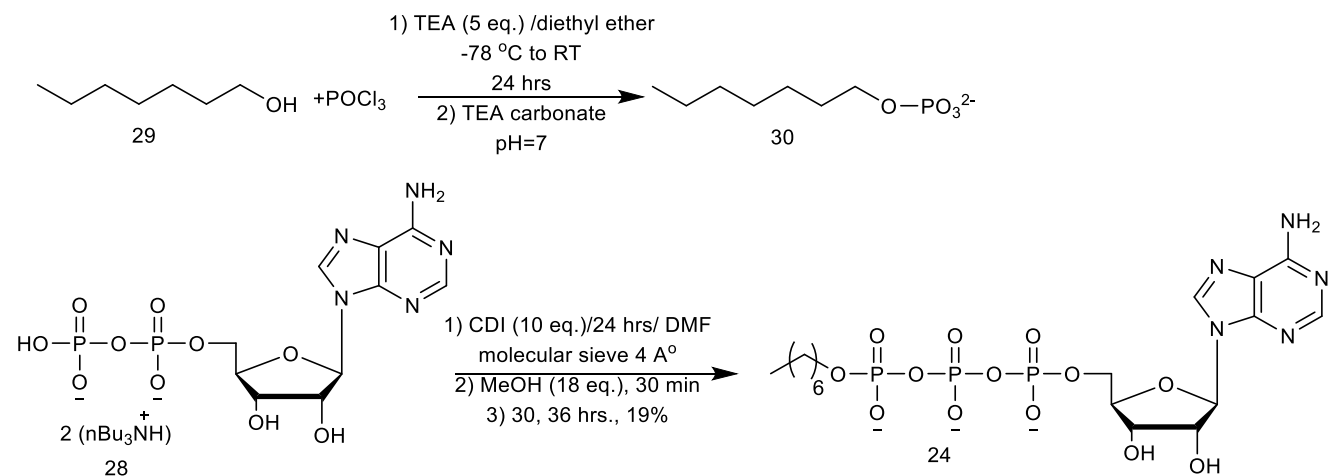
### 5.2.2 Analysis of kinase cosubstrate promiscuity using ATP-C, N, and O-heptyl (22-24)

Three $\gamma$-modified ATP analogs with same the heptyl group but different atoms of attachment on the $\gamma$-phosphate were synthesized. Since the connecting atom is the only difference in ATP analogs (**22-24**), it should be the only variable affecting the promiscuity of such ATP analogs. To investigate the effect of different bond connections on $\gamma$-modified ATP analog promiscuity, we used mass spectrometry to evaluate their ability to act as cosubstrates to kinases. The ATP analogs (**22-24**) were incubated with PKA kinase and kemptide peptide substrate and the resulting mixtures were analyzed by MALDI-TOF mass spectrometry. As a control, we analyzed the reaction mixture from the incubation of ATP, PKA, and kemptide (Ac-kemptide). The MALDI-TOF analysis of ATP revealed a peak at m/z 894.5, corresponding to [M+H] peak of phosphor-Ac-Kemptide (Figure 5.3A), which confirmed the validity of the experiment for subsequent studies. The analysis of the reaction mixtures of ATP-C-heptyl **22**, ATP-N-heptyl **23**, and ATP-O-heptyl **24** analogs revealed an [M+H] peak at m/z 975.9, 991.4, and 992.9 respectively, corresponding to modified phosphopeptide (Figure 5.3B, C, D, respectively). The data suggests that different atoms attached to $\gamma$-phosphate preserve the ability of ATP analog to act as a kinase cosubstrate but with different efficiencies.
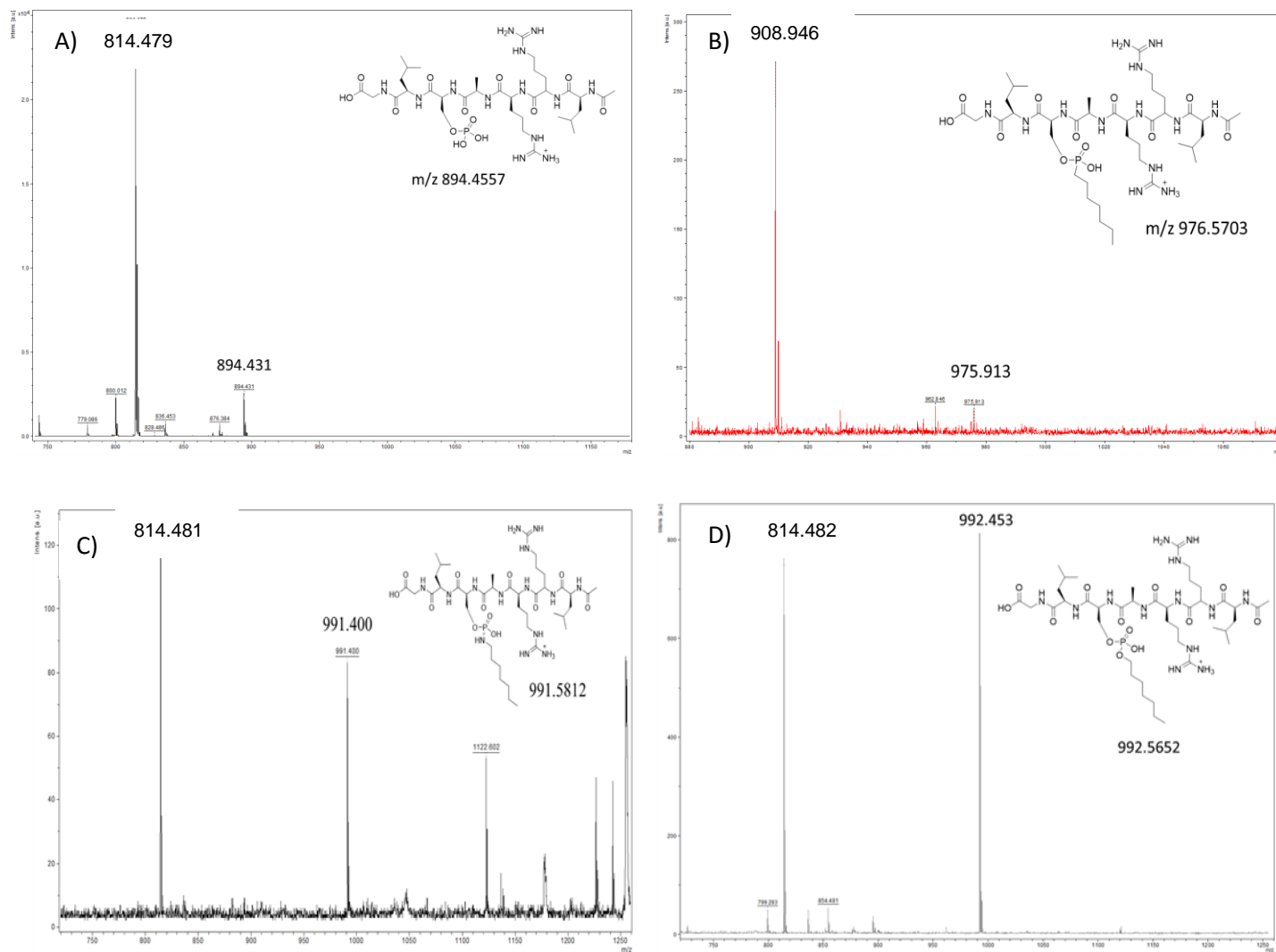
**Figure 5. 3:** MALDI mass spectrometry spectra of modified phosphorylated of Ac-kemptide using ATP analogs (**22-24**). ATP or ATP-analogs were incubated with kemptide and PKA followed by MALDI-TOF spectrometric analysis. A) ATP B) ATP-C-heptyl (**22**) C) ATP-N-heptyl (**23**) D) ATP-O-heptyl (**24**). The expected masses of each peptide products are shown. The peak at m/z 814 is for unphosphorylated Ac-kemptide (calculated m/z 814.4894). Repetitve trials are shown in figure A5.13-A5.15.

To confirm the kinase cosubstrate ability of each analog, we incubated ATP or the ATP analogs (**22-24**) with PKA and myelin basic protein (MBP) and the reaction mixture was analyzed by SDS-PAGE electrophoresis, followed by visualization of phosphoproteins using ProQ diamond stain or total proteins using Sypro Ruby stain. The reaction mixtures of ATP (Figure 5.4, lanes 2 and 9, top gel), ATP-N-heptyl (**3**)

(Figure 5.4, lane 12, top gel), and ATP-C-heptyl (**5**) (Figure 5.4, lane 6, top gel) showed

phosphorylation of MBP, while ATP-O-heptyl (**4**) (Figure 5.4, lane 4, top gel) did not

show phosphorylation. The data from ATP, ATP-N-heptyl (**3**), and ATP-C-heptyl (**5**)

confirmed the MALDI mass spectrometry data, while ATP-O-heptyl did not show

phosphorylation. We specultate that the lack of ProQ signal of ATP-O-heptyl may be

due to interference of modification with ProQ stain.



| | Pro-Q | | | | | | | | | | | |
| SYPRO Ruby | | | | | | | | | | | | |
| | 1 | 2 | 3 | 4 | 5 | 6 | 7 | 8 | 9 | 10 | 11 | 12 |
| MPB | + | + | + | + | + | + | + | + | + | + | + | + |
| PKA | | + | | + | | + | + | | + | + | | + |
| ATP | + | + | | | | | | + | + | | | |
| ATP-O-heptyl | | | + | + | | | | | | | | |
| ATP-C-heptyl | | | | | + | + | | | | | | |
| ATP-N-heptyl | | | | | | | | | | | + | + |
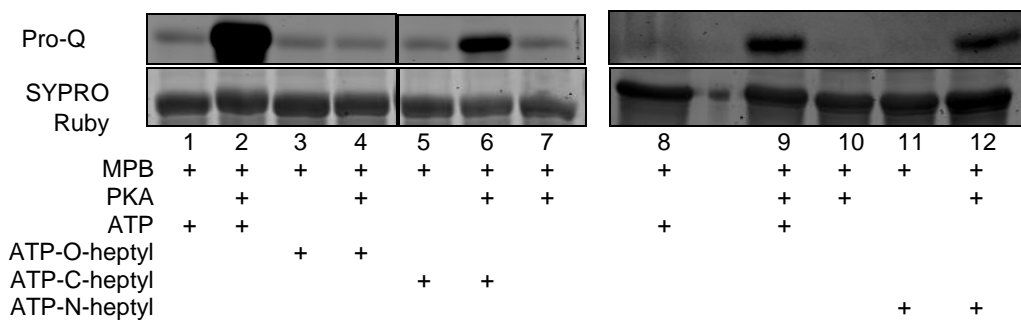
**Figure 5.4:** Analysis of MPB phosphorylation in the presence of PKA and incubated with ATP (lane 2), ATP-O-heptyl (lane 4), ATP-C-heptyl (lane 6) or ATP-N-heptyl (lane 12). The reaction mixtures were analyzed by SDS-PAGE analysis, followed by staining with ProQ diamond phosphoprotein stain (top) or SYPRO® Ruby total protein stain (bottom). As a control ATP analogs were incubated with MBP in absence of PKA (lane 1, 3, 5, 11). Repetitive trials are shown in figure A5.17.

## 5.2.3 Kinetic analysis of ATP analogs (22-24)

Since gel analysis did not confirm the kinase cosubstrate ability of all ATP-

analogs (**22-24**), we performed kinetic analysis for all analogs and compared it with ATP

using enzyme coupled assay.[184] Kinetic analysis will confirm both the kinase

cosubstrate property of all analogs and their efficiency. ATP or ATP analogs (**3-6**) were

incubated with PKA and Ac-kemptide (Figure 5.5). The $K_m$, $K_{cat}$, and $V_{max}$ were

determined for each analog (Table 5.1). As a control, we performed the reaction in the

absence of either PKA or Kemptide substrate. Kinetic analysis revealed the reactivity of

ATP analogs only in presence of PKA and kemptide, while the absence of PKA or

kemptide did not show any change in enzyme kinetics (Figure 5.5). The most efficient compound was the natural ATP ($K_{cat}/K_m$=0.3). The least efficient analog was ATP-C-heptyl **22** ($K_{cat}/K_m$=0.03), which was 10 fold less efficient than ATP. ATP-N-heptyl and ATP-O-heptyl show similar efficiency ($K_{cat}/K_m$=0.1), but three fold less than ATP. ATP-C-heptyl be the less efficient due to less electronegativity compared to nitrogen and oxygen. The nitrogen and oxygen atoms of ATP analogs (**23** and **24**) has high electronegativity and may facilitate bond breakage between $\gamma$-phosphate and $\beta$-phosphate. In summary, the kinetic analysis confirmed that all analogs are kinase-cosubstrates with different catalytic efficiencies.

## 5.3 Conclusion and future directions

In conclusion, kinase-cosubstrate promiscuity is affected by the atom attached to the $\gamma$-phosphate. Although all analogs are cosubstrates to kinases. ATP-N-heptyl (**23**) and ATP-O-heptyl (**24**) had similar efficiency, but three-fold less than to ATP. The ATP analog with carbon attached to the $\gamma$-phosphate (ATP-C-heptyl (**22**) was the least efficient ATP-analog. We note that the carbon linkage may be helpful in protein kinase studies due to its high stability.[186] In the future, ATP analogs with carbon modifications on the $\gamma$-phosphate might be designed because they are stable in both acidic and basic media.[186] ATP analogs with a carbon linker can phosphorylate kinase substrates and can withstand handling during purification of substrates in acidic and basic media.
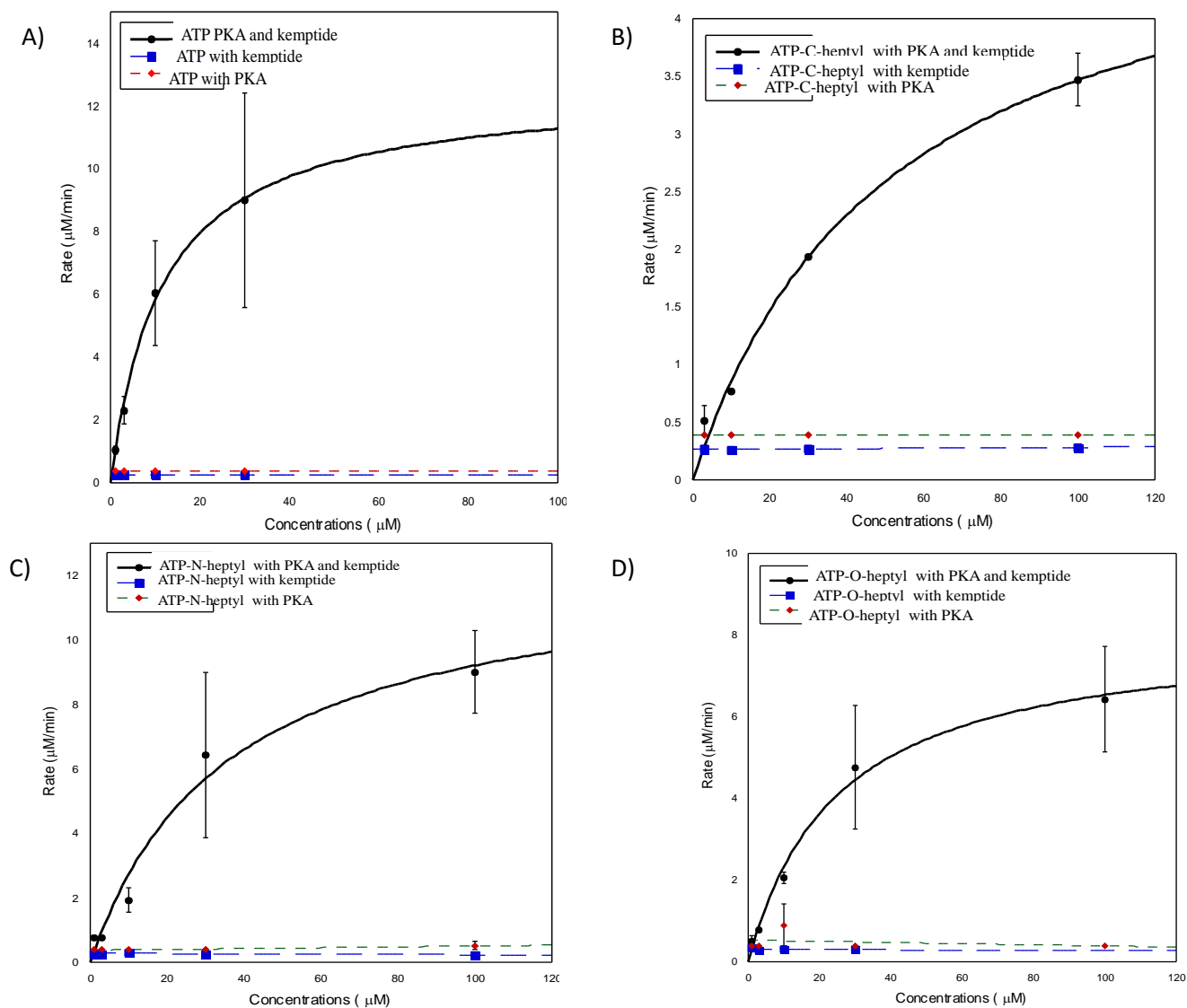
**Figure 5. 5:** Michaels Menten plot of ATP analogs (**22-24**). ATP analogs (ATP (A), ATP-C-heptyl **22** (B), ATP-N-heptyl **23 (**C), ATP-O-heptyl **24** (D)) were incubated with kemptide and PKA and kinetic data was collected by coupling this reaction NADH enzyme coupled assay. As a control, the reactions were performed in the absence of either kemptide or PKA.

**Table 5. 1:** Kinetic results of ATP analogs (22-24)

|  | $k_{cat}$ (s$^{-1}$) | $K_m$ (µM) | $K_{cat}/K_m$ (s$^{-1}$µM$^{-1}$) |
|---|---|---|---|
| ATP | 3.9±0.7 | 11.6±1.72 | 0.3 |
| ATP-C-heptyl (**5**) | 1.7±0.4 | 54±7.68 | 0.03 |
| ATP-N-heptyl (22) | 3.9±1.9 | 35.7±13 | 0.1 |
| ATP-O-heptyl (**4**) | 2.6±0.5 | 25±4.75 | 0.1 |

## 5.4    Experimental

### 5.4.1    Materials

ATP was purchased from MP Biomedicals.    1-(3-Dimethylaminopropyl)-3-ethylcarbodiimide hydrochloride (EDCI), phosphorus oxcychloride ($POCl_3$), heptyl amine, heptyl alcohol, and N,N,N',N'-Tetramethylethylenediamine (TEMED) for electrophoresis were bought from Acros. Silica, DEAE sephadex A-25, and Ammonium persulfate (APS) for electrophoresis were purchased from Fisher Scientific. Diethyl ether and dimethyl formamide (DMF) were bought from EMD. 40% Bis-acrylamide (37.5:1) for gel electrophoresis was purchases from Biorad. Pyruvate kinase, lactate dehydrogenase, NADH, and phosphoenol pyruvic acid used for kinetics were purchased from Sigma Aldrich. Myelin basic protein (MBP) was bought from Invitrogen. PKA kinase was purchased from New England Biolabs. 3-Hydroxypicolinic acid was bought from Fluka. C18 (10 µL) desalting tips were bought from ThermosFischer.

### 5.4.2    Instruments

A Lyophilizer (VirTis BT 3.3 EL Benchtop) was used during synthesis of ATP analogs. SDS-PAGE instrument were bought from BioRad (Protean III) and gels were scanned via Typhoon 9210 scanner (Amersham Biosciences). $^{1}$H NMR, $^{13}$C NMR, $^{31}$P NMR (Varian Mercury-400), and High resolution mass spectra (HRMS) (LCT Premier XT (Waters)) were used to characterize synthesized analogs. Absorbance of ATP analogs was measure by UV-Vis spectrophotometer (Shimadzu 2101 PC). GENios Plus Fluorimeter (Tecan) was used to measure absorbance during kinetic studies.

### 5.4.3 Preparation of ADP tributyl ammonium salt (28):

### 5.4.3.1 Preparation of Dowex-8H+ column:

Dowex-8H$^+$ resin (5 gm) was incubated with aqueous HCl (0.1 M, 40 mL) overnight. The resin was packed into a glass column then washed with deionized water twice (20 mL each).

### 5.4.3.2 Regeneration of Dowex-8H+:

After use, Dowex-8H+ was regenerated by washing with aqueous HCl (0.1 M, 20 mL, twice) until the elute was acidic followed by washing with deionized water until the elute was neutral. After regeneration, the resin was kept in a glass column at room temperature.

### 5.4.3.3 Preparation of ADP tributyl ammonium salt (28)

ADP. 2 Na (20 mg, 0.053 mmol) was dissolved in water (20 mL) and loaded to a Dowex-8H$^+$ column (5 gm). The column was washed with deionized water twice (20 mL) and eluted in a solution of tributyl amine (26 µl, 0.106 mmol) in ethanol (200 µL) with stirring. The solution was lyophilized, and a white powder was obtained. The ADP tributyl ammonium salt (**28**) was used directly in the synthesis of ATP analogs. The quantities were scaled up as needed except the Dowex quantity.

### 5.4.4 Synthesis of ATP-C-heptyl (22)

Compound **22** was synthesized by my colleague, Dr. Thilani Anthony, according to the following procedure.

### 5.4.4.1 Synthesis of diethyl heptylphosphonate 26

In a 50 mL round bottom flask under nitrogen, equipped with a distillation setup, triethylphosphosphite (17.147 mL, 100 mmol) and 1-bromoheptane **25** (7.85 mL, 50

mmol) were mixed. The reaction mixture was heated at 140 °C for 4 hrs. The resulting byproduct bromoethane was distilled off (~3 mL). Then the reaction mixture was cooled to room temperature and distilled under vacuum (bp 175-180 °C in 11 mmHg) affording phosphonate **26** as colorless oil (8.97 g, 76%). Characterization of molecule is in Thilani Anthony's thesis.

### 5.4.4.2    Synthesis of heptylphosphonic acid 27

TMSBr (1.0 mL, 7.8 mmol) was mixed with anhydrous dichloromethane. Compound **26** (1.3 mL, 1.3 mmol) was added at 0 °C and stirred at room temperature for 12 hrs. The solvent was evaporated under reduced pressure. Water (15 mL) was added and stirred for 10 hrs. The reaction was extracted with ethyl acetate, washed a brine and dried over $MgSO_4$.  The solid was removed under *vacuo* to yield a white solid **27 (**0.157 g, 67%). Characterization of molecule is in Thilani Anthony's thesis.

### 5.4.4.3    Synthesis of ATP-C-heptyl 22

Adenosine 5'- diphosphate tributyl ammonium salt **28** (0.066 mmol, 1.0 eq) was dissolved in molecular-sieve dried DMF (5 mL), followed by the addition of CDI (0.33 mmol, 5 eq). The mixture was stirred for 10 hrs at room temperature. Methanol (0.3 mL) was added to the reaction and stirred for 1 hr, followed by addition of trimethylamine (0.2 mL). A solution of crude **27** (section 5.4.4.2**)** in DMF (0.5 mL) was added and stirred at room temperature for 8 hrs. The mixture was mixed with 5% of 1 M TEA carbonate buffer in water (5 mL, pH=8.5) and loaded onto anion exchange sephadex A-25 (5 gm) column. 0.1-1 M triethyl ammonium carbonate buffer was used as eluent (section 2.4.6). The collected fractions were frozen and lyophilized to give white crystals of **22** (33%).^{1}H NMR (400 MHz, $D_2O$): δ 1.37 (3H, s), 1.57 (8H, m), 3.20 (2H, m), 3.82

(3, m), 4.50 (2H, s), 4.65 (1H, s), 4.80 (1H, s), 6.40 (1H, d), 8.60 (1H, s), 8.87 (1H, s).

$^{13}$C NMR (100 MHz, D$_2$O): δ 13.32, 17.57, 21.90, 22.40, 26.41, 26.70, 27.99, 29.89, 30.94, 65.02, 69.51, 70.26, 74.62, 84.42, 87.72, 120.72, 121.87, 126.84 (2C), 137.57.

$^{31}$P NMR (162 MHz, D$_2$O): δ 21.57-21.73 (d), -11.70 -11.57 (d), -23.35 (t). UV/Vis spectroscopy (H$_2$O): λ 260 nm. ESI HRMs, (M-H)$^-$ for C$_{17}$H$_{29}$N$_5$O$_{12}$P$_3$: calc. 588.1026, found 588.1028.

## 5.4.5  Synthesis of ATP-N-heptyl (23)

The disodium salt of ATP (32 mg, 0.059 mmol) was dissolved in water (5 mL) and then the pH was adjusted to 7 using NaOH (0.5 M) and pH meter. EDCI (382 mg, 2 mmol) was added and the pH was adjusted to 5.6-5.8 using aqueous HCl (0.5 M). A solution of heptyl amine (297 μL, 2 mmol) in water (2 mL) was added and the pH was readjusted to 5.6-5.8. The solution was stirred for 3 hours and the progress of reaction was monitored by TLC (isopropanol:ammonia:water in 3:1.5:0.5 ratio). The pH was brought to 8.5 by triethyl amine and the product was separated by anion exchange column (A-25 sephadex, 5 gm) with 0.1-1 M triethyl ammonium carbonate buffer (pH=8.5) as eluent (section 2.4.6). The fractions containing product were lyophilized to dryness and the solid compound was stored at -80 °C. ATP-N-heptyl (23) was obtained as a white solid (10.4 mg, 45%). $^1$HNMR (400 MHz, D$_2$O): δ 0.98 (3H, s), 1.19 (6H, m), 2.79 (2H, m), 3.42 (5H, m) 4.09 (2H, s), 4.24 (1H, s), 4.39 (1H, s), 5.99 (1H, d), 8.20 (1H, s), 8.47 (1H, s). $^{13}$C NMR (100 MHz, D$_2$O): δ 7.06, 13.18, 21.80, 25.41, 26.60, 27.76, 30.72, 58.48, 65.12, 70.30, 74.37, 87.17, 111.60, 114.11 (2C), 130.97, 156.89.

$^{31}$P NMR (162 MHz, D$_2$O): δ -10.92 (d), -11.58 (d), -23.42 (t). UV/Vis spectroscopy

(H2O): λ 260 nm. ESI HRMs, (M-H)$^-$ for $C_{17}H_{30}N_6O_{12}P_3$: calc. 603.1135, found 603.1158.

### 5.4.6 Synthesis of ATP-O-heptyl (24):

### 5.4.6.1 Synthesis of heptyl phosphate (30)

In 25 mL flask, a solution of phosphorus oxychloride (0.585 mmol, 55 uL) in diethyl ether (5 mL) was cooled to -78 °C. A solution of heptanol **29** (0.585 mmol, 85 uL) and triethyl amine (0.585 mmol, 80 uL) in diethyl ether (5 mL) was added dropwise under Argon and then stirred at room temperature for 24 hours. The reaction was quenched using TEA carbonate buffer (0.1 M, 4 mL, pH=7). The solvent was evaporated *in vacuo* and used in the next step without purification.

### 5.4.6.2 Synthesis of ATP-O-heptyl (24):

ADP. 2Na (50 mg, 0.117 mmol) was converted to the tributyl ammonium salt as in section 5.4.3.3 and then dissolved with molecular sieve (4 A°) dried DMF (3 mL), followed by addition of CDI (1.17 mmol, 190 mg, 10eq.). The reaction was stirred for 24 hours under argon. Methanol (2.1 mmol, 85 uL, 18 eq.) was added and the reaction was stirred for 30 min. Unpurified heptyl phosphate (**30**) from section 5.4.6.1 in molecular sieve (4 A°) dried DMF (3 mL) was added to the reaction mixture and the reaction was stirred for 36 hours under argon at room temperature. The mixture was mixed with 5% of 1 M TEA carbonate buffer in water (5 mL, pH=8.5) and loaded onto anion exchange sephadex A-25 (5 gm) column. 0.1-1 M triethyl ammonium carbonate buffer (pH=8.5) was used as eluent (section 2.4.6). The collected fractions were frozen and lyophilized to give white crystals (13.5 mg, 19%). $^1$H NMR (400 MHz, $D_2O$): δ 1.20 (3H, s), 1.69 (4H, m), 1.98 (2H, m), 3.40 (2H, m), 3.95 (2H, m), 4.26 (3H, m), 4.63 (2H, s), 4.76 (1H,

s), 4.92 (1H, s), 6.51 (1H, d), 8.78 (1H, s), 9.02 (1H, s). $^{13}$C NMR (100 MHz, D$_2$O): δ

13.33, 21.87, 24.77, 28.11, 29.77, 30.97, 42.16, 58.42, 66.97, 70.21, 74.69, 87.67,

142.22 (2C), 145.44(2C), 148.25.. $^{31}$P NMR (162 MHz, D$_2$O): δ -10.98 (d), -11.62 (d), -

23.38 (t). UV/Vis spectroscopy (H$_2$O): λ 259 nm. ESI HRMs (M-H)$^-$ for C$_{17}$H$_{29}$N$_5$O$_{13}$P$_3$:

calc. 604.0975, found 604.0955.

## 5.4.7 MALDI-TOF analysis of kinase-catalyzed reaction using ATP-C, N, and O-heptyl analogs (22-24)

Kinase-catalyzed reaction was performed by incubation of ATP or ATP analog (2

mM), PKA enzyme (2 µg/mL, 52.6 nM) and kemptide (1 mM) in the kinase buffer

provided by the manufacturer (50 mM Tris-HCl, 10 mM MgCl$_2$, pH 7.5). The final volume

for the reaction was 10 µL. The reaction mixture was incubated at 31°C for 2 hours

followed by desalting using C18-Tips (Pierce). The desalted reaction (2 µL) was mixed

with an equal volume of a saturated solution 3-hydroxypicolinic acid solution in 50%

acetonitrile, followed by spotting on MALDI plate (Bruker). The resulted mass spectra

were analyzed to detect either phospho-kemptide or modified phospho-kemptide.

(Figure 5.3 and A5.13-A5.15)

## 5.4.8 Procedure of desalting of kinase-catalyzed reaction before MALDI-TOF analysis adapted from Thermo-fischer scientific procedure

C18 tips (10 µL, Thermo-fischer scientific) were wetted by aspiration using 50%

acetonitrile in water (10µL). The tips were equilibrated by aspirating 0.1% TFA (10µL)

twice. The sample to be desalted was diluted to 0.1% TFA using 2.5% TFA, followed by

aspiration into the C18 tip three times. The tip was rinsed by aspirating with 0.1%

TFA/5% acetonitrile in water (10µL) twice. The sample was eluted using 0.1 % TFA in

95% acetonitrile in water (10 µL).

## 5.4.9 Pro-Q analysis of ATP-C, N, and O-heptyl analogs (22-24)

Kinase-catalyzed reaction was performed by incubation of ATP or ATP analog (3 mM), PKA enzyme (2 μg/mL, 52.6 nM) and myelin basic protein (MBP) (1 μg/ul) in the kinase buffer provided by the manufacturer (50 mM Tris-HCl, 10 mM $MgCl_2$, pH 7.5). The final volume for the reaction was 20 μL. The reaction mixture was incubated at 31°C for 2 hours. Reactions without PKA were conducted as control experiments. The reaction mixtures were separated by SDS-PAGE (16%) and visualized by SYPRO Ruby to detect total proteins or Pro-Q diamond stain to examine phosphorylation.

### 5.4.10 Synthesis of N-acetylated kemptide (AcLRRASLG)

See Chapter 2 (section 2.11.7)

### 5.4.11 Kinetics of N, O, and C-heptyl ATP analogs (22-24)

An NADH-dependent coupled assay was used to perform kinetic analysis, as previously described,[184] with some exceptions. NADH (0.5 mM), pyruvate kinase (24 units/mL), lactic acid dehydrogenase (36 units/mL), and kemptide (1.29 mM) were preincubated together for 30 min at 31 °C. ATP or ATP analogs at final concentrations of 1, 3, 10, 30 (ATP or **22**) or 1, 3, 10, 30, 100 μM (**23** or **24**) were added and preincubated for another 5 minutes at 31 °C. The reaction was initiated by addition of PKA (2 μg/mL, 52.6 nM) in a final reaction volume of 25 μL. The absorbance at 360 nm was taken every 30 second for 60 min using GENios Plus Fluorimeter (Tecan). Kaleidagraph software (Synergy Software) and non-linear regression analysis was used to obtain $K_M$ and $V_{max}$ values from the Michaelis-Mentor equation ($v = V_{max}*(S)/(K_M + (S))$, where $v$= rate of the reaction and (S)= substrate concentration). $k_{cat}$ was calculated by dividing $V_{max}$ by the concentration of PKA enzyme.

# APPENDIX A: CHAPTER 1

## 2.1 Compounds characterization
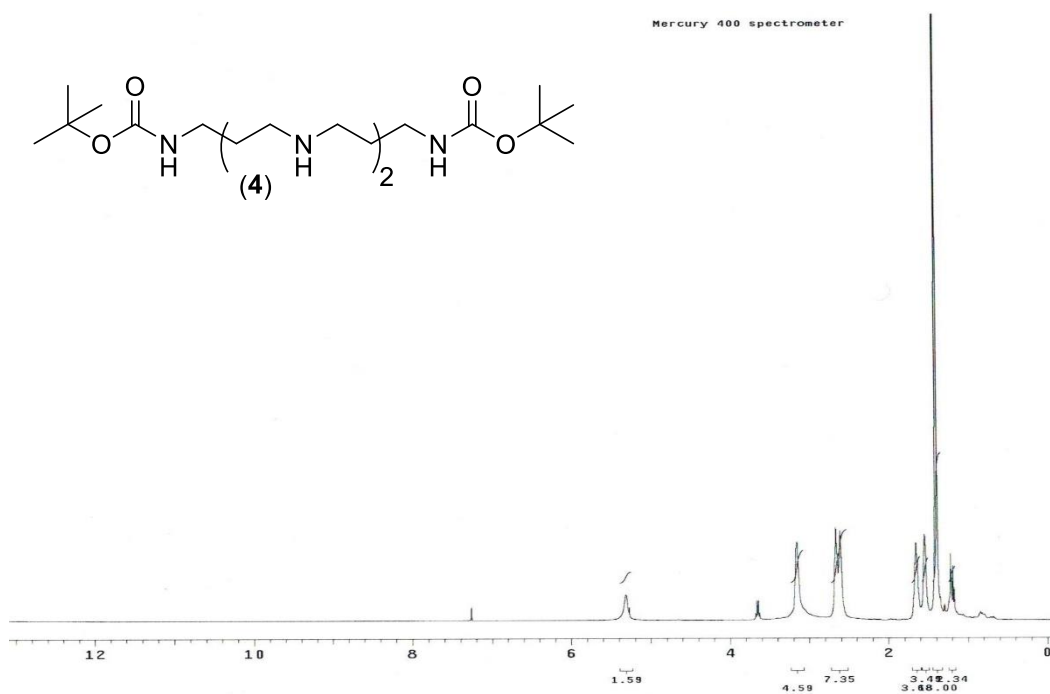


**Figure A 2.1:** $^1$H NMR of di-tert-butyl ((butane-1,4-diylbis(azanediyl))bis(propane-3,1-diyl))dicarbamate (**4**) in CDCl$_3$ at 400 MHz
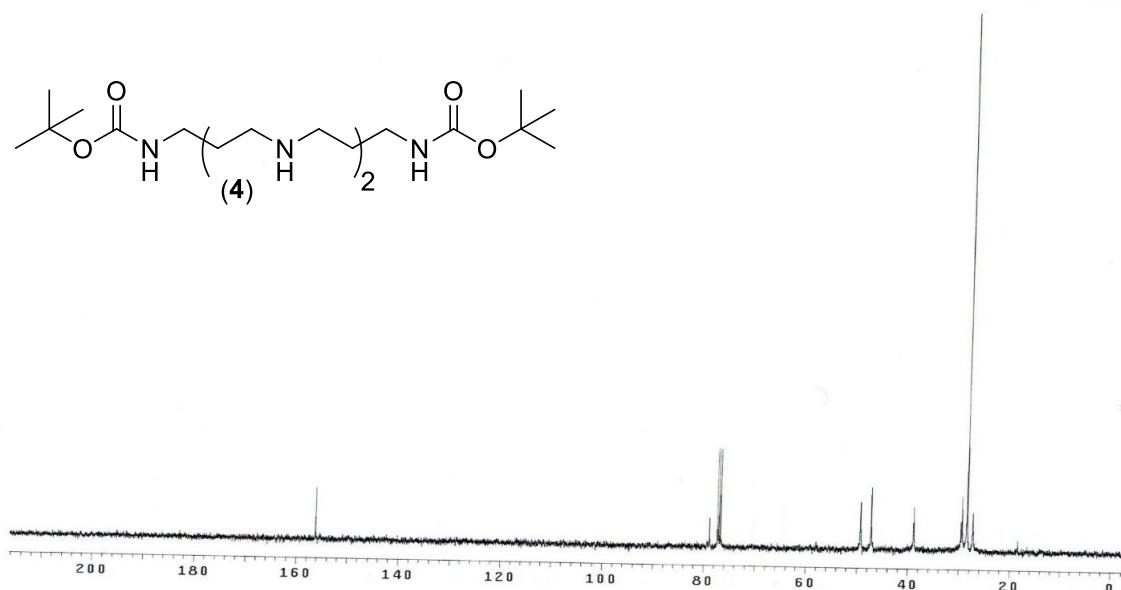


**Figure A 2.2:** $^{13}$C NMR of di-tert-butyl ((butane-1,4-diylbis(azanediyl))bis(propane-3,1-diyl))dicarbamate (**4**) in CDCl$_3$ at 400 MHz.
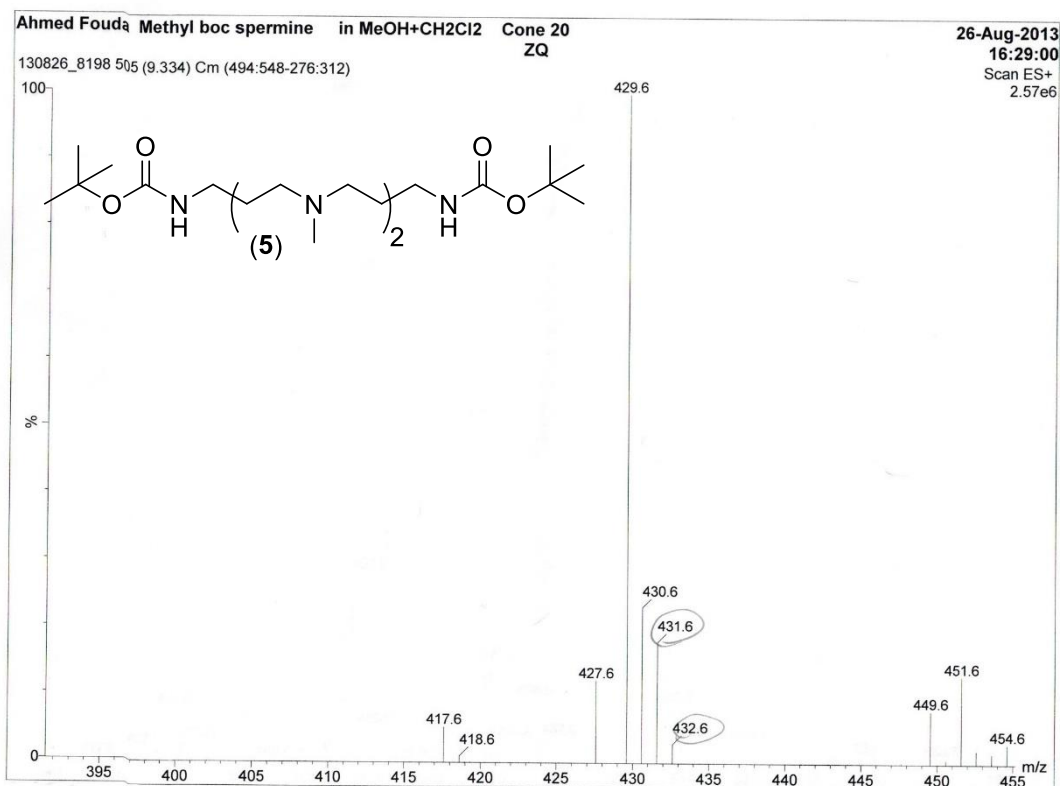
**Figure A 2.3:** Electrospray ionization (ESI) postive mode low resolution mass spectrum of di-tert-butyl ((butane-1,4-diylbis(methylazanediyl))bis(propane-3,1-diyl))dicarbamate (**5**) in methanol/methylene chloride. $(M+H)^+$ for $C_{22}H_{47}N_4O_4$: calc. 431.6, found 432.6
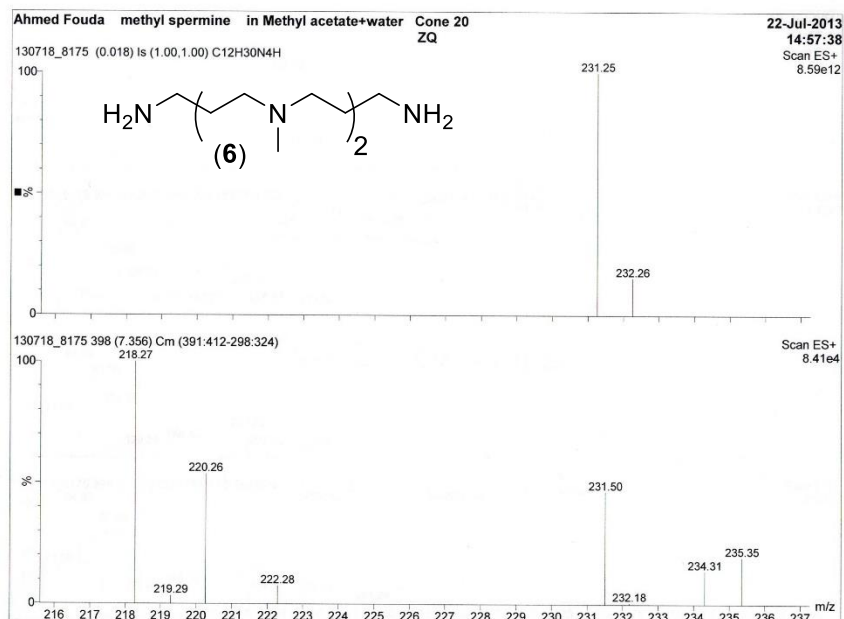


**Figure A 2.4:** Electrospray ionization (ESI) postive mode low resolution mass spectrum of N1,N1'-(butane-1,4-diyl)bis(N1-methylpropane-1,3-diamine) (**6**) in methanol/methylene chloride. $(M+H)^+$ for $C_{12}H_{31}N_4$: calc. 231.4, found 231.5
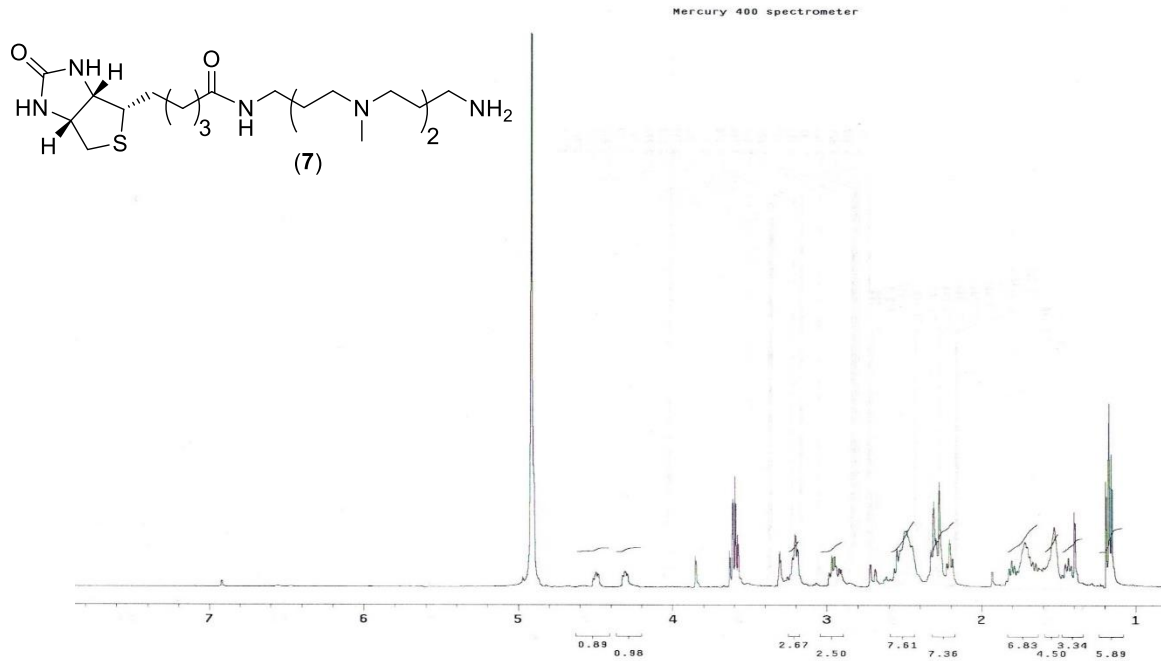
**Figure A 2.5:** $^1$H NMR of polyamine biotin (7) in CD$_3$OD at 400 MHz.
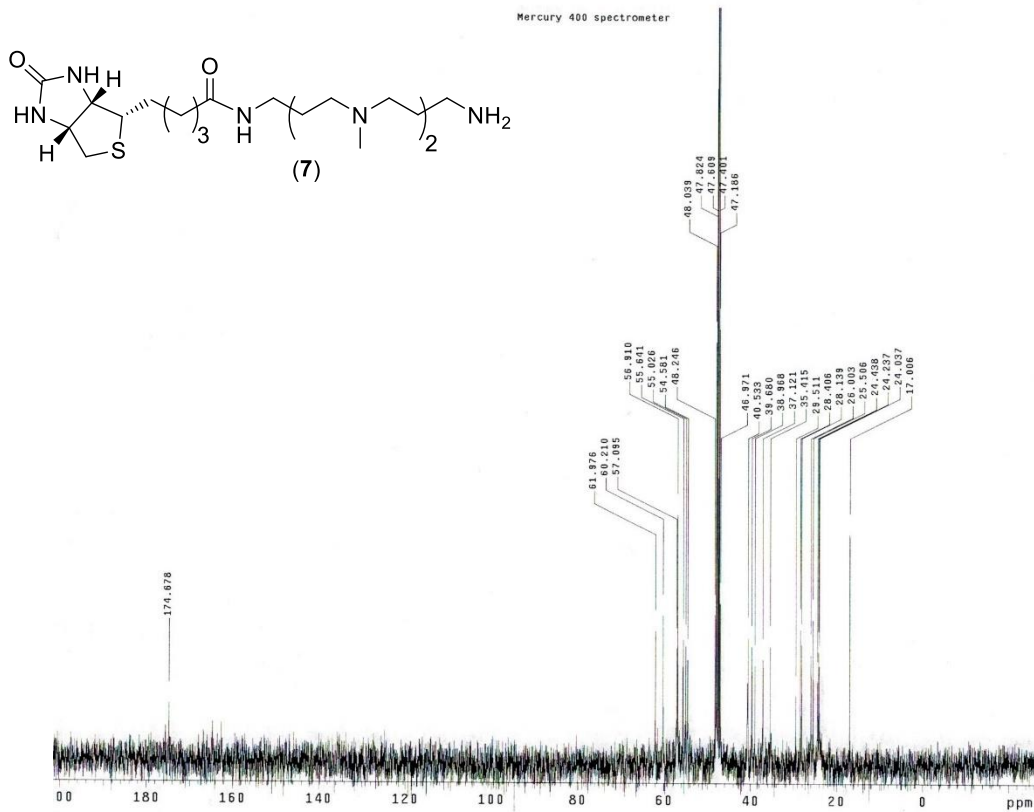


**Figure A 2.6:** $^{13}$C NMR of polyamine biotin (7) in CD$_3$OD at 100 MHz.
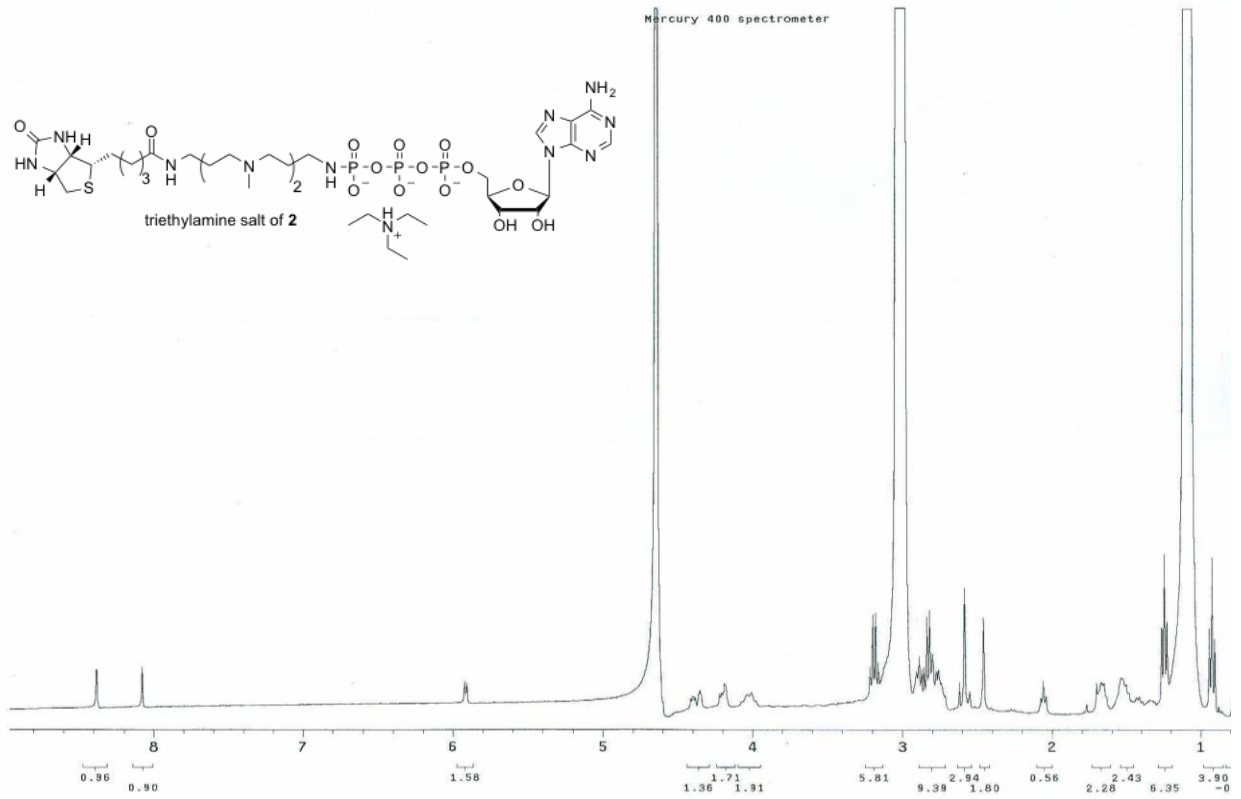
**Figure A 2.7:** ^{1}H NMR of the triethyl amine salt of ATP-polyamine-biotin (ABP) recorded in $D_2O$ at 400 MHz.
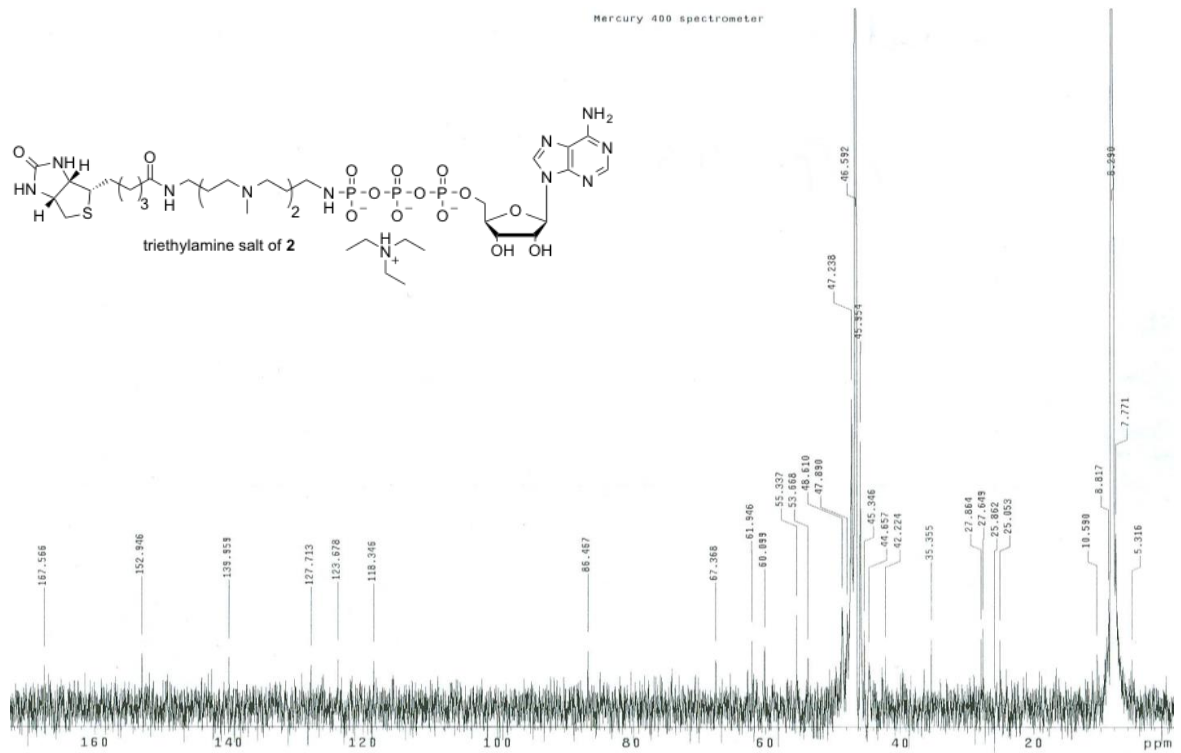
**Figure A 2.8:** ^{13}C NMR of the triethyl amine salt of ATP-polyamine-biotin (ABP) recorded in D$_2$O at 100 MHz.
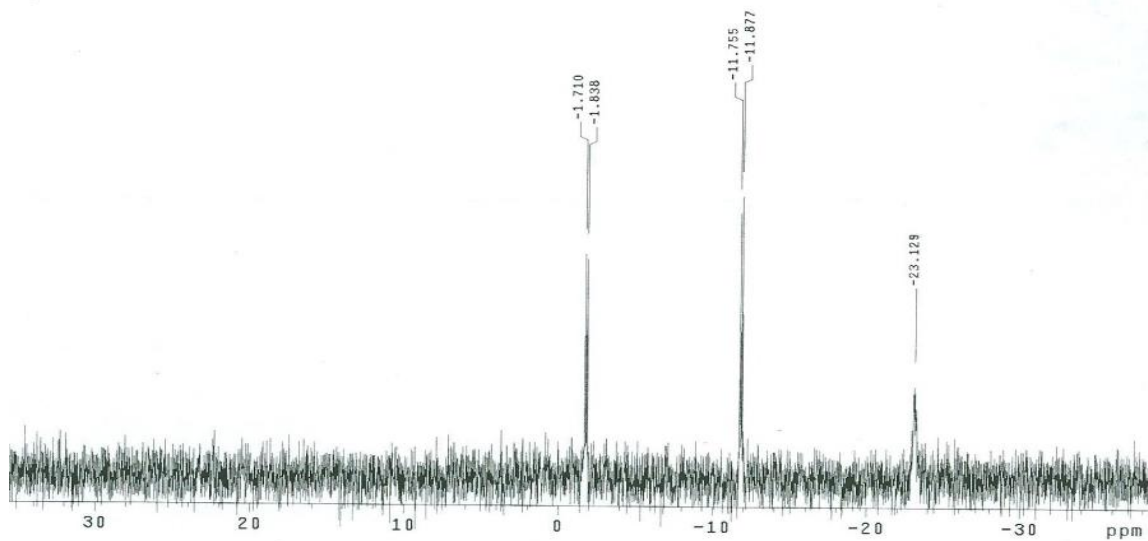


**Figure A 2.9:** ^{31}P NMR of the triethylamine salt of ATP-polyamine-biotin (ABP) recorded in D$_2$O at 162 MHz.
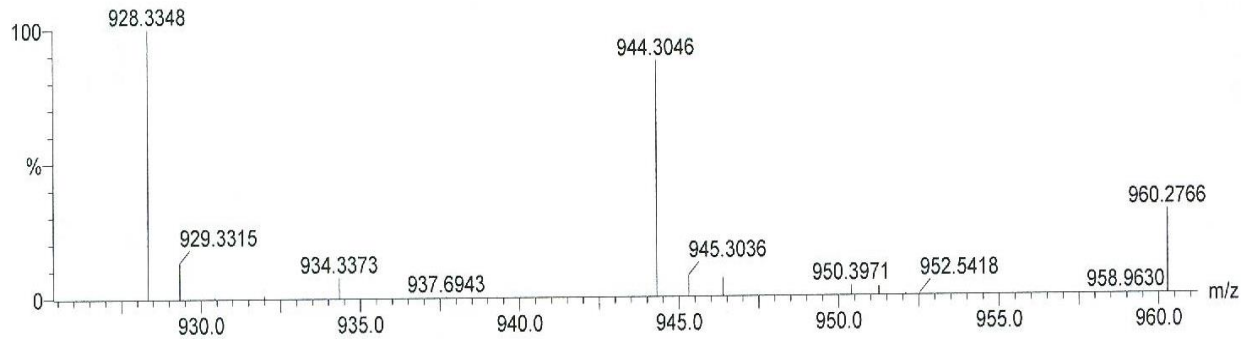
**Figure A 2.10:** Electrospray ionization (ESI) negative mode high resolution mass spectrum (HRMS) of ATP-polyamine-biotin (ABP) recorded in acetonitrile. Calculated (M-H)$^{-1}$ for $C_{32}H_{58}N_{11}O_{14}P_3S$: 944.3098; Observed: 944.3046
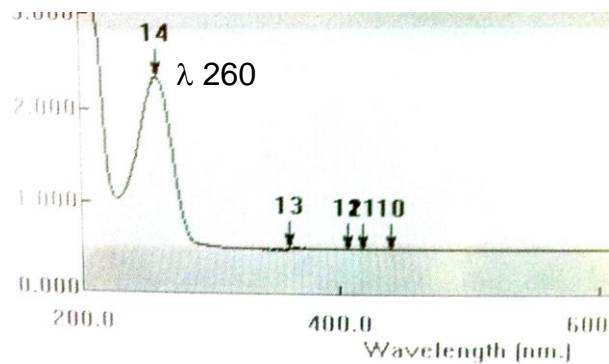


**Figure A 2.11:** UV-VIS spectrum of ATP-polyamine-biotin (ABP) recorded in water. The ABP absorbance appears at $\lambda$ 260 nm

**Auto-Scaled Chromatogram**
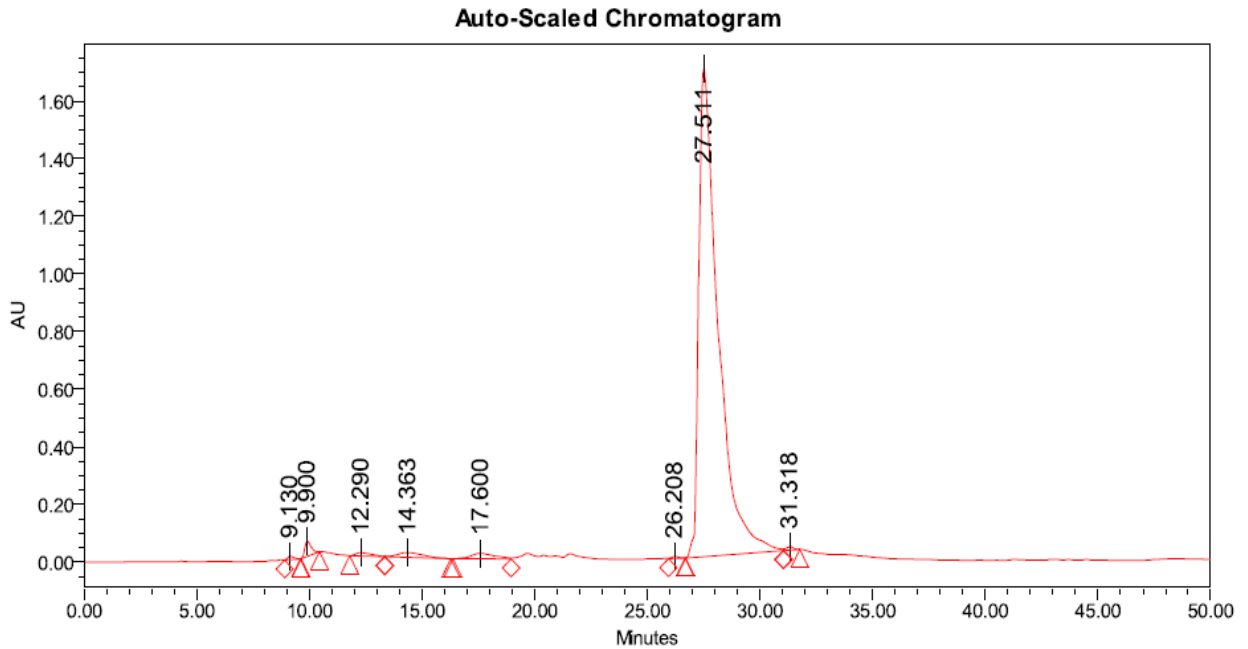


## Peak Results

|   | RT | Area | Height | % Area |
|---|---|---|---|---|
| 1 | 9.130 | 227259 | 11719 | 0.21 |
| 2 | 9.900 | 1065184 | 52685 | 1.00 |
| 3 | 12.290 | 558650 | 11098 | 0.53 |
| 4 | 14.363 | 1320540 | 16439 | 1.24 |
| 5 | 17.600 | 1390379 | 19014 | 1.31 |
| 6 | 26.208 | 145197 | 6432 | 0.14 |
| 7 | 27.511 | 101123948 | 1693568 | 95.31 |
| 8 | 31.318 | 264478 | 11226 | 0.25 |

**Figure A 2. 12:** HPLC analysis of ATP-polyamine-biotin (ABP) purity. ATP-polyamine-biotin appears at 27.511 minutes and is 95% pure.
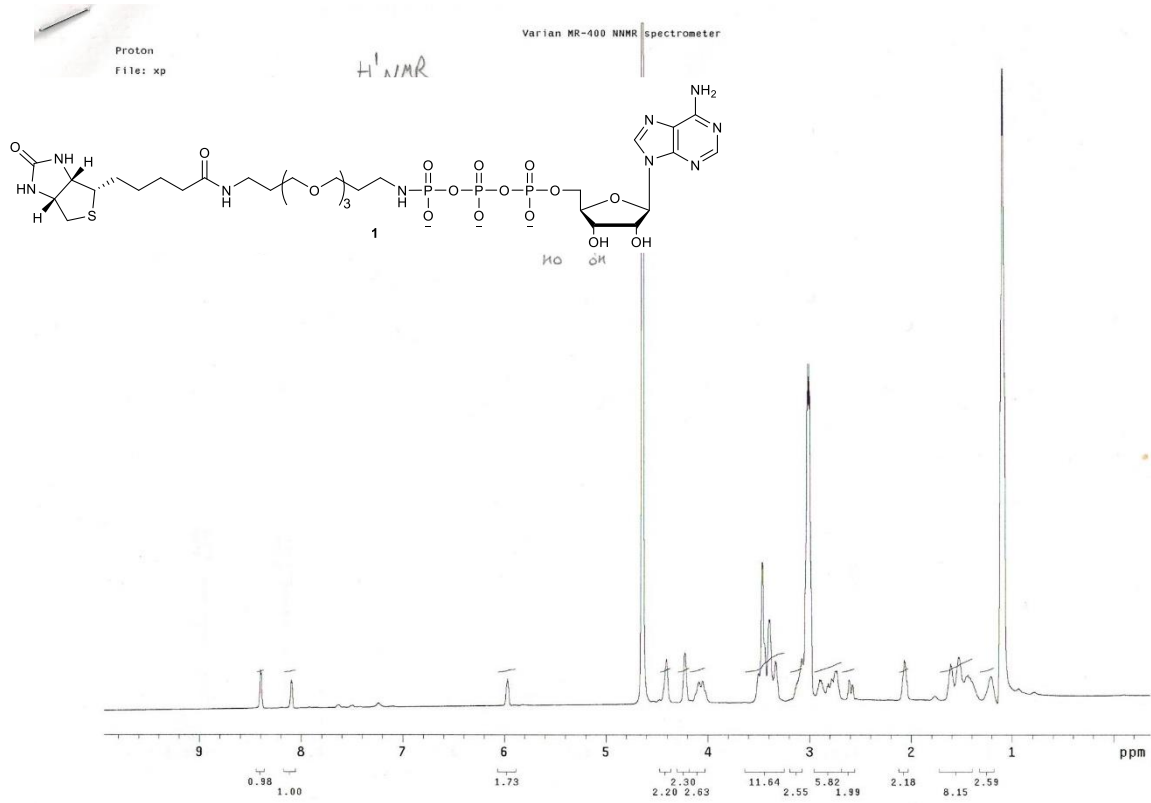
**Figure A 2. 13:** $^1$HNMR of ATP-biotin (1)
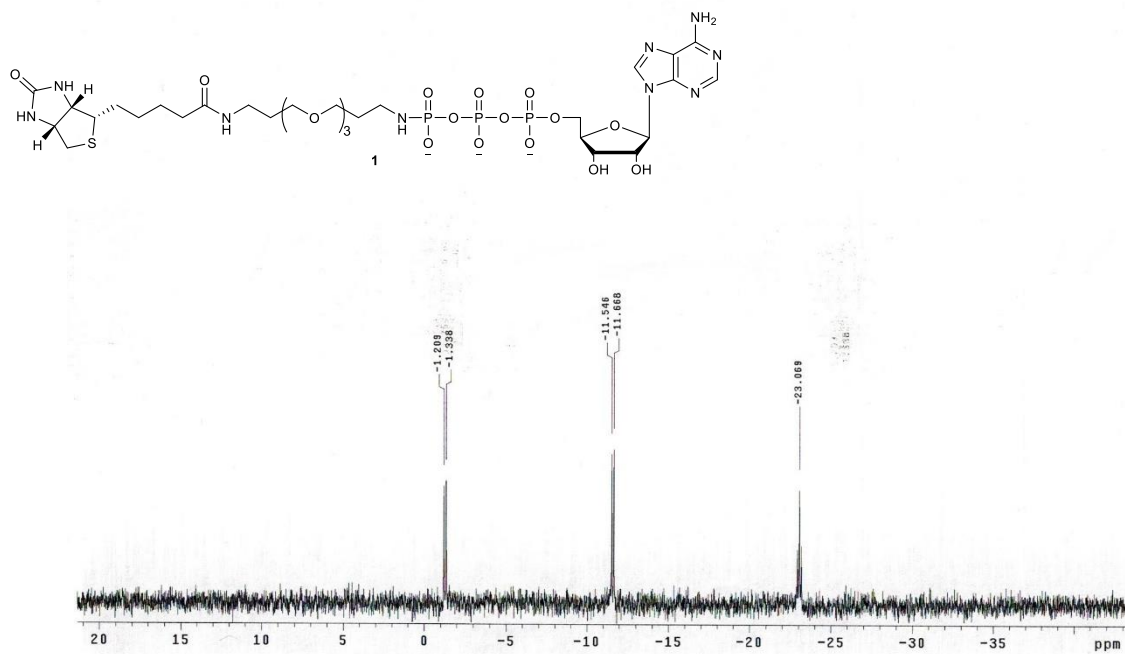


**Figure A 2. 14:** $^{31}$PNMR of ATP-biotin (1)
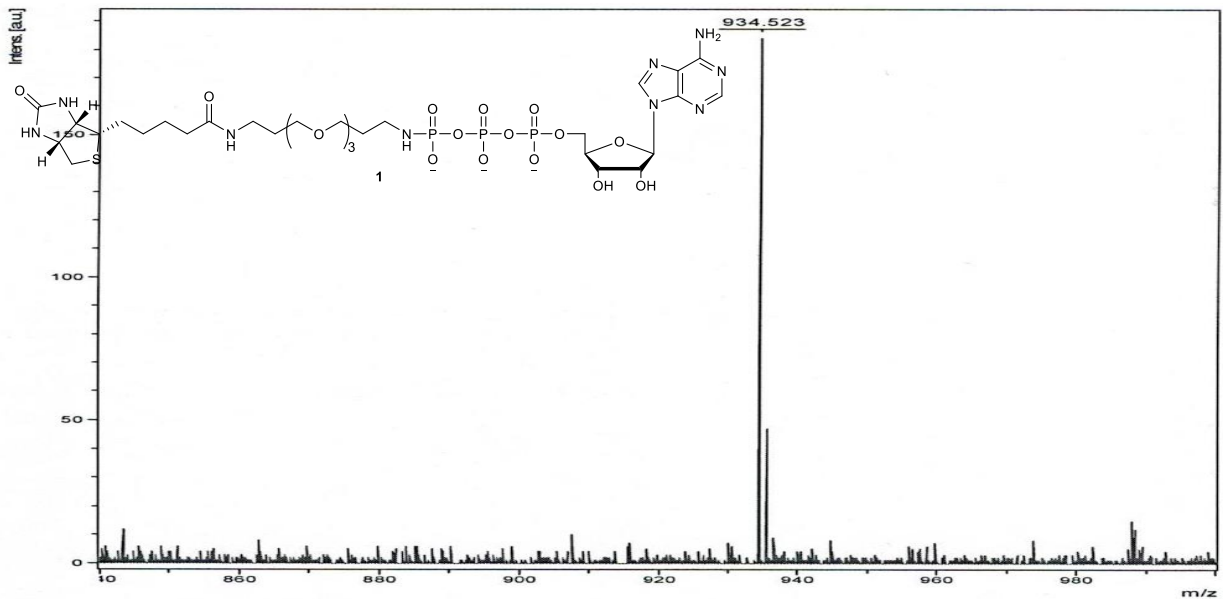
**Figure A 2. 15:** MALDI-TOF of ATP-biotin (1). (M-H)⁻ for $C_{30}H_{51}N_9O_{17}P_3S$: calc. 934.234, found 934.523.
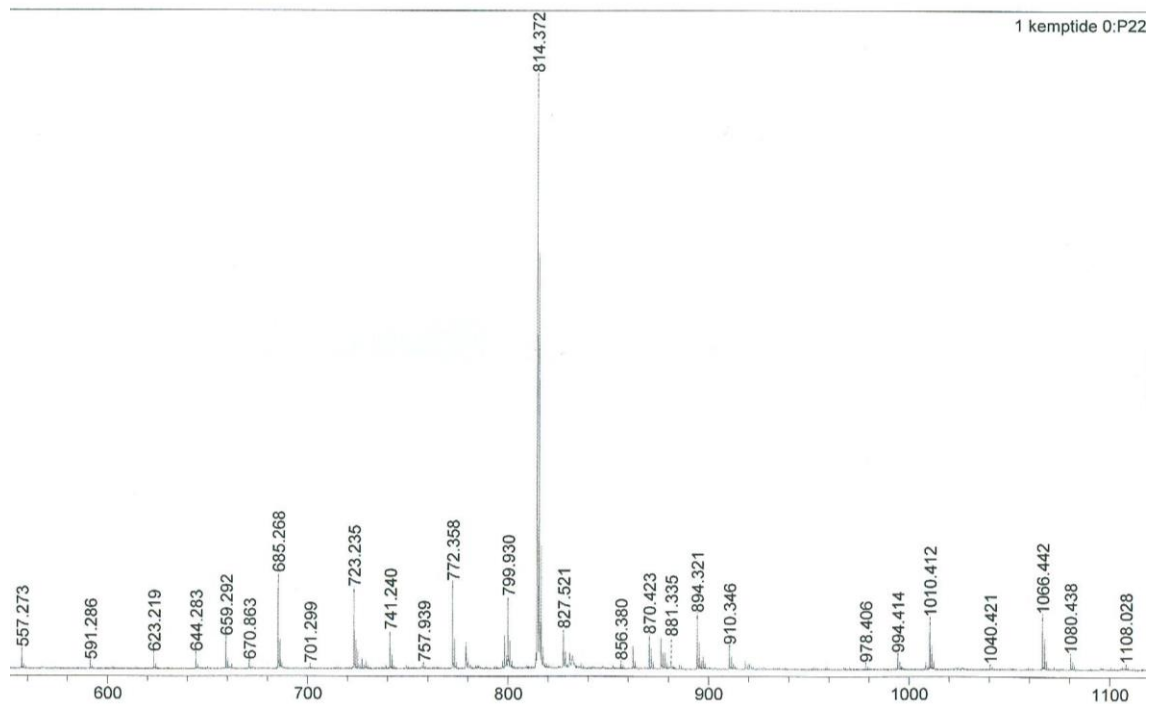


**Figure A 2. 16:** MALDI-Tof positive mode of N-acetylated kemptide peptide (AcLRRASLG). Calculated (M+H)$^{+1}$ for $C_{34}H_{63}N_{13}O_{10}^+$: 814.4894; Observed: 814.372

## 2.2 Repetitive trials of MBP labeling with APB

**Trial 1**



| | | | | | | | | |
|---|---|---|---|---|---|---|---|---|
| | 1 | 2 | 3 | 4 | 5 | 6 | 7 | 8 |
| MBP | + | + | + | + | + | + | + | + |
| PKA | - | + | - | + | + | - | + | + |
| ATP | - | + | - | - | - | - | - | - |
| APB | - | - | + | + | + | - | + | + |
| 50% TFA | - | - | - | - | + | - | - | - |
| STSP | - | - | - | - | - | - | - | + |

**Trial 2**



| | | | | | | | | |
|---|---|---|---|---|---|---|---|---|
| | 1 | 2 | 3 | 4 | 5 | 7 | 8 | 9 |
| MBP | + | + | + | + | + | + | + | + |
| PKA | - | + | - | + | + | - | + | + |
| ATP | - | + | - | - | - | - | - | - |
| APB | - | - | + | + | + | - | + | + |
| 50% TFA | - | - | - | - | + | - | - | - |
| STSP | - | - | - | - | - | - | - | + |
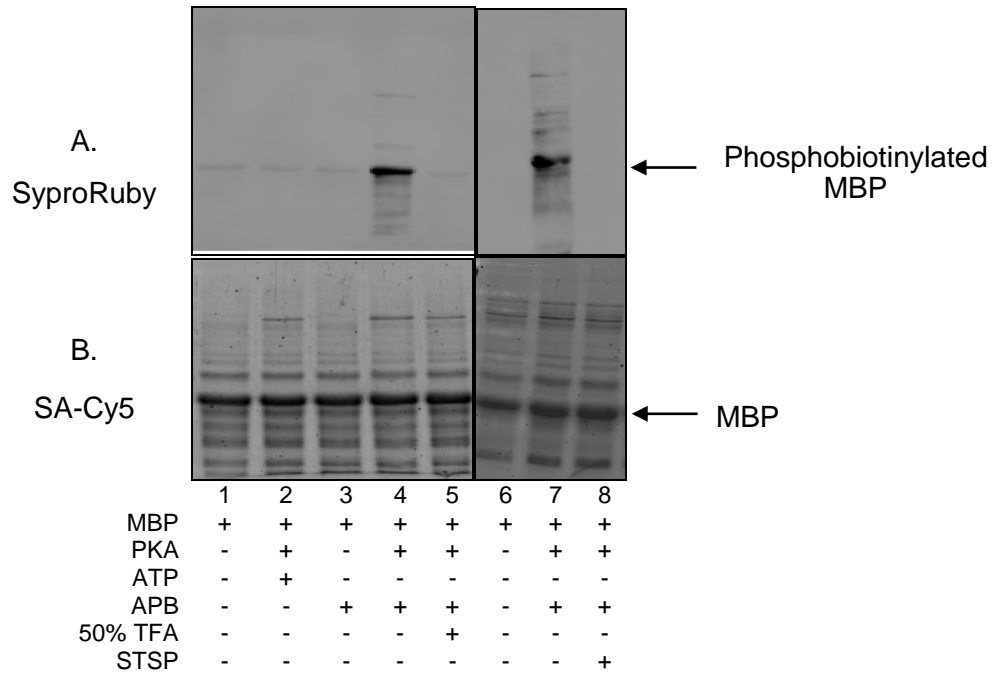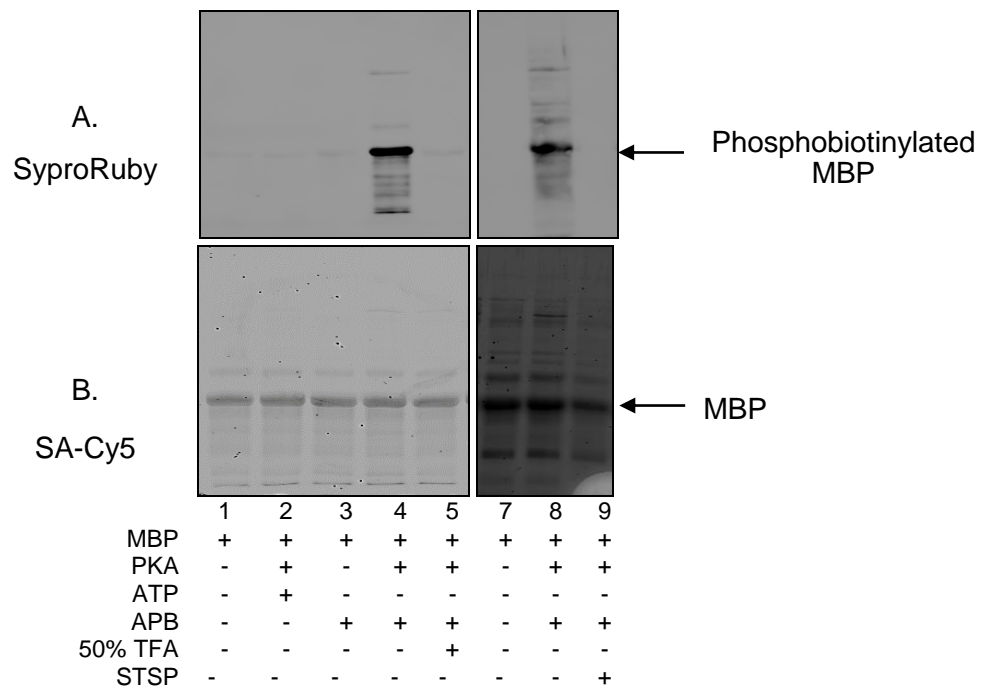
**Trial 3**
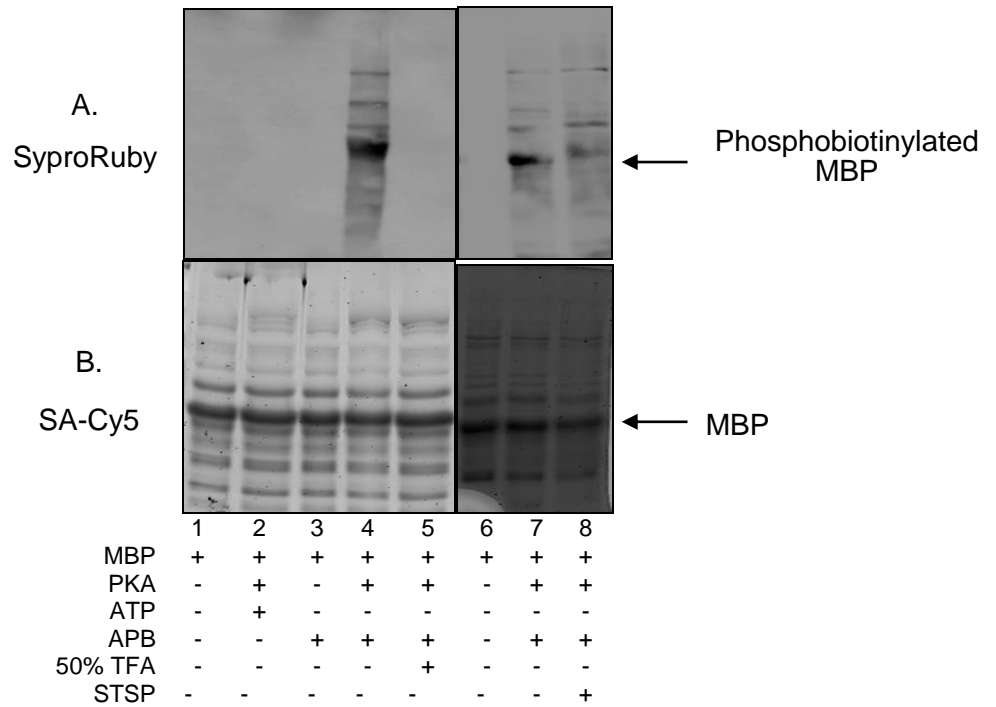


**Figure A 2.17:** Full gel images of kinase-catalyzed biotinylation with MBP, PKA, and APB. MBP was incubated with APB and PKA in the manufacture provided buffer. As a control, TFA (50%) was added after biotinylation labeling to assure biotinylation via an acid-labile phosphoramidate bond (lane 5). A kinase inhibitor, staursporine (STSP) was preincubated with PKA to confirm biotinylation via a kinase-catalyzed reaction (lane 8). The labeled mixtures were separated by SDS-PAGE and visualized by SYPRO® Ruby to see total proteins (A) or streptavdin Cy-5 (SA-Cy5, Life Technologies) to detect biotinylation (B). The images are representative of at least three independent trials.

## 2.3 Repetitive trials of Kemptide modification with APB

## Trial 2
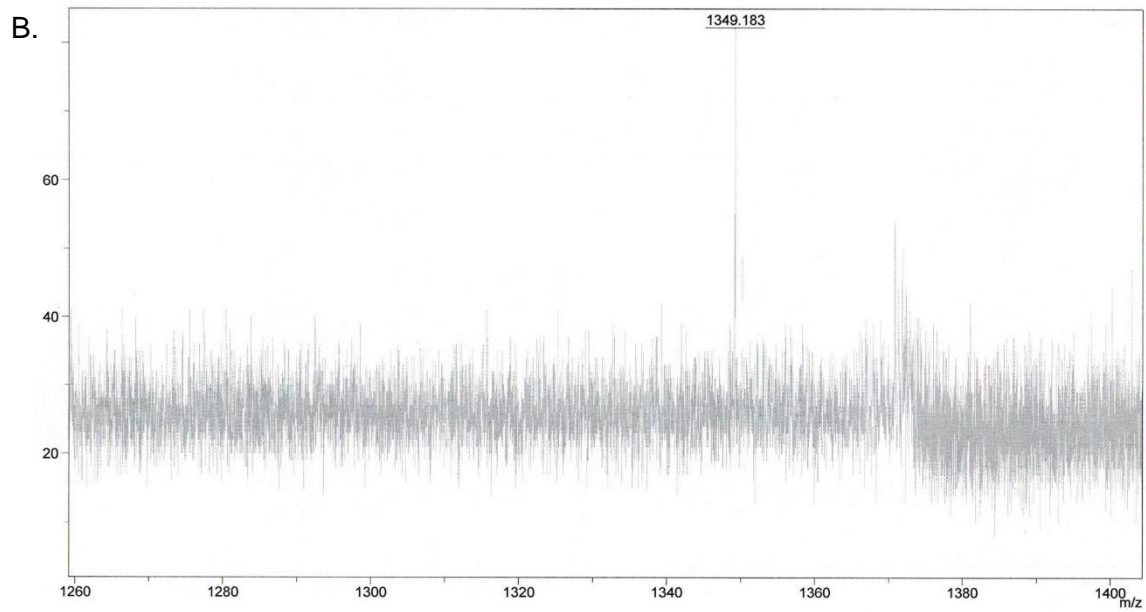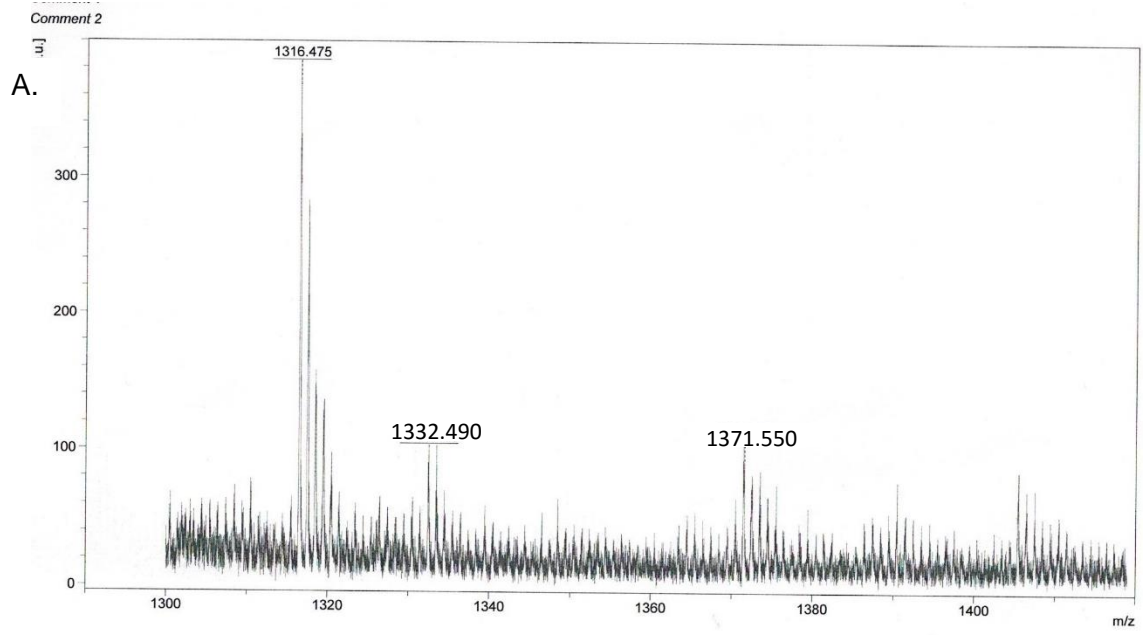
**Trial 3**
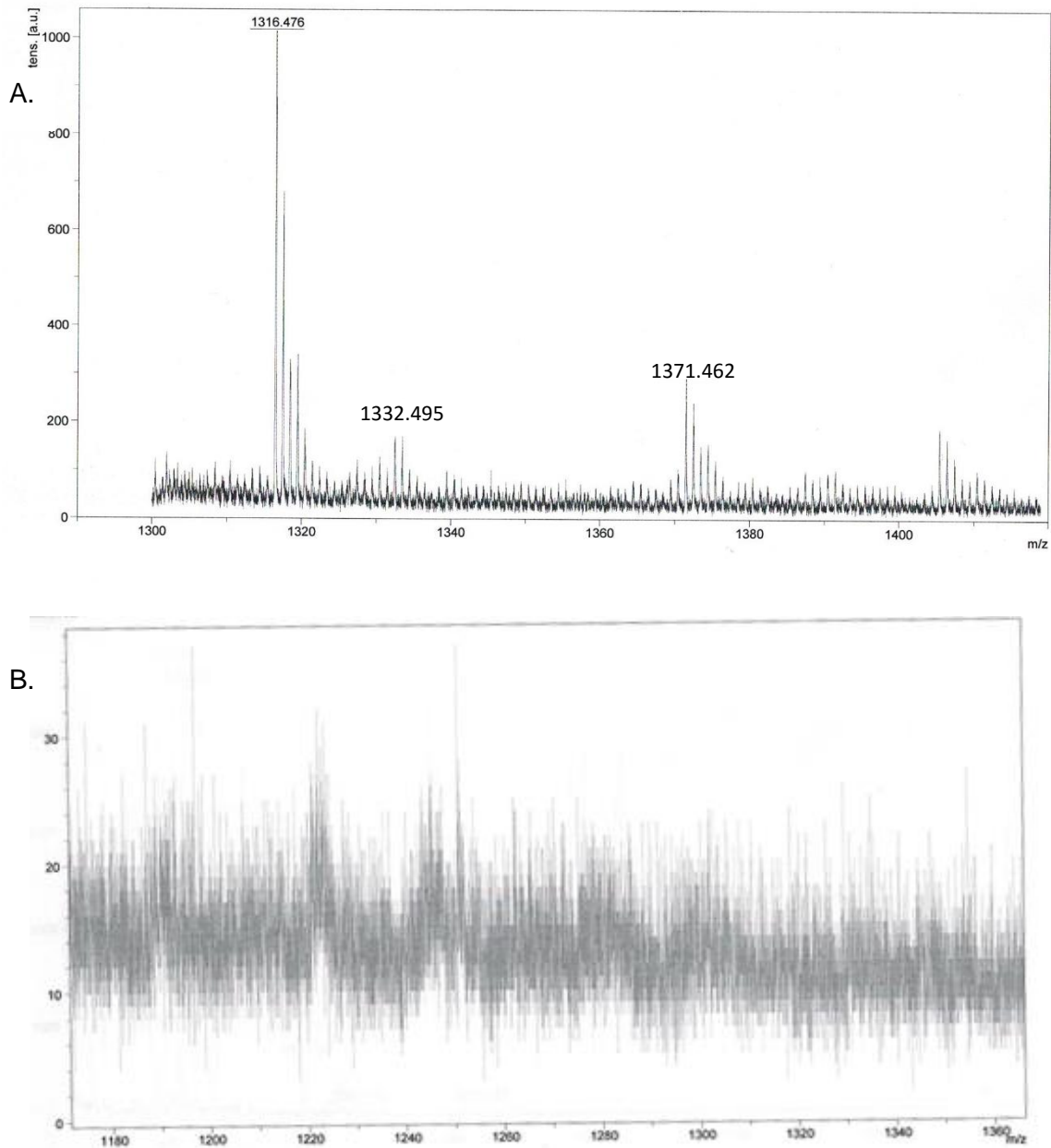


**Figure A 2.18:** Repetitive trials of MALDI-TOF spectra of a kinase-catalyzed phosphobiotinylation reaction of N-acetylated kemptide with PKA in positive ion mode. A) Reaction in the presence of APB: ((M+H)$^+$ for $C_{56}H_{107}N_{19}O_{14}PS$, Calculated: 1332.7698; Observed: 1332.490 and 1332.495 respectively for repetitive independent trials ; (M+K) $^+$ for $C_{56}H_{106}KN_{19}O_{14}PS$, Calculated: 1371.7151; Observed: 1371.550 and 1371.462 respectively for repetitive trials B) Reaction in the absence of APB showing no product peaks in the same m/z range.

## 2.4 Repetitive trials of quantification of phosphorylation of MBP using APB

**Trials 1 and 2**
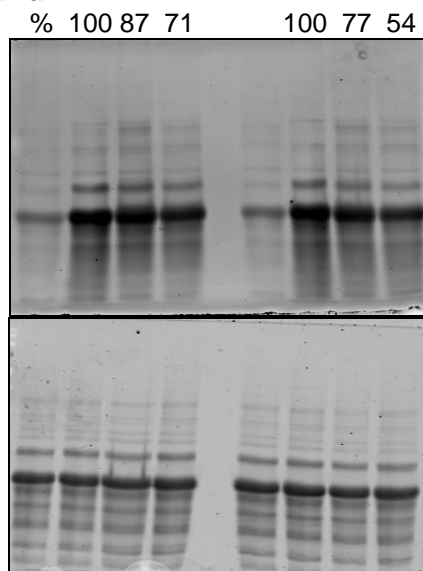


| | 1 | 2 | 3 | 4 | 5 | 6 | 7 | 8 |
|---|---|---|---|---|---|---|---|---|
| MBP | + | + | + | + | + | + | + | + |
| PKA | + | + | + | + | + | + | + | + |
| ATP | - | + | - | - | - | + | - | - |
| ATP-biotin | - | - | + | - | - | - | + | - |
| APB | - | - | - | + | - | - | - | + |

**Trials 3 and 4**
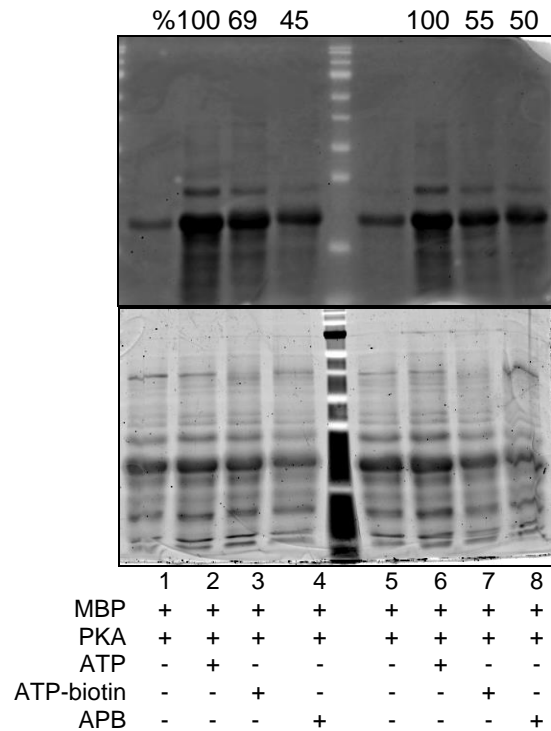


**Figure A 2.19:** Full gel images of quantitative analysis of MBP phosphorylation in presence of PKA with either ATP, ATP-biotin **1**, or APB **2**. The reaction mixtures were separated by SDS-PAGE and visualized by SYPRO® Ruby stain (top gel) to ensure homogeneity of protein loading in all lanes or ProQ diamond stain (bottom gel) to detect phosphorylation of MBP. MBP degree of phosphorylation was quantified from the ProQ diamond stained gel (bottom gel) and the percentage of phosphorylation was calculated by comparison with phosphorylation with ATP (100%). The quantitative analysis is a representation of at least three independent trials.

## 2.5 Repetitive trials of biotinylation of HeLa cell lysates with APB and ATP-biotin

**Trial 2**

**Trial 3**



| | 1 | 2 | 3 | 4 | | 5 | 6 | 7 |
|---|---|---|---|---|---|---|---|---|
| HCL | + | + | - | + | | + | - | + |
| HDL | - | - | + | - | | - | + | - |
| NHS-biotin | - | + | - | - | | - | - | - |
| APB | - | - | + | + | | + | - | - |
| 50% TFA | - | - | - | - | | + | - | - |
| ATP-biotin | - | - | - | - | | - | + | + |

| | 1 | 2 | 3 | 4 | | 5 | 6 | 7 |
|---|---|---|---|---|---|---|---|---|
| HCL | + | + | - | + | | + | - | + |
| HDL | - | - | + | - | | - | + | - |
| NHS-biotin | - | + | - | - | | - | - | - |
| APB | - | - | + | + | | + | - | - |
| 50% TFA | - | - | - | - | | + | - | - |
| ATP-biotin | - | - | - | - | | - | + | + |
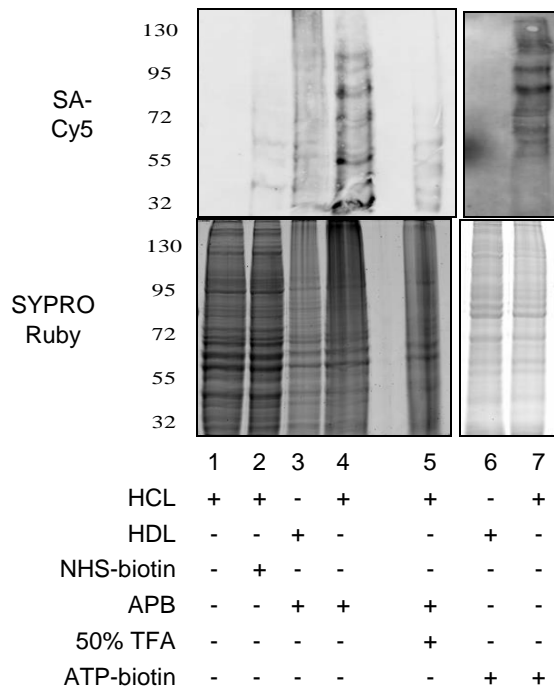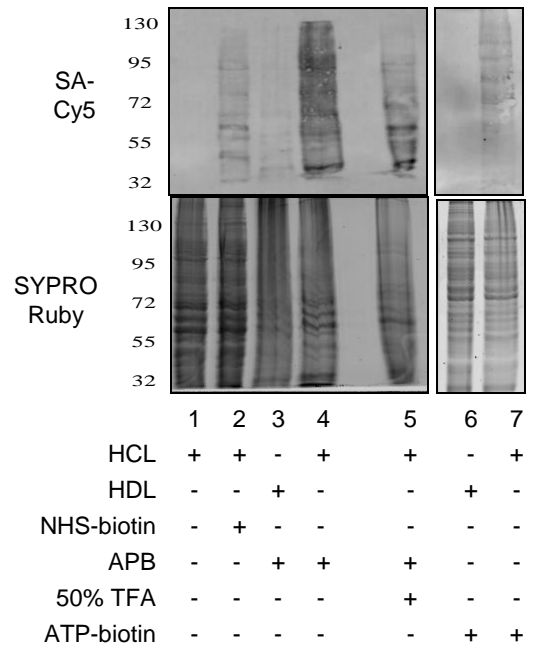
**Figure A2.20:** Kinase-catalyzed biotinylation of HeLa cell lysates (HCL) or heat-inactivated HeLa cell lysates (HDL) with APB and ATP-biotin. Acid (50% trifluoroacetic acid final concentration) was added after biotin labeling to cleave the biotin tag (lane 5). NHS-biotin was used to assess nonspecific biotinylation. Reaction mixture were separated by SDS-PAGE and visualized with streptavidin-Cy5 (SA-Cy5, top gel) or SYPRO® Ruby total protein stain (bottom gels). The third independent trial is shown in Figure 2.11.

## 2.6 Repetitive trials of direct fluorescence imaging of APB in HeLa cells

**Trial 2:**

DAPI                SA-Cy5

Untreated

ATP

ATP-biotin

APB

**Trial 3:**

DAPI　　　　　SA-Cy5



Untreated

ATP

ATP-
biotin

APB
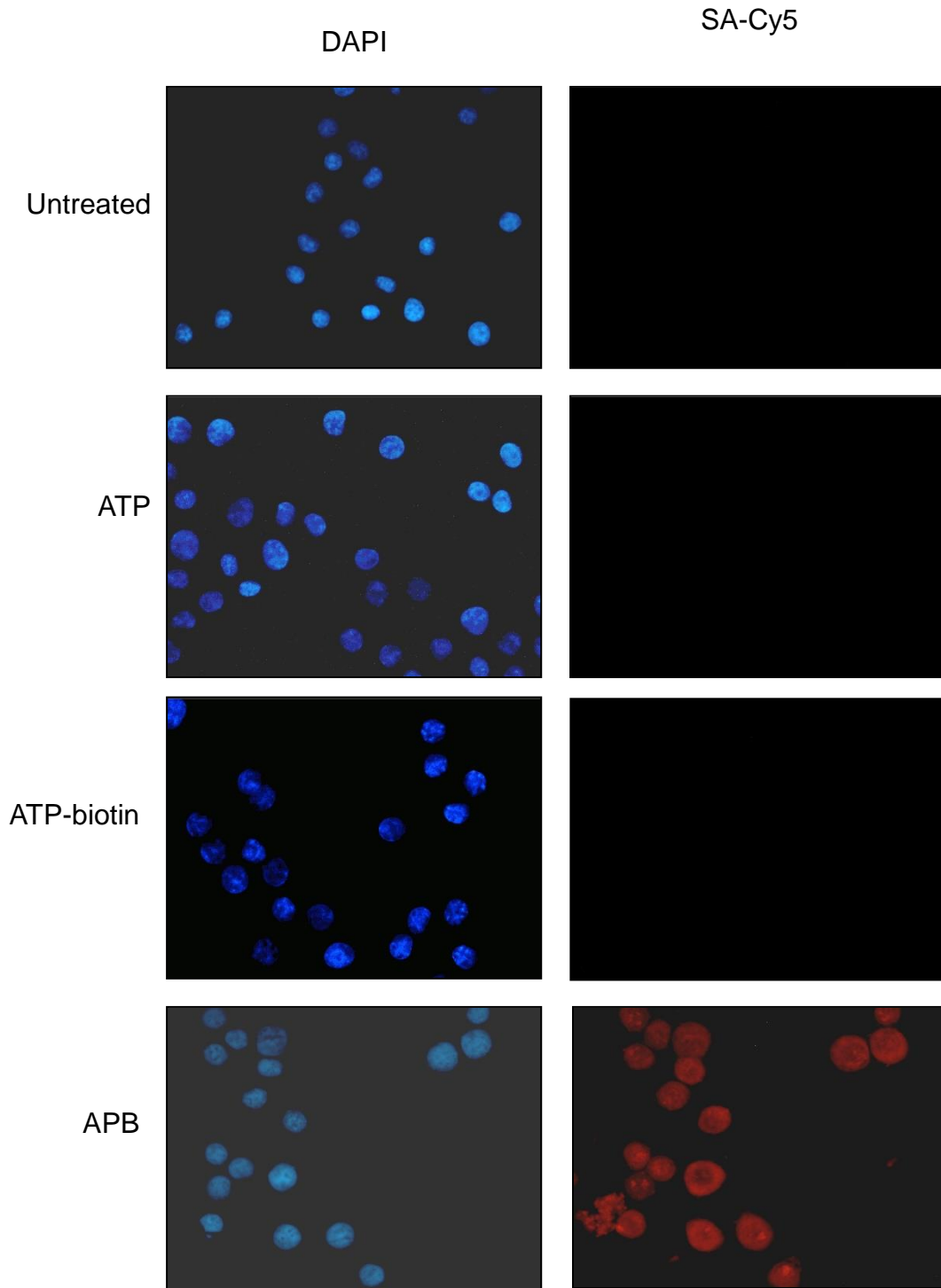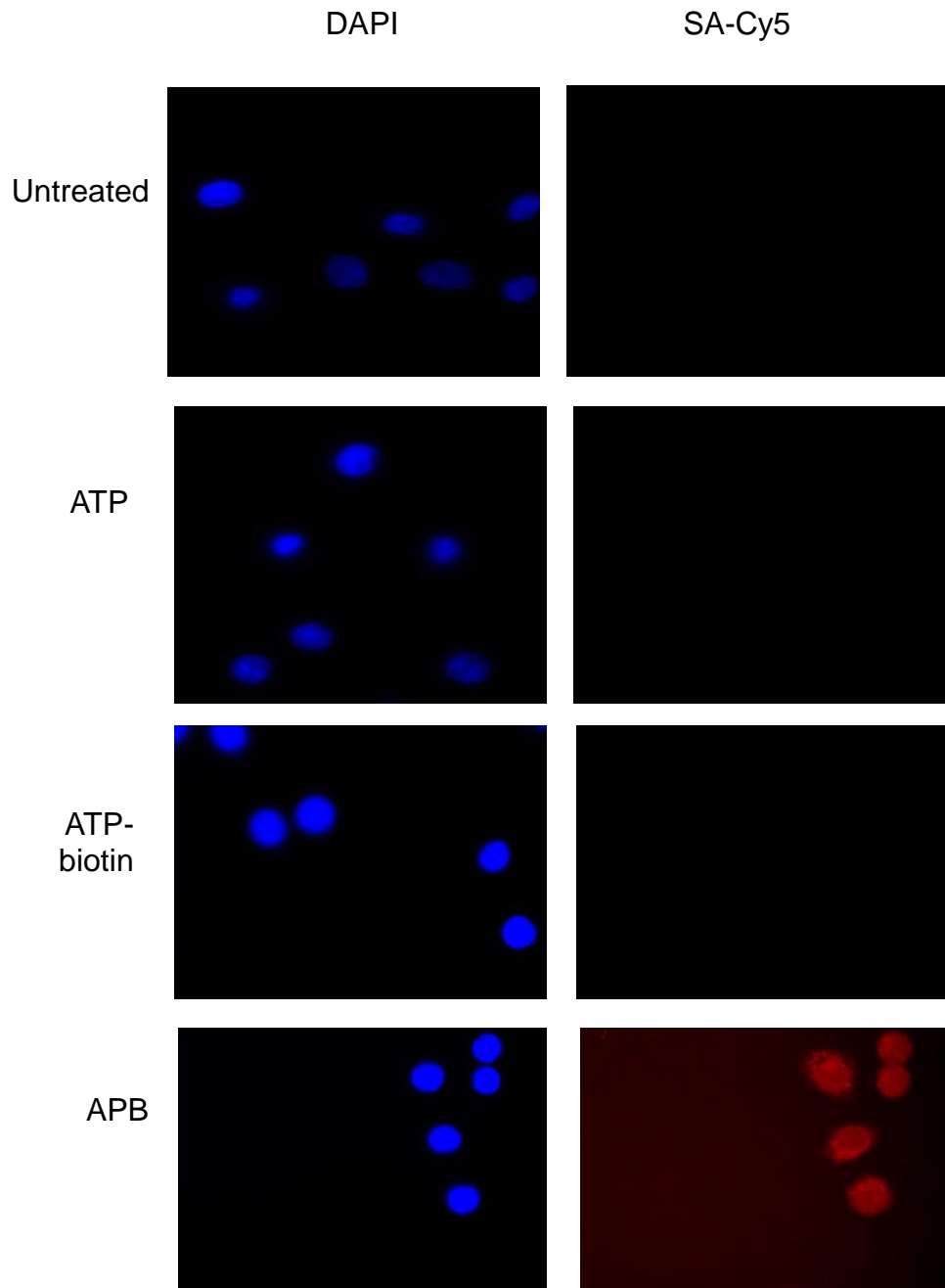
**Figure A 2.21:** Microscopy studies of ATP-biotin or APB cell permeability. HeLa cells were untreated or treated with ATP, ATP-biotin or APB before visualization with the nuclear stain DAPI or biotin stain streptavidin-Cy5 (SA-Cy5).  The third independent trial is shown in figure 2.13

## 2.7 Repetitive trials of *in cellulo* kinase-catalyzed biotinylation using APB

**Trial 2**

**Trial 3**



| | 1 | 2 | 3 | 4 |
|---|---|---|---|---|
| Hela cells | + | + | + | + |
| ATP biotin | - | + | - | - |
| APB | - | - | + | + |
| STSP | - | - | + | - |

| | 1 | 2 | 3 | 4 |
|---|---|---|---|---|
| Hela cells | + | + | + | + |
| ATP biotin | - | + | - | - |
| APB | - | - | + | + |
| STSP | - | - | + | - |
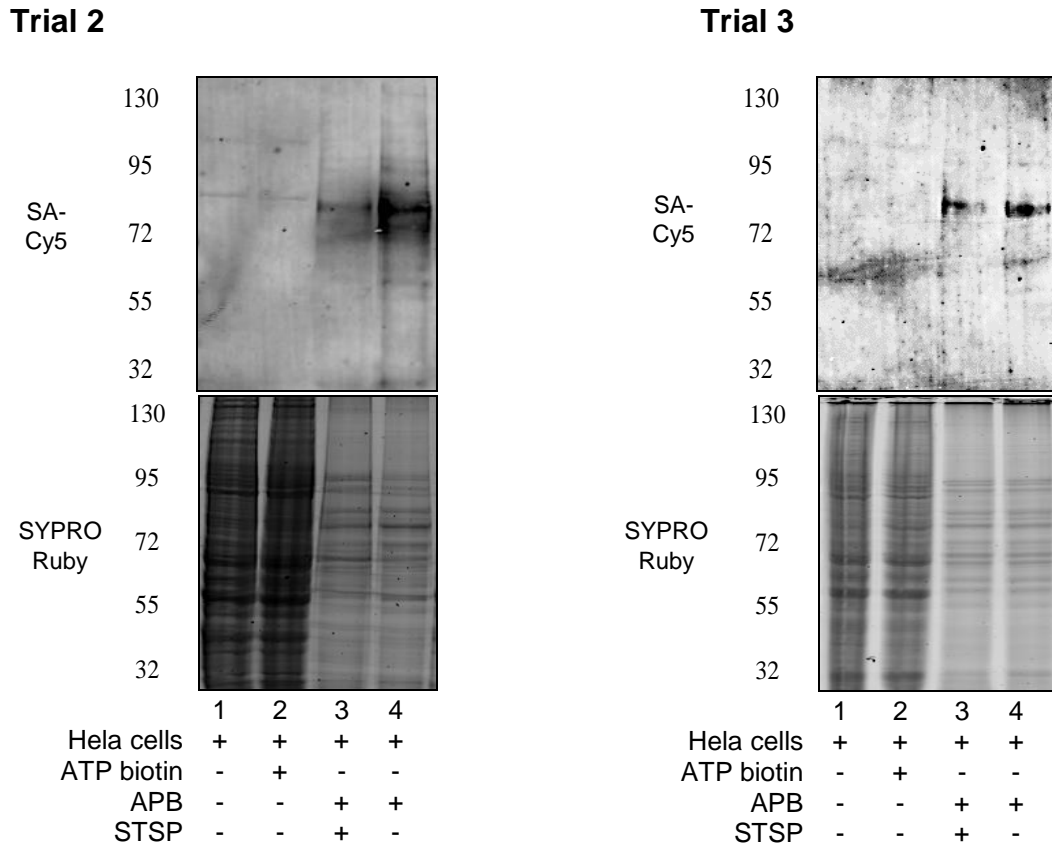
**Figure A 2.22:** *In cellulo* kinase-catalyzed biotinylation with ATP-biotin or APB in HeLa cells. As a control, kinase inhibitor staurosporine (STSP) was pre-incubated with cells to prevent kinase catalysis (lane 3). Reaction mixtures (A and C) were separated by SDS-PAGE and visualized with streptavidin-Cy5 (SA-Cy5, top gel) or SYPRO® Ruby total protein stain (bottom gels). The gels are representative of at least three independent trials.

## 2.8 Cell viability assay of APB

A)



| y = 100/(1+(x/EC50)^n) | | |
|---|---|---|
| | Value | Error |
| EC50 | 0.019 | 0.00087 |
| n | 2 | 0.22 |
| Chisq | 60 | NA |
| R | 0.99 | NA |

B)
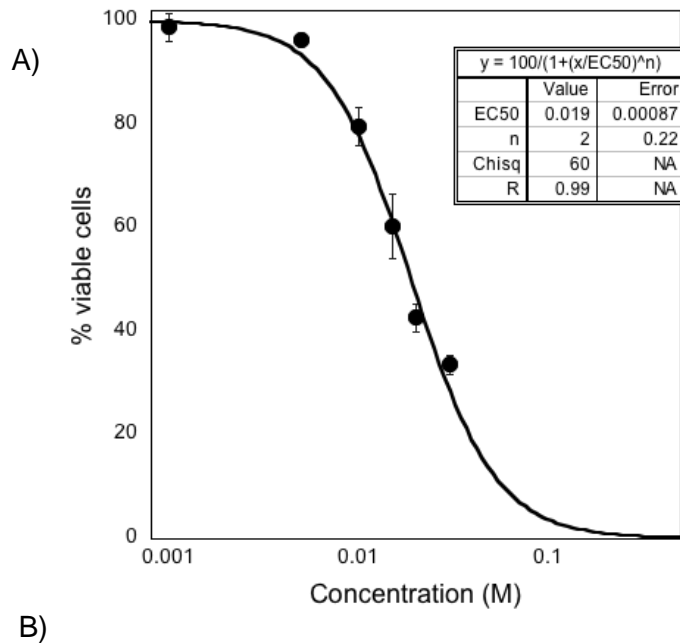
| Concentration (mM) | % cell viability |
|---|---|
| 0.0 | 100% |
| 1.0 | $99 \pm 3$ % |
| 5.0 | $96 \pm 1$ % |
| 10 | $80 \pm 4$ % |
| 15 | $60 \pm 6$ % |
| 20 | $43 \pm 3$ % |
| 30 | $34 \pm 2$ % |

**Figure A 2.23:** Cell viability assays with varying concentrations of APB. A) Dose response curve of APB with 1, 5, 10, 15, 20, 30 mM final concentrations. The $EC_{50}$ of APB is $19 \pm 1$. B) Table with the percentage viability data plotted in part A. The concentration of APB used in kinase-catalyzed labeling of cells was 5 mM.

# APPENDIX B: CHAPTER 2

## 3.1 Repetitive trial of direct fluorescence imaging of ATP-biotin/DC complex
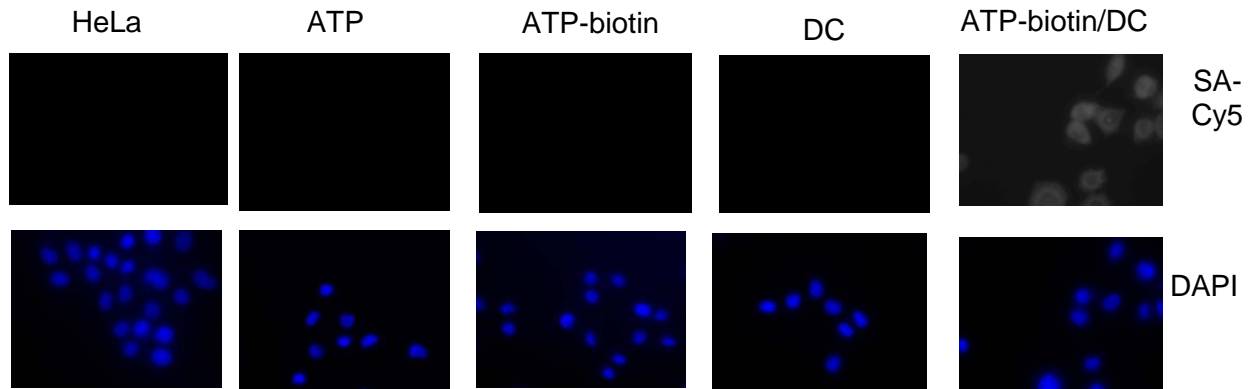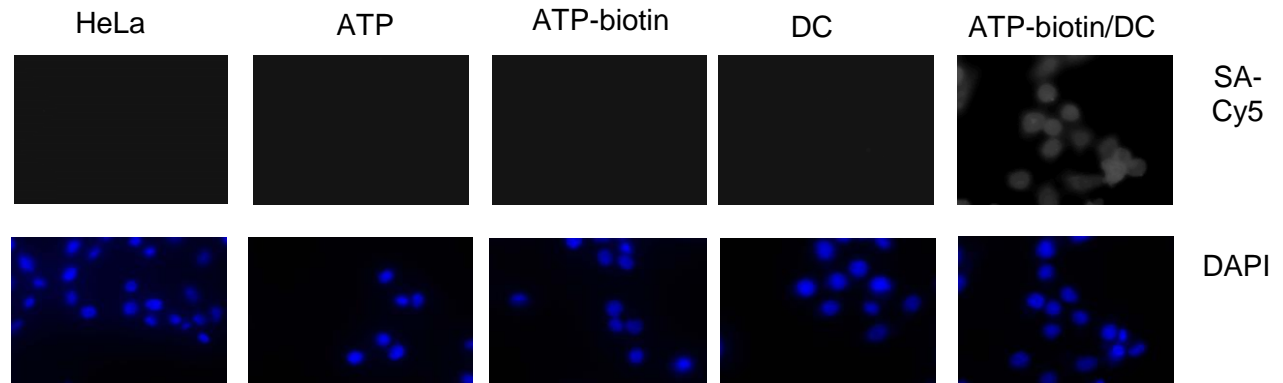
**Trial 2:**



**Trial 3:**



**Figure A 3. 1:** Repetitive trials of Fluorescence microscopy of ATP-biotin/DC complex. HeLa cells were incubated with ATP, ATP-biotin, DC, or the ATP-biotin/DC complex, followed by washing, fixing, permeabilizing, and Cells visualization with Streptavidin Cy5 (Top) and DAPI (bottom).

## 3.2 Repetitive trial of in cellulo MALDI-TOF analysis of ATP-biotin/DC complex
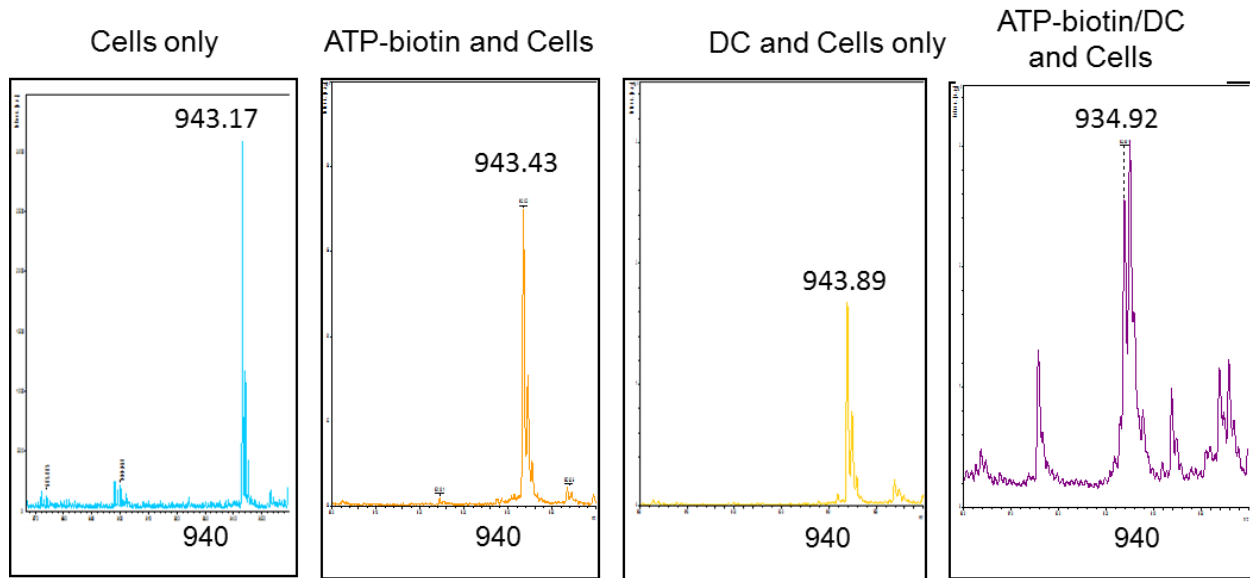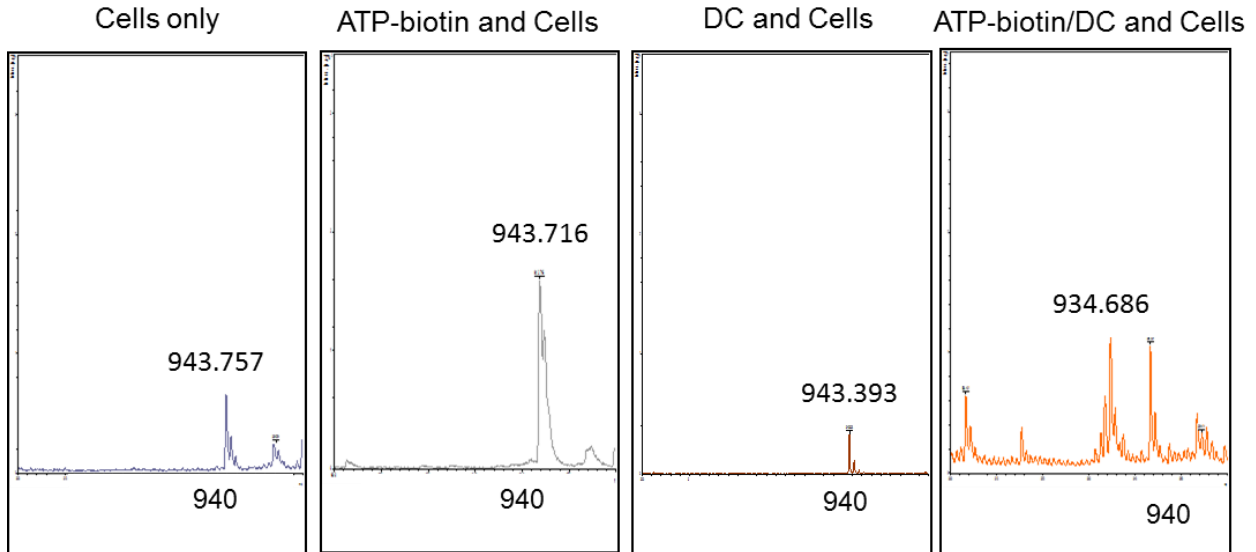
**Trial 2**



**Trial 3**



**Figure A 3. 2:** Repetitive trials of MALDI *in cellulo* imaging of ATP-biotin. HeLa cells were incubated with ATP-biotin, DC, or the ATP-biotin/DC complex followed by washing and mixing with alpha picolinic acid in 50% acetonitrile. The mixture was spotted on Bruker MALDI plate for analysis.

### 3.3 Repetitive trial of *In cellulo* and *in vitro* biotinylation comparison

**Trial 2**



| | 1 | 2 | 3 | 4 | 5 | 6 | | 7 | 8 | 9 | 10 |
|---|---|---|---|---|---|---|---|---|---|---|---|
| Protein Ladder | + | | | | | | | + | | | |
| HeLa cells | | + | + | + | + | + | | | | | |
| HCL | | | | | | | | | + | | + |
| HDL | | | | | | | | | | + | |
| ATP-biotin | | | + | | + | + | | | | + | + |
| Chitosan | | | | + | + | + | | | | | |
| STSP | | | | | + | | | | | | |

**Trial 3:**



| | 1 | 2 | 3 | 4 | 5 | 6 | | 7 | 8 | 9 | 10 |
|---|---|---|---|---|---|---|---|---|---|---|---|
| Protein Ladder | + | | | | | | | + | | | |
| HeLa cells | | + | + | + | + | + | | | | | |
| HCL | | | | | | | | | + | | + |
| HDL | | | | | | | | | | + | |
| ATP-biotin | | | + | | + | + | | | + | | + |
| Chitosan | | | | + | + | + | | | | | |
| STSP | | | | | + | | | | | | |
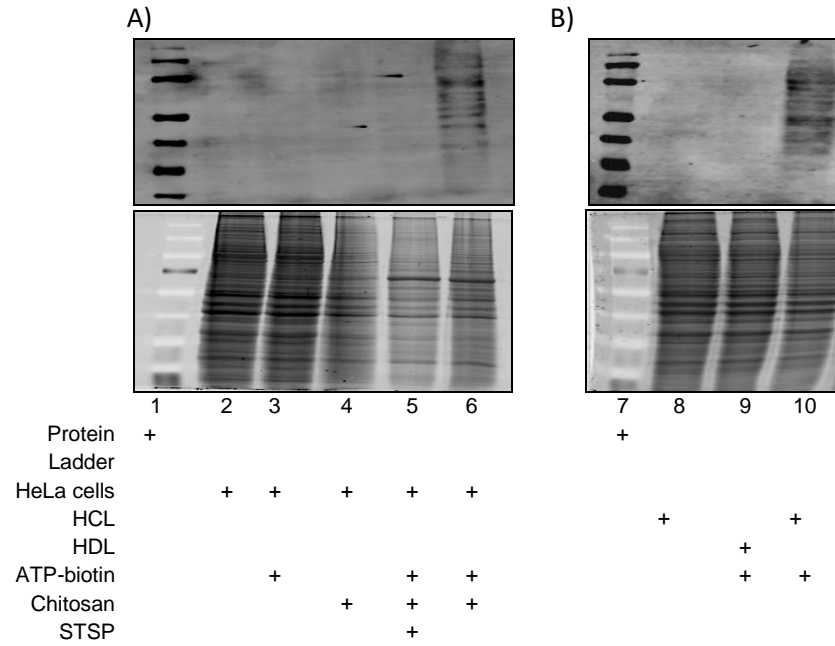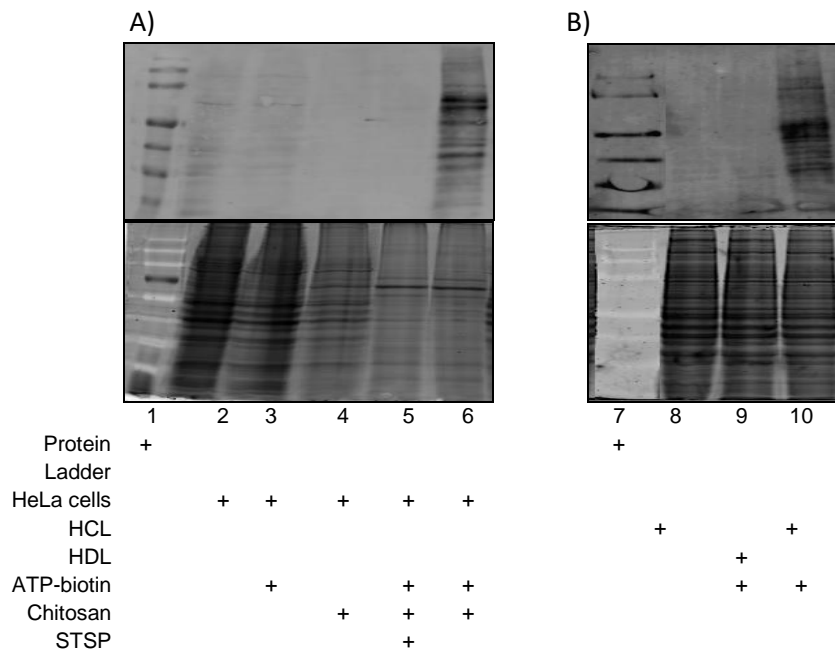
**Figure A 3. 3:** Repetitive trials of *in cellulo* and *in vitro* biotinylation A) *In cellulo* kinase-catalyzed biotinylation experiment of HeLa cells with ATP-biotin or ATP-biotin/DC complex. As a control, HeLa cells were preincubated with kinase inhibitor staurosporine (STSP) to prevent kinase catalysis (lane 5). B) In vitro kinase-catalyzed biotinylation using ATP-biotin with HeLa cell lysates (HCL). As a negative control, ATP-biotin was incubated with heat-denatured HeLa cell lysates (HDL). SDS-PAGE gel analysis was used to separate reaction mixtures and gels were visualized with streptavidin-Cy5 (top gel) or SYPRO® Ruby total protein stain (bottom gels). The protein ladder contains proteins of the following sizes: 170, 130, 100, 72, 55, 43, 34, and 26 kDa. All images are representative of at least three independent trials.

# APPENDIX C: CHAPTER 4

## 4.1 Compounds characterization



**Figure A 4. 1:** $^{1}$HNMR of N-(aminohexyl)methacrylamide (15) recorded in CD$_3$OD. Peaks at $\delta$ 5.41 and 3.83 corresponds to CD$_3$OD.
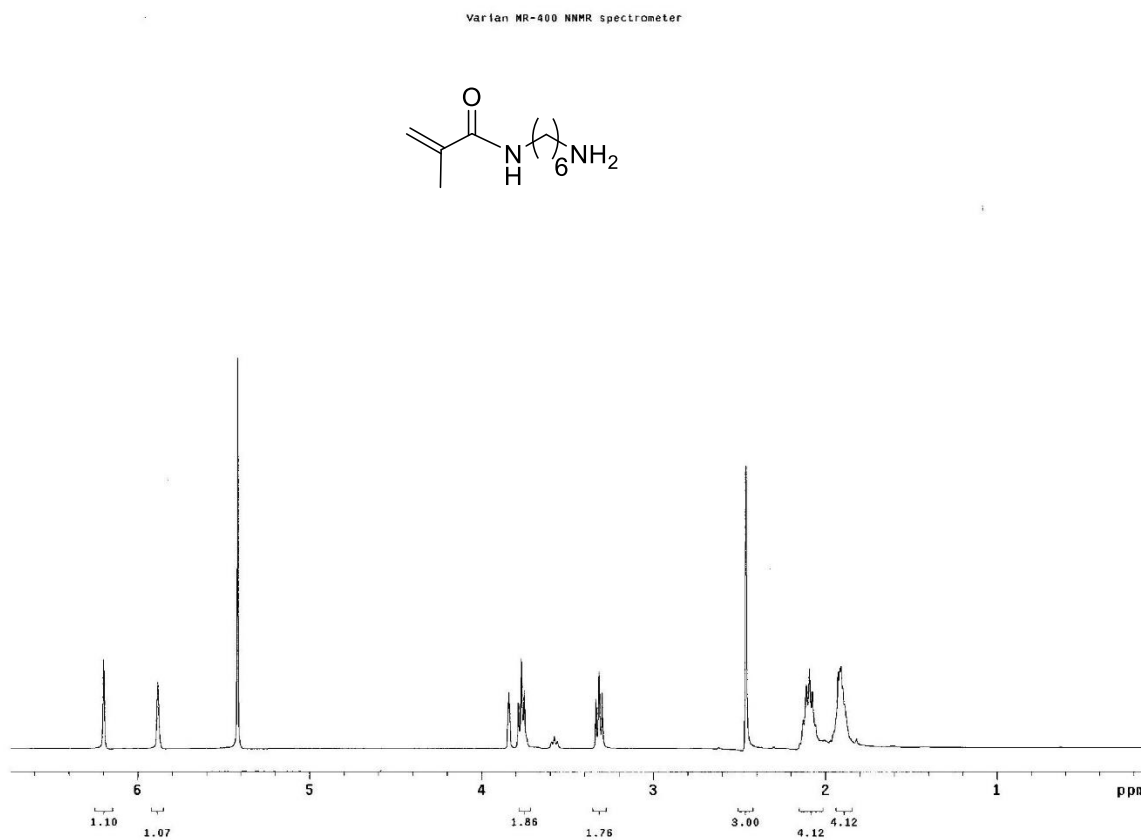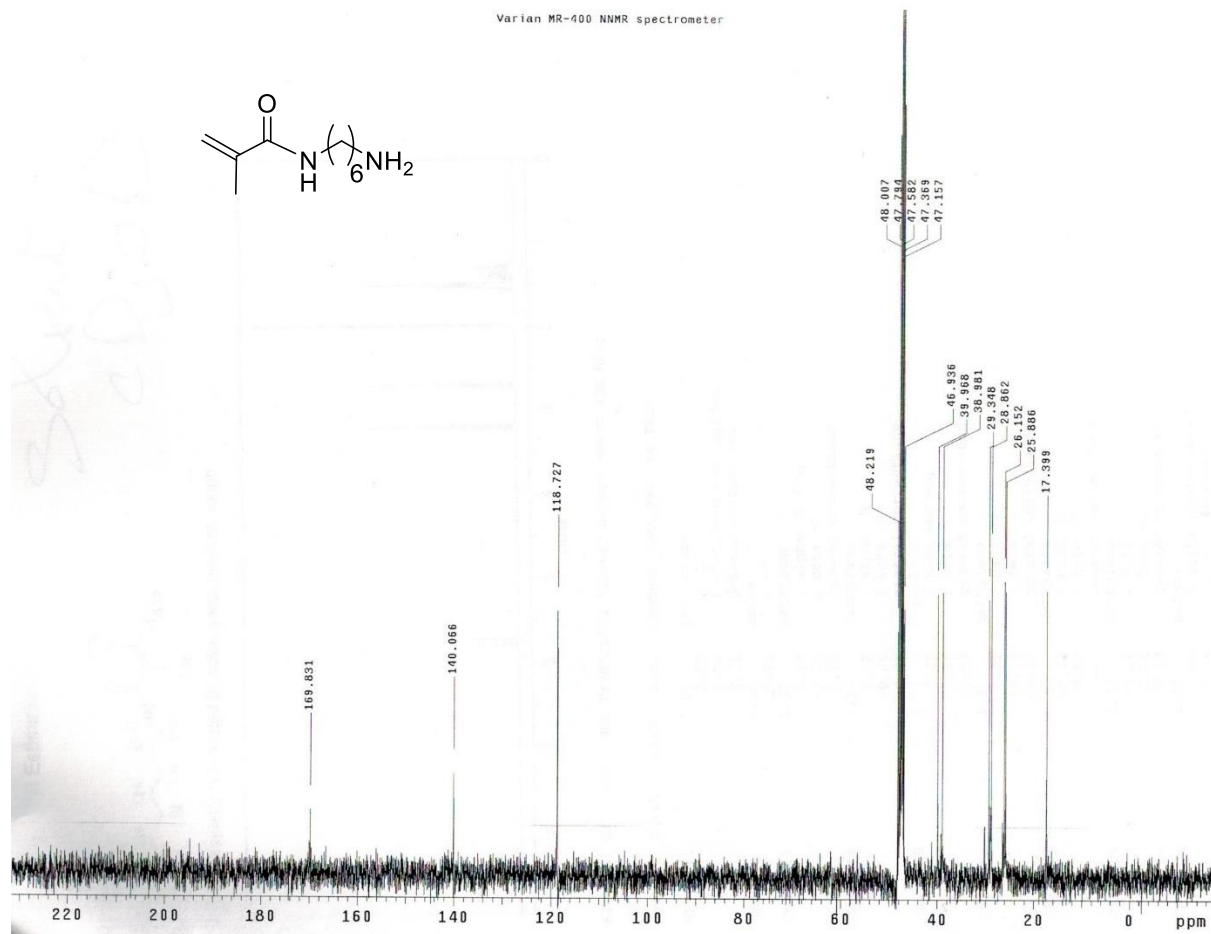
**Figure A 4. 2:** $^{13}$CNMR of N-(aminohexyl)methacrylamide (**15**) recorded in CD$_3$OD. Peaks at $\delta$ 47.56 corresponds to CD$_3$OD
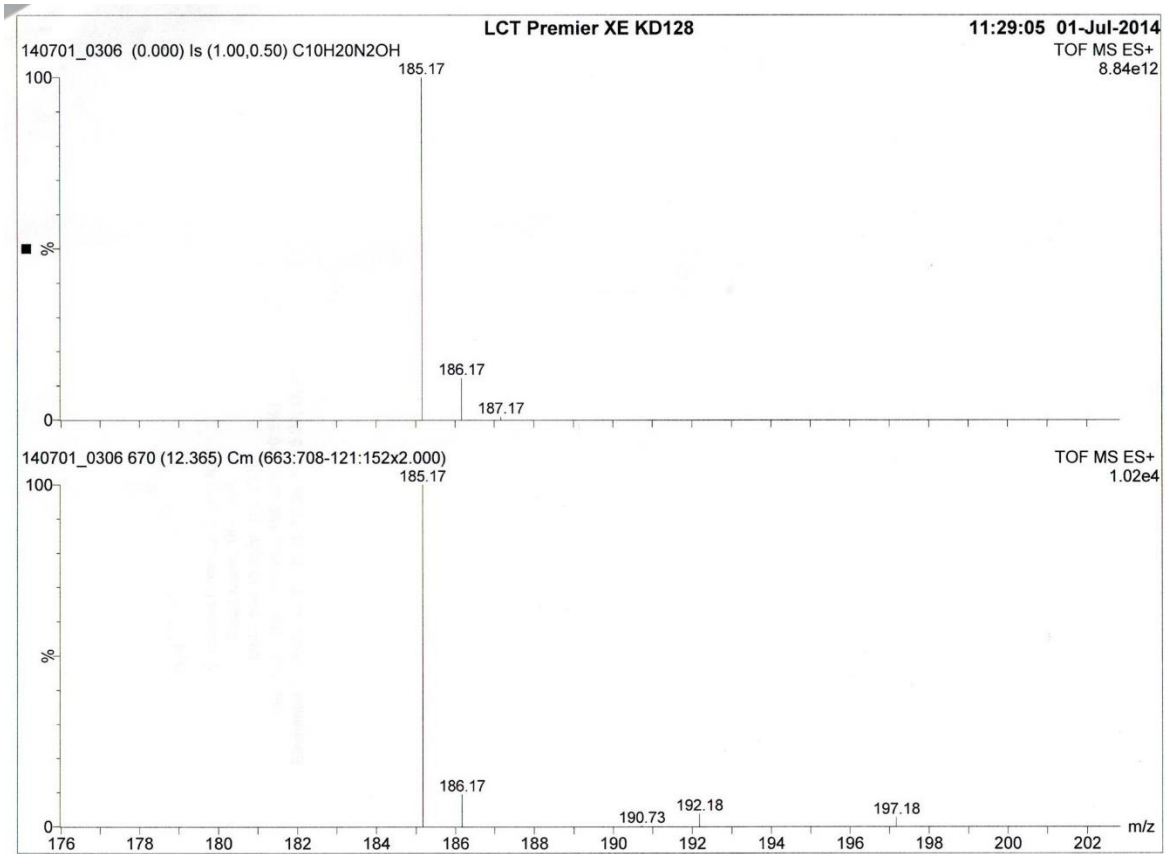
**Figure A 4. 3:** Electrospray ionization positive mode mass spectrum of N-(aminohexyl)methacrylamide (15). Calculated $(M+1)^{+1}$ for $C_{10}H_{21}N_2O$: 185.17; Observed 185.17
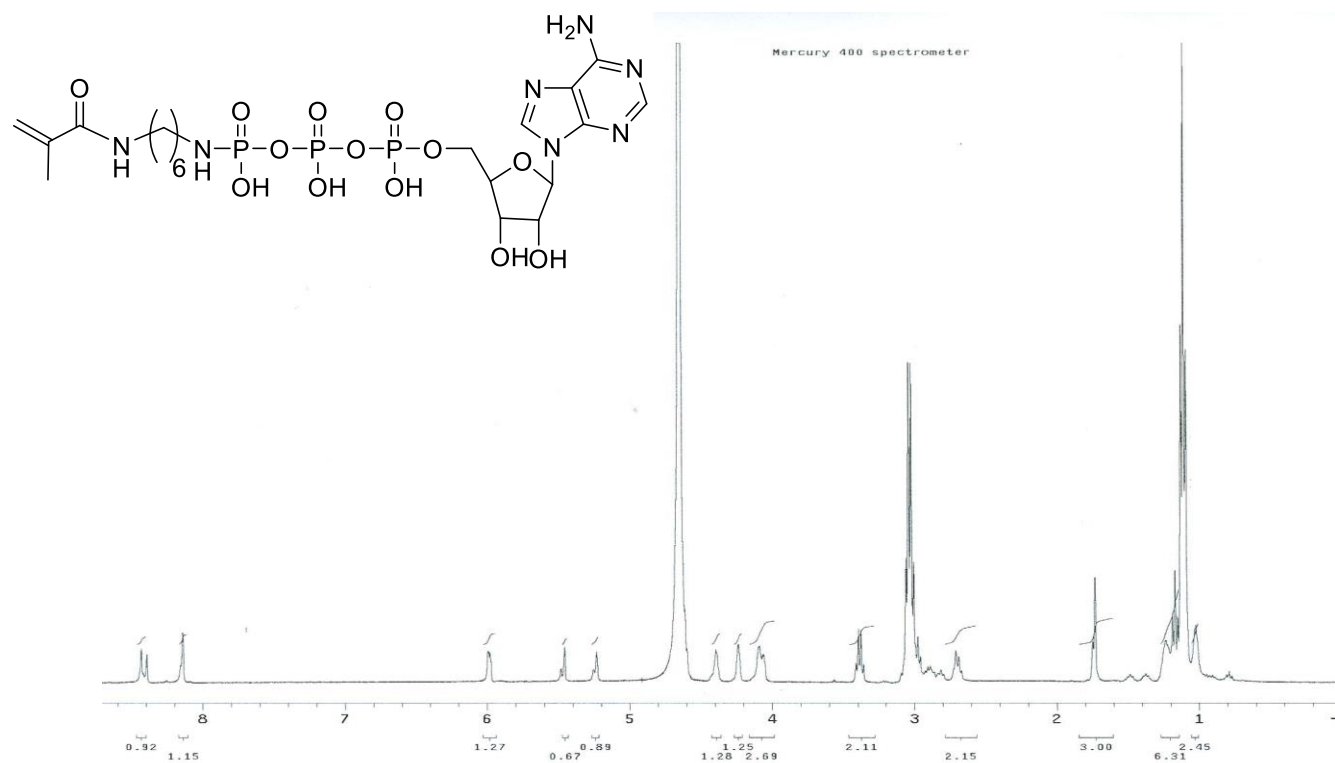
**Figure A 4. 4:** $^1$HNMR of ATP-Hex-Acr triethylamine salt (11) recorded in $D_2O$. Peaks at $\delta$ 4.61 correspond to $D_2O$ and peaks at $\delta$ 3.04 and 1.10 correspond $CH_2$ and $CH_3$ of triethylamine respectively.
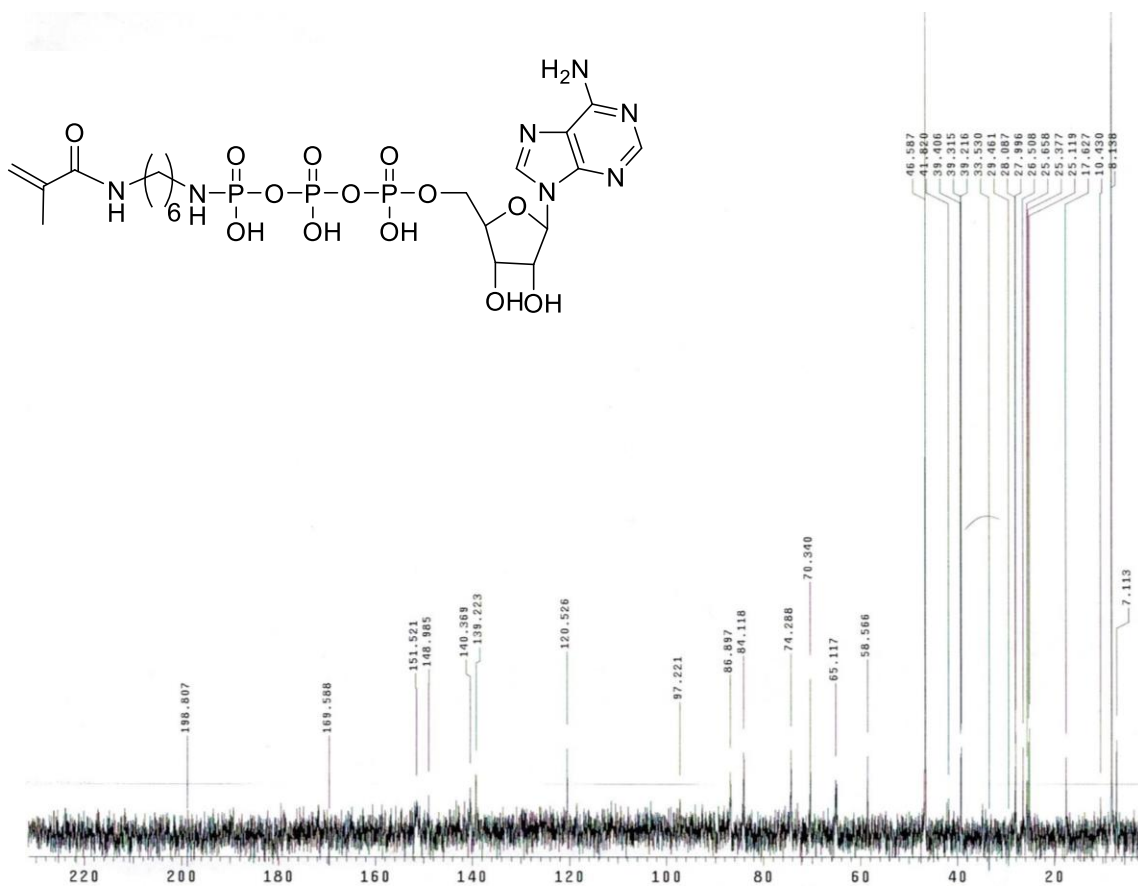
**Figure A 4. 5:** $^{13}$CNMR of ATP-Hex-Acr (**11**) recorded in D$_2$O. Peaks at δ 46.58 and 8.13 correspond CH$_2$ and CH$_3$ of triethylamine respectively. Multiplicity of C13 was observed to due to coupling with phosphorus as previously reported.[187]
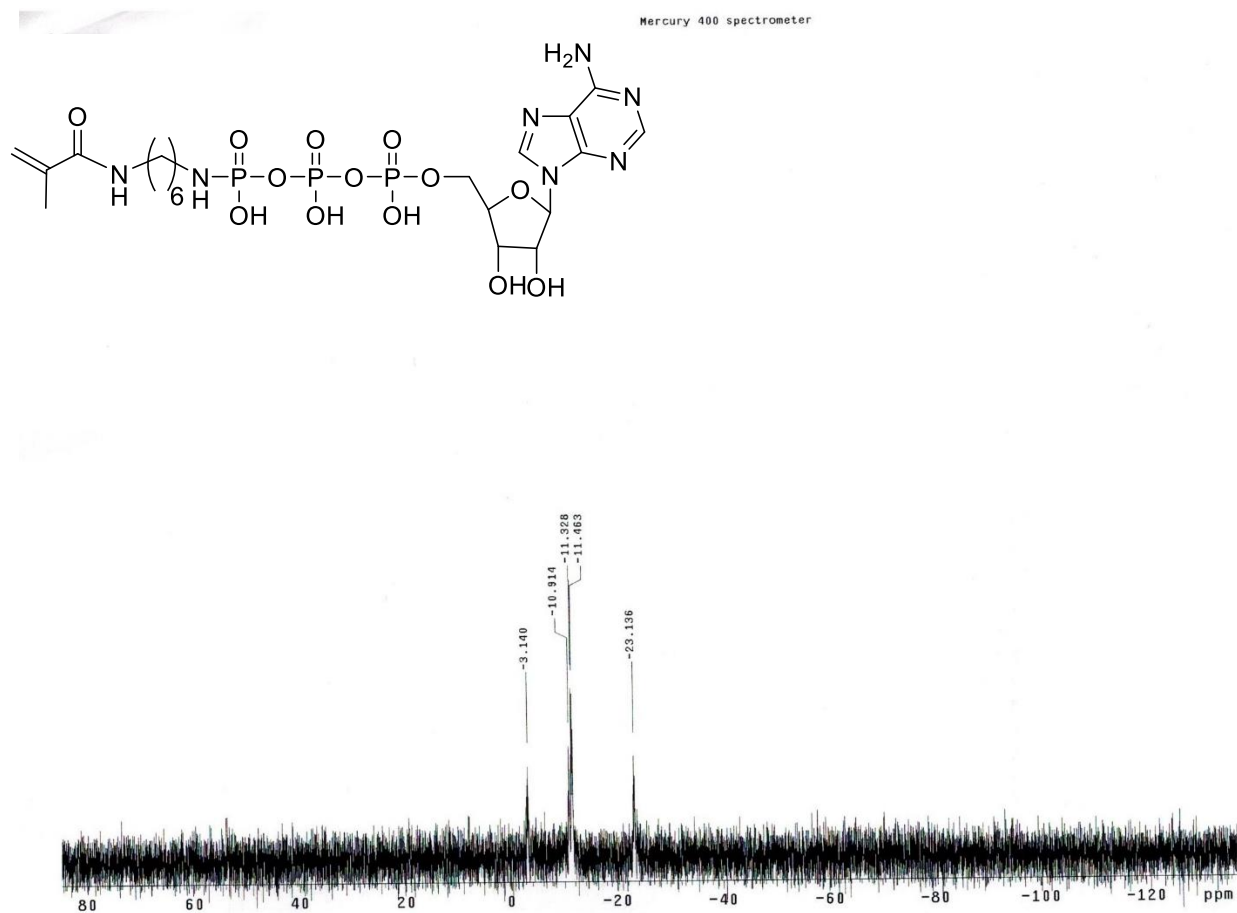
**Figure A 4. 6:** $^{31}$PNMR of ATP-Hex-Acr (**11**) recorded in D$_2$O.

**Elemental Composition Report**

**Single Mass Analysis**
Tolerance = 100.0 PPM   /   DBE: min = -1.5, max = 100.0
Element prediction: Off
Number of isotope peaks used for i-FIT = 6

Monoisotopic Mass, Even Electron Ions
686 formula(e) evaluated with 5 results within limits (all results (up to 1000) for each mass)
Elements Used:
C: 20-20   H: 0-40   N: 0-10   O: 0-15   P: 0-3

Ahmed Fouda  6-acrylamid in MeOH Cone(V)60          LCT Premier XE KD128                          12:42:57  19-Jun-2014
1400619_0306 899 (16.610) Cm (875:903-785:838x2.000)                                                          TOF MS ES-
                                                                                                              4.08e+004
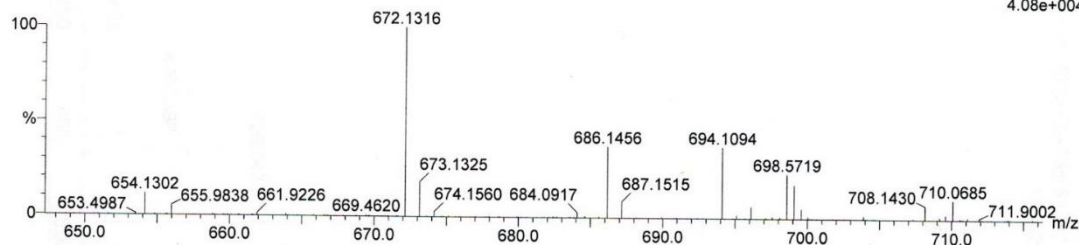


| Minimum: |  |  |  | -1.5 |  |  |  |
| Maximum: |  | 3.0 | 100.0 | 100.0 |  |  |  |

| Mass | Calc. Mass | mDa | PPM | DBE | i-FIT | i-FIT (Norm) | Formula |
|---|---|---|---|---|---|---|---|
| 672.1316 | 672.1349 | -3.3 | -4.9 | 9.5 | 74.0 | 0.6 | C20 H33 N7 O13 P3 |
|  | 672.0873 | 44.3 | 65.9 | 10.5 | 74.6 | 1.2 | C20 H29 N5 O15 P3 |
|  | 672.1825 | -50.9 | -75.7 | 8.5 | 76.2 | 2.7 | C20 H37 N9 O11 P3 |
|  | 672.1908 | -59.2 | -88.1 | 8.5 | 77.0 | 3.6 | C20 H36 N9 O13 P2 |
|  | 672.1432 | -11.6 | -17.3 | 9.5 | 77.1 | 3.7 | C20 H32 N7 O15 P2 |

**Figure A 4. 7:** Electrospray ionization (ESI) negative mode high resolution mass spectrum (HRMs) of ATP-Hex-Acr (**11**). Calculated (M-H)$^{-1}$ for $C_{20}H_{33}N_7O_{13}P_3$: 672.1349; Observed 672.1316.
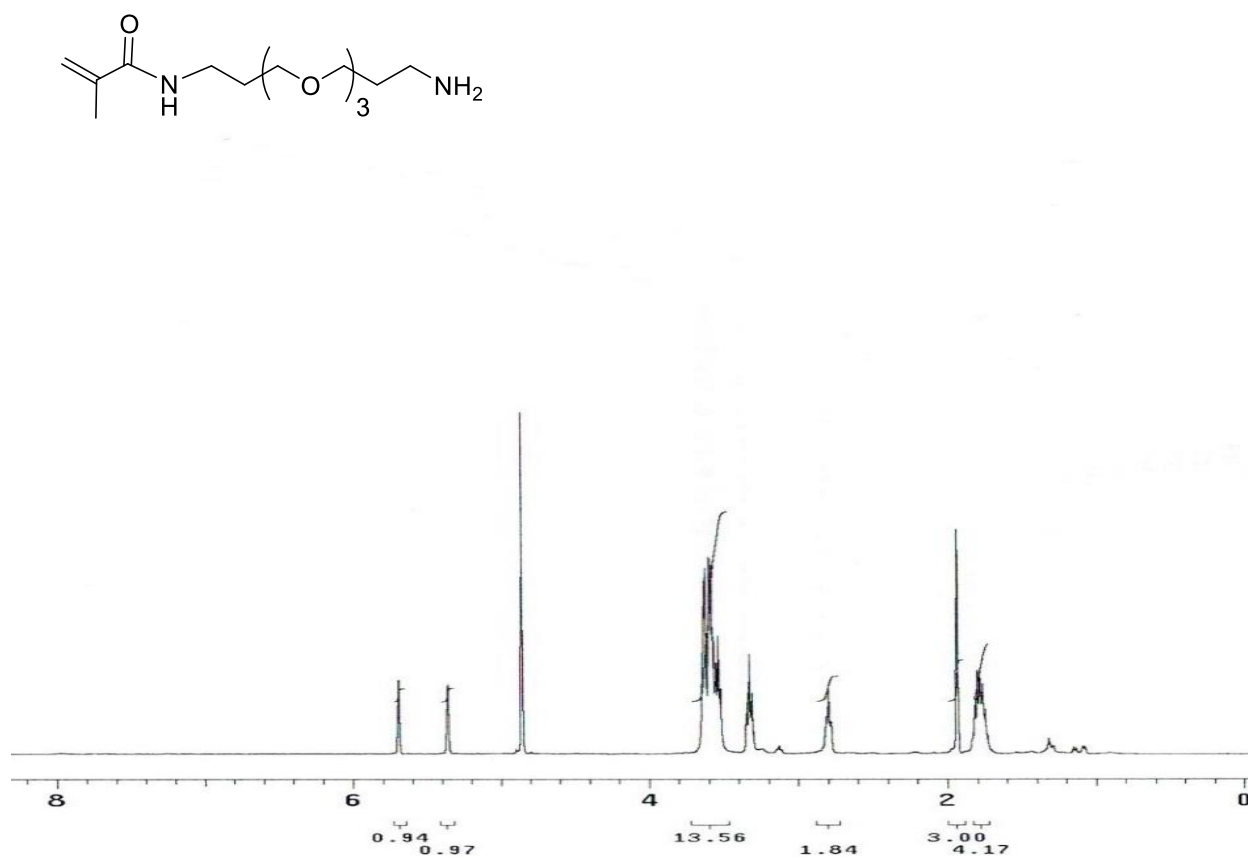
**Figure A 4. 8:** $^1$HNMR of N-(3-(2-(2-(3-aminopropoxy)ethoxy)ethoxy)propyl) methacrylamide (**17**) recorded in CD$_3$OD. Peaks at $\delta$ 3.32 and 4.85 corresponds to CD$_3$OD
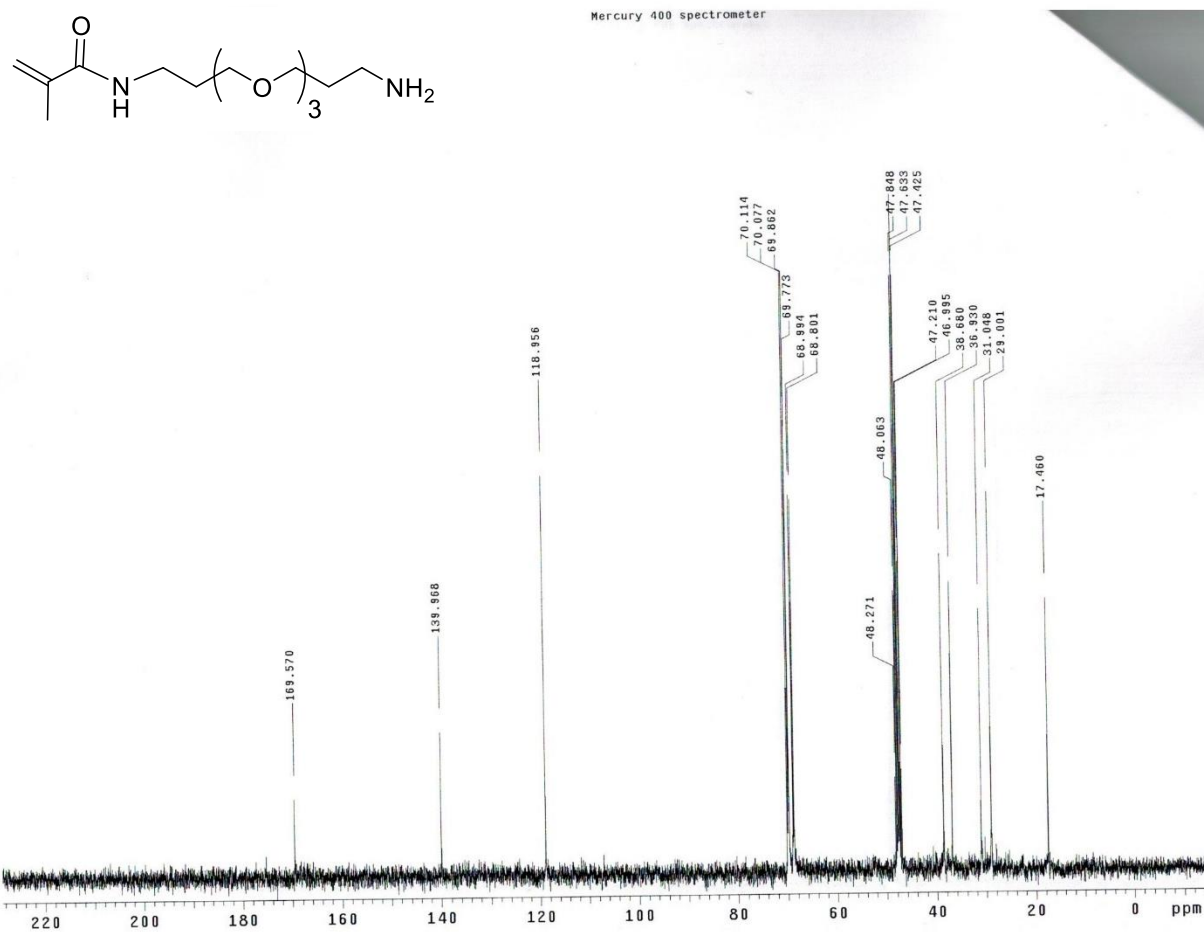
**Figure A 4. 9:** ^{13}CNMR of N-(3-(2-(2-(3-aminopropoxy)ethoxy)ethoxy)propyl) methacrylamide (**17**) recorded in CD₃OD. Peaks at δ 47.84 corresponds to CD₃OD
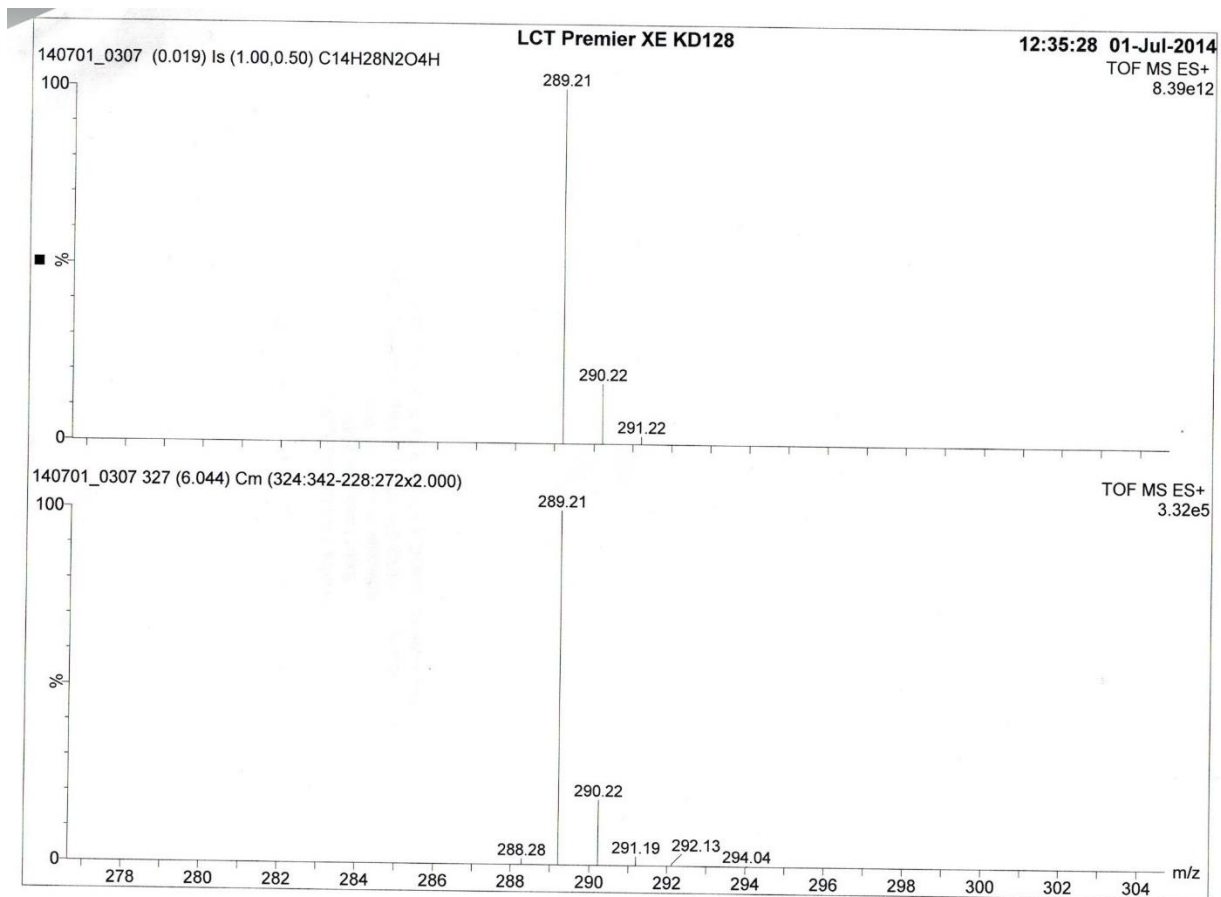
**Figure A 4. 10:** Electrospray ionization (ESI) positive mode mass spectrum of N-(3-(2-(2-(3-aminopropoxy)ethoxy)ethoxy)propyl) methacrylamide (**17**). Calculated (M+H)$^{+1}$ for $C_{14}H_{29}N_2O_4$: 289.21, observed 289.21.
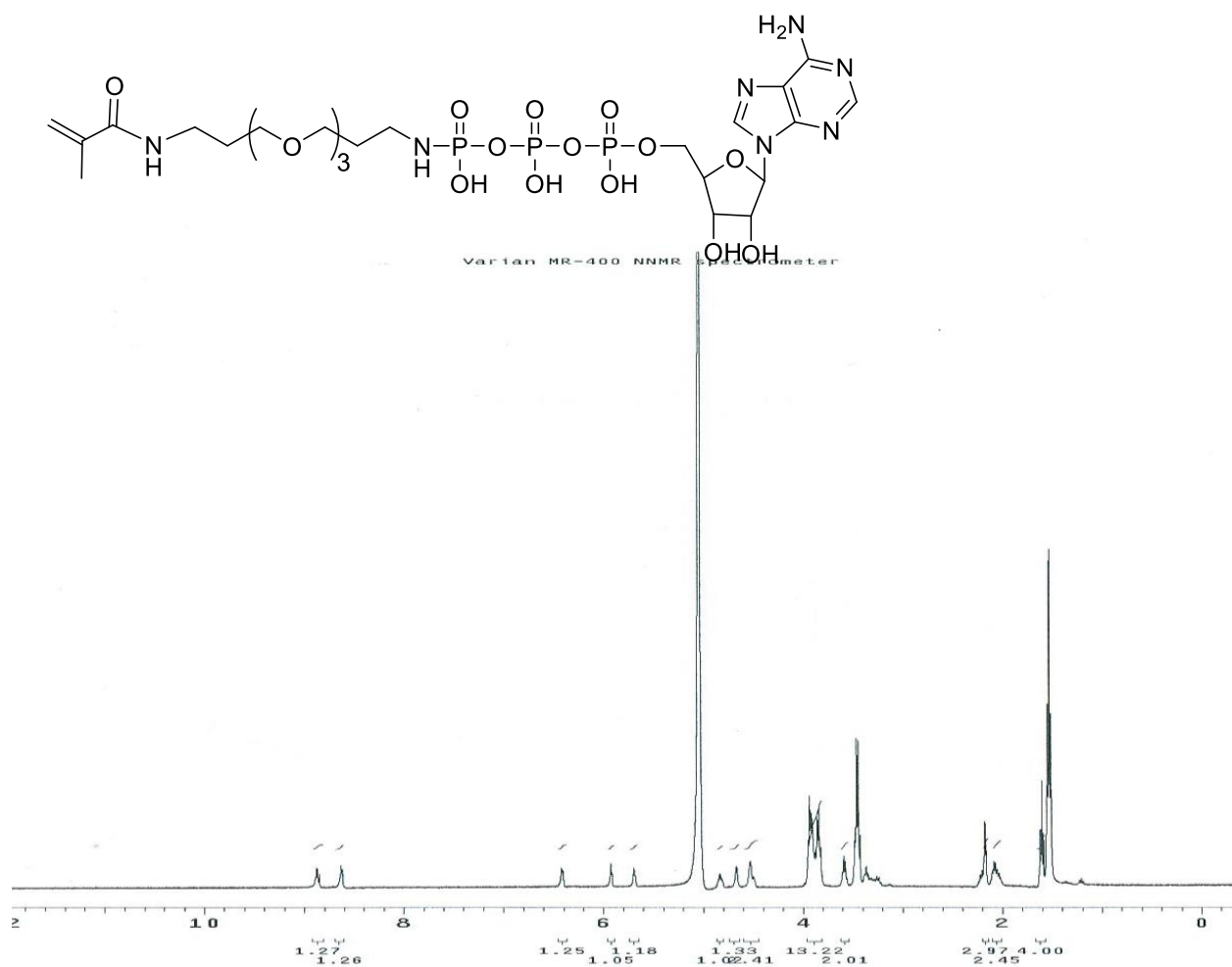
**Figure A 4. 11:** $^1$HNMR of ATP-PEG-Acr (**12**) recorded in D$_2$O. Peaks at $\delta$ 5.04 correspond to D$_2$O and peaks at $\delta$ 3.46 and 1.53 correspond CH$_2$ and CH$_3$ of triethylamine respectively.
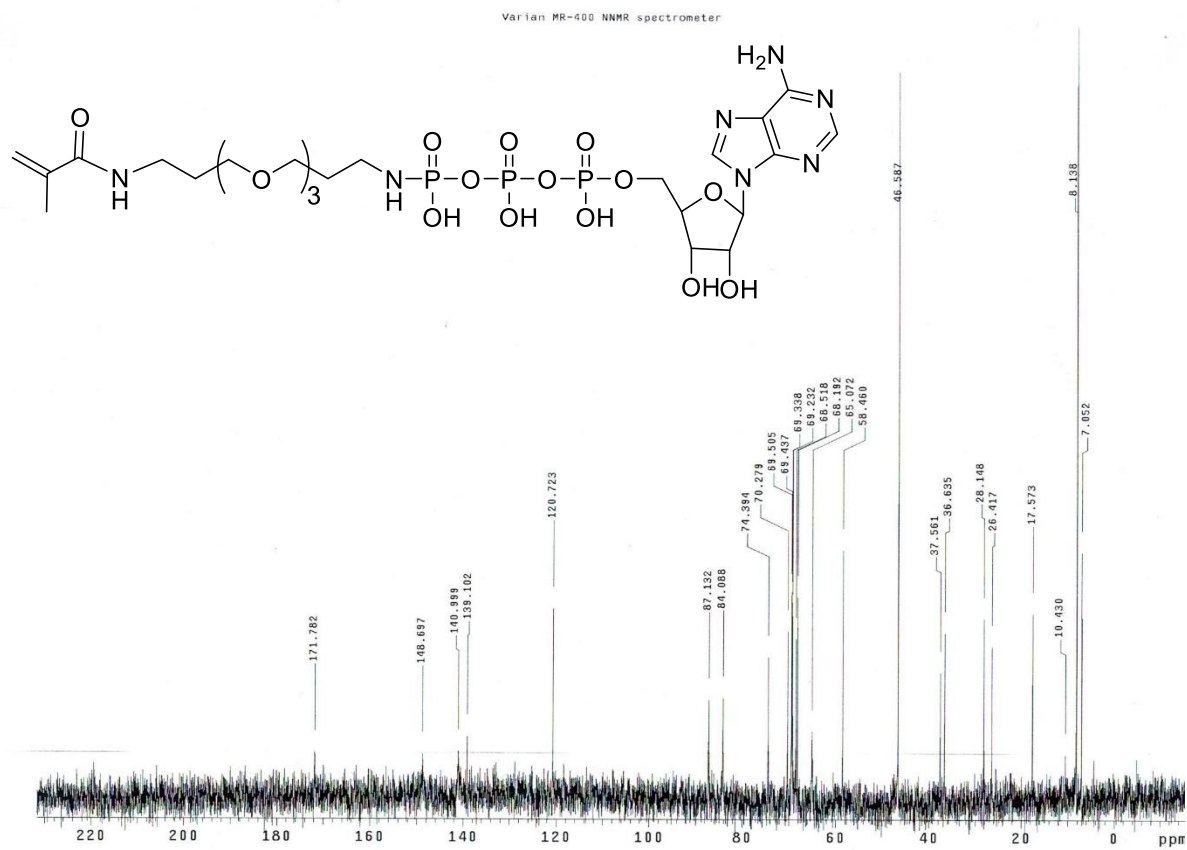
**Figure A 4. 12:** $^{13}$CNMR of ATP-PEG-Acr (**12**) recorded in D$_2$O. Peaks at $\delta$ 46.58 and 8.13 correspond CH$_2$ and CH$_3$ of triethylamine respectively. Multiplicity of C13 was observed to due to coupling with phosphorus as previously reported.[187]
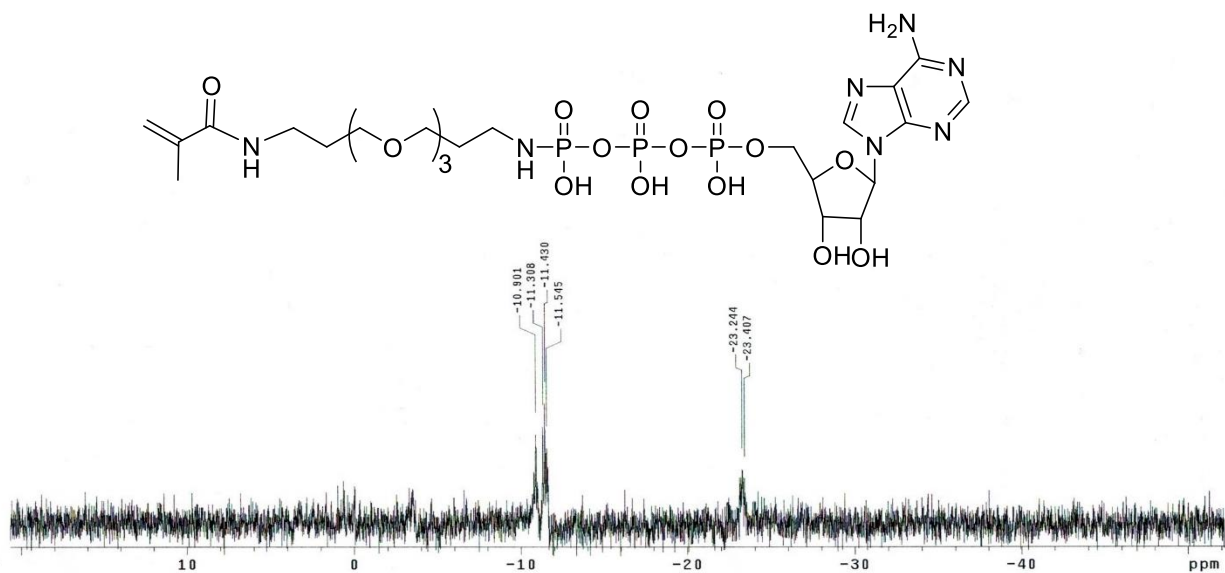


**Figure A 4. 13:** $^{31}$PNMR of ATP-PEG-Acr (**12**) recorded in D$_2$O.

**Elemental Composition Report**

**Single Mass Analysis**
Tolerance = 5.0 PPM   /   DBE: min = -1.5, max = 100.0
Element prediction: Off
Number of isotope peaks used for i-FIT = 6

Monoisotopic Mass, Odd and Even Electron Ions
891 formula(e) evaluated with 1 results within limits (all results (up to 1000) for each mass)
Elements Used:
C: 24-24   H: 0-50   N: 0-10   O: 0-20   P: 0-3
151022_0245 673 (12.429) Cm (673:675-239:317x2.000)
A. Fouda ATP-pEG-Acr in MeOH Cone(V)60
TOF MS ES-

Page 1

1.03e+005
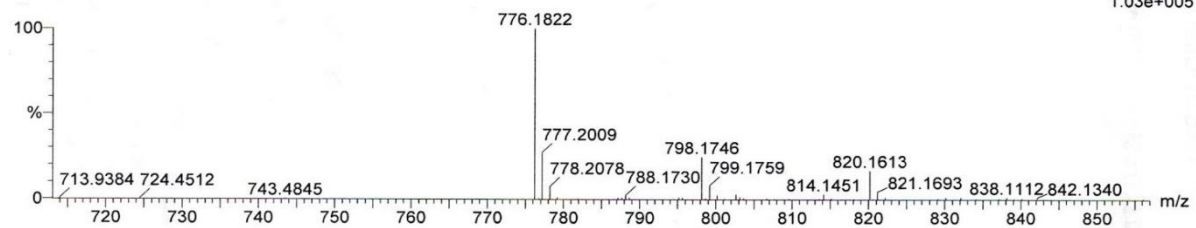


| Mass | Calc. Mass | mDa | PPM | DBE | i-FIT | i-FIT (Norm) | Formula |
|------|-----------|------|------|-----|-------|--------------|---------|
| Minimum: | | | | -1.5 | | | |
| Maximum: | | 3.0 | 5.0 | 100.0 | | | |
| 776.1822 | 776.1823 | -0.1 | -0.1 | 9.5 | 67.3 | 0.0 | C24 H41 N7 O16 P3 |

**Figure A 4. 14:** Electrospray ionization (ESI) positive mode high resolution mass spectrum (HRMs) of ATP-PEG-Acr (**12**). Calculated (M-H)$^{-1}$ for $C_{24}H_{41}N_7O_{16}P_3$: 776.1823, observed 776.1822.
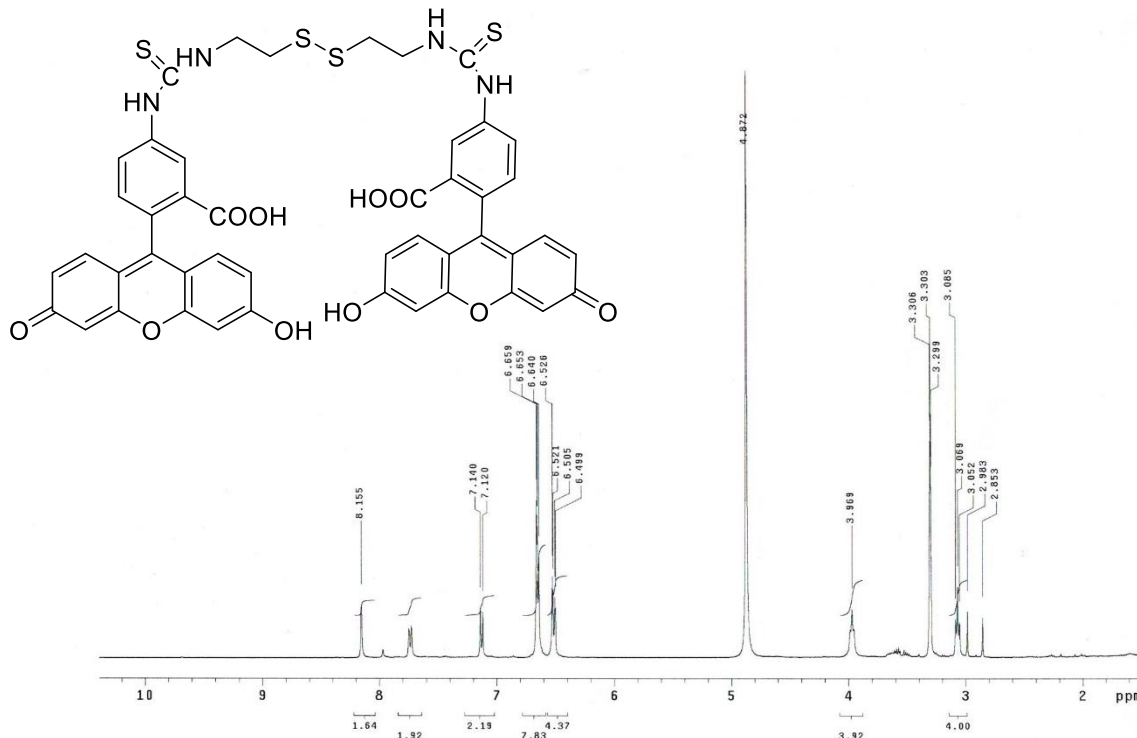


**Figure A 4. 15:** $^1$HNMR of DIFITC-cystamine (**18**) in CD$_3$OD. Peaks at 3.30 and 4.87 correspond to CD$_3$OD
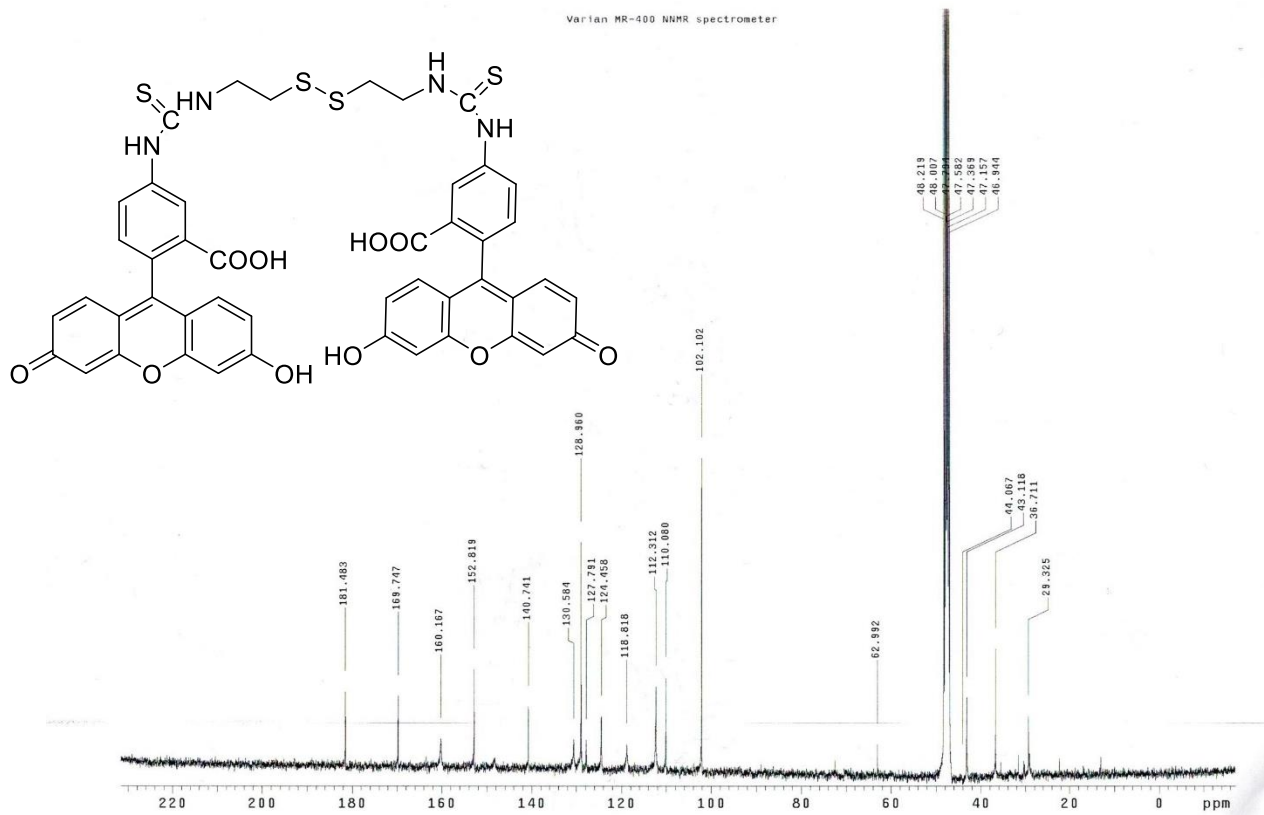
**Figure A 4. 16:** $^{13}$CNMR of DIFITC-cystamine (**18**) in CD$_3$OD. Peaks at 47.56 correspond to CD$_3$OD

**Elemental Composition Report**

**Page 1**

**Single Mass Analysis**
Tolerance = 50.0 PPM   /   DBE: min = -1.5, max = 100.0
Element prediction: Off
Number of isotope peaks used for i-FIT = 6

Monoisotopic Mass, Even Electron Ions
390 formula(e) evaluated with 4 results within limits (all results (up to 1000) for each mass)
Elements Used:
C: 46-46   H: 0-40   N: 0-5   O: 0-15   S: 0-4

Ahmed Fouda  Di FITC in MeOH Cone(V)60        LCT Premier XE KD128          16:22:11  27-Jun-2014
1400627_0317 452 (8.342) Cm (452:498-249:307x2.000)                                      TOF MS ES+
                                                                                         8.08e+005
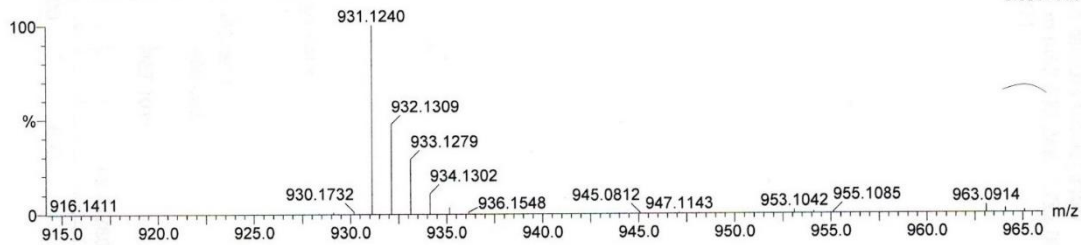


| Minimum: | | | | -1.5 | | | | | |
|---|---|---|---|---|---|---|---|---|---|
| Maximum: | | 3.0 | 50.0 | 100.0 | | | | | |
| | | | | | | | | | |
| Mass | Calc. Mass | mDa | PPM | DBE | i-FIT | i-FIT (Norm) | Formula | | |
| | | | | | | | | | |
| 931.1240 | 931.0937 | 30.3 | 32.5 | 32.5 | 55.2 | 0.7 | C46 | H31 N2 | O14 S3 |
| | 931.1414 | -17.4 | -18.7 | 31.5 | 55.6 | 1.1 | C46 | H35 N4 | O12 S3 |
| | 931.1591 | -35.1 | -37.7 | 31.5 | 56.5 | 1.9 | C46 | H35 N4 | O14 S2 |
| | 931.1236 | 0.4 | 0.4 | 31.5 | 59.7 | 5.2 | C46 | H35 N4 | O10 S4 |

**Figure A 4. 17:** Electrospray ionization (ESI) positive mode high resolution mass spectrum (HRMs) of DIFITC-cystamine (**18**). Calculated $(M+H)^{+1}$ for $C_{46}H_{35}N_4O_{10}S4$: 931.1236, observed 931.1240.

### 4.2 Full gel images and repetitive trials of kinase-catalyzed in gel fluorescence of MBP using ATP-acrylamides and DIFITIC-cystamine

**Trial 1**



| | 1 | 2 | 3 | 4 | 5 | 6 | 7 | 8 |
|---|---|---|---|---|---|---|---|---|
| MBP | + | + | + | + | + | + | + | + |
| PKA | + | + | | + | | + | + | + |
| 11 | | | + | + | | | + | |
| 12 | | | | | + | + | | + |
| STSP | | | | | | | + | + |
| 18 | | + | + | + | + | + | + | + |

**Trial 2**



| | 1 | 2 | 3 | 4 | 5 | 6 | 7 | 8 |
|------|---|---|---|---|---|---|---|---|
| MBP | + | + | + | + | + | + | + | + |
| PKA | + | + | | + | | + | + | + |
| 11 | | | + | + | | | + | |
| 12 | | | | | + | + | | + |
| STSP | | | | | | | + | + |
| 18 | | + | + | + | + | + | + | + |
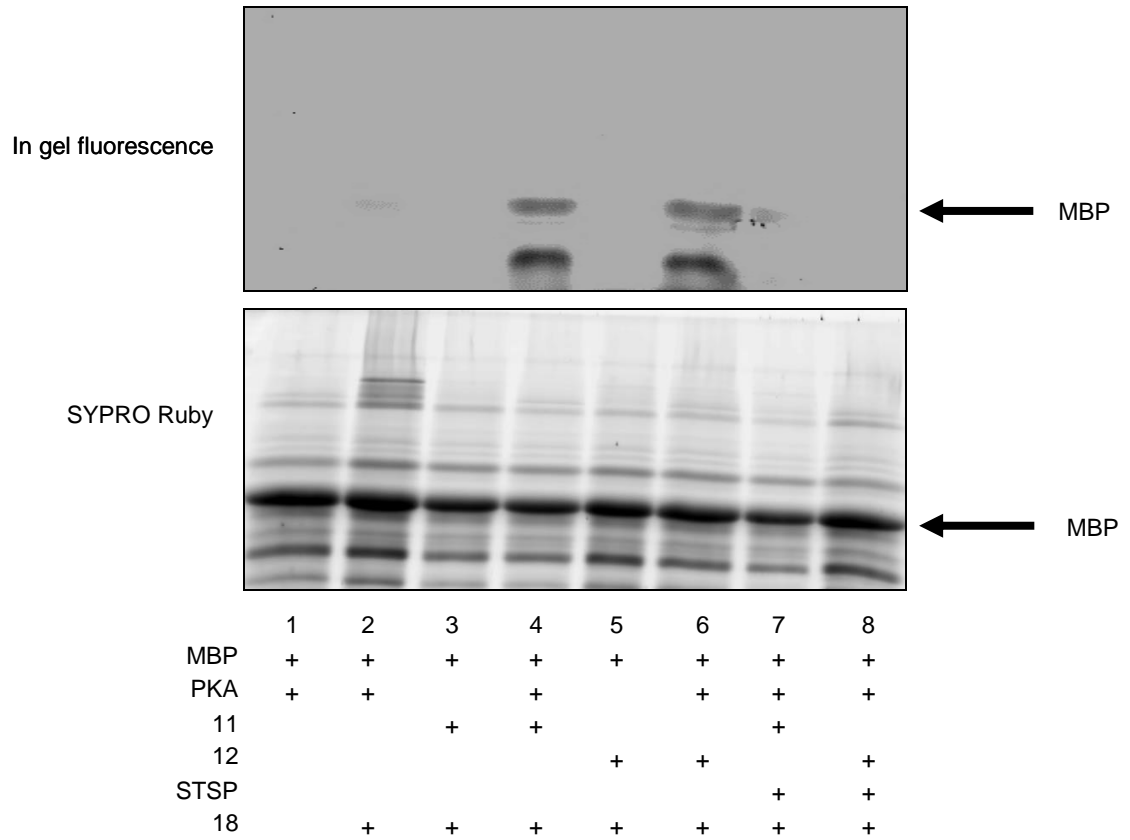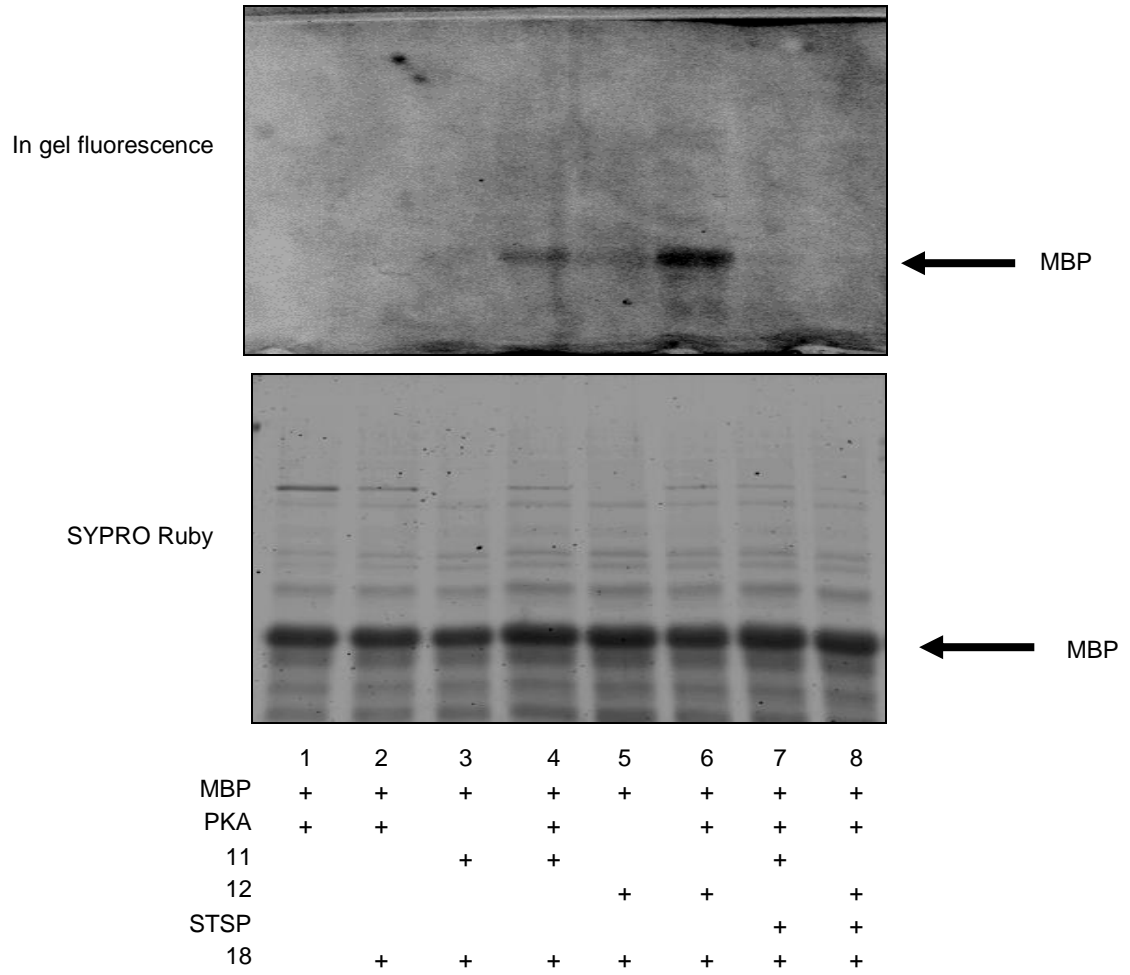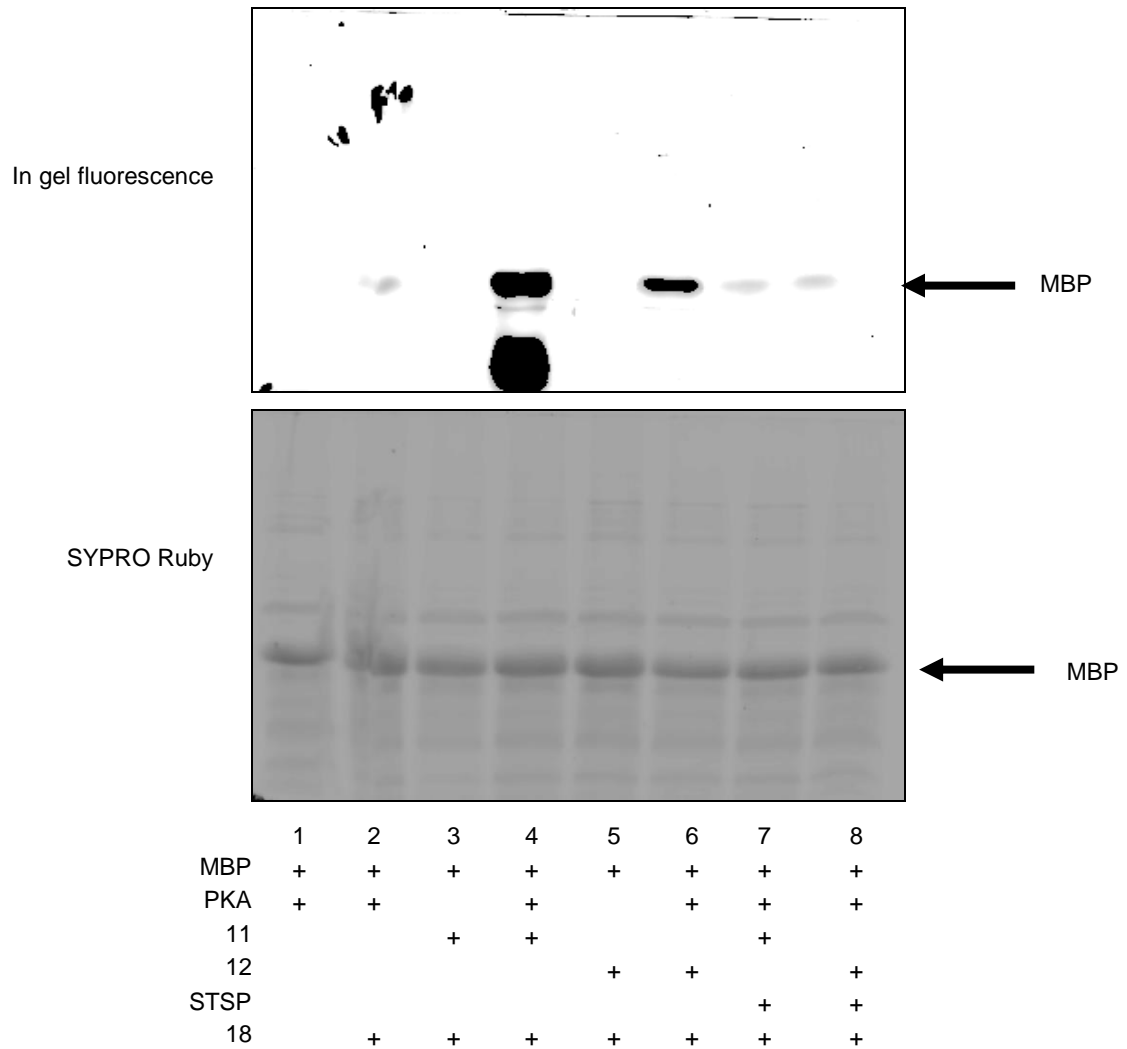
**Trial 3**



**Figure A 4.18:** Repetitive trials of detection of kinase-catalyzed phosphorylation of MPB with PKA and ATP-acrylamides in presence of DiFTC-cystamine (**18**). ATP-Hex-Acr **11** or ATP-PEG-Acr **12** were incubated with MBP, PKA, and DIFITC-cystamine (**18**). The reaction mixtures were separated by SDS-PAGE gel analysis. As a control, the reaction was performed in presence of staurosporine (STSP), kinase inhibitor. Top gel is visualized by typhoon scanning for in gel fluorescence (excitation/emission=495/519 nm) and bottom gel was visualized by SYPRO® Ruby total protein stain. Trial 1 is also shown in figure 4.16C

## 4.3 Full gel images and repetitive trials of determining the efficiency of ATP-acrylamides (11 and 12)

**Trial 1 and 2**



| | 1 | 2 | 3 | 4 | 5 | 6 | 7 | 8 |
|-----|---|---|---|---|---|---|---|---|
| MBP | + | + | + | + | + | + | + | + |
| PKA | + | + | + | + | + | + | + | + |
| ATP | - | + | - | - | - | + | - | - |
| 11 | - | - | + | | - | - | + | |
| 12 | - | - | - | + | - | - | - | + |
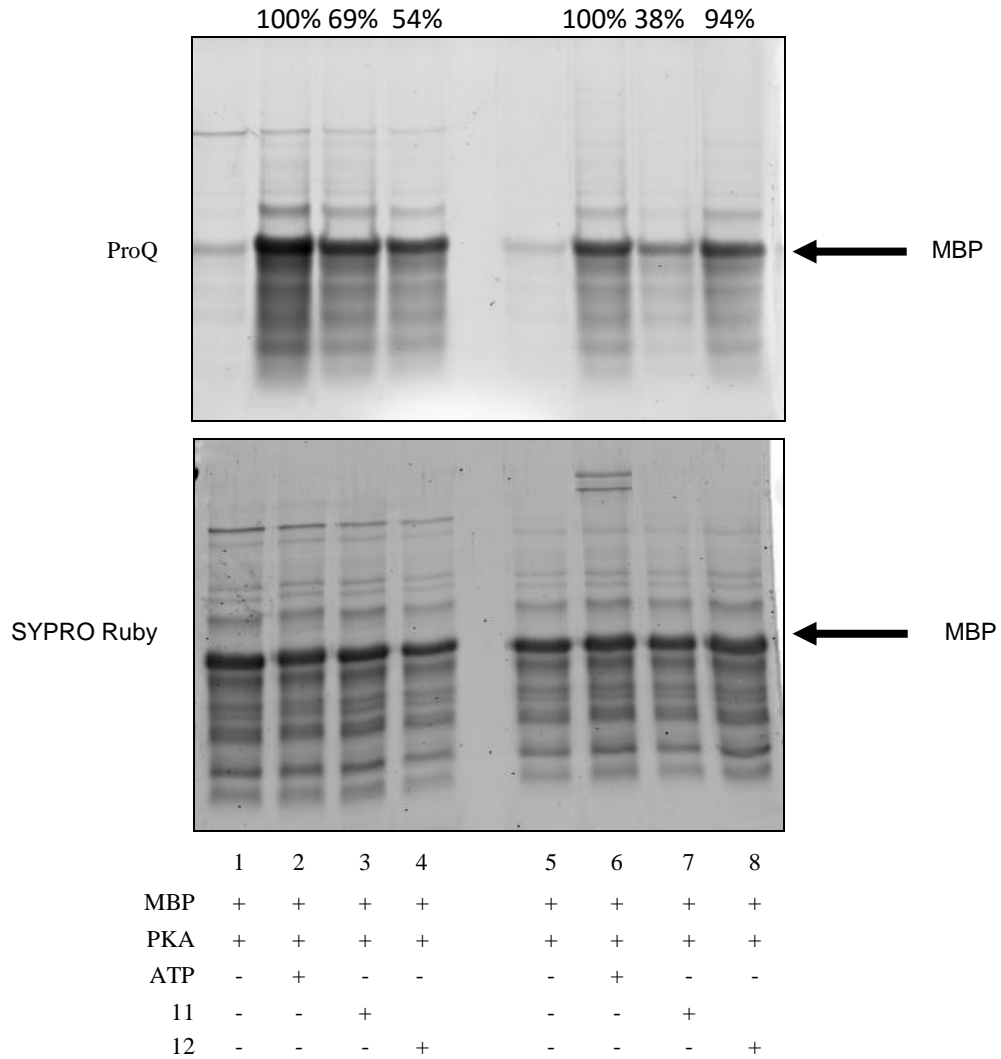
**Trial 3 and 4**
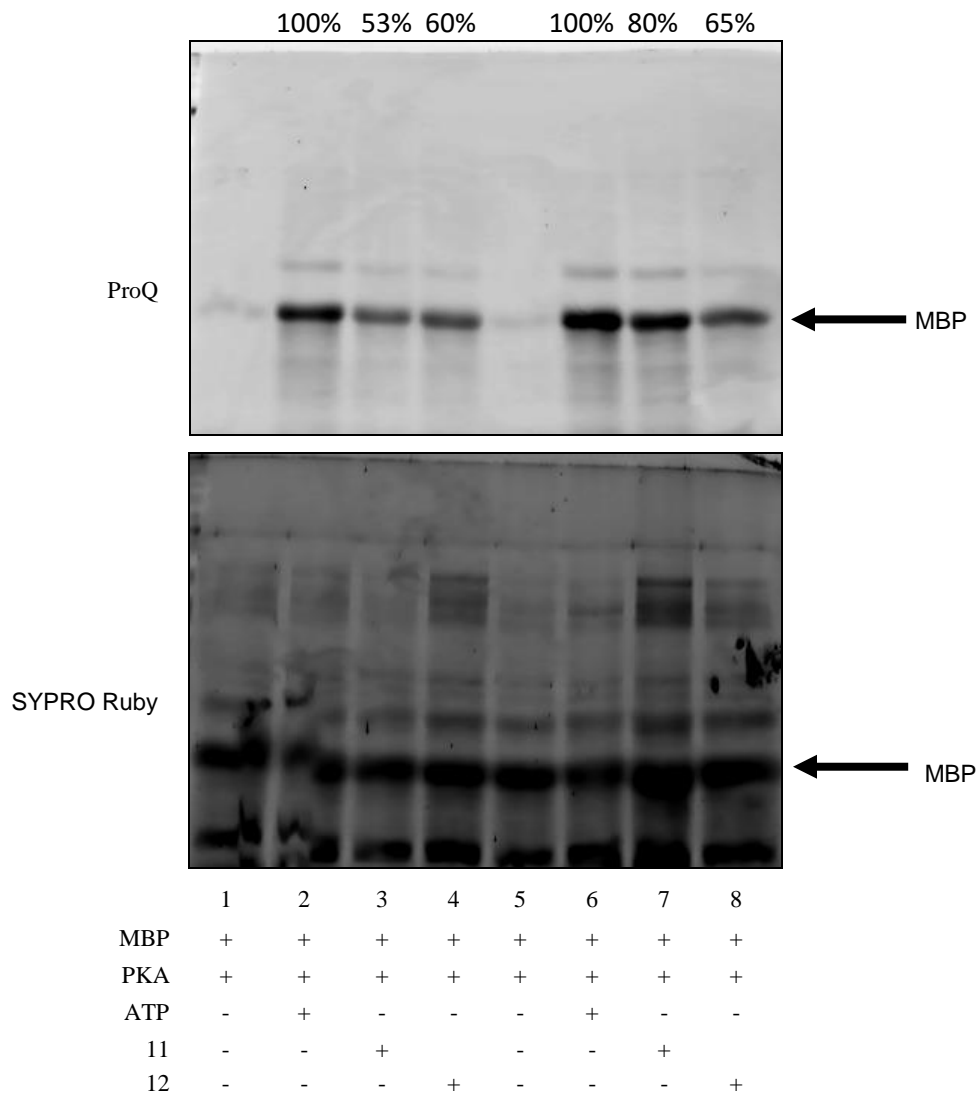


**Figure A 4.19:** Quantitative analysis of MPB phosphorylation in the presence of PKA and incubated with either ATP (lane 2 and 6), ATP-Hex-Acr (lane 3 and 7), or ATP-PEG-Acr (lane 4 and 8), then treated with TFA. The reaction mixtures were analyzed by SDS-PAGE analysis, followed by staining with ProQ diamond phosphoprotein stain (top) or SYPRO® Ruby total protein stain (bottom). MBP staining from ProQ diamond stained gel was quantified by Image quant, which corresponds to extent of phosphorylation. The mean percentage of phosphorylation of MBP from four trials is shown on the top of the ProQ diamond gel.

## 4.4 Full gel images and repetitive trials of *In vitro* Akt1 crosslinking to its substrates using ATP-acrylamides

**Trial 2:**



| | 1 | 2 | 3 | 4 | 5 |
|---|---|---|---|---|---|
| HEK293 Lysates | + | + | + | + | + |
| 11 | | + | + | | |
| 12 | | | | + | + |
| STSP | | + | | + | |
| TCEP | + | + | + | + | + |
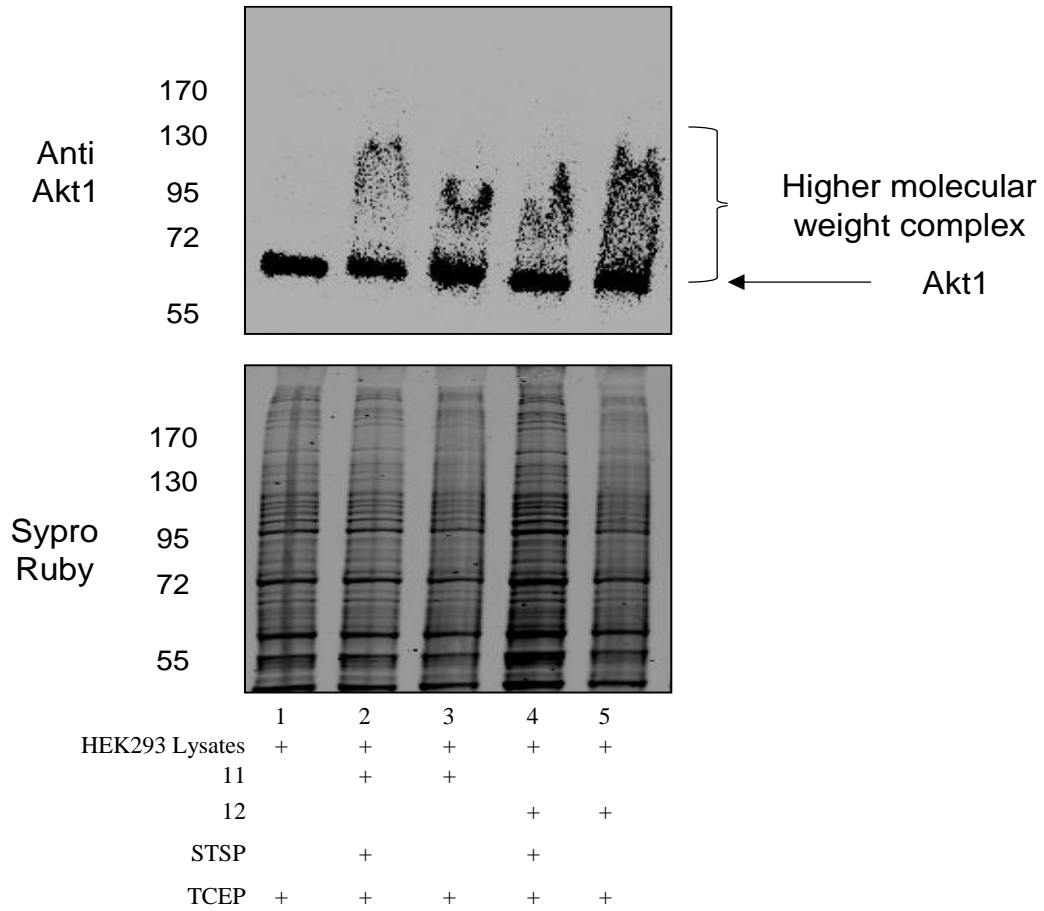
**Trial 3:**
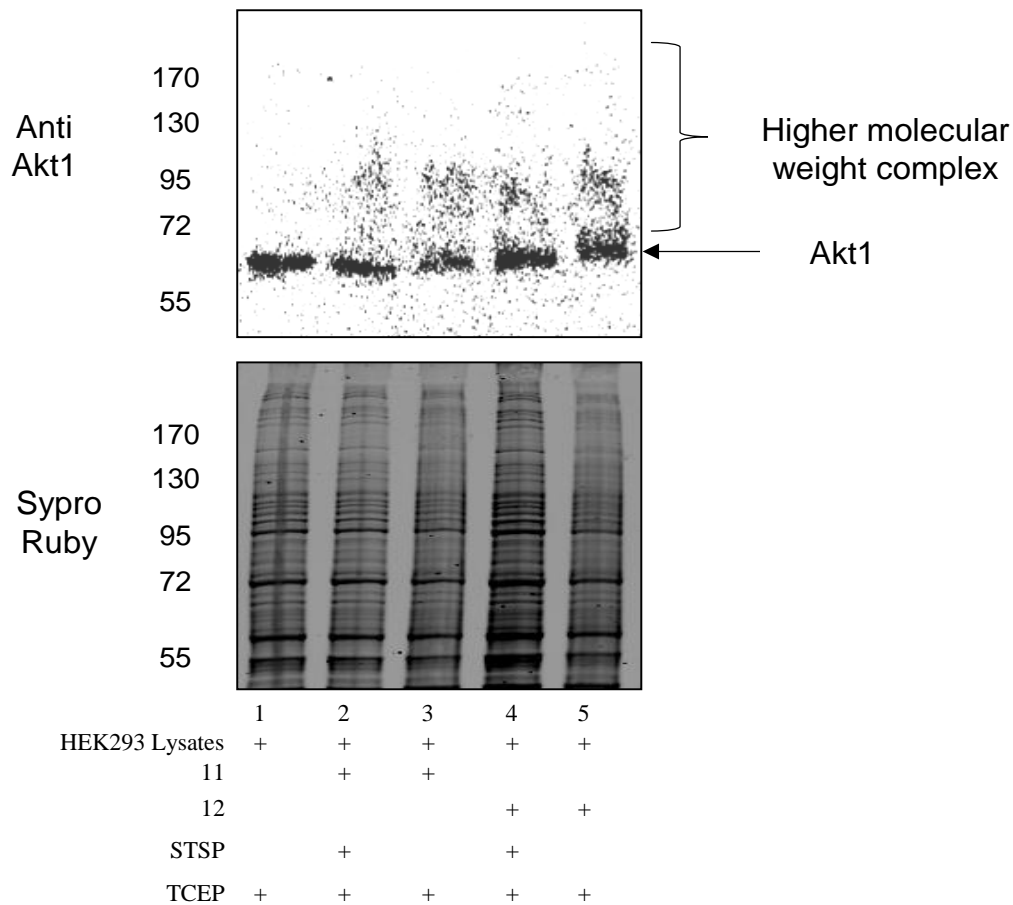


**Figure A 4.20:** Kinase-catalyzed crosslinking of AKT with its substrates in HEK293 lysates using ATP-acrylamides (**11 and 12**). HEK293 lysates were incubated with ATP-acrylamides in presence of TCEP (tris(2-carboxyethyl)phosphine). TCEP was used to form necessary reducing conditions for cysteine reactivity. As a control, the reaction was performed in presence of staurosporine (STSP), kinase inhibitor. The reaction mixtures were separated by SDS-PAGE electrophoresis and transferring onto PVDF membrane as a western blotting. Top gel is visualized by treating with anti-AKT1 antibody followed by secondary HRP, while the bottom gel was visualized by SYPRO Ruby. The third trial is shown in figure 4.19

**4.5 Repetitive trials of Akt1 substrates identification with ATP-acrylamides using K-CLIP (Kinase-CrossLinking and ImmunoPrecipitation)**

**Trial 1:**



| | 1 | 2 | 3 | 4 | 5 |
|---|---|---|---|---|---|
| HEK293 | + | + | + | + | + |
| STSP | | + | | + | |
| 11 | | + | + | | |
| 12 | | | | + | + |
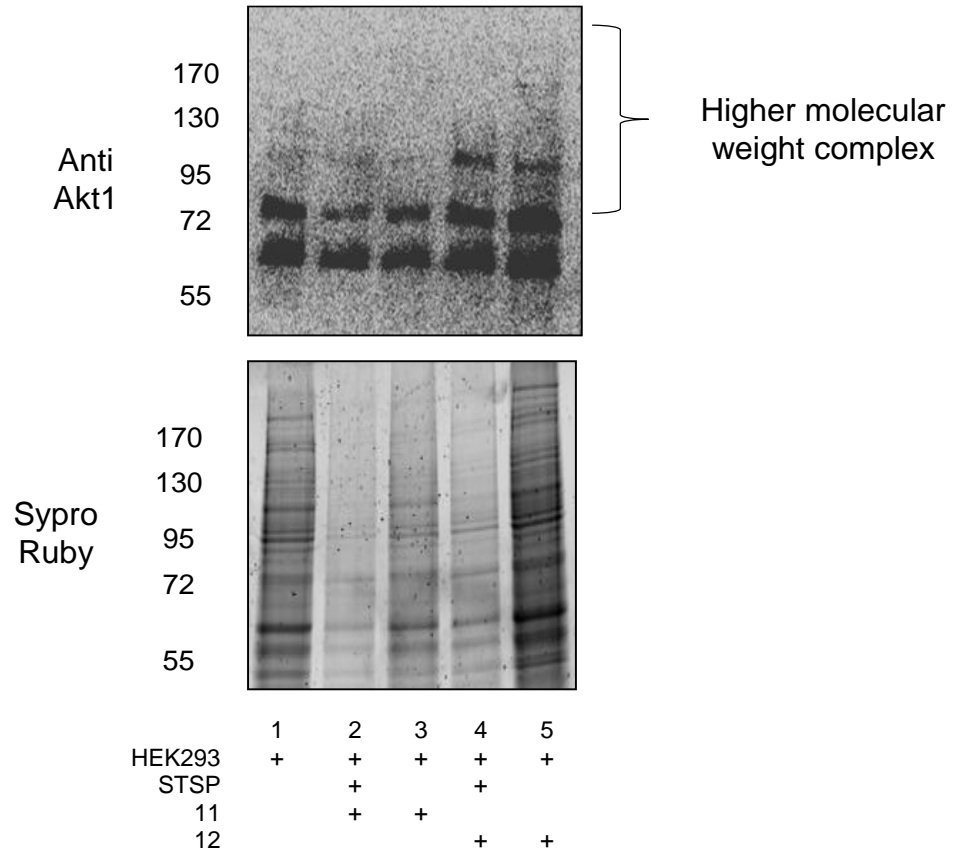
**Trial 2: Shown in Chapter 4 (Figure 4.20)**



| | 1 | 2 | 3 | 4 | 5 |
|---|---|---|---|---|---|
| HEK293 | + | + | + | + | + |
| STSP | | + | | + | |
| 11 | | + | + | | |
| 12 | | | | + | + |
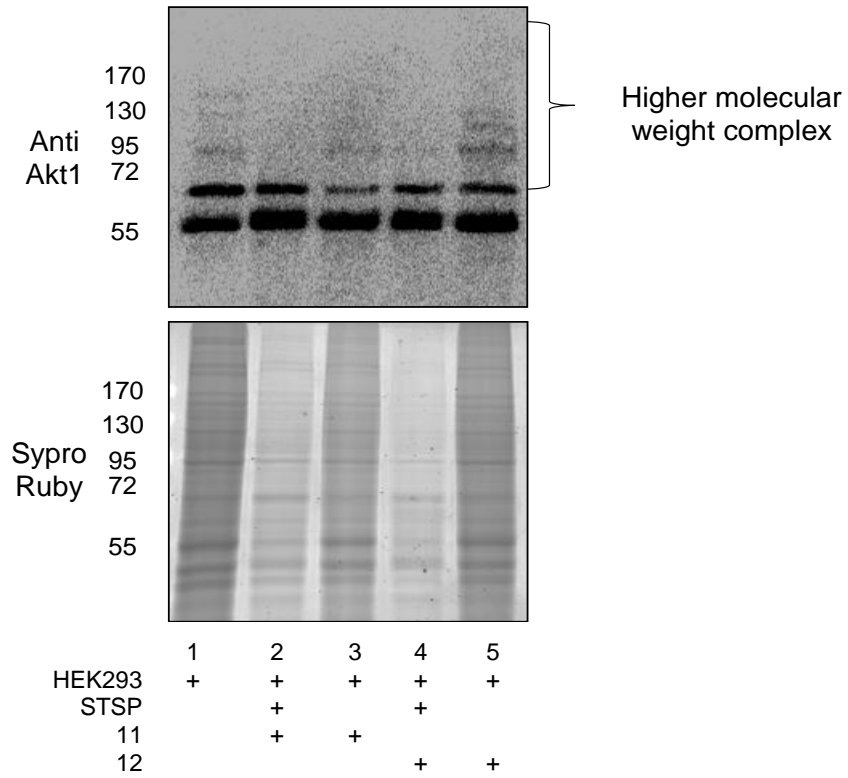
**Trial 3:**
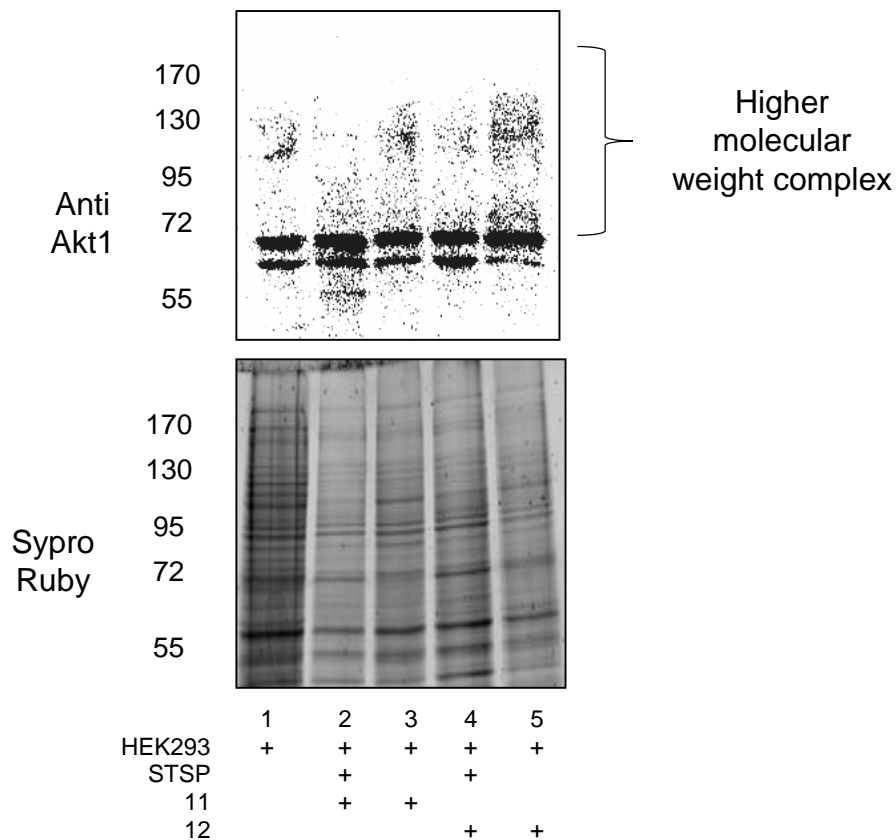


**Figure A 4.21:** Kinase-catalyzed crosslinking of AKT with its substrates in HEK293 lysates using ATP-acrylamides (**11 and 12**). HEK293 lysates were incubated with ATP-acrylamides followed by immunoprecipitation with anti Akt1 antibody and agarose beads. As a control, the reaction was performed in presence of staurosporine (STSP), kinase inhibitor. The reaction mixtures were separated by SDS-PAGE electrophoresis and transferring onto PVDF membrane as a western blotting. Top gel is visualized by treating with anti-AKT1 antibody followed by secondary HRP, while the bottom gel was visualized by SYPRO Ruby. At least three independent trials were performed but only two trials were used for in gel digestion and further MS/MS analysis (Table A4.2 and A4.3)

## 4.6 Representation of the number of unique peptides identified from Akt1 substrates identification experiment with ATP-acrylamides using K-CLIP.

**Table A.4.1: All proteins identified from crosslinking of Akt1 with ATP-PEG-Acr in HEK293 from 2 independent trials.**

After IP of Akt1 as in figure 4.20, Protein lists obtained from Ms/Ms analysis. Number of unique peptides identified for each protein in the crosslinked Akt1 with ATP-PEG-Acr lane (lane 5, Figure 4.20) were divided by number of unique peptides identified from staursporine treated HEK293 (lane 4, Figure 4.20) or non-crosslinked Akt1 (lane 1, Figure 4.20) to obtain peptide ratio of ATP-PEG-Acr. Only peptide ratio that is more than one and present in two independednt trials is considered to be solely phosphorylation dependent crosslinking and shown in the following table. Proteins from 1-7 are known Akt1 physical interactor (as reported in Biogrid database) and proteins from 8-11 are known Akt1 substrates (as reported in phosphosite database). The rest of proteins can be substrate candidates for Akt1. This data represents proteins from two independent trials

| No | Protein identified | Gene | Accession number | Mol. Wt (kDa) | Scansite motif |
|-----|--------------------|------|------------------|---------------|----------------|
| 1. | Stress-70 protein, mitochondrial | HSPA9 | GRP75 | 74 | Yes |
| 2. | Vesicle-fusing ATPase | NSF | NSF | 83 | Yes |
| 3. | Heat shock protein HSP 90-alpha | HSP90AA1 | HS90A | 85 | Yes |
| 4. | Heat shock protein HSP 90-beta | HSP90AB1 | HS90B | 83 | Yes |
| 5. | Heat shock cognate 71 kDa protein | HSPA8 | HSP7C | 71 | Yes |
| 6. | Creatine kinase B-type | CKB | KCRB | 43 | Yes |
| 7. | L-lactate dehydrogenase A chain | LDHA | LDHA | 37 | No |
| 8. | Transitional endoplasmic reticulum ATPase | VCP | TERA | 89 | Yes |
| 9. | Pre-mRNA-processing factor 19 | PRPF19 | PRP19 | 55 | Yes |
| 10. | T-complex protein 1 subunit beta | CCT2 | TCPB | 57 | Yes |
| 11. | Zyxin | ZYX | ZYX | 61 | Yes |
| 12. | Aconitate hydratase, mitochondrial | ACO2 | ACON | 85 | Yes |
| 13. | Alpha-actinin-4 | ACTN4 | ACTN4 | 105 | Yes |
| 14. | Activator of 90 kDa heat shock protein ATPase homolog 1 | AHSA1 | AHSA1 | 38 | Yes |
| 15. | Apoptosis-inducing factor 1, mitochondrial | AIFM1 | AIFM1 | 67 | Yes |
| 16. | Cytosol aminopeptidase | LAP3 | AMPL | 56 | Yes |
| 17. | ATPase family AAA domain-containing protein 3A | ATAD3A | ATD3A | 71 | Yes |

| 18. | Cytoskeleton-associated protein 4 | CKAP4 | CKAP4 | 66 | Yes |
|---|---|---|---|---|---|
| 19. | Cytosolic non-specific dipeptidase | CNDP2 | CNDP2 | 53 | Yes |
| 20. | Coatomer subunit gamma-1 | COPG1 | COPG1 | 98 | Yes |
| 21. | Cold shock domain-containing protein E1 | CSDE1 | CSDE1 | 89 | Yes |
| 22. | COP9 signalosome complex subunit 4 | COPS4 | CSN4 | 46 | Yes |
| 23. | Drebrin-like protein | DBNL | DBNL | 48 | Yes |
| 24. | ATP-dependent RNA helicase DDX1 | DDX1 | DDX1 | 82 | No |
| 25. | Probable ATP-dependent RNA helicase DDX17 | DDX17 | DDX17 | 80 | Yes |
| 26. | Peroxisomal multifunctional enzyme type 2 | HSD17B4 | DHB4 | 80 | Yes |
| 27. | Dynamin-1-like protein | DNM1L | DNM1L | 82 | Yes |
| 28. | Dihydropyrimidinase-related protein 1 | CRMP1 | DPYL1 | 62 | Yes |
| 29. | Developmentally-regulated GTP-binding protein 1 | DRG1 | DRG1 | 41 | Yes |
| 30. | Trifunctional enzyme subunit alpha, mitochondrial | HADHA | ECHA | 83 | Yes |
| 31. | Elongation factor 2 | EEF2 | EF2 | 95 | Yes |
| 32. | Eukaryotic translation initiation factor 3 subunit D | EIF3D | EIF3D | 64 | Yes |
| 33. | Eukaryotic translation initiation factor 3 subunit L | EIF3L | EIF3L | 67 | Yes |
| 34. | Epiplakin | EPPK1 | EPIPL | 556 | Yes |
| 35. | Exosome component 10 | EXOSC10 | EXOSX | 101 | Yes |
| 36. | Ezrin | EZR | EZRI | 69 | Yes |
| 37. | RNA-binding protein FUS | FUS | FUS | 53 | Yes |
| 38. | Glucose-6-phosphate isomerase | GPI | G6PI | 63 | Yes |
| 39. | Glucosidase 2 subunit beta | PRKCSH | GLU2B | 59 | Yes |
| 40. | Serine hydroxymethyltransferase, mitochondrial | SHMT2 | GLYM | 56 | Yes |
| 41. | GMP synthase (glutamine-hydrolyzing) | GMPS | GUAA | 77 | Yes |
| 42. | Heterogeneous nuclear ribonucleoproteins C1/C2 | HNRNPC | HNRPC | 34 | Yes |
| 43. | Heterogeneous nuclear ribonucleoprotein F | HNRNPF | HNRPF | 46 | Yes |
| 44. | Heterogeneous nuclear ribonucleoprotein K | HNRNPK | HNRPK | 51 | Yes |
| 45. | Heterogeneous nuclear ribonucleoprotein M | | HNRPM | 78 | Yes |
| 46. | Heterogeneous nuclear ribonucleoprotein R | HNRNPR | HNRPR | 71 | Yes |
| 47. | Hornerin | HRNR | HORN | 282 | Yes |

| 48. | Heat shock 70 kDa protein 1A | HSPA1A | HS71A | 70 | Yes |
|---|---|---|---|---|---|
| 49. | Interferon regulatory factor 2-binding protein 1 | IRF2BP1 | I2BP1 | 62 | Yes |
| 50. | Importin subunit beta-1 | KPNB1 | IMB1 | 97 | Yes |
| 51. | Pyruvate kinase PKM | PKM | KPYM | 58 | Yes |
| 52. | LETM1 and EF-hand domain-containing protein 1, mitochondrial | LETM1 | LETM1 | 83 | Yes |
| 53. | Leukotriene A-4 hydrolase | LTA4H | LKHA4 | 69 | Yes |
| 54. | Leucine-rich repeat-containing protein 40 | LRRC40 | LRC40 | 68 | Yes |
| 55. | Melanoma-associated antigen D2 | MAGED2 | MAGD2 | 65 | Yes |
| 56. | DNA replication licensing factor MCM5 | MCM5 | MCM5 | 82 | Yes |
| 57. | MICOS complex subunit MIC60 | IMMT | MIC60 | 84 | Yes |
| 58. | Mitochondrial-processing peptidase subunit alpha | PMPCA | MPPA | 58 | Yes |
| 59. | Metastasis-associated protein MTA2 | MTA2 | MTA2 | 75 | Yes |
| 60. | Nuclear autoantigenic sperm protein | NASP | NASP | 85 | Yes |
| 61. | NADH-ubiquinone oxidoreductase 75 kDa subunit, mitochondrial | NDUFS1 | NDUS1 | 79 | Yes |
| 62. | tRNA (cytosine(34)-C(5))-methyltransferase | NSUN2 | NSUN2 | 86 | Yes |
| 63. | Dihydrolipoyllysine-residue acetyltransferase component of pyruvate dehydrogenase complex, mitochondrial | DLAT | ODP2 | 69 | Yes |
| 64. | Obg-like ATPase 1 | OLA1 | OLA1 | 45 | Yes |
| 65. | Transcriptional repressor p66-alpha | GATAD2A | P66A | 68 | Yes |
| 66. | Polyadenylate-binding protein 1 | PABPC1 | PABP1 | 71 | Yes |
| 67. | Plasminogen activator inhibitor 1 RNA-binding protein | SERBP1 | PAIRB | 45 | Yes |
| 68. | Poly(rC)-binding protein 1 | PCBP1 | PCBP1 | 37 | Yes |
| 69. | Programmed cell death 6-interacting protein | PDCD6IP | PDC6I | 96 | Yes |
| 70. | 2',5'-phosphodiesterase 12 | PDE12 | PDE12 | 67 | Yes |
| 71. | Peptidyl-prolyl cis-trans isomerase D | PPID | PPID | 41 | No |
| 72. | U4/U6 small nuclear ribonucleoprotein Prp3 | PRPF3 | PRPF3 | 78 | Yes |
| 73. | 26S protease regulatory subunit 10B | PSMC6 | PRS10 | 44 | Yes |
| 74. | 26S proteasome non-ATPase regulatory subunit 2 | PSMD2 | PSMD2 | 100 | Yes |
| 75. | 26S proteasome non-ATPase regulatory subunit 3 | PSMD3 | PSMD3 | 61 | Yes |
| 76. | Bifunctional purine biosynthesis protein PURH | ATIC | PUR9 | 65 | Yes |

| 77. | Glycogen phosphorylase, liver form | PYGL | PYGL | 97 | Yes |
|---|---|---|---|---|---|
| 78. | CTP synthase 1 | CTPS1 | PYRG1 | 67 | Yes |
| 79. | Ran GTPase-activating protein 1 | RANGAP1 | RAGP1 | 64 | Yes |
| 80. | Ribonucleoprotein PTB-binding 1 | RAVER1 | RAVR1 | 64 | Yes |
| 81. | Histone-binding protein RBBP4 | RBBP4 | RBBP4 | 48 | No |
| 82. | RNA-binding protein 14 | RBM14 | RBM14 | 69 | Yes |
| 83. | RNA-binding protein 39 | RBM39 | RBM39 | 59 | Yes |
| 84. | Reticulocalbin-1 | RCN1 | RCN1 | 39 | No |
| 85. | Dolichyl-diphosphooligosaccharide--protein glycosyltransferase subunit 1 | RPN1 | RPN1 | 69 | Yes |
| 86. | Ubiquitin-40S ribosomal protein S27a | RPS27A | RS27A | 18 | No |
| 87. | 40S ribosomal protein SA | RPSA | RSSA | 33 | No |
| 88. | Protein transport protein Sec31A | SEC31A | SC31A | 133 | Yes |
| 89. | Succinate dehydrogenase (ubiquinone) flavoprotein subunit, mitochondrial | SDHA | SDHA | 73 | Yes |
| 90. | Septin-11 | SEPT11 | SEP11 | 49 | Yes |
| 91. | Serpin H1 | SERPINH1 | SERPH | 46 | Yes |
| 92. | Splicing factor 3A subunit 3 | SF3A3 | SF3A3 | 59 | No |
| 93. | Splicing factor, proline- and glutamine-rich | SFPQ | SFPQ | 76 | Yes |
| 94. | Signal recognition particle subunit SRP68 | SRP68 | SRP68 | 71 | Yes |
| 95. | Signal recognition particle receptor subunit alpha | SRPR | SRPR | 70 | Yes |
| 96. | Alanine--tRNA ligase, cytoplasmic | AARS | SYAC | 107 | Yes |
| 97. | Phenylalanine--tRNA ligase beta subunit | FARSB | SYFB | 66 | Yes |
| 98. | Glycine--tRNA ligase | GARS | SYG | 83 | Yes |
| 99. | Arginine--tRNA ligase, cytoplasmic | RARS | SYRC | 75 | Yes |
| 100. | Tyrosine--tRNA ligase, cytoplasmic | YARS | SYYC | 59 | Yes |
| 101. | T-complex protein 1 subunit alpha | TCP1 | TCPA | 60 | Yes |
| 102. | T-complex protein 1 subunit delta | CCT4 | TCPD | 58 | Yes |
| 103. | T-complex protein 1 subunit epsilon | CCT5 | TCPE | 60 | Yes |
| 104. | T-complex protein 1 subunit gamma | CCT3 | TCPG | 61 | Yes |
| 105. | T-complex protein 1 subunit theta | CCT8 | TCPQ | 60 | Yes |
| 106. | Acetyl-CoA acetyltransferase, mitochondrial | ACAT1 | THIL | 45 | Yes |
| 107. | Mitochondrial import receptor subunit TOM70 | TOMM70A | TOM70 | 67 | Yes |

| 108. | Heat shock protein 75 kDa, mitochondrial | TRAP1 | TRAP1 | 80 | Yes |
|------|------------------------------------------|-------|-------|-----|-----|
| 109. | Tetratricopeptide repeat protein 4 | TTC4 | TTC4 | 45 | No |
| 110. | Tubulin--tyrosine ligase-like protein 12 | | TTL12 | 74 | Yes |
| 111. | Ubiquitin carboxyl-terminal hydrolase 5 | USP5 | UBP5 | 96 | Yes |
| 112. | Synaptic vesicle membrane protein VAT-1 homolog | VAT1 | VAT1 | 42 | No |
| 113. | V-type proton ATPase catalytic subunit A | ATP6V1A | VATA | 68 | Yes |
| 114. | Vacuolar protein sorting-associated protein 35 | VPS35 | VPS35 | 92 | Yes |
| 115. | Exportin-T | XPOT | XPOT | 110 | Yes |
| 116. | X-ray repair cross-complementing protein 6 | XRCC6 | XRCC6 | 70 | Yes |

**Table A.4.2: Proteins identified from crosslinking of Akt1 with ATP-Hex-Acr in HEK293 from two independent trials**

After IP of Akt1 as in figure 4.20, Protein lists obtained from Ms/Ms analysis. Number of unique peptides identified for each protein in the crosslinked Akt1 with ATP-Hex-Acr lane (lane 3, Figure 4.20) were divided by number of unique peptides identified from staursporine treated HEK293 (lane 2, Figure 4.20) or non-crosslinked Akt1 (lane 1, Figure 4.20) to obtain peptide ratio of ATP-PEG-Acr. Only peptide ratio that is more than one is considered to be solely depended on phosphorylation dependednt crosslinking and shown in the following table. Proteins from 1-3 are known Akt1 physical interactor (as reported in Biogrid database).

| No | Protein identification | Gene | Accession number | Mol. Wt. (kDa) |
|---|---|---|---|---|
| 1. | Stress-70 protein, mitochondrial | HSPA9 | GRP75 | 74 |
| 2. | Creatine kinase B-type | CKB | KCRB | 43 |
| 3. | L-lactate dehydrogenase A chain | LDHA | LDHA | 37 |
| 4. | Apoptosis-inducing factor 1, mitochondrial | AIFM1 | AIFM1 | 67 |
| 5. | Far upstream element-binding protein 3 | FUBP3 | FUBP3 | 62 |
| 6. | RNA-binding protein FUS | FUS | FUS | 53 |
| 7. | Heterogeneous nuclear ribonucleoprotein Q | SYNCRIP | HNRPQ | 70 |
| 8. | KH domain-containing, RNA-binding, signal transduction-associated protein 1 | KHDRBS1 | KHDR1 | 48 |
| 9. | MICOS complex subunit MIC60 | IMMT | MIC60 | 84 |
| 10. | Nucleolar protein 56 | NOP56 | NOP56 | 66 |
| 11. | Nucleolar protein 58 | NOP58 | NOP58 | 60 |
| 12. | Protein regulator of cytokinesis 1 | PRC1 | PRC1 | 72 |
| 13. | RNA-binding protein 14 | RBM14 | RBM14 | 69 |
| 14. | Ribosomal L1 domain-containing protein 1 | RSL1D1 | RL1D1 | 55 |
| 15. | V-type proton ATPase catalytic subunit A | ATP6V1A | VATA | 68 |
| 16. | DNA repair protein XRCC1 OS=Homo sapiens | XRCC1 | XRCC1 | 69 |
| 17. | YTH domain-containing family protein 2 | YTHDF2 | YTHD2 | 62 |

**Table A. 4. 3: Representation of the number of unique peptides from Trial 1, figure A 4.21**

The table containing data for trypsinized proteins from SDS-PAGE gel of trial 1 (Appendix C, section 4.5). The data of the table represents uncrosslinked lysated (lane 1, Figure A 4.21), ATP-Hex-Acr crosslinked lysates in presence of staursporine (lane 2, Figure A 4.21), ATP-Hex-Acr crosslinked lysates (lane 3, Figure A 4.21), ATP-PEG-Acr crosslinked lysates in presence of staursporine (lane 4, Figure A 4.21), and ATP-Hex-Acr crosslinked lysates (lane 5, Figure A 4.21).

| Protein identified | Accession No. | Mol. Wt. | No. of unique peptides identified | | | | |
|---|---|---|---|---|---|---|---|
| | | | Lane 1 | Lane 2 | Lane 3 | Lane 4 | Lane 5 |
| Stress-70 protein, mitochondrial OS=Homo sapiens GN=HSPA9 PE=1 SV=2 | GRP75 | 74 kDa | 5 | 1 | 8 | 4 | 6 |
| Creatine kinase B-type OS=Homo sapiens GN=CKB PE=1 SV=1 | KCRB | 43 kDa | 0 | 1 | 5 | 5 | 10 |
| L-lactate dehydrogenase A chain OS=Homo sapiens GN=LDHA PE=1 SV=2 | LDHA | 37 kDa | 0 | 0 | 1 | 0 | 1 |
| Heat shock protein HSP 90-alpha OS=Homo sapiens GN=HSP90AA1 PE=1 SV=5 | HS90A | 85 kDa | 31 | 5 | 13 | 20 | 35 |
| Heat shock protein HSP 90-beta OS=Homo sapiens GN=HSP90AB1 PE=1 SV=4 | HS90B | 83 kDa | 20 | 2 | 14 | 9 | 22 |
| Heat shock cognate 71 kDa protein OS=Homo sapiens GN=HSPA8 PE=1 SV=1 | HSP7C | 71 kDa | 13 | 0 | 4 | 10 | 18 |
| Vesicle-fusing ATPase OS=Homo sapiens GN=NSF PE=1 SV=3 | NSF | 83 kDa | 0 | 0 | 0 | 0 | 1 |
| Transitional endoplasmic reticulum ATPase OS=Homo sapiens GN=VCP PE=1 SV=4 | TERA | 89 kDa | 0 | 0 | 0 | 0 | 3 |
| Interleukin-1 receptor-associated kinase 1 OS=Homo sapiens GN=IRAK1 PE=1 SV=2 | IRAK1 | 77 kDa | 0 | 0 | 0 | 0 | 1 |
| Actin, cytoplasmic 1 OS=Homo sapiens GN=ACTB PE=1 SV=1 | ACTB | 42 kDa | 0 | 0 | 1 | 1 | 1 |
| Alpha-enolase OS=Homo sapiens GN=ENO1 PE=1 SV=2 | ENOA | 47 kDa | 1 | 1 | 2 | 7 | 5 |
| Vimentin OS=Homo sapiens GN=VIM PE=1 SV=4 | VIME | 54 kDa | 16 | 2 | 35 | 6 | 19 |
| Kinectin OS=Homo sapiens GN=KTN1 PE=1 SV=1 | KTN1 | 156 kDa | 0 | 0 | 0 | 0 | 1 |
| Proliferation-associated protein 2G4 OS=Homo sapiens GN=PA2G4 PE=1 SV=3 | PA2G4 | 44 kDa | 0 | 0 | 0 | 0 | 1 |
| 1-phosphatidylinositol 4,5-bisphosphate phosphodiesterase gamma-1 OS=Homo sapiens GN=PLCG1 PE=1 SV=1 | PLCG1 | 149 kDa | 0 | 0 | 0 | 0 | 1 |
| DNA-dependent protein kinase catalytic subunit OS=Homo sapiens GN=PRKDC PE=1 SV=3 | PRKDC | 469 kDa | 24 | 0 | 9 | 9 | 45 |

| | | | | | | | |
|---|---|---|---|---|---|---|---|
| Dynactin subunit 1 OS=Homo sapiens GN=DCTN1 PE=1 SV=3 | DCTN1 | 142 kDa | 1 | 0 | 0 | 0 | 8 |
| DNA (cytosine-5)-methyltransferase 1 OS=Homo sapiens GN=DNMT1 PE=1 SV=2 | DNMT1 | 183 kDa | 1 | 0 | 0 | 0 | 4 |
| Probable ATP-dependent RNA helicase DDX5 OS=Homo sapiens GN=DDX5 PE=1 SV=1 | DDX5 | 69 kDa | 4 | 0 | 5 | 2 | 4 |
| Serine/threonine-protein phosphatase 2A 65 kDa regulatory subunit A alpha isoform OS=Homo sapiens GN=PPP2R1A PE=1 SV=4 | 2AAA | 65 kDa | 4 | 0 | 4 | 1 | 9 |
| Sodium/potassium-transporting ATPase subunit alpha-1 OS=Homo sapiens GN=ATP1A1 PE=1 SV=1 | AT1A1 | 113 kDa | 4 | 0 | 2 | 0 | 13 |
| Clathrin heavy chain 1 OS=Homo sapiens GN=CLTC PE=1 SV=5 | CLH1 | 192 kDa | 22 | 1 | 4 | 4 | 33 |
| Elongation factor 1-gamma OS=Homo sapiens GN=EEF1G PE=1 SV=3 | EF1G | 50 kDa | 7 | 1 | 6 | 4 | 11 |
| Heat shock 70 kDa protein 4 OS=Homo sapiens GN=HSPA4 PE=1 SV=4 | HSP74 | 94 kDa | 5 | 0 | 1 | 2 | 6 |
| Hexokinase-1 OS=Homo sapiens GN=HK1 PE=1 SV=3 | HXK1 | 102 kDa | 5 | 1 | 1 | 1 | 6 |
| Eukaryotic initiation factor 4A-I OS=Homo sapiens GN=EIF4A1 PE=1 SV=1 | IF4A1 | 46 kDa | 14 | 1 | 10 | 7 | 17 |
| Ras GTPase-activating-like protein IQGAP1 OS=Homo sapiens GN=IQGAP1 PE=1 SV=1 | IQGA1 | 189 kDa | 0 | 0 | 0 | 0 | 7 |
| Actin, cytoplasmic 2 OS=Homo sapiens GN=ACTG1 PE=1 SV=1 | ACTG | 42 kDa | 0 | 4 | 10 | 10 | 14 |
| 6-phosphogluconate dehydrogenase, decarboxylating OS=Homo sapiens GN=PGD PE=1 SV=3 | 6PGD | 53 kDa | 0 | 0 | 1 | 2 | 4 |
| Apoptosis-inducing factor 1, mitochondrial OS=Homo sapiens GN=AIFM1 PE=1 SV=1 | AIFM1 | 67 kDa | 0 | 0 | 1 | 0 | 1 |
| Cytosol aminopeptidase OS=Homo sapiens GN=LAP3 PE=1 SV=3 | AMPL | 56 kDa | 0 | 0 | 1 | 0 | 3 |
| ATP synthase subunit alpha, mitochondrial OS=Homo sapiens GN=ATP5A1 PE=1 SV=1 | ATPA | 60 kDa | 10 | 0 | 11 | 8 | 12 |
| ATP synthase subunit beta, mitochondrial OS=Homo sapiens GN=ATP5B PE=1 SV=3 | ATPB | 57 kDa | 15 | 2 | 17 | 15 | 19 |
| Calreticulin OS=Homo sapiens GN=CALR PE=1 SV=1 | CALR | 48 kDa | 1 | 0 | 2 | 2 | 6 |
| Protein DEK OS=Homo sapiens GN=DEK PE=1 SV=1 | DEK | 43 kDa | 0 | 0 | 5 | 0 | 2 |
| Desmoplakin OS=Homo sapiens GN=DSP PE=1 SV=3 | DESP | 332 kDa | 1 | 1 | 5 | 0 | 8 |
| DnaJ homolog subfamily A member 1 OS=Homo sapiens GN=DNAJA1 PE=1 SV=2 | DNJA1 | 45 kDa | 0 | 0 | 2 | 0 | 2 |
| Elongation factor Tu, mitochondrial OS=Homo sapiens GN=TUFM PE=1 SV=2 | EFTU | 50 kDa | 5 | 0 | 9 | 5 | 8 |

| Protein description | Gene | MW | | | | | |
|---|---|---|---|---|---|---|---|
| Eukaryotic translation initiation factor 3 subunit D OS=Homo sapiens GN=EIF3D PE=1 SV=1 | EIF3D | 64 kDa | 0 | 0 | 2 | 0 | 2 |
| Flap endonuclease 1 OS=Homo sapiens GN=FEN1 PE=1 SV=1 | FEN1 | 43 kDa | 0 | 0 | 1 | 1 | 2 |
| RNA-binding protein FUS OS=Homo sapiens GN=FUS PE=1 SV=1 | FUS | 53 kDa | 0 | 0 | 3 | 0 | 2 |
| Ras GTPase-activating protein-binding protein 1 OS=Homo sapiens GN=G3BP1 PE=1 SV=1 | G3BP1 | 52 kDa | 3 | 0 | 5 | 3 | 8 |
| Guanine nucleotide-binding protein-like 3 OS=Homo sapiens GN=GNL3 PE=1 SV=2 | GNL3 | 62 kDa | 1 | 0 | 2 | 0 | 3 |
| HEAT repeat-containing protein 1 OS=Homo sapiens GN=HEATR1 PE=1 SV=3 | HEAT1 | 242 kDa | 0 | 0 | 1 | 0 | 3 |
| Heterogeneous nuclear ribonucleoprotein D0 OS=Homo sapiens GN=HNRNPD PE=1 SV=1 | HNRPD | 38 kDa | 0 | 0 | 1 | 0 | 1 |
| Heterogeneous nuclear ribonucleoprotein F OS=Homo sapiens GN=HNRNPF PE=1 SV=3 | HNRPF | 46 kDa | 1 | 0 | 3 | 1 | 2 |
| Heterogeneous nuclear ribonucleoprotein M OS=Homo sapiens GN=HNRNPM PE=1 SV=3 | HNRPM | 78 kDa | 13 | 1 | 17 | 6 | 15 |
| Heterogeneous nuclear ribonucleoprotein Q OS=Homo sapiens GN=SYNCRIP PE=1 SV=2 | HNRPQ | 70 kDa | 0 | 0 | 1 | 0 | 1 |
| Eukaryotic translation initiation factor 2 subunit 2 OS=Homo sapiens GN=EIF2S2 PE=1 SV=2 | IF2B | 38 kDa | 0 | 0 | 2 | 0 | 1 |
| Eukaryotic translation initiation factor 2 subunit 3 OS=Homo sapiens GN=EIF2S3 PE=1 SV=3 | IF2G | 51 kDa | 4 | 1 | 6 | 3 | 5 |
| Eukaryotic translation initiation factor 5B OS=Homo sapiens GN=EIF5B PE=1 SV=4 | IF2P | 139 kDa | 0 | 0 | 1 | 0 | 4 |
| Eukaryotic translation initiation factor 5 OS=Homo sapiens GN=EIF5 PE=1 SV=2 | IF5 | 49 kDa | 1 | 0 | 3 | 0 | 3 |
| Ig alpha-1 chain C region OS=Homo sapiens GN=IGHA1 PE=1 SV=2 | IGHA1 | 38 kDa | 0 | 0 | 2 | 0 | 3 |
| Interleukin enhancer-binding factor 2 OS=Homo sapiens GN=ILF2 PE=1 SV=2 | ILF2 | 43 kDa | 1 | 0 | 4 | 2 | 4 |
| Importin subunit alpha-1 OS=Homo sapiens GN=KPNA2 PE=1 SV=1 | IMA1 | 58 kDa | 4 | 2 | 6 | 4 | 5 |
| Lamin-B1 OS=Homo sapiens GN=LMNB1 PE=1 SV=2 | LMNB1 | 66 kDa | 0 | 0 | 9 | 0 | 4 |
| Leucine-rich repeat-containing protein 47 OS=Homo sapiens GN=LRRC47 PE=1 SV=1 | LRC47 | 63 kDa | 0 | 0 | 1 | 0 | 5 |
| MICOS complex subunit MIC60 OS=Homo sapiens GN=IMMT PE=1 SV=1 | MIC60 | 84 kDa | 0 | 0 | 1 | 0 | 1 |
| Neurofilament light polypeptide OS=Homo sapiens GN=NEFL PE=1 SV=3 | NFL | 62 kDa | 2 | 0 | 8 | 0 | 4 |
| Neurofilament medium polypeptide OS=Homo sapiens GN=NEFM PE=1 SV=3 | NFM | 102 kDa | 6 | 1 | 9 | 0 | 7 |

| Protein | ID | kDa | | | | | |
|---|---|---|---|---|---|---|---|
| Nucleosome assembly protein 1-like 1 OS=Homo sapiens GN=NAP1L1 PE=1 SV=1 | NP1L1 | 45 kDa | 2 | 0 | 4 | 3 | 5 |
| Nuclear pore complex protein Nup205 OS=Homo sapiens GN=NUP205 PE=1 SV=3 | NU205 | 228 kDa | 0 | 0 | 1 | 0 | 1 |
| Nuclear pore complex protein Nup93 OS=Homo sapiens GN=NUP93 PE=1 SV=2 | NUP93 | 93 kDa | 0 | 0 | 2 | 0 | 2 |
| Programmed cell death protein 4 OS=Homo sapiens GN=PDCD4 PE=1 SV=2 | PDCD4 | 52 kDa | 0 | 0 | 1 | 0 | 2 |
| Retrotransposon-derived protein PEG10 OS=Homo sapiens GN=PEG10 PE=1 SV=2 | PEG10 | 80 kDa | 0 | 0 | 1 | 0 | 1 |
| Protein regulator of cytokinesis 1 OS=Homo sapiens GN=PRC1 PE=1 SV=2 | PRC1 | 72 kDa | 0 | 0 | 3 | 0 | 1 |
| U4/U6 small nuclear ribonucleoprotein Prp31 OS=Homo sapiens GN=PRPF31 PE=1 SV=2 | PRP31 | 55 kDa | 0 | 0 | 1 | 0 | 1 |
| 26S protease regulatory subunit 4 OS=Homo sapiens GN=PSMC1 PE=1 SV=1 | PRS4 | 49 kDa | 1 | 1 | 3 | 1 | 2 |
| 26S protease regulatory subunit 8 OS=Homo sapiens GN=PSMC5 PE=1 SV=1 | PRS8 | 46 kDa | 1 | 0 | 3 | 2 | 5 |
| 26S proteasome non-ATPase regulatory subunit 11 OS=Homo sapiens GN=PSMD11 PE=1 SV=3 | PSD11 | 47 kDa | 1 | 0 | 2 | 1 | 4 |
| RNA-binding protein 14 OS=Homo sapiens GN=RBM14 PE=1 SV=2 | RBM14 | 69 kDa | 2 | 0 | 7 | 1 | 4 |
| Ribosomal L1 domain-containing protein 1 OS=Homo sapiens GN=RSL1D1 PE=1 SV=3 | RL1D1 | 55 kDa | 0 | 0 | 1 | 0 | 2 |
| 40S ribosomal protein SA OS=Homo sapiens GN=RPSA PE=1 SV=4 | RSSA | 33 kDa | 0 | 0 | 2 | 3 | 7 |
| tRNA-splicing ligase RtcB homolog OS=Homo sapiens GN=RTCB PE=1 SV=1 | RTCB | 55 kDa | 1 | 0 | 2 | 0 | 2 |
| Serpin H1 OS=Homo sapiens GN=SERPINH1 PE=1 SV=2 | SERPH | 46 kDa | 0 | 0 | 1 | 2 | 3 |
| Sorting nexin-1 OS=Homo sapiens GN=SNX1 PE=1 SV=3 | SNX1 | 59 kDa | 0 | 0 | 1 | 0 | 1 |
| Phenylalanine--tRNA ligase beta subunit OS=Homo sapiens GN=FARSB PE=1 SV=3 | SYFB | 66 kDa | 0 | 0 | 2 | 2 | 4 |
| T-complex protein 1 subunit delta OS=Homo sapiens GN=CCT4 PE=1 SV=4 | TCPD | 58 kDa | 6 | 0 | 8 | 7 | 12 |
| V-type proton ATPase catalytic subunit A OS=Homo sapiens GN=ATP6V1A PE=1 SV=2 | VATA | 68 kDa | 1 | 0 | 2 | 1 | 2 |
| Serine/threonine-protein phosphatase 2A 55 kDa regulatory subunit B alpha isoform OS=Homo sapiens GN=PPP2R2A PE=1 SV=1 | 2ABA | 52 kDa | 0 | 0 | 0 | 0 | 1 |
| Neutral amino acid transporter B(0) OS=Homo sapiens GN=SLC1A5 PE=1 SV=2 | AAAT | 57 kDa | 0 | 0 | 0 | 0 | 2 |

| | | | | | | | |
|---|---|---|---|---|---|---|---|
| ATP-binding cassette sub-family E member 1 OS=Homo sapiens GN=ABCE1 PE=1 SV=1 | ABCE1 | 67 kDa | 0 | 0 | 0 | 0 | 1 |
| Acetyl-CoA carboxylase 1 OS=Homo sapiens GN=ACACA PE=1 SV=2 | ACACA | 266 kDa | 1 | 0 | 0 | 0 | 2 |
| Apoptotic chromatin condensation inducer in the nucleus OS=Homo sapiens GN=ACIN1 PE=1 SV=2 | ACINU | 152 kDa | 0 | 0 | 0 | 0 | 1 |
| Actin-like protein 6A OS=Homo sapiens GN=ACTL6A PE=1 SV=1 | ACL6A | 47 kDa | 0 | 0 | 0 | 0 | 1 |
| Aconitate hydratase, mitochondrial OS=Homo sapiens GN=ACO2 PE=1 SV=2 | ACON | 85 kDa | 2 | 1 | 1 | 1 | 3 |
| Alpha-actinin-1 OS=Homo sapiens GN=ACTN1 PE=1 SV=2 | ACTN1 | 103 kDa | 0 | 0 | 0 | 0 | 2 |
| Alpha-actinin-4 OS=Homo sapiens GN=ACTN4 PE=1 SV=2 | ACTN4 | 105 kDa | 3 | 1 | 0 | 0 | 8 |
| Alpha-centractin OS=Homo sapiens GN=ACTR1A PE=1 SV=1 | ACTZ | 43 kDa | 0 | 0 | 0 | 0 | 2 |
| Proteasomal ubiquitin receptor ADRM1 OS=Homo sapiens GN=ADRM1 PE=1 SV=2 | ADRM1 | 42 kDa | 0 | 0 | 0 | 0 | 1 |
| NADPH:adrenodoxin oxidoreductase, mitochondrial OS=Homo sapiens GN=FDXR PE=1 SV=3 | ADRO | 54 kDa | 0 | 0 | 0 | 0 | 1 |
| ADP/ATP translocase 2 OS=Homo sapiens GN=SLC25A5 PE=1 SV=7 | ADT2 | 33 kDa | 0 | 0 | 0 | 0 | 1 |
| Afadin OS=Homo sapiens GN=MLLT4 PE=1 SV=3 | AFAD | 207 kDa | 0 | 0 | 0 | 0 | 1 |
| Phosphoacetylglucosamine mutase OS=Homo sapiens GN=PGM3 PE=1 SV=1 | AGM1 | 60 kDa | 1 | 0 | 1 | 1 | 2 |
| Activator of 90 kDa heat shock protein ATPase homolog 1 OS=Homo sapiens GN=AHSA1 PE=1 SV=1 | AHSA1 | 38 kDa | 0 | 0 | 0 | 0 | 3 |
| Aldehyde dehydrogenase X, mitochondrial OS=Homo sapiens GN=ALDH1B1 PE=1 SV=3 | AL1B1 | 57 kDa | 0 | 0 | 0 | 0 | 2 |
| Aminopeptidase B OS=Homo sapiens GN=RNPEP PE=1 SV=2 | AMPB | 73 kDa | 0 | 0 | 0 | 0 | 1 |
| Rabankyrin-5 OS=Homo sapiens GN=ANKFY1 PE=1 SV=2 | ANFY1 | 128 kDa | 0 | 0 | 0 | 0 | 2 |
| Ankyrin-2 OS=Homo sapiens GN=ANK2 PE=1 SV=4 | ANK2 | 434 kDa | 0 | 0 | 0 | 0 | 1 |
| Ankyrin repeat and KH domain-containing protein 1 OS=Homo sapiens GN=ANKHD1 PE=1 SV=1 | ANKH1 | 269 kDa | 0 | 0 | 0 | 0 | 1 |
| Protein arginine N-methyltransferase 5 OS=Homo sapiens GN=PRMT5 PE=1 SV=4 | ANM5 | 73 kDa | 0 | 0 | 0 | 0 | 1 |
| Annexin A6 OS=Homo sapiens GN=ANXA6 PE=1 SV=3 | ANXA6 | 76 kDa | 0 | 0 | 0 | 0 | 1 |
| AP-2 complex subunit mu OS=Homo sapiens GN=AP2M1 PE=1 SV=2 | AP2M1 | 50 kDa | 0 | 0 | 0 | 0 | 1 |
| AP-3 complex subunit delta-1 OS=Homo sapiens GN=AP3D1 PE=1 SV=1 | AP3D1 | 130 kDa | 0 | 0 | 0 | 0 | 2 |

| | | | | | | | |
|---|---|---|---|---|---|---|---|
| Apoptosis inhibitor 5 OS=Homo sapiens GN=API5 PE=1 SV=3 | API5 | 59 kDa | 0 | 0 | 0 | 0 | 1 |
| Intron-binding protein aquarius OS=Homo sapiens GN=AQR PE=1 SV=4 | AQR | 171 kDa | 0 | 0 | 0 | 0 | 1 |
| Asparagine synthetase (glutamine-hydrolyzing) OS=Homo sapiens GN=ASNS PE=1 SV=4 | ASNS | 64 kDa | 5 | 0 | 4 | 2 | 9 |
| Sarcoplasmic/endoplasmic reticulum calcium ATPase 2 OS=Homo sapiens GN=ATP2A2 PE=1 SV=1 | AT2A2 | 115 kDa | 1 | 0 | 0 | 0 | 8 |
| Plasma membrane calcium-transporting ATPase 2 OS=Homo sapiens GN=ATP2B2 PE=1 SV=2 | AT2B2 | 137 kDa | 0 | 0 | 0 | 0 | 1 |
| ATPase family AAA domain-containing protein 3A OS=Homo sapiens GN=ATAD3A PE=1 SV=2 | ATD3A | 71 kDa | 0 | 0 | 0 | 0 | 1 |
| Transcriptional regulator ATRX OS=Homo sapiens GN=ATRX PE=1 SV=5 | ATRX | 283 kDa | 0 | 0 | 0 | 0 | 1 |
| Ataxin-10 OS=Homo sapiens GN=ATXN10 PE=1 SV=1 | ATX10 | 53 kDa | 0 | 0 | 0 | 0 | 1 |
| BRISC and BRCA1-A complex member 1 OS=Homo sapiens GN=BABAM1 PE=1 SV=1 | BABA1 | 37 kDa | 0 | 0 | 0 | 0 | 1 |
| Large proline-rich protein BAG6 OS=Homo sapiens GN=BAG6 PE=1 SV=2 | BAG6 | 119 kDa | 0 | 0 | 0 | 0 | 1 |
| BRCA2 and CDKN1A-interacting protein OS=Homo sapiens GN=BCCIP PE=1 SV=1 | BCCIP | 36 kDa | 0 | 0 | 0 | 0 | 1 |
| Bleomycin hydrolase OS=Homo sapiens GN=BLMH PE=1 SV=1 | BLMH (+1) | 53 kDa | 0 | 0 | 0 | 0 | 1 |
| E3 ubiquitin-protein ligase BRE1B OS=Homo sapiens GN=RNF40 PE=1 SV=4 | BRE1B | 114 kDa | 0 | 0 | 0 | 0 | 1 |
| Calnexin OS=Homo sapiens GN=CANX PE=1 SV=2 | CALX | 68 kDa | 4 | 0 | 0 | 1 | 5 |
| Cullin-associated NEDD8-dissociated protein 1 OS=Homo sapiens GN=CAND1 PE=1 SV=2 | CAND1 | 136 kDa | 7 | 0 | 2 | 0 | 11 |
| Histone-arginine methyltransferase CARM1 OS=Homo sapiens GN=CARM1 PE=1 SV=3 | CARM1 | 66 kDa | 0 | 0 | 0 | 0 | 1 |
| Cell division cycle and apoptosis regulator protein 1 OS=Homo sapiens GN=CCAR1 PE=1 SV=2 | CCAR1 | 133 kDa | 0 | 0 | 0 | 0 | 1 |
| Coiled-coil domain-containing protein 22 OS=Homo sapiens GN=CCDC22 PE=1 SV=1 | CCD22 | 71 kDa | 0 | 0 | 0 | 0 | 1 |
| Cell division cycle protein 20 homolog OS=Homo sapiens GN=CDC20 PE=1 SV=2 | CDC20 | 55 kDa | 0 | 0 | 0 | 0 | 1 |
| 60 kDa heat shock protein, mitochondrial OS=Homo sapiens GN=HSPD1 PE=1 SV=2 | CH60 | 61 kDa | 23 | 2 | 21 | 17 | 29 |
| Chromodomain-helicase-DNA-binding protein 4 OS=Homo sapiens GN=CHD4 PE=1 SV=2 | CHD4 | 218 kDa | 3 | 0 | 1 | 0 | 5 |

| | | | | | | | |
|---|---|---|---|---|---|---|---|
| Cytoskeleton-associated protein 4 OS=Homo sapiens GN=CKAP4 PE=1 SV=2 | CKAP4 | 66 kDa | 0 | 0 | 0 | 0 | 1 |
| Cytoskeleton-associated protein 5 OS=Homo sapiens GN=CKAP5 PE=1 SV=3 | CKAP5 | 226 kDa | 7 | 0 | 0 | 0 | 17 |
| Clustered mitochondria protein homolog OS=Homo sapiens GN=CLUH PE=1 SV=2 | CLU | 147 kDa | 0 | 0 | 0 | 0 | 3 |
| Cytosolic non-specific dipeptidase OS=Homo sapiens GN=CNDP2 PE=1 SV=2 | CNDP2 | 53 kDa | 0 | 0 | 0 | 0 | 2 |
| CCR4-NOT transcription complex subunit 1 OS=Homo sapiens GN=CNOT1 PE=1 SV=2 | CNOT1 | 267 kDa | 0 | 0 | 0 | 0 | 1 |
| Coatomer subunit alpha OS=Homo sapiens GN=COPA PE=1 SV=2 | COPA | 138 kDa | 9 | 0 | 1 | 0 | 12 |
| Coatomer subunit gamma-1 OS=Homo sapiens GN=COPG1 PE=1 SV=1 | COPG1 | 98 kDa | 5 | 0 | 1 | 1 | 10 |
| Cold shock domain-containing protein E1 OS=Homo sapiens GN=CSDE1 PE=1 SV=2 | CSDE1 | 89 kDa | 4 | 0 | 1 | 1 | 5 |
| COP9 signalosome complex subunit 3 OS=Homo sapiens GN=COPS3 PE=1 SV=3 | CSN3 | 48 kDa | 0 | 0 | 0 | 0 | 2 |
| COP9 signalosome complex subunit 4 OS=Homo sapiens GN=COPS4 PE=1 SV=1 | CSN4 | 46 kDa | 0 | 0 | 0 | 0 | 2 |
| Catenin delta-1 OS=Homo sapiens GN=CTNND1 PE=1 SV=1 | CTND1 | 108 kDa | 0 | 0 | 0 | 0 | 1 |
| RNA polymerase-associated protein CTR9 homolog OS=Homo sapiens GN=CTR9 PE=1 SV=1 | CTR9 | 134 kDa | 0 | 0 | 0 | 0 | 1 |
| Cullin-2 OS=Homo sapiens GN=CUL2 PE=1 SV=2 | CUL2 | 87 kDa | 0 | 0 | 0 | 0 | 1 |
| Cytoplasmic FMR1-interacting protein 1 OS=Homo sapiens GN=CYFIP1 PE=1 SV=1 | CYFP1 | 145 kDa | 1 | 0 | 0 | 0 | 4 |
| Dynein assembly factor 5, axonemal OS=Homo sapiens GN=DNAAF5 PE=1 SV=4 | DAAF5 | 94 kDa | 0 | 0 | 0 | 0 | 1 |
| Drebrin-like protein OS=Homo sapiens GN=DBNL PE=1 SV=1 | DBNL | 48 kDa | 0 | 0 | 0 | 0 | 1 |
| ATP-dependent RNA helicase DDX1 OS=Homo sapiens GN=DDX1 PE=1 SV=2 | DDX1 | 82 kDa | 2 | 0 | 0 | 0 | 6 |
| Probable ATP-dependent RNA helicase DDX17 OS=Homo sapiens GN=DDX17 PE=1 SV=2 | DDX17 | 80 kDa | 9 | 0 | 7 | 4 | 10 |
| Probable ATP-dependent RNA helicase DDX20 OS=Homo sapiens GN=DDX20 PE=1 SV=2 | DDX20 | 92 kDa | 0 | 0 | 0 | 0 | 1 |
| ATP-dependent RNA helicase DDX50 OS=Homo sapiens GN=DDX50 PE=1 SV=1 | DDX50 | 83 kDa | 3 | 0 | 0 | 0 | 4 |
| ATP-dependent RNA helicase DDX54 OS=Homo sapiens GN=DDX54 PE=1 SV=2 | DDX54 | 99 kDa | 0 | 0 | 0 | 0 | 1 |

| | | | | | | | |
|---|---|---|---|---|---|---|---|
| Peroxisomal multifunctional enzyme type 2 OS=Homo sapiens GN=HSD17B4 PE=1 SV=3 | DHB4 | 80 kDa | 0 | 0 | 0 | 1 | 3 |
| Putative pre-mRNA-splicing factor ATP-dependent RNA helicase DHX16 OS=Homo sapiens GN=DHX16 PE=1 SV=2 | DHX16 | 119 kDa | 0 | 0 | 0 | 0 | 1 |
| Protein diaphanous homolog 1 OS=Homo sapiens GN=DIAPH1 PE=1 SV=2 | DIAP1 | 141 kDa | 1 | 0 | 0 | 0 | 2 |
| DnaJ homolog subfamily C member 10 OS=Homo sapiens GN=DNAJC10 PE=1 SV=2 | DJC10 | 91 kDa | 0 | 0 | 0 | 0 | 1 |
| DnaJ homolog subfamily C member 7 OS=Homo sapiens GN=DNAJC7 PE=1 SV=2 | DNJC7 | 56 kDa | 0 | 0 | 0 | 0 | 1 |
| Dynamin-1-like protein OS=Homo sapiens GN=DNM1L PE=1 SV=2 | DNM1L | 82 kDa | 1 | 0 | 0 | 0 | 2 |
| Dedicator of cytokinesis protein 7 OS=Homo sapiens GN=DOCK7 PE=1 SV=4 | DOCK7 | 243 kDa | 0 | 0 | 0 | 0 | 1 |
| DNA polymerase delta catalytic subunit OS=Homo sapiens GN=POLD1 PE=1 SV=2 | DPOD1 | 124 kDa | 1 | 0 | 0 | 0 | 3 |
| DNA polymerase alpha catalytic subunit OS=Homo sapiens GN=POLA1 PE=1 SV=2 | DPOLA | 166 kDa | 0 | 0 | 0 | 0 | 2 |
| Dipeptidyl peptidase 3 OS=Homo sapiens GN=DPP3 PE=1 SV=2 | DPP3 | 83 kDa | 0 | 0 | 0 | 0 | 1 |
| Dihydropyrimidinase-related protein 1 OS=Homo sapiens GN=CRMP1 PE=1 SV=1 | DPYL1 | 62 kDa | 0 | 0 | 0 | 0 | 1 |
| Developmentally-regulated GTP-binding protein 1 OS=Homo sapiens GN=DRG1 PE=1 SV=1 | DRG1 | 41 kDa | 0 | 0 | 0 | 0 | 2 |
| Double-stranded RNA-specific adenosine deaminase OS=Homo sapiens GN=ADAR PE=1 SV=4 | DSRAD | 136 kDa | 0 | 0 | 0 | 0 | 1 |
| ATP-dependent RNA helicase DDX39A OS=Homo sapiens GN=DDX39A PE=1 SV=2 | DX39A | 49 kDa | 3 | 0 | 1 | 1 | 5 |
| Spliceosome RNA helicase DDX39B OS=Homo sapiens GN=DDX39B PE=1 SV=1 | DX39B | 49 kDa | 0 | 0 | 0 | 0 | 3 |
| Cytoplasmic dynein 1 heavy chain 1 OS=Homo sapiens GN=DYNC1H1 PE=1 SV=5 | DYHC1 | 532 kDa | 16 | 0 | 5 | 2 | 29 |
| Trifunctional enzyme subunit alpha, mitochondrial OS=Homo sapiens GN=HADHA PE=1 SV=2 | ECHA | 83 kDa | 3 | 0 | 2 | 1 | 4 |
| Proteasome-associated protein ECM29 homolog OS=Homo sapiens GN=ECM29 PE=1 SV=2 | ECM29 | 204 kDa | 0 | 0 | 0 | 0 | 6 |
| Enhancer of mRNA-decapping protein 4 OS=Homo sapiens GN=EDC4 PE=1 SV=1 | EDC4 | 152 kDa | 0 | 0 | 0 | 0 | 1 |
| Early endosome antigen 1 OS=Homo sapiens GN=EEA1 PE=1 SV=2 | EEA1 | 162 kDa | 0 | 0 | 0 | 0 | 2 |

| Protein | Gene | MW | | | | | |
|---|---|---|---|---|---|---|---|
| Elongation factor 1-alpha 1 OS=Homo sapiens GN=EEF1A1 PE=1 SV=1 | EF1A1 | 50 kDa | 17 | 3 | 14 | 10 | 19 |
| Elongation factor 2 OS=Homo sapiens GN=EEF2 PE=1 SV=4 | EF2 | 95 kDa | 35 | 5 | 24 | 24 | 38 |
| Eukaryotic translation initiation factor 2D OS=Homo sapiens GN=EIF2D PE=1 SV=3 | EIF2D | 65 kDa | 0 | 0 | 0 | 0 | 1 |
| Eukaryotic translation initiation factor 3 subunit B OS=Homo sapiens GN=EIF3B PE=1 SV=3 | EIF3B | 92 kDa | 6 | 0 | 3 | 1 | 7 |
| Eukaryotic translation initiation factor 3 subunit F OS=Homo sapiens GN=EIF3F PE=1 SV=1 | EIF3F | 38 kDa | 4 | 0 | 1 | 3 | 5 |
| Eukaryotic translation initiation factor 3 subunit L OS=Homo sapiens GN=EIF3L PE=1 SV=1 | EIF3L | 67 kDa | 2 | 0 | 1 | 0 | 5 |
| Epiplakin OS=Homo sapiens GN=EPPK1 PE=1 SV=2 | EPIPL | 556 kDa | 3 | 0 | 0 | 0 | 4 |
| Clathrin interactor 1 OS=Homo sapiens GN=CLINT1 PE=1 SV=1 | EPN4 | 68 kDa | 0 | 0 | 0 | 0 | 1 |
| ERC protein 2 OS=Homo sapiens GN=ERC2 PE=1 SV=3 | ERC2 | 111 kDa | 0 | 0 | 0 | 0 | 1 |
| Eukaryotic peptide chain release factor subunit 1 OS=Homo sapiens GN=ETF1 PE=1 SV=3 | ERF1 | 49 kDa | 0 | 0 | 0 | 0 | 1 |
| Extended synaptotagmin-1 OS=Homo sapiens GN=ESYT1 PE=1 SV=1 | ESYT1 | 123 kDa | 2 | 0 | 0 | 0 | 4 |
| Exosome component 10 OS=Homo sapiens GN=EXOSC10 PE=1 SV=2 | EXOSX | 101 kDa | 0 | 0 | 0 | 0 | 1 |
| Ezrin OS=Homo sapiens GN=EZR PE=1 SV=4 | EZRI | 69 kDa | 2 | 0 | 0 | 3 | 5 |
| Hsc70-interacting protein OS=Homo sapiens GN=ST13 PE=1 SV=2 | F10A1 | 41 kDa | 0 | 0 | 0 | 0 | 1 |
| Constitutive coactivator of PPAR-gamma-like protein 1 OS=Homo sapiens GN=FAM120A PE=1 SV=2 | F120A | 122 kDa | 1 | 0 | 0 | 0 | 2 |
| Fanconi anemia group I protein OS=Homo sapiens GN=FANCI PE=1 SV=4 | FANCI | 149 kDa | 0 | 0 | 0 | 0 | 1 |
| Fatty acid synthase OS=Homo sapiens GN=FASN PE=1 SV=3 | FAS | 273 kDa | 19 | 0 | 7 | 3 | 48 |
| FK506-binding protein 15 OS=Homo sapiens GN=FKBP15 PE=1 SV=2 | FKB15 | 134 kDa | 0 | 0 | 0 | 0 | 1 |
| Peptidyl-prolyl cis-trans isomerase FKBP4 OS=Homo sapiens GN=FKBP4 PE=1 SV=3 | FKBP4 | 52 kDa | 1 | 0 | 0 | 2 | 4 |
| Protein flightless-1 homolog OS=Homo sapiens GN=FLII PE=1 SV=2 | FLII | 145 kDa | 0 | 0 | 0 | 0 | 2 |
| Filamin-A OS=Homo sapiens GN=FLNA PE=1 SV=4 | FLNA | 281 kDa | 8 | 0 | 5 | 1 | 37 |
| Filamin-B OS=Homo sapiens GN=FLNB PE=1 SV=2 | FLNB | 278 kDa | 0 | 0 | 0 | 0 | 8 |
| Filamin-C OS=Homo sapiens GN=FLNC PE=1 SV=3 | FLNC | 291 kDa | 0 | 1 | 0 | 0 | 1 |
| Fascin OS=Homo sapiens GN=FSCN1 PE=1 SV=3 | FSCN1 | 55 kDa | 1 | 0 | 1 | 4 | 5 |

| | | | | | | | |
|---|---|---|---|---|---|---|---|
| Fumarate hydratase, mitochondrial OS=Homo sapiens GN=FH PE=1 SV=3 | FUMH | 55 kDa | 1 | 0 | 1 | 0 | 2 |
| Fragile X mental retardation syndrome-related protein 1 OS=Homo sapiens GN=FXR1 PE=1 SV=3 | FXR1 | 70 kDa | 1 | 0 | 1 | 0 | 2 |
| Glucose-6-phosphate isomerase OS=Homo sapiens GN=GPI PE=1 SV=4 | G6PI | 63 kDa | 4 | 0 | 3 | 4 | 8 |
| Neutral alpha-glucosidase AB OS=Homo sapiens GN=GANAB PE=1 SV=3 | GANAB | 107 kDa | 4 | 0 | 1 | 0 | 15 |
| Translational activator GCN1 OS=Homo sapiens GN=GCN1L1 PE=1 SV=6 | GCN1L | 293 kDa | 5 | 0 | 0 | 0 | 16 |
| Rab GDP dissociation inhibitor beta OS=Homo sapiens GN=GDI2 PE=1 SV=2 | GDIB | 51 kDa | 0 | 0 | 0 | 2 | 3 |
| Gem-associated protein 4 OS=Homo sapiens GN=GEMIN4 PE=1 SV=2 | GEMI4 | 120 kDa | 0 | 0 | 0 | 0 | 1 |
| Glomulin OS=Homo sapiens GN=GLMN PE=1 SV=2 | GLMN | 68 kDa | 0 | 0 | 0 | 0 | 1 |
| Glucosidase 2 subunit beta OS=Homo sapiens GN=PRKCSH PE=1 SV=2 | GLU2B | 59 kDa | 0 | 0 | 0 | 0 | 1 |
| Serine hydroxymethyltransferase, mitochondrial OS=Homo sapiens GN=SHMT2 PE=1 SV=3 | GLYM | 56 kDa | 8 | 0 | 6 | 5 | 9 |
| Guanine nucleotide-binding protein-like 1 OS=Homo sapiens GN=GNL1 PE=1 SV=2 | GNL1 | 69 kDa | 0 | 0 | 0 | 0 | 1 |
| Golgin subfamily A member 2 OS=Homo sapiens GN=GOLGA2 PE=1 SV=3 | GOGA2 | 113 kDa | 0 | 0 | 0 | 0 | 1 |
| Procollagen galactosyltransferase 1 OS=Homo sapiens GN=COLGALT1 PE=1 SV=1 | GT251 | 72 kDa | 0 | 0 | 0 | 0 | 1 |
| GMP synthase (glutamine-hydrolyzing) OS=Homo sapiens GN=GMPS PE=1 SV=1 | GUAA | 77 kDa | 0 | 0 | 0 | 0 | 1 |
| Histone acetyltransferase type B catalytic subunit OS=Homo sapiens GN=HAT1 PE=1 SV=1 | HAT1 | 50 kDa | 1 | 0 | 1 | 1 | 3 |
| Histone deacetylase 1 OS=Homo sapiens GN=HDAC1 PE=1 SV=1 | HDAC1 | 55 kDa | 0 | 0 | 0 | 0 | 1 |
| Histone deacetylase 2 OS=Homo sapiens GN=HDAC2 PE=1 SV=2 | HDAC2 | 55 kDa | 1 | 0 | 1 | 0 | 3 |
| E3 ubiquitin-protein ligase HECTD1 OS=Homo sapiens GN=HECTD1 PE=1 SV=3 | HECD1 | 289 kDa | 0 | 0 | 0 | 0 | 1 |
| Heterogeneous nuclear ribonucleoprotein H2 OS=Homo sapiens GN=HNRNPH2 PE=1 SV=1 | HNRH2 | 49 kDa | 1 | 0 | 1 | 0 | 2 |
| Heterogeneous nuclear ribonucleoproteins C1/C2 OS=Homo sapiens GN=HNRNPC PE=1 SV=4 | HNRPC | 34 kDa | 0 | 0 | 0 | 0 | 1 |
| Heterogeneous nuclear ribonucleoprotein K OS=Homo sapiens GN=HNRNPK PE=1 SV=1 | HNRPK | 51 kDa | 9 | 0 | 7 | 8 | 14 |

| | | | | | | | |
|---|---|---|---|---|---|---|---|
| Heterogeneous nuclear ribonucleoprotein L OS=Homo sapiens GN=HNRNPL PE=1 SV=2 | HNRPL | 64 kDa | 0 | 0 | 0 | 0 | 2 |
| Heterogeneous nuclear ribonucleoprotein R OS=Homo sapiens GN=HNRNPR PE=1 SV=1 | HNRPR | 71 kDa | 3 | 0 | 1 | 1 | 6 |
| Hornerin OS=Homo sapiens GN=HRNR PE=1 SV=2 | HORN | 282 kDa | 1 | 3 | 1 | 1 | 4 |
| Heat shock protein 105 kDa OS=Homo sapiens GN=HSPH1 PE=1 SV=1 | HS105 | 97 kDa | 3 | 0 | 0 | 2 | 5 |
| Heat shock 70 kDa protein 1A OS=Homo sapiens GN=HSPA1A PE=1 SV=1 | HS71A | 70 kDa | 22 | 10 | 18 | 18 | 29 |
| E3 ubiquitin-protein ligase HUWE1 OS=Homo sapiens GN=HUWE1 PE=1 SV=3 | HUWE1 | 482 kDa | 3 | 0 | 0 | 0 | 5 |
| Hypoxia up-regulated protein 1 OS=Homo sapiens GN=HYOU1 PE=1 SV=1 | HYOU1 | 111 kDa | 0 | 0 | 0 | 0 | 5 |
| Interferon regulatory factor 2-binding protein 1 OS=Homo sapiens GN=IRF2BP1 PE=1 SV=1 | I2BP1 | 62 kDa | 0 | 0 | 0 | 0 | 1 |
| Ig kappa chain C region OS=Homo sapiens GN=IGKC PE=1 SV=1 | IGKC | 12 kDa | 0 | 0 | 0 | 0 | 1 |
| Acetolactate synthase-like protein OS=Homo sapiens GN=ILVBL PE=1 SV=2 | ILVBL | 68 kDa | 0 | 0 | 0 | 0 | 1 |
| Importin subunit alpha-7 OS=Homo sapiens GN=KPNA6 PE=1 SV=1 | IMA7 | 60 kDa | 1 | 0 | 1 | 0 | 2 |
| Importin subunit beta-1 OS=Homo sapiens GN=KPNB1 PE=1 SV=2 | IMB1 | 97 kDa | 7 | 1 | 2 | 1 | 8 |
| Importin-11 OS=Homo sapiens GN=IPO11 PE=1 SV=1 | IPO11 | 113 kDa | 0 | 0 | 0 | 0 | 1 |
| Importin-4 OS=Homo sapiens GN=IPO4 PE=1 SV=2 | IPO4 | 119 kDa | 6 | 0 | 1 | 0 | 10 |
| Importin-5 OS=Homo sapiens GN=IPO5 PE=1 SV=4 | IPO5 | 124 kDa | 10 | 0 | 1 | 0 | 11 |
| Importin-7 OS=Homo sapiens GN=IPO7 PE=1 SV=1 | IPO7 | 120 kDa | 5 | 0 | 0 | 0 | 6 |
| C-Jun-amino-terminal kinase-interacting protein 4 OS=Homo sapiens GN=SPAG9 PE=1 SV=4 | JIP4 | 146 kDa | 0 | 0 | 0 | 0 | 1 |
| Keratin, type II cytoskeletal 6C OS=Homo sapiens GN=KRT6C PE=1 SV=3 | K2C6C | 60 kDa | 0 | 3 | 2 | 0 | 1 |
| cAMP-dependent protein kinase type II-alpha regulatory subunit OS=Homo sapiens GN=PRKAR2A PE=1 SV=2 | KAP2 | 46 kDa | 0 | 0 | 0 | 0 | 1 |
| cAMP-dependent protein kinase catalytic subunit alpha OS=Homo sapiens GN=PRKACA PE=1 SV=2 | KAPCA | 41 kDa | 0 | 0 | 0 | 0 | 1 |
| KIF1-binding protein OS=Homo sapiens GN=KIF1BP PE=1 SV=1 | KBP | 72 kDa | 0 | 0 | 0 | 0 | 1 |
| Calcium/calmodulin-dependent protein kinase type II subunit delta OS=Homo sapiens GN=CAMK2D PE=1 SV=3 | KCC2D | 56 kDa | 0 | 0 | 0 | 0 | 1 |
| Creatine kinase M-type OS=Homo sapiens GN=CKM PE=1 SV=2 | KCRM | 43 kDa | 0 | 2 | 0 | 0 | 1 |

| Creatine kinase U-type, mitochondrial OS=Homo sapiens GN=CKMT1A PE=1 SV=1 | KCRU | 47 kDa | 0 | 0 | 0 | 0 | 1 |
|---|---|---|---|---|---|---|---|
| Kinesin-like protein KIF11 OS=Homo sapiens GN=KIF11 PE=1 SV=2 | KIF11 | 119 kDa | 0 | 0 | 0 | 0 | 2 |
| Kinesin-like protein KIFC1 OS=Homo sapiens GN=KIFC1 PE=1 SV=2 | KIFC1 | 74 kDa | 0 | 0 | 0 | 0 | 1 |
| Kinesin-1 heavy chain OS=Homo sapiens GN=KIF5B PE=1 SV=1 | KINH | 110 kDa | 2 | 0 | 0 | 0 | 4 |
| Protein kinase C delta type OS=Homo sapiens GN=PRKCD PE=1 SV=2 | KPCD | 78 kDa | 0 | 0 | 0 | 0 | 1 |
| Pyruvate kinase PKM OS=Homo sapiens GN=PKM PE=1 SV=4 | KPYM | 58 kDa | 8 | 2 | 5 | 10 | 22 |
| Lethal(2) giant larvae protein homolog 1 OS=Homo sapiens GN=LLGL1 PE=1 SV=3 | L2GL1 | 115 kDa | 0 | 0 | 0 | 0 | 1 |
| Lupus La protein OS=Homo sapiens GN=SSB PE=1 SV=2 | LA | 47 kDa | 0 | 0 | 0 | 1 | 2 |
| La-related protein 4 OS=Homo sapiens GN=LARP4 PE=1 SV=3 | LARP4 | 81 kDa | 0 | 0 | 0 | 0 | 1 |
| Putative lipocalin 1-like protein 1 OS=Homo sapiens GN=LCN1P1 PE=5 SV=1 | LC1L1 (+1) | 18 kDa | 0 | 0 | 0 | 0 | 1 |
| Luc7-like protein 3 OS=Homo sapiens GN=LUC7L3 PE=1 SV=2 | LC7L3 | 51 kDa | 0 | 0 | 0 | 0 | 1 |
| LETM1 and EF-hand domain-containing protein 1, mitochondrial OS=Homo sapiens GN=LETM1 PE=1 SV=1 | LETM1 | 83 kDa | 0 | 0 | 0 | 0 | 3 |
| Leukotriene A-4 hydrolase OS=Homo sapiens GN=LTA4H PE=1 SV=2 | LKHA4 | 69 kDa | 2 | 0 | 0 | 1 | 6 |
| Lon protease homolog, mitochondrial OS=Homo sapiens GN=LONP1 PE=1 SV=2 | LONM | 106 kDa | 5 | 0 | 0 | 1 | 7 |
| Lipopolysaccharide-responsive and beige-like anchor protein OS=Homo sapiens GN=LRBA PE=1 SV=4 | LRBA | 319 kDa | 0 | 0 | 0 | 0 | 2 |
| Leucine-rich repeat-containing protein 40 OS=Homo sapiens GN=LRRC40 PE=1 SV=1 | LRC40 | 68 kDa | 0 | 0 | 0 | 0 | 1 |
| Protein LTV1 homolog OS=Homo sapiens GN=LTV1 PE=1 SV=1 | LTV1 | 55 kDa | 0 | 0 | 0 | 0 | 1 |
| Lysozyme C OS=Homo sapiens GN=LYZ PE=1 SV=1 | LYSC | 17 kDa | 0 | 0 | 0 | 0 | 1 |
| Microtubule-actin cross-linking factor 1, isoforms 1/2/3/5 OS=Homo sapiens GN=MACF1 PE=1 SV=4 | MACF1 | 838 kDa | 0 | 0 | 0 | 0 | 1 |
| Melanoma-associated antigen D2 OS=Homo sapiens GN=MAGED2 PE=1 SV=2 | MAGD2 | 65 kDa | 0 | 0 | 0 | 0 | 1 |
| Microtubule-associated protein 1B OS=Homo sapiens GN=MAP1B PE=1 SV=2 | MAP1B | 271 kDa | 0 | 0 | 0 | 0 | 3 |
| Microtubule-associated protein 4 OS=Homo sapiens GN=MAP4 PE=1 SV=3 | MAP4 | 121 kDa | 0 | 0 | 0 | 0 | 1 |

| | | | | | | | |
|---|---|---|---|---|---|---|---|
| DNA replication licensing factor MCM2 OS=Homo sapiens GN=MCM2 PE=1 SV=4 | MCM2 | 102 kDa | 11 | 0 | 2 | 2 | 12 |
| DNA replication licensing factor MCM3 OS=Homo sapiens GN=MCM3 PE=1 SV=3 | MCM3 | 91 kDa | 6 | 0 | 2 | 2 | 8 |
| DNA replication licensing factor MCM5 OS=Homo sapiens GN=MCM5 PE=1 SV=5 | MCM5 | 82 kDa | 7 | 0 | 3 | 0 | 8 |
| DNA replication licensing factor MCM6 OS=Homo sapiens GN=MCM6 PE=1 SV=1 | MCM6 | 93 kDa | 5 | 2 | 4 | 4 | 9 |
| 7SK snRNA methylphosphate capping enzyme OS=Homo sapiens GN=MEPCE PE=1 SV=1 | MEPCE | 74 kDa | 0 | 0 | 0 | 0 | 1 |
| Methionine synthase OS=Homo sapiens GN=MTR PE=1 SV=2 | METH | 141 kDa | 0 | 0 | 0 | 0 | 1 |
| Moesin OS=Homo sapiens GN=MSN PE=1 SV=3 | MOES | 68 kDa | 0 | 0 | 0 | 0 | 2 |
| Mannosyl-oligosaccharide glucosidase OS=Homo sapiens GN=MOGS PE=1 SV=5 | MOGS | 92 kDa | 0 | 0 | 0 | 0 | 1 |
| Dual specificity mitogen-activated protein kinase kinase 2 OS=Homo sapiens GN=MAP2K2 PE=1 SV=1 | MP2K2 | 44 kDa | 0 | 0 | 0 | 0 | 1 |
| Mitochondrial-processing peptidase subunit alpha OS=Homo sapiens GN=PMPCA PE=1 SV=2 | MPPA | 58 kDa | 0 | 0 | 0 | 0 | 1 |
| Cation-independent mannose-6-phosphate receptor OS=Homo sapiens GN=IGF2R PE=1 SV=3 | MPRI | 274 kDa | 0 | 0 | 0 | 0 | 2 |
| DNA mismatch repair protein Msh3 OS=Homo sapiens GN=MSH3 PE=1 SV=4 | MSH3 | 127 kDa | 0 | 0 | 0 | 0 | 1 |
| Metastasis-associated protein MTA2 OS=Homo sapiens GN=MTA2 PE=1 SV=1 | MTA2 | 75 kDa | 2 | 0 | 0 | 0 | 3 |
| Myosin-9 OS=Homo sapiens GN=MYH9 PE=1 SV=4 | MYH9 | 227 kDa | 16 | 0 | 1 | 1 | 21 |
| Unconventional myosin-VI OS=Homo sapiens GN=MYO6 PE=1 SV=4 | MYO6 | 150 kDa | 0 | 0 | 0 | 0 | 1 |
| N-alpha-acetyltransferase 15, NatA auxiliary subunit OS=Homo sapiens GN=NAA15 PE=1 SV=1 | NAA15 | 101 kDa | 6 | 0 | 2 | 0 | 7 |
| Nicotinamide phosphoribosyltransferase OS=Homo sapiens GN=NAMPT PE=1 SV=1 | NAMPT | 56 kDa | 1 | 0 | 0 | 1 | 2 |
| Nuclear autoantigenic sperm protein OS=Homo sapiens GN=NASP PE=1 SV=2 | NASP | 85 kDa | 0 | 0 | 0 | 0 | 5 |
| Nck-associated protein 1 OS=Homo sapiens GN=NCKAP1 PE=1 SV=1 | NCKP1 | 129 kDa | 0 | 0 | 0 | 0 | 1 |
| NADH-ubiquinone oxidoreductase 75 kDa subunit, mitochondrial OS=Homo sapiens GN=NDUFS1 PE=1 SV=3 | NDUS1 | 79 kDa | 0 | 0 | 0 | 0 | 2 |
| Serine/threonine-protein kinase Nek9 OS=Homo sapiens GN=NEK9 PE=1 SV=2 | NEK9 | 107 kDa | 0 | 0 | 0 | 0 | 1 |

| Negative elongation factor B OS=Homo sapiens GN=NELFB PE=1 SV=1 | NELFB | 66 kDa | 0 | 0 | 0 | 0 | 1 |
|---|---|---|---|---|---|---|---|
| Nucleolar protein 11 OS=Homo sapiens GN=NOL11 PE=1 SV=1 | NOL11 | 81 kDa | 0 | 0 | 0 | 0 | 1 |
| Nodal modulator 1 OS=Homo sapiens GN=NOMO1 PE=1 SV=5 | NOMO1 | 134 kDa | 1 | 0 | 0 | 0 | 3 |
| Probable 28S rRNA (cytosine(4447)-C(5))-methyltransferase OS=Homo sapiens GN=NOP2 PE=1 SV=2 | NOP2 | 89 kDa | 0 | 0 | 0 | 0 | 1 |
| Nucleolar protein 9 OS=Homo sapiens GN=NOP9 PE=1 SV=1 | NOP9 | 69 kDa | 0 | 0 | 0 | 0 | 1 |
| tRNA (cytosine(34)-C(5))-methyltransferase OS=Homo sapiens GN=NSUN2 PE=1 SV=2 | NSUN2 | 86 kDa | 3 | 0 | 1 | 0 | 4 |
| Nuclear pore complex protein Nup155 OS=Homo sapiens GN=NUP155 PE=1 SV=1 | NU155 | 155 kDa | 3 | 0 | 1 | 0 | 4 |
| Nucleoporin NUP188 homolog OS=Homo sapiens GN=NUP188 PE=1 SV=1 | NU188 | 196 kDa | 0 | 0 | 0 | 0 | 1 |
| Nucleolin OS=Homo sapiens GN=NCL PE=1 SV=3 | NUCL | 77 kDa | 11 | 0 | 7 | 1 | 12 |
| Nuclear migration protein nudC OS=Homo sapiens GN=NUDC PE=1 SV=1 | NUDC | 38 kDa | 0 | 0 | 0 | 0 | 1 |
| Nuclear mitotic apparatus protein 1 OS=Homo sapiens GN=NUMA1 PE=1 SV=2 | NUMA1 | 238 kDa | 2 | 0 | 2 | 0 | 8 |
| Nuclear pore complex protein Nup88 OS=Homo sapiens GN=NUP88 PE=1 SV=2 | NUP88 | 84 kDa | 0 | 0 | 0 | 0 | 1 |
| Lipoamide acyltransferase component of branched-chain alpha-keto acid dehydrogenase complex, mitochondrial OS=Homo sapiens GN=DBT PE=1 SV=3 | ODB2 | 53 kDa | 0 | 0 | 0 | 0 | 2 |
| Dihydrolipoyllysine-residue acetyltransferase component of pyruvate dehydrogenase complex, mitochondrial OS=Homo sapiens GN=DLAT PE=1 SV=3 | ODP2 | 69 kDa | 0 | 0 | 0 | 0 | 2 |
| Protein O-GlcNAcase OS=Homo sapiens GN=MGEA5 PE=1 SV=2 | OGA | 103 kDa | 0 | 0 | 0 | 0 | 2 |
| UDP-N-acetylglucosamine--peptide N-acetylglucosaminyltransferase 110 kDa subunit OS=Homo sapiens GN=OGT PE=1 SV=3 | OGT1 | 117 kDa | 0 | 0 | 0 | 0 | 1 |
| Obg-like ATPase 1 OS=Homo sapiens GN=OLA1 PE=1 SV=2 | OLA1 | 45 kDa | 0 | 0 | 0 | 0 | 2 |
| Dolichyl-diphosphooligosaccharide--protein glycosyltransferase 48 kDa subunit OS=Homo sapiens GN=DDOST PE=1 SV=4 | OST48 | 51 kDa | 2 | 0 | 0 | 0 | 3 |
| Serine/threonine-protein phosphatase 4 regulatory subunit 3A OS=Homo sapiens GN=SMEK1 PE=1 SV=1 | P4R3A | 95 kDa | 0 | 0 | 0 | 0 | 1 |
| Transcriptional repressor p66-alpha OS=Homo sapiens GN=GATAD2A PE=1 SV=1 | P66A | 68 kDa | 0 | 0 | 0 | 0 | 1 |

| | | | | | | | |
|---|---|---|---|---|---|---|---|
| Polyadenylate-binding protein 1 OS=Homo sapiens GN=PABPC1 PE=1 SV=2 | PABP1 | 71 kDa | 4 | 1 | 2 | 3 | 8 |
| Polyadenylate-binding protein 4 OS=Homo sapiens GN=PABPC4 PE=1 SV=1 | PABP4 | 71 kDa | 1 | 0 | 0 | 0 | 4 |
| Plasminogen activator inhibitor 1 RNA-binding protein OS=Homo sapiens GN=SERBP1 PE=1 SV=2 | PAIRB | 45 kDa | 2 | 1 | 2 | 2 | 3 |
| Lysophosphatidylcholine acyltransferase 1 OS=Homo sapiens GN=LPCAT1 PE=1 SV=2 | PCAT1 | 59 kDa | 0 | 0 | 0 | 0 | 1 |
| Poly(rC)-binding protein 1 OS=Homo sapiens GN=PCBP1 PE=1 SV=2 | PCBP1 | 37 kDa | 0 | 0 | 0 | 0 | 3 |
| Poly(rC)-binding protein 2 OS=Homo sapiens GN=PCBP2 PE=1 SV=1 | PCBP2 | 39 kDa | 0 | 0 | 0 | 0 | 1 |
| Programmed cell death 6-interacting protein OS=Homo sapiens GN=PDCD6IP PE=1 SV=1 | PDC6I | 96 kDa | 3 | 0 | 0 | 0 | 7 |
| 2',5'-phosphodiesterase 12 OS=Homo sapiens GN=PDE12 PE=1 SV=2 | PDE12 | 67 kDa | 0 | 0 | 0 | 0 | 1 |
| Protein disulfide-isomerase OS=Homo sapiens GN=P4HB PE=1 SV=3 | PDIA1 | 57 kDa | 0 | 0 | 0 | 0 | 1 |
| Protein disulfide-isomerase A3 OS=Homo sapiens GN=PDIA3 PE=1 SV=4 | PDIA3 | 57 kDa | 8 | 2 | 8 | 9 | 15 |
| Sister chromatid cohesion protein PDS5 homolog A OS=Homo sapiens GN=PDS5A PE=1 SV=1 | PDS5A | 151 kDa | 1 | 0 | 0 | 0 | 2 |
| Proline-, glutamic acid- and leucine-rich protein 1 OS=Homo sapiens GN=PELP1 PE=1 SV=2 | PELP1 | 120 kDa | 1 | 0 | 0 | 0 | 3 |
| PERQ amino acid-rich with GYF domain-containing protein 2 OS=Homo sapiens GN=GIGYF2 PE=1 SV=1 | PERQ2 | 150 kDa | 0 | 0 | 0 | 0 | 1 |
| Phosphoglucomutase-2 OS=Homo sapiens GN=PGM2 PE=1 SV=4 | PGM2 | 68 kDa | 0 | 0 | 0 | 0 | 1 |
| GPI transamidase component PIG-S OS=Homo sapiens GN=PIGS PE=1 SV=3 | PIGS | 62 kDa | 0 | 0 | 0 | 0 | 1 |
| Plectin OS=Homo sapiens GN=PLEC PE=1 SV=3 | PLEC | 532 kDa | 0 | 0 | 0 | 0 | 2 |
| Peptidyl-prolyl cis-trans isomerase D OS=Homo sapiens GN=PPID PE=1 SV=3 | PPID | 41 kDa | 0 | 0 | 0 | 0 | 2 |
| Pre-mRNA-processing factor 19 OS=Homo sapiens GN=PRPF19 PE=1 SV=1 | PRP19 | 55 kDa | 0 | 0 | 0 | 0 | 1 |
| Pre-mRNA-processing-splicing factor 8 OS=Homo sapiens GN=PRPF8 PE=1 SV=2 | PRP8 | 274 kDa | 2 | 0 | 0 | 0 | 13 |
| U4/U6 small nuclear ribonucleoprotein Prp3 OS=Homo sapiens GN=PRPF3 PE=1 SV=2 | PRPF3 | 78 kDa | 0 | 0 | 0 | 0 | 1 |
| 26S protease regulatory subunit 10B OS=Homo sapiens GN=PSMC6 PE=1 SV=1 | PRS10 | 44 kDa | 0 | 0 | 0 | 1 | 3 |

| | | | | | | | |
|---|---|---|---|---|---|---|---|
| 26S protease regulatory subunit 6A OS=Homo sapiens GN=PSMC3 PE=1 SV=3 | PRS6A | 49 kDa | 3 | 0 | 1 | 0 | 5 |
| 26S protease regulatory subunit 6B OS=Homo sapiens GN=PSMC4 PE=1 SV=2 | PRS6B | 47 kDa | 4 | 0 | 2 | 1 | 5 |
| 26S proteasome non-ATPase regulatory subunit 2 OS=Homo sapiens GN=PSMD2 PE=1 SV=3 | PSMD2 | 100 kDa | 12 | 1 | 2 | 3 | 13 |
| 26S proteasome non-ATPase regulatory subunit 3 OS=Homo sapiens GN=PSMD3 PE=1 SV=2 | PSMD3 | 61 kDa | 3 | 0 | 2 | 2 | 4 |
| 26S proteasome non-ATPase regulatory subunit 6 OS=Homo sapiens GN=PSMD6 PE=1 SV=1 | PSMD6 | 46 kDa | 0 | 0 | 0 | 0 | 1 |
| Polypyrimidine tract-binding protein 1 OS=Homo sapiens GN=PTBP1 PE=1 SV=1 | PTBP1 | 57 kDa | 7 | 0 | 5 | 8 | 9 |
| Trifunctional purine biosynthetic protein adenosine-3 OS=Homo sapiens GN=GART PE=1 SV=1 | PUR2 | 108 kDa | 5 | 1 | 2 | 1 | 17 |
| Adenylosuccinate lyase OS=Homo sapiens GN=ADSL PE=1 SV=2 | PUR8 | 55 kDa | 1 | 0 | 0 | 2 | 3 |
| Bifunctional purine biosynthesis protein PURH OS=Homo sapiens GN=ATIC PE=1 SV=3 | PUR9 | 65 kDa | 4 | 1 | 4 | 5 | 12 |
| Periodic tryptophan protein 2 homolog OS=Homo sapiens GN=PWP2 PE=1 SV=2 | PWP2 | 102 kDa | 0 | 0 | 0 | 0 | 1 |
| Glycogen phosphorylase, liver form OS=Homo sapiens GN=PYGL PE=1 SV=4 | PYGL | 97 kDa | 4 | 0 | 1 | 1 | 6 |
| CAD protein OS=Homo sapiens GN=CAD PE=1 SV=3 | PYR1 | 243 kDa | 4 | 0 | 3 | 2 | 18 |
| CTP synthase 1 OS=Homo sapiens GN=CTPS1 PE=1 SV=2 | PYRG1 | 67 kDa | 0 | 0 | 0 | 1 | 7 |
| CTP synthase 2 OS=Homo sapiens GN=CTPS2 PE=1 SV=1 | PYRG2 | 66 kDa | 0 | 0 | 0 | 0 | 1 |
| DNA repair protein RAD50 OS=Homo sapiens GN=RAD50 PE=1 SV=1 | RAD50 | 154 kDa | 0 | 0 | 0 | 0 | 3 |
| Ran GTPase-activating protein 1 OS=Homo sapiens GN=RANGAP1 PE=1 SV=1 | RAGP1 | 64 kDa | 2 | 0 | 0 | 0 | 7 |
| Ribonucleoprotein PTB-binding 1 OS=Homo sapiens GN=RAVER1 PE=1 SV=1 | RAVR1 | 64 kDa | 0 | 0 | 0 | 0 | 1 |
| Histone-binding protein RBBP4 OS=Homo sapiens GN=RBBP4 PE=1 SV=3 | RBBP4 | 48 kDa | 2 | 0 | 1 | 0 | 3 |
| Rab GTPase-activating protein 1 OS=Homo sapiens GN=RABGAP1 PE=1 SV=3 | RBGP1 | 122 kDa | 0 | 0 | 0 | 0 | 1 |
| Rab3 GTPase-activating protein non-catalytic subunit OS=Homo sapiens GN=RAB3GAP2 PE=1 SV=1 | RBGPR | 156 kDa | 0 | 0 | 0 | 0 | 2 |
| RNA-binding protein 12 OS=Homo sapiens GN=RBM12 PE=1 SV=1 | RBM12 | 97 kDa | 0 | 0 | 0 | 0 | 1 |
| RNA-binding protein 39 OS=Homo sapiens GN=RBM39 PE=1 SV=2 | RBM39 | 59 kDa | 1 | 0 | 1 | 0 | 2 |

| | | | | | | | |
|---|---|---|---|---|---|---|---|
| E3 SUMO-protein ligase RanBP2 OS=Homo sapiens GN=RANBP2 PE=1 SV=2 | RBP2 | 358 kDa | 0 | 0 | 0 | 0 | 1 |
| Reticulocalbin-1 OS=Homo sapiens GN=RCN1 PE=1 SV=1 | RCN1 | 39 kDa | 0 | 0 | 0 | 0 | 1 |
| UV excision repair protein RAD23 homolog B OS=Homo sapiens GN=RAD23B PE=1 SV=1 | RD23B | 43 kDa | 0 | 0 | 0 | 0 | 1 |
| ATP-dependent DNA helicase Q1 OS=Homo sapiens GN=RECQL PE=1 SV=3 | RECQ1 | 73 kDa | 0 | 0 | 0 | 0 | 1 |
| Replication initiator 1 OS=Homo sapiens GN=REPIN1 PE=1 SV=1 | REPI1 | 64 kDa | 0 | 0 | 0 | 0 | 1 |
| Ribonuclease inhibitor OS=Homo sapiens GN=RNH1 PE=1 SV=2 | RINI | 50 kDa | 0 | 0 | 0 | 0 | 1 |
| 60S ribosomal protein L27a OS=Homo sapiens GN=RPL27A PE=1 SV=2 | RL27A | 17 kDa | 0 | 0 | 0 | 0 | 1 |
| 60S ribosomal protein L3 OS=Homo sapiens GN=RPL3 PE=1 SV=2 | RL3 | 46 kDa | 5 | 0 | 4 | 0 | 7 |
| 60S ribosomal protein L6 OS=Homo sapiens GN=RPL6 PE=1 SV=3 | RL6 | 33 kDa | 1 | 0 | 1 | 1 | 4 |
| 60 kDa SS-A/Ro ribonucleoprotein OS=Homo sapiens GN=TROVE2 PE=1 SV=2 | RO60 | 61 kDa | 1 | 0 | 0 | 0 | 2 |
| Rho-associated protein kinase 2 OS=Homo sapiens GN=ROCK2 PE=1 SV=4 | ROCK2 | 161 kDa | 0 | 0 | 0 | 0 | 1 |
| DNA-directed RNA polymerase II subunit RPB1 OS=Homo sapiens GN=POLR2A PE=1 SV=2 | RPB1 | 217 kDa | 0 | 0 | 0 | 0 | 2 |
| DNA-directed RNA polymerase II subunit RPB2 OS=Homo sapiens GN=POLR2B PE=1 SV=1 | RPB2 | 134 kDa | 0 | 0 | 0 | 0 | 1 |
| DNA-directed RNA polymerase III subunit RPC3 OS=Homo sapiens GN=POLR3C PE=1 SV=1 | RPC3 | 61 kDa | 0 | 0 | 0 | 0 | 1 |
| Dolichyl-diphosphooligosaccharide--protein glycosyltransferase subunit 1 OS=Homo sapiens GN=RPN1 PE=1 SV=1 | RPN1 | 69 kDa | 2 | 0 | 2 | 1 | 5 |
| Dolichyl-diphosphooligosaccharide--protein glycosyltransferase subunit 2 OS=Homo sapiens GN=RPN2 PE=1 SV=3 | RPN2 | 69 kDa | 0 | 0 | 0 | 0 | 2 |
| RRP12-like protein OS=Homo sapiens GN=RRP12 PE=1 SV=2 | RRP12 | 144 kDa | 0 | 0 | 0 | 0 | 2 |
| Protein RRP5 homolog OS=Homo sapiens GN=PDCD11 PE=1 SV=3 | RRP5 | 209 kDa | 0 | 0 | 0 | 0 | 1 |
| Ubiquitin-40S ribosomal protein S27a OS=Homo sapiens GN=RPS27A PE=1 SV=2 | RS27A | 18 kDa | 3 | 0 | 1 | 2 | 4 |
| RNA 3'-terminal phosphate cyclase OS=Homo sapiens GN=RTCA PE=1 SV=1 | RTCA | 39 kDa | 0 | 0 | 0 | 0 | 1 |
| U1 small nuclear ribonucleoprotein 70 kDa OS=Homo sapiens GN=SNRNP70 PE=1 SV=2 | RU17 | 52 kDa | 0 | 0 | 0 | 0 | 1 |
| RuvB-like 2 OS=Homo sapiens GN=RUVBL2 PE=1 SV=3 | RUVB2 | 51 kDa | 11 | 2 | 10 | 6 | 12 |

| | | | | | | | |
|---|---|---|---|---|---|---|---|
| Solute carrier family 12 member 2 OS=Homo sapiens GN=SLC12A2 PE=1 SV=1 | S12A2 | 131 kDa | 0 | 0 | 0 | 0 | 1 |
| Protein transport protein Sec16A OS=Homo sapiens GN=SEC16A PE=1 SV=3 | SC16A | 234 kDa | 0 | 0 | 0 | 0 | 2 |
| Protein transport protein Sec31A OS=Homo sapiens GN=SEC31A PE=1 SV=3 | SC31A | 133 kDa | 1 | 0 | 0 | 0 | 3 |
| Succinate dehydrogenase (ubiquinone) flavoprotein subunit, mitochondrial OS=Homo sapiens GN=SDHA PE=1 SV=2 | SDHA | 73 kDa | 1 | 0 | 0 | 0 | 3 |
| Translocation protein SEC63 homolog OS=Homo sapiens GN=SEC63 PE=1 SV=2 | SEC63 | 88 kDa | 0 | 0 | 0 | 0 | 1 |
| Septin-11 OS=Homo sapiens GN=SEPT11 PE=1 SV=3 | SEP11 | 49 kDa | 0 | 0 | 0 | 0 | 1 |
| Septin-2 OS=Homo sapiens GN=SEPT2 PE=1 SV=1 | SEPT2 | 41 kDa | 0 | 0 | 0 | 0 | 2 |
| Splicing factor 3A subunit 1 OS=Homo sapiens GN=SF3A1 PE=1 SV=1 | SF3A1 | 89 kDa | 1 | 0 | 1 | 0 | 3 |
| Splicing factor 3A subunit 3 OS=Homo sapiens GN=SF3A3 PE=1 SV=1 | SF3A3 | 59 kDa | 1 | 0 | 0 | 0 | 2 |
| Splicing factor 3B subunit 1 OS=Homo sapiens GN=SF3B1 PE=1 SV=3 | SF3B1 | 146 kDa | 6 | 0 | 0 | 0 | 10 |
| Splicing factor 3B subunit 3 OS=Homo sapiens GN=SF3B3 PE=1 SV=4 | SF3B3 | 136 kDa | 0 | 0 | 0 | 0 | 5 |
| Splicing factor, proline- and glutamine-rich OS=Homo sapiens GN=SFPQ PE=1 SV=2 | SFPQ | 76 kDa | 4 | 1 | 0 | 4 | 9 |
| Superkiller viralicidic activity 2-like 2 OS=Homo sapiens GN=SKIV2L2 PE=1 SV=3 | SK2L2 | 118 kDa | 0 | 0 | 0 | 0 | 1 |
| STE20-like serine/threonine-protein kinase OS=Homo sapiens GN=SLK PE=1 SV=1 | SLK | 143 kDa | 0 | 0 | 0 | 0 | 1 |
| Structural maintenance of chromosomes protein 2 OS=Homo sapiens GN=SMC2 PE=1 SV=2 | SMC2 | 136 kDa | 4 | 0 | 0 | 0 | 6 |
| Structural maintenance of chromosomes protein 3 OS=Homo sapiens GN=SMC3 PE=1 SV=2 | SMC3 | 142 kDa | 6 | 0 | 3 | 1 | 8 |
| Transcription activator BRG1 OS=Homo sapiens GN=SMARCA4 PE=1 SV=2 | SMCA4 | 185 kDa | 0 | 0 | 0 | 0 | 6 |
| Structural maintenance of chromosomes flexible hinge domain-containing protein 1 OS=Homo sapiens GN=SMCHD1 PE=1 SV=2 | SMHD1 | 226 kDa | 0 | 0 | 0 | 0 | 2 |
| SWI/SNF-related matrix-associated actin-dependent regulator of chromatin subfamily D member 2 OS=Homo sapiens GN=SMARCD2 PE=1 SV=3 | SMRD2 | 59 kDa | 0 | 0 | 0 | 0 | 1 |

| Staphylococcal nuclease domain-containing protein 1 OS=Homo sapiens GN=SND1 PE=1 SV=1 | SND1 | 102 kDa | 2 | 0 | 0 | 2 | 3 |
|---|---|---|---|---|---|---|---|
| U4/U6.U5 tri-snRNP-associated protein 2 OS=Homo sapiens GN=USP39 PE=1 SV=2 | SNUT2 | 65 kDa | 0 | 0 | 0 | 0 | 1 |
| FACT complex subunit SPT16 OS=Homo sapiens GN=SUPT16H PE=1 SV=1 | SP16H | 120 kDa | 10 | 0 | 6 | 0 | 11 |
| Transcription elongation factor SPT6 OS=Homo sapiens GN=SUPT6H PE=1 SV=2 | SPT6H | 199 kDa | 0 | 0 | 0 | 0 | 1 |
| Spectrin beta chain, non-erythrocytic 1 OS=Homo sapiens GN=SPTBN1 PE=1 SV=2 | SPTB2 | 275 kDa | 0 | 0 | 0 | 0 | 2 |
| Spectrin alpha chain, non-erythrocytic 1 OS=Homo sapiens GN=SPTAN1 PE=1 SV=3 | SPTN1 | 285 kDa | 0 | 0 | 0 | 0 | 2 |
| Signal recognition particle subunit SRP68 OS=Homo sapiens GN=SRP68 PE=1 SV=2 | SRP68 | 71 kDa | 1 | 0 | 1 | 1 | 6 |
| Signal recognition particle subunit SRP72 OS=Homo sapiens GN=SRP72 PE=1 SV=3 | SRP72 | 75 kDa | 0 | 0 | 0 | 1 | 3 |
| Signal recognition particle receptor subunit alpha OS=Homo sapiens GN=SRPR PE=1 SV=2 | SRPR | 70 kDa | 0 | 0 | 0 | 0 | 2 |
| Serine/arginine-rich splicing factor 11 OS=Homo sapiens GN=SRSF11 PE=1 SV=1 | SRS11 | 54 kDa | 0 | 0 | 0 | 0 | 1 |
| Signal transducer and activator of transcription 1-alpha/beta OS=Homo sapiens GN=STAT1 PE=1 SV=2 | STAT1 | 87 kDa | 0 | 0 | 0 | 0 | 2 |
| Dolichyl-diphosphooligosaccharide--protein glycosyltransferase subunit STT3A OS=Homo sapiens GN=STT3A PE=1 SV=2 | STT3A | 81 kDa | 0 | 0 | 0 | 0 | 1 |
| SURP and G-patch domain-containing protein 2 OS=Homo sapiens GN=SUGP2 PE=1 SV=2 | SUGP2 | 120 kDa | 0 | 0 | 0 | 0 | 1 |
| Alanine--tRNA ligase, cytoplasmic OS=Homo sapiens GN=AARS PE=1 SV=2 | SYAC | 107 kDa | 1 | 0 | 0 | 1 | 7 |
| Aspartate--tRNA ligase, cytoplasmic OS=Homo sapiens GN=DARS PE=1 SV=2 | SYDC | 57 kDa | 6 | 0 | 5 | 1 | 8 |
| Aspartate--tRNA ligase, mitochondrial OS=Homo sapiens GN=DARS2 PE=1 SV=1 | SYDM | 74 kDa | 0 | 0 | 0 | 0 | 1 |
| Glycine--tRNA ligase OS=Homo sapiens GN=GARS PE=1 SV=3 | SYG | 83 kDa | 0 | 0 | 0 | 0 | 1 |
| Isoleucine--tRNA ligase, cytoplasmic OS=Homo sapiens GN=IARS PE=1 SV=2 | SYIC | 145 kDa | 10 | 0 | 1 | 0 | 15 |
| Lysine--tRNA ligase OS=Homo sapiens GN=KARS PE=1 SV=3 | SYK | 68 kDa | 2 | 0 | 1 | 0 | 3 |
| Leucine--tRNA ligase, cytoplasmic OS=Homo sapiens GN=LARS PE=1 SV=2 | SYLC | 134 kDa | 10 | 0 | 1 | 2 | 12 |

| | | | | | | | |
|---|---|---|---|---|---|---|---|
| Arginine--tRNA ligase, cytoplasmic OS=Homo sapiens GN=RARS PE=1 SV=2 | SYRC | 75 kDa | 4 | 0 | 1 | 2 | 11 |
| Valine--tRNA ligase OS=Homo sapiens GN=VARS PE=1 SV=4 | SYVC | 140 kDa | 5 | 0 | 2 | 1 | 6 |
| Tyrosine--tRNA ligase, cytoplasmic OS=Homo sapiens GN=YARS PE=1 SV=4 | SYYC | 59 kDa | 0 | 0 | 0 | 1 | 4 |
| Tyrosine--tRNA ligase, mitochondrial OS=Homo sapiens GN=YARS2 PE=1 SV=2 | SYYM | 53 kDa | 0 | 0 | 0 | 0 | 1 |
| Transforming acidic coiled-coil-containing protein 3 OS=Homo sapiens GN=TACC3 PE=1 SV=1 | TACC3 | 90 kDa | 0 | 0 | 0 | 0 | 1 |
| TBC1 domain family member 15 OS=Homo sapiens GN=TBC1D15 PE=1 SV=2 | TBC15 | 79 kDa | 0 | 0 | 0 | 0 | 1 |
| Transducin beta-like protein 2 OS=Homo sapiens GN=TBL2 PE=1 SV=1 | TBL2 | 50 kDa | 0 | 0 | 0 | 0 | 2 |
| T-complex protein 1 subunit alpha OS=Homo sapiens GN=TCP1 PE=1 SV=1 | TCPA | 60 kDa | 9 | 1 | 4 | 4 | 14 |
| T-complex protein 1 subunit beta OS=Homo sapiens GN=CCT2 PE=1 SV=4 | TCPB | 57 kDa | 9 | 2 | 6 | 6 | 16 |
| T-complex protein 1 subunit epsilon OS=Homo sapiens GN=CCT5 PE=1 SV=1 | TCPE | 60 kDa | 3 | 1 | 1 | 1 | 11 |
| T-complex protein 1 subunit gamma OS=Homo sapiens GN=CCT3 PE=1 SV=4 | TCPG | 61 kDa | 9 | 0 | 6 | 6 | 15 |
| T-complex protein 1 subunit eta OS=Homo sapiens GN=CCT7 PE=1 SV=2 | TCPH | 59 kDa | 6 | 0 | 6 | 5 | 12 |
| T-complex protein 1 subunit theta OS=Homo sapiens GN=CCT8 PE=1 SV=4 | TCPQ | 60 kDa | 6 | 1 | 5 | 4 | 12 |
| T-complex protein 1 subunit zeta OS=Homo sapiens GN=CCT6A PE=1 SV=3 | TCPZ | 58 kDa | 6 | 0 | 2 | 2 | 7 |
| Transcription elongation regulator 1 OS=Homo sapiens GN=TCERG1 PE=1 SV=2 | TCRG1 | 124 kDa | 1 | 0 | 0 | 0 | 3 |
| General transcription factor 3C polypeptide 1 OS=Homo sapiens GN=GTF3C1 PE=1 SV=4 | TF3C1 | 239 kDa | 0 | 0 | 0 | 0 | 2 |
| General transcription factor 3C polypeptide 2 OS=Homo sapiens GN=GTF3C2 PE=1 SV=2 | TF3C2 | 101 kDa | 0 | 0 | 0 | 0 | 1 |
| General transcription factor 3C polypeptide 5 OS=Homo sapiens GN=GTF3C5 PE=1 SV=2 | TF3C5 | 60 kDa | 0 | 0 | 0 | 0 | 1 |
| Acetyl-CoA acetyltransferase, mitochondrial OS=Homo sapiens GN=ACAT1 PE=1 SV=1 | THIL | 45 kDa | 0 | 0 | 0 | 0 | 3 |
| THO complex subunit 5 homolog OS=Homo sapiens GN=THOC5 PE=1 SV=2 | THOC5 | 79 kDa | 0 | 0 | 0 | 0 | 1 |
| Transketolase OS=Homo sapiens GN=TKT PE=1 SV=3 | TKT | 68 kDa | 3 | 0 | 1 | 3 | 9 |

| Talin-1 OS=Homo sapiens GN=TLN1 PE=1 SV=3 | TLN1 | 270 kDa | 0 | 0 | 0 | 0 | 6 |
|---|---|---|---|---|---|---|---|
| Mitochondrial import receptor subunit TOM70 OS=Homo sapiens GN=TOMM70A PE=1 SV=1 | TOM70 | 67 kDa | 0 | 0 | 0 | 0 | 1 |
| DNA topoisomerase 2-alpha OS=Homo sapiens GN=TOP2A PE=1 SV=3 | TOP2A | 174 kDa | 11 | 0 | 5 | 0 | 15 |
| DNA topoisomerase 2-beta OS=Homo sapiens GN=TOP2B PE=1 SV=3 | TOP2B | 183 kDa | 0 | 0 | 0 | 0 | 5 |
| Tripeptidyl-peptidase 2 OS=Homo sapiens GN=TPP2 PE=1 SV=4 | TPP2 | 138 kDa | 0 | 0 | 0 | 0 | 3 |
| Nucleoprotein TPR OS=Homo sapiens GN=TPR PE=1 SV=3 | TPR | 267 kDa | 0 | 0 | 0 | 0 | 5 |
| Heat shock protein 75 kDa, mitochondrial OS=Homo sapiens GN=TRAP1 PE=1 SV=3 | TRAP1 | 80 kDa | 4 | 0 | 2 | 6 | 11 |
| tRNA (guanine(26)-N(2))-dimethyltransferase OS=Homo sapiens GN=TRMT1 PE=1 SV=1 | TRM1 | 72 kDa | 0 | 0 | 0 | 0 | 1 |
| TRMT1-like protein OS=Homo sapiens GN=TRMT1L PE=1 SV=2 | TRM1L | 82 kDa | 0 | 0 | 0 | 0 | 1 |
| Pre-rRNA-processing protein TSR1 homolog OS=Homo sapiens GN=TSR1 PE=1 SV=1 | TSR1 | 92 kDa | 0 | 0 | 0 | 0 | 1 |
| Tetratricopeptide repeat protein 37 OS=Homo sapiens GN=TTC37 PE=1 SV=1 | TTC37 | 175 kDa | 0 | 0 | 0 | 0 | 1 |
| Tetratricopeptide repeat protein 4 OS=Homo sapiens GN=TTC4 PE=1 SV=3 | TTC4 | 45 kDa | 0 | 0 | 0 | 0 | 1 |
| Tubulin--tyrosine ligase-like protein 12 OS=Homo sapiens GN=TTLL12 PE=1 SV=2 | TTL12 | 74 kDa | 3 | 0 | 0 | 1 | 5 |
| Alpha-taxilin OS=Homo sapiens GN=TXLNA PE=1 SV=3 | TXLNA | 62 kDa | 0 | 0 | 0 | 0 | 1 |
| Thioredoxin domain-containing protein 5 OS=Homo sapiens GN=TXNDC5 PE=1 SV=2 | TXND5 | 48 kDa | 1 | 0 | 0 | 1 | 2 |
| U5 small nuclear ribonucleoprotein 200 kDa helicase OS=Homo sapiens GN=SNRNP200 PE=1 SV=2 | U520 | 245 kDa | 6 | 0 | 4 | 0 | 14 |
| 116 kDa U5 small nuclear ribonucleoprotein component OS=Homo sapiens GN=EFTUD2 PE=1 SV=1 | U5S1 | 109 kDa | 3 | 0 | 0 | 0 | 7 |
| Ubiquitin-like modifier-activating enzyme 1 OS=Homo sapiens GN=UBA1 PE=1 SV=3 | UBA1 | 118 kDa | 10 | 2 | 2 | 6 | 20 |
| Ubiquitin conjugation factor E4 A OS=Homo sapiens GN=UBE4A PE=1 SV=2 | UBE4A | 123 kDa | 0 | 0 | 0 | 0 | 1 |
| Ubiquitin carboxyl-terminal hydrolase 10 OS=Homo sapiens GN=USP10 PE=1 SV=2 | UBP10 | 87 kDa | 0 | 0 | 0 | 0 | 1 |
| Ubiquitin carboxyl-terminal hydrolase 14 OS=Homo sapiens GN=USP14 PE=1 SV=3 | UBP14 | 56 kDa | 1 | 0 | 1 | 1 | 2 |

| | | | | | | | |
|---|---|---|---|---|---|---|---|
| Ubiquitin carboxyl-terminal hydrolase 19 OS=Homo sapiens GN=USP19 PE=1 SV=2 | UBP19 | 146 kDa | 0 | 0 | 0 | 0 | 1 |
| Ubiquitin carboxyl-terminal hydrolase 24 OS=Homo sapiens GN=USP24 PE=1 SV=3 | UBP24 | 294 kDa | 0 | 0 | 0 | 0 | 2 |
| Ubiquitin carboxyl-terminal hydrolase 5 OS=Homo sapiens GN=USP5 PE=1 SV=2 | UBP5 | 96 kDa | 4 | 0 | 0 | 0 | 5 |
| Ubiquitin carboxyl-terminal hydrolase 7 OS=Homo sapiens GN=USP7 PE=1 SV=2 | UBP7 | 128 kDa | 0 | 0 | 0 | 0 | 1 |
| UDP-glucose:glycoprotein glucosyltransferase 1 OS=Homo sapiens GN=UGGT1 PE=1 SV=3 | UGGG1 | 177 kDa | 0 | 0 | 0 | 0 | 2 |
| Uridine 5'-monophosphate synthase OS=Homo sapiens GN=UMPS PE=1 SV=1 | UMPS | 52 kDa | 1 | 0 | 0 | 1 | 2 |
| General vesicular transport factor p115 OS=Homo sapiens GN=USO1 PE=1 SV=2 | USO1 | 108 kDa | 4 | 0 | 0 | 0 | 5 |
| Probable ubiquitin carboxyl-terminal hydrolase FAF-X OS=Homo sapiens GN=USP9X PE=1 SV=3 | USP9X | 292 kDa | 1 | 0 | 0 | 0 | 4 |
| Synaptic vesicle membrane protein VAT-1 homolog OS=Homo sapiens GN=VAT1 PE=1 SV=2 | VAT1 | 42 kDa | 0 | 0 | 0 | 0 | 2 |
| Vigilin OS=Homo sapiens GN=HDLBP PE=1 SV=2 | VIGLN | 141 kDa | 7 | 0 | 3 | 0 | 12 |
| Vacuolar protein sorting-associated protein 35 OS=Homo sapiens GN=VPS35 PE=1 SV=2 | VPS35 | 92 kDa | 4 | 0 | 1 | 2 | 5 |
| Vacuolar protein-sorting-associated protein 36 OS=Homo sapiens GN=VPS36 PE=1 SV=1 | VPS36 | 44 kDa | 0 | 0 | 0 | 0 | 1 |
| WASH complex subunit 7 OS=Homo sapiens GN=KIAA1033 PE=1 SV=2 | WASH7 | 136 kDa | 0 | 0 | 0 | 0 | 1 |
| WD and tetratricopeptide repeats protein 1 OS=Homo sapiens GN=WDTC1 PE=1 SV=2 | WDTC1 | 76 kDa | 0 | 0 | 0 | 0 | 1 |
| Exportin-1 OS=Homo sapiens GN=XPO1 PE=1 SV=1 | XPO1 | 123 kDa | 8 | 0 | 0 | 0 | 9 |
| Exportin-2 OS=Homo sapiens GN=CSE1L PE=1 SV=3 | XPO2 | 110 kDa | 7 | 0 | 2 | 0 | 8 |
| Exportin-5 OS=Homo sapiens GN=XPO5 PE=1 SV=1 | XPO5 | 136 kDa | 2 | 0 | 1 | 0 | 5 |
| Exportin-T OS=Homo sapiens GN=XPOT PE=1 SV=2 | XPOT | 110 kDa | 1 | 0 | 0 | 0 | 2 |
| X-ray repair cross-complementing protein 6 OS=Homo sapiens GN=XRCC6 PE=1 SV=2 | XRCC6 | 70 kDa | 16 | 0 | 12 | 3 | 20 |
| Zinc finger CCCH domain-containing protein 11A OS=Homo sapiens GN=ZC3H11A PE=1 SV=3 | ZC11A | 89 kDa | 0 | 0 | 0 | 0 | 1 |
| Zinc finger CCCH domain-containing protein 18 OS=Homo sapiens GN=ZC3H18 PE=1 SV=2 | ZCH18 | 106 kDa | 0 | 0 | 0 | 0 | 1 |
| Zinc finger protein ZPR1 OS=Homo sapiens GN=ZPR1 PE=1 SV=1 | ZPR1 | 51 kDa | 0 | 0 | 0 | 0 | 1 |

| Protein | Gene | MW | | | | | |
|---|---|---|---|---|---|---|---|
| Centromere/kinetochore protein zw10 homolog OS=Homo sapiens GN=ZW10 PE=1 SV=3 | ZW10 | 89 kDa | 0 | 0 | 0 | 0 | 1 |
| Zyxin OS=Homo sapiens GN=ZYX PE=1 SV=1 | ZYX | 61 kDa | 0 | 0 | 0 | 0 | 2 |
| AP-1 complex subunit mu-1 OS=Homo sapiens GN=AP1M1 PE=1 SV=3 | AP1M1 | 49 kDa | 0 | 0 | 1 | 0 | 0 |
| Cathepsin L2 OS=Homo sapiens GN=CTSV PE=1 SV=2 | CATL2 | 37 kDa | 0 | 0 | 1 | 0 | 0 |
| Cytoskeleton-associated protein 2 OS=Homo sapiens GN=CKAP2 PE=1 SV=1 | CKAP2 | 77 kDa | 0 | 0 | 1 | 0 | 0 |
| Probable ATP-dependent RNA helicase DDX47 OS=Homo sapiens GN=DDX47 PE=1 SV=1 | DDX47 | 51 kDa | 0 | 0 | 1 | 0 | 0 |
| Translation initiation factor eIF-2B subunit gamma OS=Homo sapiens GN=EIF2B3 PE=1 SV=1 | EI2BG | 50 kDa | 0 | 0 | 1 | 0 | 0 |
| Eukaryotic translation initiation factor 3 subunit E OS=Homo sapiens GN=EIF3E PE=1 SV=1 | EIF3E | 52 kDa | 3 | 0 | 4 | 2 | 2 |
| Eukaryotic translation initiation factor 3 subunit G OS=Homo sapiens GN=EIF3G PE=1 SV=2 | EIF3G | 36 kDa | 0 | 0 | 1 | 1 | 0 |
| Filaggrin-2 OS=Homo sapiens GN=FLG2 PE=1 SV=1 | FILA2 | 248 kDa | 0 | 0 | 1 | 0 | 0 |
| Far upstream element-binding protein 3 OS=Homo sapiens GN=FUBP3 PE=1 SV=2 | FUBP3 | 62 kDa | 0 | 0 | 1 | 0 | 0 |
| Glutathione S-transferase P OS=Homo sapiens GN=GSTP1 PE=1 SV=2 | GSTP1 | 23 kDa | 0 | 0 | 2 | 0 | 0 |
| Histone H1.2 OS=Homo sapiens GN=HIST1H1C PE=1 SV=2 | H12 | 21 kDa | 2 | 0 | 3 | 0 | 1 |
| Histone H4 OS=Homo sapiens GN=HIST1H4A PE=1 SV=2 | H4 | 11 kDa | 0 | 0 | 2 | 0 | 0 |
| Hepatoma-derived growth factor-related protein 2 OS=Homo sapiens GN=HDGFRP2 PE=1 SV=1 | HDGR2 | 74 kDa | 0 | 0 | 1 | 0 | 0 |
| Heterogeneous nuclear ribonucleoprotein H OS=Homo sapiens GN=HNRNPH1 PE=1 SV=4 | HNRH1 | 49 kDa | 5 | 0 | 8 | 4 | 5 |
| Heterogeneous nuclear ribonucleoprotein U-like protein 2 OS=Homo sapiens GN=HNRNPUL2 PE=1 SV=1 | HNRL2 | 85 kDa | 0 | 0 | 1 | 0 | 0 |
| Insulin-like growth factor 2 mRNA-binding protein 2 OS=Homo sapiens GN=IGF2BP2 PE=1 SV=2 | IF2B2 | 66 kDa | 3 | 0 | 5 | 0 | 3 |
| Eukaryotic initiation factor 4A-III OS=Homo sapiens GN=EIF4A3 PE=1 SV=4 | IF4A3 | 47 kDa | 2 | 1 | 3 | 3 | 2 |
| Eukaryotic translation initiation factor 4 gamma 2 OS=Homo sapiens GN=EIF4G2 PE=1 SV=1 | IF4G2 | 102 kDa | 0 | 0 | 2 | 0 | 0 |
| Keratin, type II cytoskeletal 75 OS=Homo sapiens GN=KRT75 PE=1 SV=2 | K2C75 | 60 kDa | 0 | 0 | 2 | 0 | 0 |

| Protein | ID | Mass | | | | | |
|---|---|---|---|---|---|---|---|
| Keratin, type II cytoskeletal 8 OS=Homo sapiens GN=KRT8 PE=1 SV=7 | K2C8 | 54 kDa | 0 | 0 | 1 | 0 | 0 |
| KH domain-containing, RNA-binding, signal transduction-associated protein 1 OS=Homo sapiens GN=KHDRBS1 PE=1 SV=1 | KHDR1 | 48 kDa | 2 | 0 | 3 | 1 | 2 |
| Keratin, type II cuticular Hb4 OS=Homo sapiens GN=KRT84 PE=2 SV=2 | KRT84 | 65 kDa | 0 | 0 | 6 | 0 | 0 |
| Putative RNA-binding protein Luc7-like 2 OS=Homo sapiens GN=LUC7L2 PE=1 SV=2 | LC7L2 | 47 kDa | 1 | 0 | 2 | 0 | 0 |
| Prelamin-A/C OS=Homo sapiens GN=LMNA PE=1 SV=1 | LMNA | 74 kDa | 0 | 0 | 4 | 0 | 0 |
| Lamin-B2 OS=Homo sapiens GN=LMNB2 PE=1 SV=3 | LMNB2 | 68 kDa | 0 | 0 | 3 | 0 | 0 |
| Non-POU domain-containing octamer-binding protein OS=Homo sapiens GN=NONO PE=1 SV=4 | NONO | 54 kDa | 7 | 2 | 8 | 7 | 7 |
| Nucleolar protein 56 OS=Homo sapiens GN=NOP56 PE=1 SV=4 | NOP56 | 66 kDa | 1 | 0 | 3 | 0 | 1 |
| Nucleolar protein 58 OS=Homo sapiens GN=NOP58 PE=1 SV=1 | NOP58 | 60 kDa | 0 | 0 | 3 | 0 | 0 |
| Nucleosome assembly protein 1-like 4 OS=Homo sapiens GN=NAP1L4 PE=1 SV=1 | NP1L4 | 43 kDa | 0 | 0 | 1 | 1 | 1 |
| Plakophilin-1 OS=Homo sapiens GN=PKP1 PE=1 SV=2 | PKP1 | 83 kDa | 0 | 0 | 1 | 0 | 0 |
| U4/U6 small nuclear ribonucleoprotein Prp4 OS=Homo sapiens GN=PRPF4 PE=1 SV=2 | PRP4 | 58 kDa | 0 | 0 | 1 | 0 | 0 |
| 26S protease regulatory subunit 7 OS=Homo sapiens GN=PSMC2 PE=1 SV=3 | PRS7 | 49 kDa | 3 | 0 | 5 | 2 | 3 |
| Pumilio homolog 2 OS=Homo sapiens GN=PUM2 PE=1 SV=2 | PUM2 | 114 kDa | 0 | 0 | 1 | 0 | 0 |
| RNA-binding motif protein, X chromosome OS=Homo sapiens GN=RBMX PE=1 SV=3 | RBMX | 42 kDa | 0 | 0 | 8 | 2 | 1 |
| Regulator of chromosome condensation OS=Homo sapiens GN=RCC1 PE=1 SV=1 | RCC1 | 45 kDa | 1 | 0 | 2 | 2 | 2 |
| Protein Red OS=Homo sapiens GN=IK PE=1 SV=3 | RED | 66 kDa | 0 | 0 | 1 | 0 | 0 |
| Ribosome biogenesis regulatory protein homolog OS=Homo sapiens GN=RRS1 PE=1 SV=2 | RRS1 | 41 kDa | 0 | 0 | 2 | 0 | 0 |
| WD40 repeat-containing protein SMU1 OS=Homo sapiens GN=SMU1 PE=1 SV=2 | SMU1 | 58 kDa | 0 | 0 | 1 | 0 | 0 |
| Sorting nexin-2 OS=Homo sapiens GN=SNX2 PE=1 SV=2 | SNX2 | 58 kDa | 0 | 0 | 1 | 1 | 0 |
| Serine/threonine-protein kinase 26 OS=Homo sapiens GN=STK26 PE=1 SV=2 | STK26 | 47 kDa | 0 | 0 | 1 | 1 | 1 |
| TAR DNA-binding protein 43 OS=Homo sapiens GN=TARDBP PE=1 SV=1 | TADBP | 45 kDa | 0 | 0 | 1 | 1 | 1 |
| Tubulin alpha-1A chain OS=Homo sapiens GN=TUBA1A PE=1 SV=1 | TBA1A | 50 kDa | 0 | 0 | 1 | 1 | 0 |

| | | | | | | | |
|---|---|---|---|---|---|---|---|
| Tubulin beta-2A chain OS=Homo sapiens GN=TUBB2A PE=1 SV=1 | TBB2A | 50 kDa | 1 | 0 | 2 | 1 | 1 |
| Deoxynucleotidyltransferase terminal-interacting protein 2 OS=Homo sapiens GN=DNTTIP2 PE=1 SV=2 | TDIF2 | 84 kDa | 0 | 0 | 1 | 0 | 0 |
| Nucleolar transcription factor 1 OS=Homo sapiens GN=UBTF PE=1 SV=1 | UBF1 | 89 kDa | 0 | 0 | 1 | 0 | 0 |
| E3 UFM1-protein ligase 1 OS=Homo sapiens GN=UFL1 PE=1 SV=2 | UFL1 | 90 kDa | 0 | 0 | 1 | 0 | 0 |
| U3 small nucleolar RNA-associated protein 18 homolog OS=Homo sapiens GN=UTP18 PE=1 SV=3 | UTP18 | 62 kDa | 1 | 0 | 2 | 0 | 1 |
| DNA repair protein XRCC1 OS=Homo sapiens GN=XRCC1 PE=1 SV=2 | XRCC1 | 69 kDa | 0 | 0 | 1 | 0 | 0 |
| 5'-3' exoribonuclease 2 OS=Homo sapiens GN=XRN2 PE=1 SV=1 | XRN2 | 109 kDa | 0 | 0 | 1 | 1 | 0 |
| YTH domain-containing family protein 2 OS=Homo sapiens GN=YTHDF2 PE=1 SV=2 | YTHD2 | 62 kDa | 0 | 0 | 1 | 1 | 1 |
| Zinc finger CCCH domain-containing protein 15 OS=Homo sapiens GN=ZC3H15 PE=1 SV=1 | ZC3HF | 49 kDa | 0 | 0 | 1 | 0 | 0 |
| Zinc finger CCCH-type antiviral protein 1 OS=Homo sapiens GN=ZC3HAV1 PE=1 SV=3 | ZCCHV | 101 kDa | 0 | 0 | 1 | 0 | 0 |

**Table A. 4. 4: Representation of the number of unique peptides from Trial 2, figure A 4.21:** The table containing data for trypsinized proteins from SDS-PAGE gel of trial 2 (Appendix C, section 4.5). The data of the table represents uncrosslinked lysated (lane 1, Figure A 4.21), ATP-Hex-Acr crosslinked lysates in presence of staursporine (lane 2, Figure A 4.21), ATP-Hex-Acr crosslinked lysates (lane 3, Figure A 4.21), ATP-PEG-Acr crosslinked lysates in presence of staursporine (lane 4, Figure A 4.21), and ATP-Hex-Acr crosslinked lysates (lane 5, Figure A 4.21)

| Identified Protein | Accession Number | Mol. Wt. | the number of unique peptides | | | | |
|---|---|---|---|---|---|---|---|
| | | | Lane 1 | Lane 2 | Lane 3 | Lane 4 | Lane 5 |
| Stress-70 protein, mitochondrial OS=Homo sapiens GN=HSPA9 PE=1 SV=2 | GRP75 | 74 kDa | 3 | 4 | 12 | 0 | 8 |
| Vesicle-fusing ATPase OS=Homo sapiens GN=NSF PE=1 SV=3 | NSF | 83 kDa | 0 | 0 | 1 | 0 | 2 |
| Heat shock protein HSP 90-alpha OS=Homo sapiens GN=HSP90AA1 PE=1 SV=5 | HS90A | 85 kDa | 19 | 13 | 19 | 1 | 30 |
| Heat shock protein HSP 90-beta OS=Homo sapiens GN=HSP90AB1 PE=1 SV=4 | HS90B | 83 kDa | 14 | 5 | 11 | 0 | 16 |
| Heat shock cognate 71 kDa protein OS=Homo sapiens GN=HSPA8 PE=1 SV=1 | HSP7C | 71 kDa | 6 | 9 | 4 | 0 | 10 |
| Creatine kinase B-type OS=Homo sapiens GN=CKB PE=1 SV=1 | KCRB | 43 kDa | 6 | 4 | 4 | 1 | 7 |
| L-lactate dehydrogenase A chain OS=Homo sapiens GN=LDHA PE=1 SV=2 | LDHA | 37 kDa | 0 | 0 | 0 | 0 | 1 |
| Transitional endoplasmic reticulum ATPase OS=Homo sapiens GN=VCP PE=1 SV=4 | TERA | 89 kDa | 0 | 0 | 0 | 0 | 1 |
| Alpha-enolase OS=Homo sapiens GN=ENO1 PE=1 SV=2 | ENOA | 47 kDa | 2 | 2 | 0 | 0 | 4 |
| Actin, cytoplasmic 1 OS=Homo sapiens GN=ACTB PE=1 SV=1 | ACTB | 42 kDa | 0 | 0 | 0 | 0 | 1 |
| Interleukin-1 receptor-associated kinase 1 OS=Homo sapiens GN=IRAK1 PE=1 SV=2 | IRAK1 | 77 kDa | 0 | 0 | 1 | 0 | 0 |
| Integrin-linked protein kinase OS=Homo sapiens GN=ILK PE=1 SV=2 | ILK | 51 kDa | 0 | 0 | 0 | 0 | 1 |
| 4F2 cell-surface antigen heavy chain OS=Homo sapiens GN=SLC3A2 PE=1 SV=3 | 4F2 | 68 kDa | 0 | 0 | 1 | 0 | 1 |
| Aconitate hydratase, mitochondrial OS=Homo sapiens GN=ACO2 PE=1 SV=2 | ACON | 85 kDa | 0 | 0 | 1 | 0 | 1 |
| Activator of 90 kDa heat shock protein ATPase homolog 1 OS=Homo sapiens GN=AHSA1 PE=1 SV=1 | AHSA1 | 38 kDa | 0 | 0 | 1 | 0 | 2 |

| | | | | | | | |
|---|---|---|---|---|---|---|---|
| Apoptosis-inducing factor 1, mitochondrial OS=Homo sapiens GN=AIFM1 PE=1 SV=1 | AIFM1 | 67 kDa | 0 | 0 | 1 | 0 | 1 |
| ATPase family AAA domain-containing protein 3A OS=Homo sapiens GN=ATAD3A PE=1 SV=2 | ATD3A | 71 kDa | 3 | 0 | 6 | 0 | 5 |
| Cytoskeleton-associated protein 4 OS=Homo sapiens GN=CKAP4 PE=1 SV=2 | CKAP4 | 66 kDa | 0 | 0 | 1 | 0 | 2 |
| Cold shock domain-containing protein E1 OS=Homo sapiens GN=CSDE1 PE=1 SV=2 | CSDE1 | 89 kDa | 0 | 0 | 1 | 0 | 1 |
| Cytoplasmic dynein 1 intermediate chain 2 OS=Homo sapiens GN=DYNC1I2 PE=1 SV=3 | DC1I2 | 71 kDa | 1 | 0 | 4 | 0 | 3 |
| Probable ATP-dependent RNA helicase DDX17 OS=Homo sapiens GN=DDX17 PE=1 SV=2 | DDX17 | 80 kDa | 6 | 4 | 7 | 0 | 8 |
| DnaJ homolog subfamily C member 2 OS=Homo sapiens GN=DNAJC2 PE=1 SV=4 | DNJC2 | 72 kDa | 0 | 0 | 2 | 0 | 1 |
| Developmentally-regulated GTP-binding protein 1 OS=Homo sapiens GN=DRG1 PE=1 SV=1 | DRG1 | 41 kDa | 0 | 0 | 1 | 0 | 1 |
| Eukaryotic translation initiation factor 3 subunit D OS=Homo sapiens GN=EIF3D PE=1 SV=1 | EIF3D | 64 kDa | 0 | 0 | 1 | 0 | 2 |
| Eukaryotic translation initiation factor 3 subunit L OS=Homo sapiens GN=EIF3L PE=1 SV=1 | EIF3L | 67 kDa | 4 | 0 | 5 | 0 | 5 |
| Pre-mRNA 3'-end-processing factor FIP1 OS=Homo sapiens GN=FIP1L1 PE=1 SV=1 | FIP1 | 67 kDa | 0 | 0 | 1 | 0 | 1 |
| RNA-binding protein FUS OS=Homo sapiens GN=FUS PE=1 SV=1 | FUS | 53 kDa | 0 | 0 | 2 | 0 | 1 |
| Glucosidase 2 subunit beta OS=Homo sapiens GN=PRKCSH PE=1 SV=2 | GLU2B | 59 kDa | 0 | 0 | 1 | 0 | 1 |
| Histone H2B type 1-C/E/F/G/I OS=Homo sapiens GN=HIST1H2BC PE=1 SV=4 | H2B1C (+8) | 14 kDa | 0 | 0 | 1 | 0 | 1 |
| Heterogeneous nuclear ribonucleoproteins C1/C2 OS=Homo sapiens GN=HNRNPC PE=1 SV=4 | HNRPC | 34 kDa | 0 | 0 | 1 | 0 | 3 |
| Insulin-like growth factor 2 mRNA-binding protein 1 OS=Homo sapiens GN=IGF2BP1 PE=1 SV=2 | IF2B1 | 63 kDa | 3 | 2 | 12 | 0 | 13 |
| Insulin-like growth factor 2 mRNA-binding protein 3 OS=Homo sapiens GN=IGF2BP3 PE=1 SV=2 | IF2B3 | 64 kDa | 3 | 1 | 7 | 0 | 6 |

| | | | | | | | |
|---|---|---|---|---|---|---|---|
| Interleukin enhancer-binding factor 3 OS=Homo sapiens GN=ILF3 PE=1 SV=3 | ILF3 | 95 kDa | 0 | 0 | 1 | 0 | 1 |
| Importin subunit alpha-5 OS=Homo sapiens GN=KPNA1 PE=1 SV=3 | IMA5 | 60 kDa | 0 | 0 | 1 | 0 | 1 |
| KH domain-containing, RNA-binding, signal transduction-associated protein 1 OS=Homo sapiens GN=KHDRBS1 PE=1 SV=1 | KHDR1 | 48 kDa | 1 | 1 | 3 | 0 | 3 |
| Lamina-associated polypeptide 2, isoform alpha OS=Homo sapiens GN=TMPO PE=1 SV=2 | LAP2A | 75 kDa | 3 | 0 | 5 | 0 | 6 |
| LETM1 and EF-hand domain-containing protein 1, mitochondrial OS=Homo sapiens GN=LETM1 PE=1 SV=1 | LETM1 | 83 kDa | 0 | 0 | 1 | 0 | 3 |
| Leukotriene A-4 hydrolase OS=Homo sapiens GN=LTA4H PE=1 SV=2 | LKHA4 | 69 kDa | 0 | 0 | 1 | 0 | 2 |
| Protein ERGIC-53 OS=Homo sapiens GN=LMAN1 PE=1 SV=2 | LMAN1 | 58 kDa | 0 | 0 | 1 | 0 | 1 |
| Melanoma-associated antigen D2 OS=Homo sapiens GN=MAGED2 PE=1 SV=2 | MAGD2 | 65 kDa | 0 | 0 | 1 | 0 | 1 |
| MICOS complex subunit MIC60 OS=Homo sapiens GN=IMMT PE=1 SV=1 | MIC60 | 84 kDa | 1 | 0 | 2 | 0 | 3 |
| Nuclear cap-binding protein subunit 1 OS=Homo sapiens GN=NCBP1 PE=1 SV=1 | NCBP1 | 92 kDa | 1 | 0 | 2 | 0 | 2 |
| NADH-ubiquinone oxidoreductase 75 kDa subunit, mitochondrial OS=Homo sapiens GN=NDUFS1 PE=1 SV=3 | NDUS1 | 79 kDa | 0 | 0 | 2 | 0 | 2 |
| Dihydrolipoyllysine-residue acetyltransferase component of pyruvate dehydrogenase complex, mitochondrial OS=Homo sapiens GN=DLAT PE=1 SV=3 | ODP2 | 69 kDa | 0 | 0 | 1 | 0 | 1 |
| Dynamin-like 120 kDa protein, mitochondrial OS=Homo sapiens GN=OPA1 PE=1 SV=3 | OPA1 | 112 kDa | 1 | 0 | 2 | 0 | 2 |
| Transcriptional repressor p66-alpha OS=Homo sapiens GN=GATAD2A PE=1 SV=1 | P66A | 68 kDa | 0 | 0 | 1 | 0 | 1 |
| Transcriptional repressor p66-beta OS=Homo sapiens GN=GATAD2B PE=1 SV=1 | P66B | 65 kDa | 0 | 0 | 2 | 0 | 1 |
| Plasminogen activator inhibitor 1 RNA-binding protein OS=Homo sapiens GN=SERBP1 PE=1 SV=2 | PAIRB | 45 kDa | 1 | 0 | 4 | 0 | 3 |

| Poly(rC)-binding protein 1 OS=Homo sapiens GN=PCBP1 PE=1 SV=2 | PCBP1 | 37 kDa | 0 | 0 | 1 | 0 | 4 |
|---|---|---|---|---|---|---|---|
| Phosphoenolpyruvate carboxykinase (GTP), mitochondrial OS=Homo sapiens GN=PCK2 PE=1 SV=3 | PCKGM | 71 kDa | 1 | 0 | 3 | 0 | 4 |
| U4/U6 small nuclear ribonucleoprotein Prp3 OS=Homo sapiens GN=PRPF3 PE=1 SV=2 | PRPF3 | 78 kDa | 0 | 0 | 1 | 0 | 1 |
| 26S proteasome non-ATPase regulatory subunit 3 OS=Homo sapiens GN=PSMD3 PE=1 SV=2 | PSMD3 | 61 kDa | 2 | 0 | 3 | 0 | 3 |
| 26S proteasome non-ATPase regulatory subunit 4 OS=Homo sapiens GN=PSMD4 PE=1 SV=1 | PSMD4 | 41 kDa | 0 | 0 | 1 | 0 | 2 |
| Cytochrome b-c1 complex subunit 1, mitochondrial OS=Homo sapiens GN=UQCRC1 PE=1 SV=3 | QCR1 | 53 kDa | 0 | 0 | 1 | 0 | 1 |
| Cytochrome b-c1 complex subunit 2, mitochondrial OS=Homo sapiens GN=UQCRC2 PE=1 SV=3 | QCR2 | 48 kDa | 0 | 0 | 1 | 0 | 3 |
| Ran GTPase-activating protein 1 OS=Homo sapiens GN=RANGAP1 PE=1 SV=1 | RAGP1 | 64 kDa | 2 | 0 | 3 | 0 | 5 |
| RNA-binding protein 14 OS=Homo sapiens GN=RBM14 PE=1 SV=2 | RBM14 | 69 kDa | 0 | 0 | 5 | 0 | 2 |
| DNA-directed RNA polymerases I and III subunit RPAC1 OS=Homo sapiens GN=POLR1C PE=1 SV=1 | RPAC1 | 39 kDa | 0 | 0 | 1 | 0 | 1 |
| Protein RUFY3 OS=Homo sapiens GN=RUFY3 PE=1 SV=1 | RUFY3 | 53 kDa | 0 | 0 | 1 | 0 | 1 |
| Signal recognition particle subunit SRP68 OS=Homo sapiens GN=SRP68 PE=1 SV=2 | SRP68 | 71 kDa | 1 | 0 | 3 | 0 | 3 |
| Stomatin-like protein 2, mitochondrial OS=Homo sapiens GN=STOML2 PE=1 SV=1 | STML2 | 39 kDa | 0 | 0 | 1 | 0 | 1 |
| Lysine--tRNA ligase OS=Homo sapiens GN=KARS PE=1 SV=3 | SYK | 68 kDa | 1 | 0 | 2 | 0 | 3 |
| Arginine--tRNA ligase, cytoplasmic OS=Homo sapiens GN=RARS PE=1 SV=2 | SYRC | 75 kDa | 1 | 0 | 4 | 0 | 7 |
| Tubulin beta-4B chain OS=Homo sapiens GN=TUBB4B PE=1 SV=1 | TBB4B | 50 kDa | 2 | 2 | 3 | 1 | 3 |
| Acetyl-CoA acetyltransferase, mitochondrial OS=Homo sapiens GN=ACAT1 PE=1 SV=1 | THIL | 45 kDa | 0 | 0 | 2 | 0 | 6 |

| Heat shock protein 75 kDa, mitochondrial OS=Homo sapiens GN=TRAP1 PE=1 SV=3 | TRAP1 | 80 kDa | 5 | 1 | 6 | 0 | 13 |
|---|---|---|---|---|---|---|---|
| V-type proton ATPase catalytic subunit A OS=Homo sapiens GN=ATP6V1A PE=1 SV=2 | VATA | 68 kDa | 0 | 0 | 1 | 0 | 3 |
| Vacuolar protein sorting-associated protein 35 OS=Homo sapiens GN=VPS35 PE=1 SV=2 | VPS35 | 92 kDa | 1 | 0 | 2 | 0 | 4 |
| X-ray repair cross-complementing protein 5 OS=Homo sapiens GN=XRCC5 PE=1 SV=3 | XRCC5 | 83 kDa | 1 | 1 | 7 | 0 | 13 |
| X-ray repair cross-complementing protein 6 OS=Homo sapiens GN=XRCC6 PE=1 SV=2 | XRCC6 | 70 kDa | 7 | 2 | 10 | 0 | 15 |
| YTH domain-containing family protein 2 OS=Homo sapiens GN=YTHDF2 PE=1 SV=2 | YTHD2 | 62 kDa | 1 | 0 | 4 | 0 | 2 |
| Zyxin OS=Homo sapiens GN=ZYX PE=1 SV=1 | ZYX | 61 kDa | 1 | 0 | 2 | 0 | 2 |
| Serine/threonine-protein phosphatase 2A 56 kDa regulatory subunit delta isoform OS=Homo sapiens GN=PPP2R5D PE=1 SV=1 | 2A5D | 70 kDa | 0 | 0 | 0 | 0 | 1 |
| Aldehyde dehydrogenase family 16 member A1 OS=Homo sapiens GN=ALDH16A1 PE=1 SV=2 | A16A1 | 85 kDa | 0 | 0 | 0 | 0 | 1 |
| Alpha-actinin-4 OS=Homo sapiens GN=ACTN4 PE=1 SV=2 | ACTN4 | 105 kDa | 1 | 1 | 0 | 0 | 6 |
| ADP/ATP translocase 2 OS=Homo sapiens GN=SLC25A5 PE=1 SV=7 | ADT2 | 33 kDa | 0 | 0 | 0 | 0 | 2 |
| AFG3-like protein 2 OS=Homo sapiens GN=AFG3L2 PE=1 SV=2 | AFG32 | 89 kDa | 0 | 0 | 0 | 0 | 1 |
| Acylglycerol kinase, mitochondrial OS=Homo sapiens GN=AGK PE=1 SV=2 | AGK | 47 kDa | 0 | 0 | 0 | 0 | 1 |
| Cytosol aminopeptidase OS=Homo sapiens GN=LAP3 PE=1 SV=3 | AMPL | 56 kDa | 2 | 0 | 1 | 0 | 4 |
| Annexin A2 OS=Homo sapiens GN=ANXA2 PE=1 SV=2 | ANXA2 | 39 kDa | 0 | 0 | 0 | 0 | 1 |
| AP-1 complex subunit beta-1 OS=Homo sapiens GN=AP1B1 PE=1 SV=2 | AP1B1 | 105 kDa | 0 | 0 | 0 | 0 | 1 |
| ADP-ribosylation factor GTPase-activating protein 1 OS=Homo sapiens GN=ARFGAP1 PE=1 SV=2 | ARFG1 | 45 kDa | 0 | 0 | 0 | 0 | 1 |
| ADP-ribosylation factor GTPase-activating protein 2 OS=Homo sapiens GN=ARFGAP2 PE=1 SV=1 | ARFG2 | 57 kDa | 0 | 0 | 0 | 0 | 1 |

| | | | | | | | |
|---|---|---|---|---|---|---|---|
| N-acetylserotonin O-methyltransferase-like protein OS=Homo sapiens GN=ASMTL PE=1 SV=3 | ASML | 69 kDa | 0 | 0 | 0 | 0 | 1 |
| ATPase family AAA domain-containing protein 3B OS=Homo sapiens GN=ATAD3B PE=1 SV=1 | ATD3B | 73 kDa | 0 | 0 | 0 | 0 | 1 |
| Calcium-binding mitochondrial carrier protein Aralar2 OS=Homo sapiens GN=SLC25A13 PE=1 SV=2 | CMC2 | 74 kDa | 1 | 0 | 0 | 0 | 3 |
| Cytosolic non-specific dipeptidase OS=Homo sapiens GN=CNDP2 PE=1 SV=2 | CNDP2 | 53 kDa | 0 | 0 | 0 | 0 | 1 |
| Coatomer subunit beta OS=Homo sapiens GN=COPB1 PE=1 SV=3 | COPB | 107 kDa | 2 | 0 | 0 | 0 | 3 |
| Coatomer subunit beta' OS=Homo sapiens GN=COPB2 PE=1 SV=2 | COPB2 | 102 kDa | 1 | 0 | 0 | 0 | 3 |
| Coatomer subunit gamma-1 OS=Homo sapiens GN=COPG1 PE=1 SV=1 | COPG1 | 98 kDa | 3 | 0 | 0 | 0 | 4 |
| Cleavage and polyadenylation specificity factor subunit 6 OS=Homo sapiens GN=CPSF6 PE=1 SV=2 | CPSF6 | 59 kDa | 0 | 0 | 0 | 0 | 1 |
| COP9 signalosome complex subunit 4 OS=Homo sapiens GN=COPS4 PE=1 SV=1 | CSN4 | 46 kDa | 0 | 0 | 0 | 0 | 2 |
| Drebrin-like protein OS=Homo sapiens GN=DBNL PE=1 SV=1 | DBNL | 48 kDa | 0 | 0 | 0 | 0 | 2 |
| ATP-dependent RNA helicase DDX1 OS=Homo sapiens GN=DDX1 PE=1 SV=2 | DDX1 | 82 kDa | 1 | 0 | 1 | 0 | 3 |
| Probable ATP-dependent RNA helicase DDX23 OS=Homo sapiens GN=DDX23 PE=1 SV=3 | DDX23 | 96 kDa | 0 | 0 | 0 | 0 | 2 |
| Probable ATP-dependent RNA helicase DDX5 OS=Homo sapiens GN=DDX5 PE=1 SV=1 | DDX5 | 69 kDa | 2 | 0 | 0 | 0 | 3 |
| Peroxisomal multifunctional enzyme type 2 OS=Homo sapiens GN=HSD17B4 PE=1 SV=3 | DHB4 | 80 kDa | 0 | 0 | 0 | 0 | 3 |
| Dynamin-1-like protein OS=Homo sapiens GN=DNM1L PE=1 SV=2 | DNM1L | 82 kDa | 0 | 0 | 0 | 0 | 1 |
| Dihydropyrimidinase-related protein 1 OS=Homo sapiens GN=CRMP1 PE=1 SV=1 | DPYL1 | 62 kDa | 0 | 0 | 0 | 0 | 1 |
| Trifunctional enzyme subunit alpha, mitochondrial OS=Homo sapiens GN=HADHA PE=1 SV=2 | ECHA | 83 kDa | 1 | 0 | 1 | 0 | 3 |
| Elongation factor 2 OS=Homo sapiens GN=EEF2 PE=1 SV=4 | EF2 | 95 kDa | 9 | 9 | 5 | 0 | 25 |

| | | | | | | | |
|---|---|---|---|---|---|---|---|
| Eukaryotic translation initiation factor 3 subunit E OS=Homo sapiens GN=EIF3E PE=1 SV=1 | EIF3E | 52 kDa | 2 | 0 | 1 | 0 | 3 |
| Eukaryotic translation initiation factor 3 subunit G OS=Homo sapiens GN=EIF3G PE=1 SV=2 | EIF3G | 36 kDa | 0 | 1 | 1 | 0 | 2 |
| Endoplasmin OS=Homo sapiens GN=HSP90B1 PE=1 SV=1 | ENPL | 92 kDa | 9 | 2 | 0 | 1 | 16 |
| Eukaryotic peptide chain release factor GTP-binding subunit ERF3A OS=Homo sapiens GN=GSPT1 PE=1 SV=1 | ERF3A | 56 kDa | 0 | 1 | 0 | 0 | 1 |
| Exosome component 10 OS=Homo sapiens GN=EXOSC10 PE=1 SV=2 | EXOSX | 101 kDa | 0 | 0 | 0 | 0 | 1 |
| Ezrin OS=Homo sapiens GN=EZR PE=1 SV=4 | EZRI | 69 kDa | 0 | 0 | 0 | 0 | 2 |
| Protein FAM98B OS=Homo sapiens GN=FAM98B PE=1 SV=1 | FA98B | 37 kDa | 0 | 0 | 0 | 0 | 1 |
| Glyceraldehyde-3-phosphate dehydrogenase OS=Homo sapiens GN=GAPDH PE=1 SV=3 | G3P | 36 kDa | 0 | 1 | 0 | 0 | 1 |
| Glucose-6-phosphate 1-dehydrogenase OS=Homo sapiens GN=G6PD PE=1 SV=4 | G6PD | 59 kDa | 0 | 0 | 0 | 0 | 1 |
| Glucose-6-phosphate isomerase OS=Homo sapiens GN=GPI PE=1 SV=4 | G6PI | 63 kDa | 3 | 1 | 0 | 0 | 5 |
| Golgi resident protein GCP60 OS=Homo sapiens GN=ACBD3 PE=1 SV=4 | GCP60 | 61 kDa | 0 | 0 | 0 | 0 | 1 |
| Glutamine--fructose-6-phosphate aminotransferase (isomerizing) 1 OS=Homo sapiens GN=GFPT1 PE=1 SV=3 | GFPT1 | 79 kDa | 0 | 0 | 0 | 0 | 1 |
| Serine hydroxymethyltransferase, mitochondrial OS=Homo sapiens GN=SHMT2 PE=1 SV=3 | GLYM | 56 kDa | 6 | 2 | 2 | 0 | 7 |
| Mannose-1-phosphate guanyltransferase alpha OS=Homo sapiens GN=GMPPA PE=1 SV=1 | GMPPA | 46 kDa | 0 | 0 | 0 | 0 | 1 |
| Golgi-associated PDZ and coiled-coil motif-containing protein OS=Homo sapiens GN=GOPC PE=1 SV=1 | GOPC | 51 kDa | 0 | 0 | 0 | 0 | 1 |
| 78 kDa glucose-regulated protein OS=Homo sapiens GN=HSPA5 PE=1 SV=2 | GRP78 | 72 kDa | 3 | 5 | 4 | 0 | 5 |

| | | | | | | | |
|---|---|---|---|---|---|---|---|
| Glutathione reductase, mitochondrial OS=Homo sapiens GN=GSR PE=1 SV=2 | GSHR | 56 kDa | 1 | 0 | 0 | 0 | 2 |
| GMP synthase (glutamine-hydrolyzing) OS=Homo sapiens GN=GMPS PE=1 SV=1 | GUAA | 77 kDa | 0 | 0 | 0 | 0 | 1 |
| Histone H4 OS=Homo sapiens GN=HIST1H4A PE=1 SV=2 | H4 | 11 kDa | 0 | 0 | 0 | 0 | 1 |
| Heterogeneous nuclear ribonucleoprotein F OS=Homo sapiens GN=HNRNPF PE=1 SV=3 | HNRPF | 46 kDa | 1 | 0 | 0 | 0 | 3 |
| Heterogeneous nuclear ribonucleoprotein K OS=Homo sapiens GN=HNRNPK PE=1 SV=1 | HNRPK | 51 kDa | 6 | 2 | 6 | 0 | 9 |
| Heterogeneous nuclear ribonucleoprotein M OS=Homo sapiens GN=HNRNPM PE=1 SV=3 | HNRPM | 78 kDa | 12 | 2 | 12 | 0 | 13 |
| Heterogeneous nuclear ribonucleoprotein R OS=Homo sapiens GN=HNRNPR PE=1 SV=1 | HNRPR | 71 kDa | 2 | 0 | 2 | 0 | 3 |
| Hornerin OS=Homo sapiens GN=HRNR PE=1 SV=2 | HORN | 282 kDa | 0 | 0 | 0 | 0 | 1 |
| Heat shock 70 kDa protein 1A OS=Homo sapiens GN=HSPA1A PE=1 SV=1 | HS71A | 70 kDa | 19 | 23 | 22 | 9 | 22 |
| Heat shock protein HSP 90-alpha A2 OS=Homo sapiens GN=HSP90AA2P PE=1 SV=2 | HS902 | 39 kDa | 0 | 0 | 0 | 0 | 1 |
| Interferon regulatory factor 2-binding protein 1 OS=Homo sapiens GN=IRF2BP1 PE=1 SV=1 | I2BP1 | 62 kDa | 0 | 0 | 0 | 0 | 1 |
| Isocitrate dehydrogenase (NAD) subunit beta, mitochondrial OS=Homo sapiens GN=IDH3B PE=1 SV=2 | IDH3B | 42 kDa | 0 | 0 | 0 | 0 | 1 |
| Ig gamma-1 chain C region OS=Homo sapiens GN=IGHG1 PE=1 SV=1 | IGHG1 | 36 kDa | 0 | 2 | 0 | 0 | 1 |
| Importin subunit alpha-3 OS=Homo sapiens GN=KPNA4 PE=1 SV=1 | IMA3 | 58 kDa | 0 | 0 | 0 | 0 | 1 |
| Importin subunit beta-1 OS=Homo sapiens GN=KPNB1 PE=1 SV=2 | IMB1 | 97 kDa | 4 | 1 | 4 | 0 | 6 |
| Inositol-3-phosphate synthase 1 OS=Homo sapiens GN=ISYNA1 PE=1 SV=1 | INO1 | 61 kDa | 0 | 0 | 0 | 0 | 1 |
| Keratin, type I cytoskeletal 10 OS=Homo sapiens GN=KRT10 PE=1 SV=6 | K1C10 | 59 kDa | 19 | 27 | 20 | 9 | 21 |
| Keratin, type I cytoskeletal 14 OS=Homo sapiens GN=KRT14 PE=1 SV=4 | K1C14 | 52 kDa | 2 | 6 | 2 | 1 | 4 |

| | | | | | | | |
|---|---|---|---|---|---|---|---|
| Keratin, type I cytoskeletal 16 OS=Homo sapiens GN=KRT16 PE=1 SV=4 | K1C16 | 51 kDa | 0 | 0 | 0 | 0 | 5 |
| Keratin, type I cytoskeletal 17 OS=Homo sapiens GN=KRT17 PE=1 SV=2 | K1C17 | 48 kDa | 0 | 0 | 0 | 0 | 3 |
| Keratin, type I cytoskeletal 9 OS=Homo sapiens GN=KRT9 PE=1 SV=3 | K1C9 | 62 kDa | 10 | 15 | 10 | 10 | 15 |
| Keratin, type I cuticular Ha1 OS=Homo sapiens GN=KRT31 PE=1 SV=3 | K1H1 | 47 kDa | 0 | 0 | 0 | 0 | 16 |
| Keratin, type I cuticular Ha2 OS=Homo sapiens GN=KRT32 PE=2 SV=3 | K1H2 | 50 kDa | 0 | 0 | 0 | 0 | 9 |
| Keratin, type II cytoskeletal 2 epidermal OS=Homo sapiens GN=KRT2 PE=1 SV=2 | K22E | 65 kDa | 12 | 30 | 19 | 11 | 19 |
| Keratin, type II cytoskeletal 1 OS=Homo sapiens GN=KRT1 PE=1 SV=6 | K2C1 | 66 kDa | 22 | 28 | 28 | 22 | 28 |
| Keratin, type II cytoskeletal 5 OS=Homo sapiens GN=KRT5 PE=1 SV=3 | K2C5 | 62 kDa | 1 | 9 | 2 | 1 | 7 |
| Keratin, type II cytoskeletal 6A OS=Homo sapiens GN=KRT6A PE=1 SV=3 | K2C6A | 60 kDa | 1 | 2 | 0 | 1 | 9 |
| Keratin, type II cytoskeletal 6C OS=Homo sapiens GN=KRT6C PE=1 SV=3 | K2C6C | 60 kDa | 0 | 1 | 0 | 0 | 1 |
| Pyruvate kinase PKM OS=Homo sapiens GN=PKM PE=1 SV=4 | KPYM | 58 kDa | 5 | 4 | 3 | 1 | 9 |
| Keratin-associated protein 11-1 OS=Homo sapiens GN=KRTAP11-1 PE=2 SV=1 | KR111 | 17 kDa | 0 | 0 | 0 | 0 | 3 |
| Keratin-associated protein 19-5 OS=Homo sapiens GN=KRTAP19-5 PE=1 SV=1 | KR195 | 8 kDa | 0 | 0 | 0 | 0 | 2 |
| Keratin-associated protein 19-7 OS=Homo sapiens GN=KRTAP19-7 PE=1 SV=1 | KR197 | 7 kDa | 0 | 0 | 0 | 0 | 1 |
| Keratin-associated protein 24-1 OS=Homo sapiens GN=KRTAP24-1 PE=2 SV=1 | KR241 | 28 kDa | 0 | 0 | 0 | 0 | 1 |
| Keratin-associated protein 2-1 OS=Homo sapiens GN=KRTAP2-1 PE=2 SV=2 | KRA21 | 14 kDa | 0 | 0 | 0 | 0 | 1 |
| Keratin-associated protein 3-1 OS=Homo sapiens GN=KRTAP3-1 PE=1 SV=1 | KRA31 | 11 kDa | 0 | 0 | 0 | 0 | 1 |
| Keratin-associated protein 6-1 OS=Homo sapiens GN=KRTAP6-1 PE=3 SV=1 | KRA61 | 7 kDa | 0 | 0 | 0 | 0 | 1 |
| Keratin-associated protein 9-1 OS=Homo sapiens GN=KRTAP9-1 PE=3 SV=1 | KRA91 | 26 kDa | 0 | 0 | 0 | 0 | 1 |
| Keratin, type I cuticular Ha4 OS=Homo sapiens GN=KRT34 PE=2 SV=2 | KRT34 | 49 kDa | 0 | 0 | 0 | 0 | 5 |

| | | | | | | | |
|---|---|---|---|---|---|---|---|
| Keratin, type I cuticular Ha5 OS=Homo sapiens GN=KRT35 PE=2 SV=5 | KRT35 | 50 kDa | 0 | 0 | 0 | 0 | 2 |
| Keratin, type II cuticular Hb2 OS=Homo sapiens GN=KRT82 PE=3 SV=3 | KRT82 | 57 kDa | 0 | 0 | 0 | 0 | 8 |
| Keratin, type II cuticular Hb5 OS=Homo sapiens GN=KRT85 PE=1 SV=1 | KRT85 | 56 kDa | 0 | 0 | 0 | 0 | 6 |
| Keratin, type II cuticular Hb6 OS=Homo sapiens GN=KRT86 PE=1 SV=1 | KRT86 | 53 kDa | 0 | 1 | 0 | 0 | 15 |
| Ribosomal protein S6 kinase alpha-3 OS=Homo sapiens GN=RPS6KA3 PE=1 SV=1 | KS6A3 | 84 kDa | 1 | 0 | 0 | 0 | 2 |
| Keratin, type I cuticular Ha3-I OS=Homo sapiens GN=KRT33A PE=2 SV=2 | KT33A | 46 kDa | 0 | 0 | 0 | 0 | 3 |
| Keratin, type I cuticular Ha3-II OS=Homo sapiens GN=KRT33B PE=1 SV=3 | KT33B | 46 kDa | 0 | 0 | 0 | 0 | 3 |
| La-related protein 6 OS=Homo sapiens GN=LARP6 PE=1 SV=1 | LARP6 | 55 kDa | 0 | 0 | 0 | 0 | 1 |
| L-lactate dehydrogenase B chain OS=Homo sapiens GN=LDHB PE=1 SV=2 | LDHB | 37 kDa | 0 | 0 | 0 | 0 | 2 |
| Leucine-rich repeat-containing protein 40 OS=Homo sapiens GN=LRRC40 PE=1 SV=1 | LRC40 | 68 kDa | 0 | 0 | 0 | 0 | 1 |
| DNA replication licensing factor MCM4 OS=Homo sapiens GN=MCM4 PE=1 SV=5 | MCM4 | 97 kDa | 1 | 0 | 1 | 0 | 3 |
| DNA replication licensing factor MCM5 OS=Homo sapiens GN=MCM5 PE=1 SV=5 | MCM5 | 82 kDa | 3 | 0 | 3 | 0 | 4 |
| DNA replication licensing factor MCM7 OS=Homo sapiens GN=MCM7 PE=1 SV=4 | MCM7 | 81 kDa | 5 | 0 | 5 | 0 | 9 |
| Mitogen-activated protein kinase 3 OS=Homo sapiens GN=MAPK3 PE=1 SV=4 | MK03 | 43 kDa | 0 | 0 | 0 | 0 | 1 |
| Mitochondrial-processing peptidase subunit alpha OS=Homo sapiens GN=PMPCA PE=1 SV=2 | MPPA | 58 kDa | 0 | 0 | 0 | 0 | 1 |
| Mitochondrial ribonuclease P protein 1 OS=Homo sapiens GN=TRMT10C PE=1 SV=2 | MRRP1 | 47 kDa | 0 | 0 | 0 | 0 | 1 |
| Metastasis-associated protein MTA2 OS=Homo sapiens GN=MTA2 PE=1 SV=1 | MTA2 | 75 kDa | 0 | 0 | 0 | 0 | 1 |
| N-alpha-acetyltransferase 15, NatA auxiliary subunit OS=Homo sapiens GN=NAA15 PE=1 SV=1 | NAA15 | 101 kDa | 0 | 0 | 0 | 0 | 2 |
| Nuclear autoantigenic sperm protein OS=Homo sapiens GN=NASP PE=1 SV=2 | NASP | 85 kDa | 0 | 0 | 0 | 0 | 2 |

| | | | | | | | |
|---|---|---|---|---|---|---|---|
| Non-POU domain-containing octamer-binding protein OS=Homo sapiens GN=NONO PE=1 SV=4 | NONO | 54 kDa | 7 | 6 | 3 | 0 | 8 |
| tRNA (cytosine(34)-C(5))-methyltransferase OS=Homo sapiens GN=NSUN2 PE=1 SV=2 | NSUN2 | 86 kDa | 1 | 0 | 0 | 0 | 3 |
| 5'-nucleotidase domain-containing protein 1 OS=Homo sapiens GN=NT5DC1 PE=1 SV=1 | NT5D1 | 52 kDa | 0 | 0 | 0 | 0 | 1 |
| Nucleoside diphosphate-linked moiety X motif 19, mitochondrial OS=Homo sapiens GN=NUDT19 PE=1 SV=1 | NUD19 | 42 kDa | 0 | 0 | 0 | 0 | 1 |
| NudC domain-containing protein 1 OS=Homo sapiens GN=NUDCD1 PE=1 SV=2 | NUDC1 | 67 kDa | 0 | 0 | 0 | 0 | 1 |
| Obg-like ATPase 1 OS=Homo sapiens GN=OLA1 PE=1 SV=2 | OLA1 | 45 kDa | 0 | 0 | 0 | 0 | 1 |
| Delta-1-pyrroline-5-carboxylate synthase OS=Homo sapiens GN=ALDH18A1 PE=1 SV=2 | P5CS | 87 kDa | 2 | 0 | 2 | 0 | 5 |
| Polyadenylate-binding protein 1 OS=Homo sapiens GN=PABPC1 PE=1 SV=2 | PABP1 | 71 kDa | 5 | 1 | 4 | 0 | 7 |
| Pantothenate kinase 4 OS=Homo sapiens GN=PANK4 PE=1 SV=1 | PANK4 | 86 kDa | 0 | 0 | 0 | 0 | 1 |
| Programmed cell death 6-interacting protein OS=Homo sapiens GN=PDCD6IP PE=1 SV=1 | PDC6I | 96 kDa | 0 | 0 | 0 | 0 | 1 |
| 2',5'-phosphodiesterase 12 OS=Homo sapiens GN=PDE12 PE=1 SV=2 | PDE12 | 67 kDa | 0 | 0 | 0 | 0 | 1 |
| Junction plakoglobin OS=Homo sapiens GN=JUP PE=1 SV=3 | PLAK | 82 kDa | 0 | 1 | 1 | 0 | 3 |
| Polyribonucleotide nucleotidyltransferase 1, mitochondrial OS=Homo sapiens GN=PNPT1 PE=1 SV=2 | PNPT1 | 86 kDa | 0 | 0 | 0 | 0 | 1 |
| Peptidyl-prolyl cis-trans isomerase D OS=Homo sapiens GN=PPID PE=1 SV=3 | PPID | 41 kDa | 0 | 0 | 0 | 0 | 1 |
| Pre-mRNA-processing factor 19 OS=Homo sapiens GN=PRPF19 PE=1 SV=1 | PRP19 | 55 kDa | 0 | 0 | 0 | 0 | 1 |
| 26S protease regulatory subunit 10B OS=Homo sapiens GN=PSMC6 PE=1 SV=1 | PRS10 | 44 kDa | 0 | 0 | 0 | 0 | 2 |
| Puromycin-sensitive aminopeptidase OS=Homo sapiens GN=NPEPPS PE=1 SV=2 | PSA | 103 kDa | 3 | 0 | 0 | 0 | 5 |

| | | | | | | | |
|---|---|---|---|---|---|---|---|
| 26S proteasome non-ATPase regulatory subunit 12 OS=Homo sapiens GN=PSMD12 PE=1 SV=3 | PSD12 | 53 kDa | 0 | 0 | 0 | 0 | 1 |
| 26S proteasome non-ATPase regulatory subunit 2 OS=Homo sapiens GN=PSMD2 PE=1 SV=3 | PSMD2 | 100 kDa | 3 | 0 | 2 | 0 | 6 |
| Paraspeckle component 1 OS=Homo sapiens GN=PSPC1 PE=1 SV=1 | PSPC1 | 59 kDa | 0 | 0 | 0 | 0 | 1 |
| Poly(U)-binding-splicing factor PUF60 OS=Homo sapiens GN=PUF60 PE=1 SV=1 | PUF60 | 60 kDa | 0 | 0 | 0 | 0 | 1 |
| Bifunctional purine biosynthesis protein PURH OS=Homo sapiens GN=ATIC PE=1 SV=3 | PUR9 | 65 kDa | 4 | 2 | 4 | 0 | 10 |
| Glycogen phosphorylase, liver form OS=Homo sapiens GN=PYGL PE=1 SV=4 | PYGL | 97 kDa | 0 | 0 | 0 | 0 | 4 |
| CTP synthase 1 OS=Homo sapiens GN=CTPS1 PE=1 SV=2 | PYRG1 | 67 kDa | 1 | 0 | 1 | 0 | 5 |
| Ribonucleoprotein PTB-binding 1 OS=Homo sapiens GN=RAVER1 PE=1 SV=1 | RAVR1 | 64 kDa | 0 | 0 | 0 | 0 | 1 |
| Histone-binding protein RBBP4 OS=Homo sapiens GN=RBBP4 PE=1 SV=3 | RBBP4 | 48 kDa | 1 | 0 | 1 | 0 | 2 |
| Histone-binding protein RBBP7 OS=Homo sapiens GN=RBBP7 PE=1 SV=1 | RBBP7 | 48 kDa | 1 | 0 | 1 | 0 | 2 |
| RNA-binding protein 39 OS=Homo sapiens GN=RBM39 PE=1 SV=2 | RBM39 | 59 kDa | 1 | 0 | 0 | 0 | 3 |
| Reticulocalbin-1 OS=Homo sapiens GN=RCN1 PE=1 SV=1 | RCN1 | 39 kDa | 0 | 0 | 0 | 0 | 1 |
| 60S ribosomal protein L24 OS=Homo sapiens GN=RPL24 PE=1 SV=1 | RL24 | 18 kDa | 0 | 0 | 0 | 0 | 1 |
| 60S ribosomal protein L29 OS=Homo sapiens GN=RPL29 PE=1 SV=2 | RL29 | 18 kDa | 0 | 0 | 0 | 0 | 1 |
| Heterogeneous nuclear ribonucleoprotein A/B OS=Homo sapiens GN=HNRNPAB PE=1 SV=2 | ROAA | 36 kDa | 0 | 0 | 0 | 0 | 1 |
| Dolichyl-diphosphooligosaccharide--protein glycosyltransferase subunit 1 OS=Homo sapiens GN=RPN1 PE=1 SV=1 | RPN1 | 69 kDa | 3 | 0 | 3 | 0 | 6 |
| Ubiquitin-40S ribosomal protein S27a OS=Homo sapiens GN=RPS27A PE=1 SV=2 | RS27A | 18 kDa | 3 | 0 | 3 | 0 | 4 |
| 40S ribosomal protein SA OS=Homo sapiens GN=RPSA PE=1 SV=4 | RSSA | 33 kDa | 3 | 1 | 2 | 0 | 5 |

| | | | | | | | |
|---|---|---|---|---|---|---|---|
| Protein S100-A8 OS=Homo sapiens GN=S100A8 PE=1 SV=1 | S10A8 | 11 kDa | 0 | 0 | 0 | 0 | 1 |
| Protein S100-A9 OS=Homo sapiens GN=S100A9 PE=1 SV=1 | S10A9 | 13 kDa | 0 | 0 | 0 | 0 | 1 |
| SUMO-activating enzyme subunit 1 OS=Homo sapiens GN=SAE1 PE=1 SV=1 | SAE1 | 38 kDa | 0 | 0 | 0 | 0 | 1 |
| SUMO-activating enzyme subunit 2 OS=Homo sapiens GN=UBA2 PE=1 SV=2 | SAE2 | 71 kDa | 2 | 1 | 2 | 0 | 3 |
| Adenosylhomocysteinase OS=Homo sapiens GN=AHCY PE=1 SV=4 | SAHH | 48 kDa | 0 | 0 | 0 | 0 | 1 |
| Suprabasin OS=Homo sapiens GN=SBSN PE=1 SV=2 | SBSN | 61 kDa | 0 | 0 | 0 | 0 | 1 |
| Protein transport protein Sec23A OS=Homo sapiens GN=SEC23A PE=1 SV=2 | SC23A | 86 kDa | 1 | 0 | 1 | 0 | 3 |
| Protein transport protein Sec31A OS=Homo sapiens GN=SEC31A PE=1 SV=3 | SC31A | 133 kDa | 0 | 0 | 0 | 0 | 1 |
| Succinate dehydrogenase (ubiquinone) flavoprotein subunit, mitochondrial OS=Homo sapiens GN=SDHA PE=1 SV=2 | SDHA | 73 kDa | 0 | 0 | 0 | 0 | 1 |
| Septin-11 OS=Homo sapiens GN=SEPT11 PE=1 SV=3 | SEP11 | 49 kDa | 0 | 0 | 0 | 0 | 1 |
| D-3-phosphoglycerate dehydrogenase OS=Homo sapiens GN=PHGDH PE=1 SV=4 | SERA | 57 kDa | 12 | 2 | 6 | 0 | 14 |
| Phosphoserine aminotransferase OS=Homo sapiens GN=PSAT1 PE=1 SV=2 | SERC | 40 kDa | 0 | 0 | 0 | 0 | 4 |
| Serpin H1 OS=Homo sapiens GN=SERPINH1 PE=1 SV=2 | SERPH | 46 kDa | 2 | 1 | 1 | 0 | 4 |
| Splicing factor 3A subunit 3 OS=Homo sapiens GN=SF3A3 PE=1 SV=1 | SF3A3 | 59 kDa | 0 | 0 | 0 | 0 | 1 |
| Splicing factor, proline- and glutamine-rich OS=Homo sapiens GN=SFPQ PE=1 SV=2 | SFPQ | 76 kDa | 1 | 1 | 0 | 0 | 6 |
| Shootin-1 OS=Homo sapiens GN=KIAA1598 PE=1 SV=4 | SHOT1 | 72 kDa | 0 | 0 | 0 | 0 | 1 |
| Serpin B3 OS=Homo sapiens GN=SERPINB3 PE=1 SV=2 | SPB3 | 45 kDa | 0 | 0 | 0 | 0 | 1 |
| Signal recognition particle 54 kDa protein OS=Homo sapiens GN=SRP54 PE=1 SV=1 | SRP54 | 56 kDa | 0 | 0 | 0 | 0 | 1 |
| Signal recognition particle receptor subunit alpha OS=Homo sapiens GN=SRPR PE=1 SV=2 | SRPR | 70 kDa | 0 | 0 | 0 | 0 | 3 |

| | | | | | | | |
|---|---|---|---|---|---|---|---|
| Succinyl-CoA ligase (ADP-forming) subunit beta, mitochondrial OS=Homo sapiens GN=SUCLA2 PE=1 SV=3 | SUCB1 | 50 kDa | 0 | 0 | 0 | 0 | 1 |
| Succinyl-CoA ligase (GDP-forming) subunit beta, mitochondrial OS=Homo sapiens GN=SUCLG2 PE=1 SV=2 | SUCB2 | 47 kDa | 0 | 0 | 0 | 0 | 1 |
| ATP-dependent RNA helicase SUPV3L1, mitochondrial OS=Homo sapiens GN=SUPV3L1 PE=1 SV=1 | SUV3 | 88 kDa | 0 | 0 | 0 | 0 | 1 |
| Alanine--tRNA ligase, cytoplasmic OS=Homo sapiens GN=AARS PE=1 SV=2 | SYAC | 107 kDa | 0 | 0 | 0 | 0 | 1 |
| Phenylalanine--tRNA ligase beta subunit OS=Homo sapiens GN=FARSB PE=1 SV=3 | SYFB | 66 kDa | 0 | 0 | 0 | 0 | 3 |
| Glycine--tRNA ligase OS=Homo sapiens GN=GARS PE=1 SV=3 | SYG | 83 kDa | 0 | 0 | 0 | 0 | 1 |
| Methionine--tRNA ligase, cytoplasmic OS=Homo sapiens GN=MARS PE=1 SV=2 | SYMC | 101 kDa | 4 | 0 | 0 | 0 | 8 |
| Glutamine--tRNA ligase OS=Homo sapiens GN=QARS PE=1 SV=1 | SYQ | 88 kDa | 1 | 0 | 1 | 0 | 3 |
| Tyrosine--tRNA ligase, cytoplasmic OS=Homo sapiens GN=YARS PE=1 SV=4 | SYYC | 59 kDa | 2 | 1 | 1 | 0 | 3 |
| T-complex protein 1 subunit alpha OS=Homo sapiens GN=TCP1 PE=1 SV=1 | TCPA | 60 kDa | 3 | 1 | 2 | 0 | 8 |
| T-complex protein 1 subunit beta OS=Homo sapiens GN=CCT2 PE=1 SV=4 | TCPB | 57 kDa | 6 | 4 | 2 | 1 | 7 |
| T-complex protein 1 subunit delta OS=Homo sapiens GN=CCT4 PE=1 SV=4 | TCPD | 58 kDa | 3 | 3 | 0 | 0 | 7 |
| T-complex protein 1 subunit epsilon OS=Homo sapiens GN=CCT5 PE=1 SV=1 | TCPE | 60 kDa | 2 | 1 | 1 | 0 | 3 |
| T-complex protein 1 subunit gamma OS=Homo sapiens GN=CCT3 PE=1 SV=4 | TCPG | 61 kDa | 4 | 2 | 4 | 1 | 6 |
| T-complex protein 1 subunit theta OS=Homo sapiens GN=CCT8 PE=1 SV=4 | TCPQ | 60 kDa | 4 | 2 | 3 | 0 | 7 |
| Transcription factor p65 OS=Homo sapiens GN=RELA PE=1 SV=2 | TF65 | 60 kDa | 0 | 0 | 0 | 0 | 1 |
| Thimet oligopeptidase OS=Homo sapiens GN=THOP1 PE=1 SV=2 | THOP1 | 79 kDa | 0 | 0 | 0 | 0 | 1 |
| Mitochondrial import inner membrane translocase subunit TIM44 OS=Homo sapiens GN=TIMM44 PE=1 SV=2 | TIM44 | 51 kDa | 0 | 0 | 0 | 0 | 2 |

| | | | | | | | |
|---|---|---|---|---|---|---|---|
| Mitochondrial import receptor subunit TOM70 OS=Homo sapiens GN=TOMM70A PE=1 SV=1 | TOM70 | 67 kDa | 0 | 0 | 0 | 0 | 1 |
| Trypsin-2 OS=Homo sapiens GN=PRSS2 PE=1 SV=1 | TRY2 | 26 kDa | 0 | 0 | 0 | 0 | 1 |
| Tetratricopeptide repeat protein 4 OS=Homo sapiens GN=TTC4 PE=1 SV=3 | TTC4 | 45 kDa | 0 | 0 | 0 | 0 | 1 |
| Tubulin--tyrosine ligase-like protein 12 OS=Homo sapiens GN=TTLL12 PE=1 SV=2 | TTL12 | 74 kDa | 1 | 0 | 1 | 0 | 4 |
| Ubiquitin carboxyl-terminal hydrolase 5 OS=Homo sapiens GN=USP5 PE=1 SV=2 | UBP5 | 96 kDa | 0 | 0 | 0 | 0 | 2 |
| Protein unc-45 homolog A OS=Homo sapiens GN=UNC45A PE=1 SV=1 | UN45A | 103 kDa | 0 | 0 | 0 | 0 | 1 |
| Synaptic vesicle membrane protein VAT-1 homolog OS=Homo sapiens GN=VAT1 PE=1 SV=2 | VAT1 | 42 kDa | 2 | 0 | 0 | 0 | 3 |
| V-set and immunoglobulin domain-containing protein 8 OS=Homo sapiens GN=VSIG8 PE=2 SV=1 | VSIG8 | 44 kDa | 0 | 0 | 0 | 0 | 2 |
| WD repeat-containing protein 1 OS=Homo sapiens GN=WDR1 PE=1 SV=4 | WDR1 | 66 kDa | 0 | 0 | 0 | 0 | 1 |
| Exportin-T OS=Homo sapiens GN=XPOT PE=1 SV=2 | XPOT | 110 kDa | 1 | 0 | 0 | 0 | 2 |
| Neutral amino acid transporter B(0) OS=Homo sapiens GN=SLC1A5 PE=1 SV=2 | AAAT | 57 kDa | 0 | 0 | 2 | 0 | 0 |
| ADP/ATP translocase 3 OS=Homo sapiens GN=SLC25A6 PE=1 SV=4 | ADT3 | 33 kDa | 0 | 0 | 1 | 0 | 0 |
| Phosphoacetylglucosamine mutase OS=Homo sapiens GN=PGM3 PE=1 SV=1 | AGM1 | 60 kDa | 0 | 0 | 1 | 0 | 0 |
| AP-2 complex subunit mu OS=Homo sapiens GN=AP2M1 PE=1 SV=2 | AP2M1-DECOY | ? | 0 | 0 | 1 | 0 | 0 |
| Rho guanine nucleotide exchange factor 7 OS=Homo sapiens GN=ARHGEF7 PE=1 SV=2 | ARHG7 | 90 kDa | 0 | 0 | 1 | 0 | 0 |
| E3 ubiquitin-protein ligase ARIH1 OS=Homo sapiens GN=ARIH1 PE=1 SV=2 | ARI1 | 64 kDa | 0 | 0 | 1 | 0 | 0 |
| Bone morphogenetic protein 1 OS=Homo sapiens GN=BMP1 PE=1 SV=2 | BMP1-DECOY | ? | 0 | 0 | 1 | 0 | 0 |
| Basic leucine zipper and W2 domain-containing protein 1 OS=Homo sapiens GN=BZW1 PE=1 SV=1 | BZW1 | 48 kDa | 0 | 0 | 1 | 0 | 0 |
| Coatomer subunit delta OS=Homo sapiens GN=ARCN1 PE=1 SV=1 | COPD | 57 kDa | 1 | 1 | 2 | 0 | 1 |

| Protein | Gene | Mass | | | | | |
|---|---|---|---|---|---|---|---|
| Cullin-4B OS=Homo sapiens GN=CUL4B PE=1 SV=4 | CUL4B | 104 kDa | 0 | 0 | 1 | 0 | 0 |
| Nucleolar RNA helicase 2 OS=Homo sapiens GN=DDX21 PE=1 SV=5 | DDX21 | 87 kDa | 5 | 0 | 7 | 0 | 5 |
| ATP-dependent RNA helicase DDX50 OS=Homo sapiens GN=DDX50 PE=1 SV=1 | DDX50 | 83 kDa | 0 | 0 | 2 | 0 | 0 |
| Dynein heavy chain 14, axonemal OS=Homo sapiens GN=DNAH14 PE=2 SV=3 | DYH14 | 400 kDa | 0 | 0 | 1 | 0 | 0 |
| Eukaryotic translation initiation factor 2D OS=Homo sapiens GN=EIF2D PE=1 SV=3 | EIF2D | 65 kDa | 0 | 0 | 1 | 0 | 0 |
| RNA-binding protein EWS OS=Homo sapiens GN=EWSR1 PE=1 SV=1 | EWS | 68 kDa | 0 | 0 | 1 | 0 | 0 |
| Exocyst complex component 3 OS=Homo sapiens GN=EXOC3 PE=1 SV=2 | EXOC3 | 87 kDa | 0 | 0 | 1 | 0 | 0 |
| Far upstream element-binding protein 3 OS=Homo sapiens GN=FUBP3 PE=1 SV=2 | FUBP3 | 62 kDa | 1 | 0 | 2 | 0 | 1 |
| Fragile X mental retardation syndrome-related protein 1 OS=Homo sapiens GN=FXR1 PE=1 SV=3 | FXR1 | 70 kDa | 0 | 0 | 2 | 0 | 0 |
| Guanine nucleotide-binding protein subunit beta-like protein 1 OS=Homo sapiens GN=GNB1L PE=1 SV=2 | GNB1L | 36 kDa | 0 | 0 | 1 | 0 | 0 |
| Heterogeneous nuclear ribonucleoprotein Q OS=Homo sapiens GN=SYNCRIP PE=1 SV=2 | HNRPQ | 70 kDa | 1 | 0 | 2 | 0 | 1 |
| Insulin-like growth factor 2 mRNA-binding protein 2 OS=Homo sapiens GN=IGF2BP2 PE=1 SV=2 | IF2B2 | 66 kDa | 4 | 0 | 7 | 0 | 4 |
| La-related protein 7 OS=Homo sapiens GN=LARP7 PE=1 SV=1 | LARP7 | 67 kDa | 1 | 0 | 2 | 0 | 1 |
| Prolow-density lipoprotein receptor-related protein 1 OS=Homo sapiens GN=LRP1 PE=1 SV=2 | LRP1-DECOY | ? | 0 | 0 | 1 | 0 | 0 |
| Myristoylated alanine-rich C-kinase substrate OS=Homo sapiens GN=MARCKS PE=1 SV=4 | MARCS | 32 kDa | 0 | 0 | 1 | 0 | 0 |
| Mitotic spindle assembly checkpoint protein MAD1 OS=Homo sapiens GN=MAD1L1 PE=1 SV=2 | MD1L1 | 83 kDa | 0 | 0 | 2 | 0 | 0 |
| 7SK snRNA methylphosphate capping enzyme OS=Homo sapiens GN=MEPCE PE=1 SV=1 | MEPCE | 74 kDa | 0 | 0 | 1 | 0 | 0 |

| Double-strand break repair protein MRE11A OS=Homo sapiens GN=MRE11A PE=1 SV=3 | MRE11 | 81 kDa | 0 | 0 | 1 | 0 | 0 |
|---|---|---|---|---|---|---|---|
| NADH dehydrogenase (ubiquinone) 1 alpha subcomplex subunit 2 OS=Homo sapiens GN=NDUFA2 PE=1 SV=3 | NDUA2 | 11 kDa | 0 | 0 | 1 | 0 | 0 |
| Nucleolar protein 56 OS=Homo sapiens GN=NOP56 PE=1 SV=4 | NOP56 | 66 kDa | 1 | 0 | 3 | 0 | 1 |
| Nucleolar protein 58 OS=Homo sapiens GN=NOP58 PE=1 SV=1 | NOP58 | 60 kDa | 1 | 0 | 2 | 0 | 0 |
| Nucleophosmin OS=Homo sapiens GN=NPM1 PE=1 SV=2 | NPM | 33 kDa | 0 | 0 | 1 | 0 | 0 |
| PiggyBac transposable element-derived protein 1 OS=Homo sapiens GN=PGBD1 PE=1 SV=1 | PGBD1 | 93 kDa | 0 | 0 | 1 | 0 | 0 |
| Protein regulator of cytokinesis 1 OS=Homo sapiens GN=PRC1 PE=1 SV=2 | PRC1 | 72 kDa | 0 | 0 | 3 | 0 | 0 |
| CAD protein OS=Homo sapiens GN=CAD PE=1 SV=3 | PYR1 | 243 kDa | 4 | 1 | 5 | 0 | 0 |
| 60S ribosomal protein L15 OS=Homo sapiens GN=RPL15 PE=1 SV=2 | RL15 | 24 kDa | 0 | 0 | 1 | 0 | 0 |
| Ribosomal L1 domain-containing protein 1 OS=Homo sapiens GN=RSL1D1 PE=1 SV=3 | RL1D1 | 55 kDa | 1 | 0 | 2 | 0 | 1 |
| 60S ribosomal protein L8 OS=Homo sapiens GN=RPL8 PE=1 SV=2 | RL8 | 28 kDa | 0 | 0 | 1 | 0 | 0 |
| RING finger protein 214 OS=Homo sapiens GN=RNF214 PE=1 SV=2 | RN214 | 78 kDa | 0 | 0 | 1 | 0 | 0 |
| Septin-9 OS=Homo sapiens GN=SEPT9 PE=1 SV=2 | SEPT9 | 65 kDa | 0 | 0 | 1 | 0 | 0 |
| Suppressor of SWI4 1 homolog OS=Homo sapiens GN=PPAN PE=1 SV=1 | SSF1 | 53 kDa | 0 | 0 | 1 | 0 | 0 |
| Pre-mRNA-splicing factor SYF1 OS=Homo sapiens GN=XAB2 PE=1 SV=2 | SYF1 | 100 kDa | 0 | 0 | 1 | 0 | 0 |
| Tubulin beta-6 chain OS=Homo sapiens GN=TUBB6 PE=1 SV=1 | TBB6 | 50 kDa | 0 | 0 | 1 | 0 | 0 |
| Testis-expressed sequence 10 protein OS=Homo sapiens GN=TEX10 PE=1 SV=2 | TEX10 | 106 kDa | 0 | 0 | 1 | 0 | 0 |
| General transcription factor 3C polypeptide 5 OS=Homo sapiens GN=GTF3C5 PE=1 SV=2 | TF3C5 | 60 kDa | 0 | 0 | 2 | 0 | 0 |
| TRMT1-like protein OS=Homo sapiens GN=TRMT1L PE=1 SV=2 | TRM1L | 82 kDa | 0 | 0 | 1 | 0 | 0 |

| | | | | | | | |
|---|---|---|---|---|---|---|---|
| DNA repair protein XRCC1 OS=Homo sapiens GN=XRCC1 PE=1 SV=2 | XRCC1 | 69 kDa | 0 | 0 | 1 | 0 | 0 |
| YTH domain-containing family protein 1 OS=Homo sapiens GN=YTHDF1 PE=1 SV=1 | YTHD1 | 61 kDa | 0 | 0 | 1 | 0 | 0 |
| Zinc finger CCCH domain-containing protein 14 OS=Homo sapiens GN=ZC3H14 PE=1 SV=1 | ZC3HE | 83 kDa | 0 | 0 | 1 | 0 | 0 |

**Table A. 4. 5: Representation of the protein identification probability (Identification confidence) of proteins with peptide ratio more than 1, from Trial 1 and Trial 2, figure A 4.21**

The table containing data for trypsinized proteins from SDS-PAGE gel of trial 1 and trial 2 (Appendix C, section 4.5). The data of the table represents uncrosslinked lysated (lane 1, Figure A 4.21), ATP-Hex-Acr crosslinked lysates in presence of staursporine (lane 2, Figure A 4.21), ATP-Hex-Acr crosslinked lysates (lane 3, Figure A 4.21), ATP-PEG-Acr crosslinked lysates in presence of staursporine (lane 4, Figure A 4.21), and ATP-Hex-Acr crosslinked lysates (lane 5, Figure A 4.21)

| Identified Proteins (900) | Mol. Wt | Protein identification probability | | | | | | | | | |
| | | Trial 1 | | | | | Trial 2 | | | | |
| | | 1 | 2 | 3 | 4 | 5 | 1 | 2 | 3 | 4 | 5 |
| Aconitate hydratase, mitochondrial OS=Homo sapiens GN=ACO2 PE=1 SV=2 | 85 | 100% | 100% | 99% | 100% | 100% | 0 | 93% | 99% | 0 | 100% |
| Alpha-actinin-4 OS=Homo sapiens GN=ACTN4 PE=1 SV=2 | 105 | 100% | 100% | 0 | 100% | 100% | 100% | 100% | 0 | 0 | 100% |
| Activator of 90  heat shock protein ATPase homolog 1 OS=Homo sapiens GN=AHSA1 PE=1 SV=1 | 38 | 0 | 0 | 0 | 100% | 100% | 0 | 94% | 99% | 0 | 100% |
| Apoptosis-inducing factor 1, mitochondrial OS=Homo sapiens GN=AIFM1 PE=1 SV=1 | 67 | 0 | 0 | 100% | 6% | 100% | 0 | 0 | 99% | 0 | 100% |
| Cytosol aminopeptidase OS=Homo sapiens GN=LAP3 PE=1 SV=3 | 56 | 0 | 0 | 99% | 0 | 100% | 100% | 0 | 100% | 0 | 100% |
| ATPase family AAA domain-containing protein 3A OS=Homo sapiens GN=ATAD3A PE=1 SV=2 | 71 | 100% | 0 | 21% | 100% | 100% | 100% | 89% | 100% | 0 | 100% |
| Cytoskeleton-associated protein 4 OS=Homo sapiens GN=CKAP4 PE=1 SV=2 | 66 | 99% | 99% | 0 | 0 | 100% | 83% | 0 | 100% | 0 | 100% |
| Cytosolic non-specific dipeptidase OS=Homo sapiens GN=CNDP2 PE=1 SV=2 | 53 | 0 | 66% | 0 | 0 | 100% | 0 | 0 | 0 | 20% | 99% |
| Coatomer subunit gamma-1 OS=Homo sapiens GN=COPG1 PE=1 SV=1 | 98 | 100% | 65% | 99% | 100% | 100% | 100% | 0 | 100% | 0 | 100% |
| Cold shock domain-containing protein E1 OS=Homo sapiens GN=CSDE1 PE=1 SV=2 | 89 | 100% | 100% | 100% | 100% | 100% | 99% | 100% | 100% | 0 | 100% |
| COP9 signalosome complex subunit 4 OS=Homo sapiens GN=COPS4 PE=1 SV=1 | 46 | 0 | 0 | 0 | 100% | 100% | 0 | 0 | 0 | 0 | 100% |
| Drebrin-like protein OS=Homo sapiens GN=DBNL PE=1 SV=1 | 48 | 0 | 0 | 0 | 0 | 99% | 0 | 0 | 0 | 0 | 100% |

| | | | | | | | | | | | |
|---|---|---|---|---|---|---|---|---|---|---|---|
| ATP-dependent RNA helicase DDX1 OS=Homo sapiens GN=DDX1 PE=1 SV=2 | 82 | 100% | 54% | 100% | 100% | 100% | 100% | 100% | 100% | 0 | 100% |
| Probable ATP-dependent RNA helicase DDX17 OS=Homo sapiens GN=DDX17 PE=1 SV=2 | 80 | 100% | 67% | 100% | 100% | 100% | 100% | 100% | 100% | 0 | 100% |
| Peroxisomal multifunctional enzyme type 2 OS=Homo sapiens GN=HSD17B4 PE=1 SV=3 | 80 | 0 | 57% | 0 | 100% | 100% | 0 | 0 | 92% | 0 | 100% |
| Dynamin-1-like protein OS=Homo sapiens GN=DNM1L PE=1 SV=2 | 82 | 100% | 0 | 99% | 0 | 100% | 80% | 0 | 100% | 0 | 100% |
| Dihydropyrimidinase-related protein 1 OS=Homo sapiens GN=CRMP1 PE=1 SV=1 | 62 | 0 | 0 | 0 | 98% | 99% | 0 | 0 | 0 | 84% | 99% |
| Developmentally-regulated GTP-binding protein 1 OS=Homo sapiens GN=DRG1 PE=1 SV=1 | 41 | 0 | 0 | 0 | 0 | 100% | 0 | 0 | 99% | 0 | 100% |
| Trifunctional enzyme subunit alpha, mitochondrial OS=Homo sapiens GN=HADHA PE=1 SV=2 | 83 | 100% | 0 | 100% | 100% | 100% | 99% | 0 | 100% | 0 | 100% |
| Elongation factor 2 OS=Homo sapiens GN=EEF2 PE=1 SV=4 | 95 | 100% | 100% | 100% | 100% | 100% | 100% | 100% | 100% | 0 | 100% |
| Eukaryotic translation initiation factor 3 subunit D OS=Homo sapiens GN=EIF3D PE=1 SV=1 | 64 | 100% | 73% | 100% | 0 | 100% | 100% | 57% | 100% | 0 | 100% |
| Eukaryotic translation initiation factor 3 subunit L OS=Homo sapiens GN=EIF3L PE=1 SV=1 | 67 | 100% | 0 | 100% | 100% | 100% | 100% | 100% | 100% | 0 | 100% |
| Epiplakin OS=Homo sapiens GN=EPPK1 PE=1 SV=2 | 556 | 100% | 0 | 100% | 100% | 100% | 100% | 0 | 71% | 100% | 0 |
| Exosome component 10 OS=Homo sapiens GN=EXOSC10 PE=1 SV=2 | 101 | 0 | 0 | 0 | 99% | 99% | 0 | 0 | 0 | 0 | 99% |
| Ezrin OS=Homo sapiens GN=EZR PE=1 SV=4 | 69 | 100% | 0 | 0 | 100% | 100% | 53% | 100% | 100% | 0 | 100% |
| RNA-binding protein FUS OS=Homo sapiens GN=FUS PE=1 SV=1 | 53 | 99% | 0 | 100% | 0 | 100% | 100% | 70% | 100% | 0 | 100% |
| Glucose-6-phosphate isomerase OS=Homo sapiens GN=GPI PE=1 SV=4 | 63 | 100% | 99% | 100% | 100% | 100% | 100% | 100% | 96% | 0 | 100% |
| Glucosidase 2 subunit beta OS=Homo sapiens GN=PRKCSH PE=1 SV=2 | 59 | 96% | 49% | 84% | 0 | 100% | 72% | 97% | 100% | 0 | 99% |
| Serine hydroxymethyltransferase, mitochondrial OS=Homo sapiens GN=SHMT2 PE=1 SV=3 | 56 | 100% | 100% | 100% | 100% | 100% | 100% | 100% | 100% | 0 | 100% |

| | | | | | | | | | | |
|---|---|---|---|---|---|---|---|---|---|---|
| Stress-70 protein, mitochondrial OS=Homo sapiens GN=HSPA9 PE=1 SV=2 | 74 | 100% | 100% | 100% | 100% | 100% | 100% | 100% | 100% | 0 | 100% |
| GMP synthase [glutamine-hydrolyzing] OS=Homo sapiens GN=GMPS PE=1 SV=1 | 77 | 0 | 0 | 0 | 100% | 99% | 0 | 0 | 0 | 0 | 99% |
| Heterogeneous nuclear ribonucleoproteins C1/C2 OS=Homo sapiens GN=HNRNPC PE=1 SV=4 | 34 | 0 | 0 | 0 | 0 | 99% | 0 | 0 | 100% | 0 | 100% |
| Heterogeneous nuclear ribonucleoprotein M OS=Homo sapiens GN=HNRNPM PE=1 SV=3 | 78 | 100% | 100% | 100% | 100% | 100% | 100% | 100% | 100% | 96% | 100% |
| Heterogeneous nuclear ribonucleoprotein R OS=Homo sapiens GN=HNRNPR PE=1 SV=1 | 71 | 100% | 100% | 100% | 100% | 100% | 100% | 0 | 100% | 0 | 100% |
| Hornerin OS=Homo sapiens GN=HRNR PE=1 SV=2 | 282 | 100% | 100% | 100% | 100% | 100% | 0 | 100% | 100% | 0 | 100% |
| Heat shock 70 protein 1A OS=Homo sapiens GN=HSPA1A PE=1 SV=1 | 70 | 100% | 100% | 100% | 100% | 100% | 100% | 100% | 100% | 100% | 100% |
| Heat shock protein HSP 90-alpha OS=Homo sapiens GN=HSP90AA1 PE=1 SV=5 | 85 | 100% | 100% | 100% | 100% | 100% | 100% | 100% | 100% | 100% | 100% |
| Heat shock protein HSP 90-beta OS=Homo sapiens GN=HSP90AB1 PE=1 SV=4 | 83 | 100% | 100% | 100% | 100% | 100% | 100% | 100% | 100% | 79% | 100% |
| Heat shock cognate 71 protein OS=Homo sapiens GN=HSPA8 PE=1 SV=1 | 71 | 100% | 100% | 100% | 100% | 100% | 100% | 100% | 100% | 99% | 100% |
| Interferon regulatory factor 2-binding protein 1 OS=Homo sapiens GN=IRF2BP1 PE=1 SV=1 | 62 | 0 | 0 | 0 | 0 | 99% | 0 | 0 | 0 | 0 | 100% |
| Importin subunit beta-1 OS=Homo sapiens GN=KPNB1 PE=1 SV=2 | 97 | 100% | 100% | 100% | 100% | 100% | 100% | 100% | 100% | 0 | 100% |
| Creatine kinase B-type OS=Homo sapiens GN=CKB PE=1 SV=1 | 43 | 0 | 100% | 100% | 100% | 100% | 100% | 100% | 100% | 100% | 100% |
| Pyruvate kinase PKM OS=Homo sapiens GN=PKM PE=1 SV=4 | 58 | 100% | 100% | 100% | 100% | 100% | 100% | 100% | 100% | 100% | 100% |
| L-lactate dehydrogenase A chain OS=Homo sapiens GN=LDHA PE=1 SV=2 | 37 | 0 | 0 | 100% | 100% | 100% | 0 | 99% | 0 | 0 | 100% |
| LETM1 and EF-hand domain-containing protein 1, mitochondrial OS=Homo sapiens GN=LETM1 PE=1 SV=1 | 83 | 77% | 0 | 0 | 0 | 100% | 0 | 0 | 100% | 0 | 100% |
| Leukotriene A-4 hydrolase OS=Homo sapiens GN=LTA4H PE=1 SV=2 | 69 | 100% | 0 | 100% | 100% | 100% | 93% | 96% | 99% | 0 | 100% |
| Leucine-rich repeat- | 68 | 0 | 0 | 0 | 0 | 99% | 0 | 0 | 0 | 0 | 99% |

| | | | | | | | | | | |
|---|---|---|---|---|---|---|---|---|---|---|
| containing protein 40 OS=Homo sapiens GN=LRRC40 PE=1 SV=1 | | | | | | | | | | |
| Melanoma-associated antigen D2 OS=Homo sapiens GN=MAGED2 PE=1 SV=2 | 65 | 100% | 74% | 56% | 100% | 100% | 0 | 58% | 100% | 40% | 100% |
| DNA replication licensing factor MCM5 OS=Homo sapiens GN=MCM5 PE=1 SV=5 | 82 | 100% | 0 | 100% | 100% | 100% | 100% | 0 | 100% | 0 | 100% |
| MICOS complex subunit MIC60 OS=Homo sapiens GN=IMMT PE=1 SV=1 | 84 | 83% | 0 | 100% | 0 | 99% | 100% | 0 | 100% | 0 | 100% |
| Mitochondrial-processing peptidase subunit alpha OS=Homo sapiens GN=PMPCA PE=1 SV=2 | 58 | 0 | 0 | 0 | 0 | 99% | 90% | 0 | 31% | 0 | 99% |
| Metastasis-associated protein MTA2 OS=Homo sapiens GN=MTA2 PE=1 SV=1 | 75 | 100% | 0 | 96% | 0 | 100% | 99% | 0 | 100% | 0 | 100% |
| Nuclear autoantigenic sperm protein OS=Homo sapiens GN=NASP PE=1 SV=2 | 85 | 0 | 0 | 0 | 99% | 100% | 100% | 0 | 99% | 0 | 100% |
| NADH-ubiquinone oxidoreductase 75 subunit, mitochondrial OS=Homo sapiens GN=NDUFS1 PE=1 SV=3 | 79 | 0 | 32% | 99% | 0 | 100% | 87% | 0 | 100% | 0 | 100% |
| Vesicle-fusing ATPase OS=Homo sapiens GN=NSF PE=1 SV=3 | 83 | 100% | 73% | 0 | 0 | 100% | 100% | 0 | 100% | 62% | 100% |
| tRNA (cytosine(34)-C(5))-methyltransferase OS=Homo sapiens GN=NSUN2 PE=1 SV=2 | 86 | 100% | 0 | 100% | 0 | 100% | 100% | 0 | 0 | 0 | 100% |
| Dihydrolipoyllysine-residue acetyltransferase component of pyruvate dehydrogenase complex, mitochondrial OS=Homo sapiens GN=DLAT PE=1 SV=3 | 69 | 0 | 0 | 0 | 0 | 100% | 0 | 41% | 99% | 0 | 100% |
| Obg-like ATPase 1 OS=Homo sapiens GN=OLA1 PE=1 SV=2 | 45 | 0 | 0 | 0 | 0 | 100% | 100% | 97% | 0 | 0 | 99% |
| Transcriptional repressor p66-alpha OS=Homo sapiens GN=GATAD2A PE=1 SV=1 | 68 | 99% | 0 | 0 | 100% | 99% | 99% | 0 | 99% | 0 | 99% |
| Polyadenylate-binding protein 1 OS=Homo sapiens GN=PABPC1 PE=1 SV=2 | 71 | 100% | 100% | 100% | 100% | 100% | 100% | 100% | 100% | 0 | 100% |
| Plasminogen activator inhibitor 1 RNA-binding protein OS=Homo sapiens GN=SERBP1 PE=1 SV=2 | 45 | 100% | 100% | 100% | 100% | 100% | 100% | 94% | 100% | 0 | 100% |
| Poly(rC)-binding protein 1 | 37 | 0 | 0 | 0 | 99% | 100 | 0 | 0 | 100 | 0 | 100 |

| Protein | | | | | | | | | | | |
|---|---|---|---|---|---|---|---|---|---|---|---|
| OS=Homo sapiens GN=PCBP1 PE=1 SV=2 | | | | | | % | | % | | % | |
| Programmed cell death 6-interacting protein OS=Homo sapiens GN=PDCD6IP PE=1 SV=1 | 96 | 100% | 89% | 0 | 100% | 100% | 98% | 57% | 0 | 0 | 100% |
| 2',5'-phosphodiesterase 12 OS=Homo sapiens GN=PDE12 PE=1 SV=2 | 67 | 0 | 0 | 0 | 0 | 99% | 0 | 0 | 0 | 0 | 99% |
| Peptidyl-prolyl cis-trans isomerase D OS=Homo sapiens GN=PPID PE=1 SV=3 | 41 | 0 | 0 | 0 | 100% | 100% | 0 | 0 | 0 | 26% | 99% |
| Pre-mRNA-processing factor 19 OS=Homo sapiens GN=PRPF19 PE=1 SV=1 | 55 | 99% | 0 | 100% | 100% | 100% | 100% | 0 | 99% | 0 | 100% |
| U4/U6 small nuclear ribonucleoprotein Prp3 OS=Homo sapiens GN=PRPF3 PE=1 SV=2 | 78 | 62% | 84% | 100% | 0 | 99% | 0 | 0 | 100% | 0 | 100% |
| 26S protease regulatory subunit 10B OS=Homo sapiens GN=PSMC6 PE=1 SV=1 | 44 | 0 | 0 | 0 | 100% | 100% | 0 | 0 | 0 | 0 | 100% |
| 26S proteasome non-ATPase regulatory subunit 2 OS=Homo sapiens GN=PSMD2 PE=1 SV=3 | 100 | 100% | 100% | 100% | 100% | 100% | 100% | 96% | 100% | 0 | 100% |
| 26S proteasome non-ATPase regulatory subunit 3 OS=Homo sapiens GN=PSMD3 PE=1 SV=2 | 61 | 100% | 97% | 100% | 100% | 100% | 100% | 0 | 100% | 0 | 100% |
| Bifunctional purine biosynthesis protein PURH OS=Homo sapiens GN=ATIC PE=1 SV=3 | 65 | 100% | 100% | 100% | 100% | 100% | 100% | 100% | 100% | 0 | 100% |
| Glycogen phosphorylase, liver form OS=Homo sapiens GN=PYGL PE=1 SV=4 | 97 | 100% | 100% | 100% | 100% | 100% | 99% | 95% | 0 | 0 | 100% |
| CTP synthase 1 OS=Homo sapiens GN=CTPS1 PE=1 SV=2 | 67 | 0 | 0 | 100% | 100% | 100% | 100% | 0 | 100% | 0 | 100% |
| Ran GTPase-activating protein 1 OS=Homo sapiens GN=RANGAP1 PE=1 SV=1 | 64 | 100% | 0 | 100% | 100% | 100% | 100% | 0 | 100% | 0 | 100% |
| Ribonucleoprotein PTB-binding 1 OS=Homo sapiens GN=RAVER1 PE=1 SV=1 | 64 | 0 | 0 | 0 | 0 | 99% | 82% | 77% | 98% | 0 | 100% |
| Histone-binding protein RBBP4 OS=Homo sapiens GN=RBBP4 PE=1 SV=3 | 48 | 100% | 0 | 100% | 99% | 100% | 100% | 0 | 99% | 0 | 100% |
| RNA-binding protein 14 OS=Homo sapiens GN=RBM14 PE=1 SV=2 | 69 | 100% | 0 | 100% | 100% | 100% | 32% | 0 | 100% | 0 | 100% |
| RNA-binding protein 39 OS=Homo sapiens GN=RBM39 PE=1 SV=2 | 59 | 100% | 0 | 100% | 0 | 100% | 100% | 0 | 88% | 0 | 100% |

| Protein | | | | | | | | | | | |
|---|---|---|---|---|---|---|---|---|---|---|---|
| Reticulocalbin-1 OS=Homo sapiens GN=RCN1 PE=1 SV=1 | 39 | 0 | 0 | 0 | 76% | 99% | 99% | 0 | 99% | 0 | 100% |
| Dolichyl-diphosphooligosaccharide--protein glycosyltransferase subunit 1 OS=Homo sapiens GN=RPN1 PE=1 SV=1 | 69 | 100% | 0 | 100% | 100% | 100% | 100% | 100% | 100% | 0 | 100% |
| Ubiquitin-40S ribosomal protein S27a OS=Homo sapiens GN=RPS27A PE=1 SV=2 | 18 | 100% | 100% | 100% | 100% | 100% | 100% | 100% | 100% | 41% | 100% |
| 40S ribosomal protein SA OS=Homo sapiens GN=RPSA PE=1 SV=4 | 33 | 0 | 0 | 100% | 100% | 100% | 100% | 100% | 100% | 90% | 100% |
| Protein transport protein Sec31A OS=Homo sapiens GN=SEC31A PE=1 SV=3 | 133 | 100% | 0 | 99% | 0 | 100% | 100% | 0 | 0 | 0 | 100% |
| Succinate dehydrogenase [ubiquinone] flavoprotein subunit, mitochondrial OS=Homo sapiens GN=SDHA PE=1 SV=2 | 73 | 99% | 0 | 95% | 0 | 100% | 0 | 0 | 0 | 0 | 100% |
| Septin-2 OS=Homo sapiens GN=SEPT2 PE=1 SV=1 | 49 | 0 | 0 | 0 | 0 | 100% | 0 | 0 | 0 | 0 | 99% |
| Serpin H1 OS=Homo sapiens GN=SERPINH1 PE=1 SV=2 | 46 | 0 | 0 | 99% | 100% | 100% | 100% | 100% | 100% | 0 | 100% |
| Splicing factor 3A subunit 3 OS=Homo sapiens GN=SF3A3 PE=1 SV=1 | 59 | 99% | 0 | 96% | 99% | 100% | 100% | 0 | 99% | 0 | 100% |
| Splicing factor, proline- and glutamine-rich OS=Homo sapiens GN=SFPQ PE=1 SV=2 | 76 | 100% | 100% | 99% | 100% | 100% | 100% | 100% | 0 | 0 | 100% |
| Signal recognition particle subunit SRP68 OS=Homo sapiens GN=SRP68 PE=1 SV=2 | 71 | 100% | 0 | 100% | 100% | 100% | 100% | 0 | 100% | 0 | 100% |
| Signal recognition particle receptor subunit alpha OS=Homo sapiens GN=SRPR PE=1 SV=2 | 70 | 0 | 0 | 0 | 0 | 100% | 72% | 0 | 0 | 0 | 100% |
| Alanine--tRNA ligase, cytoplasmic OS=Homo sapiens GN=AARS PE=1 SV=2 | 107 | 100% | 100% | 0 | 100% | 100% | 93% | 0 | 0 | 0 | 100% |
| Phenylalanine--tRNA ligase beta subunit OS=Homo sapiens GN=FARSB PE=1 SV=3 | 66 | 100% | 83% | 100% | 100% | 100% | 100% | 90% | 100% | 48% | 100% |
| Glycine--tRNA ligase OS=Homo sapiens GN=GARS PE=1 SV=3 | 83 | 0 | 0 | 0 | 0 | 100% | 0 | 0 | 0 | 0 | 99% |
| Arginine--tRNA ligase, cytoplasmic OS=Homo sapiens GN=RARS PE=1 SV=2 | 75 | 100% | 39% | 100% | 100% | 100% | 100% | 95% | 100% | 0 | 100% |
| Tyrosine--tRNA ligase, cytoplasmic OS=Homo | 59 | 0 | 0 | 0 | 100% | 100% | 100% | 100% | 99% | 0 | 100% |

| | | | | | | | | | | | |
|---|---|---|---|---|---|---|---|---|---|---|---|
| sapiens GN=YARS PE=1 SV=4 | | | | | | | | | | | |
| T-complex protein 1 subunit alpha OS=Homo sapiens GN=TCP1 PE=1 SV=1 | 60 | 100% | 100% | 100% | 100% | 100% | 100% | 100% | 100% | 68% | 100% |
| T-complex protein 1 subunit beta OS=Homo sapiens GN=CCT2 PE=1 SV=4 | 57 | 100% | 100% | 100% | 100% | 100% | 100% | 100% | 100% | 100% | 100% |
| T-complex protein 1 subunit delta OS=Homo sapiens GN=CCT4 PE=1 SV=4 | 58 | 100% | 100% | 100% | 100% | 100% | 100% | 100% | 100% | 0 | 100% |
| T-complex protein 1 subunit epsilon OS=Homo sapiens GN=CCT5 PE=1 SV=1 | 60 | 100% | 100% | 100% | 100% | 100% | 100% | 100% | 100% | 0 | 100% |
| T-complex protein 1 subunit gamma OS=Homo sapiens GN=CCT3 PE=1 SV=4 | 61 | 100% | 100% | 100% | 100% | 100% | 100% | 100% | 100% | 100% | 100% |
| T-complex protein 1 subunit theta OS=Homo sapiens GN=CCT8 PE=1 SV=4 | 60 | 100% | 100% | 100% | 100% | 100% | 100% | 100% | 100% | 53% | 100% |
| Transitional endoplasmic reticulum ATPase OS=Homo sapiens GN=VCP PE=1 SV=4 | 89 | 100% | 0 | 0 | 97% | 100% | 95% | 0 | 0 | 0 | 100% |
| Acetyl-CoA acetyltransferase, mitochondrial OS=Homo sapiens GN=ACAT1 PE=1 SV=1 | 45 | 0 | 0 | 0 | 100% | 100% | 0 | 0 | 100% | 0 | 100% |
| Mitochondrial import receptor subunit TOM70 OS=Homo sapiens GN=TOMM70A PE=1 SV=1 | 67 | 0 | 0 | 0 | 0 | 99% | 0 | 0 | 0 | 0 | 100% |
| Heat shock protein 75 , mitochondrial OS=Homo sapiens GN=TRAP1 PE=1 SV=3 | 80 | 100% | 52% | 100% | 100% | 100% | 100% | 100% | 100% | 0 | 100% |
| Tetratricopeptide repeat protein 4 OS=Homo sapiens GN=TTC4 PE=1 SV=3 | 45 | 0 | 0 | 0 | 0 | 99% | 100% | 0 | 0 | 0 | 99% |
| Tubulin--tyrosine ligase-like protein 12 OS=Homo sapiens GN=TTLL12 PE=1 SV=2 | 74 | 100% | 37% | 100% | 100% | 100% | 100% | 0 | 100% | 0 | 100% |
| Ubiquitin carboxyl-terminal hydrolase 5 OS=Homo sapiens GN=USP5 PE=1 SV=2 | 96 | 100% | 69% | 99% | 92% | 100% | 100% | 0 | 70% | 0 | 100% |
| Synaptic vesicle membrane protein VAT-1 homolog OS=Homo sapiens GN=VAT1 PE=1 SV=2 | 42 | 0 | 0 | 0 | 0 | 100% | 100% | 0 | 0 | 0 | 100% |
| V-type proton ATPase catalytic subunit A OS=Homo sapiens GN=ATP6V1A PE=1 SV=2 | 68 | 100% | 0 | 100% | 100% | 100% | 54% | 0 | 100% | 0 | 100% |
| Vacuolar protein sorting-associated protein 35 OS=Homo sapiens GN=VPS35 PE=1 SV=2 | 92 | 100% | 78% | 100% | 100% | 100% | 100% | 0 | 100% | 0 | 100% |

| | | | | | | | | | | | |
|---|---|---|---|---|---|---|---|---|---|---|---|
| Exportin-T OS=Homo sapiens GN=XPOT PE=1 SV=2 | 110 | 100% | 0 | 6% | 71% | 100% | 100% | 0 | 11% | 0 | 100% |
| X-ray repair cross-complementing protein 6 OS=Homo sapiens GN=XRCC6 PE=1 SV=2 | 70 | 100% | 100% | 100% | 100% | 100% | 100% | 100% | 100% | 0 | 100% |
| Zyxin OS=Homo sapiens GN=ZYX PE=1 SV=1 | 61 | 0 | 0 | 29% | 0 | 100% | 100% | 0 | 100% | 0 | 100% |

# APPENDIX D: CHAPTER 5

## 5.1 Compound characterization
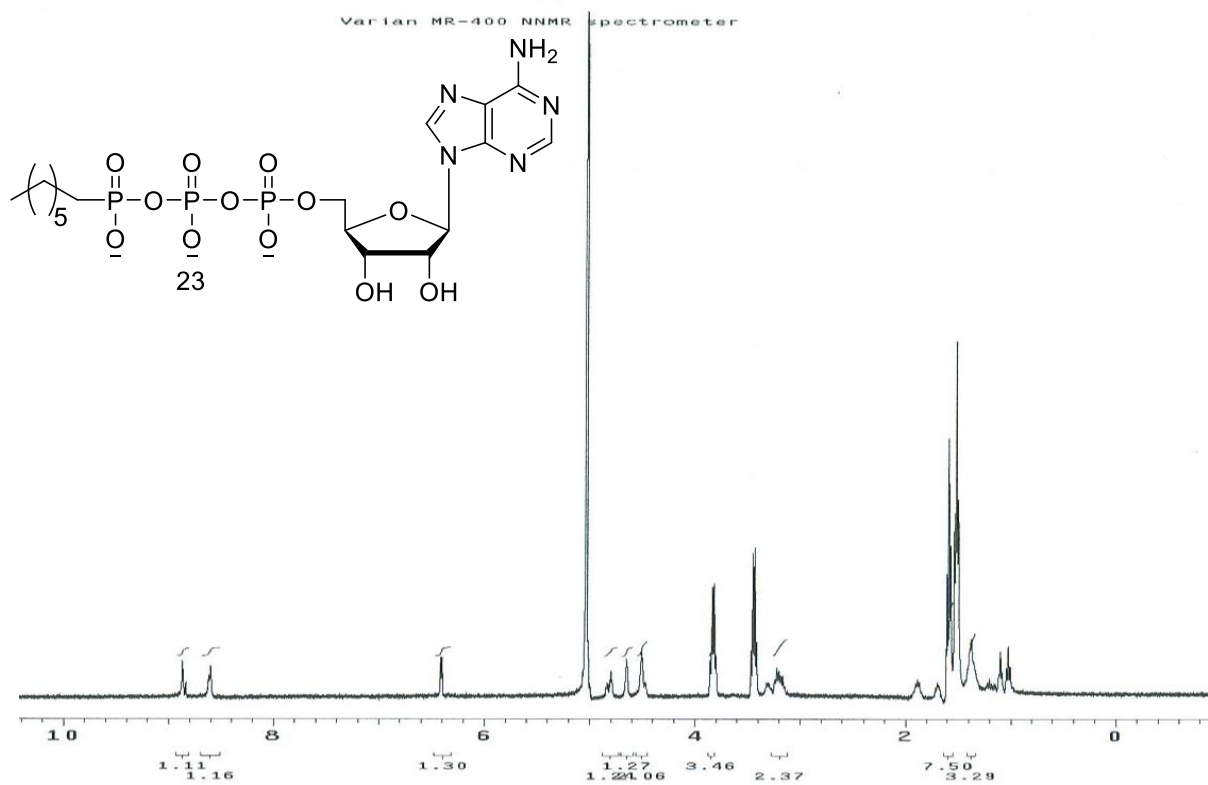


**Figure A 5. 1:** $^1$HNMR of ATP-C-heptyl (5) recorded in $D_2O$. Peaks at $\delta$ 5.03 correspond to $D_2O$ and peaks at $\delta$ 3.43 and 1.52 correspond $CH_2$ and $CH_3$ of triethylamine respectively**.**
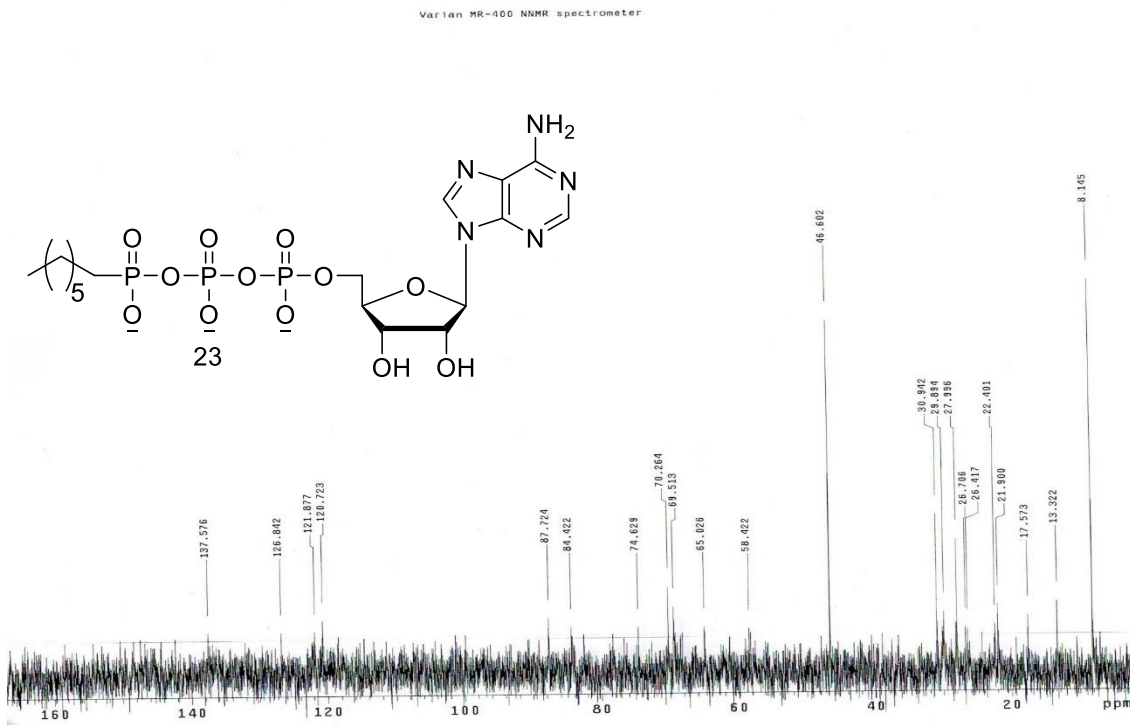
**Figure A 5. 2:** $^{13}$CNMR of ATP-C-heptyl (**5**) recorded in D$_2$O. Peaks at δ 46.59 and 8.14 correspond CH$_2$ and CH$_3$ of triethylamine respectively. Multiplicity of C13 was observed to due to coupling with phosphorus as previously reported.[187]
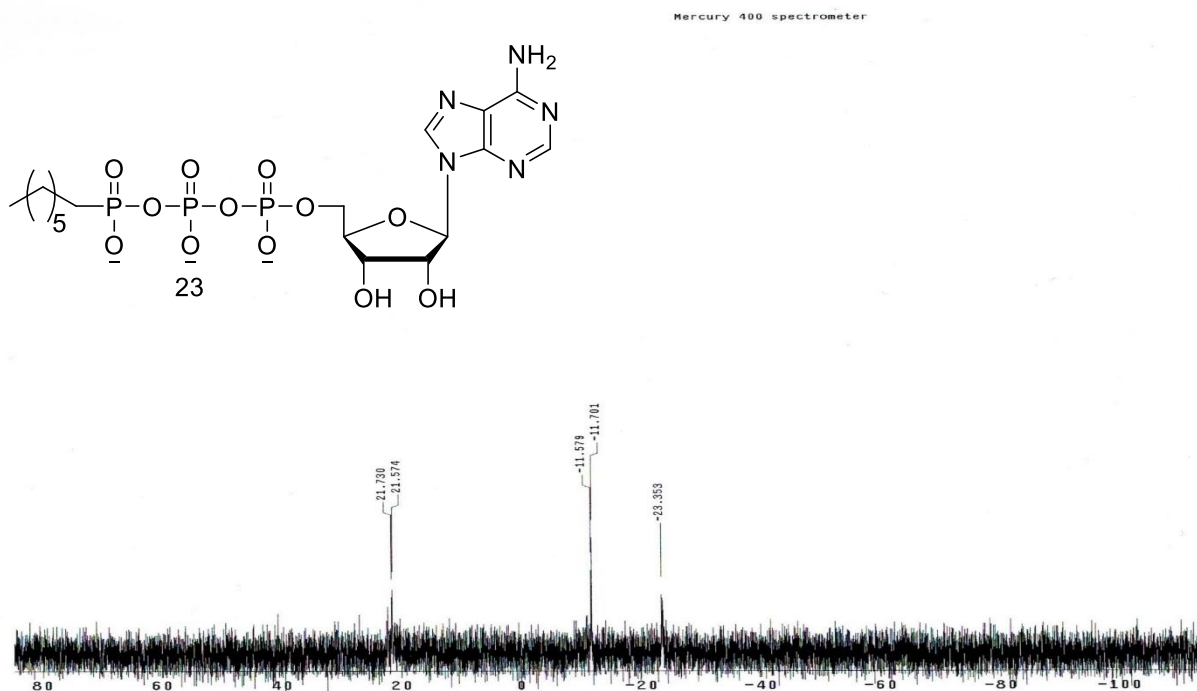


**Figure A 5. 3:** $^{31}$PNMR of ATP-C-heptyl (5) recorded in D$_2$O.

**Single Mass Analysis**
Tolerance = 5.0 PPM / DBE: min = -1.5, max = 100.0
Element prediction: Off
Number of isotope peaks used for i-FIT = 6

Monoisotopic Mass, Even Electron Ions
906 formula(e) evaluated with 1 results within limits (all results (up to 1000) for each mass)
Elements Used:
C: 17-17   H: 0-50   N: 0-10   O: 0-20   31P: 0-3

Ahmed Fouda ATP-C(3) in MeOH+W Cone(V)40

LCT Premier KD128
TOF MS ES-
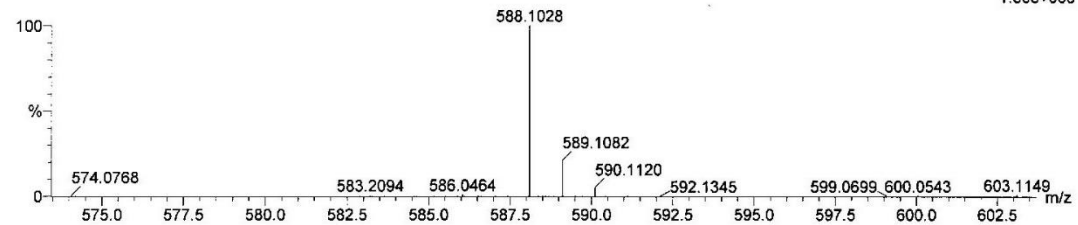
1.30e+005



| Mass | Calc. Mass | mDa | PPM | DBE | i-FIT | i-FIT (Norm) | Formula |
|---|---|---|---|---|---|---|---|
| | | | | Minimum: | | | -1.5 |
| | | 3.0 | 5.0 | Maximum: | | | 100.0 |
| 588.1028 | 588.1026 | 0.2 | 0.3 | 7.5 | 93.2 | 0.0 | C17 H29 N5 O12 31P3 |

**Figure A 5. 4:** Electrospray ionization (ESI) negative mode high resolution mass spectrum (HRMs) of ATP-C-heptyl (**5**). Calculated (M-H)$^{-1}$ for $C_{17}H_{29}N_5O_{12}P_3$: calc. 588.1026, found 588.1028
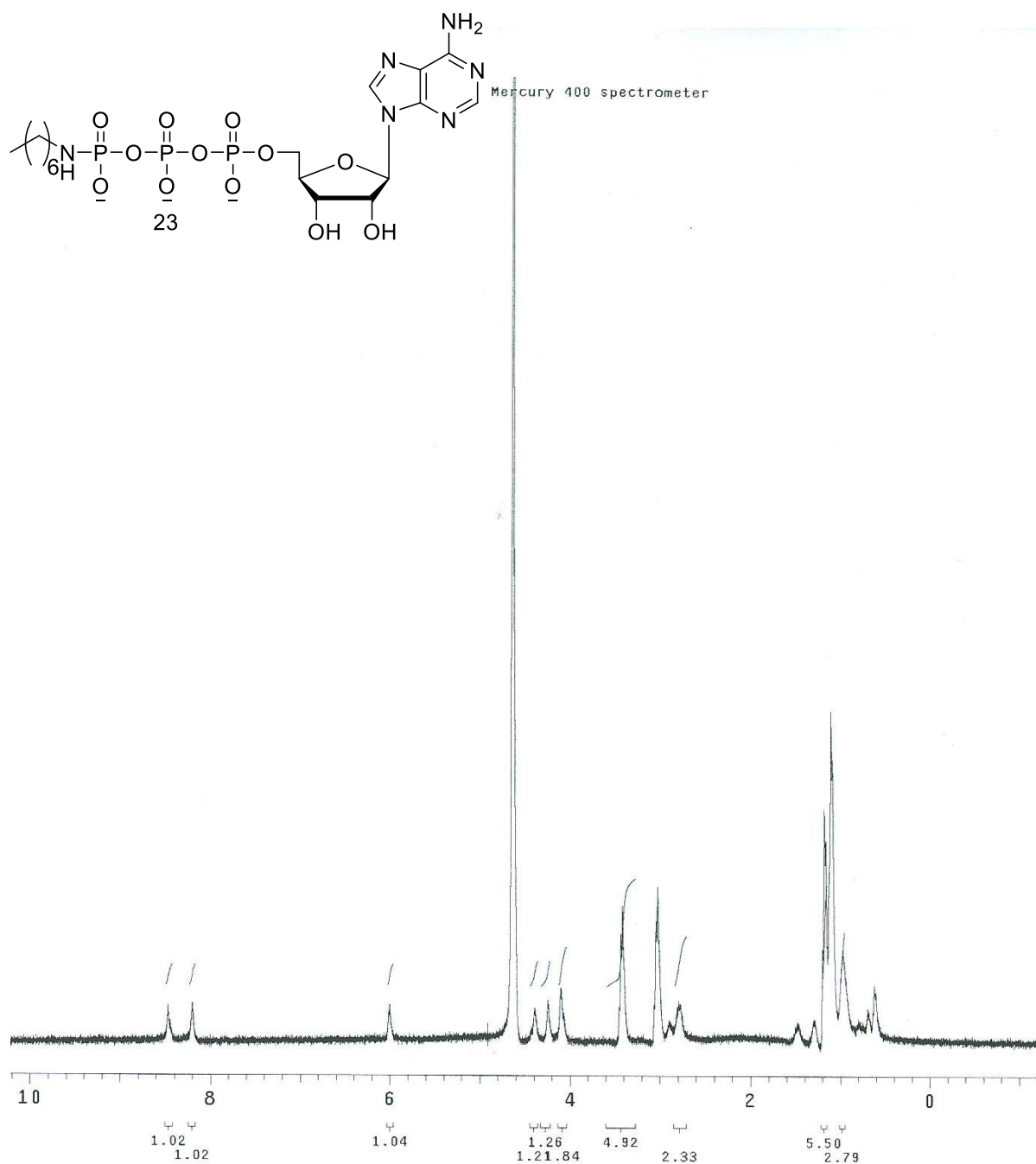
**Figure A 5. 5:** $^1$HNMR of ATP-N-heptyl (**23**) recorded in D$_2$O. Peaks at $\delta$ 4.65 correspond to D$_2$O and peaks at $\delta$ 3.03 and 1.11 correspond CH$_2$ and CH$_3$ of triethylamine respectively.
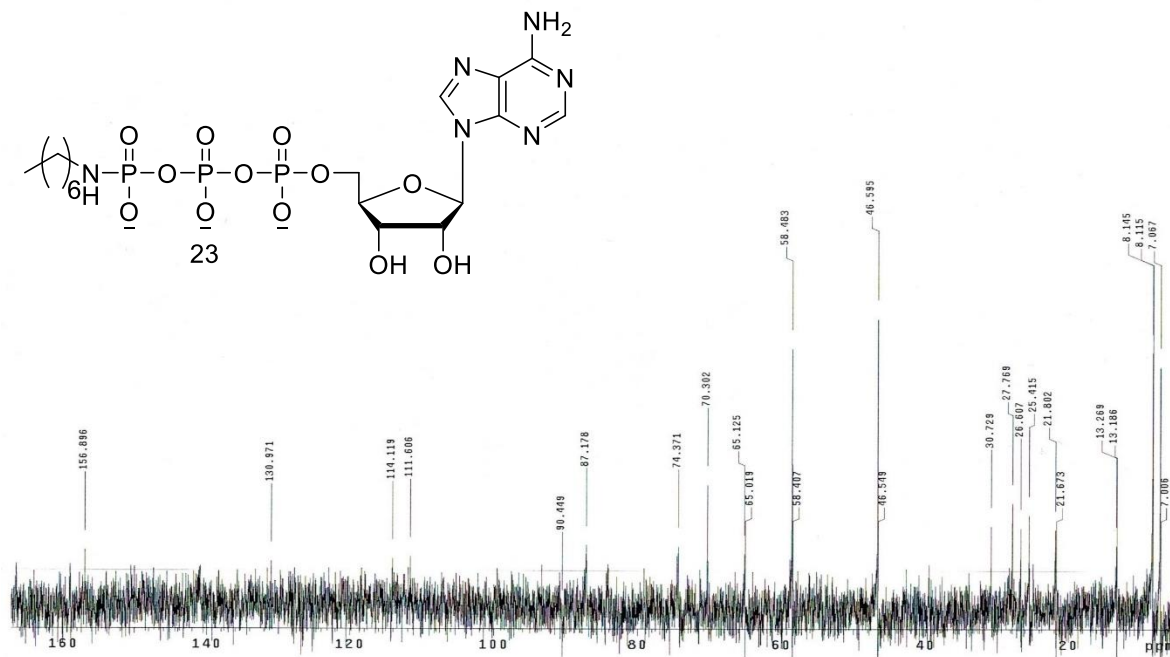
**Figure A 5. 6:**$^{13}$CNMR of ATP-N-heptyl (23) recorded in D$_2$O. Peaks at δ 46.58 and 8.11 correspond CH$_2$ and CH$_3$ of triethylamine respectively. Multiplicity of C13 was observed to due to coupling with phosphorus as previously reported.[187]
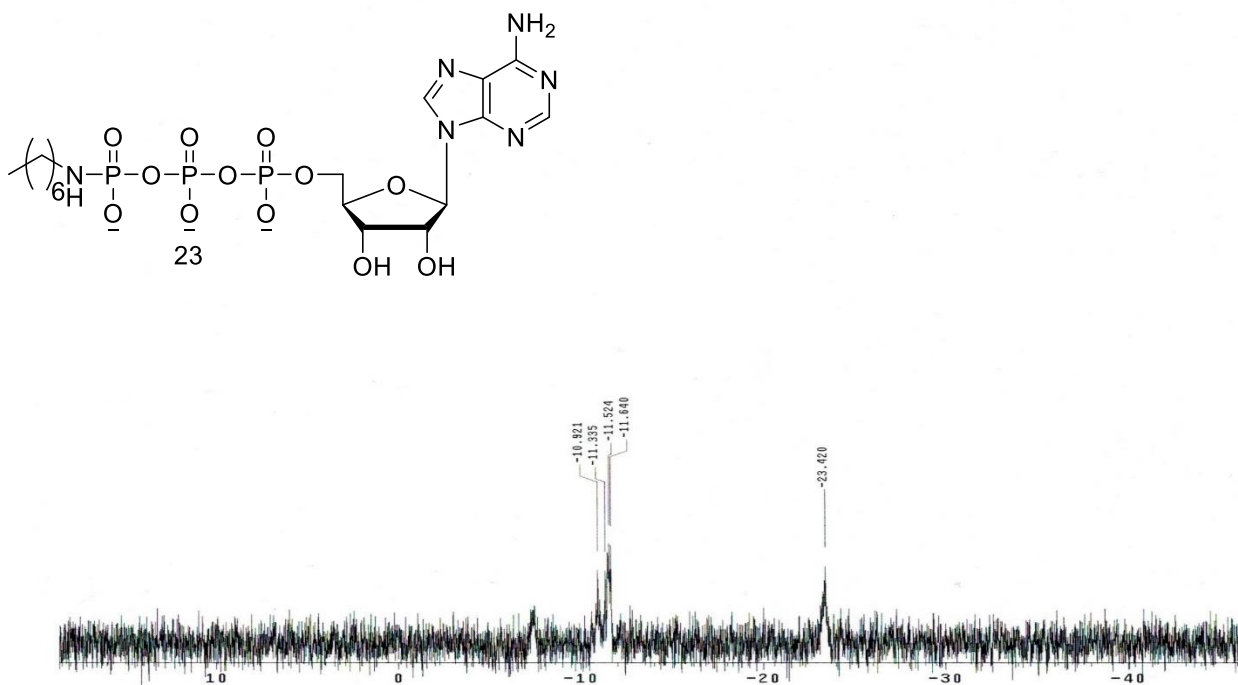
**Figure A 5. 7:** $^{31}$PNMR of ATP-N-heptyl (23) recorded in D$_2$O.

**Elemental Composition Report**

**Single Mass Analysis**
Tolerance = 5.0 PPM / DBE: min = -1.5, max = 100.0
Element prediction: Off
Number of isotope peaks used for i-FIT = 6

Monoisotopic Mass, Even Electron Ions
908 formula(e) evaluated with 1 results within limits (all results (up to 1000) for each mass)
Elements Used:
C: 17-17   H: 0-50   N: 0-10   O: 0-20   31P: 0-3
160413_128 559 (10.320)                     Ahmad Fouda ATP-N(1) in MeOH Cone(V)40
LCT Premier KD128
TOF MS ES-

4.02e+004
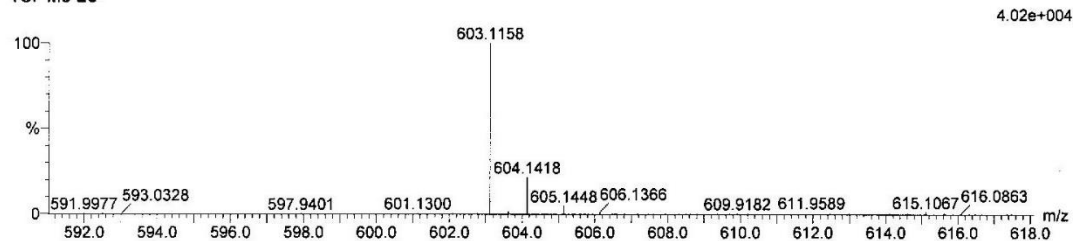


| Minimum: | | | | -1.5 | | | |
|---|---|---|---|---|---|---|---|
| Maximum: | | 3.0 | 5.0 | 100.0 | | | |
| | | | | | | | |
| Mass | Calc. Mass | mDa | PPM | DBE | i-FIT | i-FIT (Norm) | Formula |
| | | | | | | | |
| 603.1158 | 603.1135 | 2.3 | 3.8 | 7.5 | 138.4 | 0.0 | C17 H30 N6 O12 31P3 |

**Figure A 5. 8:** Electrospray ionization (ESI) positive mode high resolution mass spectrum (HRMs) of ATP-N-heptyl (**23**). Calculated (M-H)$^{-1}$ for $C_{17}H_{30}N_6O_{12}P_3$: 603.1135, observed 603.1158.
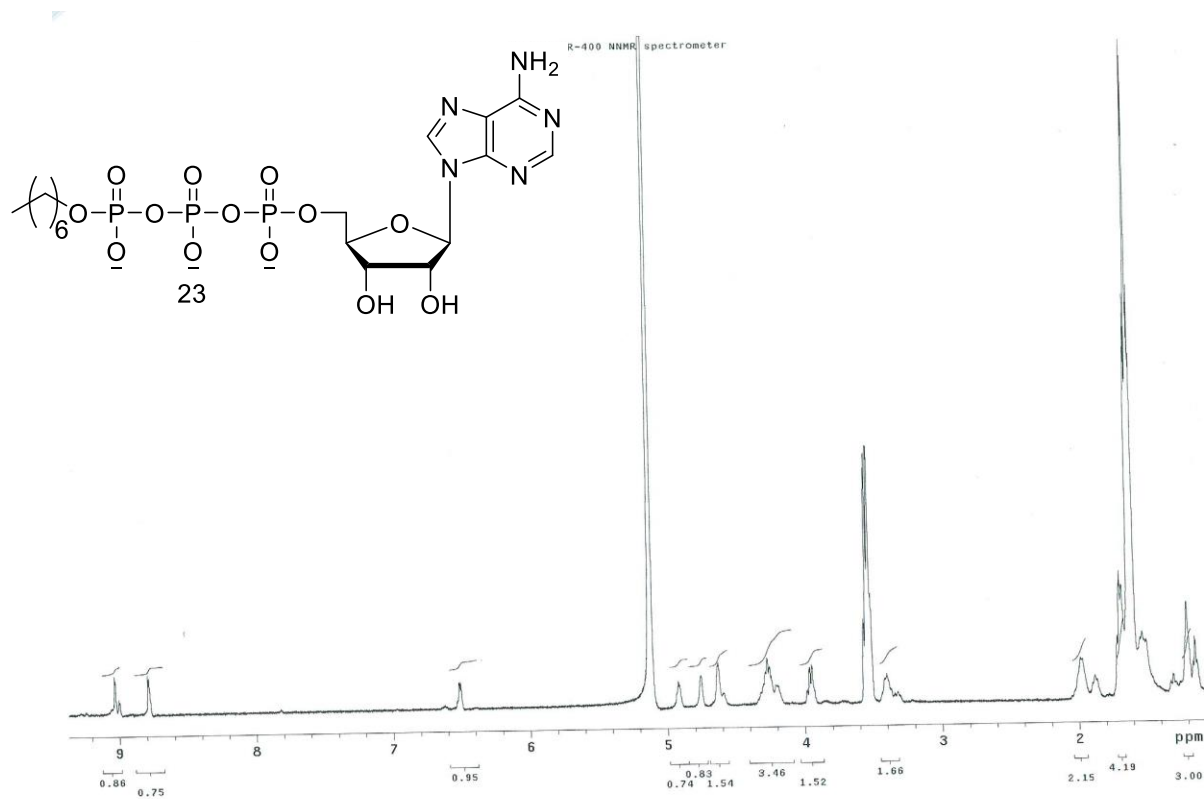
**Figure A 5. 9:** $^1$HNMR of ATP-O-heptyl (**24**) recorded in D$_2$O. Peaks at $\delta$ 5.12 correspond to D$_2$O and peaks at $\delta$ 3.54 and 1.61 correspond CH$_2$ and CH$_3$ of triethylamine respectively.
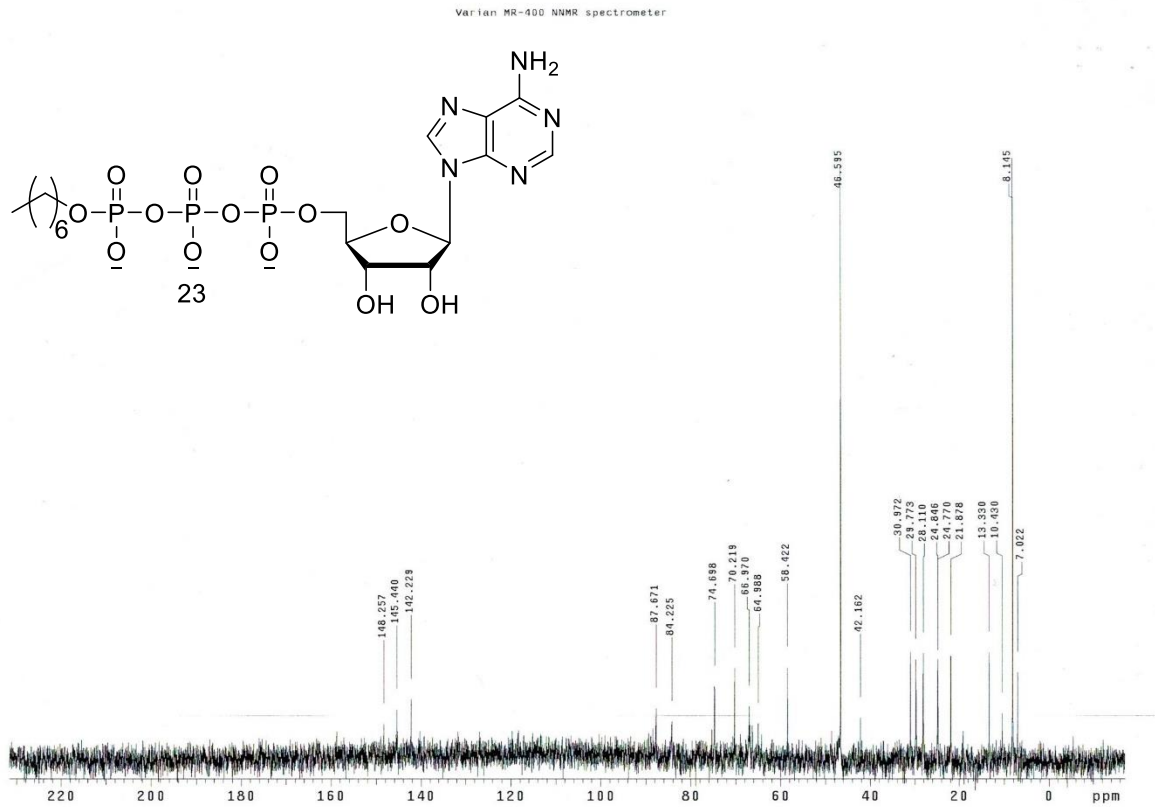
**Figure A 5. 10**:$^{13}$CNMR of ATP-O-heptyl (**24**) recorded in D$_2$O. Peaks at δ 46.59 and 8.14 correspond CH$_2$ and CH$_3$ of triethylamine respectively. Multiplicity of C13 was observed to due to coupling with phosphorus as previously reported.[187]
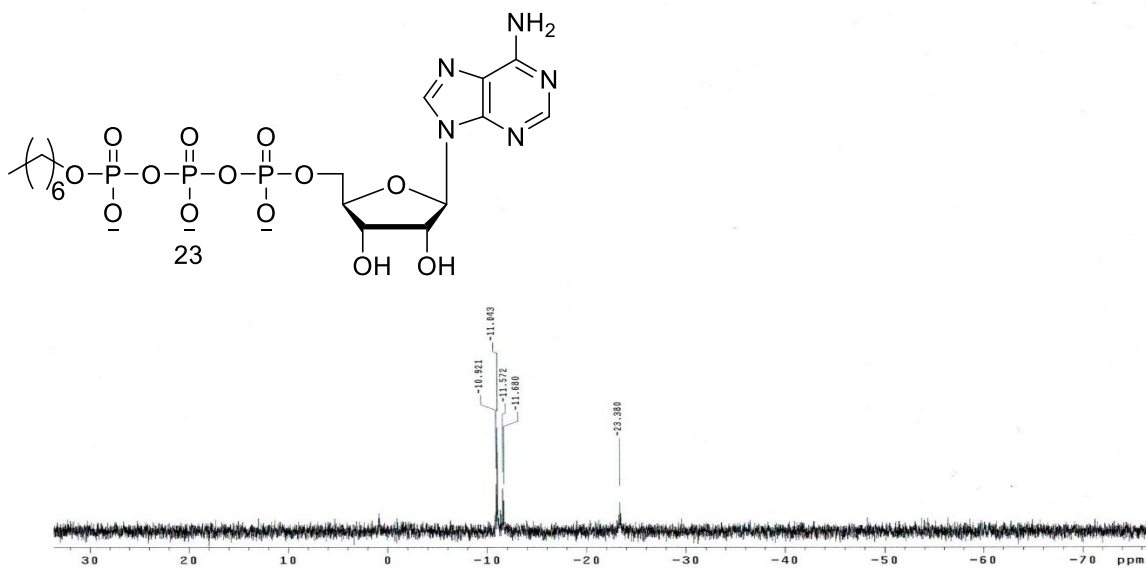


**Figure A 5. 11:** $^{31}$PNMR of ATP-O-heptyl (**24**) recorded in D$_2$O.

**Elemental Composition Report**

**Single Mass Analysis**
Tolerance = 5.0 PPM  /  DBE: min = -1.5, max = 100.0
Element prediction: Off
Number of isotope peaks used for i-FIT = 6

Monoisotopic Mass, Even Electron Ions
907 formula(e) evaluated with 1 results within limits (all results (up to 1000) for each mass)
Elements Used:
C: 17-17   H: 0-50   N: 0-10   O: 0-20   31P: 0-3

Ahmad Fouda ATP-O(2) in MeOH+W Cone(V)40

LCT Premier KD128
TOF MS ES-

2.93e+004
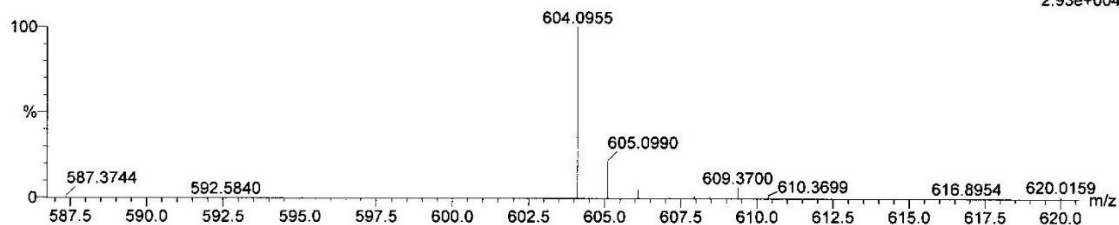


| Minimum: | | | | -1.5 | | | |
|---|---|---|---|---|---|---|---|
| Maximum: | | 3.0 | 5.0 | 100.0 | | | |
| | | | | | | | |
| Mass | Calc. Mass | mDa | PPM | DBE | i-FIT | i-FIT (Norm) | Formula |
| | | | | | | | |
| 604.0955 | 604.0975 | -2.0 | -3.3 | 7.5 | 73.1 | 0.0 | C17 H29 N5 O13 31P3 |

**Figure A 5. 12:** Electrospray ionization (ESI) positive mode high resolution mass spectrum (HRMs) of ATP-O-heptyl (**24**). Calculated (M-H)$^{-1}$ for $C_{17}H_{29}N_5O_{13}P_3$: 604.975, observed 604.0955.

## 5.2 Repetitive trials of MALDI-TOF analysis of kinase-catalyzed reaction using ATP-C, N, and O-heptyl analogs (22-24)

### a) Kemptide phosphorylation using ATP

**Trial 2**



m/z 894.4557
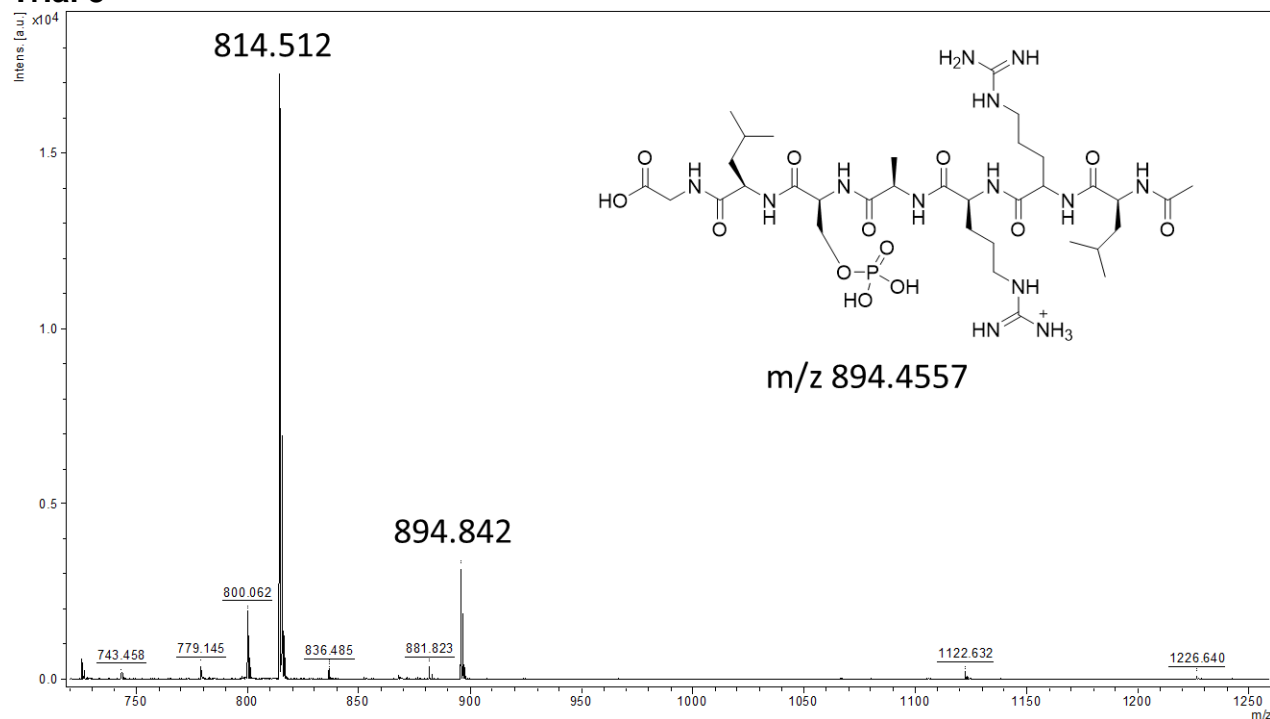
**Trial 3**



**Figure A 5. 13:** MALDI mass spectrometry spectra of modified phosphorylation of Ac-kemptide using ATP. ATP was incubated with kemptide and PKA followed by MALDI-TOF spectrometric analysis. Two trials are shown here, with the third trial in Figure 5.3A.

**b) Kemptide phosphorylation using ATP-C-heptyl (22)**

**Trial 2**

**Trial 3**



m/z 976.5703
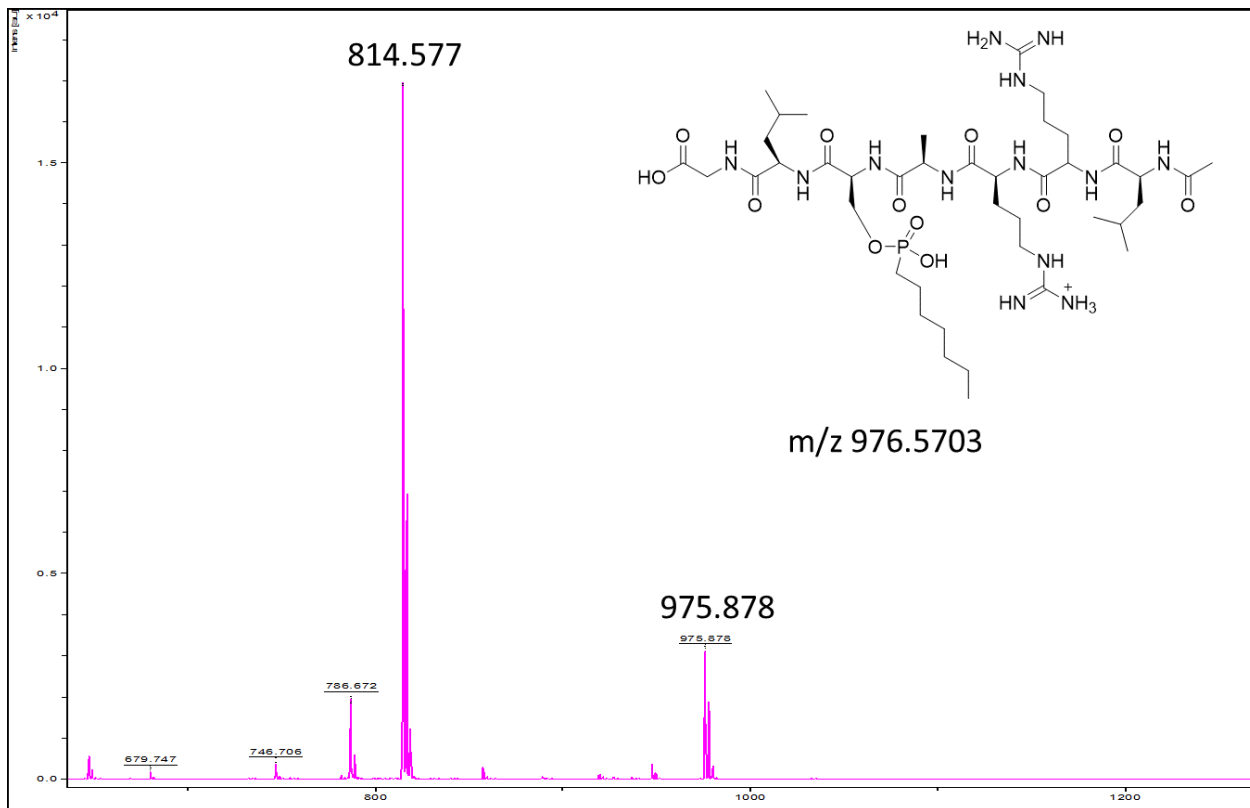
**Trial 4**



**Figure A 5. 14:** MALDI mass spectrometry spectra of modified phosphorylation of Ac-kemptide using ATP-C-heptyl (**22**). ATP was incubated with kemptide and PKA followed by MALDI-TOF spectrometric analysis. Two trials are shown here, with the third trial in Figure 5.3B.

## c) Kemptide phosphorylation using ATP-N-heptyl (23)

### Trial 2
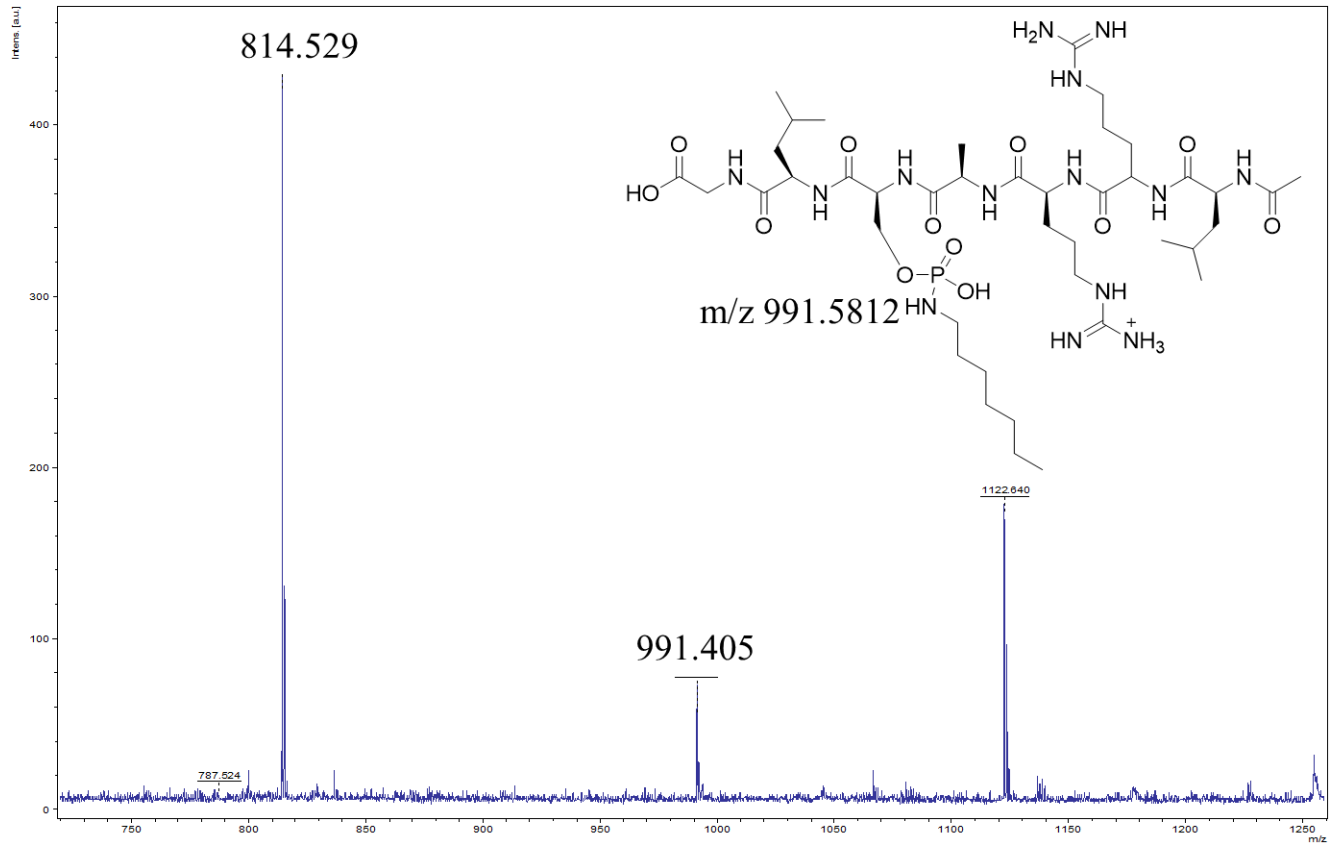
**Trial 3**
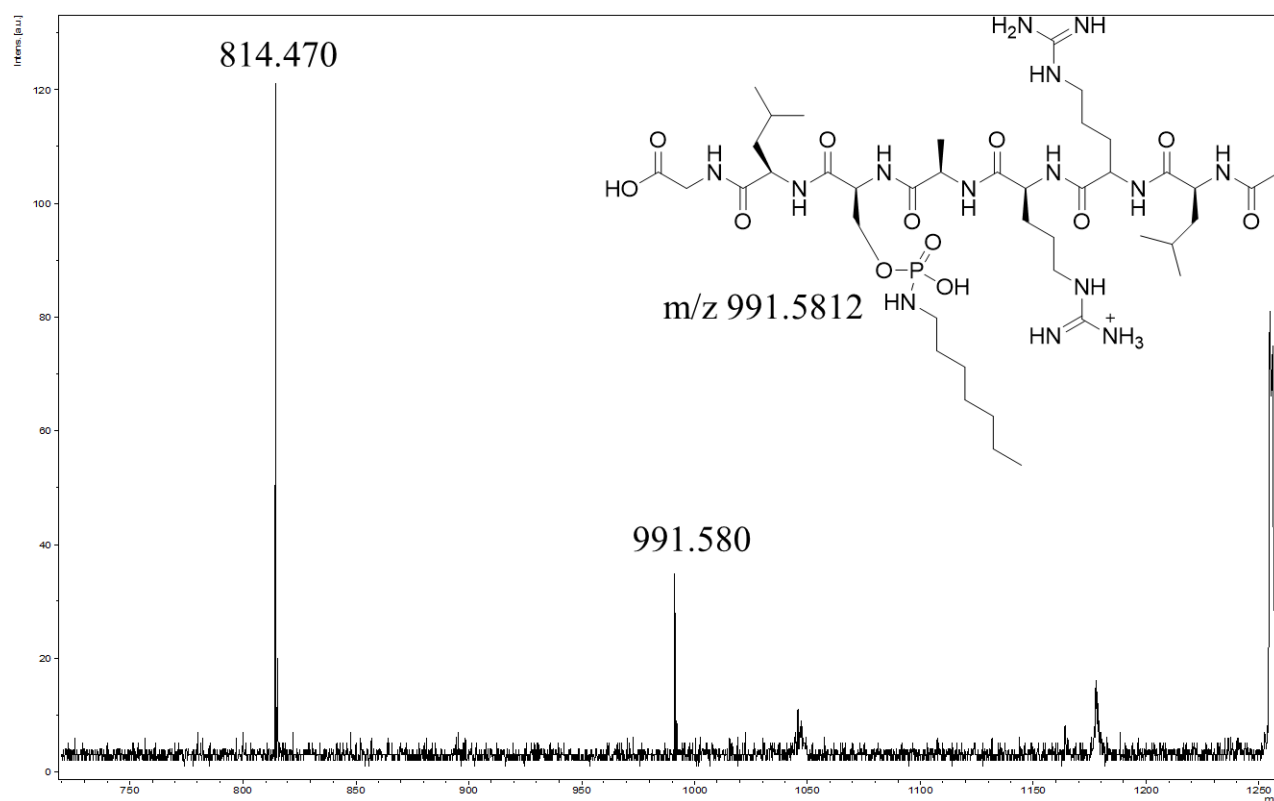


**Figure A 5.15:** MALDI mass spectrometry spectra of modified phosphorylation of Ac-kemptide using ATP-N-heptyl. ATP-N-heptyl was incubated with kemptide and PKA followed by MALDI-TOF spectrometric analysis. Two trials are shown here, with the third trial in Figure 5.3C

## d) Kemptide phosphorylation using ATP-O-heptyl (24)

**Trial 2:**



m/z 992.5652
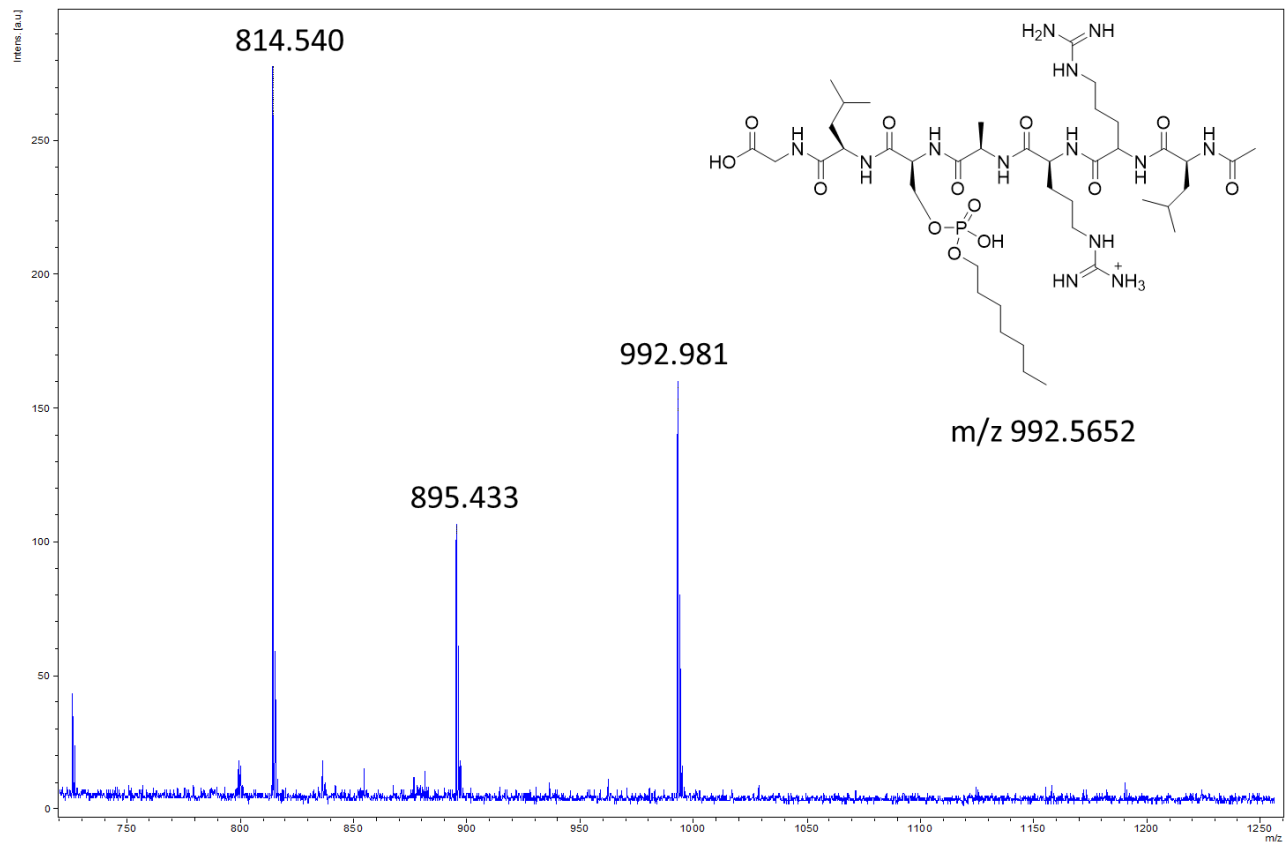
**Trial 3:**



**Figure A 5.16:** MALDI mass spectrometry spectra of modified phosphorylation of Ac-kemptide using ATP-O-heptyl. ATP-O-heptyl was incubated with kemptide and PKA followed by MALDI-TOF spectrometric analysis. . Two trials are shown here, with the third trial in Figure 5.3D

## 5.3 Full gel images and repetitive trial of Pro-Q analysis of ATP-C, N, and O-heptyl analogs (22-24)

**Trial 1**



| | 1 | 2 | 3 | 4 | 5 | 6 | 7 | | 8 | 9 | 10 | 11 | 12 |
|---|---|---|---|---|---|---|---|---|---|---|---|---|---|
| MPB | + | + | + | + | + | + | + | | + | + | + | + | + |
| PKA | | + | | + | | + | + | | | + | + | | + |
| ATP | + | + | | | | | | | + | + | | | |
| ATP-O-heptyl | | | + | + | | | | | | | | | |
| ATP-C-heptyl | | | | | + | + | | | | | | | |
| ATP-N-heptyl | | | | | | | | | | | | + | + |

**Trial 2**



| | 1 | 2 | 3 | 4 | 5 | 6 | 7 | 11 | 12 |
|---|---|---|---|---|---|---|---|---|---|
| MPB | + | + | + | + | + | + | + | + | + |
| PKA | | + | | + | | + | + | | + |
| ATP | + | + | | | | | | | |
| ATP-O-heptyl | | | + | + | | | | | |
| ATP-C-heptyl | | | | | + | + | | | |
| ATP-N-heptyl | | | | | | | | + | + |

**Trial 3**



| | 1 | 2 | 3 | 4 | 5 | 6 | 7 |
|---|---|---|---|---|---|---|---|
| MPB | + | + | + | + | + | + | + |
| PKA | | + | | + | | + | + |
| ATP | + | + | | | | | |
| ATP-O-heptyl | | | + | + | | | |
| ATP-C-heptyl | | | | | + | + | |

**Trial 4**



| | 1 | 2 | 3 | 4 | 5 | 6 | 7 | 8 |
|---|---|---|---|---|---|---|---|---|
| MBP | + | + | + | + | + | + | + | + |
| PKA | + | | + | + | + | - | - | |
| ATP-O-heptyl | - | - | + | - | - | + | - | - |
| ATP-N-heptyl | - | - | - | + | - | - | + | - |
| ATP-C-heptyl | - | - | - | - | + | - | - | + |
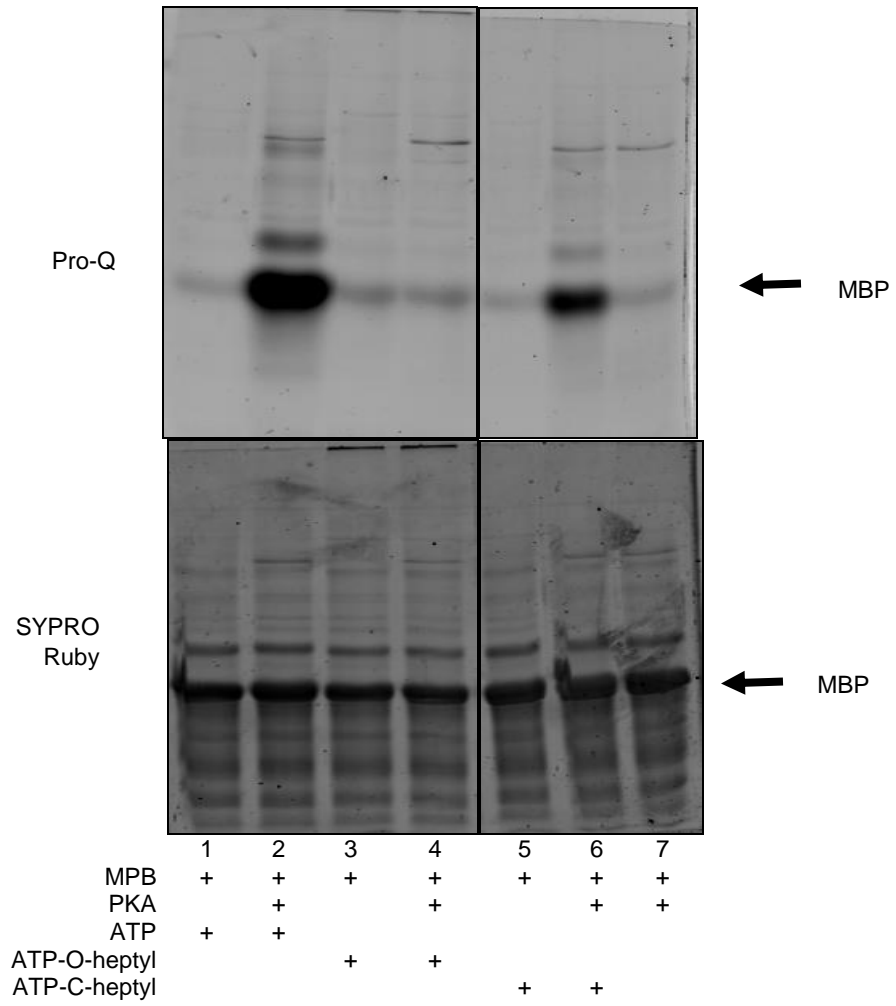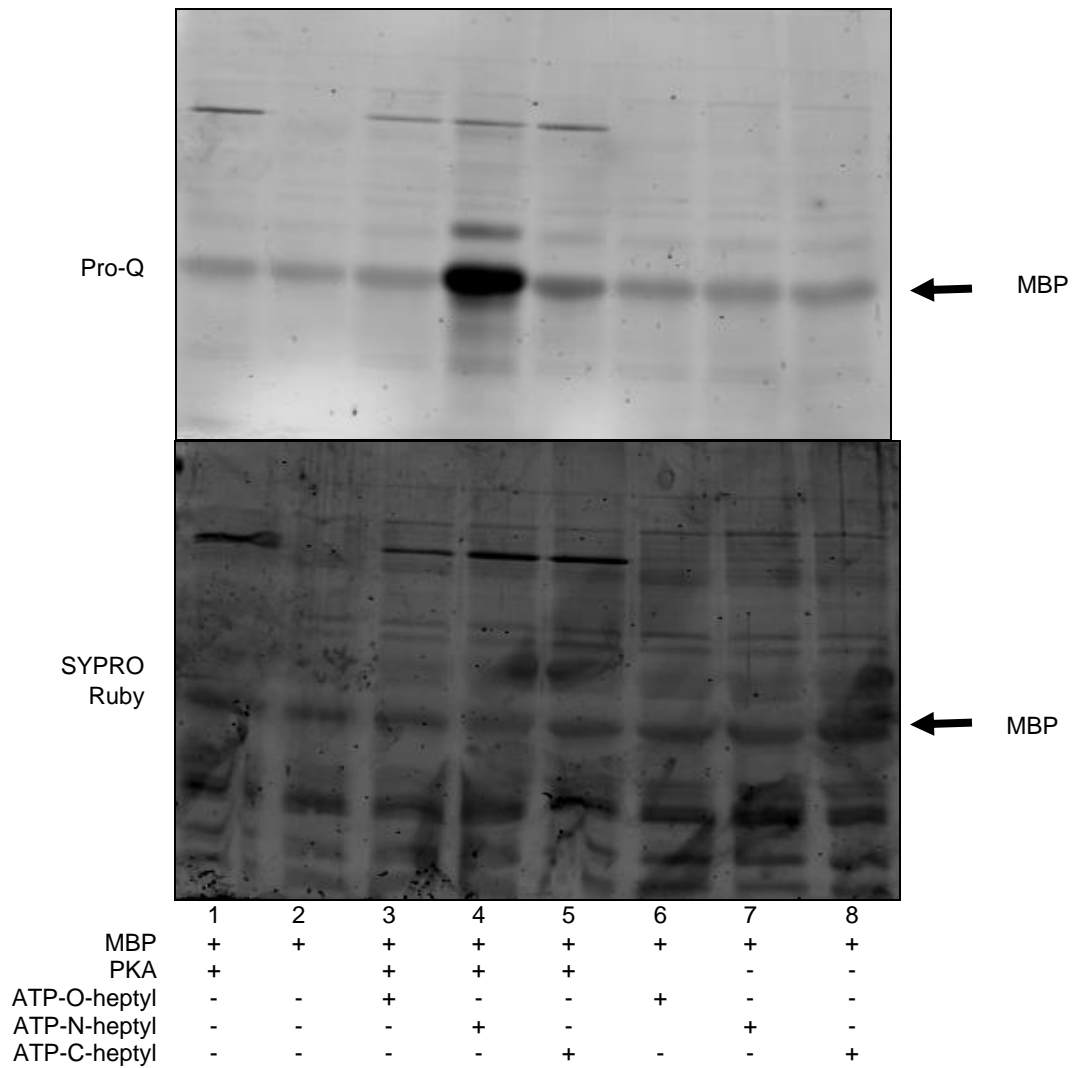
**Figure A 5.17:** Analysis of MPB phosphorylation in the presence of PKA and incubated with either ATP, ATP-O-heptyl, ATP-C-heptyl or ATP-N-heptyl. The reaction mixtures were analyzed by SDS-PAGE analysis, followed by staining with ProQ diamond phosphoprotein stain (top) or SYPRO® Ruby total protein stain (bottom). As a control ATP analogs were incubated with MBP in absence of PKA. Four trials are shown here, with the full gel image of the trial in Figure 5.4 shown as trial 1.

### 5.4 Michaelis-Menton plots of ATP, ATP-C-heptyl, ATP-N-heptyl, and ATP-O-heptyl
#### A) ATP



| v=Vmax*S/Km+S | | |
|---|---|---|
| | Value | Error |
| Vmax | 12.591 | 0.74768 |
| Km | 11.629 | 1.6667 |
| Chisq | 0.1278 | NA |
| R | 0.99838 | NA |

#### B) ATP-C-heptyl



| v=Vmax*S/Km+S | | |
|---|---|---|
| | Value | Error |
| Vmax | 5.3469 | 0.35201 |
| Km | 53.882 | 7.6424 |
| Chisq | 0.01534 | NA |
| R | 0.99867 | NA |

**C) ATP-N-heptyl**



| v=Vmax*S/Km+S | | |
|---|---|---|
| | Value | Error |
| Vmax | 12.501 | 1.8792 |
| Km | 35.731 | 13.166 |
| Chisq | 1.4403 | NA |
| R | 0.98702 | NA |

**D) ATP-O-heptyl**



| v=Vmax*S/Km+S | | |
|---|---|---|
| | Value | Error |
| Vmax | 8.171 | 0.57176 |
| Km | 25.024 | 4.7672 |
| Chisq | 0.22978 | NA |
| R | 0.99571 | NA |
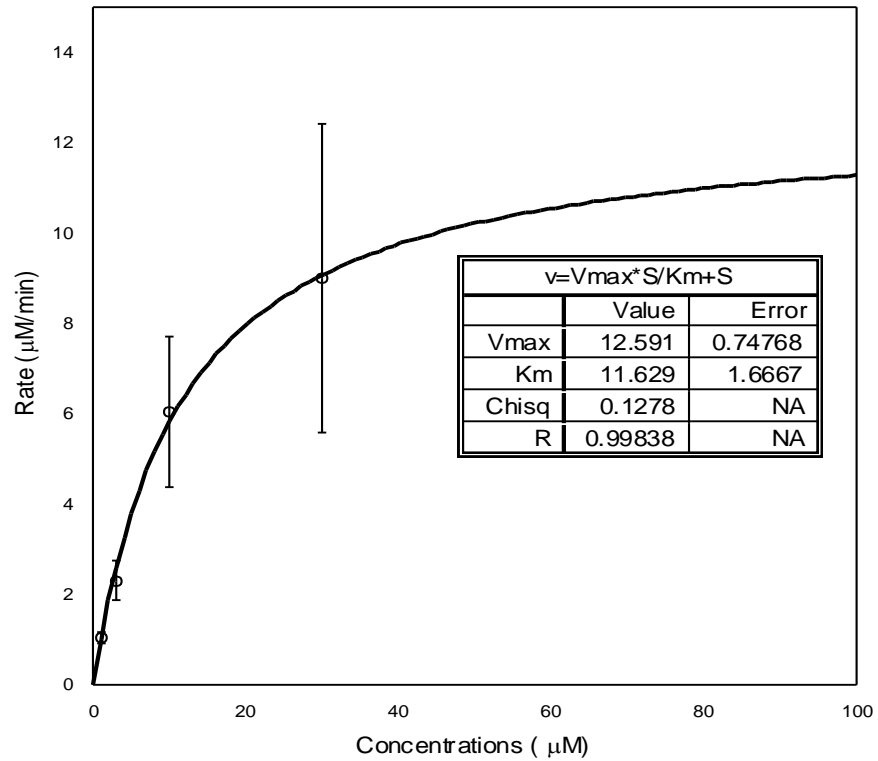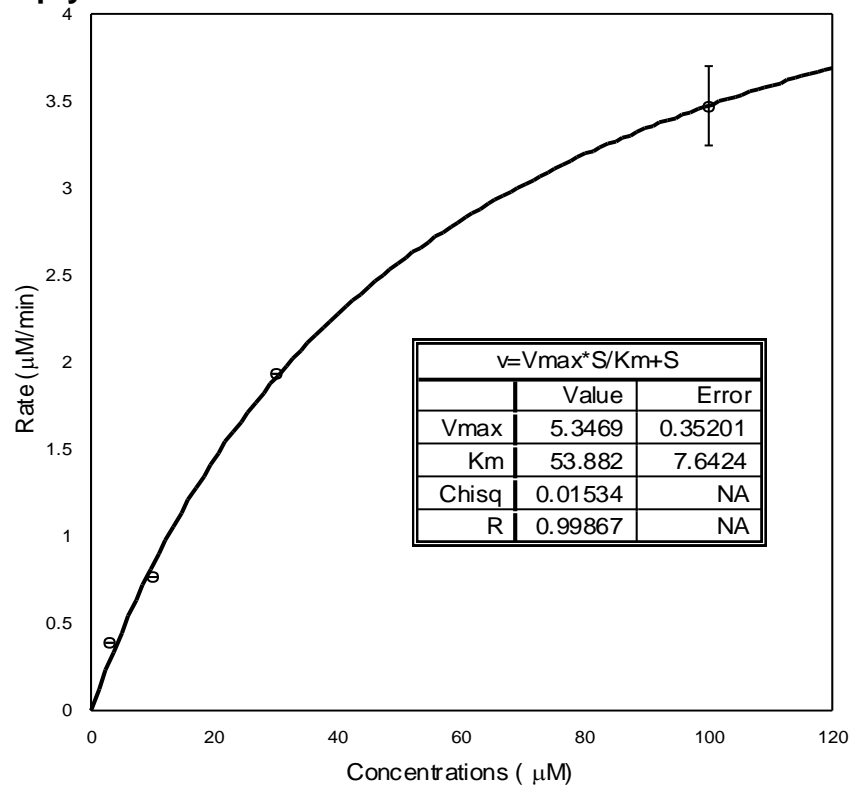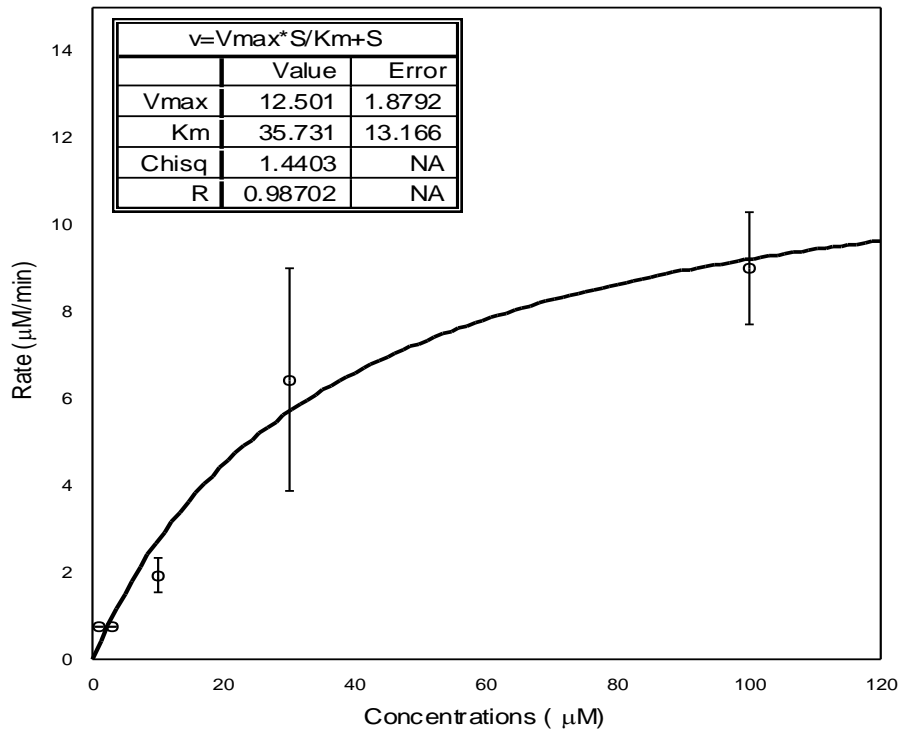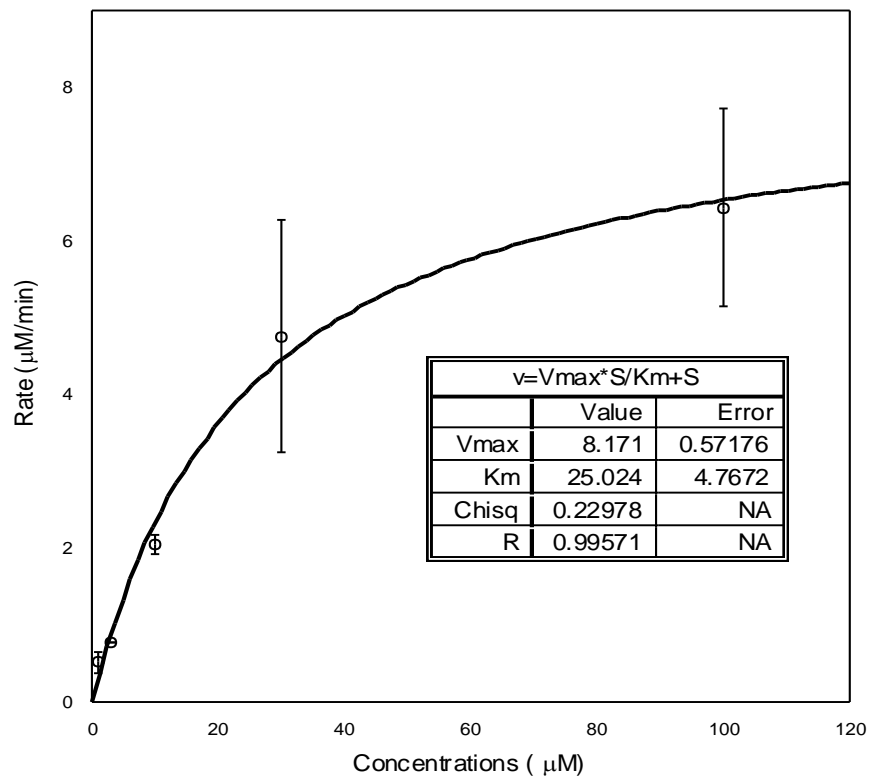
**Figure A 5.18:** Michaelis-Menton curve fits for reaction containing ATP, ATP-C-heptyl, ATP-N-heptyl, and ATP-O-heptyl.

## APPENDIX E: REPRINT AUTHORIZATIONS

- **Reprint authorization for "A cell permeable ATP analog for kinase-catalyzed biotinylation".** *Angew. Chem. Int. Ed.*, 2015, 54, 9618

**JOHN WILEY AND SONS LICENSE
TERMS AND CONDITIONS**

Jun 07, 2016

This Agreement between Ahmed E Fouda ("You") and John Wiley and Sons ("John Wiley and Sons") consists of your license details and the terms and conditions provided by John Wiley and Sons and Copyright Clearance Center.

| | |
|---|---|
| License Number | 3883691172808 |
| License date | Jun 07, 2016 |
| Licensed Content Publisher | John Wiley and Sons |
| Licensed Content Publication | Angewandte Chemie International Edition |
| Licensed Content Title | A Cell-Permeable ATP Analogue for Kinase-Catalyzed Biotinylation |
| Licensed Content Author | Ahmed E. Fouda,Mary Kay H. Pflum |
| Licensed Content Date | Jun 26, 2015 |
| Licensed Content Pages | 4 |
| Type of use | Dissertation/Thesis |
| Requestor type | Author of this Wiley article |
| Format | Print and electronic |
| Portion | Full article |
| Will you be translating? | Yes, including English rights |
| Number of languages | 1 |
| Languages | English |
| Title of your thesis / dissertation | Development of gamma-modified ATP analogs to study kinase-catalyzed phosphorylation |
| Expected completion date | Jul 2016 |
| Expected size (number of pages) | 300 |
| Requestor Location | Ahmed E Fouda 4643 chrysler dr DETROIT, MI 48201 United States Attn: Ahmed E Fouda |
| Publisher Tax ID | EU826007151 |
| Billing Type | Invoice |
| Billing Address | Ahmed E Fouda 4643 chrysler dr DETROIT, MI 48201 United States Attn: Ahmed E Fouda |

Total                          0.00 USD

Terms and Conditions

## TERMS AND CONDITIONS

This copyrighted material is owned by or exclusively licensed to John Wiley & Sons, Inc. or one of its group companies (each a"Wiley Company") or handled on behalf of a society with which a Wiley Company has exclusive publishing rights in relation to a particular work (collectively "WILEY"). By clicking "accept" in connection with completing this licensing transaction, you agree that the following terms and conditions apply to this transaction (along with the billing and payment terms and conditions established by the Copyright Clearance Center Inc., ("CCC's Billing and Payment terms and conditions"), at the time that you opened your RightsLink account (these are available at any time at http://myaccount.copyright.com).

**Terms and Conditions**

- The materials you have requested permission to reproduce or reuse (the "Wiley Materials") are protected by copyright.

- You are hereby granted a personal, non-exclusive, non-sub licensable (on a stand-alone basis), non-transferable, worldwide, limited license to reproduce the Wiley Materials for the purpose specified in the licensing process. This license, **and any CONTENT (PDF or image file) purchased as part of your order,** is for a one-time use only and limited to any maximum distribution number specified in the license. The first instance of republication or reuse granted by this license must be completed within two years of the date of the grant of this license (although copies prepared before the end date may be distributed thereafter). The Wiley Materials shall not be used in any other manner or for any other purpose, beyond what is granted in the license. Permission is granted subject to an appropriate acknowledgement given to the author, title of the material/book/journal and the publisher. You shall also duplicate the copyright notice that appears in the Wiley publication in your use of the Wiley Material. Permission is also granted on the understanding that nowhere in the text is a previously published source acknowledged for all or part of this Wiley Material. Any third party content is expressly excluded from this permission.

- With respect to the Wiley Materials, all rights are reserved. Except as expressly granted by the terms of the license, no part of the Wiley Materials may be copied, modified, adapted (except for minor reformatting required by the new Publication), translated, reproduced, transferred or distributed, in any form or by any means, and no derivative works may be made based on the Wiley Materials without the prior permission of the respective copyright owner.**For STM Signatory Publishers clearing permission under the terms of the STM Permissions Guidelines only, the terms of the license are extended to include subsequent editions and for editions in other languages, provided such editions are for the work as a whole in situ and does not involve the separate exploitation of the permitted figures or extracts,** You may not alter, remove or suppress in any manner any copyright, trademark or other notices displayed by the Wiley Materials. You may not license, rent, sell, loan, lease, pledge, offer as security, transfer or assign the Wiley Materials on a stand-alone basis, or any of the rights granted to you hereunder to any other person.

- The Wiley Materials and all of the intellectual property rights therein shall at all times remain the exclusive property of John Wiley & Sons Inc, the Wiley Companies, or their respective licensors, and your interest therein is only that of having possession of and the right to reproduce the Wiley Materials pursuant to Section 2 herein during the continuance of this Agreement. You agree that you own no right, title or interest in or to the Wiley Materials or any of the intellectual property rights therein. You shall have no rights hereunder other than the license as provided for above in Section 2. No right, license or interest to any trademark, trade name, service mark or other branding ("Marks") of WILEY or its licensors is granted hereunder, and you agree that you shall not assert any such right, license or interest with respect thereto

- NEITHER WILEY NOR ITS LICENSORS MAKES ANY WARRANTY OR REPRESENTATION OF ANY KIND TO YOU OR ANY THIRD PARTY, EXPRESS, IMPLIED OR STATUTORY, WITH RESPECT TO THE MATERIALS OR THE ACCURACY OF ANY INFORMATION CONTAINED IN THE MATERIALS, INCLUDING, WITHOUT LIMITATION, ANY IMPLIED WARRANTY OF MERCHANTABILITY, ACCURACY, SATISFACTORY QUALITY, FITNESS FOR A PARTICULAR PURPOSE, USABILITY, INTEGRATION OR NON-INFRINGEMENT AND ALL SUCH WARRANTIES ARE HEREBY EXCLUDED BY WILEY AND ITS LICENSORS AND WAIVED BY YOU.

- WILEY shall have the right to terminate this Agreement immediately upon breach of this Agreement by you.

- You shall indemnify, defend and hold harmless WILEY, its Licensors and their respective directors, officers, agents and employees, from and against any actual or threatened claims, demands, causes of action or proceedings arising from any breach of this Agreement by you.

- IN NO EVENT SHALL WILEY OR ITS LICENSORS BE LIABLE TO YOU OR ANY OTHER PARTY OR ANY OTHER PERSON OR ENTITY FOR ANY SPECIAL, CONSEQUENTIAL, INCIDENTAL, INDIRECT, EXEMPLARY OR PUNITIVE DAMAGES, HOWEVER CAUSED, ARISING OUT OF OR IN CONNECTION WITH THE DOWNLOADING, PROVISIONING, VIEWING OR USE OF THE MATERIALS REGARDLESS OF THE FORM OF ACTION, WHETHER FOR BREACH OF CONTRACT, BREACH OF WARRANTY, TORT, NEGLIGENCE, INFRINGEMENT OR OTHERWISE (INCLUDING, WITHOUT LIMITATION, DAMAGES BASED ON LOSS OF PROFITS, DATA, FILES, USE, BUSINESS OPPORTUNITY OR CLAIMS OF THIRD PARTIES), AND WHETHER OR NOT THE PARTY HAS BEEN ADVISED OF THE POSSIBILITY OF SUCH DAMAGES. THIS LIMITATION SHALL APPLY NOTWITHSTANDING ANY FAILURE OF ESSENTIAL PURPOSE OF ANY LIMITED REMEDY PROVIDED HEREIN.

- Should any provision of this Agreement be held by a court of competent jurisdiction to be illegal, invalid, or unenforceable, that provision shall be deemed amended to achieve as nearly as possible the same economic effect as the original provision, and the legality, validity and enforceability of the remaining provisions of this Agreement

shall not be affected or impaired thereby.

- The failure of either party to enforce any term or condition of this Agreement shall not constitute a waiver of either party's right to enforce each and every term and condition of this Agreement. No breach under this agreement shall be deemed waived or excused by either party unless such waiver or consent is in writing signed by the party granting such waiver or consent. The waiver by or consent of a party to a breach of any provision of this Agreement shall not operate or be construed as a waiver of or consent to any other or subsequent breach by such other party.

- This Agreement may not be assigned (including by operation of law or otherwise) by you without WILEY's prior written consent.

- Any fee required for this permission shall be non-refundable after thirty (30) days from receipt by the CCC.

- These terms and conditions together with CCC's Billing and Payment terms and conditions (which are incorporated herein) form the entire agreement between you and WILEY concerning this licensing transaction and (in the absence of fraud) supersedes all prior agreements and representations of the parties, oral or written. This Agreement may not be amended except in writing signed by both parties. This Agreement shall be binding upon and inure to the benefit of the parties' successors, legal representatives, and authorized assigns.

- In the event of any conflict between your obligations established by these terms and conditions and those established by CCC's Billing and Payment terms and conditions, these terms and conditions shall prevail.

- WILEY expressly reserves all rights not specifically granted in the combination of (i) the license details provided by you and accepted in the course of this licensing transaction, (ii) these terms and conditions and (iii) CCC's Billing and Payment terms and conditions.

- This Agreement will be void if the Type of Use, Format, Circulation, or Requestor Type was misrepresented during the licensing process.

- This Agreement shall be governed by and construed in accordance with the laws of the State of New York, USA, without regards to such state's conflict of law rules. Any legal action, suit or proceeding arising out of or relating to these Terms and Conditions or the breach thereof shall be instituted in a court of competent jurisdiction in New York County in the State of New York in the United States of America and each party hereby consents and submits to the personal jurisdiction of such court, waives any objection to venue in such court and consents to service of process by registered or certified mail, return receipt requested, at the last known address of such party.

## WILEY OPEN ACCESS TERMS AND CONDITIONS

Wiley Publishes Open Access Articles in fully Open Access Journals and in Subscription journals offering Online Open. Although most of the fully Open Access journals publish open access articles under the terms of the Creative Commons Attribution (CC BY) License only, the subscription journals and a few of the Open Access Journals offer a choice of Creative Commons Licenses. The license type is clearly identified on the article.

**The Creative Commons Attribution License**
The Creative Commons Attribution License (CC-BY) allows users to copy, distribute and transmit an article, adapt the article and make commercial use of the article. The CC-BY license permits commercial and non-

**Creative Commons Attribution Non-Commercial License**
The Creative Commons Attribution Non-Commercial (CC-BY-NC)License permits use, distribution and reproduction in any medium, provided the original work is properly cited and is not used for commercial purposes.(see below)


**Creative Commons Attribution-Non-Commercial-NoDerivs License**
The Creative Commons Attribution Non-Commercial-NoDerivs License (CC-BY-NC-ND) permits use, distribution and reproduction in any medium, provided the original work is properly cited, is not used for commercial purposes and no modifications or adaptations are made. (see below)

**Use by commercial "for-profit" organizations**
Use of Wiley Open Access articles for commercial, promotional, or marketing purposes requires further explicit permission from Wiley and will be subject to a fee.
Further details can be found on Wiley Online Library
http://olabout.wiley.com/WileyCDA/Section/id-410895.html


**Other Terms and Conditions:**



**v1.10 Last updated September 2015**

**Questions?** customercare@copyright.com **or +1-855-239-3415 (toll free in the US) or +1-978-646-2777.**

- **Reprint authorization for Figure 4.14 from "Diverse functional roles of reactive cysteines"; Nicholas J. Pace, Eranthie Weerapana. *ACS Chem Bio***

Copyright Clearance Center

RightsLink®

Home | Create Account | Help | Live Chat

ACS Publications
Most Trusted. Most Cited. Most Read.

**Title:** Diverse Functional Roles of Reactive Cysteines
**Author:** Nicholas J. Pace, Eranthie Weerapana
**Publication:** ACS Chemical Biology
**Publisher:** American Chemical Society
**Date:** Feb 1, 2013

Copyright © 2013, American Chemical Society

LOGIN

If you're a copyright.com user, you can login to RightsLink using your copyright.com credentials.
Already a RightsLink user or want to learn more?

## PERMISSION/LICENSE IS GRANTED FOR YOUR ORDER AT NO CHARGE

This type of permission/license, instead of the standard Terms & Conditions, is sent to you because no fee is being charged for your order. Please note the following:

- Permission is granted for your request in both print and electronic formats, and translations.
- If figures and/or tables were requested, they may be adapted or used in part.
- Please print this page for your records and send a copy of it to your publisher/graduate school.
- Appropriate credit for the requested material should be given as follows: "Reprinted (adapted) with permission from (COMPLETE REFERENCE CITATION). Copyright (YEAR) American Chemical Society." Insert appropriate information in place of the capitalized words.
- One-time permission is granted only for the use specified in your request. No additional uses are granted (such as derivative works or other editions). For any other uses, please submit a new request.

If credit is given to another source for the material you requested, permission must be obtained from that source.

BACK | CLOSE WINDOW

# REFERENCES

(1)     Fouda, A. E.; Pflum, M. K.: A Cell-Permeable ATP Analogue for Kinase-Catalyzed Biotinylation. *Angew Chem Int Ed Engl* **2015**, *54*, 9618-21.

(2)     Walsh, C. T.; Garneau-Tsodikova, S.; Gatto, G. J.: Protein posttranslational modifications: The chemistry of proteome diversifications. *Angew Chem Int Edit* **2005**, *44*, 7342-7372.

(3)     Maniatis, T.; Tasic, B.: Alternative pre-mRNA splicing and proteome expansion in metazoans. *Nature* **2002**, *418*, 236-43.

(4)     Manning, G.; Whyte, D. B.; hunter, T.; Sudarsanam, S.: The Protein Kinase Complement of the Human Genome. *Science* **2002**, *298*, 1912-1926.

(5)     Jackson, M. D.; Denu, J. M.: Molecular Reactions of Protein PhosphatasessInsights from Structure and Chemistry. *Chem. Rev.* **2001**, *101*, 2313−2340.

(6)     Adams, J. A.: Kinetic and catalytic mechanisms of protein kinases. *Chem. Rev.* **2001**, *101*, 2271-2290.

(7)     Lawrence, D. S.: Chemical Probes of Signal-Transducing Proteins. *Accounts of Chemical Research* **2003**, *36*, 401-409.

(8)     Parang, K.; Till, J. H.; Ablooglu, A. J.; Kohanski, R. A.; Hubbard, S. R.; Cole, P. A.: Mechanism-based design of a protein kinase inhibitor. *Nature structural biology* **2001**, *8*, 37-41.

(9)     Nelson, D. L.; Cox, M. N.: *Lehninger Principles of Biochemistry*, *Fourth Edition*.

(10)    Cohen, P.: Protein Kinase the major drug targets of the twenty-first century. *Nat. Rev. Drug Discov.* **2002**, *1*, 309-315.

(11)    Manning, G.; Plowman, G. D.; Hunter, T.; Sudarsanam, S.: Evolution of protein kinase signaling from yeast to man. *Trends in biochemical sciences* **2002**, *27*, 514-20.

(12)    Manning, G.; Whyte, D. B.; Martinez, R.; Hunter, T.; Sudarsanam, S.: The protein kinase complement of the human genome. *Science* **2002**, *298*, 1912-34.

(13)    Rautio, J.: Inhibitors of LRRK2 Kinase Activity To Probe the Treatment Option in Parkinson's Disease. *J. Med. Chem.* **2012**, *55*, 9414–9415.

(14)    Estrada, A. A.; Liu, X.; Baker-Glenn, C.; Beresford, A.; Burdick, D. J.; Chambers, M.; Chan, B. K.; Chen, H.; Ding, X.; DiPasquale, A. G.; Dominguez, S. L.; Dotson, J.; Drummond, J.; Flagella, M.; Flynn, S.; Fuji, R.; Gill, A.; Gunzner-Toste, J.; Harris, S. F.; Heffron, T. P.; Kleinheinz, T.; Lee, D. W.; Pichon, C. E. L.; Lyssikatos, J. P.; Medhurst, A. D.; Moffat, J. G.; Mukund, S.; Nash, K.; Scearce-Levie, K.; Shore, Z. S. D. G.; Tran, T.; Trivedi, N.; Wang, S.; Zhang, S.; Zhang, X.; Zhao, G.; Zhu, H.; Sweeney, Z. K.: Discovery of Highly Potent, Selective, and Brain-Penetrable Leucine-Rich Repeat Kinase 2 (LRRK2) Small Molecule Inhibitors. *J. Med. Chem.* **2012**, *55*, 9416−9433.

(15)    Capdeville, R.; Buchdunger, E.; Zimmermann, J.; Matter, A. G.: a rationally developed, targeted anticancer. *Nat. Rev. Drug Discov.* **2002**, *14*, 493-502.

(16)    Siegel-Lakhai, W. S.; Rodenstein, D. O.; Beijnen, J. H.; Gianella-Borradori, A.; Schellens, J. H.; Talbot, D. C.: Phase I study of seliciclib (CYC202 or R-roscovitine) in combination with gemcitabine (gem)/cisplatin (cis) in patients with advanced Non-Small Cell Lung Cancer (NSCLC). *J. Clin. Oncology ASCO Annual Meeting Proceedings* **2005**, *26S*, 2060.

(17)    Pellegrini, S.; Dusanter-Fourt, I.: The structure, regulation and function of the Janus kinases (JAKs) and the signal transducers and activators of transcription (STATs). *European journal of biochemistry / FEBS* **1997**, *248*, 615-33.

(18)    Starr, R.; Hilton, D. J.: Negative regulation of the JAK/STAT pathway. *BioEssays : news and reviews in molecular, cellular and developmental biology* **1999**, *21*, 47-52.

(19)    Gibbs, K. L.; Greensmith, L.; Schiavo, G.: Regulation of Axonal Transport by Protein Kinases. *Trends in biochemical sciences* **2015**, *40*, 597-610.

(20)    Toren, P.; Zoubeidi, A.: Targeting the PI3K/Akt pathway in prostate cancer: challenges and opportunities (review). *International journal of oncology* **2014**, *45*, 1793-801.

(21)    Carnero, A.; Paramio, J. M.: The PTEN/PI3K/AKT Pathway in vivo, Cancer Mouse Models. *Frontiers in oncology* **2014**, *4*, 252.

(22)    Shimamura, H.; Terada, Y.; Okado, T.; Tanaka, H.; Inoshita, S.; Sasaki, S.: The PI3-kinase-Akt pathway promotes mesangial cell survival and inhibits apoptosis in vitro via NF-kappa B and Bad. *Journal of the American Society of Nephrology : JASN* **2003**, *14*, 1427-34.

(23)    Altomare, D. A.; Testa, J. R.: Perturbations of the AKT signaling pathway in human cancer. *Oncogene* **2005**, *24*, 7455-64.

(24)    Crowell, J. A.; Steele, V. E.; Fay, J. R.: Targeting the AKT protein kinase for cancer chemoprevention. *Molecular cancer therapeutics* **2007**, *6*, 2139-48.

(25)    Chrivia, J. C.; Kwok, R. P.; Lamb, N.; Hagiwara, M.; Montminy, M. R.; Goodman, R. H.: Phosphorylated CREB binds specifically to the nuclear protein CBP. *Nature* **1993**, *365*, 855-9.

(26)    Parker, D.; Ferreri, K.; Nakajima, T.; Morte, V. J. L.; Evans, R.; Koerber, S. C.; Hoeger, C.; Montminy, M. R.: Phosphorylation of CREB at Ser-133 induces complex formation with CREB-binding protein via a direct mechanism. *Molecular and cellular biology* **1996**, *16*, 694-703.

(27)    Okamoto, H.; Kobayashi, A.: Tyrosine kinases in rheumatoid arthritis. *Journal of Inflammation* **2011**, *8*, 21.

(28)    Koya, D.; King, G. L.: Protein Kinase C Activation and the Development of Diabetic complications. *Perspectives in Diabetes* **1998**, *47*, 859-866.

(29)    Dachsel, J. C.; Farrerl, M. J.: LRRK2 and Parkinson disease. *Arch. Neurol.* **2010**, *67*, 542−547.

(30)    Satake, W.; Nakabayashi, Y.; Mizuta, I.; Hirota, Y.; Ito, C.; Kubo, M.; Kawaguchi, T.; Tsunoda, T.; Watanabe, M.; Takeda, A.; Tomiyama, H.; Nakashima, K.; Hasegawa, K.; Obata, F.; Yoshikawa, T.; Kawakami, H.; Sakoda, S.; Yamamoto, M.; Hattori, N.; Murata, M.; Nakamura, Y.; Toda, T.: Genome-wide association study identifies common variants at four loci as genetic risk factors for Parkinson's disease. . *Nat. Genet.* **2009**, *41* 1303−1307.

(31)    Pandya, N.; Santani, D.; Jain, S.: Role of Mitogen-Activated Protein (MAP) Kinases in Cardiovascular Diseases. *Cardiovascular Drug Reviews* **2005**, *23*.

(32)    Thomas Force; Pombo, C. M.; Avruch, J. A.; Bonventre, J. V.; Kyriakis, J. M.: Stress-Activated Protein Kinases in Cardiovascular Disease. *Circulation Research.* **1996**, *78* 947-953.

(33)    Grant, S. K.: Therapeutic Protein Kinase Inhibitors. *Cell. Mol. Life Sci.* **2009**, *66*, 1163 - 1177.

(34)    Vlahovic, G.; Crawford, J.: Activation of Tyrsoine Kinase in Cancer. *The Oncologist* **2003**, *8*, 531-538.

(35)    Davies, H.; Bignell, G. R.; Cox, C.; Stephens, P.; Edkins, S.; Clegg, S.; Teague, J.; Woffendin, H.; Garnett, M. J.; Bottomley, W.; Davis, N.; Dicks, E.; Ewing, R.; Floyd, Y.; Gray, K.; Hall, S.; Hawes, R.; Hughes, J.; Kosmidou, V.; Menzies, A.; Mould, C.; Parker, A.; Stevens, C.; Watt, S.; Hooper, S.; Wilson, R.; Jayatilake, H.; Gusterson, B. A.; Cooper, C.; Shipley, J.; Hargrave, D.; Pritchard-Jones, K.; Maitland, N.; Chenevix-Trench, G.; Riggins, G. J.; Bigner, D. D.; Palmieri, G.; Cossu, A.; Flanagan, A.; Nicholson, A.; Ho, J. W.; Leung, S. Y.; Yuen, S. T.; Weber, B. L.; Seigler, H. F.; Darrow, T. L.; Paterson, H.; Marais, R.; Marshall, C. J.; Wooster, R.; Stratton, M. R.; Futreal, P. A.: Mutations of the BRAF gene in human cancer. *Nature* **2002**, *417*, 949-54.

(36)    WestcAndrew, B.; Darren, J. M.; Saskia, B.; Artem, B.; Wanli, W. S.; Christopher, A. R.; Valina, L. D.; Ted, M. D.: Parkinson's disease-associated mutations in leucine-rich repeat kinase 2 augment kinase activity. *Proceedings of the National Academy of Sciences of the United States of America* **2005**, *102* 16842-16847

(37)    Wu, P.; Nielsen, T. E.; Clausen, M. H.: FDA-approved small-molecule kinase inhibitors. *Trends in pharmacological sciences* **2015**, *36*, 422-39.

(38)    Wu, P.; Nielsen, T. E.; Clausen, M. H.: Small-molecule kinase inhibitors: an analysis of FDA-approved drugs. *Drug discovery today* **2016**, *21*, 5-10.

(39)    Garber, K.: The second wave in kinase cancer drugs. *Nature biotechnology* **2006**, *24*, 127-30.

(40)    Niefind, K.; Putter, M.; Guerra, B.; Issinger, O. G.; Schomburg, D.: GTP plus water mimic ATP in the active site of protein kinase CK2. *Nature structural biology* **1999**, *6*, 1100-3.

(41)    Hanks, S. K.: Homology probing: identification of cDNA clones encoding members of the protein-serine kinase family. *Proceedings of the National Academy of Sciences of the United States of America* **1987**, *84*, 388-392.

(42)    Ablooglu, A. J.; Till, J. H.; Kim, K.; Parang, K.; Cole, P. A.; Hubbard, S. R.; Kohanski, R. A.: Probing the catalytic mechanism of the insulin receptor kinase with a tetrafluorotyrosine-containing peptide substrate. *The Journal of biological chemistry* **2000**, *275*, 30394-8.

(43)    Cole, P. A.; Courtney, A. D.; Shen, K.; Zhang, Z.; Qiao, Y.; Lu, W.; Williams, D. M.: Chemical approaches to reversible protein phosphorylation. *Acc Chem Res* **2003**, *36*, 444-52.

(44)    Knighton, D. R.; Zheng, J. H.; Ten Eyck, L. F.; Ashford, V. A.; Xuong, N. H.; Taylor, S. S.; Sowadski, J. M.: Crystal structure of the catalytic subunit of cyclic adenosine monophosphate-dependent protein kinase. *Science* **1991**, *253*, 407-14.

(45)    Grant, B. D.; Adams, J. A.: Pre-steady-state kinetic analysis of cAMP-dependent protein kinase using rapid quench flow techniques. *Biochemistry* **1996**, *35*, 2022-9.

(46)    Kemp, B. E.; Graves, D. J.; Benjamini, E.; Krebs, E. G.: Role of multiple basic residues in determining the substrate specificity of cyclic AMP-dependent protein kinase. *The Journal of biological chemistry* **1977**, *252*, 4888-94.

(47)    Wu, J. J.; Afar, D. E.; Phan, H.; Witte, O. N.; Lam, K. S.: Recognition of multiple substrate motifs by the c-ABL protein tyrosine kinase. *Combinatorial chemistry & high throughput screening* **2002**, *5*, 83-91.

(48)    Meggio, F.; Marin, O.; Pinna, L. A.: Substrate specificity of protein kinase CK2. *Cellular & molecular biology research* **1994**, *40*, 401-9.

(49)    Olsen, J. V.; Blagoev, B.; Gnad, F.; Macek, B.; Kumar, C.; Mortensen, P.; Mann, M.: Global, in vivo, and site-specific phosphorylation dynamics in signaling networks. *Cell* **2006**, *127*, 635-48.

(50)    Charron, G.; Zhang, M. M.; Yount, J. S.; Wilson, J.; Raghavan, A. S.; Shamir, E.; Hang, H. C.: Robust fluorescent detection of protein fatty-acylation with chemical reporters. *J Am Chem Soc* **2009**, *131*, 4967-75.

(51)    Du, J.; Jiang, H.; Lin, H.: Investigating the ADP-ribosyltransferase activity of sirtuins with NAD analogues and 32P-NAD. *Biochemistry* **2009**, *48*, 2878-90.

(52)    Duckworth, B. P.; Zhang, Z.; Hosokawa, A.; Distefano, M. D.: Selective labeling of proteins by using protein farnesyltransferase. *Chembiochem* **2007**, *8*, 98-105.

(53)    Grammel, M.; Luong, P.; Orth, K.; Hang, H. C.: A chemical reporter for protein AMPylation. *J Am Chem Soc* **2011**, *133*, 17103-5.

(54)    Hang, H. C.; Geutjes, E. J.; Grotenbreg, G.; Pollington, A. M.; Bijlmakers, M. J.; Ploegh, H. L.: Chemical probes for the rapid detection of Fatty-acylated proteins in Mammalian cells. *J Am Chem Soc* **2007**, *129*, 2744-5.

(55)    Hang, H. C.; Wilson, J. P.; Charron, G.: Bioorthogonal chemical reporters for analyzing protein lipidation and lipid trafficking. *Acc Chem Res* **2011**, *44*, 699-708.

(56)    Heal, W. P.; Wickramasinghe, S. R.; Leatherbarrow, R. J.; Tate, E. W.: N-Myristoyl transferase-mediated protein labelling in vivo. *Organic & biomolecular chemistry* **2008**, *6*, 2308-15.

(57)    Hwang, Y.; Thompson, P. R.; Wang, L.; Jiang, L.; Kelleher, N. L.; Cole, P. A.: A selective chemical probe for coenzyme A-requiring enzymes. *Angew Chem Int Ed Engl* **2007**, *46*, 7621-4.

(58)    Jeger, S.; Zimmermann, K.; Blanc, A.; Grunberg, J.; Honer, M.; Hunziker, P.; Struthers, H.; Schibli, R.: Site-specific and stoichiometric modification of antibodies by bacterial transglutaminase. *Angew Chem Int Ed Engl* **2010**, *49*, 9995-7.

(59)    Jiang, H.; Kim, J. H.; Frizzell, K. M.; Kraus, W. L.; Lin, H.: Clickable NAD analogues for labeling substrate proteins of poly(ADP-ribose) polymerases. *J Am Chem Soc* **2010**, *132*, 9363-72.

(60)    Anthony, T. M.; Dedigama-Arachchige, P. M.; Embogama, D. M.; Faner, T. R.; Fouda, A. E.; Pflum, M. K. H.: ATP Analogs in Protein Kinase Research. In *Kinomics*; Wiley-VCH Verlag GmbH & Co. KGaA, 2015; pp 137-168.

(61)    Cassel, D.; Glaser, L.: Resistance to phosphatase of thiophosphorylated epidermal growth factor receptor in A431 membranes. *Proceedings of the National Academy of Sciences of the United States of America* **1982**, *79*, 2231-2235.

(62)    Facemyer, K. C.; Cremo, C. R.: A new method to specifically label thiophosphorylatable proteins with extrinsic probes. Labeling of serine-19 of the regulatory light chain of smooth muscle myosin. *Bioconjugate Chem.* **1992**, *3*, 408-413.

(63)    Eckstein, F.: Nucleoside phosphorothioates. *Annu. Rev. Biochem* **1985**, *54*, 367-402.

(64)    Orr, G. A.; Simon, J.; Jones, S. R.; Chin, G. J.; Knowles, J. R.: Adenosine 5'-O-([gamma-18O]gamma-thio)triphosphate chiral at the gamma-phosphorus: stereochemical consequences of reactions catalyzed by pyruvate kinase, glycerol kinase, and hexokinase. *Proceedings of the National Academy of Sciences of the United States of America* **1978**, *75*, 2230-3.

(65)    Kwon, S. W.; Kim, S. C.; Jaunbergs, J.; Falck, J. R.; Zhao, Y.: Selective enrichment of thiophosphorylated polypeptides as a tool for the analysis of protein phosphorylation. *Molecular & cellular proteomics : MCP* **2003**, *2*, 242-7.

(66)    Jeong, S.; Nikiforov, T. T.: Kinase assay based on thiophosphorylation and biotinylation. *BioTechniques* **1999**, *27*, 1232-8.

(67)    Lee, S. E.; Elphick, L. M.; Kramer, H. B.; Jones, A. M.; Child, E. S.; Anderson, A. A.; Bonnac, L.; Suwaki, N.; Kessler, B. M.; Gouverneur, V.; Mann, D. J.: The chemoselective one-step alkylation and isolation of thiophosphorylated cdk2 substrates in the presence of native cysteine. *Chembiochem* **2011**, *12*, 633-40.

(68)    Carlson, S. M.; Chouinard, C. R.; Labadorf, A.; Lam, C. J.; Schmelzle, K.; Fraenkel, E.; White, F. M.: Large-scale discovery of ERK2 substrates identifies ERK-mediated transcriptional regulation by ETV3. *Science signaling* **2011**, *4*, rs11.

(69)    Blethrow, J. D.; Glavy, J. S.; Morgan, D. O.; Shokat, K. M.: Covalent capture of kinase-specific phosphopeptides reveals Cdk1-cyclin B substrates. *Proceedings of the National Academy of Sciences of the United States of America* **2008**, *105*, 1442-7.

(70)    Garber, K. C.; Carlson, E. E.: Thiol-ene enabled detection of thiophosphorylated kinase substrates. *ACS chemical biology* **2013**, *8*, 1671-6.

(71)     Kerman, K.; Kraatz, H. B.: Electrochemical detection of protein tyrosine kinase-catalysed phosphorylation using gold nanoparticles. *Biosens Bioelectron* **2009**, *24*, 1484-1489.

(72)     Chi, Y.; Welcker, M.; Hizli, A. A.; Posakony, J. J.; Aebersold, R.; Clurman, B. E.: Identification of CDK2 substrates in human cell lysates. *Genome Biol* **2008**, *9.*

(73)     Blasius, M.; Forment, J. V.; Thakkar, N.; Wagner, S. A.; Choudhary, C.; Jackson, S. P.: A phospho-proteomic screen identifies substrates of the checkpoint kinase Chk1. *Genome Biol* **2011**, *12*, R78.

(74)     Allen, J. J.; Lazerwith, S. E.; Shokat, K. M.: Bio-orthogonal Affinity Purification of Direct Kinase Substrates. *J. Am. Chem. Soc.* **2005**, *127*, 5288-5289.

(75)     Allen, J. J.; Li, M.; Brinkworth, C. S.; Paulson, J. L.; Wang, D.; Hubner, A.; Chou, W.-H.; Davis, R. J.; Burlingame, A. L.; Messing, R. O.; Katayama, C. D.; Hedrick, S. M.; Shokat, K. M.: A semisynthetic epitope for kinase substrates. *Nat. Methods* **2007**, *4*, 511-516.

(76)     Uhalte, E. C.; Kirchner, M.; Hellwig, N.; Allen, J. J.; Donat, S.; Shokat, K. M.; Selbach, M.; Abdelilah-Seyfried, S.: In Vivo Conditions to Identify Prkci Phosphorylation Targets Using the Analog-Sensitive Kinase Method in Zebrafish. *PloS one* **2012**, *7.*

(77)     Green, K. D.; Pflum, M. K. H.: Kinase-Catalyzed Biotinylation for Phosphoprotein Detection. *J. Am. Chem. Soc.* **2007**, *129*, 10-11.

(78)     Senevirathne, C.; Green, K. D.; Pflum, M. K. H.: Kinase-Catalyzed Biotinylation of Peptides, Proteins, and Lysates. In *Current Protocols in Chemical Biology*; John Wiley & Sons, Inc., 2012; Vol. 4.

(79)    Senevirathne, C.; Embogama, D. M.; Anthony, T. A.; Fouda, A. E.; Pflum, M. K.: The generality of kinase-catalyzed biotinylation. *Bioorg Med Chem* **2016**, *24*, 12-9.

(80)    Senevirathne, C.; Pflum, M. K. H.: Biotinylated Phosphoproteins from Kinase-Catalyzed Biotinylation are Stable to Phosphatases: Implications for Phosphoproteomics. *ChemBioChem* **2013**, 381-387.

(81)    Senevirathne, C.; Green, K. D.; Pflum, M. K. H.: Kinase-Catalyzed Biotinylation of Peptides, Proteins and Lysates. *In Curr. Prot. Chem. Bio., John Wiley & Sons* **2009**, *4*.

(82)    Green, K. D.; Pflum, M. H.: Exploring Kinase Cosubstrate Promiscuity: Monitoring Kinase Activity through dansylation. *ChemBioChem* **2009**, *10*, 234-237.

(83)    Suwal, S.; Pflum, M. K. H.: Phosphorylation-Dependent Kinase-Substrate Cross-Linking,. *Angew Chem Int Ed Engl* **2010**, *49* 1627-1630.

(84)    Martić, S.; Gabriel, M.; Turowec, J. P.; Litchfield, D. W.; Kraatz, H.-B.: Versatile Strategy for Biochemical, Electrochemical and Immunoarray Detection of Protein Phosphorylations. *J. Am. Chem. Soc.* **2012**.

(85)    Song, H.; Kerman, K.; Kraatz, H. B.: Electrochemical detection of kinase-catalyzed phosphorylation using ferrocene-conjugated ATP. *Chem Commun (Camb)* **2008**, 502-4.

(86)    Lee, S. E.; Elphick, L. M.; Anderson, A. A.; Bonnac, L.; Child, E. S.; Mann, D. J.; Gouverneur, V.: Synthesis and reactivity of novel gamma-phosphate modified ATP analogues. *Bioorg Med Chem Lett* **2009**, *19*, 3804-7.

(87)    Wang, N.; She, Z.; Lin, Y. C.; Martic, S.; Mann, D. J.; Kraatz, H. B.: Clickable 5 '-gamma-Ferrocenyl Adenosine Triphosphate Bioconjugates in Kinase-Catalyzed Phosphorylations. *Chem-Eur J* **2015**, *21*, 4988-4999.

(88)    Patricelli, M. P.; Szardenings, A. K.; Liyanage, M.; Nomanbhoy, T. K.; Wu, M.; Weissig, H.; Aban, A.; Chun, D.; Tanner, S.; Kozarich, J. W.: Functional interrogation of the kinome using nucleotide acyl phosphates. *Biochemistry* **2007**, *46*, 350-358.

(89)    Patricelli, M. P.; Nomanbhoy, T. K.; Wu, J.; Brown, H.; Zhou, D.; Zhang, J.; Jagannathan, S.; Aban, A.; Okerberg, E.; Herring, C.; Nordin, B.; Weissig, H.; Yang, Q.; Lee, J. D.; Gray, N. S.; Kozarich, J. W.: In situ kinase profiling reveals functionally relevant properties of native kinases. *Chemistry & biology* **2011**, *18*, 699-710.

(90)    Hanks, S. K.; Hunter, T.: Protein kinases 6. The eukaryotic protein kinase superfamily: kinase (catalytic) domain structure and classification. *FASEB journal : official publication of the Federation of American Societies for Experimental Biology* **1995**, *9*, 576-96.

(91)    Zheng, J.; Knighton, D. R.; ten Eyck, L. F.; Karlsson, R.; Xuong, N.; Taylor, S. S.; Sowadski, J. M.: Crystal structure of the catalytic subunit of cAMP-dependent protein kinase complexed with MgATP and peptide inhibitor. *Biochemistry* **1993**, *32*, 2154-61.

(92)    Green, K. D.; Pflum, M. H.: Kinase-Catalyzed Biotinylation for Phosphoprotein Detection. *J. Am. Chem. Soc.* **2007**, *129*, 10-11.

(93)    Wilke, K. E.; Francis, S.; Carlson, E. E.: Activity-based probe for histidine kinase signaling. *J Am Chem Soc* **2012**, *134*, 9150-3.

(94)    Suwal, S.; Senevirathne, C.; Garre, S.; Pflum, M. K.: Structural Analysis of ATP

Analogues Compatible with Kinase-Catalyzed Labeling. *Bioconjugate chemistry* **2012**,

*23*, 2386–2391.

(95)    Senevirathne, C.; Pflum, M. K.: Biotinylated phosphoproteins from kinase-

catalyzed biotinylation are stable to phosphatases: implications for phosphoproteomics.

*ChemBioChem* **2013**, *14*, 381-7.

(96)    Suwal, S.; Pflum, M. H.: Phosphorylation-dependent kinase-substrate cross-

linking. *Angew Chem Int Ed Engl* **2010**, *49*, 1627-30.

(97)    Garre, S.; Senevirathne, C.; Pflum, M. K.: A comparative study of ATP analogs

for phosphorylation-dependent kinase-substrate crosslinking. *Bioorg Med Chem* **2014**,

*22*, 1620-5.

(98)    Gao, X.; Schutz-Geschwender, A.; Hardwidge, P. R.: Near-infrared fluorescence

detection of ATP-biotin-mediated phosphoprotein labeling. *Biotechnology letters* **2009**,

*31*, 113-7.

(99)    Dunn, J. D.; Reid, G. E.; Bruening, M. L.: Techniques for phosphopeptide

enrichment prior to analysis by mass spectrometry. *Mass Spectrometry Reviews* **2010**,

*29*, 29-54.

(100)  Goncalves, C. A.; Gottfried, C.; Dunkley, P. R.: The use of permeabilized cells to

assay protein phosphorylation and catecholamine release. *Neurochemical research*

**2000**, *25*, 885-94.

(101)  Laketa, V.; Zarbakhsh, S.; Morbier, E.; Subramanian, D.; Dinkel, C.; Brumbaugh,

J.; Zimmermann, P.; Pepperkok, R.; Schultz, C.: Membrane-Permeant Phosphoinositide

Derivatives as Modulators of Growth Factor Signaling and Neurite Outgrowth. *Chem. & Bio.* **2009**, *16* 1190-1196.

(102)  Webster, M. R.; Zhao, M.; Rudek, M. A.; Hann, C. L.; Meyers, C. L. F.: Bisphosphonamidate clodronate prodrug exhibits potent anticancer activity in non-small-cell lung cancer cells. *J. Med. Chem.* **2011**, *54* 6647-56.

(103)  Mentel, M.; Laketa, V.; Subramanian, D.; Gillandt, H.; Schultz, C.: Photoactivatable and cellmembrane-permeable phosphatidylinositol 3,4,5-trisphosphate. *Angewandte Chemie* **2011**, *50*, 3811-4.

(104)  Ozaki, S.; DeWald, D. B.; Shope, J. C.; Chen, J.; Prestwich, G. D.: Intracellular delivery of phosphoinositides and inositol phosphates using polyamine carriers. *Proceedings of the National Academy of Sciences of the United States of America* **2000**, *97*, 11286-91.

(105)  Duan, S. Y.; Ge, X. M.; Lu, N.; Wu, F.; Yuan, W.; Jin, T.: Synthetic polyspermine imidazole-4, 5-amide as an efficient and cytotoxicity-free gene delivery system. *International journal of nanomedicine* **2012**, *7*, 3813-22.

(106)  Shah, S.; Solanki, A.; Sasmal, P. K.; Lee, K. B.: Single vehicular delivery of siRNA and small molecules to control stem cell differentiation. *J Am Chem Soc* **2013**, *135*, 15682-5.

(107)  Kovalevsky, A. Y.; Johnson, H.; Hanson, B. L.; Waltman, M. J.; Fisher, S. Z.; Taylor, S.; Langan, P.: Low- and room-temperature X-ray structures of protein kinase A ternary complexes shed new light on its activity. *Acta crystallographica. Section D, Biological crystallography* **2012**, *68*, 854-60.

(108) Morris, G. M.; Huey, R.; Lindstrom, W.; Sanner, M. F.; Belew, R. K.; Goodsell, D. S.; Olson, A. J.: AutoDock4 and AutoDockTools4: Automated docking with selective receptor flexibility. *Journal of computational chemistry* **2009**, *30*, 2785-2791.

(109) García, J.; Pereira, R.; de Lera, A. R.: Total synthesis of the natural isoprenylcysteine carboxyl methyltransferase inhibitor spermatinamine. *Tet Lett* **2009**, *50*, 5028-5030.

(110) Chaturvedi, D. N.; Knittel, J. J.; Hruby, V. J.; Castrucci, A. M. d. L.; Hadley, M. E.: Synthesis and Biological Actions of Highly Potent and Prolonged Acting Biotin-Labeled Melanotropins. *J. Med. Chem.* **1984**, *27*, 1406-1410.

(111) Albarella, J. P.; Minegar, R. L.; Patterson, W. L.; Dattaguptal, N.; Carlson, E.: Monoadduct forming photochemical reagents for labeling nucleic acids for hybridization. *Nucl. Acids Res.* **1989**, *17*, 4293-4308.

(112) Parang, K.; Kohn, J. A.; Saldanha, S. A.; Cole, P. A.: Development of photo-crosslinking reagents for protein kinase-substrate interactions. *FEBS Lett.* **2002**, *520*, 156.

(113) Ulrich, S. M.; Kenski, D. M.; Shokat, K. M.: Engineering a "methionine clamp" into Src family kinases enhances specificity toward unnatural ATP analogues. *Biochemistry* **2003**, *42*, 7915-21.

(114) Liu, Y.; Shah, K.; Yang, F.; Witucki, L.; Shokata, K. M.: A Molecular Gate which Controls Unnatural ATP Analogue Recognition by the Tyrosine Kinase V-Src. *Bioorganic & Medicinal Chemistry* **1998**, *6*, 1219-1226.

(115) Kelner, K. L.; Morita, K.; Rossen, J. S.; Pollard, H. B.: Restricted diffusion of tyrosine hydroxylase and phenylethanolamine N-methyltransferase from digitonin-

permeabilized adrenal chromaffin cells. *Proceedings of the National Academy of Sciences of the United States of America* **1986**, *83*, 2998-3002.

(116) Sarafian, T.; Aunis, D.; Bader, M. F.: Loss of proteins from digitonin-permeabilized adrenal chromaffin cells essential for exocytosis. *The Journal of biological chemistry* **1987**, *262*, 16671-6.

(117) Hoyer, J.; Schatzschneider, U.; Schulz-Siegmund, M.; Neundorf, I.: Dimerization of a cell-penetrating peptide leads to enhanced cellular uptake and drug delivery. *Beilstein J. Org. Chem.* **2012**, *8*, 1788-1797.

(118) García, J.; Pereira, R.; de Lera, A. R.: Total synthesis of the natural isoprenylcysteine carboxyl methyltransferase inhibitor spermatinamine. *Tetrahedron Letters* **2009**, *50*, 5028-5030.

(119) Albarella, J. P.; Minegar, R. L.; Patterson, W. L.; Dattaguptal, N.; Carlson, E.: Monoadduct forming photochemical reagents for labeling nucleic acids for hybridization. *Nucleic acid research* **1989**, *17*, 4293-4308.

(120) Warthaka, M.; Karwowska-Desaulniers, P.; Pflum, M. H.: Phosphopeptide Modification and Enrichment by Oxidation–Reduction Condensation. *ACS Chem. Biol.* **2006**, *1*, 697-701.

(121) Sambrook, J.; Russel, D.: Molecular Cloning: A Laboratory Manual. *Third edition ed.,* **2011**, *Cold Spring Harbor Press, New York*.

(122) Senevirathne, K. A. C.: Development of kinase catalyzed biotinylation to study phsophoproteomics. *Wayne State University, Detroit, MI, 48202, USA* **2013**.

(123) Stoddart, M. J.: *Mammalian Cell Viability*; Humana Press, 2011; Vol. 740.

(124)  Goncalves, C. A.; Hall, A.; Sim, A. T.; Bunn, S. J.; Marley, P. D.; Cheah, T. B.; Dunkley, P. R.: Tyrosine hydroxylase phosphorylation in digitonin-permeabilized bovine adrenal chromaffin cells: the effect of protein kinase and phosphatase inhibitors on Ser19 and Ser40 phosphorylation. *Journal of neurochemistry* **1997**, *69*, 2387-96.

(125)  Banko, M. R.; Allen, J. J.; Schaffer, B. E.; Wilker, E. W.; Tsou, P.; White, J. L.; Villen, J.; Wang, B.; Kim, S. R.; Sakamoto, K.; Gygi, S. P.; Cantley, L. C.; Yaffe, M. B.; Shokat, K. M.; Brunet, A.: Chemical genetic screen for AMPKalpha2 substrates uncovers a network of proteins involved in mitosis. *Molecular cell* **2011**, *44*, 878-92.

(126)  Delouche, B.; Pradel, L. A.; Henry, J. P.: Phosphorylation by protein kinase C of annexin 2 in chromaffin cells stimulated by nicotine. *Journal of neurochemistry* **1997**, *68*, 1720-7.

(127)  Giacalone, G.; Bochot, A.; Fattal, E.; Hillaireau, H.: Drug-induced nanocarrier assembly as a strategy for the cellular delivery of nucleotides and nucleotide analogues. *Biomacromolecules* **2013**, *14*, 737-42.

(128)  Senevirathne, C.; Pflum, M. K. H.: Biotinylated Phosphoproteins from Kinase-Catalyzed Biotinylation are Stable to Phosphatases: Implications for Phosphoproteomics. *ChemBioChem* **2013**, *14*, 381-387.

(129)  Phizicky, E. M.; Fields, S.: Protein-protein interactions: methods for detection and analysis. *Microbiological reviews* **1995**, *59*, 94-123.

(130)  Sinz, A.: Chemical cross-linking and mass spectrometry to map three-dimensional protein structures and protein-protein interactions. *Mass Spectrom Rev* **2006**, *25*, 663-82.

(131)  Hemaprabha, E.: Chemical crosslinking of proteins. *Journal of pharmaceutical and scientific inovation* **2012**, 22.

(132)  Shannon, D. A.; Banerjee, R.; Webster, E. R.; Bak, D. W.; Wang, C.; Weerapana, E.: Investigating the proteome reactivity and selectivity of aryl halides. *J Am Chem Soc* **2014**, *136*, 3330-3.

(133)  Riel-Mehan, M. M.; Shokat, K. M.: A crosslinker based on a tethered electrophile for mapping kinase-substrate networks. *Chemistry & biology* **2014**, *21*, 585-90.

(134)  Schwaid, A. G.; Shannon, D. A.; Ma, J.; Slavoff, S. A.; Levin, J. Z.; Weerapana, E.; Saghatelian, A.: Chemoproteomic discovery of cysteine-containing human short open reading frames. *J Am Chem Soc* **2013**, *135*, 16750-3.

(135)  Garske, A. L.; Peters, U.; Cortesi, A. T.; Perez, J. L.; Shokat, K. M.: Chemical genetic strategy for targeting protein kinases based on covalent complementarity. *Proceedings of the National Academy of Sciences of the United States of America* **2011**, *108*, 15046-52.

(136)  Singh, A.; Thornton, E. R.; Westheimer, F. H.: The photolysis of diazoacetylchymotrypsin. *The Journal of biological chemistry* **1962**, *237*, 3006-8.

(137)  Smith, R. A.; Knowles, J. R.: Letter: Aryldiazirines. Potential reagents for photolabeling of biological receptor sites. *J Am Chem Soc* **1973**, *95*, 5072-3.

(138)  Chowdhry, V.; Vaughan, R.; Westheimer, F. H.: 2-diazo-3,3,3-trifluoropropionyl chloride: reagent for photoaffinity labeling. *Proceedings of the National Academy of Sciences of the United States of America* **1976**, *73*, 1406-8.

(139)  Brunner, J.; Senn, H.; Richards, F. M.: 3-Trifluoromethyl-3-phenyldiazirine. A new carbene generating group for photolabeling reagents. *The Journal of biological chemistry* **1980**, *255*, 3313-8.

(140)  Nielsen, P. E.; Hansen, J. B.; Thomsen, T.; Buchardt, O.: Reagents for photoaffinity labeling. I. Photobinding efficiency of aryl azido-, diazocyclopentadienyl- and ethyl diazomalonyl-derivatives of 9-aminoacridine. *Experientia*, *39*, 1063-1072.

(141)  Goeldner, M. P.; Hawkinson, J. E.; Casida, J. E.: Diazocyclohexadienones as photoaffinity ligands: Syntheses of trioxabicyclooctane probes for the convulsant binding site of the GABAA receptor. *Tetrahedron Letters* **1989**, *30*, 823-826.

(142)  Galardy, R. E.; Craig, L. C.; Printz, M. P.: Benzophenone triplet: a new photochemical probe of biological ligand-receptor interactions. *Nature: New biology* **1973**, *242*, 127-8.

(143)  Wilhelm, S.; Christfriede, S.; Hans, S.: Lipids with Photosensitive Groups as Chemical Probes for the Structural Analysis of Biological Membranes. On the Localization of the G- and M-Protein of Vesicular Stomatitis Virus. In *Hoppe-Seyler´s Zeitschrift für physiologische Chemie*, 1978; Vol. 359; pp 923.

(144)  Young, M. J. T.; Platz, M. S.: Polyfluorinated aryl azides as photoaffinity labelling reagents; the room temperature CH insertion reactions of singlet pentafluorophenyl nitrene with alkanes. *Tetrahedron Letters* **1989**, *30*, 2199-2202.

(145)  Kolpashchikov, D. M.; Zakharenko, A. L.; Dezhurov, S. V.; Rechkunova, N. I.; Khodyreva, S. N.; Degtiarev, S.; Litvak, V. V.; Lavrik, O. I.: [New reagents for affinity modification of biopolymers. Photoaffinity modification of Tte-DNA polymerase]. *Bioorganicheskaia khimiia* **1999**, *25*, 129-36.

(146)  Goeldner, M. P.; Hirth, C. G.: Specific photoaffinity labeling induced by energy transfer: application to irreversible inhibition of acetylcholinesterase. *Proceedings of the National Academy of Sciences of the United States of America* **1980**, *77*, 6439-42.

(147)  Vodovozova, E. L.: Photoaffinity labeling and its application in structural biology. *Biochemistry. Biokhimiia* **2007**, *72*, 1-20.

(148)  Reiser, A.; Willets, F. W.; Terry, G. C.; Williams, V.; Marley, R.: Photolysis of aromatic azides. Part 4.-Lifetimes of aromatic nitrenes and absolute rates of some of their reactions. *Transactions of the Faraday Society* **1968**, *64*, 3265-3275.

(149)  Geiger, M. W.; Elliot, M. M.; Karacostas, V. D.; Moricone, T. J.; Salmon, J. B.; Sideli, V. L.; Onge, M. A. S.: ARYL AZIDES AS PROTEIN PHOTOLABELS: ABSORPTION SPECTRAL PROPERTIES AND QUANTUM YIELDS OF PHOTODISSOCIATION. *Photochemistry and photobiology* **1984**, *40*, 545-548.

(150)  Hall, J. H.; Hill, J. W.; Tsai, H.-c.: Insertion reactions of aryl nitrenes. *Tetrahedron Letters* **1965**, *6*, 2211-2216.

(151)  Blencowe, A.; Hayes, W.: Development and application of diazirines in biological and synthetic macromolecular systems. *Soft Matter* **2005**, *1*, 178-205.

(152)  Dürr, H.: Carbenes, Nitrenes and Arynes. Von T. L. Gilchrist u. C. W. Rees. Th. Nelson and Sons Ltd., London 1969. 1. Aufl., 131 S., geb. $ 21.—. *Angewandte Chemie* **1971**, *83*, 812-812.

(153)  Bayley, H.: Preface. In *Laboratory Techniques in Biochemistry and Molecular Biology*; T.S, W., R.H, B., Eds.; Elsevier, 1983; Vol. Volume 12; pp vii-viii.

(154)   Wittelsberger, A.; Thomas, B. E.; Mierke, D. F.; Rosenblatt, M.: Methionine acts as a "magnet" in photoaffinity crosslinking experiments. *FEBS Letters* **2006**, *580*, 1872-1876.

(155)   Dorman, G.; Prestwich, G. D.: Benzophenone Photophores in Biochemistry. *Biochemistry* **1994**, *33*, 5661-5673.

(156)   Hastie, C. J.; McLauchlan, H. J.; Cohen, P.: Assay of protein kinases using radiolabeled ATP: a protocol. *Nat. Protocols* **2006**, *1*, 968-971.

(157)   Shah, K.; Liu, Y.; Deirmengian, C.; Shokat, K. M.: Engineering unnatural nucleotide specificity for Rous sarcoma virus tyrosine kinase to uniquely label its direct substrates. *Proc. Natl. Acad. Sci. USA* **1997**, *94*, 3565-3570.

(158)   Fujimoto, T.; Hatano, N.; Nozaki, N.; Yurimoto, S.; Kobayashi, R.; Tokumitsu, H.: Identification of a novel CaMKK substrate. *Biochemical and biophysical research communications* **2011**, *410*, 45-51.

(159)   Shah, K.; Shokat, K. M.: A chemical genetic screen for direct v-Src substrates reveals ordered assembly of a retrograde signaling pathway. *Chemistry & biology* **2002**, *9*, 35-47.

(160)   Eblen, S. T.; Kumar, N. V.; Shah, K.; Henderson, M. J.; Watts, C. K.; Shokat, K. M.; Weber, M. J.: Identification of novel ERK2 substrates through use of an engineered kinase and ATP analogs. *The Journal of biological chemistry* **2003**, *278*, 14926-35.

(161)   Ubersax, J. A.; Woodbury, E. L.; Quang, P. N.; Paraz, M.; Blethrow, J. D.; Shah, K.; Shokat, K. M.; Morgan, D. O.: Targets of the cyclin-dependent kinase Cdk1. *Nature* **2003**, *425*, 859-64.

(162)  Larochelle, S.; Batliner, J.; Gamble, M. J.; Barboza, N. M.; Kraybill, B. C.; Blethrow, J. D.; Shokat, K. M.; Fisher, R. P.: Dichotomous but stringent substrate selection by the dual-function Cdk7 complex revealed by chemical genetics. *Nature structural & molecular biology* **2006**, *13*, 55-62.

(163)  Chaudhary, A.; Brugge, J. S.; Cooper, J. A.: Direct phosphorylation of focal adhesion kinase by c-Src: evidence using a modified nucleotide pocket kinase and ATP analog. *Biochemical and biophysical research communications* **2002**, *294*, 293-300.

(164)  Schauble, S.; King, C. C.; Darshi, M.; Koller, A.; Shah, K.; Taylor, S. S.: Identification of ChChd3 as a novel substrate of the cAMP-dependent protein kinase (PKA) using an analog-sensitive catalytic subunit. *The Journal of biological chemistry* **2007**, *282*, 14952-9.

(165)  Fields, S.; Song, O.: A novel genetic system to detect protein-protein interactions. *Nature* **1989**, *340*, 245-6.

(166)  Staudinger, J.; Zhou, J.; Burgess, R.; Elledge, S. J.; Olson, E. N.: PICK1: a perinuclear binding protein and substrate for protein kinase C isolated by the yeast two-hybrid system. *The Journal of cell biology* **1995**, *128*, 263-71.

(167)  Wankhede, D. P.; Misra, M.; Singh, P.; Sinha, A. K.: Rice mitogen activated protein kinase kinase and mitogen activated protein kinase interaction network revealed by in-silico docking and yeast two-hybrid approaches. *PloS one* **2013**, *8*, e65011.

(168)  Liang, W.; Yang, B.; Yu, B. J.; Zhou, Z.; Li, C.; Jia, M.; Sun, Y.; Zhang, Y.; Wu, F.; Zhang, H.; Wang, B.; Deyholos, M. K.; Jiang, Y. Q.: Identification and analysis of MKK and MPK gene families in canola (Brassica napus L.). *BMC genomics* **2013**, *14*, 392.

(169)  Maly, D. J.; Allen, J. A.; Shokat, K. M.: A mechanism-based cross-linker for the identification of kinase-substrate pairs. *J Am Chem Soc* **2004**, *126*, 9160-1.

(170)  Liu, K.; Kalesh, K. A.; Ong, L. B.; Yao, S. Q.: An improved mechanism-based cross-linker for multiplexed kinase detection and inhibition in a complex proteome. *Chembiochem* **2008**, *9*, 1883-8.

(171)  Statsuk, A. V.; Maly, D. J.; Seeliger, M. A.; Fabian, M. A.; Biggs, W. H., 3rd; Lockhart, D. J.; Zarrinkar, P. P.; Kuriyan, J.; Shokat, K. M.: Tuning a three-component reaction for trapping kinase substrate complexes. *J Am Chem Soc* **2008**, *130*, 17568-74.

(172)  Pace, N. J.; Weerapana, E.: Diverse functional roles of reactive cysteines. *ACS chemical biology* **2013**, *8*, 283-96.

(173)  Shevchenko, A.; Wilm, M.; Vorm, O.; Mann, M.: Mass spectrometric sequencing of proteins silver-stained polyacrylamide gels. *Analytical chemistry* **1996**, *68*, 850-8.

(174)  Nesvizhskii, A. I.; Keller, A.; Kolker, E.; Aebersold, R.: A Statistical Model for Identifying Proteins by Tandem Mass Spectrometry. *Analytical chemistry* **2003**, *75*, 4646-4658.

(175)  Kalume, D. E.; Molina, H.; Pandey, A.: Tackling the phosphoproteome: tools and strategies. *Current opinion in chemical biology* **2003**, *7*, 64-9.

(176)  Garcia, B. A.; Shabanowitz, J.; Hunt, D. F.: Analysis of protein phosphorylation by mass spectrometry. *Methods* **2005**, *35*, 256-64.

(177)  Steinberg, T. H.; Agnew, B. J.; Gee, K. R.; Leung, W. Y.; Goodman, T.; Schulenberg, B.; Hendrickson, J.; Beechem, J. M.; Haugland, R. P.; Patton, W. F.:

Global quantitative phosphoprotein analysis using Multiplexed Proteomics technology. *Proteomics* **2003**, *3*, 1128-44.

(178)  Mann, M.; Ong, S. E.; Gronborg, M.; Steen, H.; Jensen, O. N.; Pandey, A.: Analysis of protein phosphorylation using mass spectrometry: deciphering the phosphoproteome. *Trends in biotechnology* **2002**, *20*, 261-8.

(179)  Posewitz, M. C.; Tempst, P.: Immobilized gallium(III) affinity chromatography of phosphopeptides. *Analytical chemistry* **1999**, *71*, 2883-92.

(180)  Sun, T.; Campbell, M.; Gordon, W.; Arlinghaus, R. B.: Preparation and application of antibodies to phosphoamino acid sequences. *Biopolymers* **2001**, *60*, 61-75.

(181)  Fouda, A. E.; Pflum, M. K. H.: A Cell-Permeable ATP Analogue for Kinase-Catalyzed Biotinylation. *Angew. Chem. Int. Ed.* **2015**, *54*, 9618-9621.

(182)  Senevirathne, C.; Green, K. D.; Pflum, M. K.: Kinase-Catalyzed Biotinylation. *Current protocols in chemical biology* **2012**, *4*, 83-100.

(183)  Anthony, T. M.; Dedigama-Arachchige, P. M.; Embogama, D. M.; Faner, T. R.; Fouda, A. E.; Pflum, M. K. H.: ATP Analogs in Protein Kinase Research, in Kinomics: Approaches and Applications (eds H.-B. Kraatz and S. Martic). *Wiley-VCH Verlag GmbH & Co. KGaA, Weinheim, Germany* **2015**, *Ch6*.

(184)  Green, K. D.; Pflum, M. K.: Exploring kinase cosubstrate promiscuity: monitoring kinase activity through dansylation. *Chembiochem* **2009**, *10*, 234-7.

(185)  Suwal, S.; Pflum, M. K.: Phosphorylation-dependent kinase-substrate cross-linking. *Angewandte Chemie* **2010**, *49*, 1627-30.

(186)  Hacker, S. M.; Mex, M.; Marx, A.: Synthesis and Stability of Phosphate Modified ATP Analogues. *Journal of Organic Chemistry* **2012**, *77*, 10450-10454.

(187)  Davisson, V. J.; Woodside, A. B.; Neal, T. R.; Stremler, K. E.; Muehlbacher, M.; Poulter, C. D.: Phosphorylation of isoprenoid alcohols. *The Journal of organic chemistry* **1986**, *51*, 4768-4779.

(188) Wingender, E.; Arellano, A: Synthesis and properties of the new thiol-specific reagent difluorescein disulfide: Its application on histone-histone and histone-DNA interactions. *Analytical biochemistry*, **1982**, 127, 351-360.

# ABSTRACT

# DEVELOPMENT OF γ-MODIFIED ATP ANALOGS TO STUDY KINASE-CATALYZED PHOSPHORYLATIONS

by

## AHMED EID FOUDA

### August 2016

**Advisor:** Dr. Mary Kay Pflum

**Major:** Chemistry (Organic)

**Degree:** Doctor of Philosophy

Kinase-catalyzed protein phosphorylation is one of the most important post-translational modifications that controls cascades of biochemical reactions. Irregularities in phosphorylation result in many diseases, such as diabetes mellitus, Parkinsons, and cancer. The development of new methods to monitor kinase-catalyzed phosphorylation is needed to decipher details of normal and diseased cell signaling. The Pflum lab recently developed several γ-modified ATP analogs to study kinase catalyzed phosphorylation reactions. The γ-modified ATP analogs have different tags, such as biotin for substrate labeling or aryl-azide for kinase substrates identification. Unfortunately, use of γ-modified ATP analogs was limited to in vitro studies due to the cell impermeability of ATP analogs. Here, we report the first cell permeable ATP analog compatible with kinase-catalyzed labeling. Cell permeable ATP-biotin showed *in vitro* protein labeling similar to the previously reported ATP-biotin. Importantly, biotin labeling of kinase substrates in living cells was also observed. Also, we report an alternative method to permeabilize ATP analogs in cases where synthesis of cell

permeable ATP analog is not feasible. Permeabilizing ATP analogs will aid in monitoring kinase-catalyzed phosphorylation in living cells, which will enhance studies on cell signaling cascades and disease formation. Furthermore, we developed new crosslinking ATP analogs to identify substrates to kinases. We report affinity-based crosslinking ATP analogs, ATP-acrylamides. ATP-acrylamides crosslinked cysteine containing kinases to their substrates through specific proximal cysteine residues on kinases. ATP-acrylamides will solve problems accompanied with the previously reported ATP-Ar-azide that suffer from nonspecific crosslinking due to the very reactive crosslinking azide group. ATP-acrylamides will provide the details of cell signaling of specific kinases, which is supporting biomedical studies. Lastly, we are studying the effect of different bonds between the $\gamma$-phosphate and the attached group on kinase cosubstrate promiscuity phenomenon. This study revealed the electronic effect of several atoms on the ability of ATP-analogs to act as kinase-cosubstrates. Understanding the factors governing the ability of ATP analogs to act as cosubstrate will lead to development of more suitable ATP analogs for kinase catalyzed phosphorylation studies.

# AUTOBIOGRAPHICAL STATEMENT

## AHMED EID FOUDA

### Educational background

**2011-2016: Ph.D. in Chemistry**, (organic chemistry major and biochemistry minor), Wayne State University, Detroit, MI, 48202, USA

**2005-2009: M.Sc. in Pharmaceutical sciences** (pharmaceutical organic chemistry), Faculty of Pharmacy, Cairo University, Cairo, Egypt

**1999-2004: Bachelor of pharmacy and pharmaceutical sciences,** Faculty of Pharmacy, Cairo University, Cairo, Egypt

### Awards, fellowships and honors

- **2016**: Graduate school citation for excellence in teaching award, Wayne State University, Detroit, Michigan, USA.
- **2015-2016**: Thomas C. Rumble University Graduate Fellowship, Wayne State University.
- **2015**: Willard R. Lenz, Jr. Endowed Memorial Scholarship, Wayne State University.
- **2015**: Calvin Stevens memorial scholarship (travel award), Wayne State University.
- **2015**: Graduate school citation for excellence in teaching award, Wayne State University.
- **2013**: Norman A. LeBel Endowed Graduate travel Award in Organic Chemistry, Wayne State University, Detroit, Michigan, USA.
- **2004**: Honors, Faculty of Pharmacy, Cairo University, Cairo, Egypt.

### Publications

- **Ahmed E. Fouda**, Aparni Kaushalya, and Mary Kay H. Pflum. Development of affinity based crosslinking ATP analogs for cysteine containing kinases-substrate identification (In preparation)
- **Ahmed E. Fouda**, Thilani Anthony, and Mary Kay H. Pflum. "Comparative study of the effect of different bond linkage on the γ-phosphate of ATP analogs on kinase-cosubstrate promiscuity" (final stage of preparation)
- **Ahmed E. Fouda**, D. Maheeka Embogama, and Mary Kay H. Pflum. "Carbohydrate assisted ATP-Biotin cell delivery for *in cellulo* kinase-catalyzed biotinylation" (Submitted)
- Chamara Senevirathne, D. Maheeka Embogama, Thilani M. Anthony, **Ahmed E. Fouda**, and Mary Kay H. Pflum. "The Generality of Kinase-Catalyzed Biotinylation". ***Bioorg. and med. Chem.,*** **2016**, 24, 12.
- **Ahmed E. Fouda** and Mary Kay H. Pflum. "A cell permeable ATP analog for kinase-catalyzed biotinylation". ***Angew. Chem. Int. Ed.,*** **2015**, 54, 9618. (This paper was highlighted as a very important paper).
- Thilani M. Anthony, Pavithra M. Dedigama Arachchige, D. Maheeka Embogama, Todd R. Faner, **Ahmed E. Fouda***, and Mary Kay H. Pflum. ATP analogs in protein kinase research. *Kinomics: Approaches and Applications*, Heinz-Bernhard Kraatz, Sanela Martic, Eds. *Wiley-VCH Verlag GmbH. ISBN: 9783527337651*. August **2015 (All authors contributed equally to this work).**
- **Ahmed E. Fouda**, Suzan M. Abuel-Maaty, Ashraf F. Zaher, Hamdy M. Ragab. "Synthesis of new 4-Quinolones of expected anticancer activity- Synthesis, Drug Design and Biological Assay", *LAP LAMBERT Academic Publishing GmbH & Co. KG, Saarbrücken*, Germany, ISBN978-3-8433-6809-4, November **2010**.
- Hamdy M. Ragab, Ashraf F. Zaher, Suzan M. Abuel-Maaty and **Ahmed E. Fouda**. "Synthesis of certain 4-Quinolones of expected antitumor activity", *Journal Bull. Fac. Pharm, Cairo Univ.*, Elsevier, Vol. 47, No. 1, **2009**, P. 9-17.